INVESTIGATION OF VARIATION OF TRIAXIALTY AND LODE ANGLE PARAMETER VALUES IN SHEET METAL FORMING PROCESSES

A THESIS SUBMITTED TO
THE GRADUATE SCHOOL OF NATURAL AND APPLIED SCIENCES
OF
MIDDLE EAST TECHNICAL UNIVERSITY

BY

TOLUNAY GÜZELDEREN

IN PARTIAL FULFILLMENT OF THE REQUIREMENTS
FOR
THE DEGREE OF MASTER OF SCIENCE
IN
MECHANICAL ENGINEERING

AUGUST 2022

Approval of the thesis:

INVESTIGATION OF VARIATION OF TRIAXIALTY AND LODE ANGLE PARAMETER VALUES IN SHEET METAL FORMING PROCESSES

submitted by **TOLUNAY GÜZELDEREN** in partial fulfillment of the requirements for the degree of **Master of Science** i**n Mechanical Engineering, Middle East Technical University** by,

Prof. Dr. Halil Kalıpçılar
Dean, Graduate School of **Natural and Applied Sciences** _____

Prof. Dr. M.A. Sahir Arıkan
Head of the Department, **Mechanical Engineering, METU** _____

Prof. Dr. Haluk Darendeliler
Supervisor, **Mechanical Engineering, METU** _____

Examining Committee Members:

Prof. Dr. Suha Oral
Mechanical Engineering, METU _____

Prof. Dr. Haluk Darendeliler
Mechanical Engineering, METU _____

Prof. Dr. F. Suat Kadıoğlu
Mechanical Engineering, METU _____

Assistant Prof. Dr. Orkun Özşahin
Mechanical Engineering, METU _____

Prof. Dr. Can Çoğun
Mechatronics Engineering, ÇANKAYA University _____

Date: 29.08.2022

I hereby declare that all information in this document has been obtained and presented in accordance with academic rules and ethical conduct. I also declare that, as required by these rules and conduct, I have fully cited and referenced all material and results that are not original to this work.

Name, Last name : Tolunay Güzelderen

Signature :

ABSTRACT

INVESTIGATION OF VARIATION OF TRIAXIALTY AND LODE ANGLE PARAMETER VALUES IN SHEET METAL FORMING PROCESSES

Güzelderen, Tolunay

Master of Science, Mechanical Engineering
Supervisor: Prof. Dr. Haluk Darendeliler

August 2022, 273 pages

The aim of this study is to find out the relations of stress triaxiality and Lode angle parameter with the deformation characteristics of deep drawing process. For this purpose, deep drawing process is analyzed numerically by using different yield criteria, ductile criteria and hardening models for two different sheet materials. The simulations are carried out by using the finite element method.

Square and cylindrical cups made of Al-2024 aluminum and AISI 304 steel are formed. Von Mises and Hill'48 yield criteria are applied with the Johnson-Cook and the Hosford Coulomb ductile criteria. For hardening Johnson-Cook model and direct implementation of the plastic stress-plastic strain relations are used.

The results are presented in terms of effective plastic strain, triaxiality and Lode parameter distributions within the deformed blank. The tensile, compressive and shear nature of the deformation is evaluated by referring the corresponding triaxiality and Lode angle parameter values. Triaxiality and Lode angle parameter values are also considered the verify the type of the fracture. For the fractured points in the deformed cups the variation of triaxiality and Lode angle parameter values with

respect to equivalent plastic strain are presented by considering the two different ductile fracture criteria.

Keywords: Sheet Metal, Deep Drawing, Lode Parameter, Triaxiality, Yield Criteria

ÖZ

SAÇ METAL ŞEKİLLENDİRME SÜREÇLERİNDE ÜÇ EKSENLİLİK VE LODE AÇISI PARAMETRE DEĞERLERİNİN DEĞİŞİMİNİN İNCELENMESİ

Güzelderen, Tolunay
Yüksek Lisans, Makina Mühendisliği
Tez Yöneticisi: Prof. Dr. Haluk Darendeliler

Ağustos 2022, 273 sayfa

Bu çalışmanın amacı, derin çekme işleminin şekil değiştirme davranışı ile gerilme üç eksenliliği ve Lode açı parametresi arasındaki ilişkileri bulmaktır. Bu amaçla, iki farklı sac malzeme için farklı akma kriterleri, süneklik kriterleri ve pekleşme modelleri kullanılarak derin çekme işlemi sayısal olarak analiz edilmiştir. Simülasyonlar sonlu elemanlar yöntemi kullanılarak gerçekleştirilmiştir.

Al-2024 alüminyum ve AISI 304 çelik malzemeleri kullanılarak kare ve silindirik kaplar şekillendirilmiştir. Von Mises ve Hill'48 akma kriterleri, Johnson-Cook ve Hosford Coulomb sünek kopma kriterleri ile birlikte uygulanmıştır. Pekleşme için Johnson-Cook modeli kullanılmış veya plastik gerilme-plastik gerinim ilişkileri doğrudan uygulanmıştır.

Sonuçlar, şekil değiştirmiş taslak için eşdeğer plastik gerinim, üç eksenlilik ve Lode açı parametre dağılımları verilerek sunulmuştur. Şekil değiştirmenin çekme, sıkıştırma ve kesme doğası, ilgili üç eksenlilik ve Lode açı parametre değerleri kullanılarak değerlendirmiştir. Üç eksenlilik ve Lode açı parametre değerleri kırılma tipini doğrulamak için de kullanılmıştır. Şekil değiştirmiş taslaktan kopma noktaları için üç eksenlilik ve Lode parametre değerlerinin değişimi, her iki sünek kopma kriterini göz önüne alarak verilmiştir.

Anahtar Kelimeler: Sac Malzeme, Derin Çekme, Lode Parametresi, Üç Eksenlilik, Akma Kriterleri

To My Family

ACKNOWLEDGMENTS

First of all, I would like to express my sincere thanks to my supervisor, Prof. Dr. Haluk DARENDELİLER for his support, encouragement, valuable advices and guidance. I am also grateful for the time he devoted to me.

Finally, I would like to express my gratitude to my beloved family for their unwavering support; I would like to thank my dear wife Yazgı Beriy ALTUN GÜZELDEREN, my mother Sönmez GÜZELDEREN, and my brother Koray GÜZELDEREN for their understanding, effort, encouragement, and unending patience throughout the studies.

TABLE OF CONTENTS

ABSTRACT v

ÖZ vii

ACKNOWLEDGMENTS x

TABLE OF CONTENTS xi

LIST OF TABLES xiv

LIST OF FIGURES xv

LIST OF ABBREVIATIONS xxxvii

LIST OF SYMBOLS xxxviii

CHAPTERS

1 INTRODUCTION 1

1.1 Background and Motivation 1

1.2 Objective of the Thesis 2

1.3 Scope of the Thesis 2

1.4 Outline of the Thesis 2

2 LITERATURE SURVEY 5

3 THEORETICAL BACKGROUND 9

3.1 Yield Criteria 9

3.1.1 Von Mises Yield Criterion 9

3.1.2 Hill'48 Yield Criterion 10

3.2 Hardening 12

3.2.1 Isotropic Hardening 12

3.2.2 Kinematic Hardening 12

3.2.3 Combined Hardening 13
3.2.4 Johnson Cook Hardening 13
3.3 Ductile Fracture Criteria 14
3.3.1 Johnson Cook Damage Initiation Criterion 14
3.3.2 Hosford Coulomb Damage Initiation Criteria 14
3.4 Triaxiality and Lode Parameter 15
3.4.1 Triaxiality 15
3.4.2 Lode Parameter 16
4 FINITE ELEMENT ANALYZES 21
4.1 Finite Element Method 21
4.2 Finite Element Model 22
4.2.1 Square Cup Drawing 22
4.2.1.1 Model Geometry and Mesh 22
4.2.1.2 Boundary Conditions and Load 25
4.2.2 Materials 26
4.2.2.1 AL-2024 26
4.2.2.2 AISI 304 27
5 RESULTS 31
5.1 Square Bottom Punch Deep-Drawing Analyzes 31
5.1.1 Case 1: Square-Al2024-von Mises-Discrete-Johnson Cook Model .. 33
5.1.2 Case 2: Square-Al2024-von Mises-Discrete-Hosford Coulomb Model 46
5.1.3 Case 3: Square-Al2024-von Mises -Johnson Cook-Johnson Cook Model 68

5.1.4 Case 4: Square-Al2024-von Mises -Johnson Cook-Hosford Coulomb Model 84

5.1.5 Case 5: Square-Al2024-Hill48-Discrete-Johnson Cook Model 111

5.1.6 Case 6: Square-Al2024- Hill48-Discrete-Hosford Coulomb Model 127

5.1.7 Case 7: Square- AISI304-von Mises-Discrete-Johnson Cook Model 148

5.1.8 Case 8: Square- AISI304-von Mises-Discrete-Hosford Coulomb Model 166

5.1.9 Case 9: Square- AISI304-von Mises -Johnson Cook-Johnson Cook Model 181

5.1.10 Case 10: Square-AISI304-von Mises-Johnson Cook-Hosford Coulomb Model 205

5.1.11 Case 11: Square-AISI304-Hill48-Discrete-Johnson Cook Model.. 220

5.1.12 Case 12: Square-AISI304-Hill48-Discrete-Hosford Coulomb Model 238

5.2 Cylindrical Bottom Punch Deep-Drawing Analysis 253

5.2.1 Case 13-Al2024-von Mises-Johnson Cook-Hosford Coulomb Model 253

6 CONCLUSION & FUTURE WORKS.....263

6.1 Conclusion..... 263

6.2 Future Works..... 265

REFERENCES 267

LIST OF TABLES

TABLES

Table 4.1 Geometric Parameters of Model.....22
Table 4.2. Hill'48 r values and coefficients for Al-2024 [51], [52] 26
Table 4.3. Johnson Cook damage initiation coefficients for Al-2024 [53].....27
Table 4.4. Hosford Coulomb Coefficients for Al-2024 [54].....27
Table 4.5. Hill'48 r values and coefficients for AISI-304 [56], [57] 28
Table 4.6. Johnson Cook damage initiation coefficients for AISI-304 [58] 28
Table 4.7. Hosford Coulomb Coefficients for AISI-304 [59].....29
Table 5.1 Model of Analyzes 32

LIST OF FIGURES

FIGURES

Figure 3.1. The change of new combination of the Lode and Stress Triaxiality [42] 17
Figure 3.2. Three types of coordinate system in the space of principal stresses [44] 18
Figure 3.3. The stress state of the specimen with inclined notch in the Wierzbicki stress state diagram [43]..... 19
Figure 4.1. Blank Meshed..... 23
Figure 4.2. Die Meshed..... 23
Figure 4.3. Holder Meshed 24
Figure 4.4. Punch Meshed 24
Figure 4.5. Boundary Conditions of Parts on Assembly 25
Figure 4.6. Al-2024 true strain-true stress curve[50]..... 26
Figure 4.7. AISI-304 strain-true stress curve [55] 28
Figure 5.1. Assembly of Square Bottom Punch Model 31
Figure 5.2. First Rupture Moment of Case 1 34
Figure 5.3. The variation of (a) Equivalent Plastic Strain (b) Stress Triaxiality and (c) Lode Angle Parameter along the rolling direction of the blank at 2 mm cup depth for Al2024 aluminum (VM-Disc-JC) 35
Figure 5.4. The variation of (a) Equivalent Plastic Strain (b) Stress Triaxiality and (c) Lode Angle Parameter along the rolling direction of the blank at 4 mm cup depth for Al2024 aluminum (VM-Disc-JC) 36
Figure 5.5. The variation of (a) Equivalent Plastic Strain (b) Stress Triaxiality and (c) Lode Angle Parameter along the rolling direction of the blank at 6 mm cup depth for Al2024 aluminum (VM-Disc-JC) 37
Figure 5.6. The variation of (a) Equivalent Plastic Strain (b) Stress Triaxiality and (c) Lode Angle Parameter along the rolling direction of the blank at 8 mm cup depth for Al2024 aluminum (VM-Disc-JC) 38

Figure 5.7. The variation of (a) Equivalent Plastic Strain (b) Stress Triaxiality and (c) Lode Angle Parameter along the diagonal of the blank at 2 mm cup depth for Al2024 aluminum (VM-Disc-JC)..... 39
Figure 5.8. The variation of (a) Equivalent Plastic Strain (b) Stress Triaxiality and (c) Lode Angle Parameter along the diagonal of the blank at 4 mm cup depth for Al2024 aluminum (VM-Disc-JC)..... 40
Figure 5.9. The variation of (a) Equivalent Plastic Strain (b) Stress Triaxiality and (c) Lode Angle Parameter along the diagonal of the blank at 6 mm cup depth for Al2024 aluminum (VM-Disc-JC)..... 41
Figure 5.10. The variation of (a) Equivalent Plastic Strain and Thickness Plastic Strain (b) Stress Triaxiality and (c) Lode Angle Parameter along the diagonal of the blank at 8 mm cup depth for Al2024 aluminum (VM-Disc-JC) 42
Figure 5.11. Equivalent Plastic Strain - Stress Triaxiality variations Plot of First Rupture Element (VM-Disc-JC)..... 43
Figure 5.12. Equivalent Plastic Strain - Lode Angle Parameter Plot of First Rupture Element (VM-Disc-JC) 43
Figure 5.13. First Rupture Moment of Case 2..... 47
Figure 5.14. The variation of (a) Equivalent Plastic Strain (b) Stress Triaxiality and (c) Lode Angle Parameter along the rolling direction of the blank at 2 mm cup depth for Al2024 aluminum (VM-Disc-HC)..... 48
Figure 5.15. The variation of (a) Equivalent Plastic Strain (b) Stress Triaxiality and (c) Lode Angle Parameter along the rolling direction of the blank at 4 mm cup depth for Al2024 aluminum (VM-Disc-HC)..... 49
Figure 5.16. The variation of (a) Equivalent Plastic Strain (b) Stress Triaxiality and (c) Lode Angle Parameter along the rolling direction of the blank at 6 mm cup depth for Al2024 aluminum (VM-Disc-HC)..... 50
Figure 5.17. The variation of (a) Equivalent Plastic Strain (b) Stress Triaxiality and (c) Lode Angle Parameter along the rolling direction of the blank at 8 mm cup depth for Al2024 aluminum (VM-Disc-HC)..... 51

Figure 5.18. The variation of (a) Equivalent Plastic Strain (b) Stress Triaxiality and (c) Lode Angle Parameter along the rolling direction of the blank at 10 mm cup depth for Al2024 aluminum (VM-Disc-HC) 52
Figure 5.19 The variation of (a) Equivalent Plastic Strain (b) Stress Triaxiality and (c) Lode Angle Parameter along the rolling direction of the blank at 12 mm cup depth for Al2024 aluminum (VM-Disc-HC) 53
Figure 5.20. The variation of (a) Equivalent Plastic Strain (b) Stress Triaxiality and (c) Lode Angle Parameter along the transverse direction of the blank at 2 mm cup depth for Al2024 aluminum (VM-Disc-HC) 54
Figure 5.21. The variation of (a) Equivalent Plastic Strain (b) Stress Triaxiality and (c) Lode Angle Parameter along the transverse direction of the blank at 4 mm cup depth for Al2024 aluminum (VM-Disc-HC) 55
Figure 5.22. The variation of (a) Equivalent Plastic Strain (b) Stress Triaxiality and (c) Lode Angle Parameter along the transverse direction of the blank at 6 mm cup depth for Al2024 aluminum (VM-Disc-HC) 56
Figure 5.23. The variation of (a) Equivalent Plastic Strain (b) Stress Triaxiality and (c) Lode Angle Parameter along the transverse direction of the blank at 8 mm cup depth for Al2024 aluminum (VM-Disc-HC) 57
Figure 5.24. The variation of (a) Equivalent Plastic Strain (b) Stress Triaxiality and (c) Lode Angle Parameter along the transverse direction of the blank at 10 mm cup depth for Al2024 aluminum (VM-Disc-HC) 58
Figure 5.25. The variation of (a) Equivalent Plastic Strain (b) Stress Triaxiality and (c) Lode Angle Parameter along the transverse direction of the blank at 12 mm cup depth for Al2024 aluminum (VM-Disc-HC) 59
Figure 5.26. The variation of (a) Equivalent Plastic Strain (b) Stress Triaxiality and (c) Lode Angle Parameter along the diagonal of the blank at 2 mm cup depth for Al2024 aluminum (VM-Disc-HC)..... 60
Figure 5.27. The variation of (a) Equivalent Plastic Strain (b) Stress Triaxiality and (c) Lode Angle Parameter along the diagonal of the blank at 4 mm cup depth for Al2024 aluminum (VM-Disc-HC)..... 61

Figure 5.28 The variation of (a) Equivalent Plastic Strain (b) Stress Triaxiality and (c) Lode Angle Parameter along the diagonal of the blank at 6 mm cup depth for Al2024 aluminum (VM-Disc-HC) 62
Figure 5.29 The variation of (a) Equivalent Plastic Strain (b) Stress Triaxiality and (c) Lode Angle Parameter along the diagonal of the blank at 8 mm cup depth for Al2024 aluminum (VM-Disc-HC) 63
Figure 5.30. The variation of (a) Equivalent Plastic Strain (b) Stress Triaxiality and (c) Lode Angle Parameter along the diagonal of the blank at 10 mm cup depth for Al2024 aluminum (VM-Disc-HC) 64
Figure 5.31. The variation of (a) Equivalent Plastic Strain and Thickness Plastic Strain (b) Stress Triaxiality and (c) Lode Angle Parameter along the diagonal of the blank at 12 mm cup depth for Al2024 aluminum (VM-Disc-HC) 65
Figure 5.32. Equivalent Plastic Strain - Stress Triaxiality Plot of First Rupture Element (VM-Disc-HC) 66
Figure 5.33. Equivalent Plastic Strain – Lode Angle Parameter Plot of First Rupture Element (VM-Disc-HC) 66
Figure 5.34. First Rupture Moment of Case 3 69
Figure 5.35. The variation of (a) Equivalent Plastic Strain (b) Stress Triaxiality and (c) Lode Angle Parameter along the rolling direction of the blank at 2 mm cup depth for Al2024 aluminum (VM-JC-JC) 70
Figure 5.36. The variation of (a) Equivalent Plastic Strain (b) Stress Triaxiality and (c) Lode Angle Parameter along the rolling direction of the blank at 4 mm cup depth for Al2024 aluminum (VM-JC-JC) 71
Figure 5.37. The variation of (a) Equivalent Plastic Strain (b) Stress Triaxiality and (c) Lode Angle Parameter along the rolling direction of the blank at 6 mm cup depth for Al2024 aluminum (VM-JC-JC) 72
Figure 5.38. The variation of (a) Equivalent Plastic Strain (b) Stress Triaxiality and (c) Lode Angle Parameter along the rolling direction of the blank at 8 mm cup depth for Al2024 aluminum (VM-JC-JC) 73

Figure 5.39. The variation of (a) Equivalent Plastic Strain (b) Stress Triaxiality and (c) Lode Angle Parameter along the transverse direction of the blank at 2 mm cup depth for Al2024 aluminum (VM-JC-JC)..... 74
Figure 5.40. The variation of (a) Equivalent Plastic Strain (b) Stress Triaxiality and (c) Lode Angle Parameter along the transverse direction of the blank at 4 mm cup depth for Al2024 aluminum (VM-JC-JC)..... 75
Figure 5.41. The variation of (a) Equivalent Plastic Strain (b) Stress Triaxiality and (c) Lode Angle Parameter along the transverse direction of the blank at 6 mm cup depth for Al2024 aluminum (VM-JC-JC)..... 76
Figure 5.42. The variation of (a) Equivalent Plastic Strain (b) Stress Triaxiality and (c) Lode Angle Parameter along the transverse direction of the blank at 8 mm cup depth for Al2024 aluminum (VM-JC-JC)..... 77
Figure 5.43. The variation of (a) Equivalent Plastic Strain (b) Stress Triaxiality and (c) Lode Angle Parameter along the diagonal of the blank at 2 mm cup depth for Al2024 aluminum (VM-JC-JC) 78
Figure 5.44. The variation of (a) Equivalent Plastic Strain (b) Stress Triaxiality and (c) Lode Angle Parameter along the diagonal of the blank at 4 mm cup depth for Al2024 aluminum (VM-JC-JC) 79
Figure 5.45. The variation of (a) Equivalent Plastic Strain (b) Stress Triaxiality and (c) Lode Angle Parameter along the diagonal of the blank at 6 mm cup depth for Al2024 aluminum (VM-JC-JC) 80
Figure 5.46. The variation of (a) Equivalent Plastic Strain and Thickness Plastic Strain (b) Stress Triaxiality and (c) Lode Angle Parameter along the diagonal of the blank at 8 mm cup depth for Al2024 aluminum (VM-JC-JC)..... 81
Figure 5.47. Equivalent Plastic Strain - Stress Triaxiality Plot of First Rupture Element (VM-JC-JC) 82
Figure 5.48. Equivalent Plastic Strain – Lode Angle Parameter Plot of First Rupture Element (VM-JC-JC) 82
Figure 5.49. First Rupture Moment of Case 4 84

Figure 5.50. The variation of (a) Equivalent Plastic Strain (b) Stress Triaxiality and (c) Lode Angle Parameter along the rolling direction of the blank at 2 mm cup depth for Al2024 aluminum (VM-JC-HC) 85
Figure 5.51. The variation of (a) Equivalent Plastic Strain (b) Stress Triaxiality and (c) Lode Angle Parameter along the rolling direction of the blank at 4 mm cup depth for Al2024 aluminum (VM-JC-HC) 86
Figure 5.52. The variation of (a) Equivalent Plastic Strain (b) Stress Triaxiality and (c) Lode Angle Parameter along the rolling direction of the blank at 6 mm cup depth for Al2024 aluminum (VM-JC-HC) 87
Figure 5.53. The variation of (a) Equivalent Plastic Strain (b) Stress Triaxiality and (c) Lode Angle Parameter along the rolling direction of the blank at 8 mm cup depth for Al2024 aluminum (VM-JC-HC) 88
Figure 5.54. The variation of (a) Equivalent Plastic Strain (b) Stress Triaxiality and (c) Lode Angle Parameter along the rolling direction of the blank at 10 mm cup depth for Al2024 aluminum (VM-JC-HC) 89
Figure 5.55 The variation of (a) Equivalent Plastic Strain (b) Stress Triaxiality and (c) Lode Angle Parameter along the rolling direction of the blank at 12 mm cup depth for Al2024 aluminum (VM-JC-HC) 90
Figure 5.56. The variation of (a) Equivalent Plastic Strain (b) Stress Triaxiality and (c) Lode Angle Parameter along the transverse direction of the blank at 2 mm cup depth for Al2024 aluminum (VM-JC-HC) 91
Figure 5.57. The variation of (a) Equivalent Plastic Strain (b) Stress Triaxiality and (c) Lode Angle Parameter along the transverse direction of the blank at 4 mm cup depth for Al2024 aluminum (VM-JC-HC) 92
Figure 5.58. The variation of (a) Equivalent Plastic Strain (b) Stress Triaxiality and (c) Lode Angle Parameter along the transverse direction of the blank at 6 mm cup depth for Al2024 aluminum (VM-JC-HC) 93
Figure 5.59. The variation of (a) Equivalent Plastic Strain (b) Stress Triaxiality and (c) Lode Angle Parameter along the transverse direction of the blank at 8 mm cup depth for Al2024 aluminum (VM-JC-HC) 94

Figure 5.60. The variation of (a) Equivalent Plastic Strain (b) Stress Triaxiality and (c) Lode Angle Parameter along the transverse direction of the blank at 10 mm cup depth for Al2024 aluminum (VM-JC-HC) 95
Figure 5.61. The variation of (a) Equivalent Plastic Strain (b) Stress Triaxiality and (c) Lode Angle Parameter along the transverse direction of the blank at 12 mm cup depth for Al2024 aluminum (VM-JC-HC) 96
Figure 5.62. The variation of (a) Equivalent Plastic Strain (b) Stress Triaxiality and (c) Lode Angle Parameter along the diagonal of the blank at 2 mm cup depth for Al2024 aluminum (VM-JC-HC)..... 97
Figure 5.63. The variation of (a) Equivalent Plastic Strain (b) Stress Triaxiality and (c) Lode Angle Parameter along the diagonal of the blank at 4 mm cup depth for Al2024 aluminum (VM-JC-HC)..... 98
Figure 5.64 The variation of (a) Equivalent Plastic Strain (b) Stress Triaxiality and (c) Lode Angle Parameter along the diagonal of the blank at 6 mm cup depth for Al2024 aluminum (VM-JC-HC)..... 99
Figure 5.65. The variation of (a) Equivalent Plastic Strain (b) Stress Triaxiality and (c) Lode Angle Parameter along the diagonal of the blank at 8 mm cup depth for Al2024 aluminum (VM-JC-HC)..... 100
Figure 5.66. The variation of (a) Equivalent Plastic Strain (b) Stress Triaxiality and (c) Lode Angle Parameter along the diagonal of the blank at 10 mm cup depth for Al2024 aluminum (VM-JC-HC)..... 101
Figure 5.67. The variation of (a) Equivalent Plastic Strain and Thickness Plastic Strain (b) Stress Triaxiality and (c) Lode Angle Parameter along the diagonal of the blank at 12 mm cup depth for Al2024 aluminum (VM-JC-HC) 102
Figure 5.68. Equivalent Plastic Strain - Stress Triaxiality Plot of First Rupture Element (VM-JC-HC)..... 103
Figure 5.69. Equivalent Plastic Strain – Lode Angle Parameter Plot of First Rupture Element (VM-JC-HC)..... 103
Figure 5.70. The variation of triaxiality values with respect to Lode angle parameter values in rolling direction (a) for punch (b) for punch shoulder or corner

(c) for the clearance between die and punch (d) for die shoulder or corner and (e) for the blank holder regions of the blank at 12 mm cup depth for Al2024 aluminum (VM-JC-HC).....105
Figure 5.71. The variation of triaxiality values with respect to Lode angle parameter values in transverse direction (a) for punch (b) for punch shoulder or corner (c) for the clearance between die and punch (d) for die shoulder or corner and (e) for the blank holder regions of the blank at 12 mm cup depth for Al2024 aluminum (VM-JC-HC) 107
Figure 5.72. The variation of triaxiality values with respect to Lode angle parameter values in diagonal direction (a) for punch (b) for punch shoulder or corner (c) for the clearance between die and punch (d) for die shoulder or corner and (e) for the blank holder regions of the blank at 12 mm cup depth for Al2024 aluminum (VM-JC-HC) 109
Figure 5.73. First Rupture Moment of Case 5.....111
Figure 5.74. The variation of (a) Equivalent Plastic Strain (b) Stress Triaxiality and (c) Lode Angle Parameter along the rolling direction of the blank at 2 mm cup depth for Al2024 aluminum (Hill'48-Disc-JC).....112
Figure 5.75. The variation of (a) Equivalent Plastic Strain (b) Stress Triaxiality and (c) Lode Angle Parameter along the rolling direction of the blank at 4 mm cup depth for Al2024 aluminum (Hill'48-Disc-JC).....113
Figure 5.76. The variation of (a) Equivalent Plastic Strain (b) Stress Triaxiality and (c) Lode Angle Parameter along the rolling direction of the blank at 6 mm cup depth for Al2024 aluminum (Hill'48-Disc-JC).....114
Figure 5.77. The variation of (a) Equivalent Plastic Strain (b) Stress Triaxiality and (c) Lode Angle Parameter along the rolling direction of the blank at 8 mm cup depth for Al2024 aluminum (Hill'48-Disc-JC).....115
Figure 5.78. The variation of (a) Equivalent Plastic Strain (b) Stress Triaxiality and (c) Lode Angle Parameter along the transverse direction of the blank at 2 mm cup depth for Al2024 aluminum (Hill'48-Disc-JC).....116

Figure 5.79. The variation of (a) Equivalent Plastic Strain (b) Stress Triaxiality and (c) Lode Angle Parameter along the transverse direction of the blank at 4 mm cup depth for Al2024 aluminum (Hill'48-Disc-JC) 117
Figure 5.80. The variation of (a) Equivalent Plastic Strain (b) Stress Triaxiality and (c) Lode Angle Parameter along the transverse direction of the blank at 6 mm cup depth for Al2024 aluminum (Hill'48-Disc-JC) 118
Figure 5.81. The variation of (a) Equivalent Plastic Strain (b) Stress Triaxiality and (c) Lode Angle Parameter along the transverse direction of the blank at 8 mm cup depth for Al2024 aluminum (Hill'48-Disc-JC) 119
Figure 5.82. The variation of (a) Equivalent Plastic Strain (b) Stress Triaxiality and (c) Lode Angle Parameter along the diagonal of the blank at 2 mm cup depth for Al2024 aluminum (Hill'48-Disc-JC) 120
Figure 5.83. The variation of (a) Equivalent Plastic Strain (b) Stress Triaxiality and (c) Lode Angle Parameter along the diagonal of the blank at 4 mm cup depth for Al2024 aluminum (Hill'48-Disc-JC) 121
Figure 5.84. The variation of (a) Equivalent Plastic Strain (b) Stress Triaxiality and (c) Lode Angle Parameter along the diagonal of the blank at 6 mm cup depth for Al2024 aluminum (Hill'48-Disc-JC) 122
Figure 5.85. The variation of (a) Equivalent Plastic Strain and Thickness Plastic Strain (b) Stress Triaxiality and (c) Lode Angle Parameter along the diagonal of the blank at 8 mm cup depth for Al2024 aluminum (Hill'48-Disc-JC) 123
Figure 5.86. Equivalent Plastic Strain - Stress Triaxiality Plot of First Rupture Element (Hill'48-Disc-JC) 124
Figure 5.87. Equivalent Plastic Strain – Lode Angle Parameter Plot of First Rupture Element (Hill'48-Disc-JC) 124
Figure 5.88. First Rupture Moment of Case 6 127
Figure 5.89. The variation of (a) Equivalent Plastic Strain (b) Stress Triaxiality and (c) Lode Angle Parameter along the rolling direction of the blank at 2 mm cup depth for Al2024 aluminum (Hill'48-Disc-HC) 128

Figure 5.90. The variation of (a) Equivalent Plastic Strain (b) Stress Triaxiality and (c) Lode Angle Parameter along the rolling direction of the blank at 4 mm cup depth for Al2024 aluminum (Hill'48-Disc-HC).....129
Figure 5.91. The variation of (a) Equivalent Plastic Strain (b) Stress Triaxiality and (c) Lode Angle Parameter along the rolling direction of the blank at 6 mm cup depth for Al2024 aluminum (Hill'48-Disc-HC).....130
Figure 5.92. The variation of (a) Equivalent Plastic Strain (b) Stress Triaxiality and (c) Lode Angle Parameter along the rolling direction of the blank at 8 mm cup depth for Al2024 aluminum (Hill'48-Disc-HC).....131
Figure 5.93. The variation of (a) Equivalent Plastic Strain (b) Stress Triaxiality and (c) Lode Angle Parameter along the rolling direction of the blank at 10 mm cup depth for Al2024 aluminum (Hill'48-Disc-HC).....132
Figure 5.94 The variation of (a) Equivalent Plastic Strain (b) Stress Triaxiality and (c) Lode Angle Parameter along the rolling direction of the blank at 12 mm cup depth for Al2024 aluminum (Hill'48-Disc-HC).....133
Figure 5.95. The variation of (a) Equivalent Plastic Strain (b) Stress Triaxiality and (c) Lode Angle Parameter along the transverse direction of the blank at 2 mm cup depth for Al2024 aluminum (Hill'48-Disc-HC).....134
Figure 5.96. The variation of (a) Equivalent Plastic Strain (b) Stress Triaxiality and (c) Lode Angle Parameter along the transverse direction of the blank at 4 mm cup depth for Al2024 aluminum (Hill'48-Disc-HC).....135
Figure 5.97. The variation of (a) Equivalent Plastic Strain (b) Stress Triaxiality and (c) Lode Angle Parameter along the transverse direction of the blank at 6 mm cup depth for Al2024 aluminum (Hill'48-Disc-HC).....136
Figure 5.98. The variation of (a) Equivalent Plastic Strain (b) Stress Triaxiality and (c) Lode Angle Parameter along the transverse direction of the blank at 8 mm cup depth for Al2024 aluminum (Hill'48-Disc-HC).....137
Figure 5.99. The variation of (a) Equivalent Plastic Strain (b) Stress Triaxiality and (c) Lode Angle Parameter along the transverse direction of the blank at 10 mm cup depth for Al2024 aluminum (Hill'48-Disc-HC).....138

Figure 5.100. The variation of (a) Equivalent Plastic Strain (b) Stress Triaxiality and (c) Lode Angle Parameter along the transverse direction of the blank at 12 mm cup depth for Al2024 aluminum (Hill'48-Disc-HC) 139
Figure 5.101. The variation of (a) Equivalent Plastic Strain (b) Stress Triaxiality and (c) Lode Angle Parameter along the diagonal of the blank at 2 mm cup depth for Al2024 aluminum (Hill'48-Disc-HC) 140
Figure 5.102. The variation of (a) Equivalent Plastic Strain (b) Stress Triaxiality and (c) Lode Angle Parameter along the diagonal of the blank at 4 mm cup depth for Al2024 aluminum (Hill'48-Disc-HC) 141
Figure 5.103 The variation of (a) Equivalent Plastic Strain (b) Stress Triaxiality and (c) Lode Angle Parameter along the diagonal of the blank at 6 mm cup depth for Al2024 aluminum (Hill'48-Disc-HC) 142
Figure 5.104 The variation of (a) Equivalent Plastic Strain (b) Stress Triaxiality and (c) Lode Angle Parameter along the diagonal of the blank at 8 mm cup depth for Al2024 aluminum (Hill'48-Disc-HC) 143
Figure 5.105. The variation of (a) Equivalent Plastic Strain (b) Stress Triaxiality and (c) Lode Angle Parameter along the diagonal of the blank at 10 mm cup depth for Al2024 aluminum (Hill'48-Disc-HC) 144
Figure 5.106. The variation of (a) Equivalent Plastic Strain and Thickness Plastic Strain (b) Stress Triaxiality and (c) Lode Angle Parameter along the diagonal of the blank at 12 mm cup depth for Al2024 aluminum (Hill'48-Disc-HC) 145
Figure 5.107. Equivalent Plastic Strain - Stress Triaxiality Plot of First Rupture Element (Hill'48-Disc-HC) 146
Figure 5.108. Equivalent Plastic Strain – Lode Angle Parameter Plot of First Rupture Element (Hill'48-Disc-HC) 146
Figure 5.109. First Rupture Moment of Case 7 148
Figure 5.110. The variation of (a) Equivalent Plastic Strain (b) Stress Triaxiality and (c) Lode Angle Parameter along the rolling direction of the blank at 4 mm cup depth for AISI 304 steel (VM-Disc-JC) 149

Figure 5.111. The variation of (a) Equivalent Plastic Strain (b) Stress Triaxiality and (c) Lode Angle Parameter along the rolling direction of the blank at 8 mm cup depth for AISI 304 steel (VM-Disc-JC) 150
Figure 5.112. The variation of (a) Equivalent Plastic Strain (b) Stress Triaxiality and (c) Lode Angle Parameter along the rolling direction of the blank at 12 mm cup depth for AISI 304 steel (VM-Disc-JC) 151
Figure 5.113. The variation of (a) Equivalent Plastic Strain (b) Stress Triaxiality and (c) Lode Angle Parameter along the rolling direction of the blank at 16 mm cup depth for AISI 304 steel (VM-Disc-JC) 152
Figure 5.114. The variation of (a) Equivalent Plastic Strain (b) Stress Triaxiality and (c) Lode Angle Parameter along the rolling direction of the blank at 20 mm cup depth for AISI 304 steel (VM-Disc-JC) 153
Figure 5.115. The variation of (a) Equivalent Plastic Strain (b) Stress Triaxiality and (c) Lode Angle Parameter along the transverse direction of the blank at 4 mm cup depth for AISI 304 steel (VM-Disc-JC) 154
Figure 5.116. The variation of (a) Equivalent Plastic Strain (b) Stress Triaxiality and (c) Lode Angle Parameter along the transverse direction of the blank at 8 mm cup depth for AISI 304 steel (VM-Disc-JC) 155
Figure 5.117. The variation of (a) Equivalent Plastic Strain (b) Stress Triaxiality and (c) Lode Angle Parameter along the transverse direction of the blank at 12 mm cup depth for AISI 304 steel (VM-Disc-JC) 156
Figure 5.118. The variation of (a) Equivalent Plastic Strain (b) Stress Triaxiality and (c) Lode Angle Parameter along the transverse direction of the blank at 16 mm cup depth for AISI 304 steel (VM-Disc-JC) 157
Figure 5.119. The variation of (a) Equivalent Plastic Strain (b) Stress Triaxiality and (c) Lode Angle Parameter along the transverse direction of the blank at 20 mm cup depth for AISI 304 steel (VM-Disc-JC) 158
Figure 5.120. The variation of (a) Equivalent Plastic Strain (b) Stress Triaxiality and (c) Lode Angle Parameter along the diagonal of the blank at 4 mm cup depth for AISI 304 steel (VM-Disc-JC) 159

Figure 5.121. The variation of (a) Equivalent Plastic Strain (b) Stress Triaxiality and (c) Lode Angle Parameter along the diagonal of the blank at 8 mm cup depth for AISI 304 steel (VM-Disc-JC) 160
Figure 5.122 The variation of (a) Equivalent Plastic Strain (b) Stress Triaxiality and (c) Lode Angle Parameter along the diagonal of the blank at 12 mm cup depth for AISI 304 steel (VM-Disc-JC) 161
Figure 5.123 The variation of (a) Equivalent Plastic Strain (b) Stress Triaxiality and (c) Lode Angle Parameter along the diagonal of the blank at 16 mm cup depth for AISI 304 steel (VM-Disc-JC) 162
Figure 5.124. The variation of (a) Equivalent Plastic Strain and Thickness Plastic Strain (b) Stress Triaxiality and (c) Lode Angle Parameter along the diagonal of the blank at 20 mm cup depth for AISI 304 steel (VM-Disc-JC)..... 163
Figure 5.125. Equivalent Plastic Strain - Stress Triaxiality Plot of First Rupture Element (VM-Disc-JC)..... 164
Figure 5.126. Equivalent Plastic Strain – Lode Angle Parameter Plot of First Rupture Element (VM-Disc-JC) 164
Figure 5.127. First Rupture Moment of Case 8 166
Figure 5.128. The variation of (a) Equivalent Plastic Strain (b) Stress Triaxiality and (c) Lode Angle Parameter along the rolling direction of the blank at 4 mm cup depth for AISI 304 steel (VM-Disc-HC) 167
Figure 5.129. The variation of (a) Equivalent Plastic Strain (b) Stress Triaxiality and (c) Lode Angle Parameter along the rolling direction of the blank at 8 mm cup depth for AISI 304 steel (VM-Disc-HC) 168
Figure 5.130. The variation of (a) Equivalent Plastic Strain (b) Stress Triaxiality and (c) Lode Angle Parameter along the rolling direction of the blank at 12 mm cup depth for AISI 304 steel (VM-Disc-HC) 169
Figure 5.131. The variation of (a) Equivalent Plastic Strain (b) Stress Triaxiality and (c) Lode Angle Parameter along the rolling direction of the blank at 16 mm cup depth for AISI 304 steel (VM-Disc-HC) 170

Figure 5.132. The variation of (a) Equivalent Plastic Strain (b) Stress Triaxiality and (c) Lode Angle Parameter along the transverse direction of the blank at 4 mm cup depth for AISI 304 steel (VM-Disc-HC) 171
Figure 5.133. The variation of (a) Equivalent Plastic Strain (b) Stress Triaxiality and (c) Lode Angle Parameter along the transverse direction of the blank at 8 mm cup depth for AISI 304 steel (VM-Disc-HC) 172
Figure 5.134. The variation of (a) Equivalent Plastic Strain (b) Stress Triaxiality and (c) Lode Angle Parameter along the transverse direction of the blank at 12 mm cup depth for AISI 304 steel (VM-Disc-HC) 173
Figure 5.135. The variation of (a) Equivalent Plastic Strain (b) Stress Triaxiality and (c) Lode Angle Parameter along the transverse direction of the blank at 16 mm cup depth for AISI 304 steel (VM-Disc-HC) 174
Figure 5.136. The variation of (a) Equivalent Plastic Strain (b) Stress Triaxiality and (c) Lode Angle Parameter along the diagonal of the blank at 4 mm cup depth for AISI 304 steel (VM-Disc-HC) 175
Figure 5.137. The variation of (a) Equivalent Plastic Strain (b) Stress Triaxiality and (c) Lode Angle Parameter along the diagonal of the blank at 8 mm cup depth for AISI 304 steel (VM-Disc-HC) 176
Figure 5.138 The variation of (a) Equivalent Plastic Strain (b) Stress Triaxiality and (c) Lode Angle Parameter along the diagonal of the blank at 12 mm cup depth for AISI 304 steel (VM-Disc-HC) 177
Figure 5.139 The variation of (a) Equivalent Plastic Strain and Thickness Plastic Strain (b) Stress Triaxiality and (c) Lode Angle Parameter along the diagonal of the blank at 16 mm cup depth for AISI 304 steel (VM-Disc-HC) 178
Figure 5.140. Equivalent Plastic Strain - Stress Triaxiality Plot of First Rupture Element (VM-Disc-HC) 179
Figure 5.141. Equivalent Plastic Strain – Lode Angle Parameter Plot of First Rupture Element (VM-Disc-HC) 179
Figure 5.142. First Rupture Moment of Case 9 181

Figure 5.143. The variation of (a) Equivalent Plastic Strain (b) Stress Triaxiality and (c) Lode Angle Parameter along the rolling direction of the blank at 4 mm cup depth for AISI 304 steel (VM-JC-JC)..... 182
Figure 5.144. The variation of (a) Equivalent Plastic Strain (b) Stress Triaxiality and (c) Lode Angle Parameter along the rolling direction of the blank at 8 mm cup depth for AISI 304 steel (VM-JC-JC)..... 183
Figure 5.145. The variation of (a) Equivalent Plastic Strain (b) Stress Triaxiality and (c) Lode Angle Parameter along the rolling direction of the blank at 12 mm cup depth for AISI 304 steel (VM-JC-JC)..... 184
Figure 5.146. The variation of (a) Equivalent Plastic Strain (b) Stress Triaxiality and (c) Lode Angle Parameter along the rolling direction of the blank at 16 mm cup depth for AISI 304 steel (VM-JC-JC)..... 185
Figure 5.147. The variation of (a) Equivalent Plastic Strain (b) Stress Triaxiality and (c) Lode Angle Parameter along the rolling direction of the blank at 20 mm cup depth for AISI 304 steel (VM-JC-JC)..... 186
Figure 5.148. The variation of (a) Equivalent Plastic Strain (b) Stress Triaxiality and (c) Lode Angle Parameter along the transverse direction of the blank at 4 mm cup depth for AISI 304 steel (VM-JC-JC)..... 187
Figure 5.149. The variation of (a) Equivalent Plastic Strain (b) Stress Triaxiality and (c) Lode Angle Parameter along the transverse direction of the blank at 8 mm cup depth for AISI 304 steel (VM-JC-JC)..... 188
Figure 5.150. The variation of (a) Equivalent Plastic Strain (b) Stress Triaxiality and (c) Lode Angle Parameter along the transverse direction of the blank at 12 mm cup depth for AISI 304 steel (VM-JC-JC)..... 189
Figure 5.151. The variation of (a) Equivalent Plastic Strain (b) Stress Triaxiality and (c) Lode Angle Parameter along the transverse direction of the blank at 16 mm cup depth for AISI 304 steel (VM-JC-JC)..... 190
Figure 5.152. The variation of (a) Equivalent Plastic Strain (b) Stress Triaxiality and (c) Lode Angle Parameter along the transverse direction of the blank at 20 mm cup depth for AISI 304 steel (VM-JC-JC)..... 191

Figure 5.153. The variation of (a) Equivalent Plastic Strain (b) Stress Triaxiality and (c) Lode Angle Parameter along the diagonal of the blank at 4 mm cup depth for AISI 304 steel (VM-JC-JC) 192
Figure 5.154. The variation of (a) Equivalent Plastic Strain (b) Stress Triaxiality and (c) Lode Angle Parameter along the diagonal of the blank at 8 mm cup depth for AISI 304 steel (VM-JC-JC) 193
Figure 5.155 The variation of (a) Equivalent Plastic Strain (b) Stress Triaxiality and (c) Lode Angle Parameter along the diagonal of the blank at 12 mm cup depth for AISI 304 steel (VM-JC-JC) 194
Figure 5.156 The variation of (a) Equivalent Plastic Strain (b) Stress Triaxiality and (c) Lode Angle Parameter along the diagonal of the blank at 16 mm cup depth for AISI 304 steel (VM-JC-JC) 195
Figure 5.157. The variation of (a) Equivalent Plastic Strain (b) Stress Triaxiality and (c) Lode Angle Parameter along the diagonal of the blank at 20 mm cup depth for AISI 304 steel (VM-JC-JC) 196
Figure 5.158. Equivalent Plastic Strain - Stress Triaxiality Plot of First Rupture Element (VM-JC-JC) 197
Figure 5.159. Equivalent Plastic Strain – Lode Angle Parameter Plot of First Rupture Element (VM-JC-JC) 197
Figure 5.160. The variation of triaxiality values with respect to Lode angle parameter values in rolling direction (a) for punch (b) for punch shoulder or corner (c) for the clearance between die and punch (d) for die shoulder or corner and (e) for the blank holder regions of the blank at 20 mm cup depth for AISI304 steel (VM-JC-JC) 199
Figure 5.161. The variation of triaxiality values with respect to Lode angle parameter values in transverse direction (a) for punch (b) for punch shoulder or corner (c) for the clearance between die and punch (d) for die shoulder or corner and (e) for the blank holder regions of the blank at 20 mm cup depth for AISI304 steel (VM-JC-JC) 201

Figure 5.162. The variation of triaxiality values with respect to Lode angle parameter values in diagonal direction (a) for punch (b) for punch shoulder or corner (c) for the clearance between die and punch (d) for die shoulder or corner and (e) for the blank holder regions of the blank at 20 mm cup depth for AISI304 steel (VM-JC-JC) 203
Figure 5.163. First Fracture Moment of Case 10 205
Figure 5.164. The variation of (a) Equivalent Plastic Strain (b) Stress Triaxiality and (c) Lode Angle Parameter along the rolling direction of the blank at 4 mm cup depth for AISI 304 steel (VM-JC-HC) 206
Figure 5.165. The variation of (a) Equivalent Plastic Strain (b) Stress Triaxiality and (c) Lode Angle Parameter along the rolling direction of the blank at 8 mm cup depth for AISI 304 steel (VM-JC-HC) 207
Figure 5.166. The variation of (a) Equivalent Plastic Strain (b) Stress Triaxiality and (c) Lode Angle Parameter along the rolling direction of the blank at 12 mm cup depth for AISI 304 steel (VM-JC-HC) 208
Figure 5.167. The variation of (a) Equivalent Plastic Strain (b) Stress Triaxiality and (c) Lode Angle Parameter along the rolling direction of the blank at 16 mm cup depth for AISI 304 steel (VM-JC-HC) 209
Figure 5.168. The variation of (a) Equivalent Plastic Strain (b) Stress Triaxiality and (c) Lode Angle Parameter along the transverse direction of the blank at 4 mm cup depth for AISI 304 steel (VM-JC-HC)..... 210
Figure 5.169. The variation of (a) Equivalent Plastic Strain (b) Stress Triaxiality and (c) Lode Angle Parameter along the transverse direction of the blank at 8 mm cup depth for AISI 304 steel (VM-JC-HC)..... 211
Figure 5.170. The variation of (a) Equivalent Plastic Strain (b) Stress Triaxiality and (c) Lode Angle Parameter along the transverse direction of the blank at 12 mm cup depth for AISI 304 steel (VM-JC-HC)..... 212
Figure 5.171. The variation of (a) Equivalent Plastic Strain (b) Stress Triaxiality and (c) Lode Angle Parameter along the transverse direction of the blank at 16 mm cup depth for AISI 304 steel (VM-JC-HC)..... 213

Figure 5.172. The variation of (a) Equivalent Plastic Strain (b) Stress Triaxiality and (c) Lode Angle Parameter along the diagonal of the blank at 4 mm cup depth for AISI 304 steel (VM-JC-HC) 214
Figure 5.173. The variation of (a) Equivalent Plastic Strain (b) Stress Triaxiality and (c) Lode Angle Parameter along the diagonal of the blank at 8 mm cup depth for AISI 304 steel (VM-JC-HC) 215
Figure 5.174 The variation of (a) Equivalent Plastic Strain (b) Stress Triaxiality and (c) Lode Angle Parameter along the diagonal of the blank at 12 mm cup depth for AISI 304 steel (VM-JC-HC) 216
Figure 5.175 The variation of (a) Equivalent Plastic Strain and Thickness Plastic Strain (b) Stress Triaxiality and (c) Lode Angle Parameter along the diagonal of the blank at 16 mm cup depth for AISI 304 steel (VM-JC-HC) 217
Figure 5.176. Equivalent Plastic Strain - Stress Triaxiality Plot of First Fracture Element (VM-JC-HC) 218
Figure 5.177. Equivalent Plastic Strain – Lode Angle Parameter Plot of First Fracture Element (VM-JC-HC) 218
Figure 5.178. First Fracture Moment of Case 11 220
Figure 5.179. The variation of (a) Equivalent Plastic Strain (b) Stress Triaxiality and (c) Lode Angle Parameter along the rolling direction of the blank at 4 mm cup depth for AISI 304 steel (Hill’48-Disc-JC) 221
Figure 5.180. The variation of (a) Equivalent Plastic Strain (b) Stress Triaxiality and (c) Lode Angle Parameter along the rolling direction of the blank at 8 mm cup depth for AISI 304 steel (Hill’48-Disc-JC) 222
Figure 5.181. The variation of (a) Equivalent Plastic Strain (b) Stress Triaxiality and (c) Lode Angle Parameter along the rolling direction of the blank at 12 mm cup depth for AISI 304 steel (Hill’48-Disc-JC) 223
Figure 5.182. The variation of (a) Equivalent Plastic Strain (b) Stress Triaxiality and (c) Lode Angle Parameter along the rolling direction of the blank at 16 mm cup depth for AISI 304 steel (Hill’48-Disc-JC) 224

Figure 5.183. The variation of (a) Equivalent Plastic Strain (b) Stress Triaxiality and (c) Lode Angle Parameter along the rolling direction of the blank at 20 mm cup depth for AISI 304 steel (Hill'48-Disc-JC) 225
Figure 5.184. The variation of (a) Equivalent Plastic Strain (b) Stress Triaxiality and (c) Lode Angle Parameter along the transverse direction of the blank at 4 mm cup depth for AISI 304 steel (Hill'48-Disc-JC)..... 226
Figure 5.185. The variation of (a) Equivalent Plastic Strain (b) Stress Triaxiality and (c) Lode Angle Parameter along the transverse direction of the blank at 8 mm cup depth for AISI 304 steel (Hill'48-Disc-JC)..... 227
Figure 5.186. The variation of (a) Equivalent Plastic Strain (b) Stress Triaxiality and (c) Lode Angle Parameter along the transverse direction of the blank at 12 mm cup depth for AISI 304 steel (Hill'48-Disc-JC)..... 228
Figure 5.187. The variation of (a) Equivalent Plastic Strain (b) Stress Triaxiality and (c) Lode Angle Parameter along the transverse direction of the blank at 16 mm cup depth for AISI 304 steel (Hill'48-Disc-JC)..... 229
Figure 5.188. The variation of (a) Equivalent Plastic Strain (b) Stress Triaxiality and (c) Lode Angle Parameter along the transverse direction of the blank at 20 mm cup depth for AISI 304 steel (Hill'48-Disc-JC)..... 230
Figure 5.189. The variation of (a) Equivalent Plastic Strain (b) Stress Triaxiality and (c) Lode Angle Parameter along the diagonal of the blank at 4 mm cup depth for AISI 304 steel (Hill'48-Disc-JC) 231
Figure 5.190. The variation of (a) Equivalent Plastic Strain (b) Stress Triaxiality and (c) Lode Angle Parameter along the diagonal of the blank at 8 mm cup depth for AISI 304 steel (Hill'48-Disc-JC) 232
Figure 5.191 The variation of (a) Equivalent Plastic Strain (b) Stress Triaxiality and (c) Lode Angle Parameter along the diagonal of the blank at 12 mm cup depth for AISI 304 steel (Hill'48-Disc-JC) 233
Figure 5.192 The variation of (a) Equivalent Plastic Strain (b) Stress Triaxiality and (c) Lode Angle Parameter along the diagonal of the blank at 16 mm cup depth for AISI 304 steel (Hill'48-Disc-JC) 234

Figure 5.193. The variation of (a) Equivalent Plastic Strain and Thickness Plastic Strain (b) Stress Triaxiality and (c) Lode Angle Parameter along the diagonal of the blank at 20 mm cup depth for AISI 304 steel (Hill'48-Disc-JC) 235
Figure 5.194. Equivalent Plastic Strain - Stress Triaxiality Plot of First Fracture Element (Hill'48-Disc-JC) 236
Figure 5.195. Equivalent Plastic Strain – Lode Angle Parameter Plot of First Fracture Element (Hill'48-Disc-JC) 236
Figure 5.196. First Fracture Moment of Case 12 238
Figure 5.197. The variation of (a) Equivalent Plastic Strain (b) Stress Triaxiality and (c) Lode Angle Parameter along the rolling direction of the blank at 4 mm cup depth for AISI 304 steel (Hill'48-Disc-HC) 239
Figure 5.198. The variation of (a) Equivalent Plastic Strain (b) Stress Triaxiality and (c) Lode Angle Parameter along the rolling direction of the blank at 8 mm cup depth for AISI 304 steel (Hill'48-Disc-HC) 240
Figure 5.199. The variation of (a) Equivalent Plastic Strain (b) Stress Triaxiality and (c) Lode Angle Parameter along the rolling direction of the blank at 12 mm cup depth for AISI 304 steel (Hill'48-Disc-HC) 241
Figure 5.200. The variation of (a) Equivalent Plastic Strain (b) Stress Triaxiality and (c) Lode Angle Parameter along the rolling direction of the blank at 16 mm cup depth for AISI 304 steel (Hill'48-Disc-HC) 242
Figure 5.201. The variation of (a) Equivalent Plastic Strain (b) Stress Triaxiality and (c) Lode Angle Parameter along the transverse direction of the blank at 4 mm cup depth for AISI 304 steel (Hill'48-Disc-HC) 243
Figure 5.202. The variation of (a) Equivalent Plastic Strain (b) Stress Triaxiality and (c) Lode Angle Parameter along the transverse direction of the blank at 8 mm cup depth for AISI 304 steel (Hill'48-Disc-HC) 244
Figure 5.203. The variation of (a) Equivalent Plastic Strain (b) Stress Triaxiality and (c) Lode Angle Parameter along the transverse direction of the blank at 12 mm cup depth for AISI 304 steel (Hill'48-Disc-HC) 245

Figure 5.204. The variation of (a) Equivalent Plastic Strain (b) Stress Triaxiality and (c) Lode Angle Parameter along the transverse direction of the blank at 16 mm cup depth for AISI 304 steel (Hill'48-Disc-HC) 246
Figure 5.205. The variation of (a) Equivalent Plastic Strain (b) Stress Triaxiality and (c) Lode Angle Parameter along the diagonal of the blank at 4 mm cup depth for AISI 304 steel (Hill'48-Disc-HC) 247
Figure 5.206. The variation of (a) Equivalent Plastic Strain (b) Stress Triaxiality and (c) Lode Angle Parameter along the diagonal of the blank at 8 mm cup depth for AISI 304 steel (Hill'48-Disc-HC) 248
Figure 5.207 The variation of (a) Equivalent Plastic Strain (b) Stress Triaxiality and (c) Lode Angle Parameter along the diagonal of the blank at 12 mm cup depth for AISI 304 steel (Hill'48-Disc-HC) 249
Figure 5.208 The variation of (a) Equivalent Plastic Strain and Thickness Plastic Strain (b) Stress Triaxiality and (c) Lode Angle Parameter along the diagonal of the blank at 16 mm cup depth for AISI 304 steel (Hill'48-Disc-HC) 250
Figure 5.209. Equivalent Plastic Strain - Stress Triaxiality Plot of First Fracture Element (Hill'48-Disc-HC) 251
Figure 5.210. Equivalent Plastic Strain – Lode Angle Parameter Plot of First Fracture Element (Hill'48-Disc-HC) 251
Figure 5.211. First Fracture Moment of Case 13 253
Figure 5.212. The variation of (a) Equivalent Plastic Strain (b) Stress Triaxiality and (c) Lode Angle Parameter of the blank at 5 mm cup depth for Al2024 aluminum (VM-JC-HC) 254
Figure 5.213. The variation of (a) Equivalent Plastic Strain (b) Stress Triaxiality and (c) Lode Angle Parameter of the blank at 10 mm cup depth for Al2024 aluminum (VM-JC-HC) 255
Figure 5.214. The variation of (a) Equivalent Plastic Strain (b) Stress Triaxiality and (c) Lode Angle Parameter of the blank at 15 mm cup depth for Al2024 aluminum (VM-JC-HC) 256

Figure 5.215. The variation of (a) Equivalent Plastic Strain and Thickness Plastic Strain (b) Stress Triaxiality and (c) Lode Angle Parameter of the blank at 20 mm cup depth for Al2024 aluminum (VM-JC-HC) 257
Figure 5.216. Equivalent Plastic Strain - Stress Triaxiality Plot of First Fracture Element (VM-JC-HC) 258
Figure 5.217. Equivalent Plastic Strain – Lode Angle Parameter Plot of First Fracture Element (VM-JC-HC) 258
Figure 5.218. The variation of triaxiality values with respect to Lode angle parameter values (a) for punch (b) for punch shoulder or corner (c) for the clearance between die and punch (d) for die shoulder or corner and (e) for the blank holder regions of the blank at 20 mm cup depth for Al2024 aluminum (VM-JC-HC) 260

LIST OF ABBREVIATIONS

ABBREVIATIONS

2D	2 Dimensional
3D	3 Dimensional
BHF	Blank Holder Force
BC	Boundary Conditions
DOF	Degree of Freedom
FE	Finite Element
FEA	Finite Element Analysis
FEM	Finite Element Method
FFLD	Fracture Forming Limit Diagrams
FLC	Forming Limit Curves
PEEQ	Equivalent Plastic Strain
SMF	Sheet Metal Forming
TRIA	Triaxiality
UTS	Ultimate Tensile Strength

LIST OF SYMBOLS

SYMBOLS

ρ	Density, (kg/mm^3)
σ	True Stress, (MPa)
σ_0	Nominal (Engineering) Stress, (MPa)
τ	Shear Stress, (MPa)
t	Time (s)
ε	True Strain, (mm/mm)
ε_0	Nominal (Engineering) Strain, (mm/mm)
ν	Poisson ratio
A	Area, (mm^2)
L	Length, (mm)
l	Elongation, (mm)
F	Force, (N)
E	Young's (Elastic) Modulus, (GPa)

SUBSCRIPTS / SUPERSCRIPTS

u	Ultimate
f	Fracture
Y	Yield
l	Limit
0	Initial State / Condition
i	Any Certain State Between Initial and Final
p	Plastic
e	Elastic

CHAPTER 1

INTRODUCTION

1.1 Background and Motivation

Several industries employ sheet metal forming to make a variety of components. Deep drawing is a significant sheet metal forming process that plastically deforms materials into various forms. Through precise deep drawing, intricate forms may be made with precision. Deep-drawn sheet metal is used to create cans, cups, gasoline tanks, shell containers, pressure vessels, and vehicle body pieces, among other goods. In deep drawing, a thin blank is plastically distorted with the use of forming tools to obtain the required shape, which is defined by a die. The blank holder forces hold the blank as the punch moves progressively toward the die blank. To get a defect-free blank during the deep drawing process, it is essential to select the proper process parameters. If the process parameters are selected properly, the blank will acquire the desired form without defect. This will reduce the manufacturing expenses and help to eliminate operational flaws. Process factors such as die radius, blank holding force, coefficient of friction, punch speed, and blank thickness can be set or improved based on their effect on the sheet metal forming qualities [1]–[7].

In finite element analyses, the constitutive model is as crucial to the accuracy of simulations of sheet metal forming processes as the forming variables such as geometry of parts, holder force, friction between parts, etc. To get precise stress and strain distributions in the produced material, constitutive models are required to characterize the material's deformation property [8], [9].

Material’s stress state can be calculated by elastic constitutive relations before the plastic deformation occurs. A yield criterion, often expressed as yield surface, or yield locus, is a hypothesis concerning the limit of elasticity under any combination

of stresses and also forms the plastic constitutive relations. Von-Misses yield criterion and Hill'48 yield criterion are utilized to explain the material behavior in this thesis. First yield criterion in this study is von Mises which is the most common and oldest yield criteria for isotropic materials. Second one is the Hill'48 yield criterion which was developed for quadratic anisotropic materials in 1948 [10]–[12]. Also, two different ductile fracture criteria which are Johnson Cook and Hosford Coulomb are considered as they are used in the recent studies to predict ductile materials' behaviors upon fracture [13], [14]. In this way the effect of triaxiality and Lode angle parameter on deformation behavior of material is investigated.

1.2 Objective of the Thesis

Previous studies have shown that on ductile materials, Lode parameter and triaxiality are critical for estimation of material behaviors [15]–[18]. The objective of this study is to find out the effects of Lode parameter and triaxiality with different yield criteria and different ductile criteria on simulation of different deep drawing processes.

1.3 Scope of the Thesis

In this study, analyzes are made with Al2024 and AISI 304 materials. Von Mises and Hill'48 yield criteria are used with Johnson Cook and Hosford Coulomb ductile criterion in the simulations. Triaxiality is also defined by using Hill'48 equivalent stress and strain in addition to the von Mises criterion, and its effect is examined. Analyzes have performed on ABAQUS software.

1.4 Outline of the Thesis

There are six chapters in this thesis. The first chapter provides general information about the thesis's content as well as background knowledge about plasticity and the deep drawing process to the reader.

In the second chapter, a review of the associated literature survey is provided. It is about past studies which contents similar subjects. A brief summary and results of the articles written on triaxiality, Lode parameter, ductile fracture criteria, new yield criteria etc. are given.

Third chapter is about theoretical background mainly, yield criteria, hardening, ductile criteria and parameters explained theoretically and general information of these topics is given. Theoretical information on Triaxiality and Lode parameters are also included in this section.

Fourth chapter contains finite element analyzes made for this thesis. Finite element model, boundaries, constrictions, drawing types and materials are given. Many analyzes have made for this thesis. From these analyzes, to evaluate and contrast various combinations of outcomes, numerous figures have been created.

In fifth chapter, is about the results and interpretations of the analyzes. Analyzes are performed on ABAQUS software. Then, the model types, the collected data, the obtained graphics and the results of the analyzes were compared and interpreted together with the previous studies.

Finally, main results are presented and discussed in sixth chapter. Interpretations and evaluation of the results of the analysis are included in this section. In addition, possible studies as a continuation of the work that can be done in the future are included.

CHAPTER 2

LITERATURE SURVEY

There is a great deal of information in the literature about constitutive models and their applications to various forming processes. In this part of the thesis, the founding models from this large amount of information in the literature are reserved for research studies that include the subject of the thesis or have similar topics.

Extension of a shear-controlled ductile fracture criteria for more accurate prediction of fracture forming limit diagrams (FFLD) in sheet metal forming processes is the focus of the work by Huh et al. [19]. This criterion is extended to 3D stress space with dependence on the Lode parameter and stress triaxiality. Al 2024-T351 material is used. A shear-controlled ductile fracture criterion was compared with the Mohr-Coulomb criterion and for this purpose, Mohr's circle technique was used. The comparison shows that, with the exception of two data points in the high stress triaxiality, fracture loci created using two criteria are close to experimental results. The Mohr-Coulomb criterion has limitations; thus, the new criterion is more appropriate to characterize ductile fracture in metal-forming processes.

In the research by Bao and Wierzbicki [20], a series of experiments were undertaken on the aluminum alloy Al2024-T351, including upsetting tests, shear tests, and tensile tests. These tests showed the fracture ductility of the alloy over a broad range of stress triaxiality. Stress triaxiality, in addition to strain intensity, is the most critical factor affecting the start of ductile fracture. ABAQUS has been utilized to simulate each test numerically. There was a close association between numerical simulation and experiment. This association allowed the link between the equivalent strain to fracture and stress triaxiality to be determined. The mechanism of fracture for negative stress triaxialities is determined by shear. For large triaxialities, void growth

is the major failure mode. However, for low stress triaxialities between the two regimes described above, a mix of shear and void growth modes may arise.

According to the study by Mohr et al. [21], it is necessary to employ sheet materials with a high strength-to-weight ratio in order to increase fuel economy and reduce the cost of transportation vehicle materials. Consequently, the seek for lighter structural materials continues**.** It intends to use advanced high-strength steels with tensile strengths that are more than twice as high as standard low-carbon or HSLA steels. Usually, the formability and resistance to fracture of light metal structures are restricted by ductile fracture. In order to model the behavior of these specified ductile materials, the most appropriate ductility criterion must be determined. To do this, comparative experimental investigations must be conducted. Early investigations by McClintock [22] and Rice and Tracey [23] examined how spherical and cylindrical holes develop in a ductile matrix. Their findings demonstrate that the triaxiality of the stress controls the formation of voids. A porous plasticity model with the void volume as an internal variable was proposed by Gurson [24]. Basic ductile fracture tests were performed to observe the material structure on test specimens extracted from TRIP780 steel sheets. Different types of test specimens were used, such as central holes and circular notches. The outcome of both test of punch and stress specimen, show that equivalent strains of more than 0.8 can be achieved at constant triaxialities to fracture of about 0.30 and 0.66.

In Bai and Wierzbicki [25] study, past studies on metal plasticity assumes that hydrostatic pressure has negligible effect and independent of the Lode parameter which is named as third deviatoric stress invariant. On the other hand, recent experiments have shown that the third invariant and hydrostatic pressure have an effect on material behaviors. The material model (a new form of an asymmetric metal plasticity model) created by considering the effect of these parameters was tested on Al-2024 and the results were verified. Moreover, the proposed 3D asymmetric fracture locus was validated by the test results of Bao [26] on aluminum 2024-T351 and the data points of A710 steel.

Hancock and MacKenzie [27], examined the relationship between the ductility and stress triaxiality of three different steels. Using smooth and U-notched axisymmetric tensile specimens, they determined that the ductility of all investigated materials decreases with increasing stress triaxiality. In addition, their experimental findings and the predictions of Rice and Tracey's [28] fracture model were found to be in good accord.

In Bai and Wierzbicki study [29], the Modified Mohr-Coulomb model using the weighting function based on the Lode angle was obtained by transforming the stress-based Mohr-Coulomb refractive criterion into the stress triaxiality domain by Bai and Wierzbicki. Lode parameter and equivalent plastic strain on the basis of an isotropic but stress-state dependent plasticity model (Bai and Wierzbicki [30]). Other methods for estimating ductile fracture involve the modeling of the localization of deformation using theoretical embranchment analysis (e.g., Li and Karr, [31]), micromechanics-based analysis (Sun et al. [32]), and Forming Limit Curves (FLC).

CHAPTER 3

THEORETICAL BACKGROUND

3.1 Yield Criteria

The yield criteria are crucial in determining the constitutive models that are used to simulate plastically deformed materials. In this study, von-Mises and Hill'48 yield criteria have been used with different hardening and ductile fracture criteria which were embedded into the ABAQUS software.

3.1.1 Von Mises Yield Criterion

There are a lot of researches that used the von Mises yield criterion in literature. If the is material assumed as fully isotropic then von Mises yield function is generally used for the analysis because it can be easily differentiated, which makes it very convenient to implement. This criterion is only dependent on the second invariant, J_2'.

When the second invariant J_2' reaches a critical value, κ^2 yielding occurs [12]. Then, the von Mises Yield Criterion can be written as:

$$J_2' - \kappa^2 = 0$$

$$\frac{1}{6}[(\sigma_1 - \sigma_2)^2 + (\sigma_2 - \sigma_3)^2 + (\sigma_3 - \sigma_1)^2] = \kappa^2$$

The tension test determines that as $\kappa = \sigma_Y/\sqrt{3}$ where, σ_Y is the initial yield stress in simple tension. Von Mises is the standard yield criterion when plastic coefficients are provided on the ABAQUS interface without parameters are specifying any other.

Equivalent von Mises stress is defined as,

$$\bar{\sigma}_{VM} = \frac{1}{\sqrt{2}}\sqrt{(\sigma_1 - \sigma_2)^2 + (\sigma_2 - \sigma_3)^2(\sigma_3 - \sigma_1)^2}$$

and equivalent von Mises strain is,

$$\bar{\varepsilon}^P = $$

$$= \frac{\sqrt{2}}{3}\sqrt{[(\varepsilon_{xx}^P - \varepsilon_{yy}^P)^2 + (\varepsilon_{yy}^P - \varepsilon_{zz}^P)^2 + (\varepsilon_{zz}^P - \varepsilon_{xx}^P)^2 + 6(\varepsilon_{xy}^P)^2 + 6(\varepsilon_{xz}^P)^2 + 6(\varepsilon_{yz}^P)^2]}$$

3.1.2 Hill'48 Yield Criterion

The Hill'48 yield criterion, developed by Rodney Hill, is one of several yield criteria for describing anisotropic plastic deformations. Hill created a quadratic yield function in order to characterize the orthotropic plasticity of sheet metals. Hill'48 yield criterion [12], [33] assumes that hydrostatic stress has no effect on yielding. It is a simple extension of von Mises' yield criteria and had a quadratic shape. This model was eventually extended by including an exponent *m*. Variations of these criteria are often applied to metals, polymers, and certain composites. The criterion is,

$$F(\sigma_{yy} - \sigma_{zz})^2 + G(\sigma_{zz} - \sigma_{xx})^2 + H(\sigma_{xx} - \sigma_{yy})^2 + 2L{\sigma_{yz}}^2 + 2M{\sigma_{xz}}^2 + 2N{\sigma_{xy}}^2 - 1 = 2f$$

where the constants *F*, *G*, *H*, *L*, *M* and *N* are calculated experimentally. These values change according to the anisotropy of the material.

$$F = \frac{1}{2}\left(\frac{1}{Y^2} + \frac{1}{Z^2} - \frac{1}{X^2}\right)$$

$$G = \frac{1}{2}\left(\frac{1}{Z^2} + \frac{1}{X^2} - \frac{1}{Y^2}\right)$$

$$H = \frac{1}{2}\left(\frac{1}{Y^2} + \frac{1}{X^2} - \frac{1}{Z^2}\right)$$

$$L = \frac{1}{2R^2}$$

$$M = \frac{1}{2S^2}$$

$$N = \frac{1}{2T^2}$$

In the above equations *X, Y, Z* are the tensile yield stresses for corresponding principal directions and *R, S, T* are the pure shear stresses for corresponding planes of anisotropy.

Lankford anisotropy coefficients [34], which can be used in Hill'48 criterion; are

$$r_0 = \frac{H}{G}$$

$$r_{45} = \frac{N}{F+G} - \frac{1}{2}$$

$$r_{90} = \frac{H}{F}$$

and $X=\sigma_0$, $Y=\sigma_{90}$, $Z=\sigma_{45}$, where σ_0, σ_{90} and σ_{45} is the yield strength values in 0º, 90º and 45º to the rolling direction. Then the criterion is,

$$\sigma_{xx}^2 - \frac{2r_0}{1+r_0}\sigma_{xx}\sigma_{yy} + \frac{r_0(1+r_{90})}{r_{90}(1+r_0)}\sigma_{yy}^2 + \frac{r_0+r_{90}}{r_{90}(1+r_0)}(2r_{45}+1)\sigma_{xy}^2 = \sigma_0^2$$

Briefly, the quadratic Hill yield criterion depends only on the deviatoric stresses. It is pressure independent and predicts the same yield stress in tension and in compression.

Equivalent Hill'48 stress is,

$$\bar{\sigma}_H = \sqrt{\frac{3}{2}\left(\frac{F\left(\sigma_{yy}-\sigma_{zz}\right)^2 + G(\sigma_{zz}-\sigma_{xx})^2 + H\left(\sigma_{xx}-\sigma_{yy}\right)^2 + 2L{\sigma_{yz}}^2 + 2M{\sigma_{xz}}^2 + 2N{\sigma_{xy}}^2}{F+G+H}\right)}$$

and equivalent Hill'48 strain is,

$$\bar{\varepsilon}^P = \sqrt{\frac{F(\varepsilon_{xx}^P)^2 + G(\varepsilon_{yy}^P)^2 + H(\varepsilon_{zz}^P)^2}{FG + GH + HF} + \frac{2(\varepsilon_{yz}^P)^2}{L} + \frac{2(\varepsilon_{xz}^P)^2}{M} + \frac{2(\varepsilon_{xy}^P)^2}{N}}$$

3.2 Hardening

There are several approaches to describe strain hardening of a material. Isotropic hardening, kinematic hardening and combined hardening will be explained in the following sections.

3.2.1 Isotropic Hardening

In the case of isotropic hardening [34], [35], if a solid is deformed plastically, then unloaded, and reloaded again, it will be discovered that its yield stress (or elastic limit) has risen relative to the first cycle. In the isotropic hardening model, the yield surface expands continuously and without spatial displacement. The hardening can be represented as

$$F = f(\sigma) - \sigma_Y(\beta) = 0$$

where σ_Y is the current uni-axial yield strength that depends on hardening variable β. It does not take Bauschinger effect into account.

3.2.2 Kinematic Hardening

Isotropic hardening [34]–[36] is not useful in situations where components are subjected to cyclic loading. The size and geometry of the yield surface do not change during kinematic hardening. It is possible to express the yield surface as,

$$F = f(\sigma, \alpha) - \kappa = 0$$

where κ represents a material constant that depends on the size of the yield surface and α is often called as back stress.

Isotropic hardening does not account for the Bauschinger effect [35], [36]. In kinematic hardening cyclic behavior and the Bauschinger effect, is represented.

3.2.3 Combined Hardening

The materials often exhibit a mixture of isotropic and kinematic hardening properties. During combined hardening, the material yield surface simultaneously expands and moves. In forming processes, the combination type hardening (short for combined hardening) law more accurately forecasts the spring back and failure behaviors. In combined hardening, the material hardens isotropically and kinematically, although kinematic hardening predominates [35], [36].

$$F = f(\sigma, \alpha) - \sigma_Y(\beta) = 0$$

3.2.4 Johnson Cook Hardening

Johnson-Cook hardening is a particular type of isotropic hardening where the yield stress, σ, is assumed to be of the form,

$$\sigma = [A + B(\bar{\varepsilon}^P)^n](1 - \hat{\theta}^m)$$

where $\bar{\varepsilon}^P$ is the equivalent plastic strain and $A, B, n,$ and m are material parameters. $\hat{\theta}$ is the nondimensional temperature defined as,

$$\hat{\theta} \equiv 0 \text{ for } \theta < \theta_{transition}$$

$$\hat{\theta} \equiv (\theta - \theta_{transition}) / (\theta_{\text{melt}} - \theta_{transition}) \text{ for } \theta_{transition} < \theta < \theta_{\text{melt}}$$

$$\hat{\theta} \equiv \{1 \text{ for } \theta > \theta_{\text{melt}}\}$$

3.3 Ductile Fracture Criteria

Two different ductile fracture criteria have been used. These are Johnson-Cook, and Hosford-Coulomb criteria.

3.3.1 Johnson Cook Damage Initiation Criterion

According to the Johnson-Cook model, the equivalent plastic strain at the initiation of damage is a function of stress triaxiality and strain rate. The Johnson-Cook criterion is compatible with the von Mises, Johnson-Cook, and Hill models of plasticity, as well as the equation of state. Johnson-Cook Damage Initiation Criteria Parameters are given below [37],

$$\overline{\varepsilon}_D^P = [d_1 + d_2 exp(-d_3\eta)]\left(1 + d_4\, ln\left(\frac{\dot{\overline{\varepsilon}}^P}{\dot{\varepsilon}_0}\right)\right)(1 + d_5\hat{\theta})$$

where, $\hat{\theta}$ is the nondimensional temperature and, d_1, d_2, d_3, d_4, d_5 are Johnson-Cook failure parameters, η is the stress triaxiality, θ_{melt} is the melting temperature, $\theta_{transition}$ is the transition temperature and $\dot{\varepsilon}_0$ is the reference strain rate.

3.3.2 Hosford Coulomb Damage Initiation Criteria

Based on strain rate, the Hosford-Coulomb damage model predicts anisotropic damage. Triaxiality and Lode angle characteristics of Hosford Coulomb Damage Initiation Criteria are relevant [38].

According to the equation which is based on the work of Roth and Mohr [39], the equivalent plastic strain at the onset of damage $\overline{\varepsilon}_D^{pl}$ is,

$$\bar{\varepsilon}_D^p = b\left(1 + d\ ln\left(\frac{\dot{\bar{\varepsilon}}^p}{\dot{\varepsilon}_0}\right)\right)(1+c)^{\frac{1}{n}}\left(\left\{\frac{1}{2}((f_1 - f_2)^a + (f_2 - f_3)^a + (f_1 - f_3)^a)\right\}^{\frac{1}{a}} + c(2\eta + f_1 + f_3)\right)^{-\frac{1}{n}}$$

where, η is the stress triaxiality, *a, b, c, d* and n are material parameters, $\dot{\varepsilon}_0$ is the reference strain rate and $f_1,\ f_2, f_3$ are functions of the Lode Angle Parameter.

3.4 Triaxiality and Lode Parameter

3.4.1 Triaxiality

Stress triaxiality is given as [40],

$$\eta = \frac{\sigma_m}{\bar{\sigma}_{VM}}$$

where mean stress is,

$$\sigma_m = \frac{\sigma_1 + \sigma_2 + \sigma_3}{3}$$

and equivalent von Mises stress is

$$\bar{\sigma}_{VM} = \frac{1}{\sqrt{2}}\sqrt{(\sigma_1 - \sigma_2)^2 + (\sigma_2 - \sigma_3)^2(\sigma_3 - \sigma_1)^2}$$

Stress triaxiality formulae can also be defined as,

$$\eta = \frac{\sqrt{2}}{3}\frac{\sigma_1 + \sigma_2 + \sigma_3}{\sqrt{(\sigma_1 - \sigma_2)^2 + (\sigma_2 - \sigma_3)^2(\sigma_3 - \sigma_1)^2}}$$

It is known that for, uniaxial tension η = 0.33, equi-biaxial tension η = 0.66, simple shear η = 0 and uniaxial compression $\eta = -0.33$ [26], [41].

Stress triaxiality is a parameter that is used to understand the stress situation at a point. As seen in tension it is positive, and in compression it is negative.

Also, the stress triaxiality is recently defined by using Hill'48 criterion for anisotropic materials as using,

$$\eta_{\mathrm{H}} = \frac{\sigma_m}{\bar{\sigma}_{\mathrm{H}}} = \frac{1}{3}\frac{\sigma_1 + \sigma_2 + \sigma_3}{\sqrt{(\sigma_3 - \sigma_1)^2 \mathrm{T}}}$$

and

$$T = F\left(\frac{1+L}{2}cos^2\omega + sin^2\omega\right)^2 + G\left(\frac{1+L}{2}sin^2\omega + cos^2\omega\right)^2 + \left(Hcos^2 2\omega + \frac{N}{2}sin^2 2\omega\right)\left(\frac{1-L_l}{2}\right)^2$$

where, σ_1, σ_2, σ_3 are the principal stresses; L is the Lode parameter; ω is the rotation angle between the anisotropic coordinate system and the principal stress coordinate system.

3.4.2 Lode Parameter

The Load Parameter, L is position of the intermediate principal stress and defined as,

$$L = \frac{\sigma_2 - \sigma_N}{\tau}$$

where, σ_N is normal stress on plane of maximum shear

$$\sigma_N = \frac{\sigma_1 + \sigma_3}{2}$$

and τ is maximum shear stress which is described below

$$\tau = \frac{\sigma_1 - \sigma_3}{2}$$

then, Load Parameter can also be defined as,

$$L = \frac{2\sigma_2 - \sigma_1 - \sigma_3}{\sigma_1 - \sigma_3}$$

Figure 3.1. shows that stress situation according to Lode parameter and stress triaxiality.

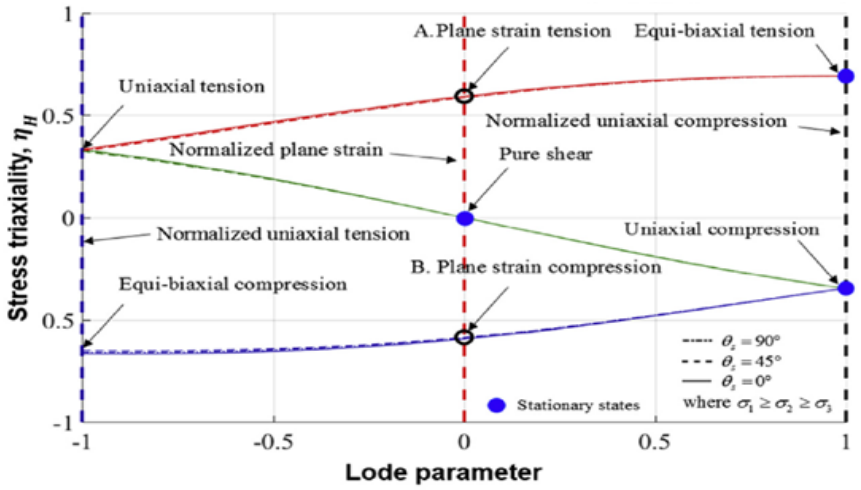

Figure 3.1. The change of new combination of the Lode and Stress Triaxiality [42]

The Lode angle [43], θ is defined as,

$$\theta = \frac{1}{3}\arccos(\xi) = \theta = \frac{1}{3}\arccos\left(\frac{3\sqrt{3}}{2}\frac{J_3}{\sqrt{J_2^3}}\right)$$

where ξ is the third deviatoric stress and J_3 is the third invariant of the deviatoric Cauchy stress tensor [40], [41], ξ can be defined as,

$$\xi = \frac{3\sqrt{3}}{2}\frac{J_3}{\sqrt{J_2^3}}$$

Since the range of the Lode angle is $0 \leq \theta \leq \pi/3$, the range of ξ is $-1 \leq \xi \leq 1$. The geometrical representation of the Lode angle is shown below in Figure 3.2,

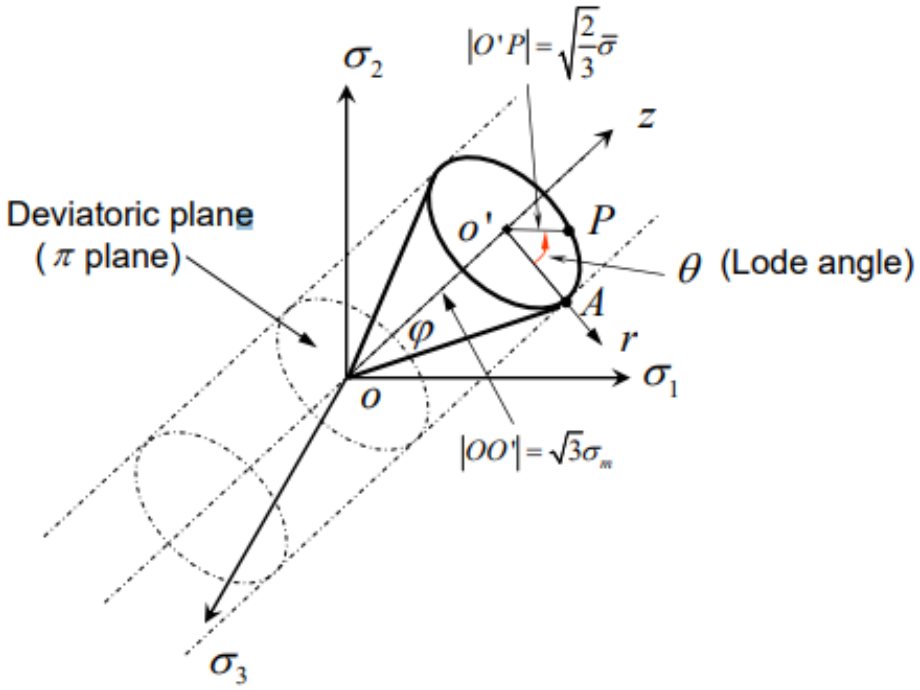

Figure 3.2. Three types of coordinate system in the space of principal stresses [44]

The Lode angle parameter is $\bar{\theta}$ $(-1 \leq \bar{\theta} \leq 1)$ is also a function of the normalized third invariant, J_3, of the deviatoric Cauchy stress tensor [40], [41],

$$\bar{\theta} = 1 - \frac{2}{\pi}\arccos\left(\frac{3\sqrt{3}}{2}\frac{J_3}{\sqrt{J_2^3}}\right)$$

$$\bar{\theta} = 1 - \frac{6\theta}{\pi}$$

The Lode angle parameter may be interpreted as a measure of the magnitude of the second principal stress, σ_2, with respect to the maximum and minimum principal stresses, σ_1 and σ_3 respectively. It is a monotonically decreasing function of the ratio of the second and first principal deviatoric stresses. Some important values are, $\bar{\theta} = -1$ when $\sigma_2 = \sigma_1$ (e.g., equi-biaxial tension or uniaxial compression), $\bar{\theta} = 0$ when $\sigma_2 = (1/2)\,(\sigma_1 + \sigma_3)$ (e.g., pure shear), and $\bar{\theta} = 1$ when $\sigma_2 = \sigma_3$ (e.g., uniaxial tension).

The normal stress acting on the plane of maximum shear is monotonically related to both the stress triaxiality and the Lode angle parameter; it increases with increasing

stress triaxiality and increasing Lode angle parameter. In Figure 3.3 stress situations according to Lode angle parameter and stress triaxiality are given.

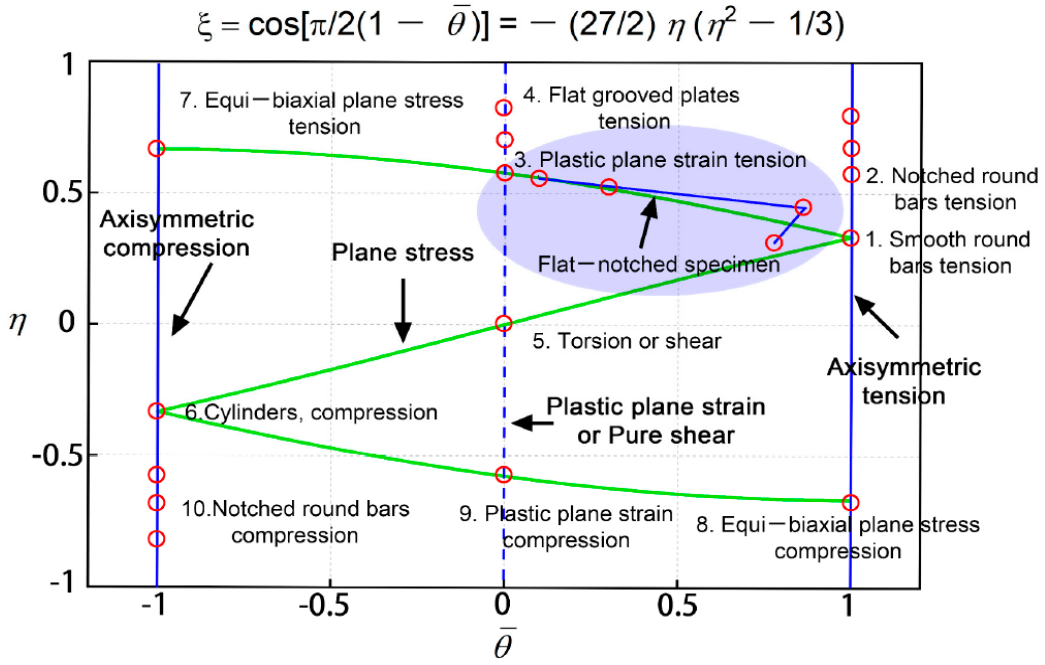

Figure 3.3. The stress state of the specimen with inclined notch in the Wierzbicki stress state diagram [43].

CHAPTER 4

FINITE ELEMENT ANALYZES

4.1 Finite Element Method

Modern engineering applications need products that are always developing and ideal in terms of pricing, durability, strength, and repeatability. Engineers design product models and simulate environmental effects to work on material behaviors without experiments that take so much time [45]. The simulation approaches play a crucial role throughout the design process since they are methodical and under control. Due to cost and time considerations, engineering assessments using simulation models are typically used to adequately depict the actual system and surroundings. Engineering assessments using simulation models are typically used to adequately depict the actual system and surroundings due to cost and time considerations. One of the approaches for this modeling and simulation is Finite Element Method. In this method to minimize the error in the solution, the technique essentially entails assuming the piecewise continuous function for the solution and determining the parameters of the functions [46]–[48]. The fundamental concept of FEM is to split a component into tiny parts. In this way, it makes the part easier to solve by examining a larger number of smaller elements. Finite element analyses take into account a number of features to produce accurate results as quickly as possible. Of course, one should optimize the number of elements and not detract from the purpose of the finite element method. Because as the number of elements increases, even though the simplicity and accuracy of the solution increase, too much detail may be elaborated and a lot of time may be lost [48], [49].

4.2 Finite Element Model

Analyzes are conducted using the FEA program ABAQUS 2022. In this work, simulations of deep drawing were performed with two different die sets; square and flat bottom cylindrical punches. Both Al-2024 and AISI 304, are used in the simulations.

Due to symmetry conditions, a square cup drawing is modeled as a quarter model and cylindrical cup drawing is model as axisymmetric model. The punch, holder and die are modeled as rigid parts. Only the blank is modelled as a deformable body.

4.2.1 Square Cup Drawing

4.2.1.1 Model Geometry and Mesh

There are four different parts in assembly. These parts are designated as blank, die, blank holder, and punch. Essentially, punch is the component that provides force and punch and die provide the form with punch. Additionally, the die guides the blank to avoid scattering. Also, blank holder is the component that prevents wrinkling.

Geometric parameters of model are given as table on Table 4.1.

Table 4.1 Geometric Parameters of Model

Deep drawing with square bottom punch	
Blank Dimension (mm)	80x80
Punch Dimension (mm)	40x40
Punch Shoulder Radius (mm)	4.5
Punch Corner Radius (mm)	12.5
Die Dimension (mm)	42x42
Die Shoulder Radius (mm)	4.5
Sheet Thickness (mm)	1

Blank Holder Inner Dimension (mm)	21x21
Blank Holder Outer Dimension (mm)	50x50

Meshed blank, die, blank holder and punch are given in Figure 4.1, Figure 4.2, Figure 4.3 and Figure 4.4, respectively.

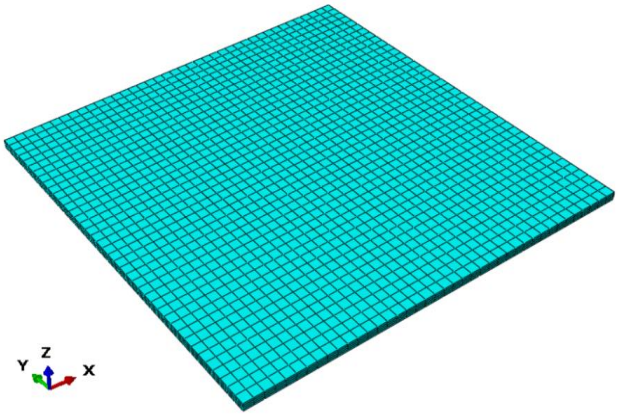

Figure 4.1. Blank Meshed

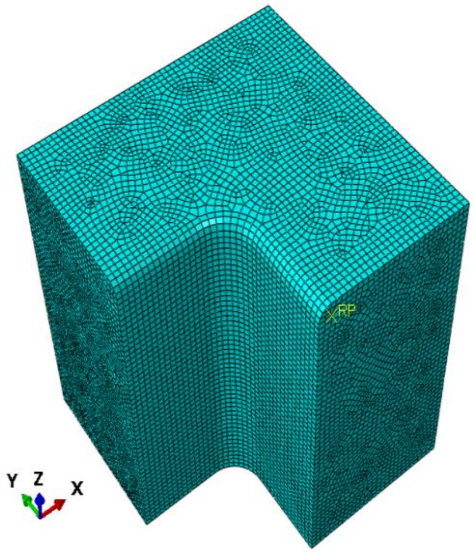

Figure 4.2. Die Meshed

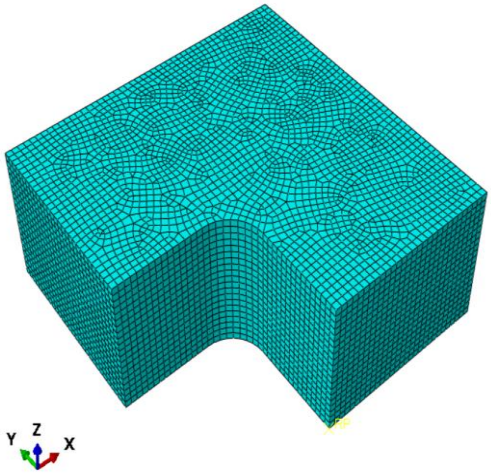

Figure 4.3. Holder Meshed

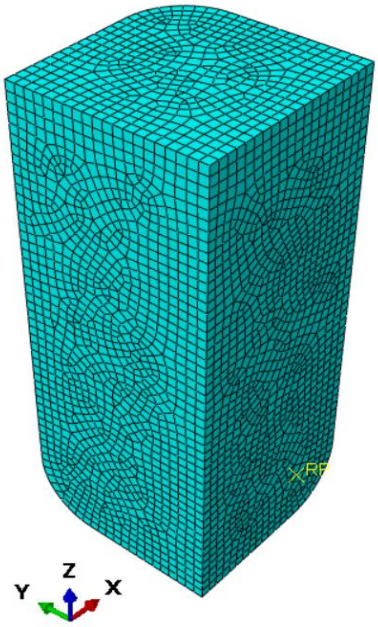

Figure 4.4. Punch Meshed

4.2.1.2 Boundary Conditions and Load

There are six BC's in this simulation. BC's on assembly are shown in Figure 4.5.

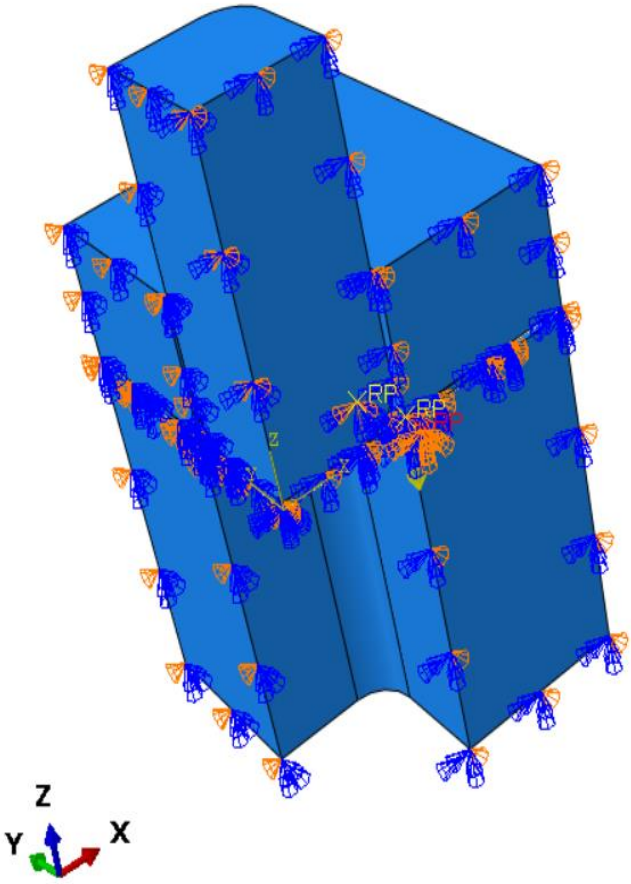

Figure 4.5. Boundary Conditions of Parts on Assembly

First of all, die is fixed and not allowed to move. Blank holder is permitted to move in z direction only as punch. There are two options to simulate motion: Displacement and Velocity. Velocity preferred because it is easier to use with time. Punch Velocity is equal to -1000 mm/s in z direction. Symmetry conditions are defined with respect to x and y axes.

4.2.2 Materials

4.2.2.1 AL-2024

The first material used in this study is Al-2024 alloy. Numerous investigations have been conducted on the Al-2024 alloy. Materials true strain-true stress curve is taken from $\sigma = K\varepsilon^n$ [50], Hill'48 r values and coefficients taken from [51], [52] Johnson Cook damage initiation coefficients taken from [53] and the Hosford Coulomb damage initiation coefficients taken from [54]. Values are given in Figure 4.6, Table 4.2, Table 4.3 and Table 4.4 respectively.

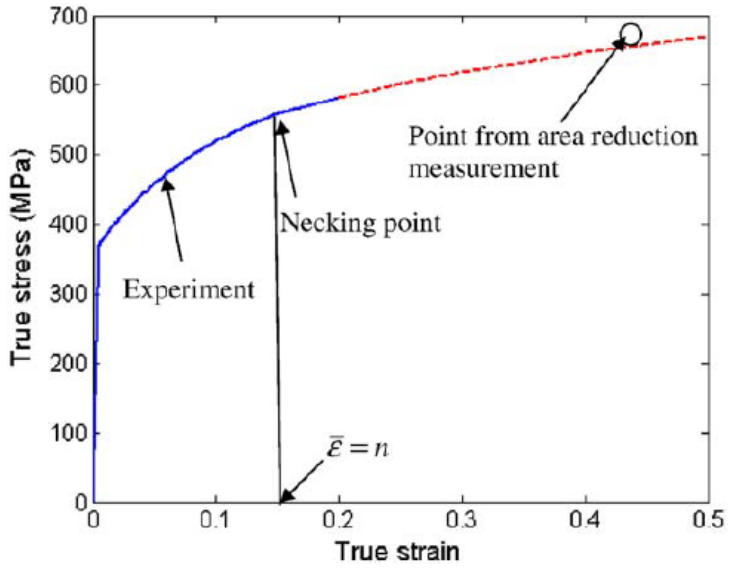

Figure 4.6. Al-2024 true strain-true stress curve[50]

A good power law fit $\sigma = K\varepsilon^n$ of the entire stress–strain curve gives the amplitude K = 744 MPa and the hardening exponent n = 0.153.

Table 4.2. Hill'48 r values and coefficients for Al-2024 [51], [52]

r_0	r_{45}	r_{90}
0.643	0.939	0.545

Table 4.3. Johnson Cook damage initiation coefficients for Al-2024 [53]

Description	Notations	Constants
Modulus of elasticity (MPa)	E	71000
Poisson's ratio	υ	0.33
Density	ρ	2710
Yield stress constant	A	369
	B	684
Strain hardening constant	n	0.73
Viscous effect	C	0.0083
Thermal softening constant	m	1.7
Reference strain rate	$\dot{\varepsilon}_0$	1
Melting temperature (K)	θ_{melt}	893
Transition temperature (K)	$\theta_{transition}$	293
Fracture strain constant	d_1	0.13
	d_2	0.13
	d_3	-1.5
	d_4	0.011
	d_5	0

Table 4.4. Hosford Coulomb Coefficients for Al-2024 [54]

a	b	c	n	d	$\dot{\varepsilon}_0$
1.21	0.21	0.076	0.1	0.71	1

4.2.2.2 AISI 304

The second selected material is the AISI304 alloy, which is a stainless steel. Materials true strain-true stress curve is taken from [55], Hill'48 r values and coefficients taken from [56], [57], Johnson Cook damage initiation coefficients taken from [58] and the Hosford Coulomb damage initiation coefficients taken from [59]. Values are given in Figure 4.7, Table 4.5, Table 4.6 and Table 4.7 respectively.

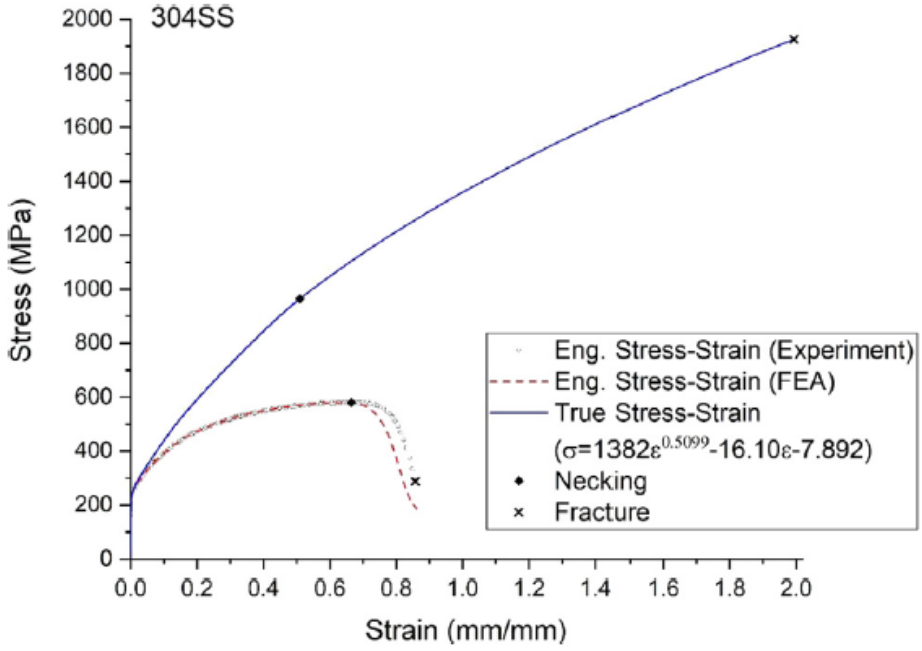

Figure 4.7. AISI-304 strain-true stress curve [55]

From Figure 4.7, $\sigma = 1382\boldsymbol{\varepsilon}^{0.5099}$-$16.10\boldsymbol{\varepsilon}$-7.892 is taken.

Table 4.5. Hill'48 r values and coefficients for AISI-304 [56], [57]

r_0	r_{45}	r_{90}
0.923	1.011	0.840

Table 4.6. Johnson Cook damage initiation coefficients for AISI-304 [58]

Description	**Notations**	**Constants**
Modulus of elasticity (MPa)	E	207.8
Poisson's ratio	υ	0.3
Density	ρ	8000
Yield stress constant	A	280
	B	802.5
Strain hardening constant	n	0.622
Viscous effect	C	0.0799
Thermal softening constant	m	1.0
Reference strain rate	$\dot{\varepsilon}_0$	1
Melting temperature (K)	θ_{melt}	1673
Transition temperature (K)	$\theta_{transition}$	1000

Fracture strain constant	d_1	0.69
	d_2	0
	d_3	0
	d_4	0.0546
	d_5	0

Table 4.7. Hosford Coulomb Coefficients for AISI-304 [59]

a	b	c	n	d	$\dot{\varepsilon}_0$
0.623	1.671	0.096	0.1	0.193	1

CHAPTER 5

RESULTS

Twelve different cases were analyzed by FEM on ABAQUS 2022 with explicit solver for square cup deep drawing model (Figure 5.1). As mentioned on Table 5.1 von Mises and Hill'48 yield criteria, direct use of strain-stress curve and Johnson Cook hardening and Johnson Cook and Hosford Coulomb ductile fracture criteria are used for analyzes. Also, one cylindrical cup drawing model is analyzed with cylindrical punch punch bottom deep drawing. This axisymmetric case is applied just to see the main differences.The results are presented below.

5.1 Square Bottom Punch Deep-Drawing Analyzes

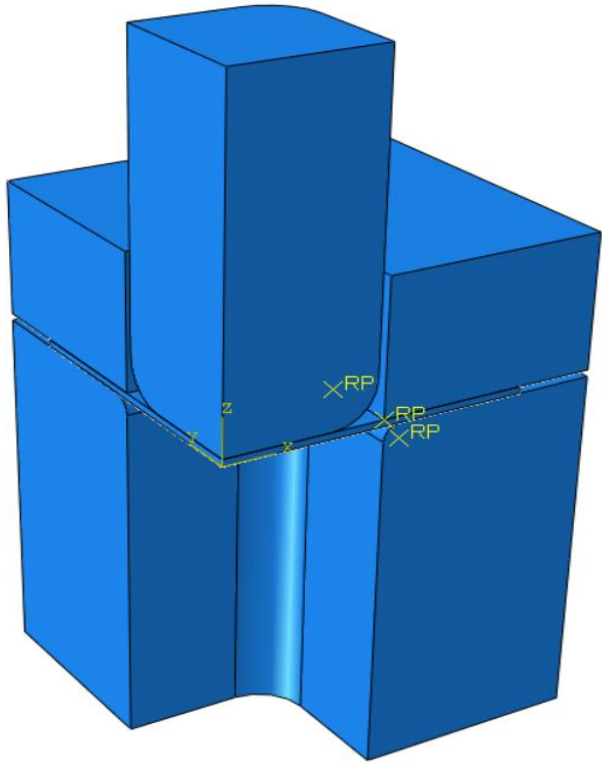

Figure 5.1. Assembly of Square Bottom Punch Model

Table 5.1 Model of Analyzes

Case No	Model	Punch	Material	Yield Criteria	Hardening	Ductile Fracture Criteria
1	Quarter	Square Punch	AL-2024	Von Mises	Discrete	Johnson Cook
2	Quarter	Square Punch	AL-2024	Von Mises	Discrete	Hosford Coulomb
3	Quarter	Square Punch	AL-2024	Von Mises	Johnson Cook	Johnson Cook
4	Quarter	Square Punch	AL-2024	Von Mises	Johnson Cook	Hosford Coulomb
5	Quarter	Square Punch	AL-2024	Hill-48	Discrete	Johnson Cook
6	Quarter	Square Punch	AL-2024	Hill-48	Discrete	Hosford Coulomb
7	Quarter	Square Punch	AISI-304	Von Mises	Discrete	Johnson Cook
8	Quarter	Square Punch	AISI-304	Von Mises	Discrete	Hosford Coulomb
9	Quarter	Square Punch	AISI-304	Von Mises	Johnson Cook	Johnson Cook
10	Quarter	Square Punch	AISI-304	Von Mises	Johnson Cook	Hosford Coulomb
11	Quarter	Square Punch	AISI-304	Hill-48	Discrete	Johnson Cook
12	Quarter	Square Punch	AISI-304	Hill-48	Discrete	Hosford Coulomb

The plastic equivalent strain is zero where the center and farthest side of the blank when the punch starts to move. This indicates that plastic deformation occurs only in the elements in the position where the punch first starts to compress between the center of the blank and the farthest point, which is expected. In positions where the triaxiality value is positive, it is in tension, and in positions where it is negative, it is in compression. In addition, we can see that as the Lode angle parameter goes to the -1, the compression becomes +1 point, and the tension becomes. After sharing this general information obtained from the literature and seen from all graphics, the results and comments on a case-by-case basis are in their respective fields.

5.1.1 Case 1: Square-Al2024-von Mises-Discrete-Johnson Cook Model

For the first case, von Mises yield criterion was applied with discrete hardening and the Johnson Cook ductile fracture criterion was used. It was observed that the fracture had started after 8 mm punch travel as shown in Figure 5.2. The variation of equivalent plastic strain, stress triaxiality and Lode angle parameter values are presented as a function of the distance from the center of the blank for different cup heights up to the fracture. The results are shown for rolling direction in Figure 5.3 to Figure 5.6 and for diagonal direction in in Figure 5.7 to Figure 5.10. The thickness plastic strain distribution is also inserted into Figure 5.10 (a) in order to better visualize the deformation. Further, the variations of stress triaxiality values with respect to equivalent plastic strain are given by considering both von Mises and Hill'48 criteria as a function of the path of the element that fractured first in Figure 5.11. Along the same path, the variation of the Lode parameter with respect to equivalent plastic strain is also illustrated in Figure 5.12.

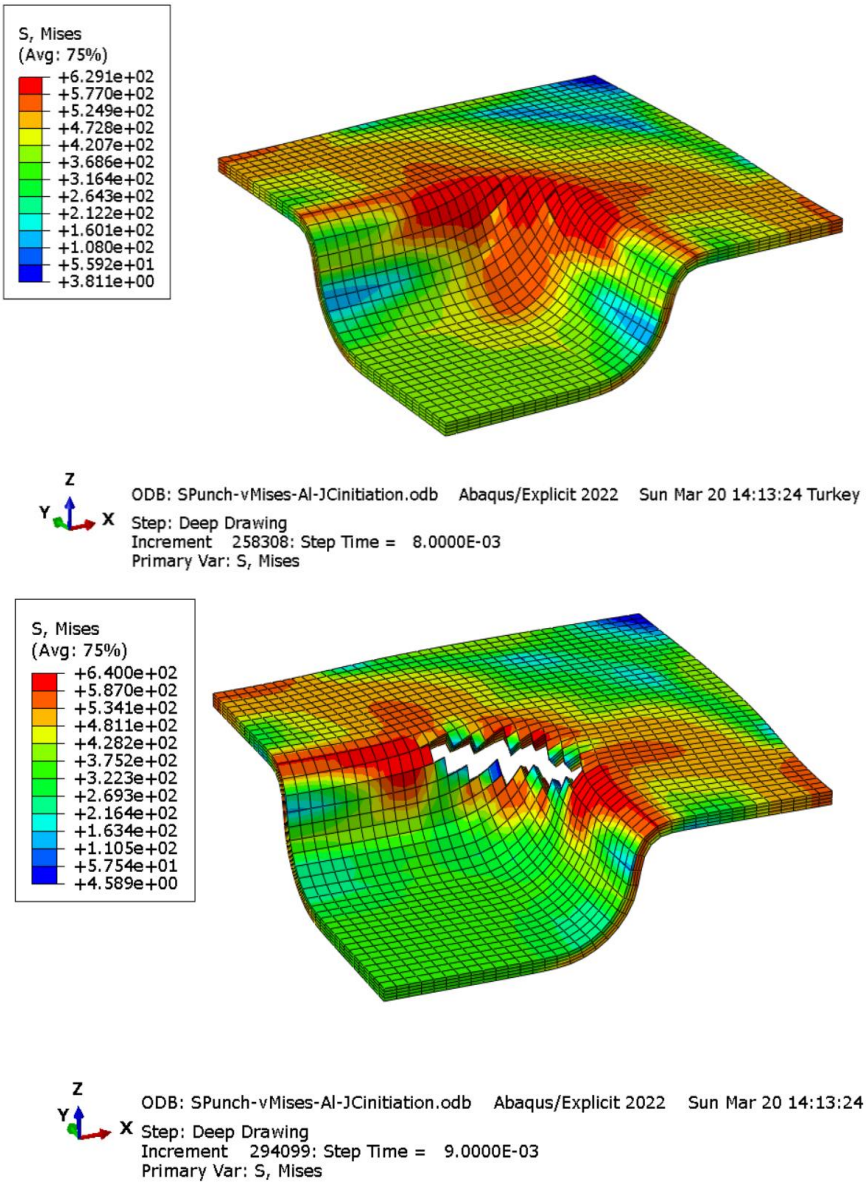

Figure 5.2. First Rupture Moment of Case 1

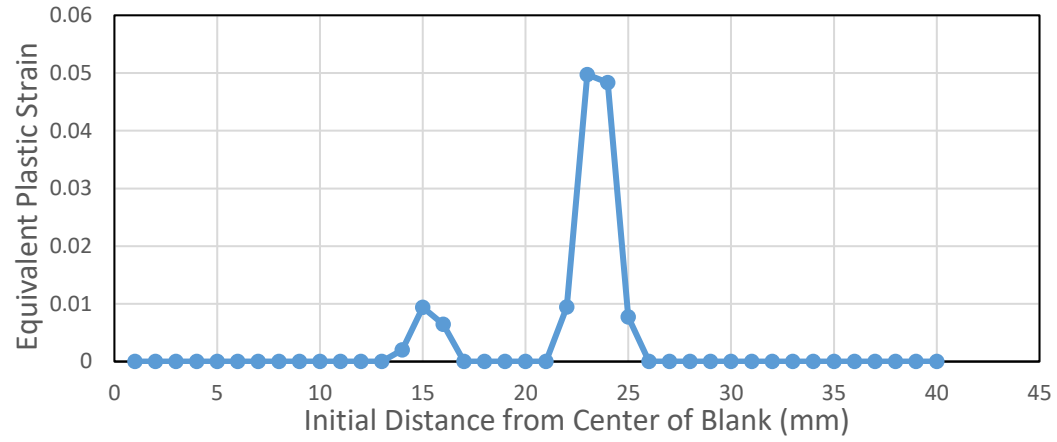

(a)

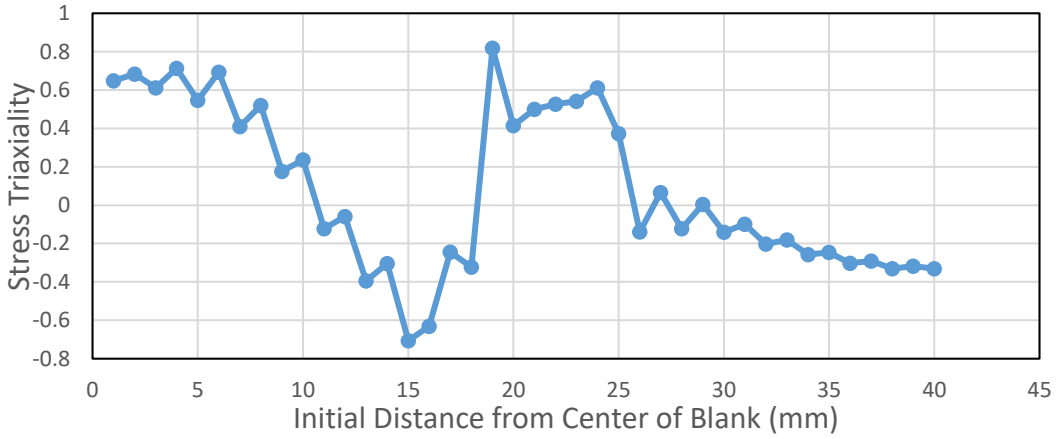

(b)

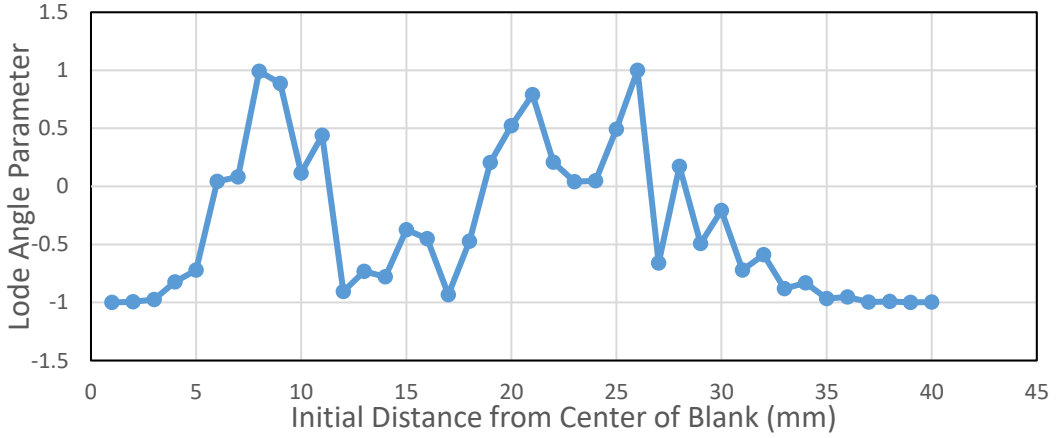

(c)

Figure 5.3. The variation of (a) Equivalent Plastic Strain (b) Stress Triaxiality and (c) Lode Angle Parameter along the rolling direction of the blank at 2 mm cup depth for Al2024 aluminum (VM-Disc-JC)

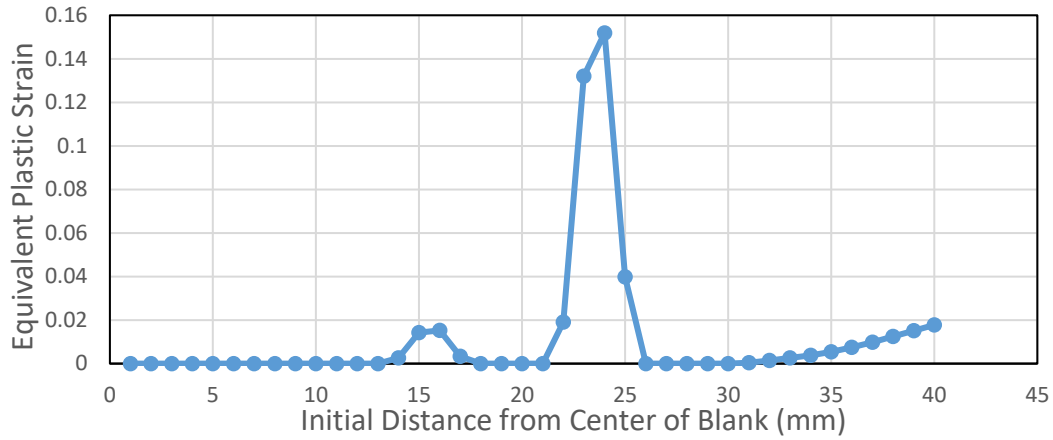

(a)

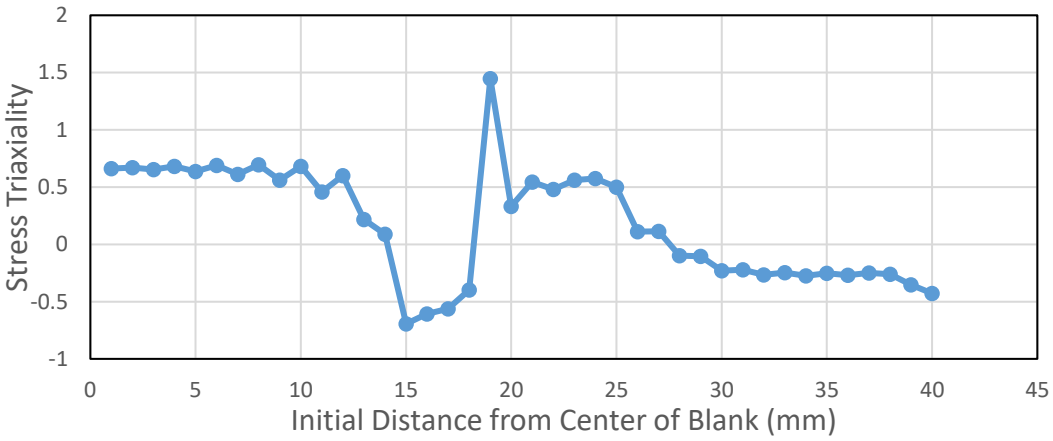

(b)

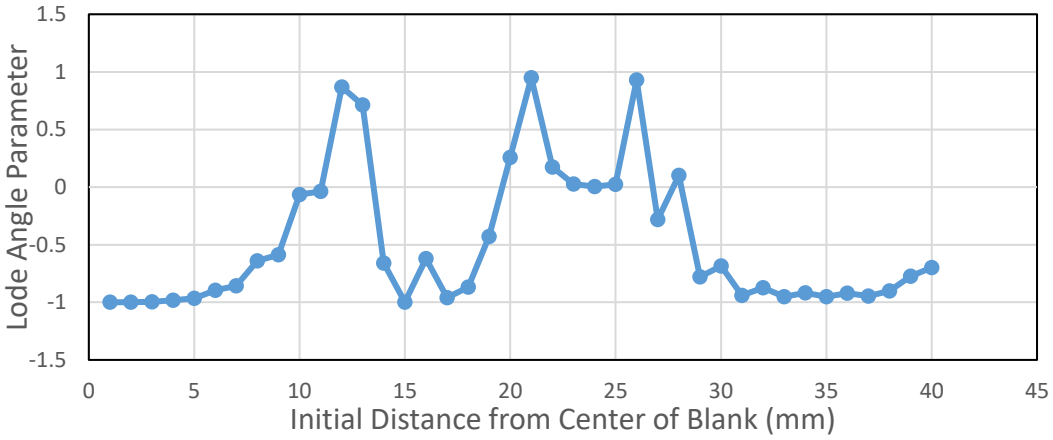

(c)

Figure 5.4. The variation of (a) Equivalent Plastic Strain (b) Stress Triaxiality and (c) Lode Angle Parameter along the rolling direction of the blank at 4 mm cup depth for Al2024 aluminum (VM-Disc-JC)

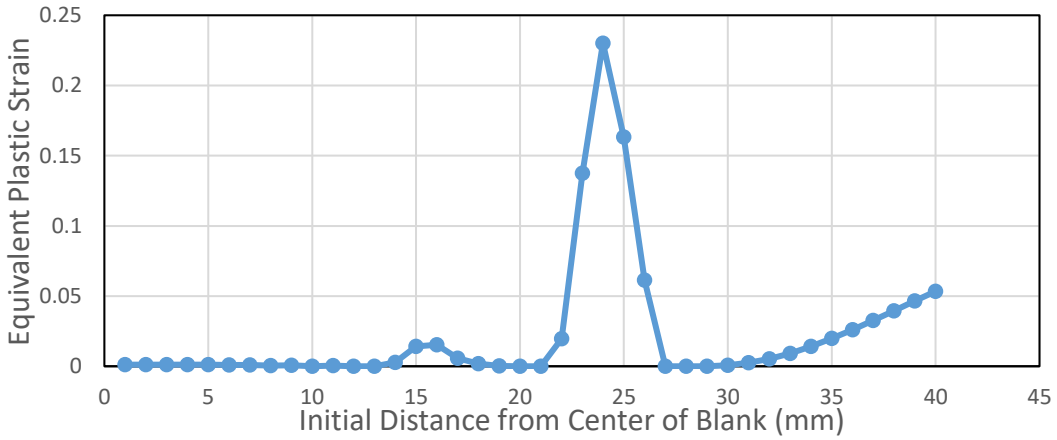

(a)

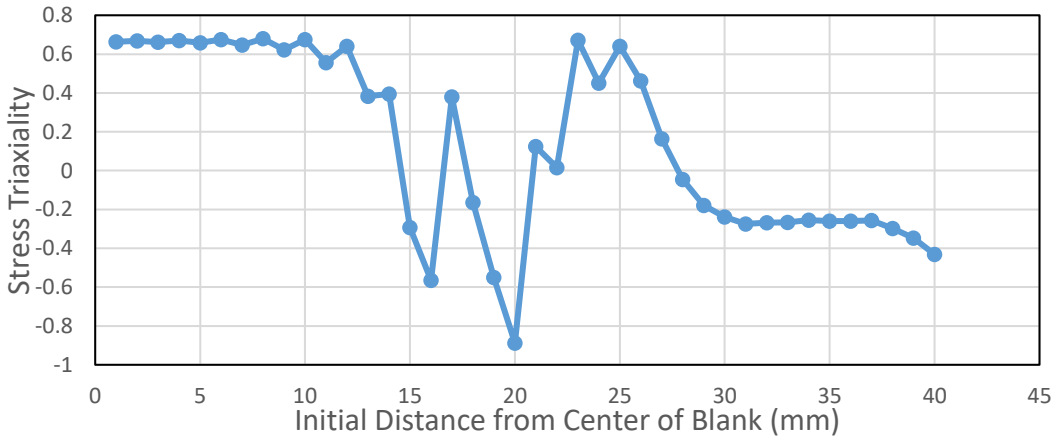

(b)

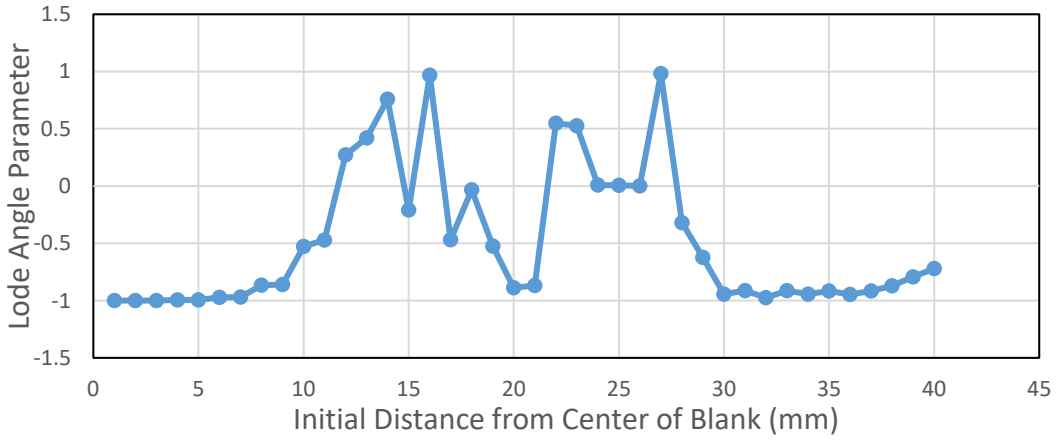

(c)

Figure 5.5. The variation of (a) Equivalent Plastic Strain (b) Stress Triaxiality and (c) Lode Angle Parameter along the rolling direction of the blank at 6 mm cup depth for Al2024 aluminum (VM-Disc-JC)

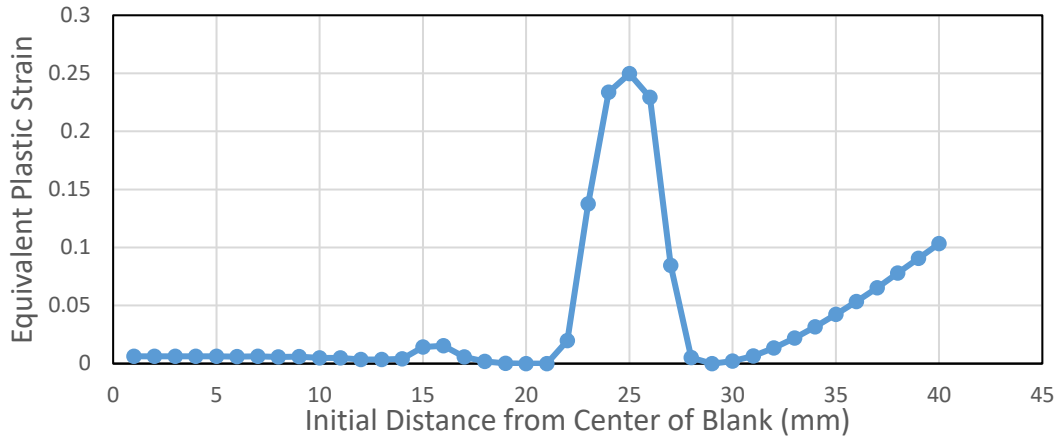

(a)

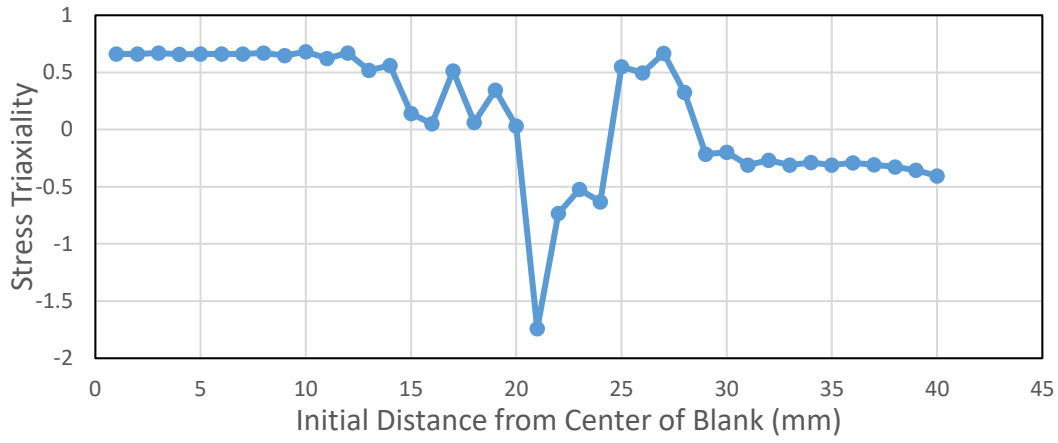

(b)

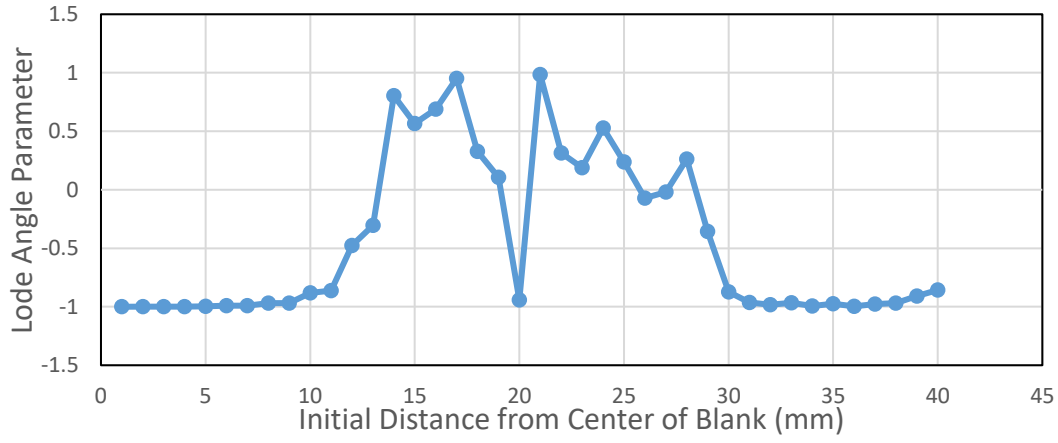

(c)

Figure 5.6. The variation of (a) Equivalent Plastic Strain (b) Stress Triaxiality and (c) Lode Angle Parameter along the rolling direction of the blank at 8 mm cup depth for Al2024 aluminum (VM-Disc-JC)

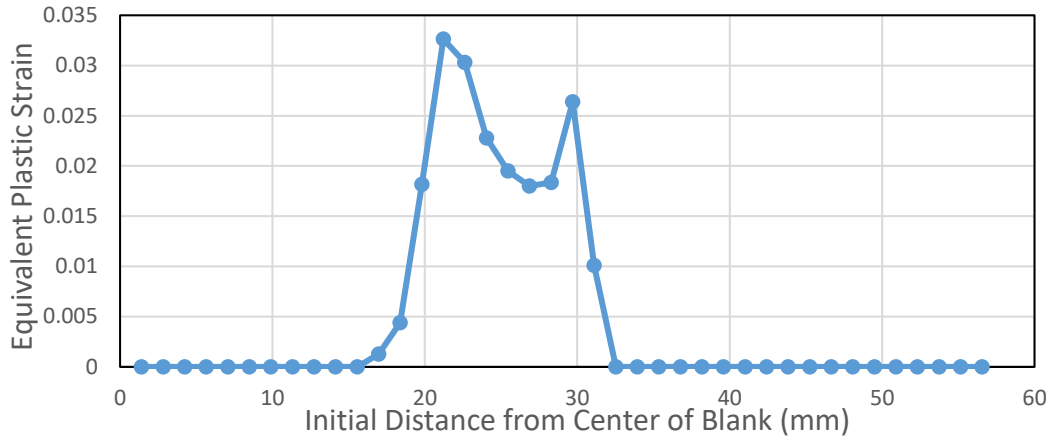

(a)

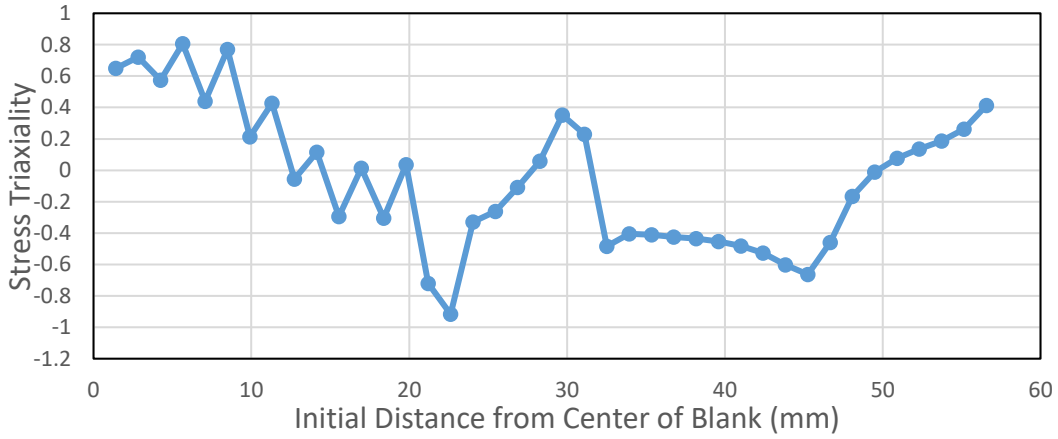

(b)

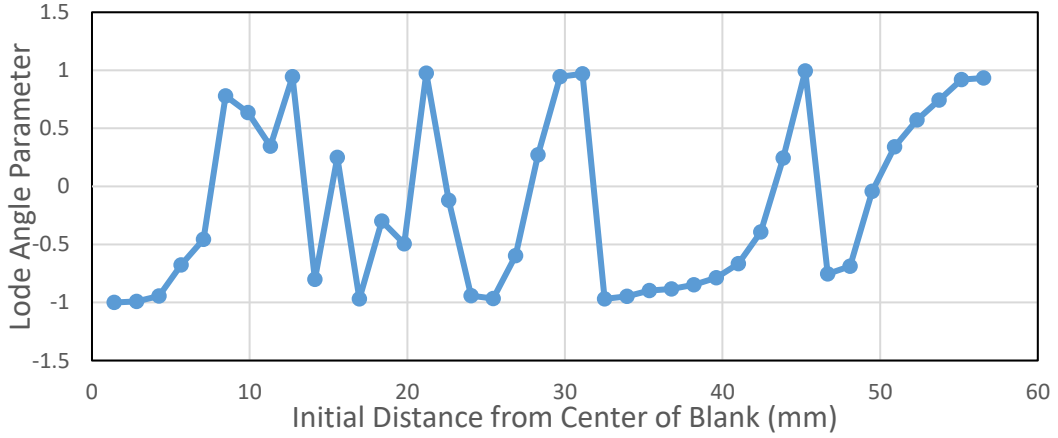

(c)

Figure 5.7. The variation of (a) Equivalent Plastic Strain (b) Stress Triaxiality and (c) Lode Angle Parameter along the diagonal of the blank at 2 mm cup depth for Al2024 aluminum (VM-Disc-JC)

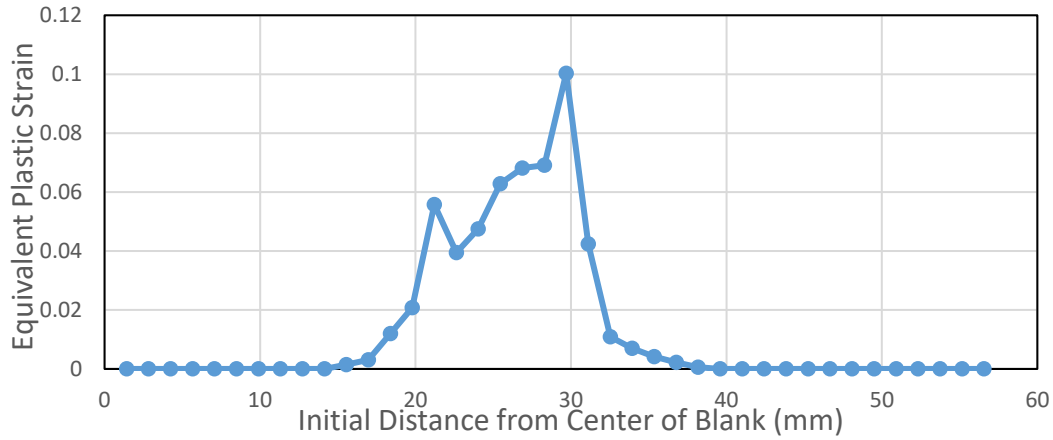

(a)

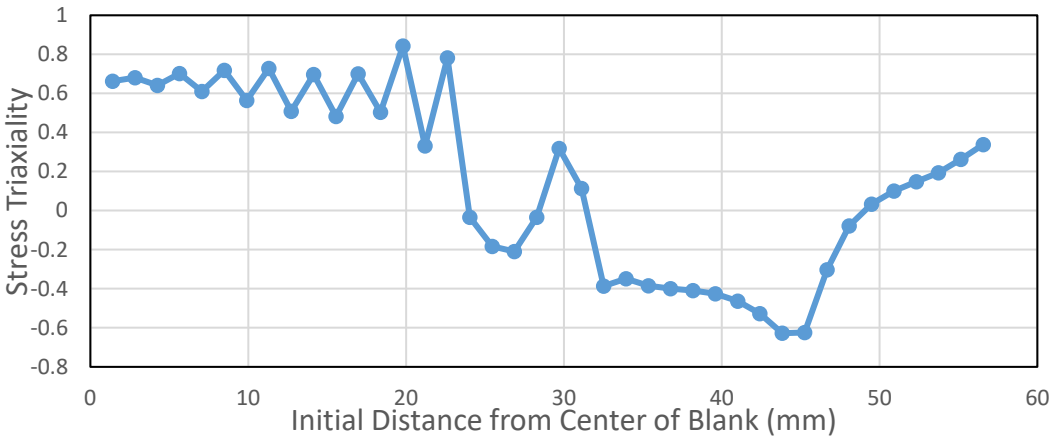

(b)

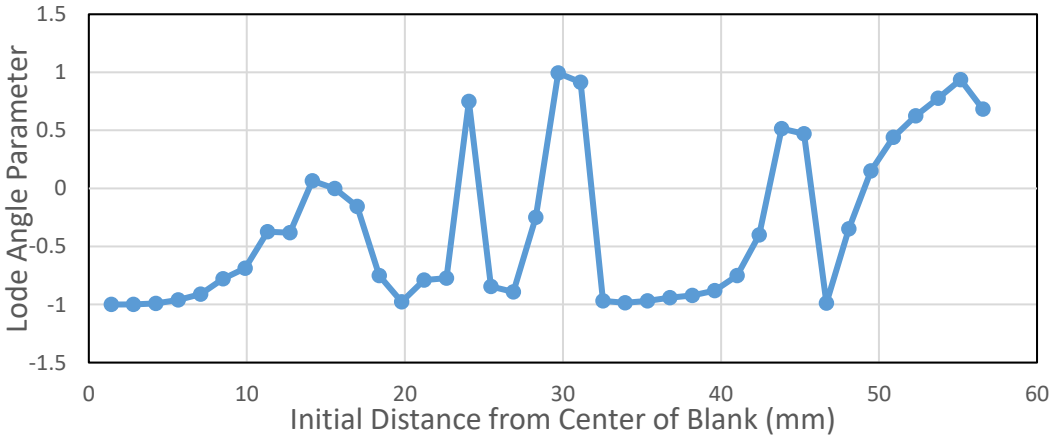

(c)

Figure 5.8. The variation of (a) Equivalent Plastic Strain (b) Stress Triaxiality and (c) Lode Angle Parameter along the diagonal of the blank at 4 mm cup depth for Al2024 aluminum (VM-Disc-JC)

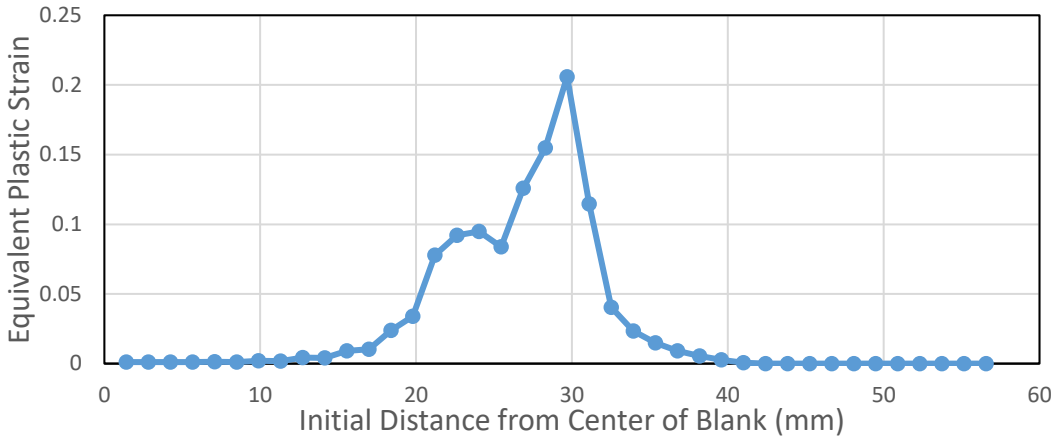

(a)

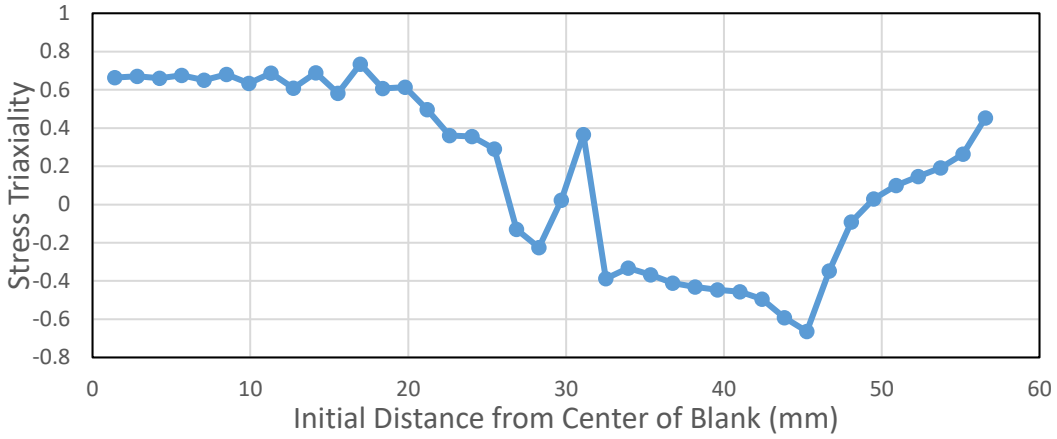

(b)

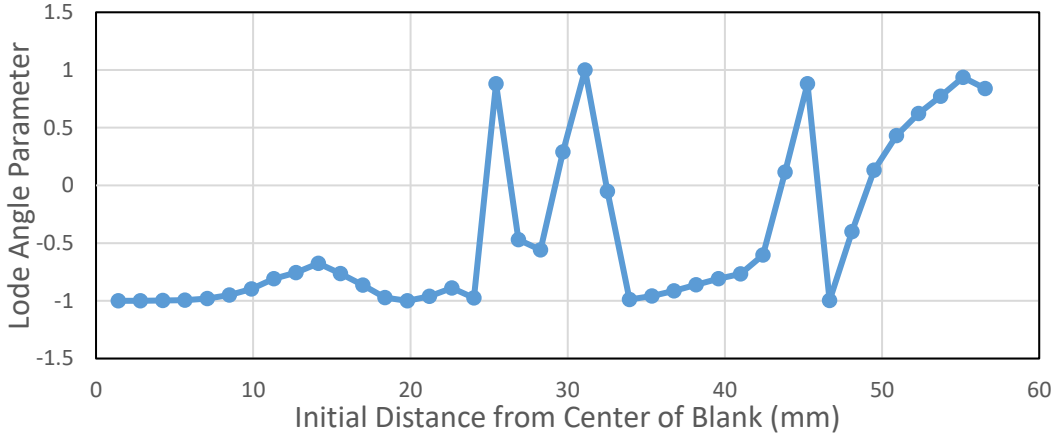

(c)

Figure 5.9. The variation of (a) Equivalent Plastic Strain (b) Stress Triaxiality and (c) Lode Angle Parameter along the diagonal of the blank at 6 mm cup depth for Al2024 aluminum (VM-Disc-JC)

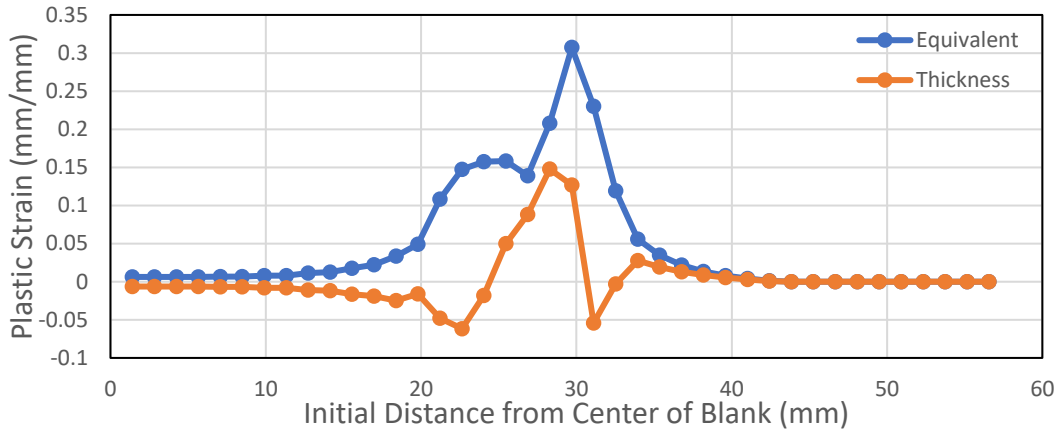

(a)

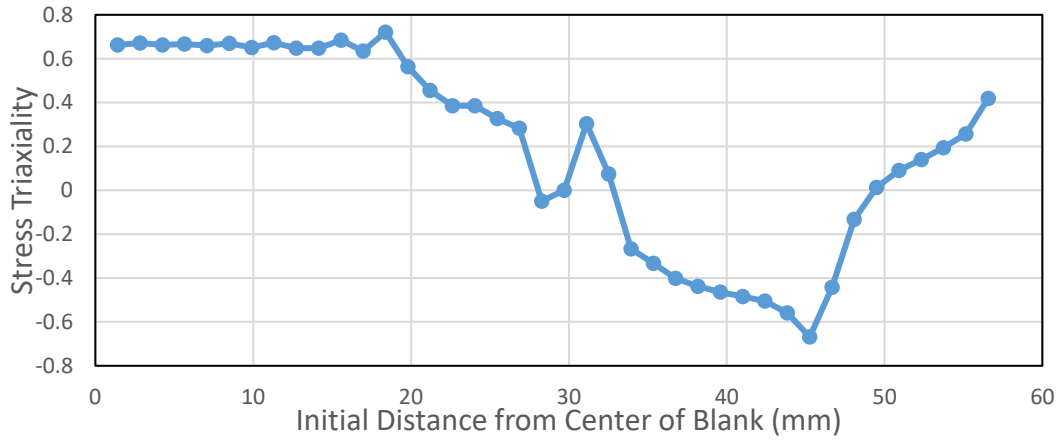

(b)

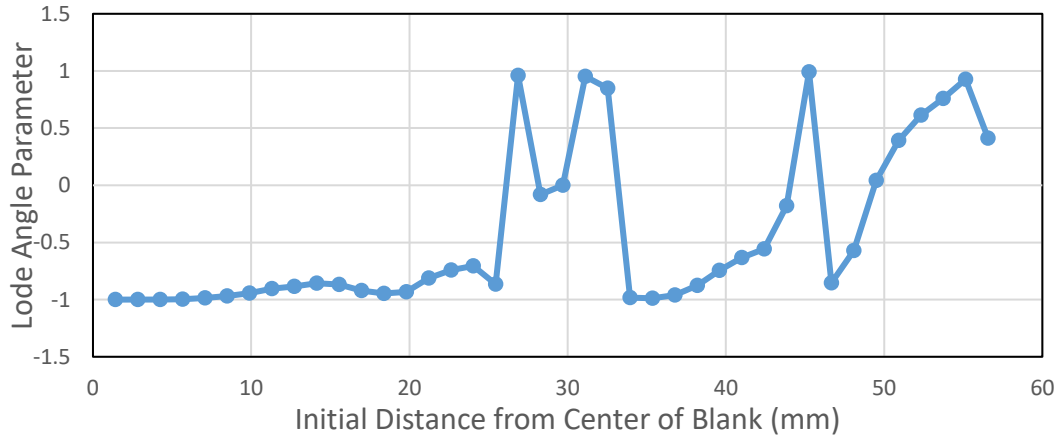

(c)

Figure 5.10. The variation of (a) Equivalent Plastic Strain and Thickness Plastic Strain (b) Stress Triaxiality and (c) Lode Angle Parameter along the diagonal of the blank at 8 mm cup depth for Al2024 aluminum (VM-Disc-JC)

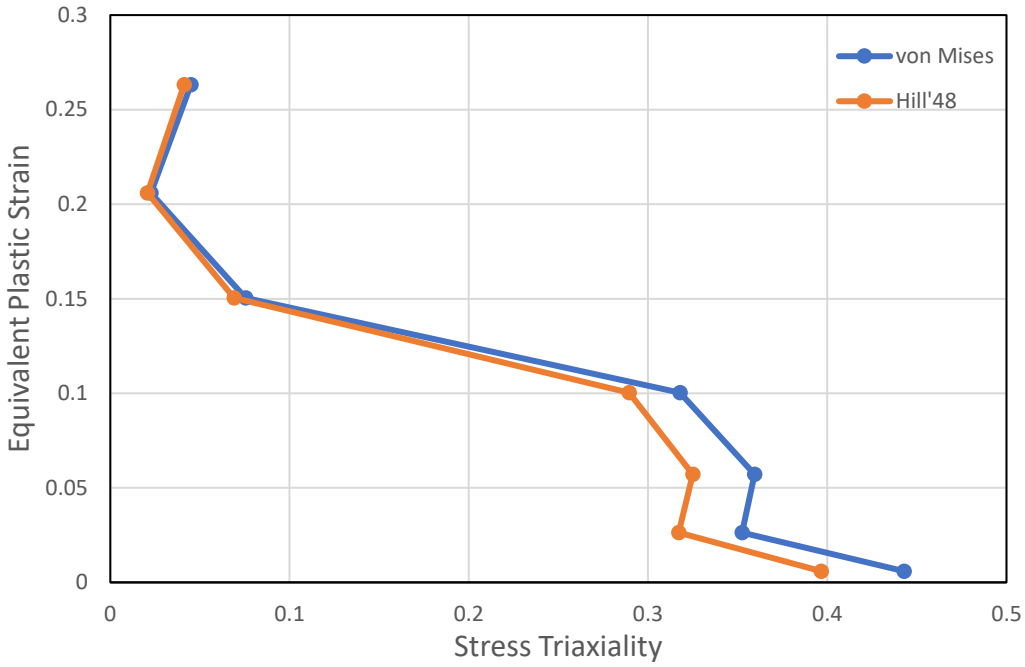

Figure 5.11. Equivalent Plastic Strain - Stress Triaxiality variations Plot of First Rupture Element (VM-Disc-JC)

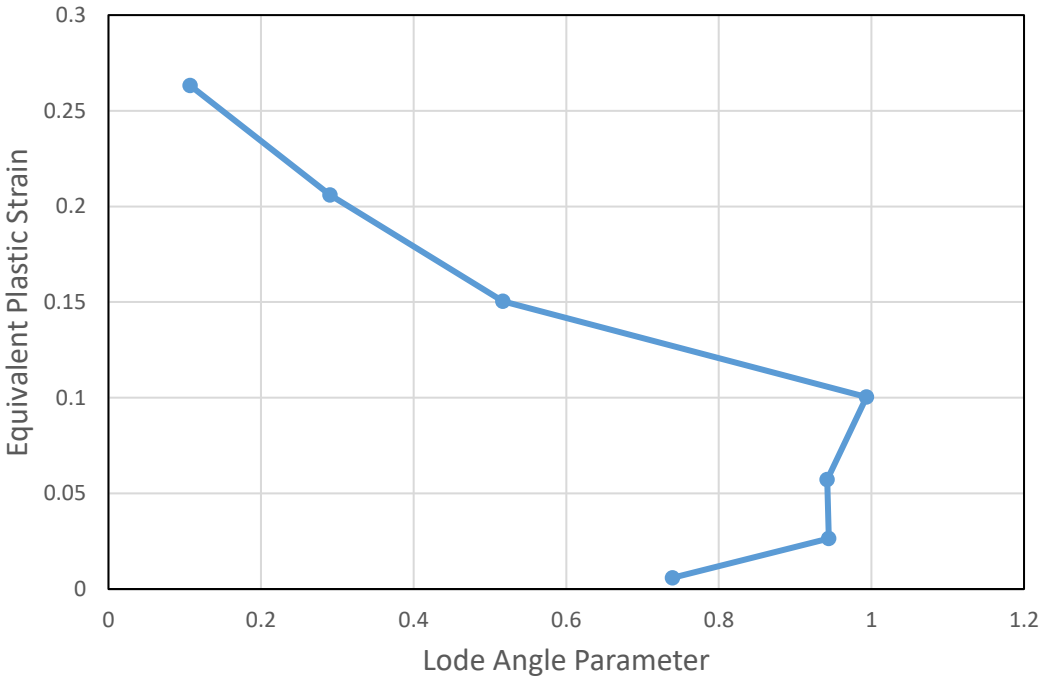

Figure 5.12. Equivalent Plastic Strain - Lode Angle Parameter Plot of First Rupture Element (VM-Disc-JC)

In the rolling direction, the triaxiality values vary generally between 0.6 and 0.8 under the punch whereas the Lode angle parameter values change between -0.5 and -1. Up to the punch shoulder, it can be said that the deformation behavior is in equi-biaxial tension condition. However, for 2 mm punch travel the compressive punch force on the sheet surface dominates towards the punch shoulder where triaxiality values change towards negative where Lode angle parameter values show the same tendency. Here, only in the regions close to the center of the blank i.e., up to a distance of 5 mm from the center, the equi-biaxial tension conditions are observed. As the punch continues to move, the region with equi-biaxial tension conditions extend and reaches 10 mm from the center of the blank. When the pre-rupture state of sheet is examined, it is seen that equi-biaxial stress conditions dominates up to 15 mm from the center of the blank. At the punch shoulder triaxiality values are still positive but decreasing as the distance increases from the blank center. On the other hand, the Lode angle parameter values increases as with distance from the center of the blank. Hence, there is a tensile type deformation in this region. At the clearance between die and punch thinning continues. At the die shoulder, the triaxiality values are mostly positive with varying Lode angle parameter values. The deformation nature begins to change towards thickening. Under the blank holder the triaxiality values and Lode angle parameter values are negative, indicating thickening towards the rim.

In the diagonal direction, as in the rolling direction, equi-biaxial stress condition is observed under the punch. Still, for 2 mm punch travel the compressive punch force on the sheet surface dominates towards the punch corner. Here, the triaxiality values change towards negative whereas Lode angle parameter values show the same tendency. Only in the regions close to the center of the blank i.e., up to a distance of 5 mm from the center, the equi-biaxial tension conditions are observed. At the punch corner, triaxiality values are still positive but decreasing and the Lode angle parameter values are increasing, as the distance increases from the blank center. Hence there is a tensile type deformation in this region. At the clearance between die and punch thinning continues, by changing the nature of deformation from equi-

biaxial tension towards unidirectional tension. At the die corner the triaxiality values start to became negative, indication compressive type deformation with the Lode angle parameter values. Under the blank holder, the triaxiality values are negative and decreases, and finally become positive, similarly negative Lode angle parameter values turn into positive, indicating thickening towards the rim where the nature of the deformation changes from uniaxial dominant compression to equi-biaxial dominant compression.

5.1.2 Case 2: Square-Al2024-von Mises-Discrete-Hosford Coulomb Model

For the second case, von Mises yield criterion was applied with discrete hardening and the Hosford Coulomb ductile fracture criterion was used. It was observed that the fracture had started after 12 mm punch travel as shown in Figure 5.13. The variation of equivalent plastic strain, stress triaxiality and Lode angle parameter values are presented as a function of the distance from the center of the blank for different cup heights up to the fracture. The results are shown for rolling direction in Figure 5.14 to Figure 5.19, for transverse direction in Figure 5.20 to Figure 5.25 and for diagonal direction in Figure 5.26 to Figure 5.31. The thickness plastic strain distribution is also inserted into Figure 5.31 (a) in order to better visualize the deformation. Further, the variations of stress triaxiality values with respect to equivalent plastic strain are given by considering both von Mises and Hill'48 criteria as a function of the path of the element that fractured first in Figure 5.32. Along the same path, the variation of the Lode parameter with respect to equivalent plastic strain is also illustrated in Figure 5.33.

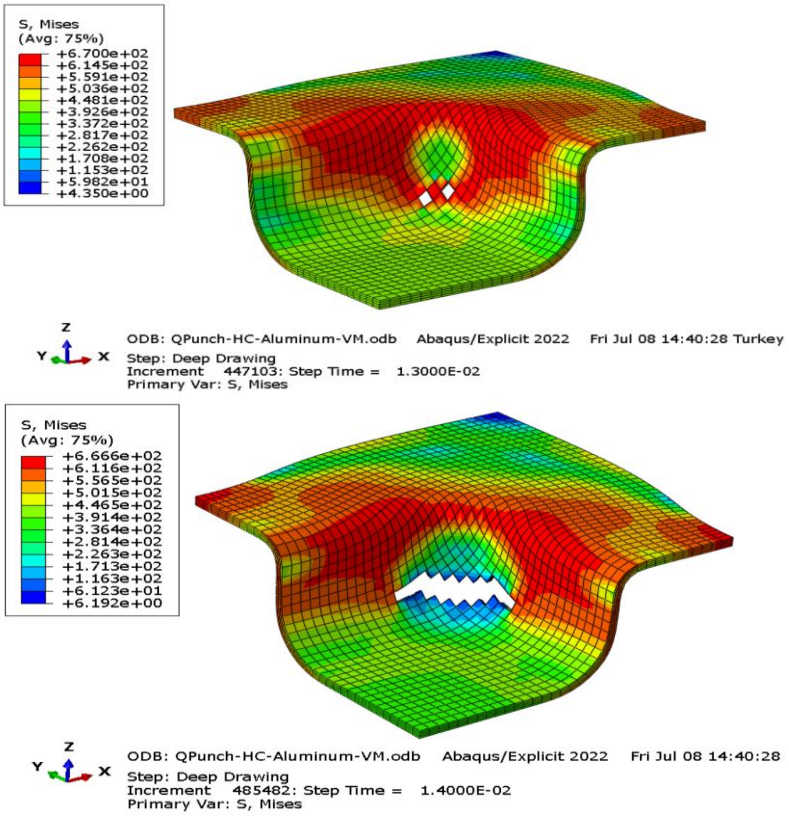

Figure 5.13. First Rupture Moment of Case 2

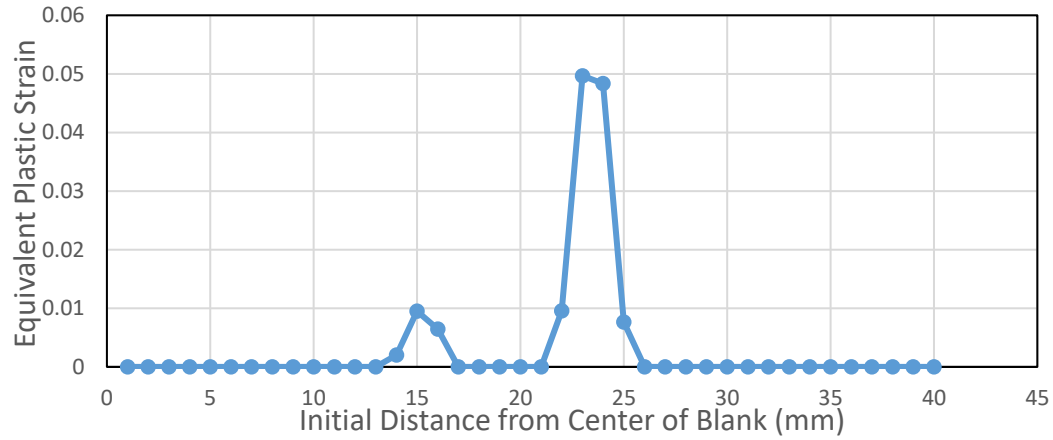

(a)

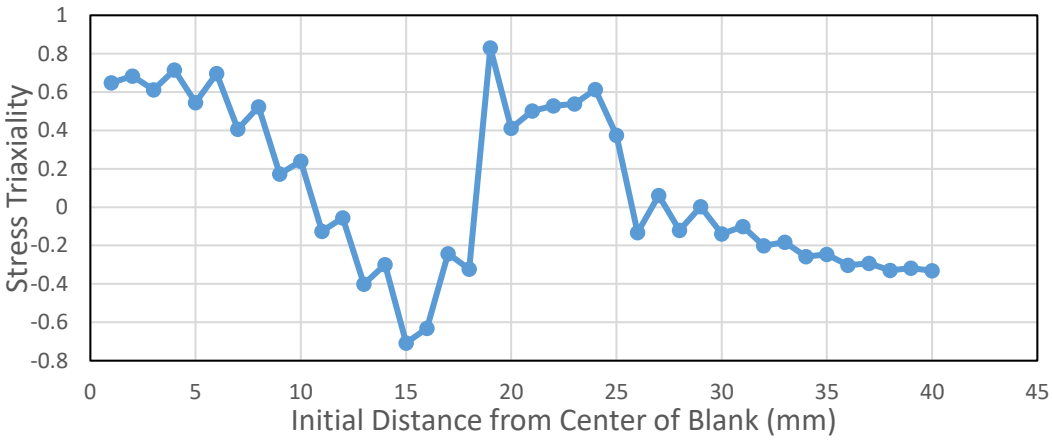

(b)

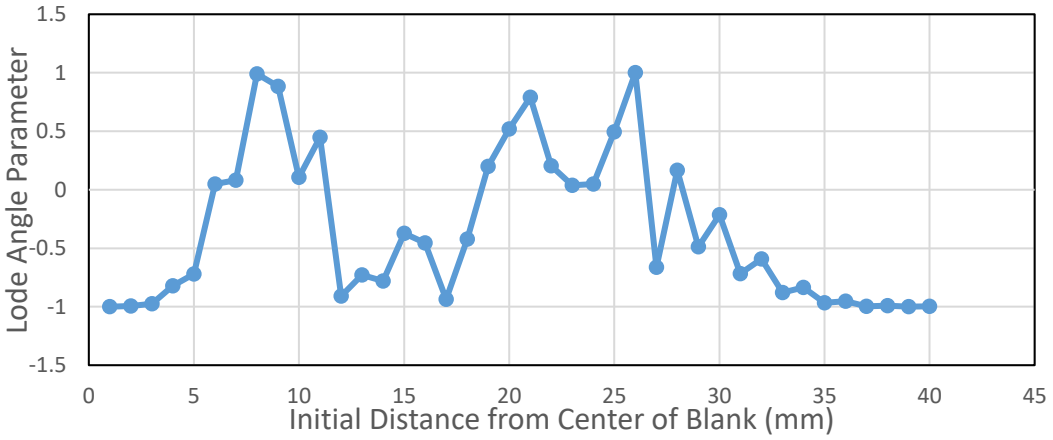

(c)

Figure 5.14. The variation of (a) Equivalent Plastic Strain (b) Stress Triaxiality and (c) Lode Angle Parameter along the rolling direction of the blank at 2 mm cup depth for Al2024 aluminum (VM-Disc-HC)

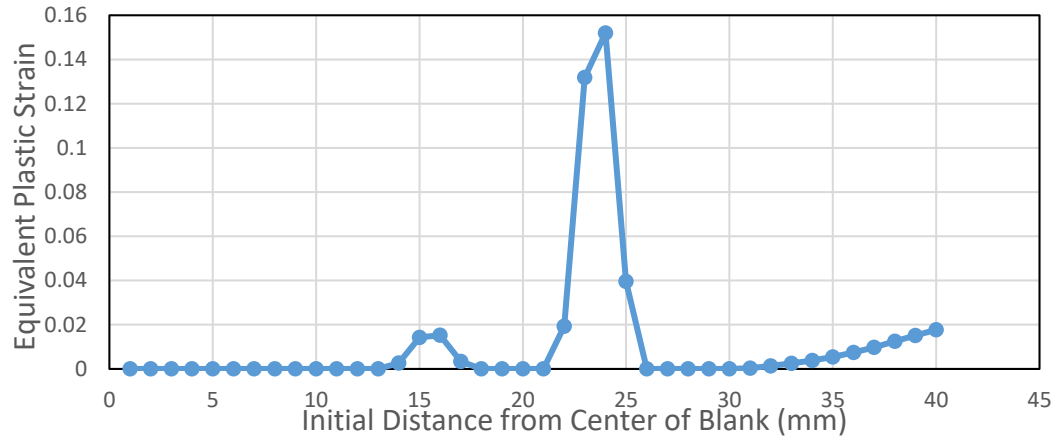

(a)

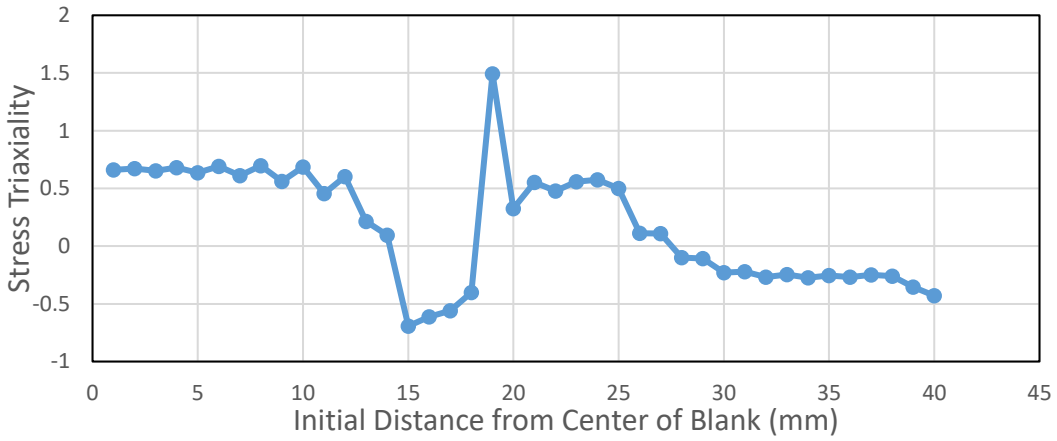

(b)

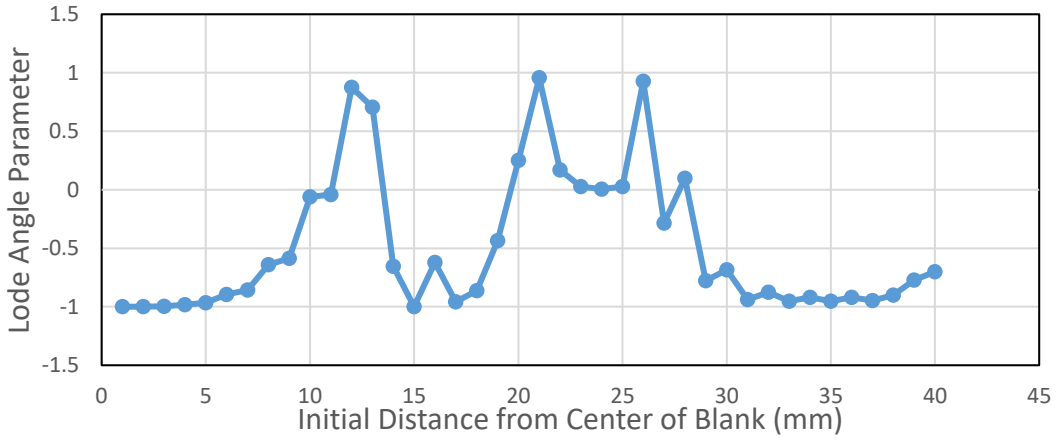

(c)

Figure 5.15. The variation of (a) Equivalent Plastic Strain (b) Stress Triaxiality and (c) Lode Angle Parameter along the rolling direction of the blank at 4 mm cup depth for Al2024 aluminum (VM-Disc-HC)

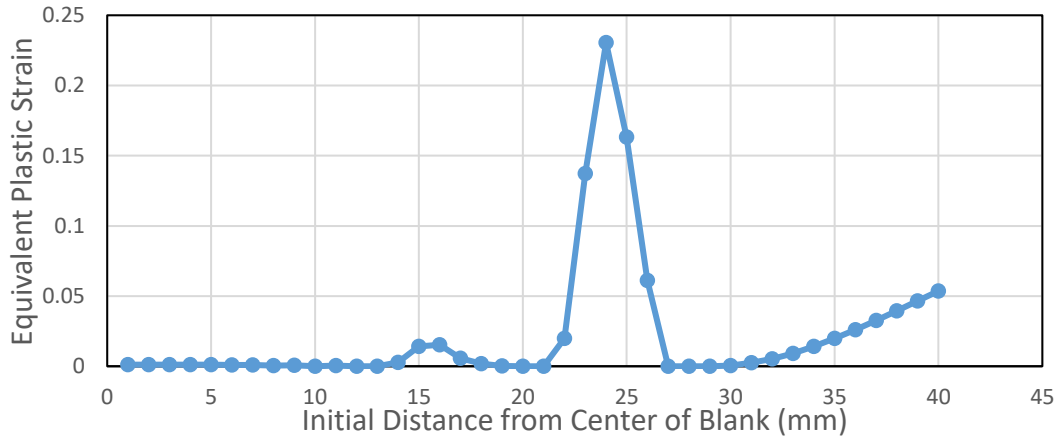

(a)

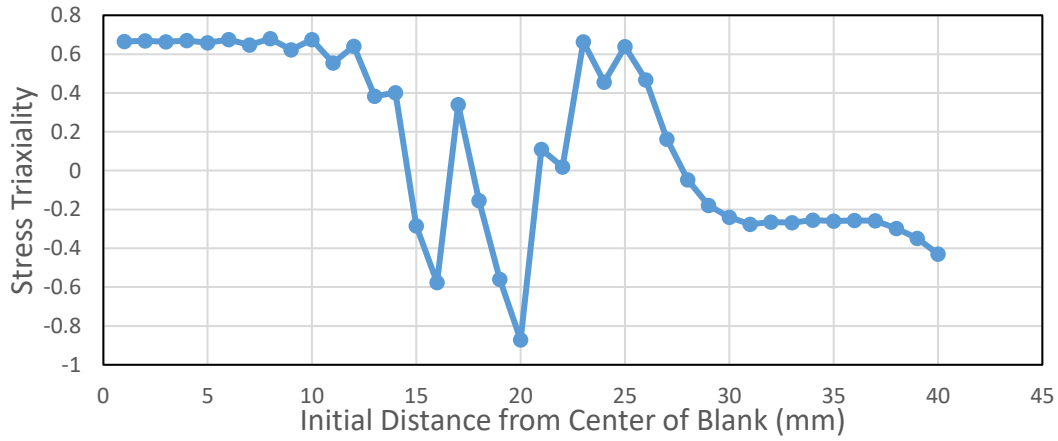

(b)

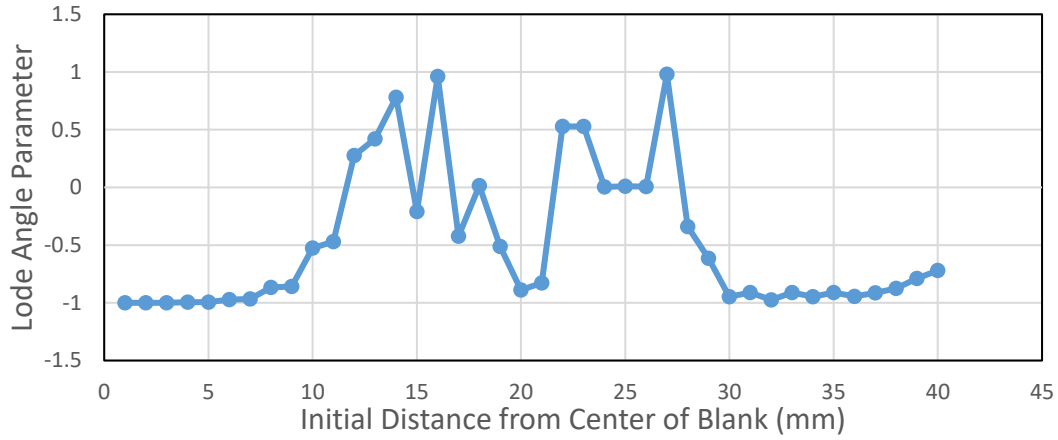

(c)

Figure 5.16. The variation of (a) Equivalent Plastic Strain (b) Stress Triaxiality and (c) Lode Angle Parameter along the rolling direction of the blank at 6 mm cup depth for Al2024 aluminum (VM-Disc-HC)

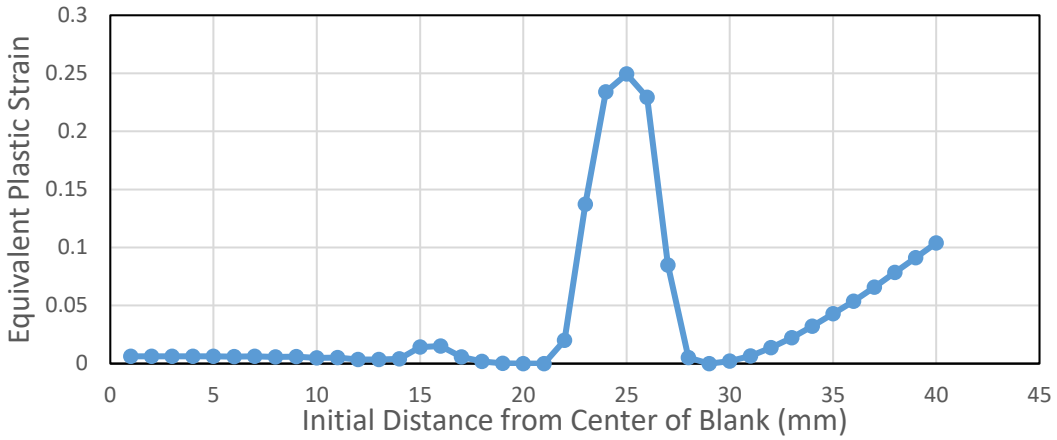

(a)

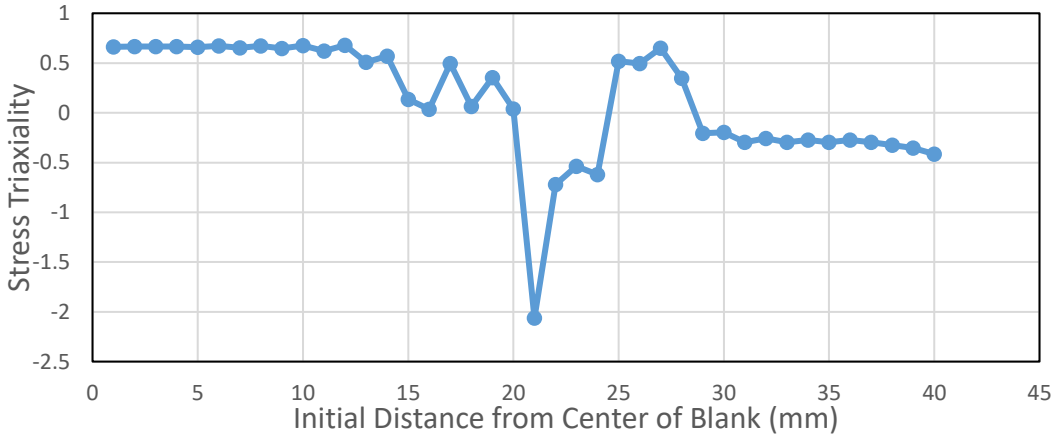

(b)

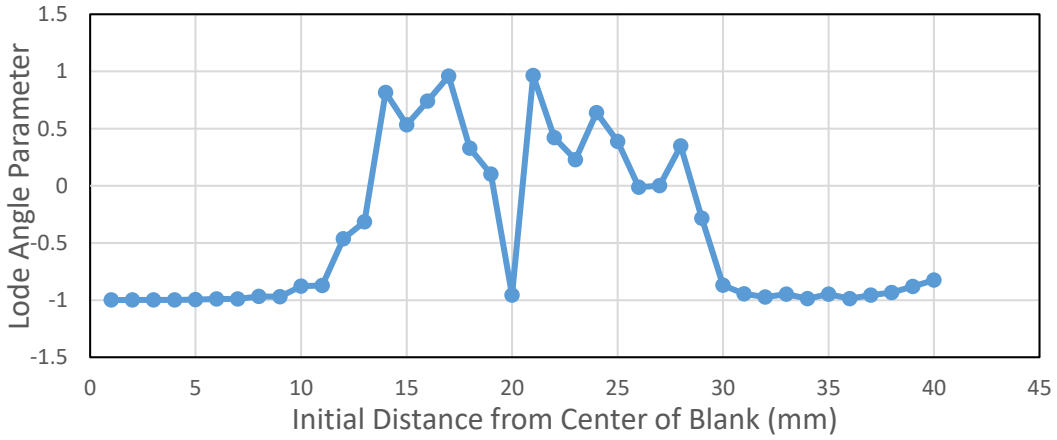

(c)

Figure 5.17. The variation of (a) Equivalent Plastic Strain (b) Stress Triaxiality and (c) Lode Angle Parameter along the rolling direction of the blank at 8 mm cup depth for Al2024 aluminum (VM-Disc-HC)

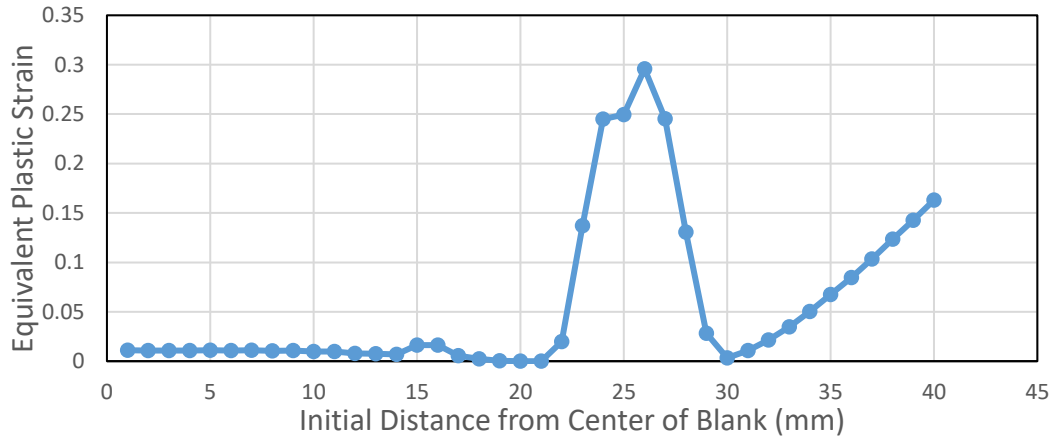

(a)

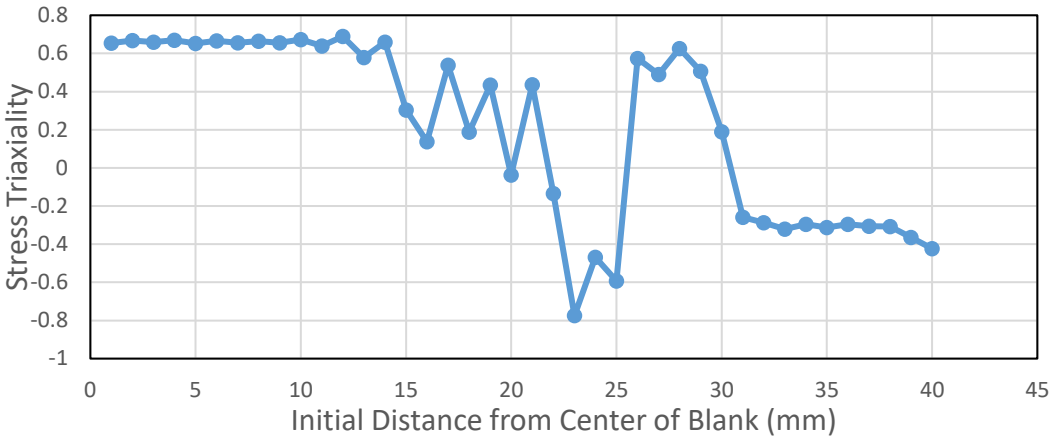

(b)

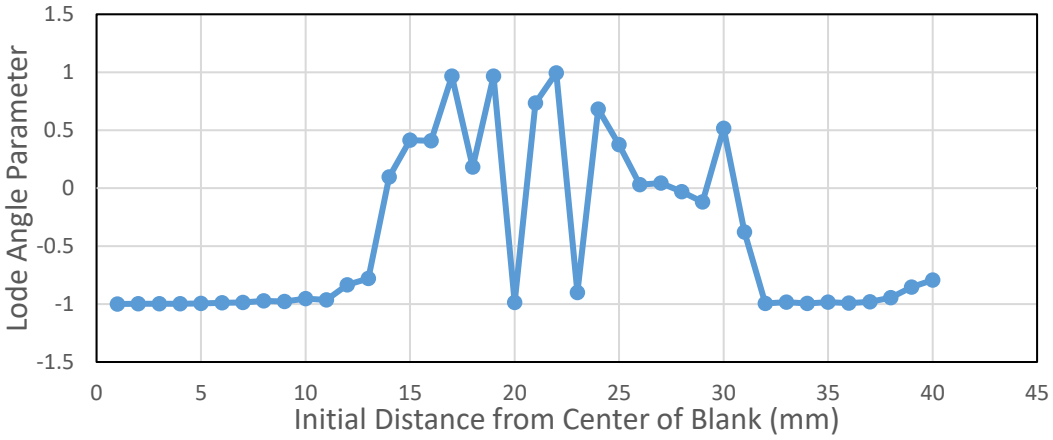

(c)

Figure 5.18. The variation of (a) Equivalent Plastic Strain (b) Stress Triaxiality and (c) Lode Angle Parameter along the rolling direction of the blank at 10 mm cup depth for Al2024 aluminum (VM-Disc-HC)

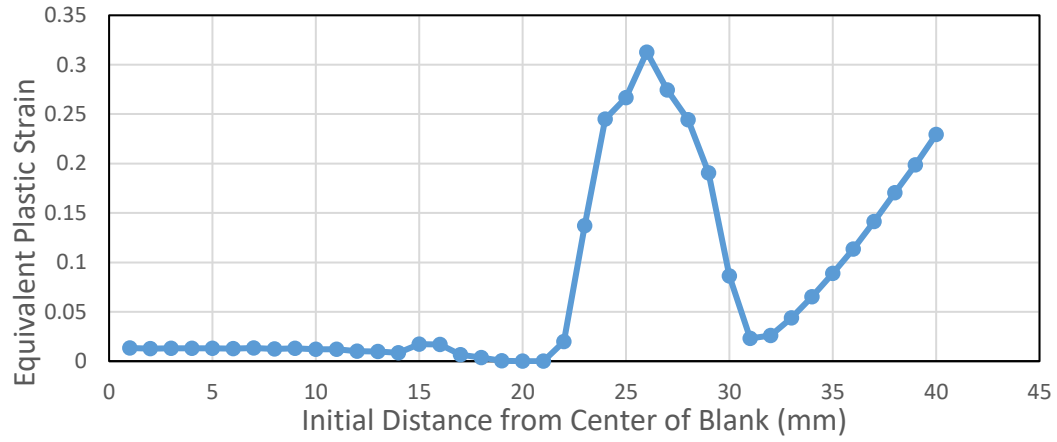

(a)

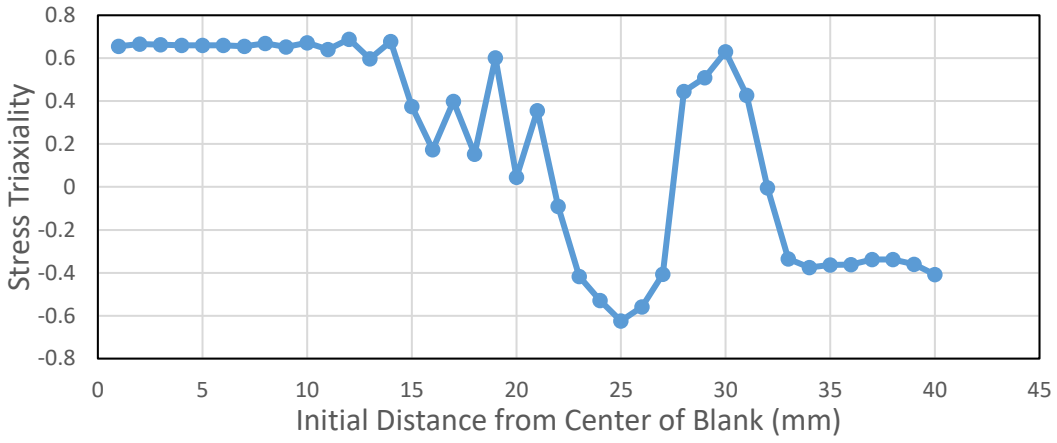

(b)

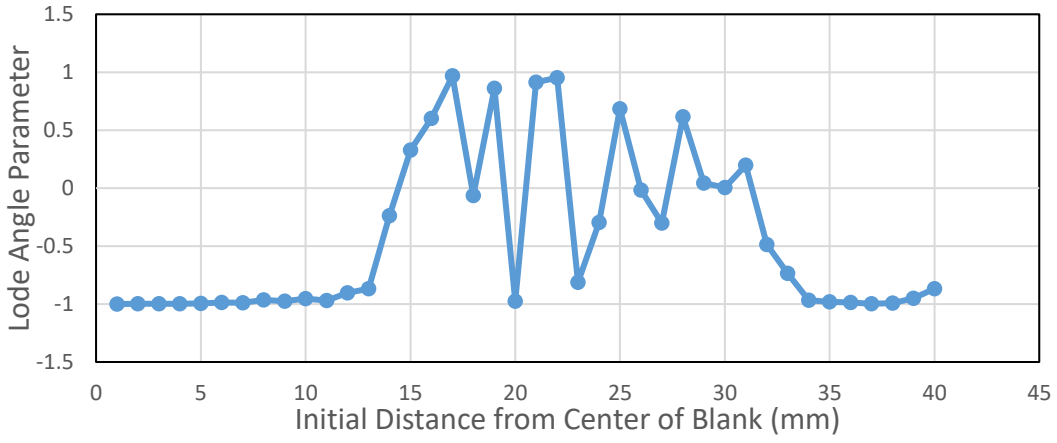

(c)

Figure 5.19 The variation of (a) Equivalent Plastic Strain (b) Stress Triaxiality and (c) Lode Angle Parameter along the rolling direction of the blank at 12 mm cup depth for Al2024 aluminum (VM-Disc-HC)

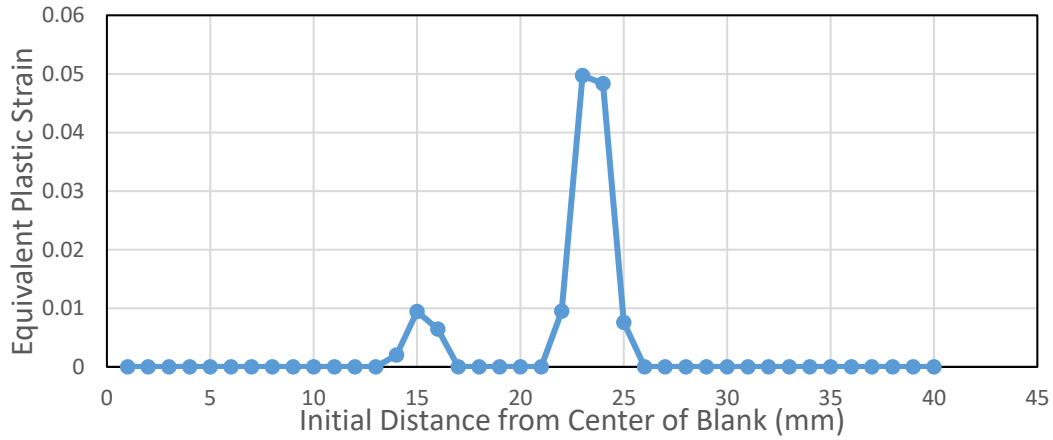

(a)

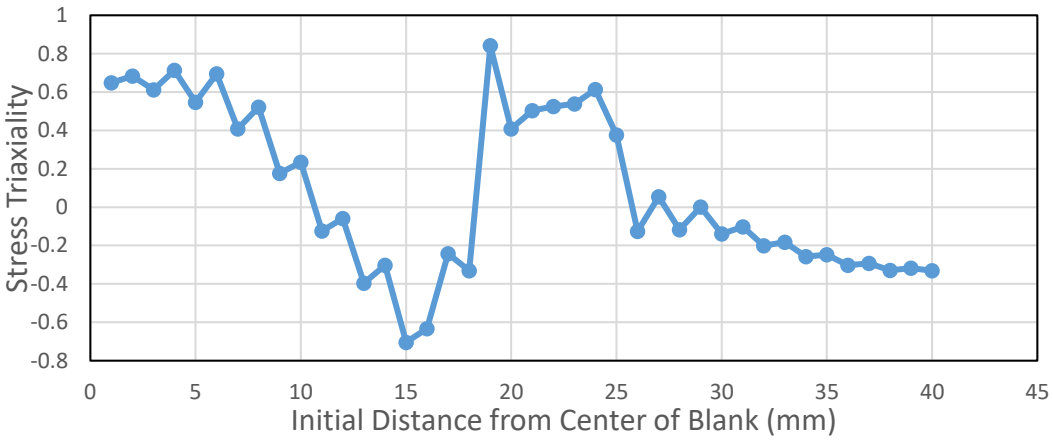

(b)

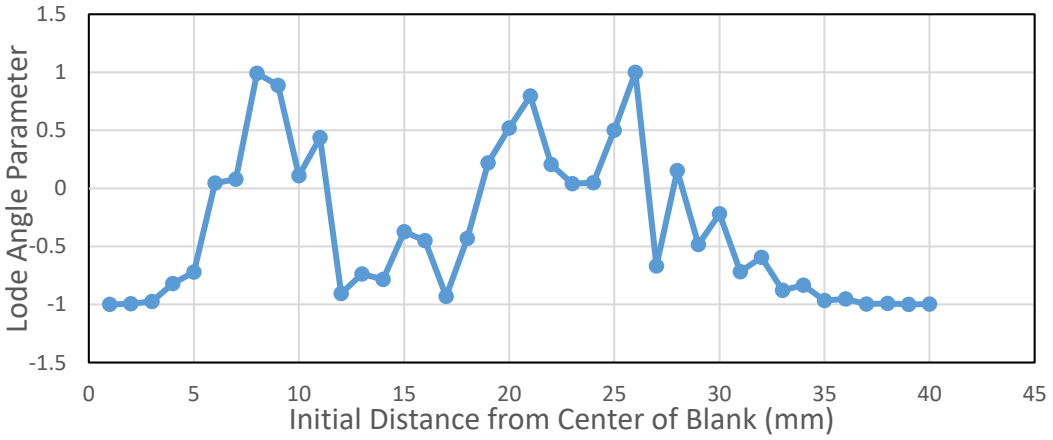

(c)

Figure 5.20. The variation of (a) Equivalent Plastic Strain (b) Stress Triaxiality and (c) Lode Angle Parameter along the transverse direction of the blank at 2 mm cup depth for Al2024 aluminum (VM-Disc-HC)

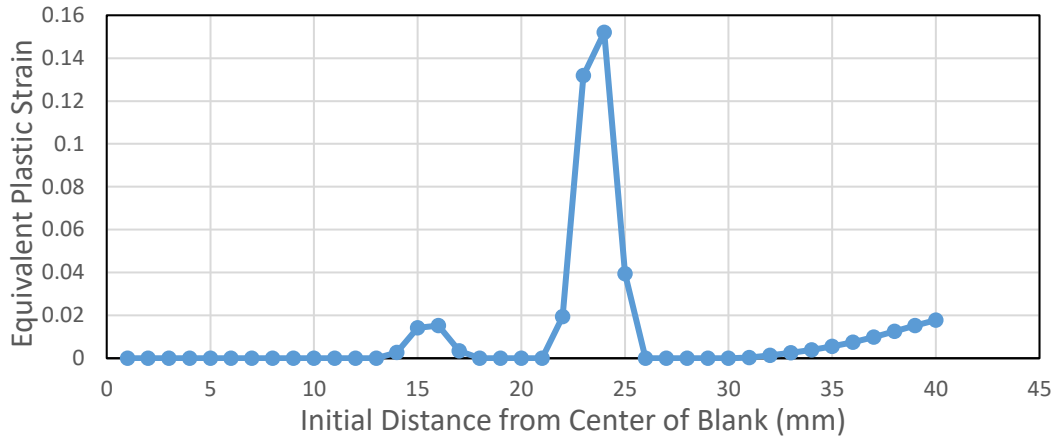

(a)

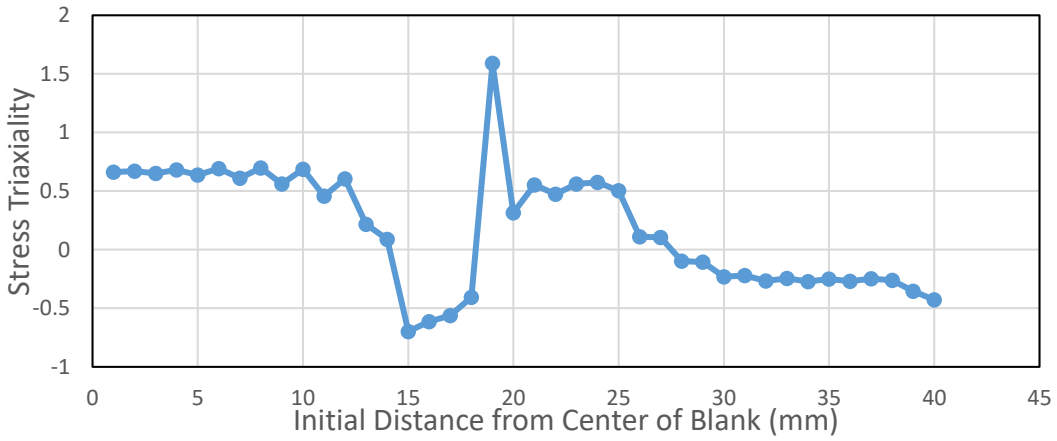

(b)

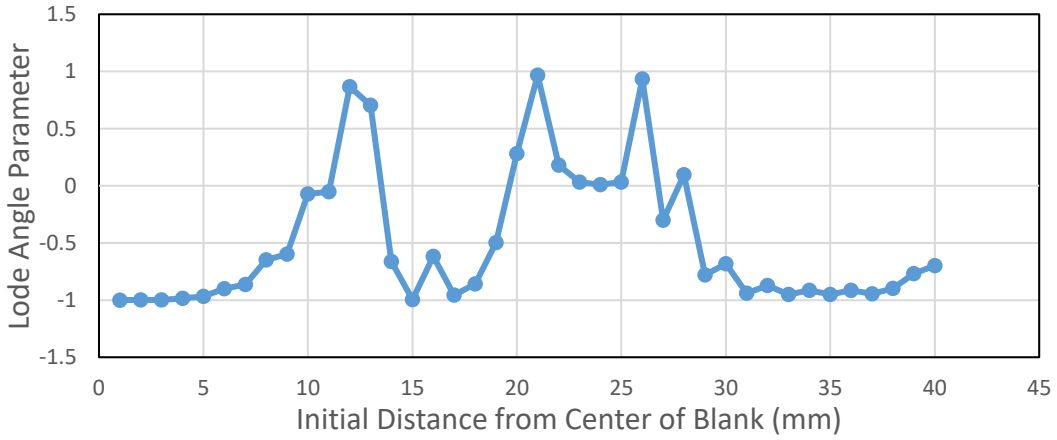

(c)

Figure 5.21. The variation of (a) Equivalent Plastic Strain (b) Stress Triaxiality and (c) Lode Angle Parameter along the transverse direction of the blank at 4 mm cup depth for Al2024 aluminum (VM-Disc-HC)

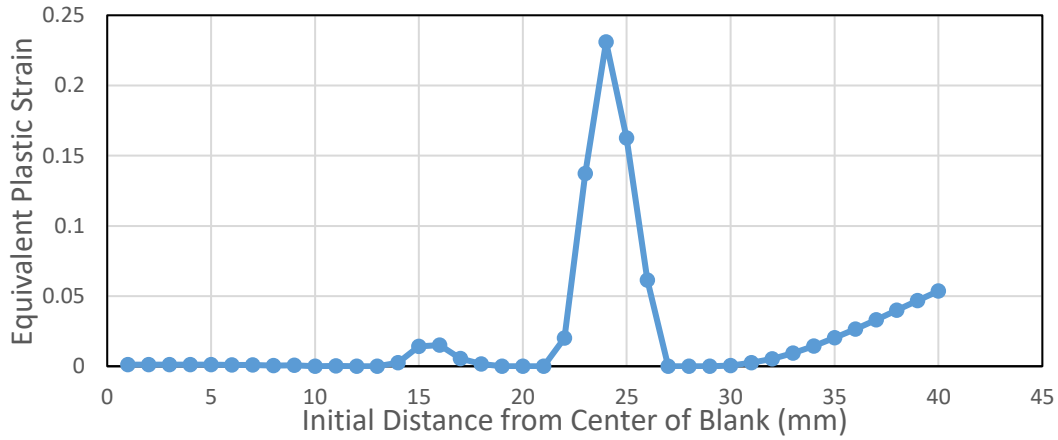

(a)

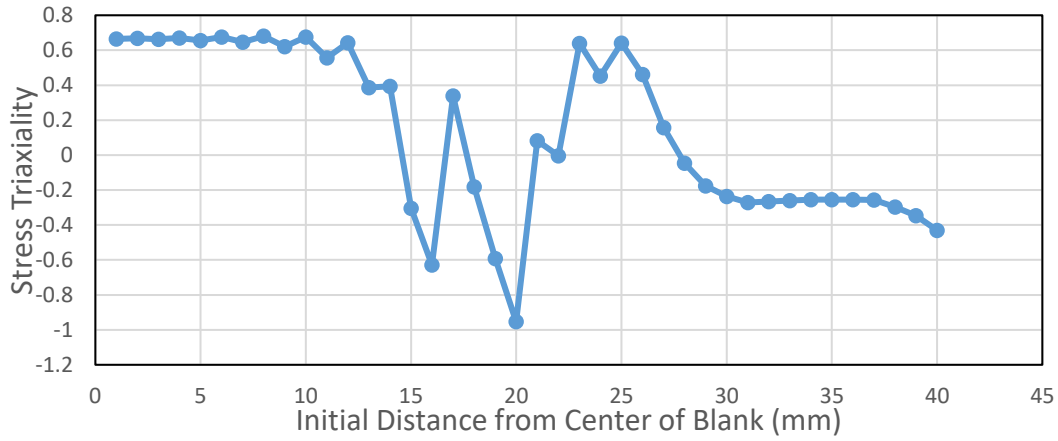

(b)

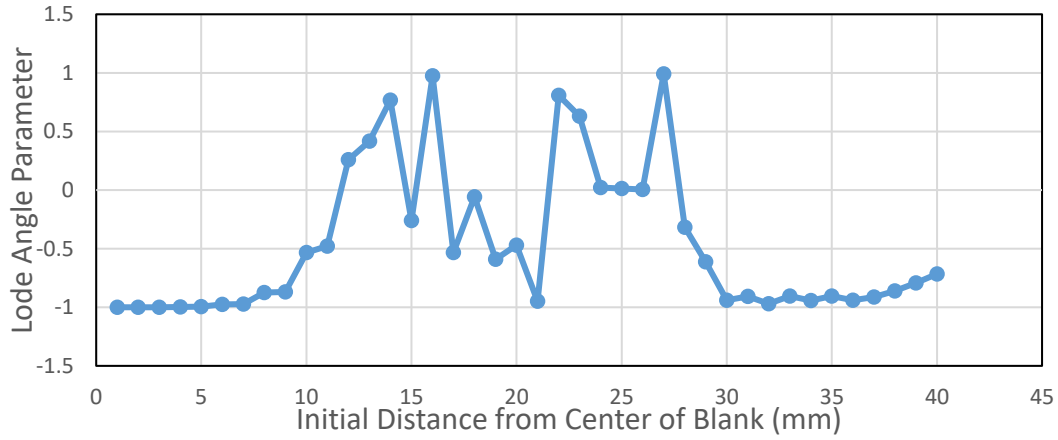

(c)

Figure 5.22. The variation of (a) Equivalent Plastic Strain (b) Stress Triaxiality and (c) Lode Angle Parameter along the transverse direction of the blank at 6 mm cup depth for Al2024 aluminum (VM-Disc-HC)

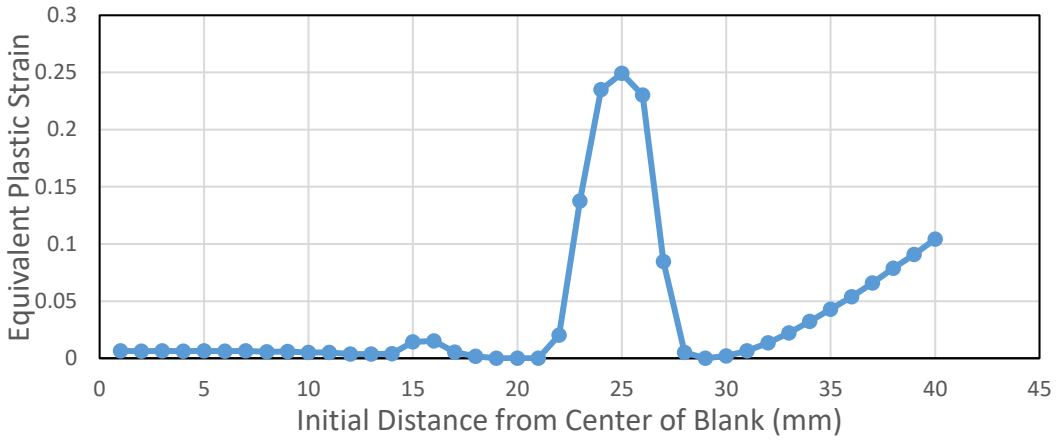

(a)

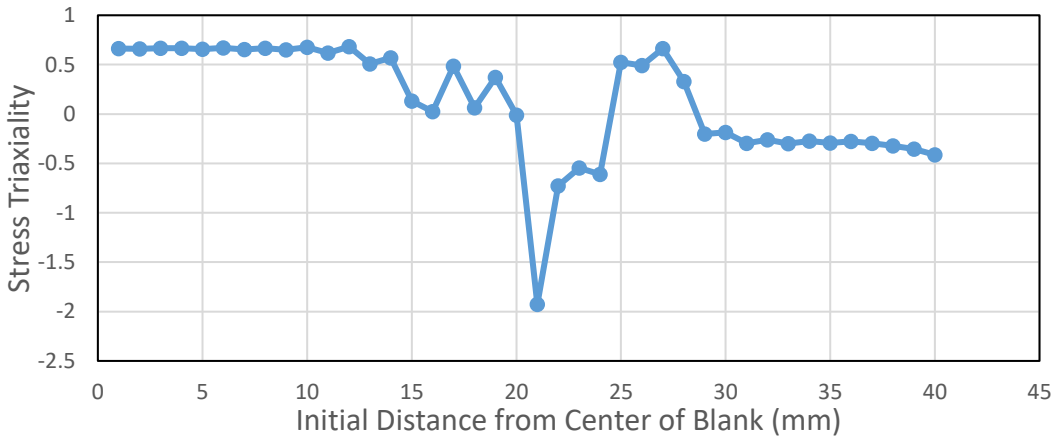

(b)

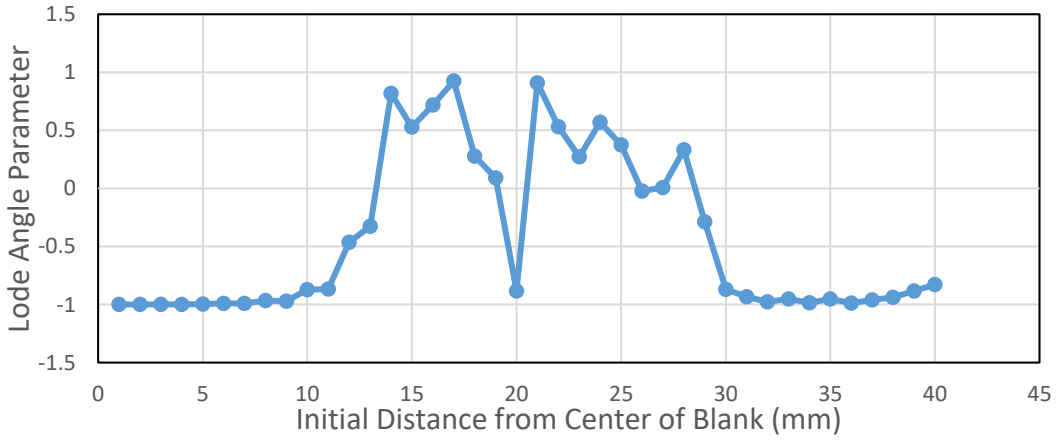

(c)

Figure 5.23. The variation of (a) Equivalent Plastic Strain (b) Stress Triaxiality and (c) Lode Angle Parameter along the transverse direction of the blank at 8 mm cup depth for Al2024 aluminum (VM-Disc-HC)

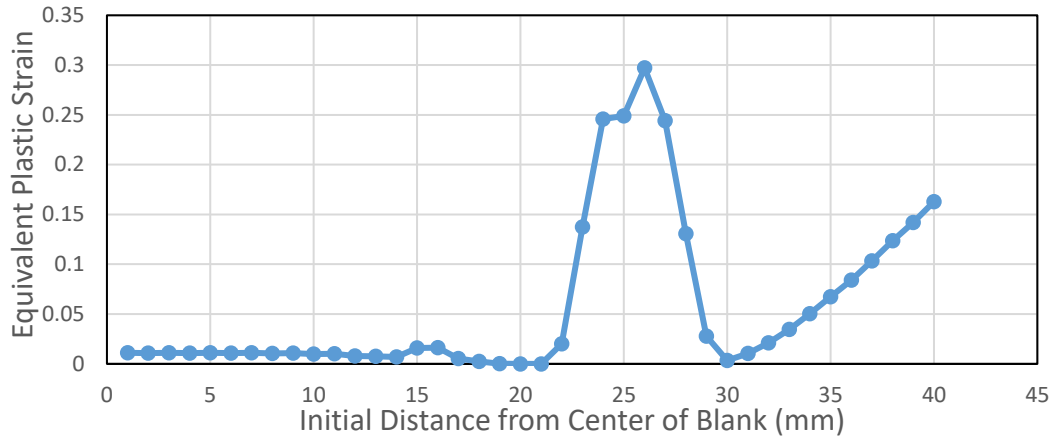

(a)

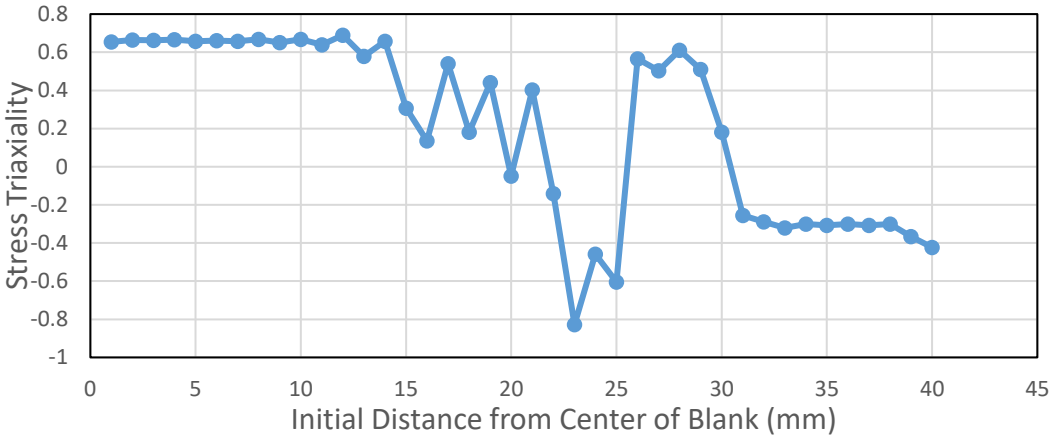

(b)

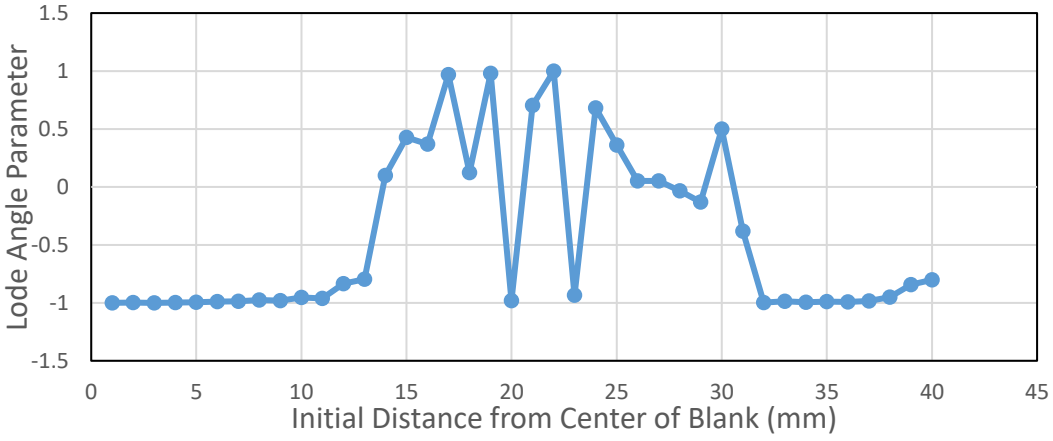

(c)

Figure 5.24. The variation of (a) Equivalent Plastic Strain (b) Stress Triaxiality and (c) Lode Angle Parameter along the transverse direction of the blank at 10 mm cup depth for Al2024 aluminum (VM-Disc-HC)

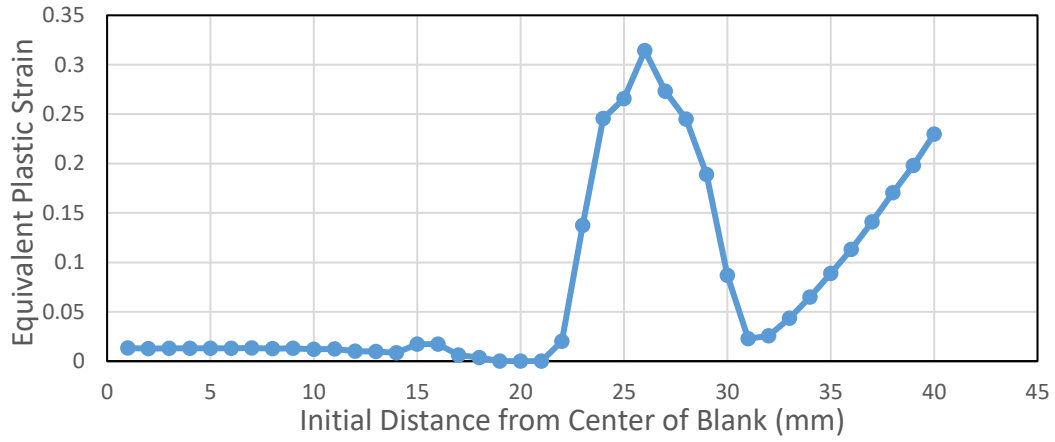

(a)

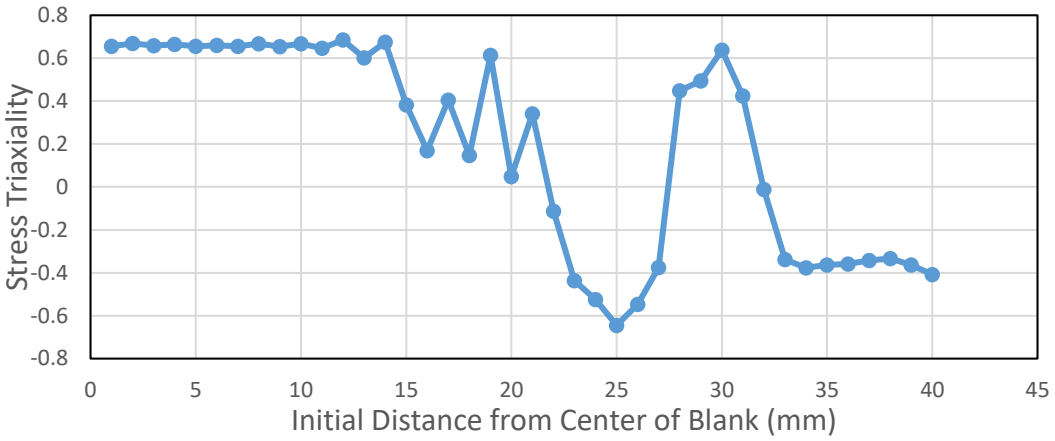

(b)

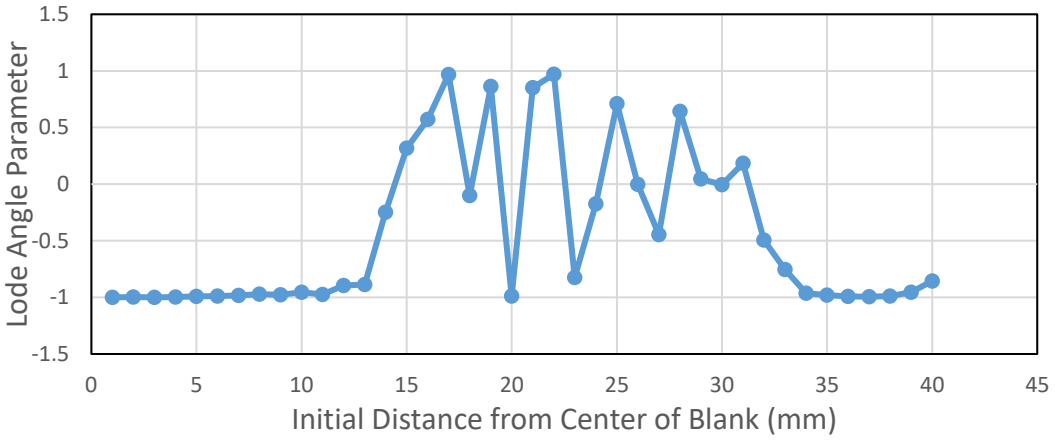

(c)

Figure 5.25. The variation of (a) Equivalent Plastic Strain (b) Stress Triaxiality and (c) Lode Angle Parameter along the transverse direction of the blank at 12 mm cup depth for Al2024 aluminum (VM-Disc-HC)

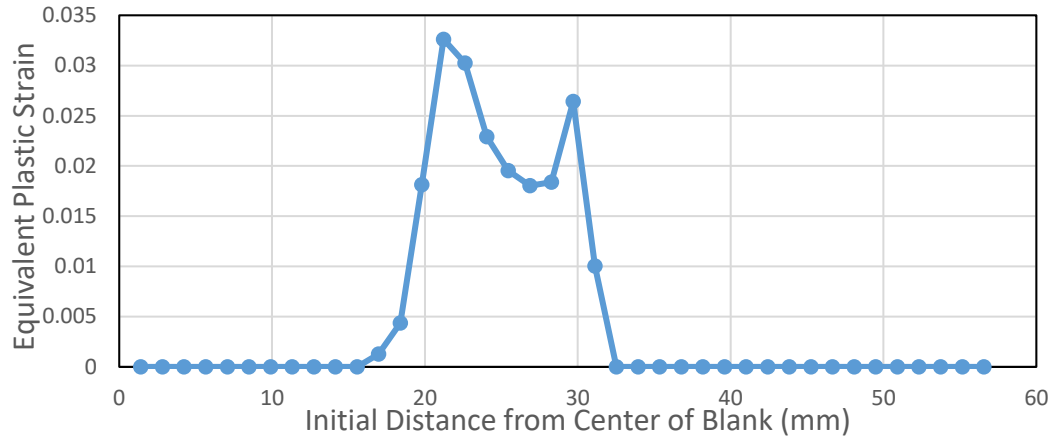

(a)

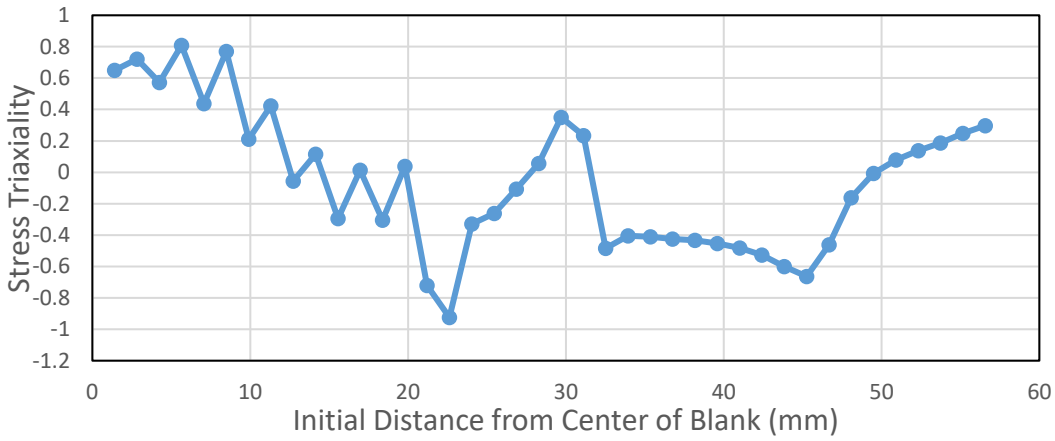

(b)

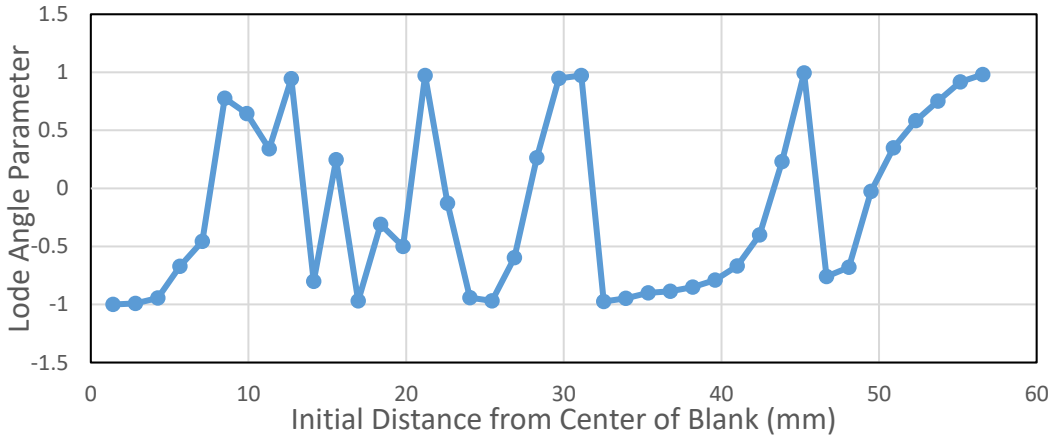

(c)

Figure 5.26. The variation of (a) Equivalent Plastic Strain (b) Stress Triaxiality and (c) Lode Angle Parameter along the diagonal of the blank at 2 mm cup depth for Al2024 aluminum (VM-Disc-HC)

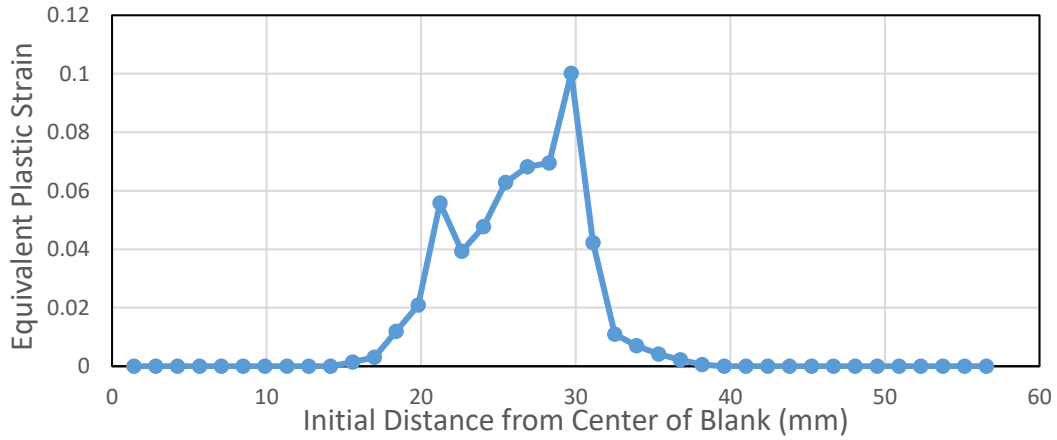

(a)

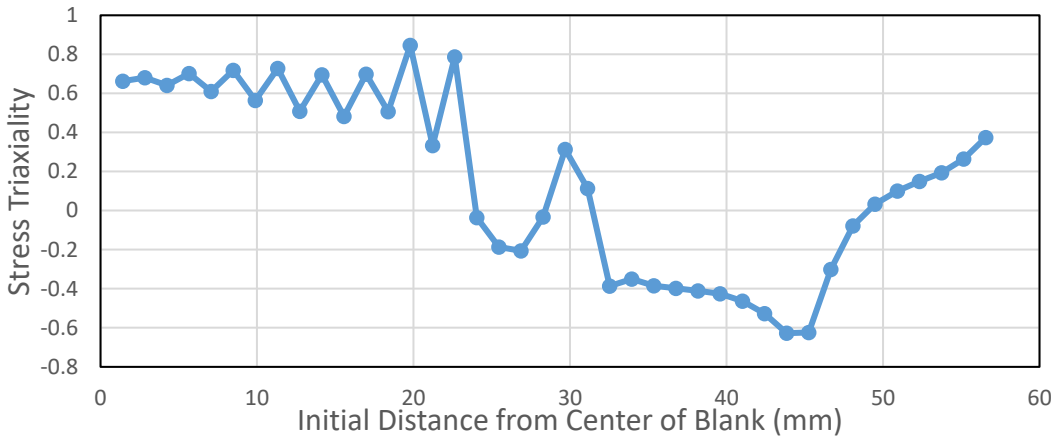

(b)

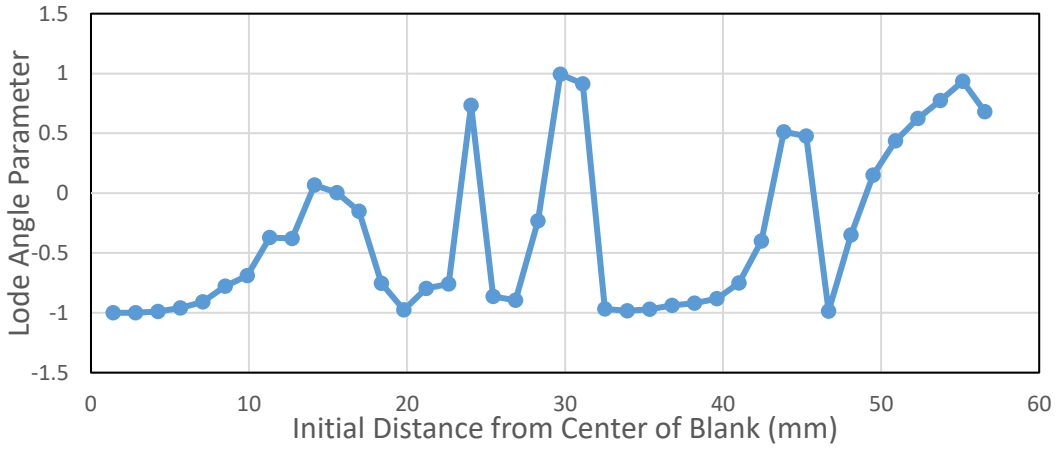

(c)

Figure 5.27. The variation of (a) Equivalent Plastic Strain (b) Stress Triaxiality and (c) Lode Angle Parameter along the diagonal of the blank at 4 mm cup depth for Al2024 aluminum (VM-Disc-HC)

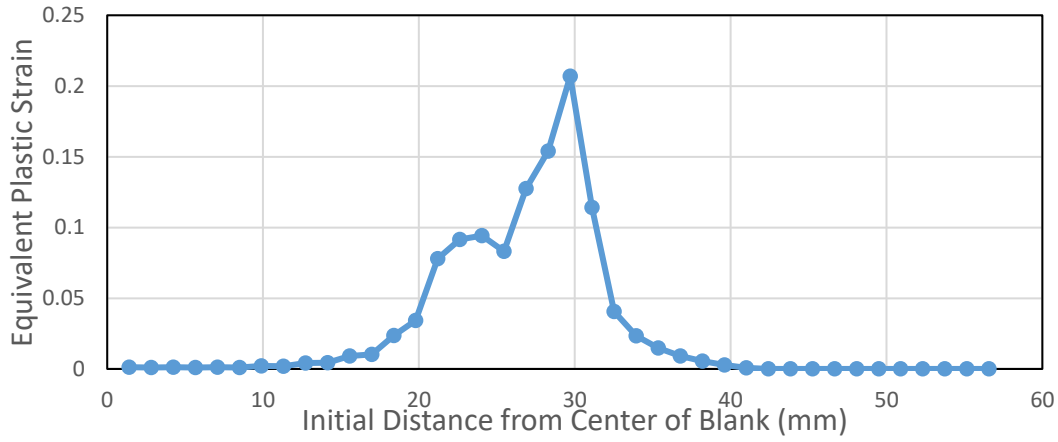

(a)

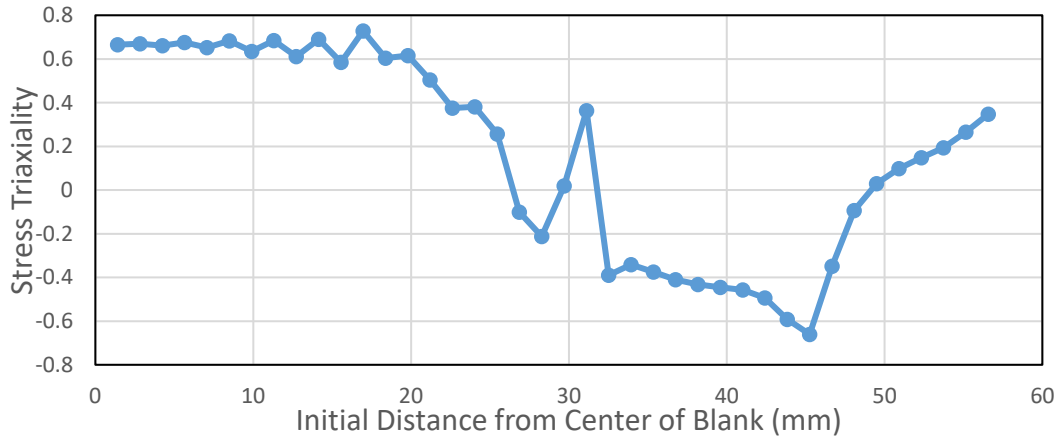

(b)

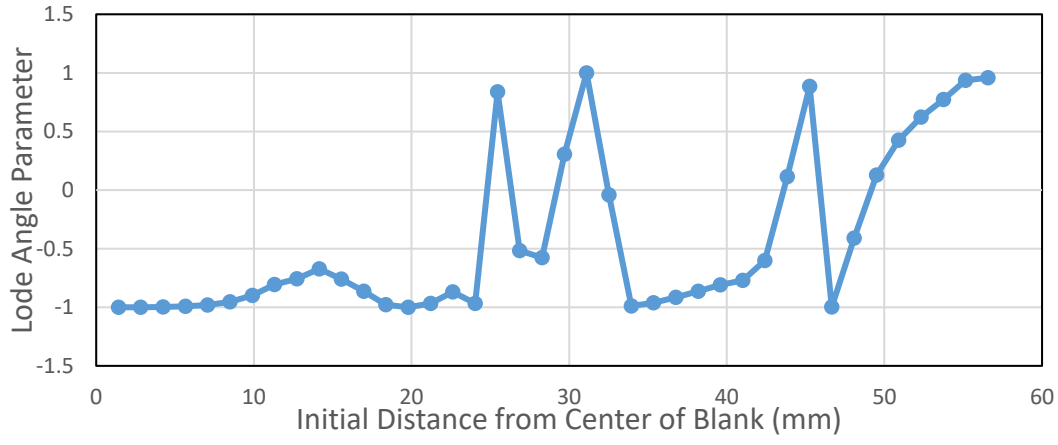

(c)

Figure 5.28 The variation of (a) Equivalent Plastic Strain (b) Stress Triaxiality and (c) Lode Angle Parameter along the diagonal of the blank at 6 mm cup depth for Al2024 aluminum (VM-Disc-HC)

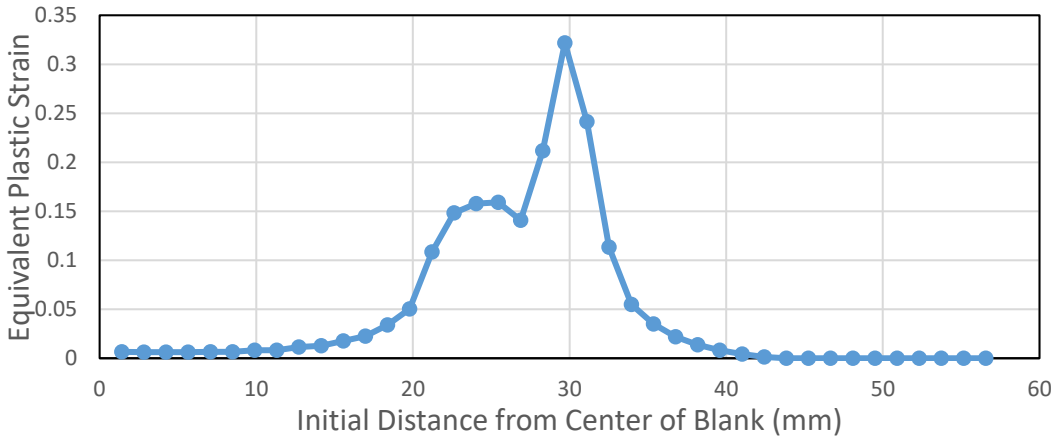

(a)

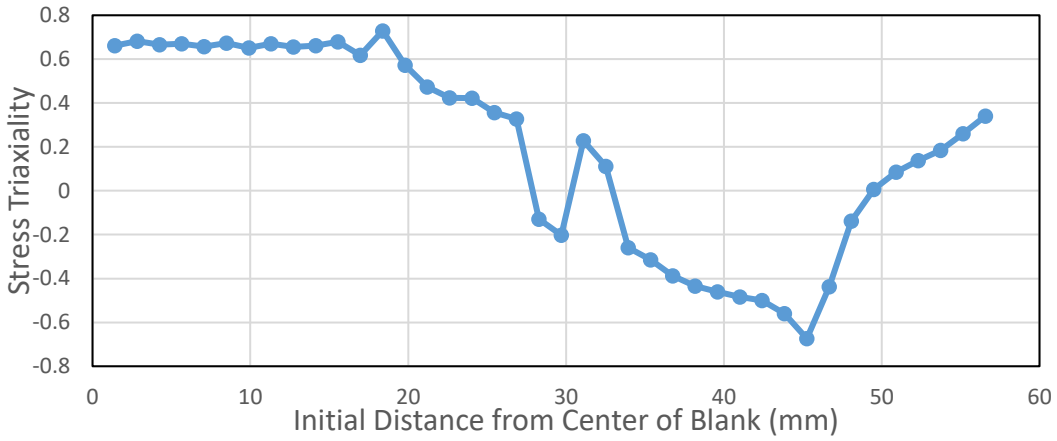

(b)

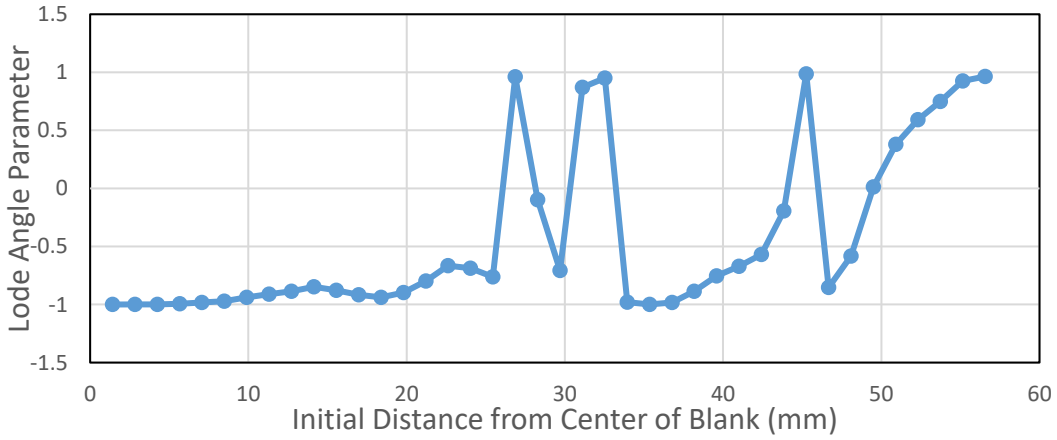

(c)

Figure 5.29 The variation of (a) Equivalent Plastic Strain (b) Stress Triaxiality and (c) Lode Angle Parameter along the diagonal of the blank at 8 mm cup depth for Al2024 aluminum (VM-Disc-HC)

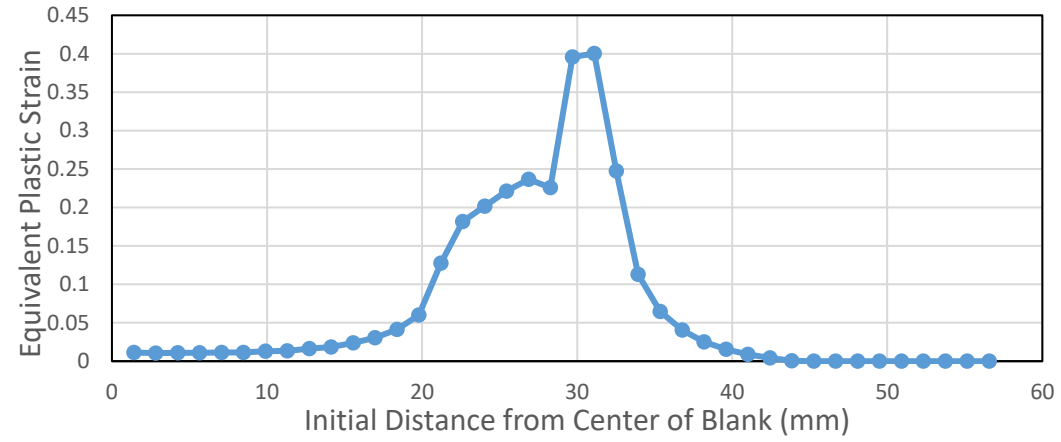

(a)

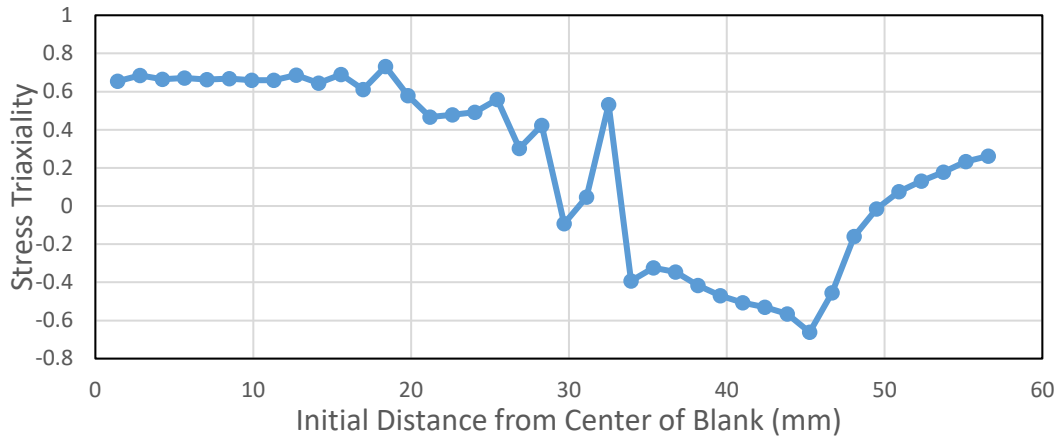

(b)

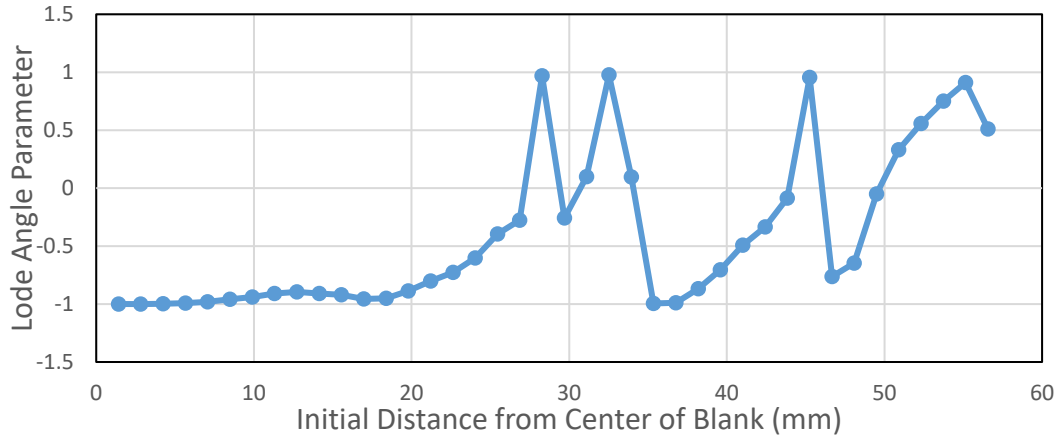

(c)

Figure 5.30. The variation of (a) Equivalent Plastic Strain (b) Stress Triaxiality and (c) Lode Angle Parameter along the diagonal of the blank at 10 mm cup depth for Al2024 aluminum (VM-Disc-HC)

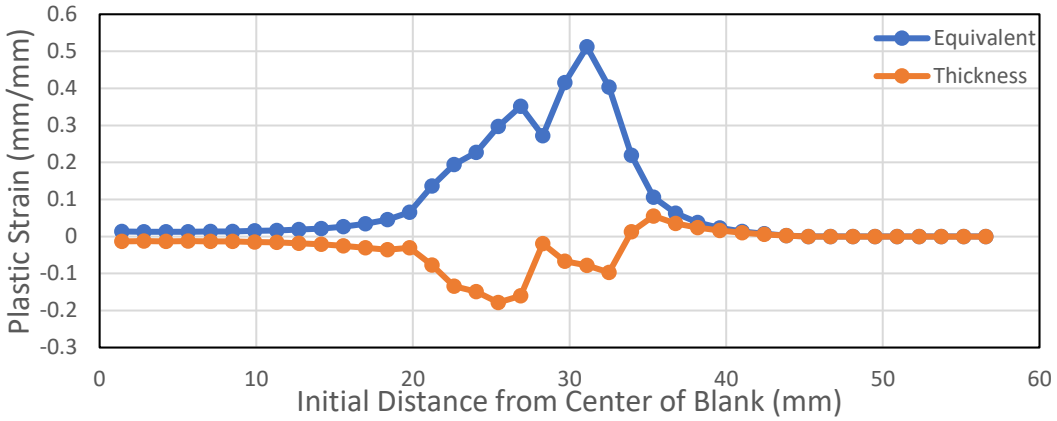

(a)

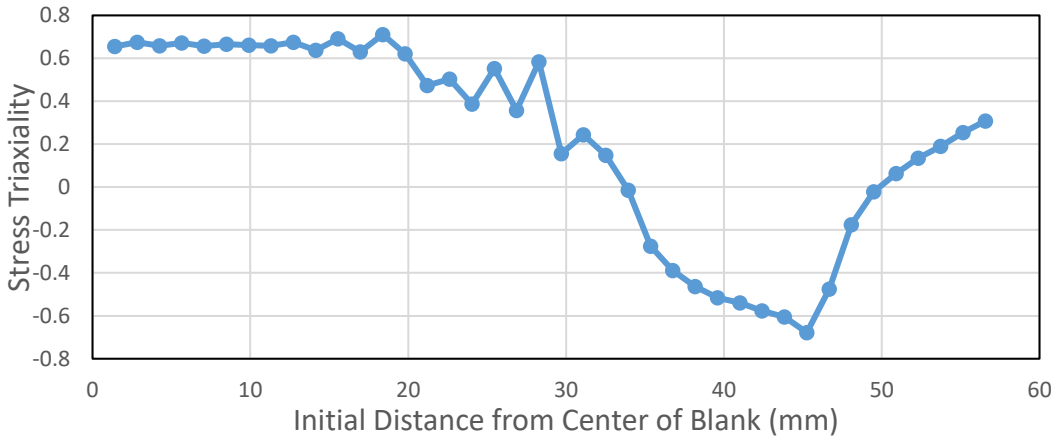

(b)

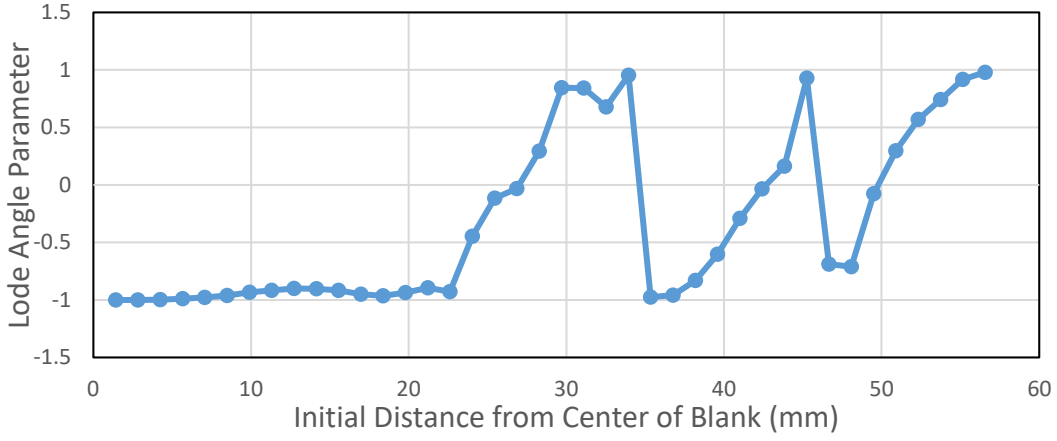

(c)

Figure 5.31. The variation of (a) Equivalent Plastic Strain and Thickness Plastic Strain (b) Stress Triaxiality and (c) Lode Angle Parameter along the diagonal of the blank at 12 mm cup depth for Al2024 aluminum (VM-Disc-HC)

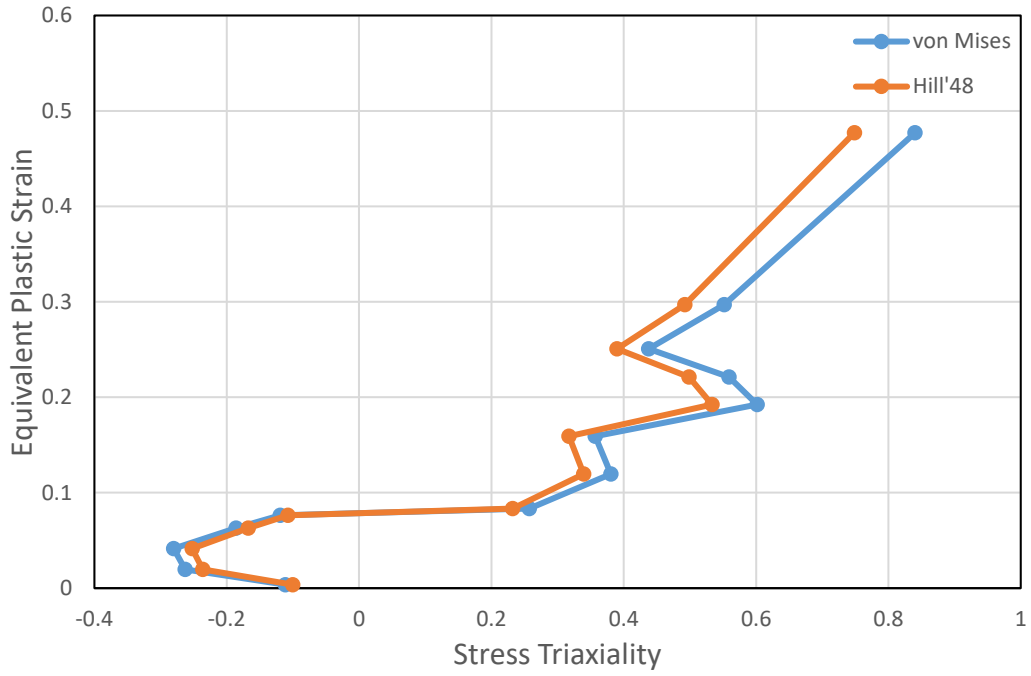

Figure 5.32. Equivalent Plastic Strain - Stress Triaxiality Plot of First Rupture Element (VM-Disc-HC)

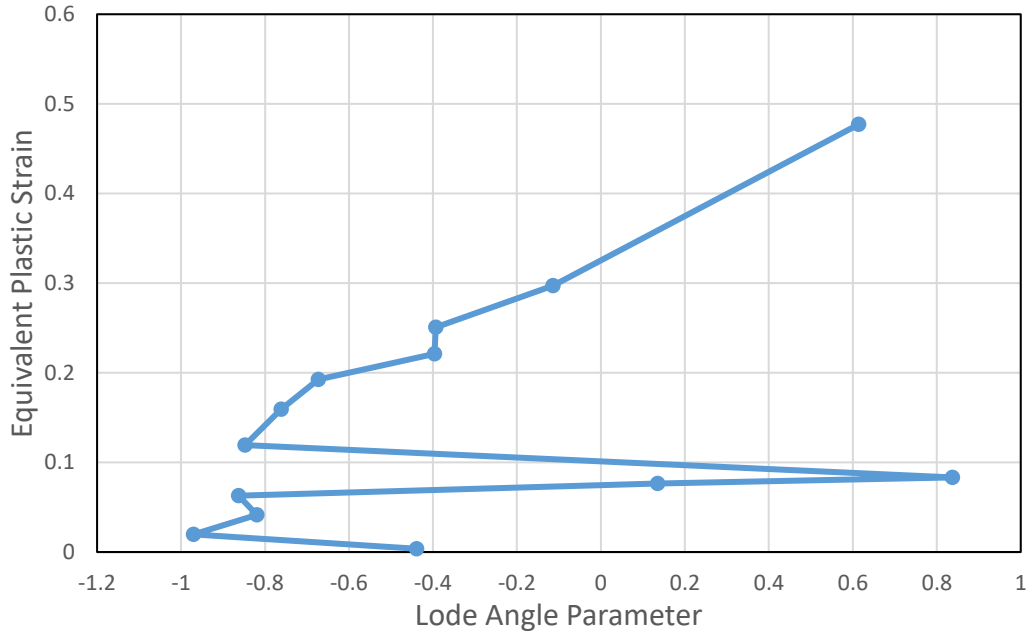

Figure 5.33. Equivalent Plastic Strain – Lode Angle Parameter Plot of First Rupture Element (VM-Disc-HC)

In the rolling direction, the triaxiality values vary generally between 0.6 and 0.8 under the punch whereas the Lode angle parameter values change between -0.5 and -1. Up to the punch shoulder, it can be said that the deformation behavior is in equi-biaxial tension condition. However, for 2 mm punch travel the compressive punch force on the sheet surface dominates towards the punch shoulder where triaxiality values change towards negative where Lode angle parameter values show the same tendency. Here, only in the regions close to the center of the blank i.e., up to a distance of 5 mm from the center, the equi-biaxial tension conditions are observed. As the punch continues to move, the region with equi-biaxial tension conditions extend and reaches 10 mm from the center of the blank. At the punch shoulder triaxiality values are still positive but decreasing as the distance increases from the blank center. At the clearance between die and punch thinning continues. At the punch shoulder, the triaxiality values are mostly positive with varying Lode angle parameter values. From die shoulder to end of the blank, uniaxial compression may be noticed.

The same tendency of rolling direction is observed in the transverse direction also. The differences are a result of anisotropy of the material.

In the diagonal direction, as in the transverse and rolling directions, equi-biaxial stress condition is observed under the punch. At the punch corner, triaxiality values are still positive but decreasing and the Lode angle parameter values are increasing, as the distance increases from the blank center. Hence there is a tensile type deformation in this region. At the die corner the triaxiality values start to became negative, indication compressive type deformation with the Lode angle parameter values. Under the blank holder, the triaxiality values are negative and increases, and finally become positive, similarly negative Lode angle parameter values turn into positive, indicating thickening towards the rim where the nature of the deformation changes from uniaxial compression to tension dominant situation and fracture occurs in tension situation.

5.1.3 Case 3: Square-Al2024-von Mises -Johnson Cook-Johnson Cook Model

For the third case, von Mises yield criterion was applied with Johnson Cook hardening and the Johnson Cook ductile fracture criterion was used. It was observed that the fracture had started after 8 mm punch travel as shown in Figure 5.34. The variation of equivalent plastic strain, stress triaxiality and Lode angle parameter values are presented as a function of the distance from the center of the blank for different cup heights up to the fracture. The results are shown for rolling direction in Figure 5.35 to Figure 5.38, for transverse direction in Figure 5.39 to Figure 5.42 and for diagonal direction in Figure 5.43 to Figure 5.46. The thickness plastic strain distribution is also inserted into Figure 5.46 (a) in order to better visualize the deformation. Further, the variations of stress triaxiality values with respect to equivalent plastic strain are given by considering both von Mises and Hill'48 criteria as a function of the path of the element that fractured first in Figure 5.47 Along the same path, the variation of the Lode parameter with respect to equivalent plastic strain is also illustrated in Figure 5.48.

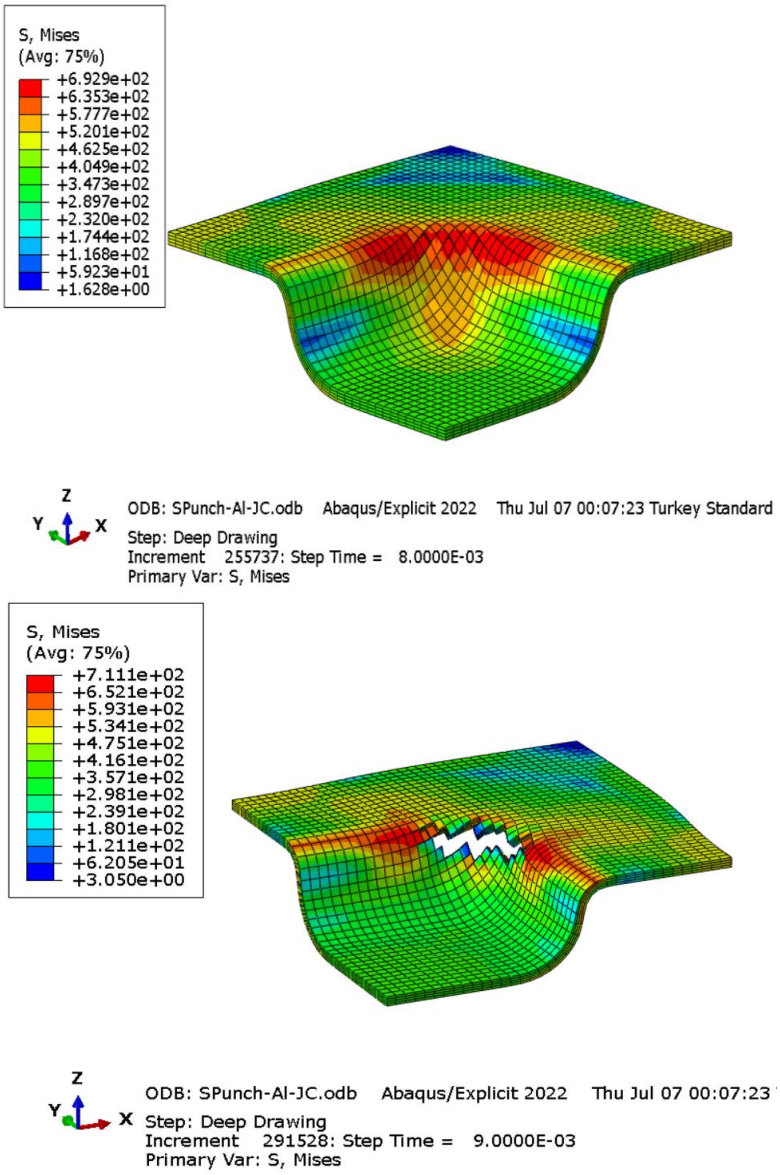

Figure 5.34. First Rupture Moment of Case 3

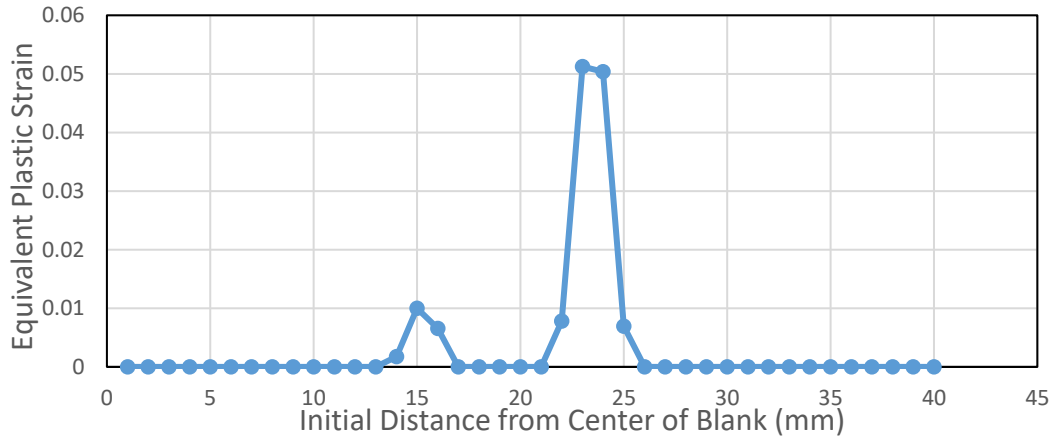

(a)

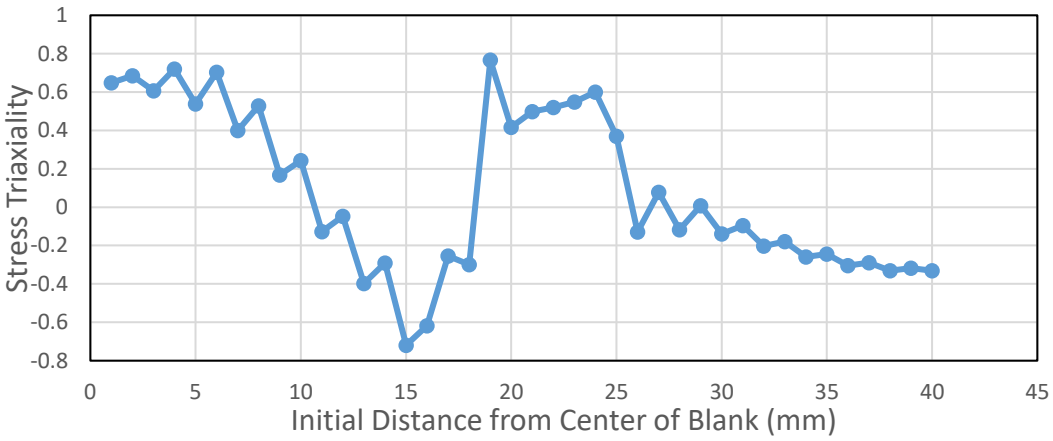

(b)

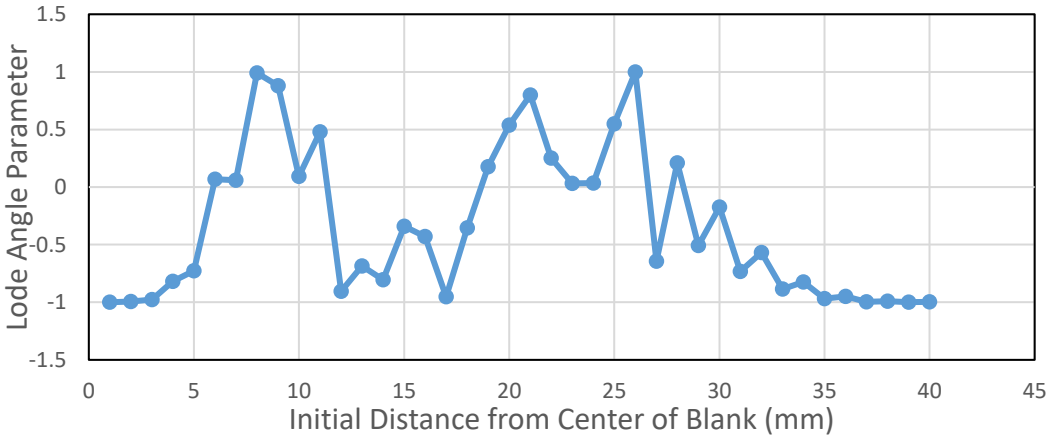

(c)

Figure 5.35. The variation of (a) Equivalent Plastic Strain (b) Stress Triaxiality and (c) Lode Angle Parameter along the rolling direction of the blank at 2 mm cup depth for Al2024 aluminum (VM-JC-JC)

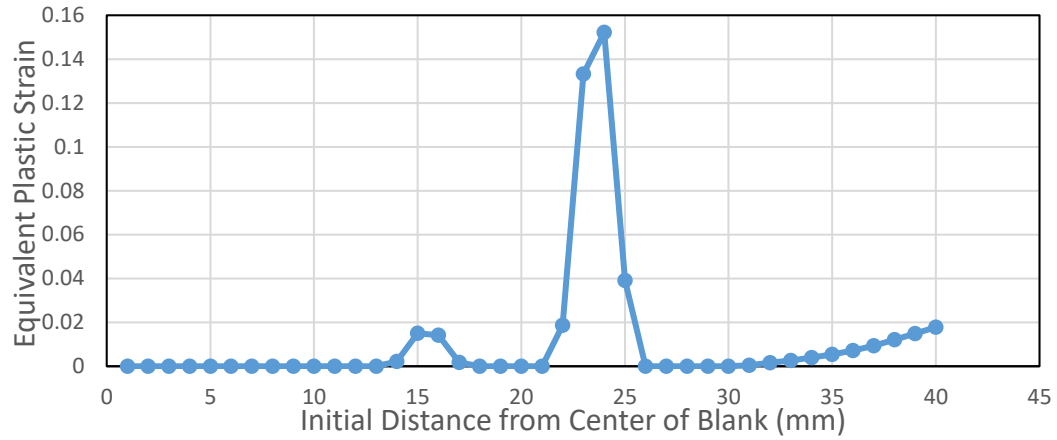

(a)

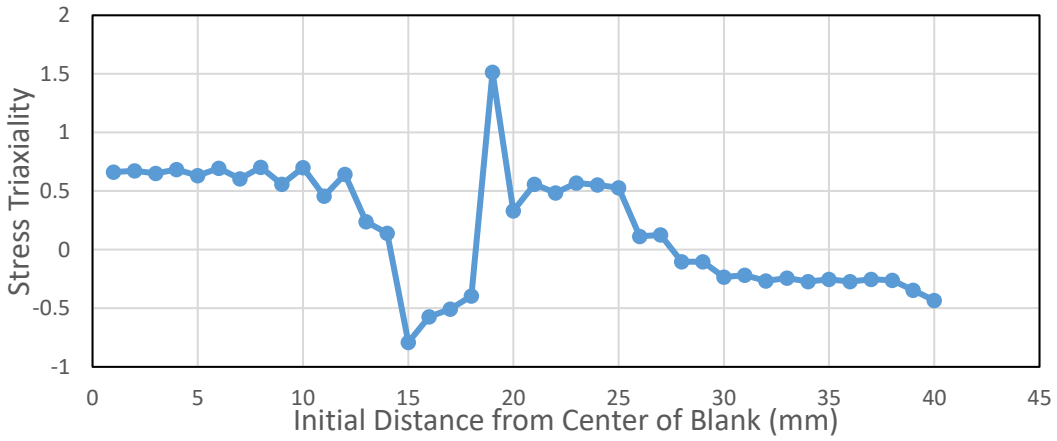

(b)

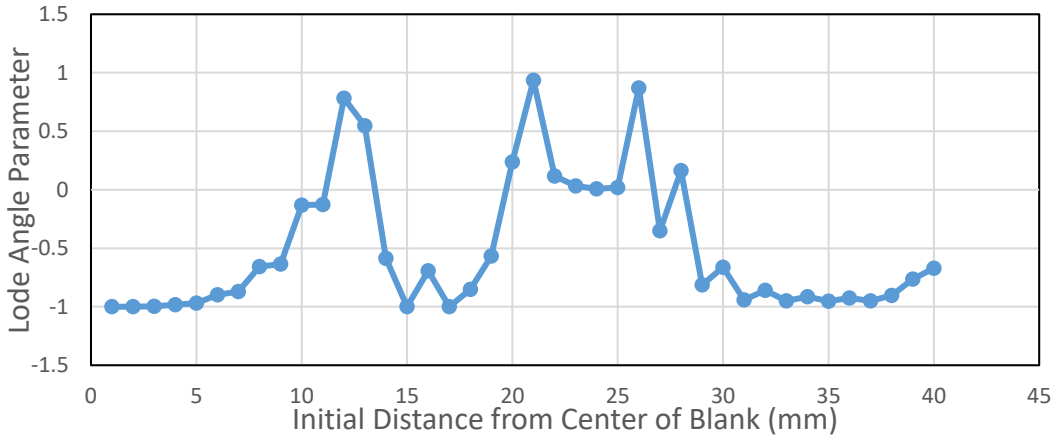

(c)

Figure 5.36. The variation of (a) Equivalent Plastic Strain (b) Stress Triaxiality and (c) Lode Angle Parameter along the rolling direction of the blank at 4 mm cup depth for Al2024 aluminum (VM-JC-JC)

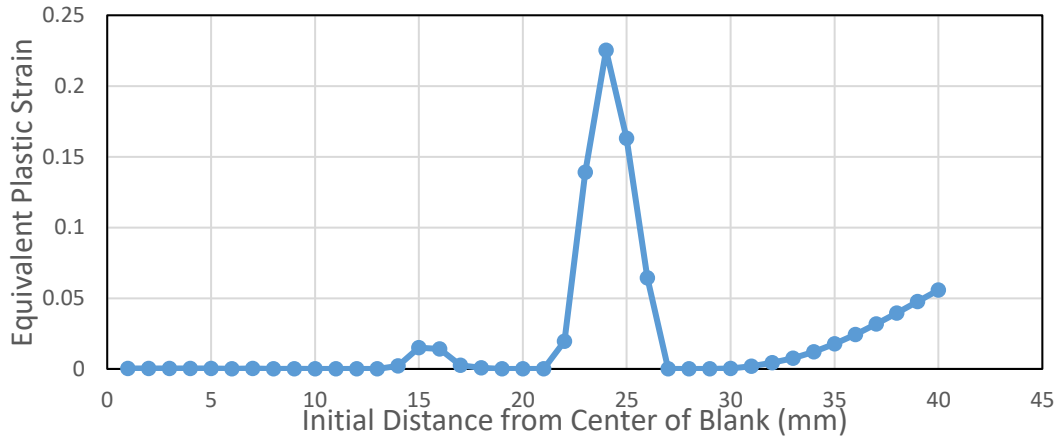

(a)

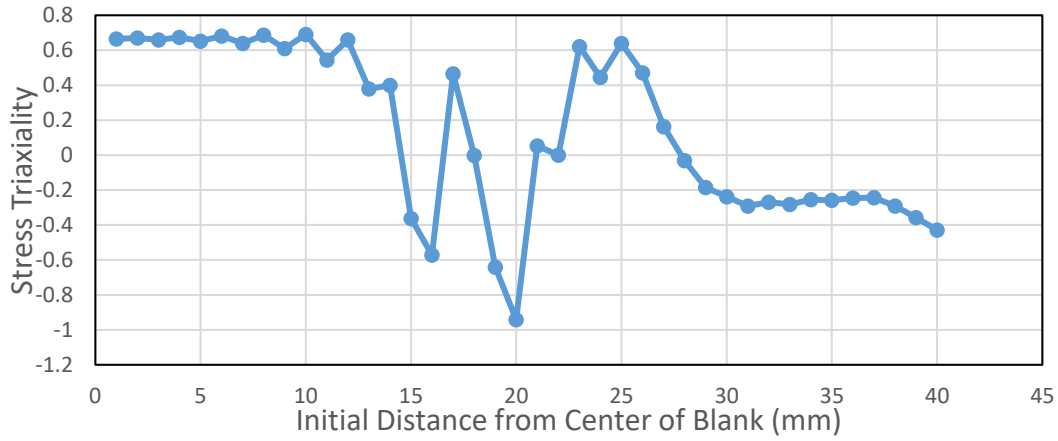

(b)

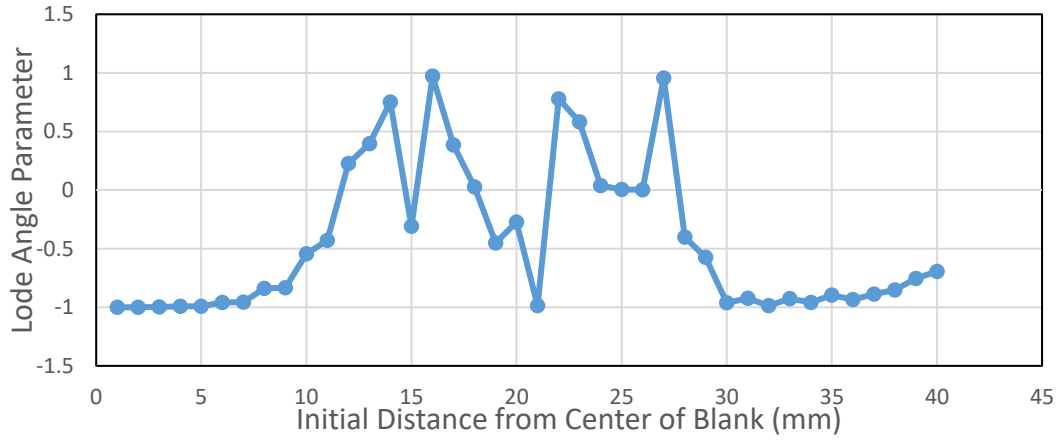

(c)

Figure 5.37. The variation of (a) Equivalent Plastic Strain (b) Stress Triaxiality and (c) Lode Angle Parameter along the rolling direction of the blank at 6 mm cup depth for Al2024 aluminum (VM-JC-JC)

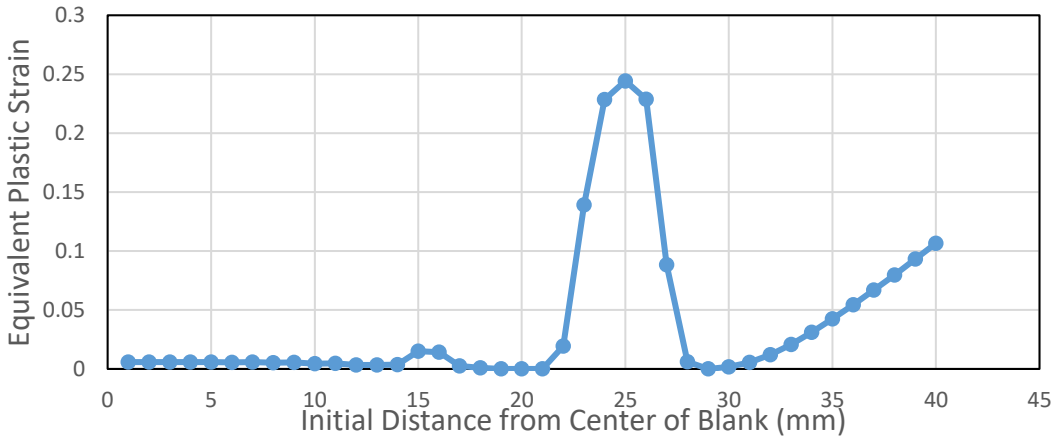

(a)

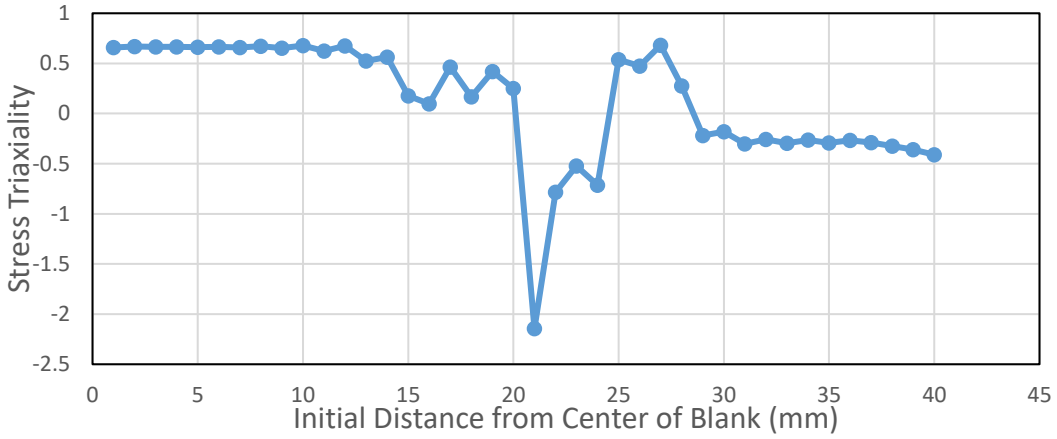

(b)

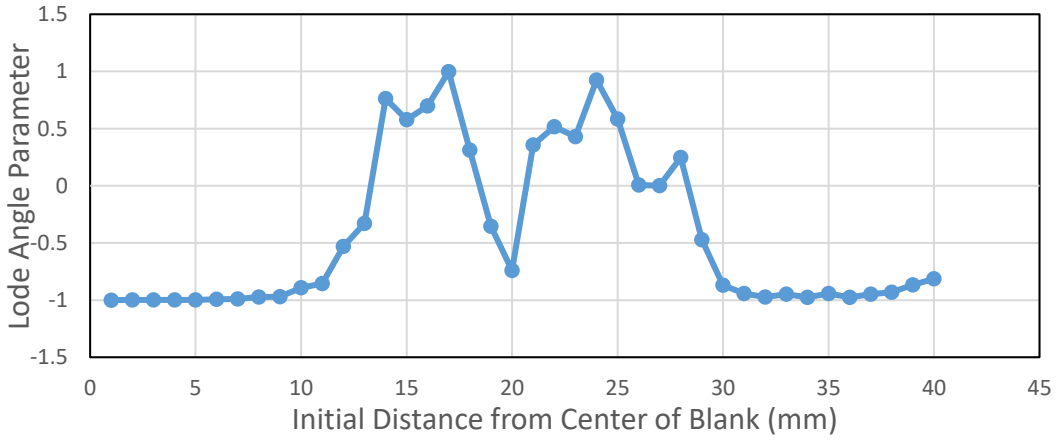

(c)

Figure 5.38. The variation of (a) Equivalent Plastic Strain (b) Stress Triaxiality and (c) Lode Angle Parameter along the rolling direction of the blank at 8 mm cup depth for Al2024 aluminum (VM-JC-JC)

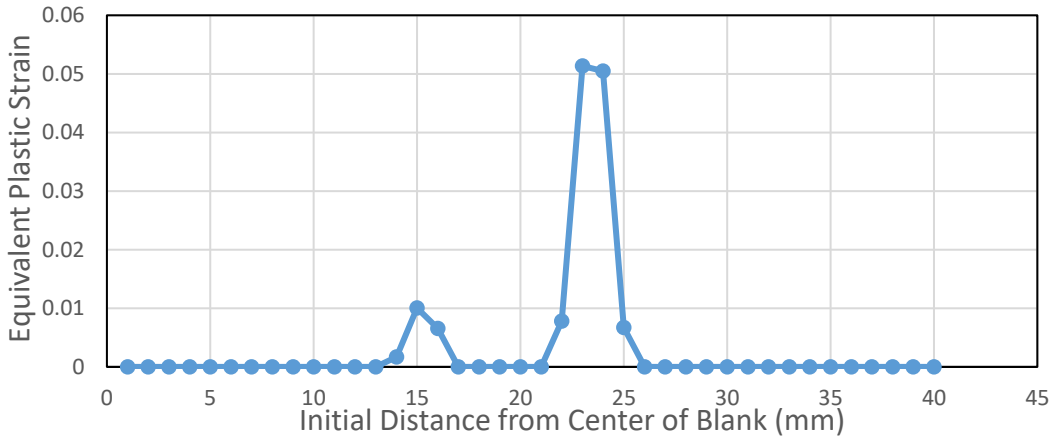

(a)

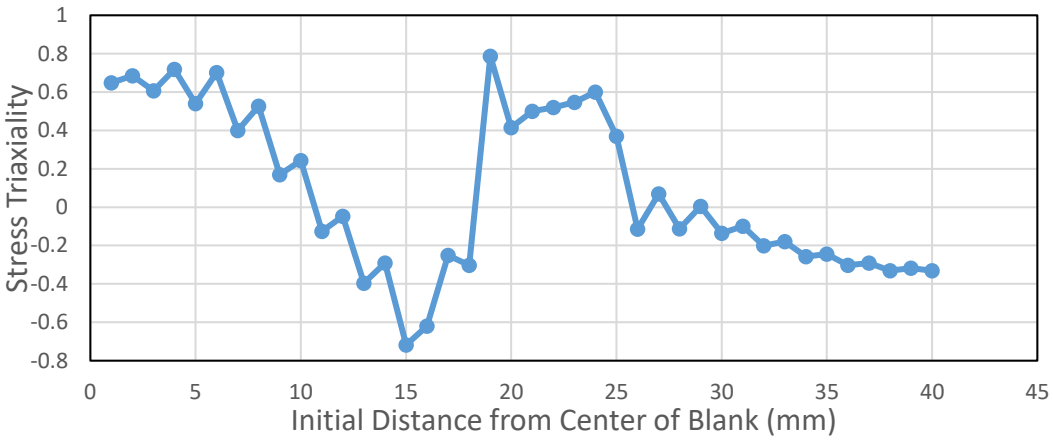

(b)

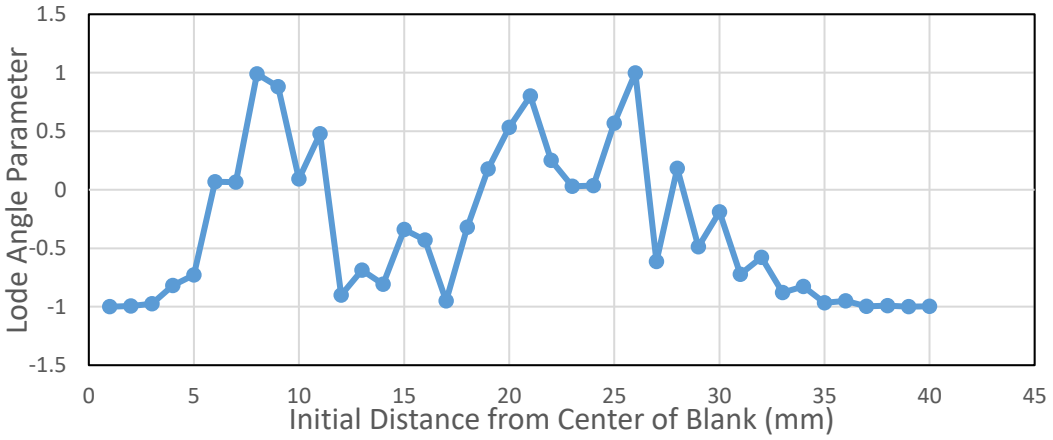

(c)

Figure 5.39. The variation of (a) Equivalent Plastic Strain (b) Stress Triaxiality and (c) Lode Angle Parameter along the transverse direction of the blank at 2 mm cup depth for Al2024 aluminum (VM-JC-JC)

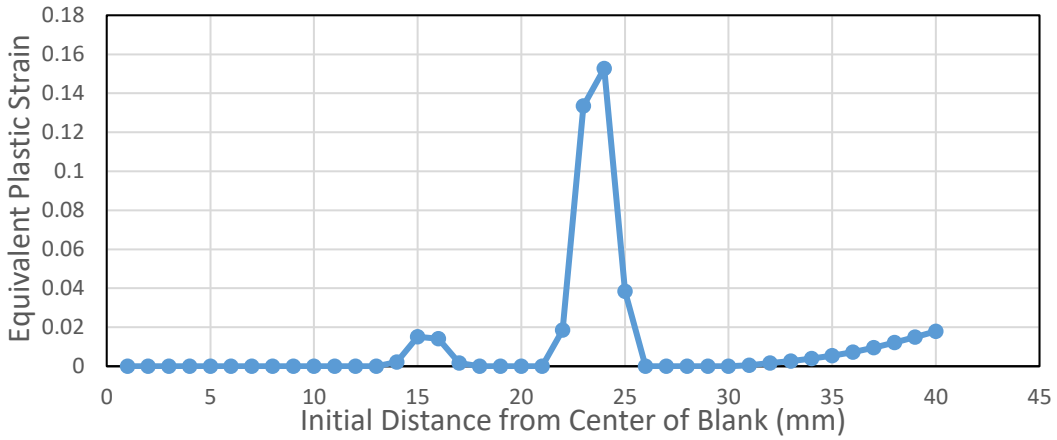

(a)

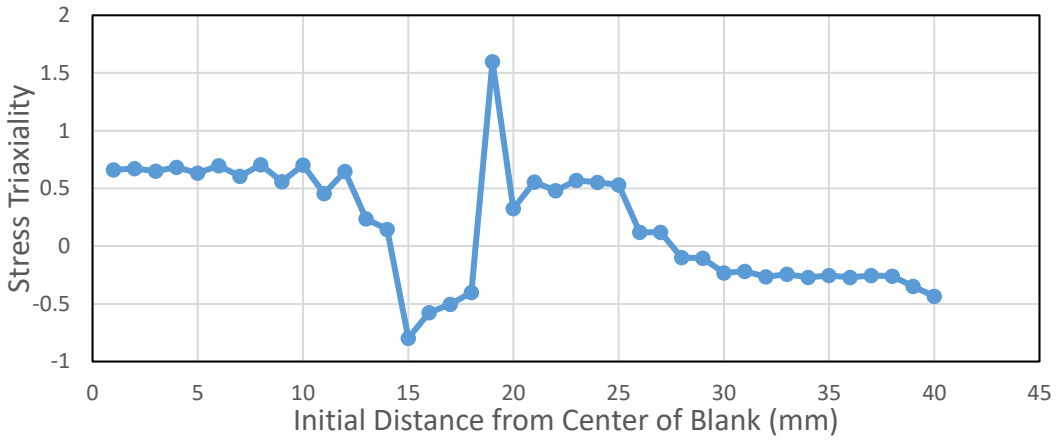

(b)

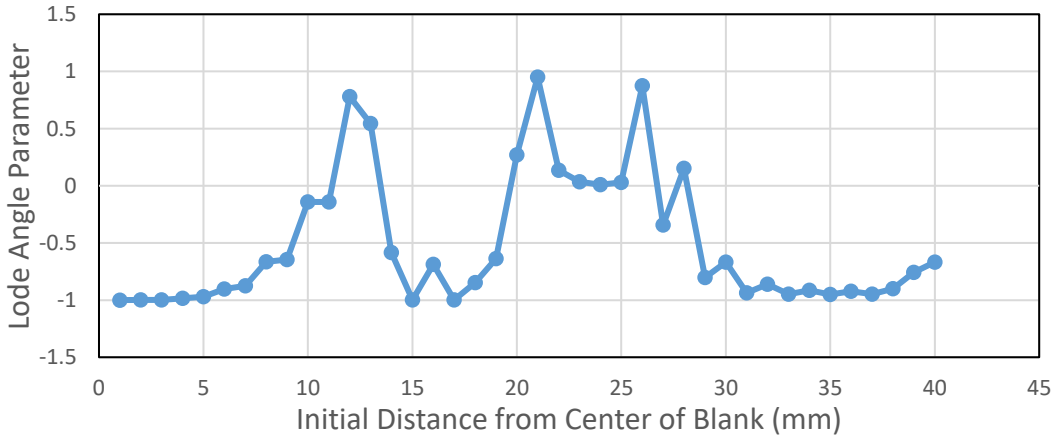

(c)

Figure 5.40. The variation of (a) Equivalent Plastic Strain (b) Stress Triaxiality and (c) Lode Angle Parameter along the transverse direction of the blank at 4 mm cup depth for Al2024 aluminum (VM-JC-JC)

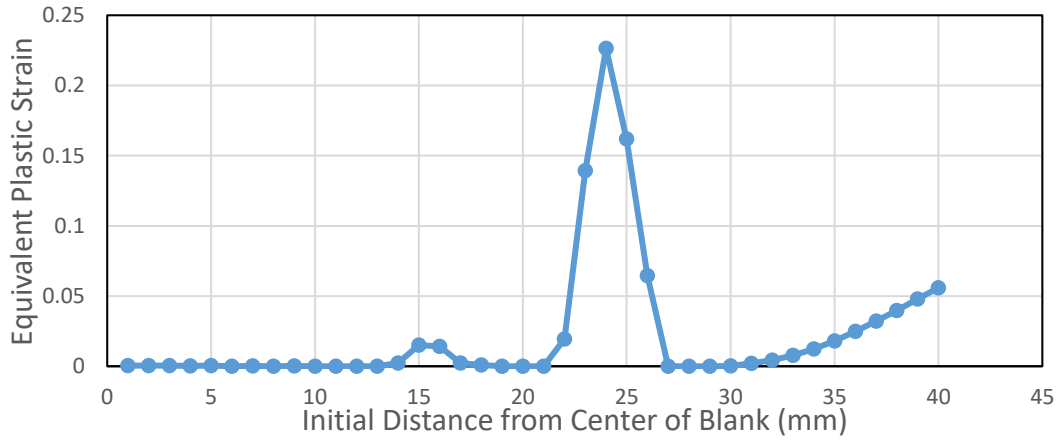

(a)

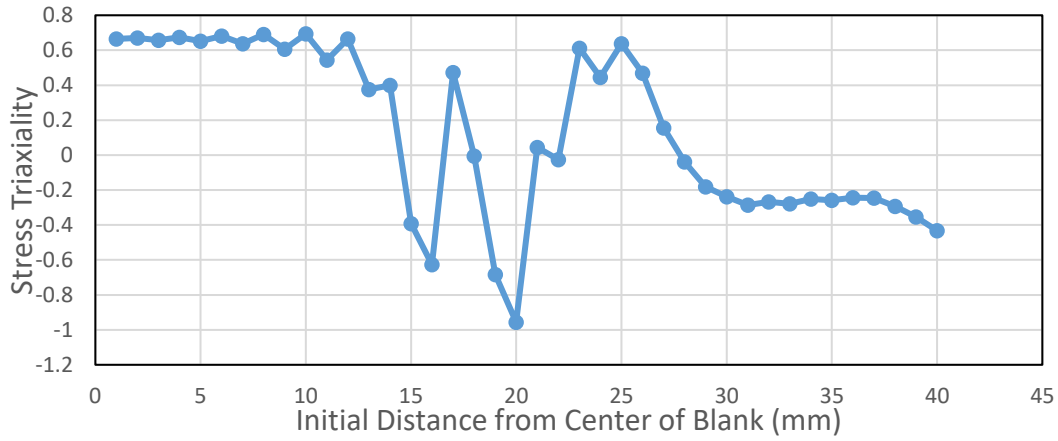

(b)

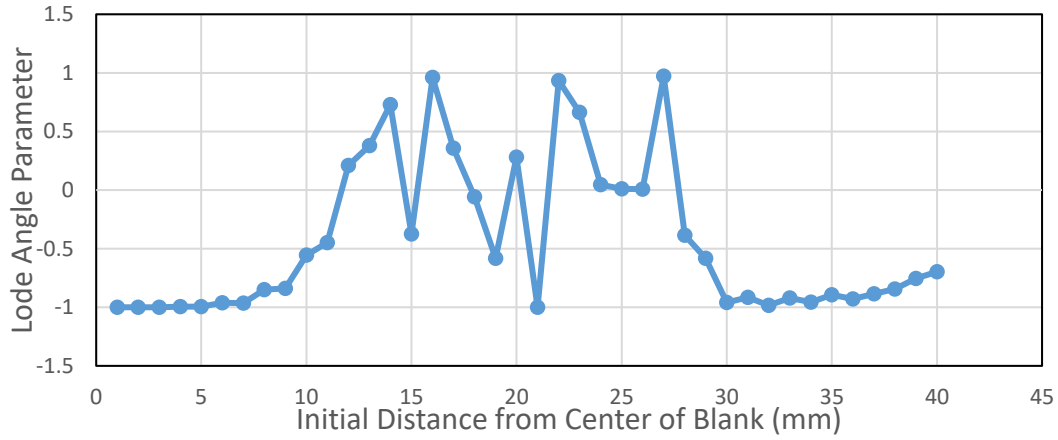

(c)

Figure 5.41. The variation of (a) Equivalent Plastic Strain (b) Stress Triaxiality and (c) Lode Angle Parameter along the transverse direction of the blank at 6 mm cup depth for Al2024 aluminum (VM-JC-JC)

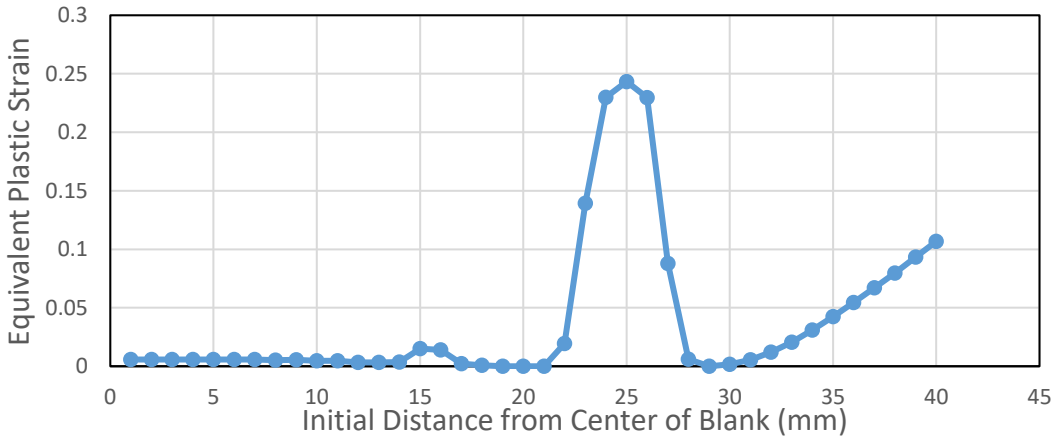

(a)

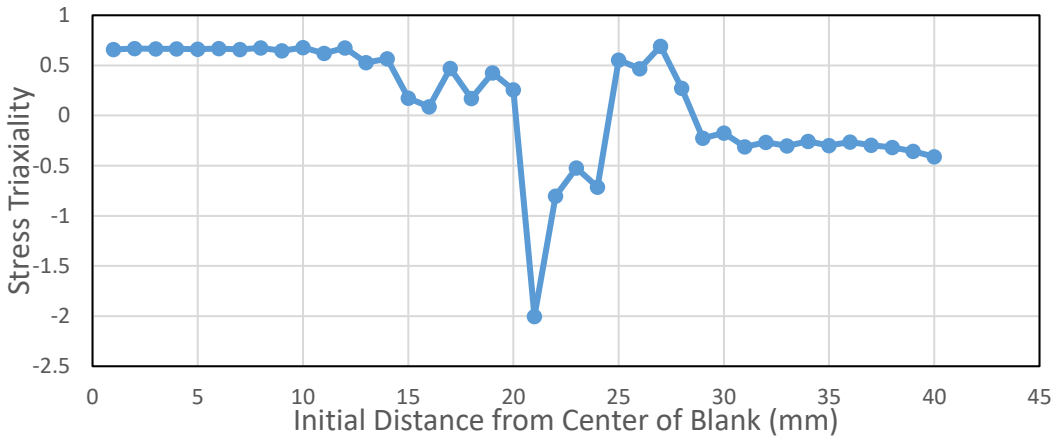

(b)

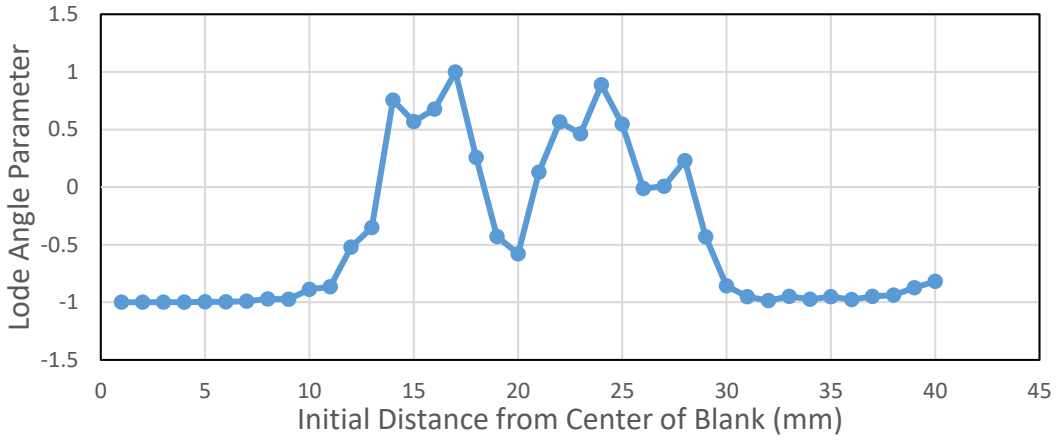

(c)

Figure 5.42. The variation of (a) Equivalent Plastic Strain (b) Stress Triaxiality and (c) Lode Angle Parameter along the transverse direction of the blank at 8 mm cup depth for Al2024 aluminum (VM-JC-JC)

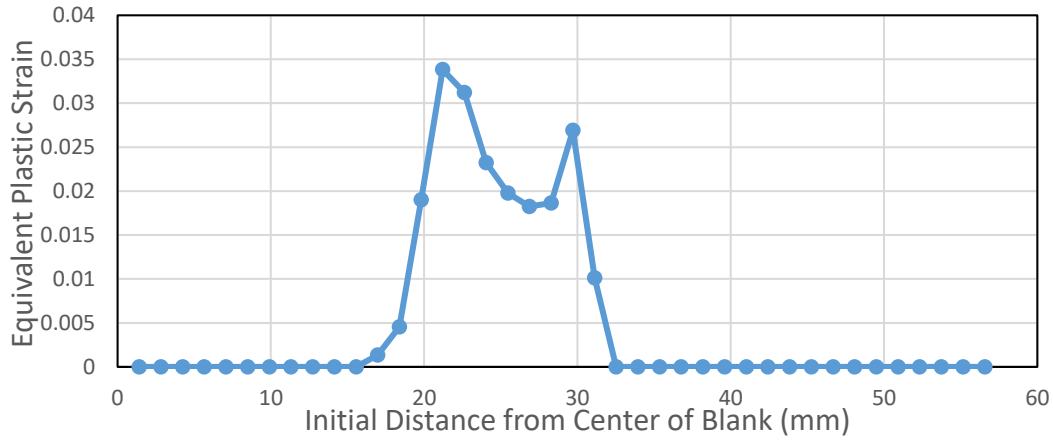

(a)

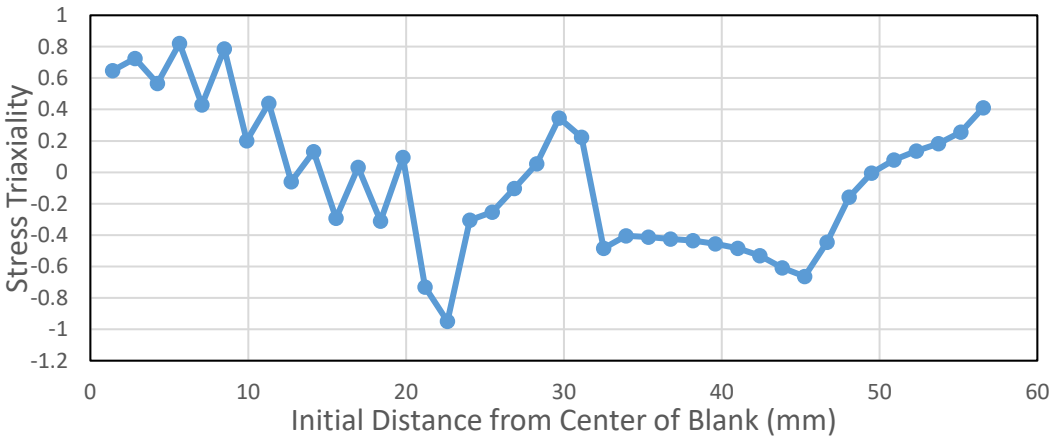

(b)

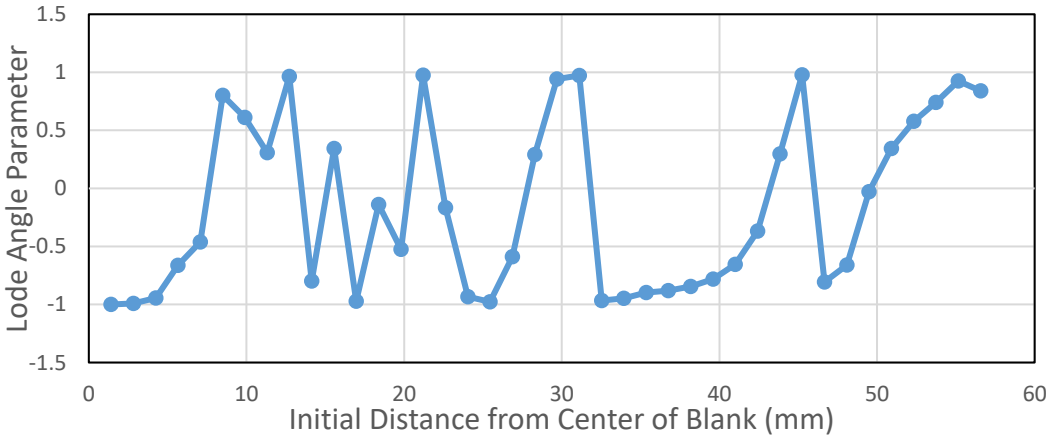

(c)

Figure 5.43. The variation of (a) Equivalent Plastic Strain (b) Stress Triaxiality and (c) Lode Angle Parameter along the diagonal of the blank at 2 mm cup depth for Al2024 aluminum (VM-JC-JC)

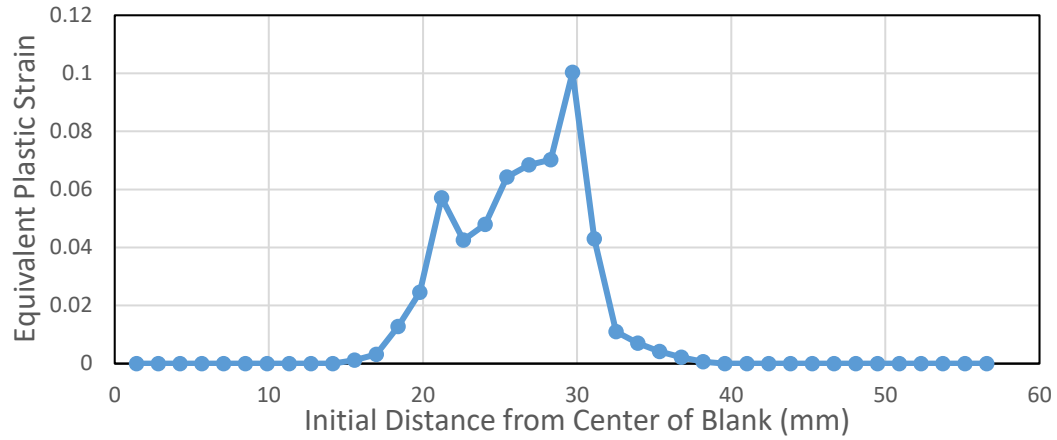

(a)

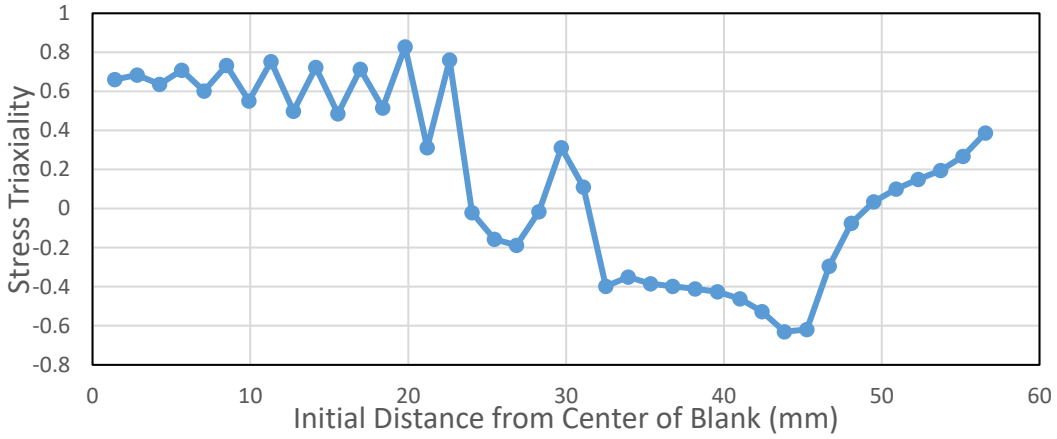

(b)

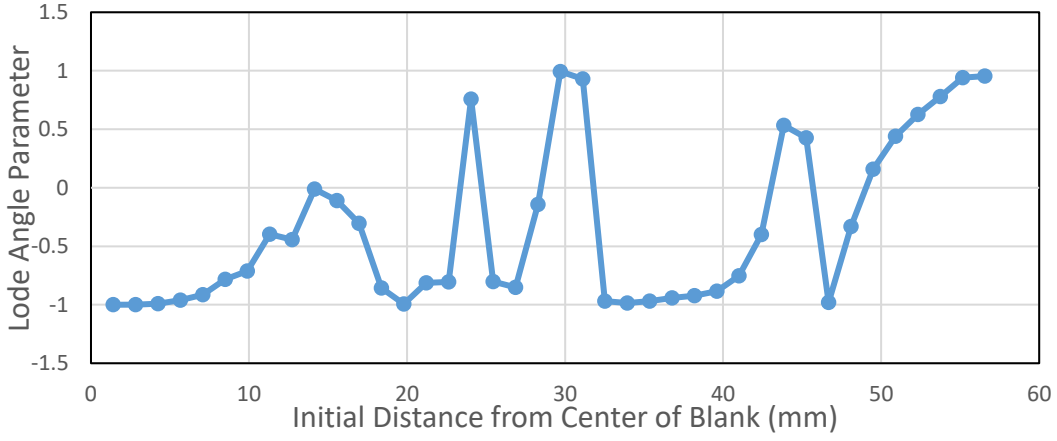

(c)

Figure 5.44. The variation of (a) Equivalent Plastic Strain (b) Stress Triaxiality and (c) Lode Angle Parameter along the diagonal of the blank at 4 mm cup depth for Al2024 aluminum (VM-JC-JC)

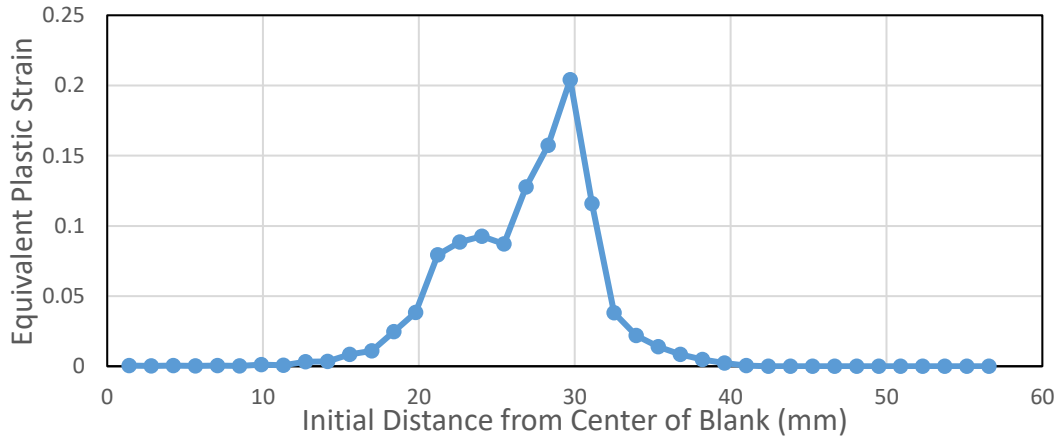

(a)

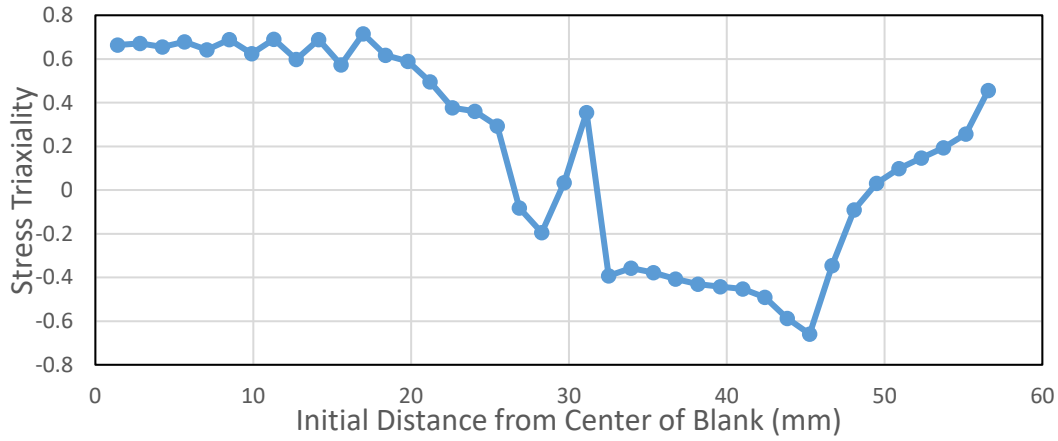

(b)

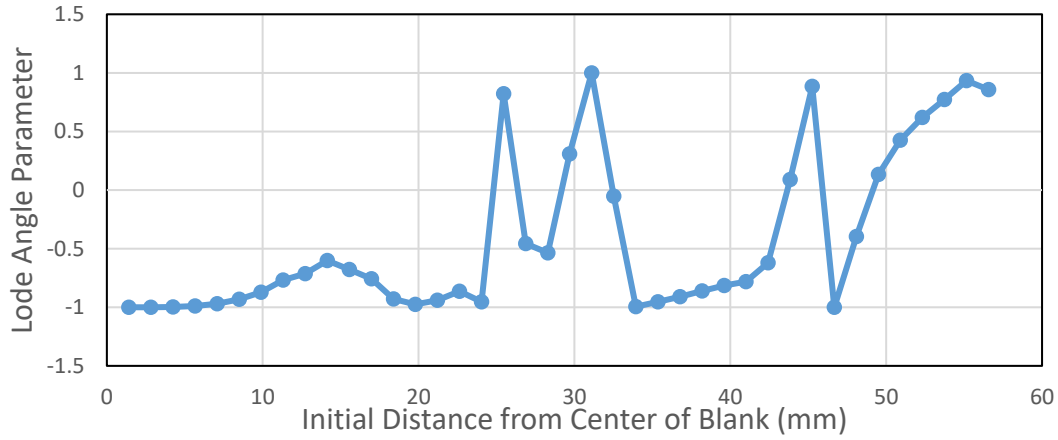

(c)

Figure 5.45. The variation of (a) Equivalent Plastic Strain (b) Stress Triaxiality and (c) Lode Angle Parameter along the diagonal of the blank at 6 mm cup depth for Al2024 aluminum (VM-JC-JC)

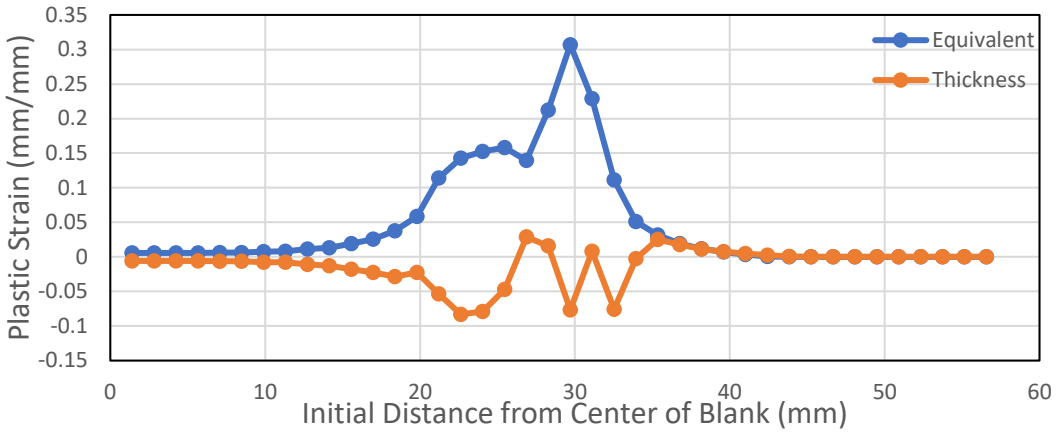

(a)

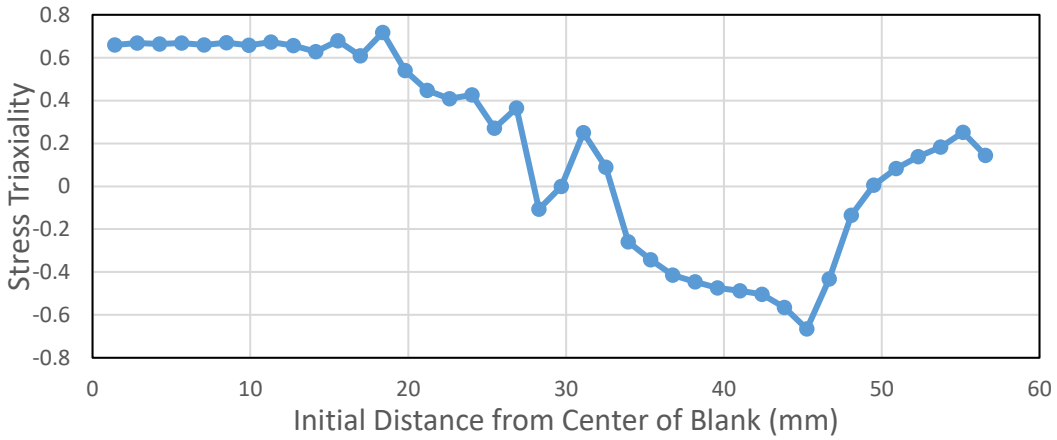

(b)

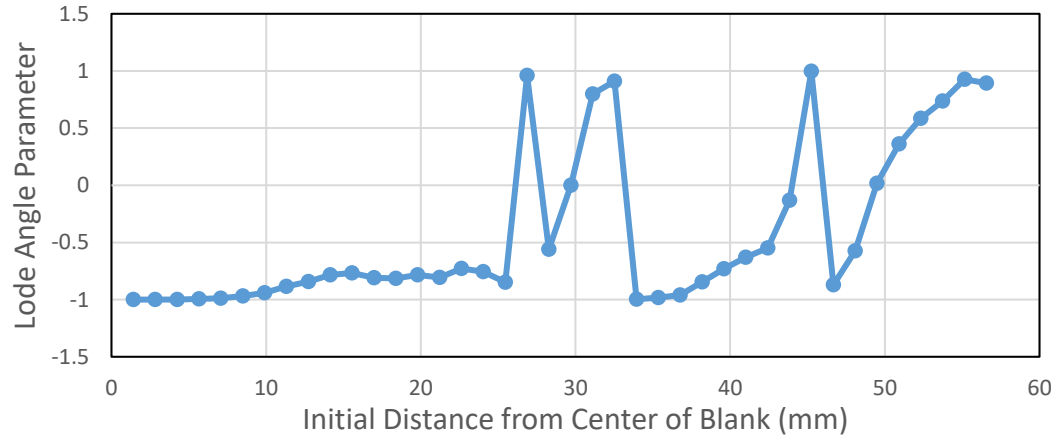

(c)

Figure 5.46. The variation of (a) Equivalent Plastic Strain and Thickness Plastic Strain (b) Stress Triaxiality and (c) Lode Angle Parameter along the diagonal of the blank at 8 mm cup depth for Al2024 aluminum (VM-JC-JC)

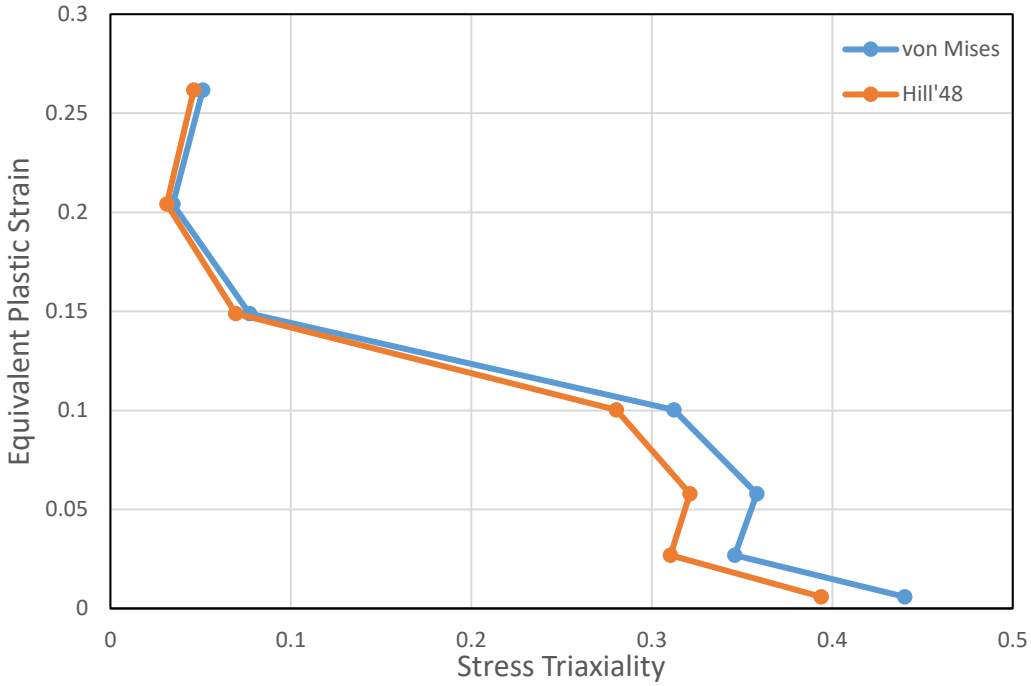

Figure 5.47. Equivalent Plastic Strain - Stress Triaxiality Plot of First Rupture Element (VM-JC-JC)

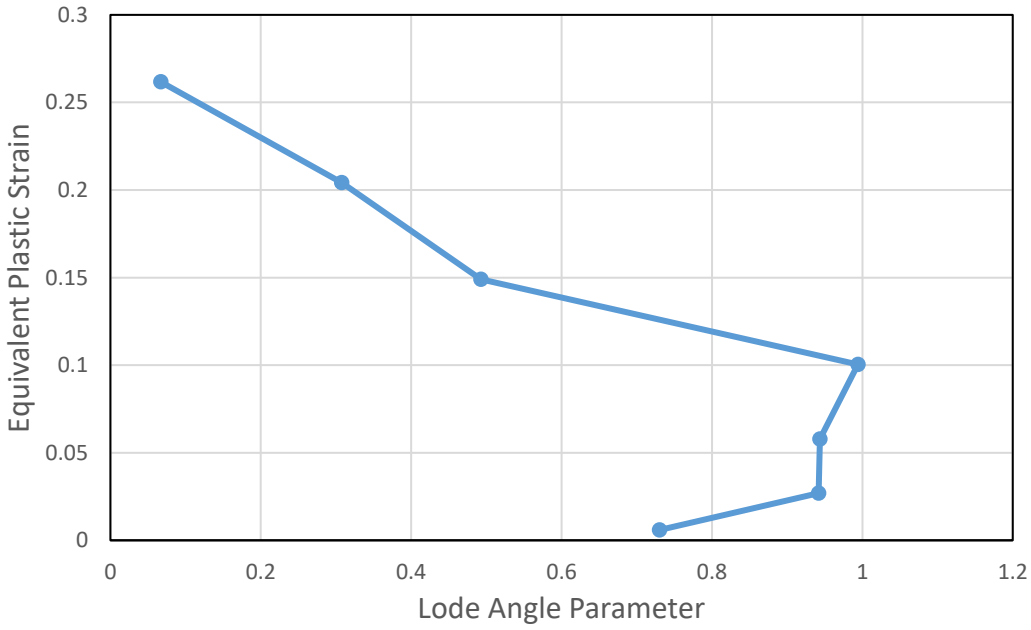

Figure 5.48. Equivalent Plastic Strain – Lode Angle Parameter Plot of First Rupture Element (VM-JC-JC)

In the rolling direction, the triaxiality values vary generally between 0.6 and 0.8 under the punch whereas the Lode angle parameter values change between -0.5 and -1 in the regions close to the center of the blank i.e., up to a distance of 5 mm from the center, the equi-biaxial tension conditions are observed. As the punch continues to move, the region with equi-biaxial tension conditions extend and reaches 10 mm from the center of the blank. When the pre-rupture state of sheet is examined, it is seen that equi-biaxial stress conditions dominates up to 15 mm from the center of the blank. At the punch shoulder triaxiality values are still positive but decreasing as the distance increases from the blank center. On the other hand, the Lode angle parameter values increases as with distance from the center of the blank. Hence, there is a tensile type deformation in this region. At the clearance between die and punch thinning continues. At the die shoulder, the triaxiality values are mostly positive with varying Lode angle parameter values. The deformation nature begins to change towards thickening. Under the blank holder the triaxiality values and Lode angle parameter values are negative, indicating thickening towards the rim.

The same tendency of rolling direction is observed in the transverse direction also. The differences are a result of anisotropy of the material.

In the diagonal direction, equi-biaxial stress condition is observed under the punch as in the transverse and rolling directions. It is observed that as the distance from the center of the blank increases, the stress state of the regions changes from tension to compression. The triaxiality values start to turn negative near the die corner, indicating compressive type deformation based on the Lode angle parameter values. The triaxiality values are negative under the blank holder but increases and become positive, same as negative Lode angle parameter values turn into positive, signify thickening toward the rim, where equi-biaxial dominant compression replaces uniaxial dominant compression as the dominating type of deformation.

5.1.4 Case 4: Square-Al2024-von Mises -Johnson Cook-Hosford Coulomb Model

For the fourth case, von Mises yield criterion was applied with Johnson Cook hardening and the Hosford Coulomb ductile fracture criterion was used. It was observed that the fracture had started after 12 mm punch travel as shown in Figure 5.49. The variation of equivalent plastic strain, stress triaxiality and Lode angle parameter values are presented as a function of the distance from the center of the blank for different cup heights up to the fracture. The results are shown for rolling direction in Figure 5.50 to Figure 5.55, for transverse direction in Figure 5.56 to Figure 5.61 and for diagonal direction in Figure 5.62 to Figure 5.67. The thickness plastic strain distribution is also inserted into Figure 5.67 (a) in order to better visualize the deformation. Further, the variations of stress triaxiality values with respect to equivalent plastic strain are given by considering both von Mises and Hill'48 criteria as a function of the path of the element that fractured first in Figure 5.68. Along the same path, the variation of the Lode parameter with respect to equivalent plastic strain is also illustrated in Figure 5.69. Finally, the variation of triaxiality values with respect to Lode angle parameter values are given in Figure 5.70 to Figure 5.72 for rolling direction in Figure 5.70, for transverse direction Figure 5.71 and, in Figure 5.72 for diagonal direction. The variations are first given for the whole deformation and then for punch, punch shoulder or corner, the clearance between die and punch, punch shoulder or corner and for the blank holder regions.

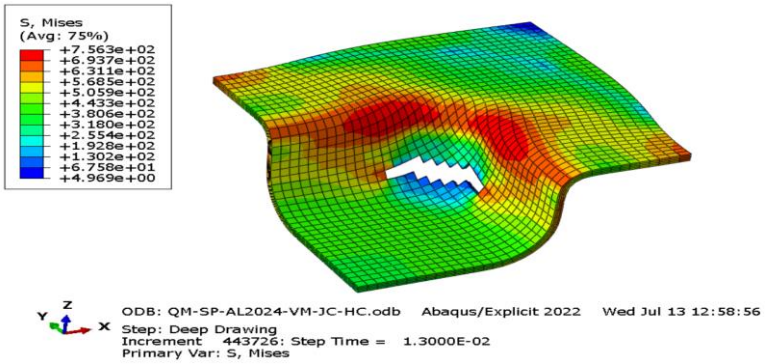

Figure 5.49. First Rupture Moment of Case 4

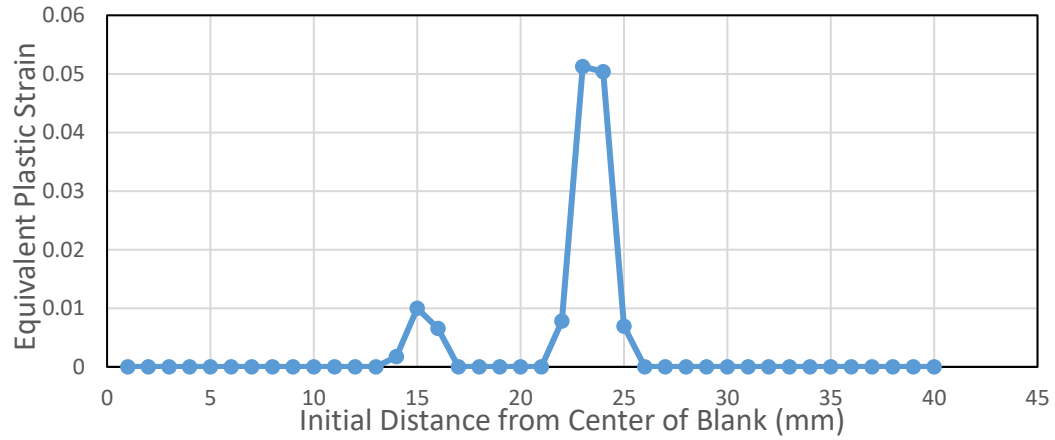

(a)

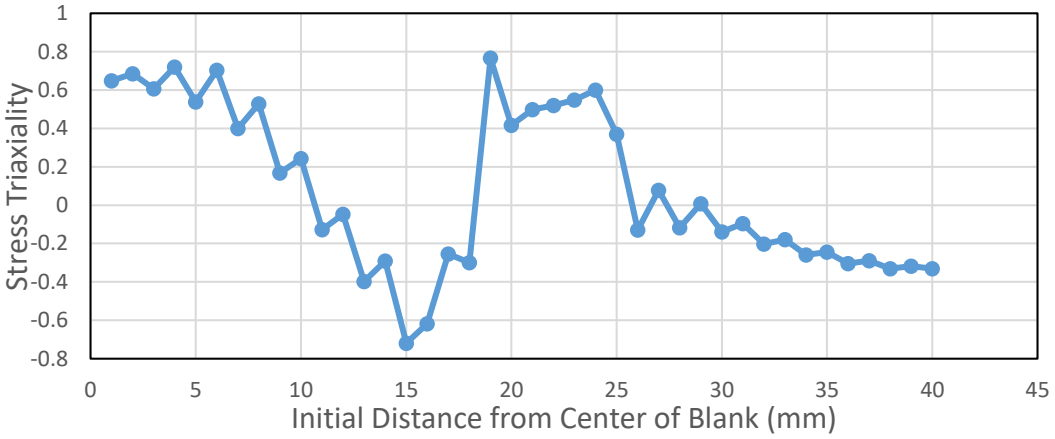

(b)

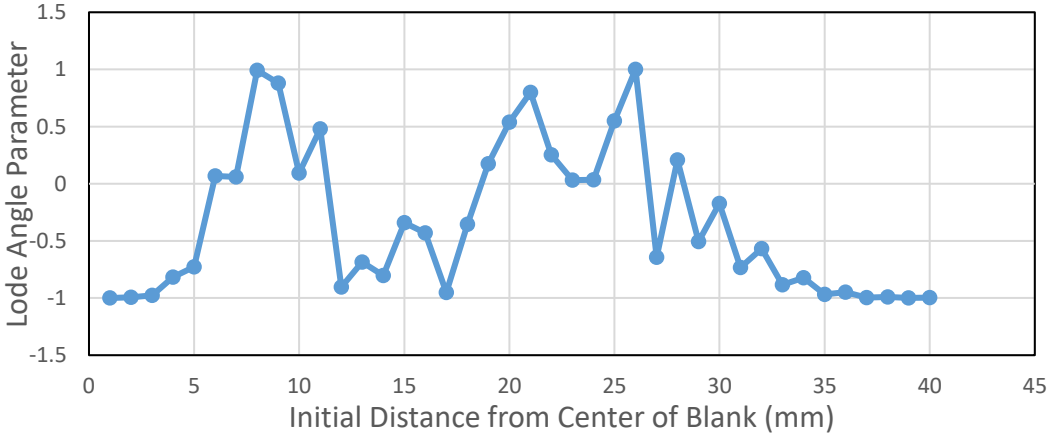

(c)

Figure 5.50. The variation of (a) Equivalent Plastic Strain (b) Stress Triaxiality and (c) Lode Angle Parameter along the rolling direction of the blank at 2 mm cup depth for Al2024 aluminum (VM-JC-HC)

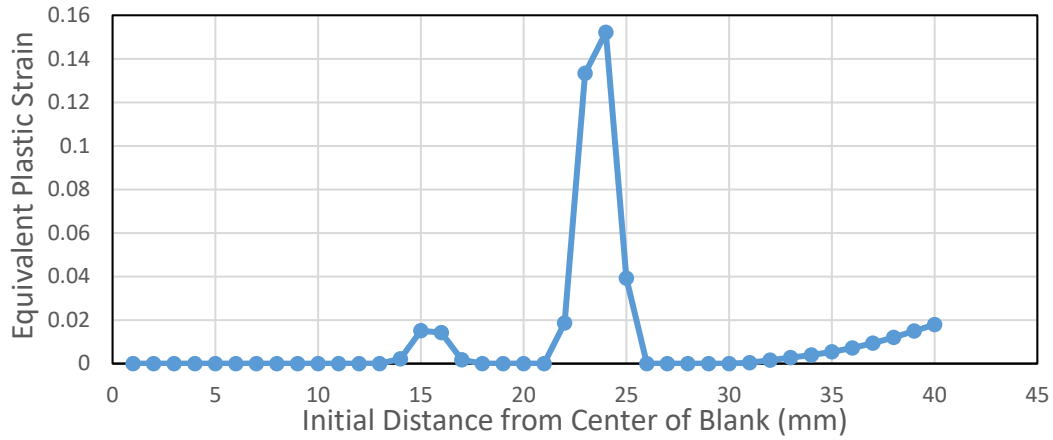

(a)

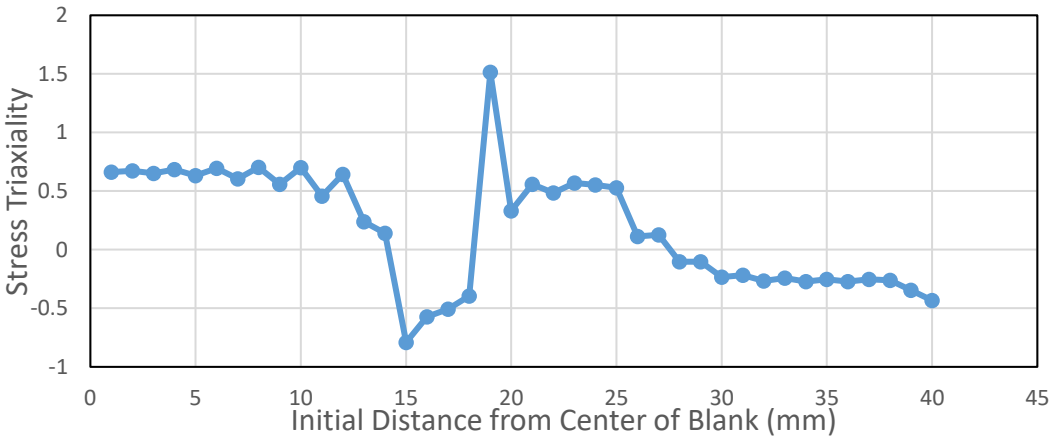

(b)

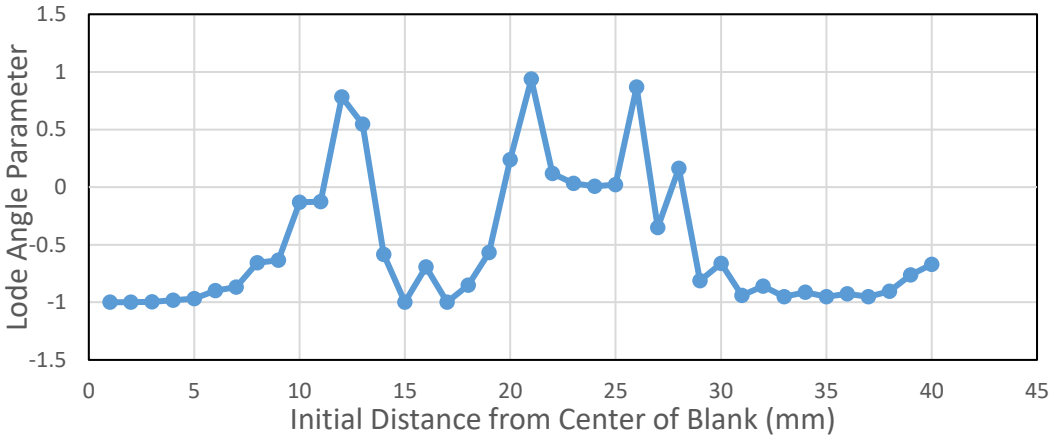

(c)

Figure 5.51. The variation of (a) Equivalent Plastic Strain (b) Stress Triaxiality and (c) Lode Angle Parameter along the rolling direction of the blank at 4 mm cup depth for Al2024 aluminum (VM-JC-HC)

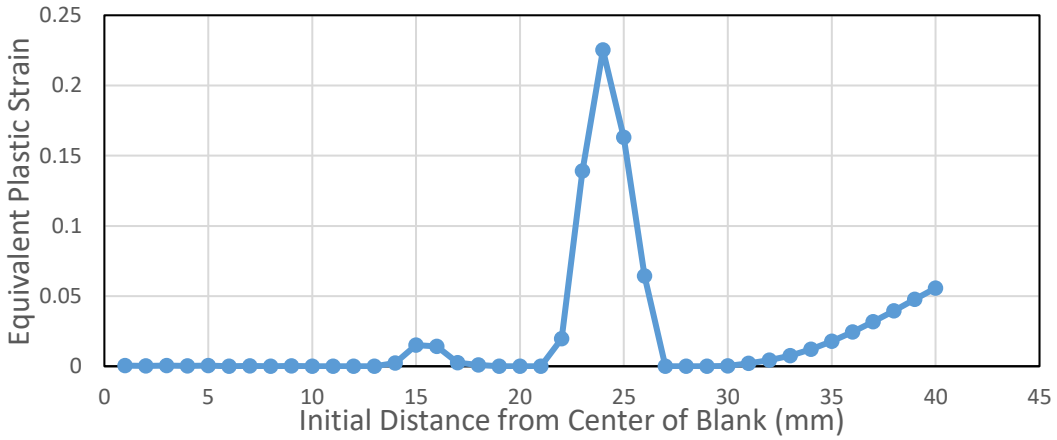

(a)

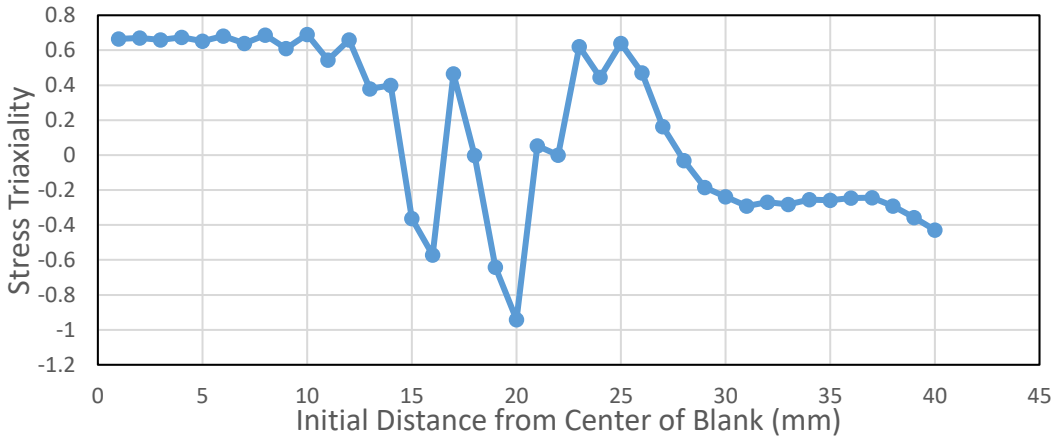

(b)

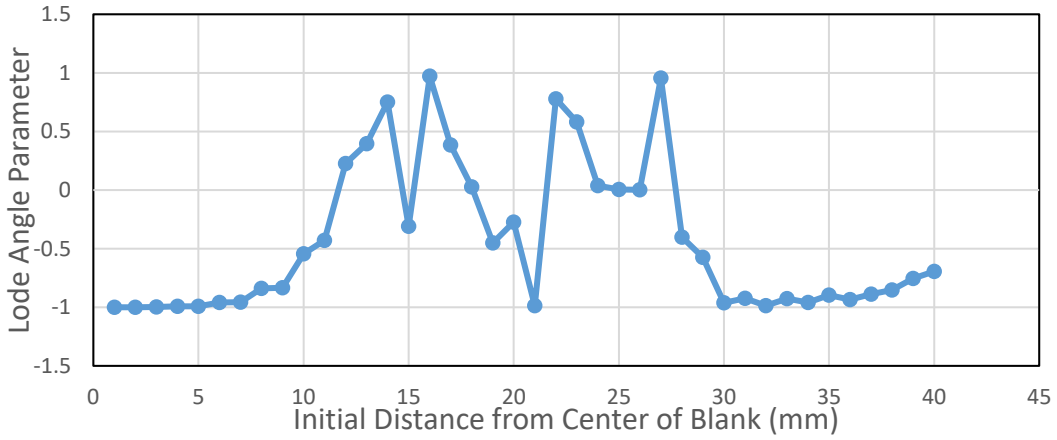

(c)

Figure 5.52. The variation of (a) Equivalent Plastic Strain (b) Stress Triaxiality and (c) Lode Angle Parameter along the rolling direction of the blank at 6 mm cup depth for Al2024 aluminum (VM-JC-HC)

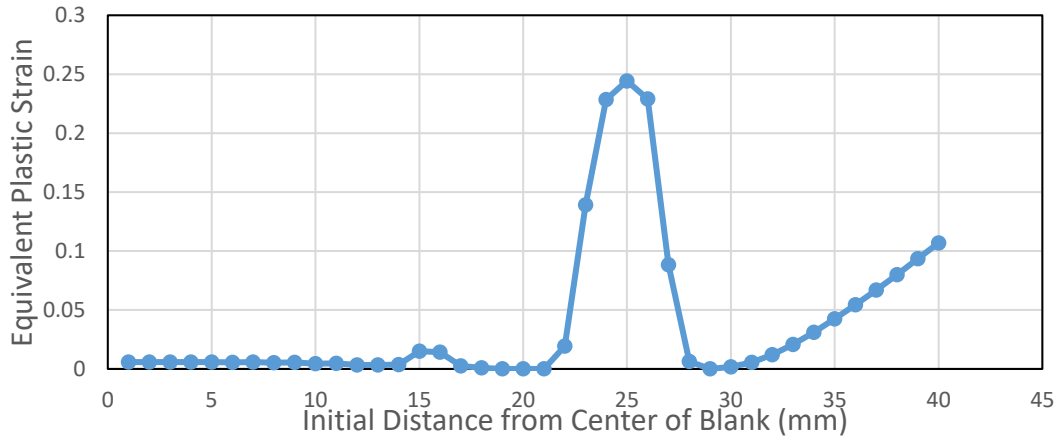

(a)

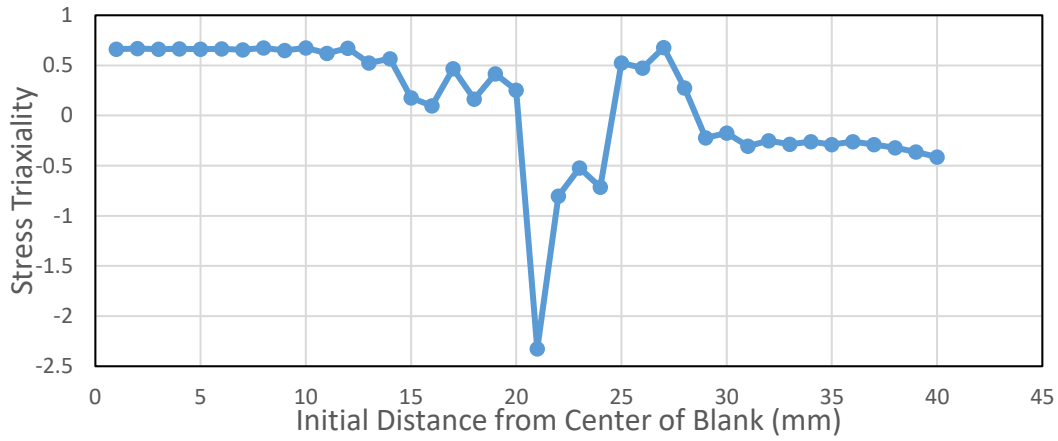

(b)

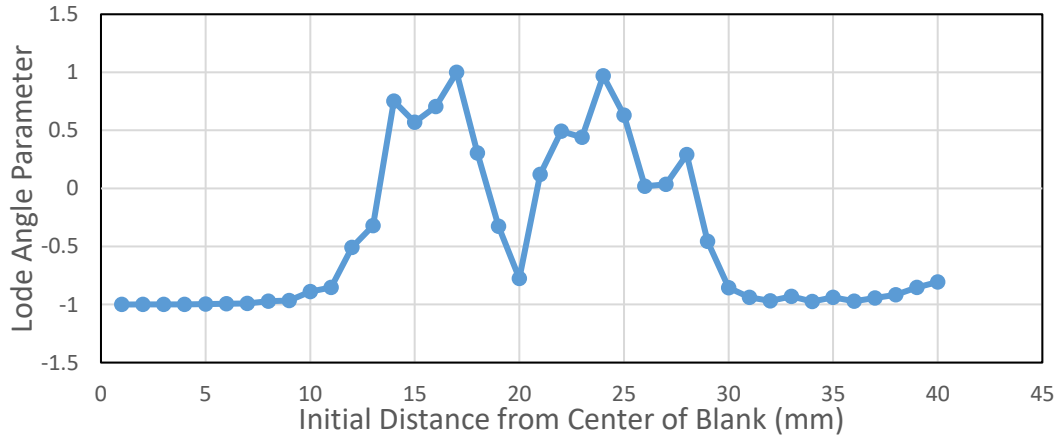

(c)

Figure 5.53. The variation of (a) Equivalent Plastic Strain (b) Stress Triaxiality and (c) Lode Angle Parameter along the rolling direction of the blank at 8 mm cup depth for Al2024 aluminum (VM-JC-HC)

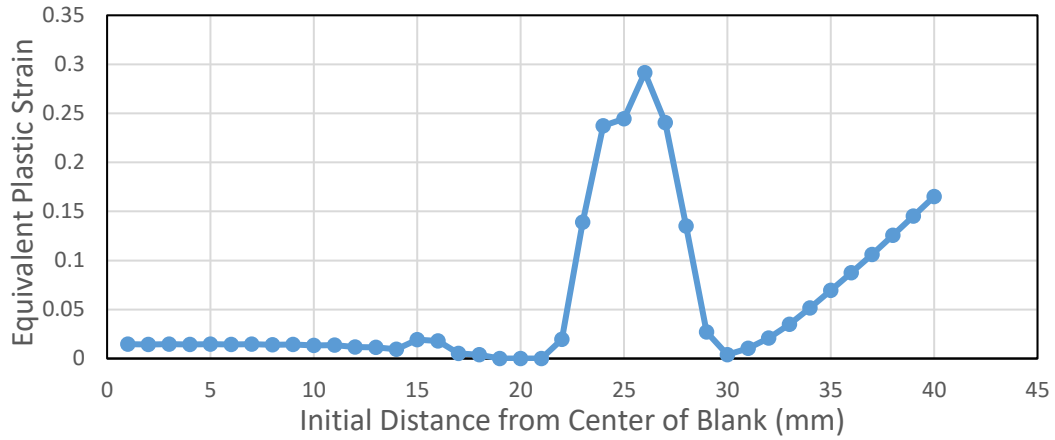

(a)

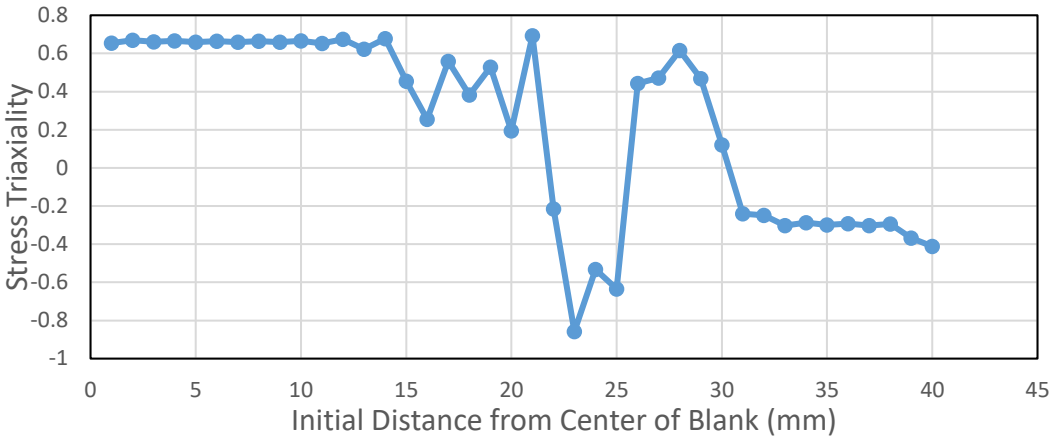

(b)

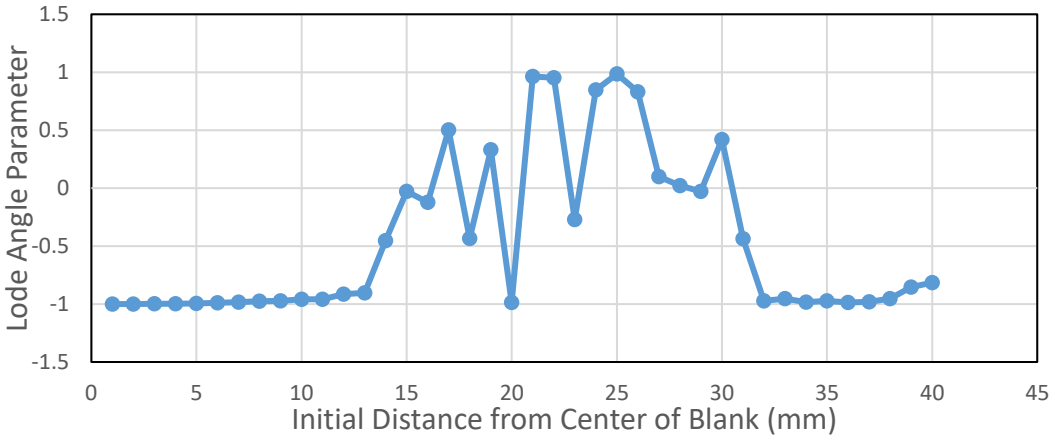

(c)

Figure 5.54. The variation of (a) Equivalent Plastic Strain (b) Stress Triaxiality and (c) Lode Angle Parameter along the rolling direction of the blank at 10 mm cup depth for Al2024 aluminum (VM-JC-HC)

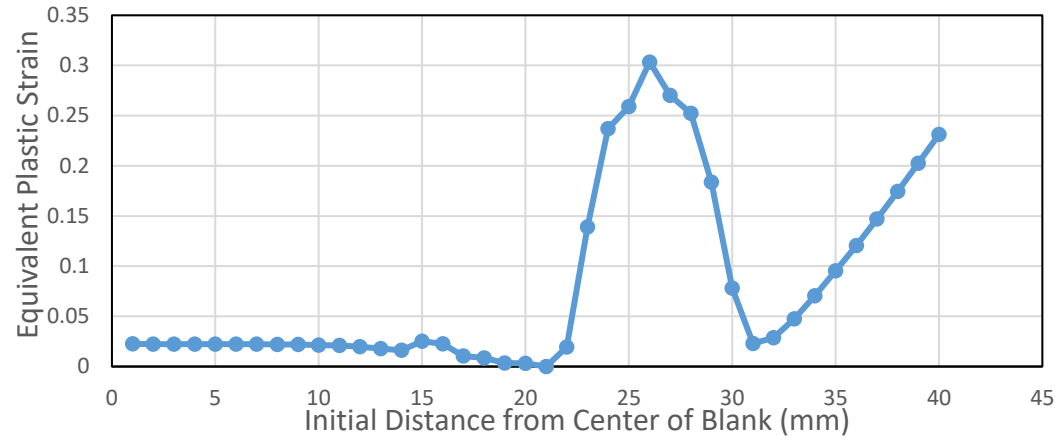

(a)

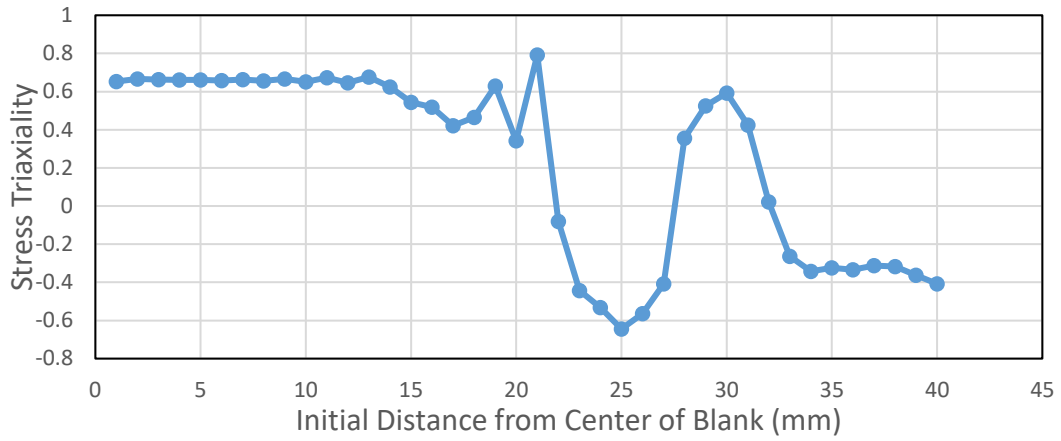

(b)

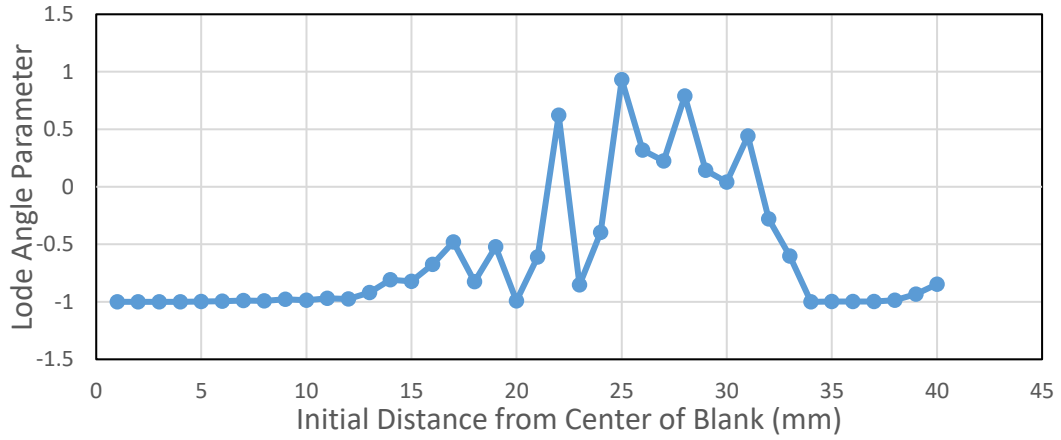

(c)

Figure 5.55 The variation of (a) Equivalent Plastic Strain (b) Stress Triaxiality and (c) Lode Angle Parameter along the rolling direction of the blank at 12 mm cup depth for Al2024 aluminum (VM-JC-HC)

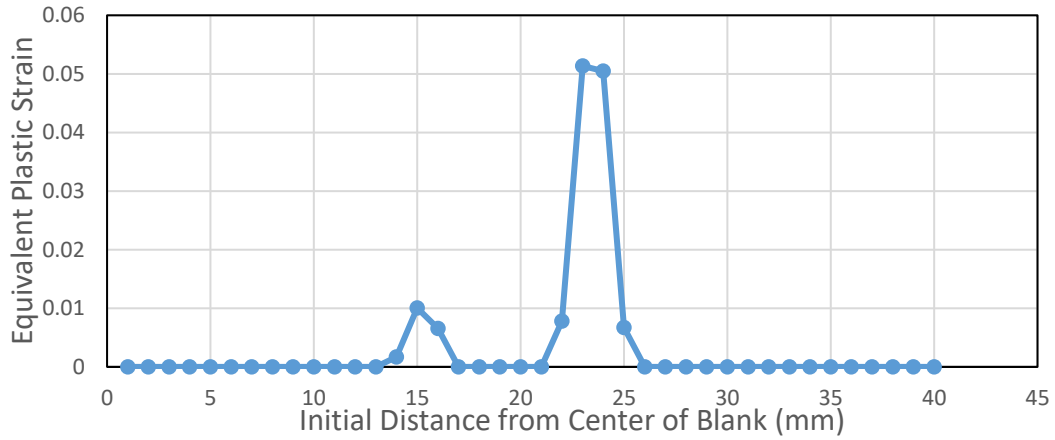

(a)

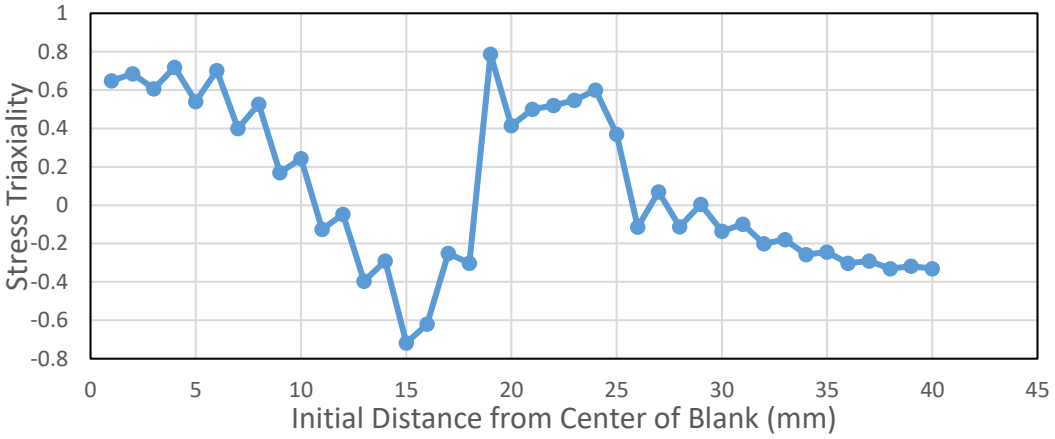

(b)

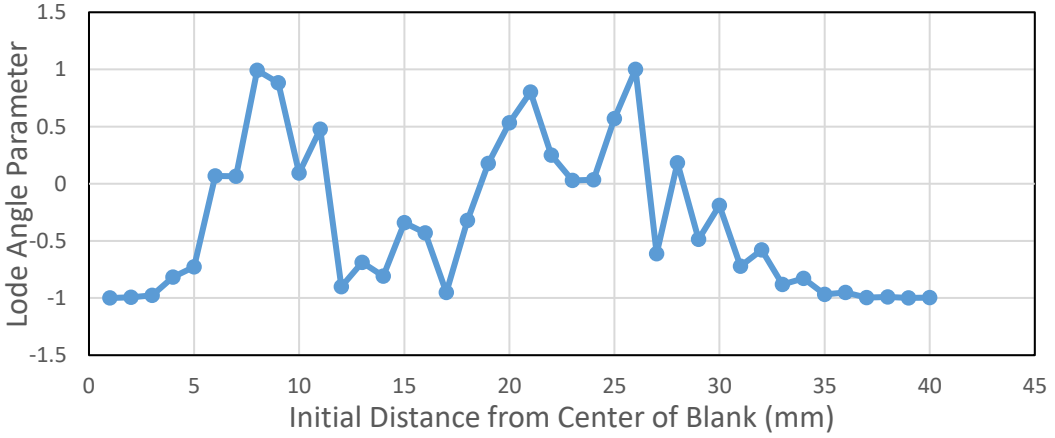

(c)

Figure 5.56. The variation of (a) Equivalent Plastic Strain (b) Stress Triaxiality and (c) Lode Angle Parameter along the transverse direction of the blank at 2 mm cup depth for Al2024 aluminum (VM-JC-HC)

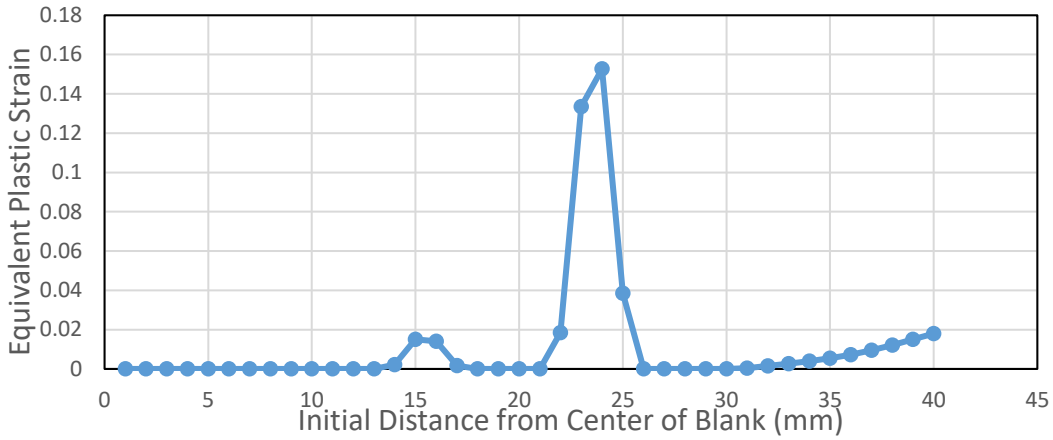

(a)

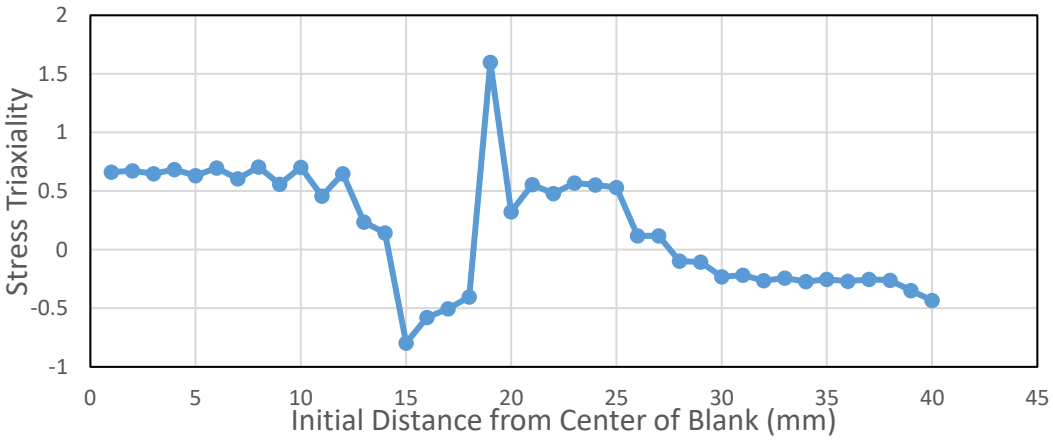

(b)

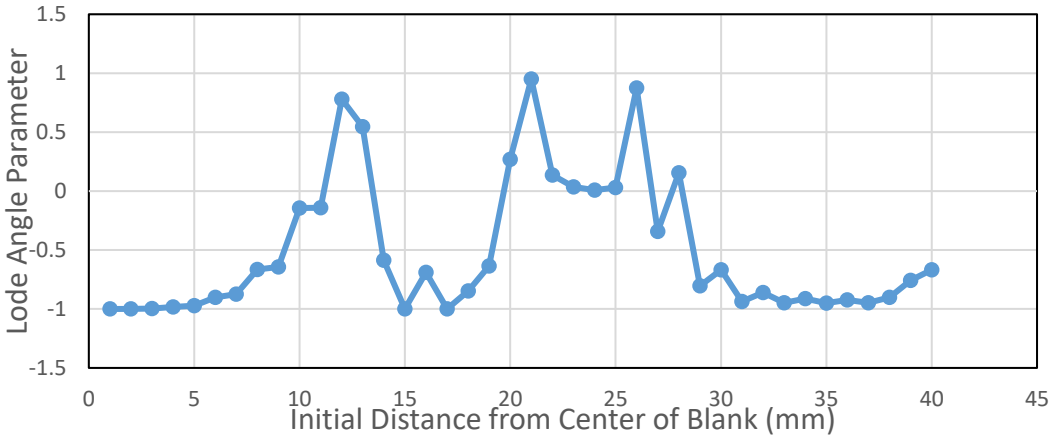

(c)

Figure 5.57. The variation of (a) Equivalent Plastic Strain (b) Stress Triaxiality and (c) Lode Angle Parameter along the transverse direction of the blank at 4 mm cup depth for Al2024 aluminum (VM-JC-HC)

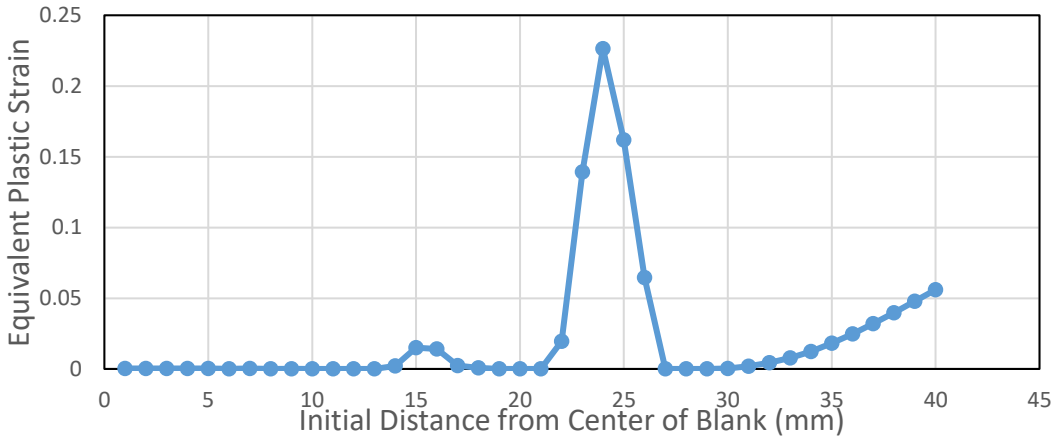

(a)

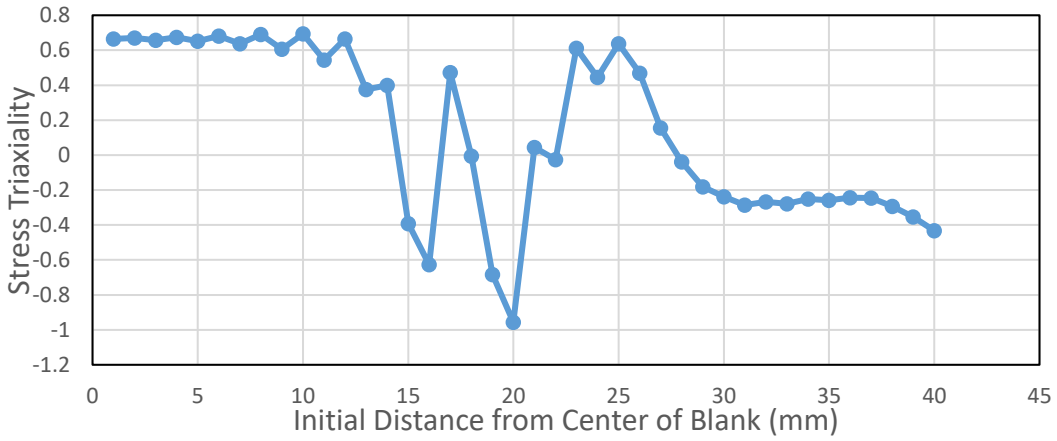

(b)

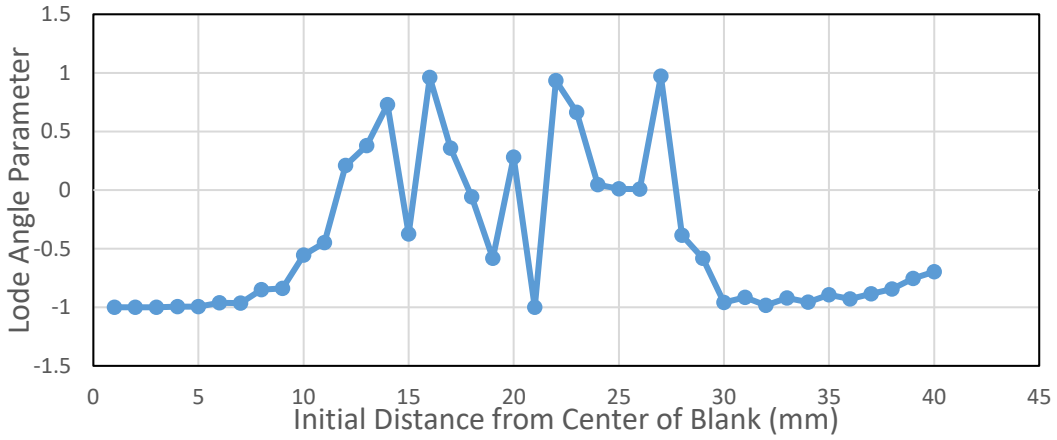

(c)

Figure 5.58. The variation of (a) Equivalent Plastic Strain (b) Stress Triaxiality and (c) Lode Angle Parameter along the transverse direction of the blank at 6 mm cup depth for Al2024 aluminum (VM-JC-HC)

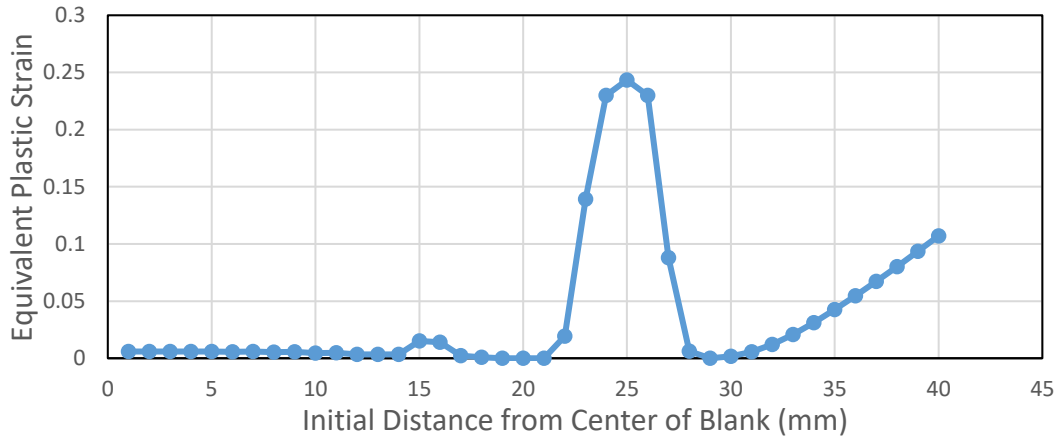

(a)

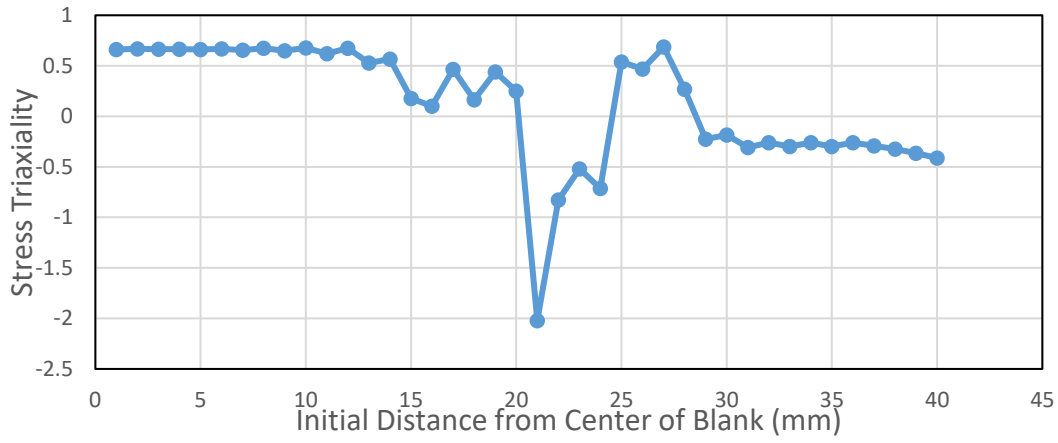

(b)

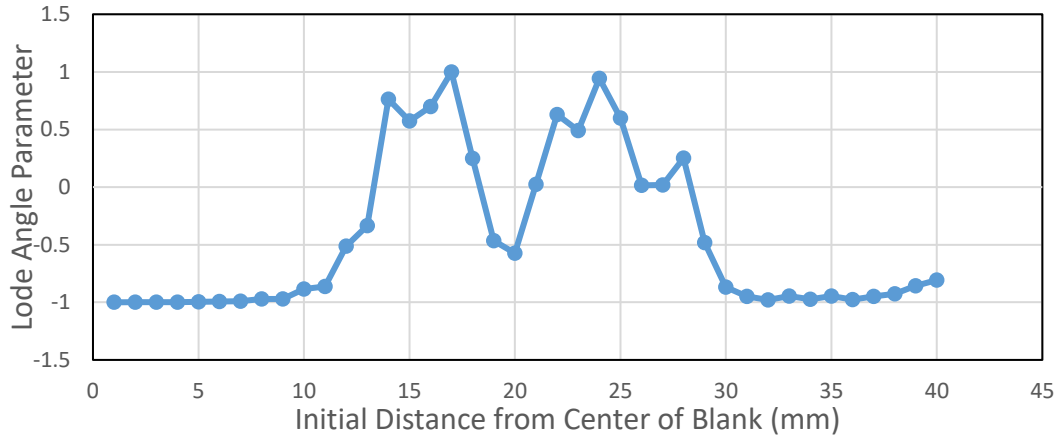

(c)

Figure 5.59. The variation of (a) Equivalent Plastic Strain (b) Stress Triaxiality and (c) Lode Angle Parameter along the transverse direction of the blank at 8 mm cup depth for Al2024 aluminum (VM-JC-HC)

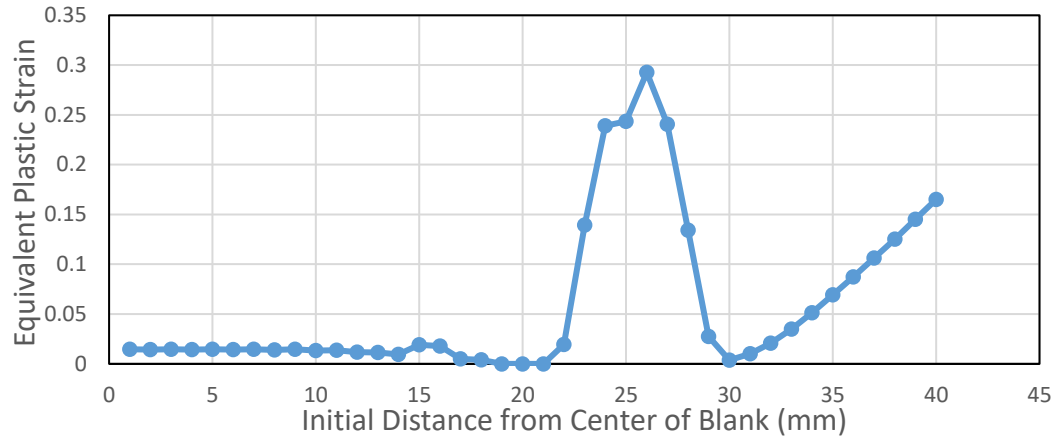

(a)

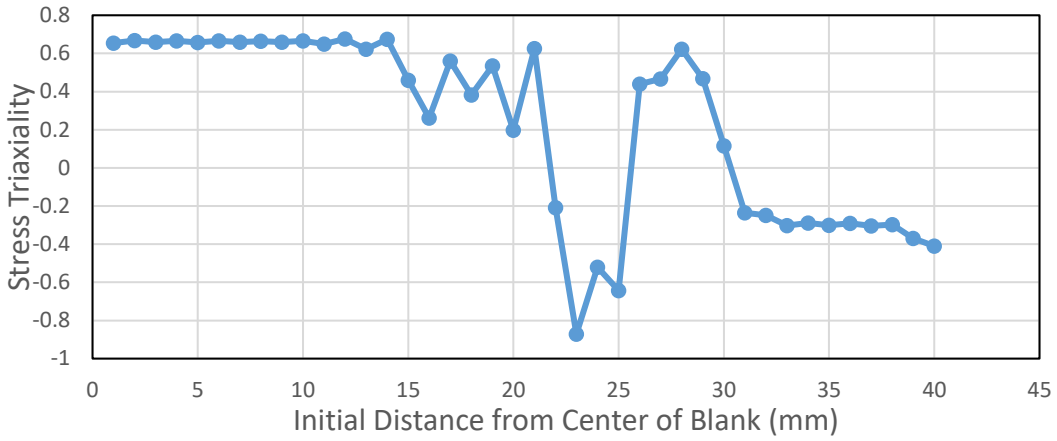

(b)

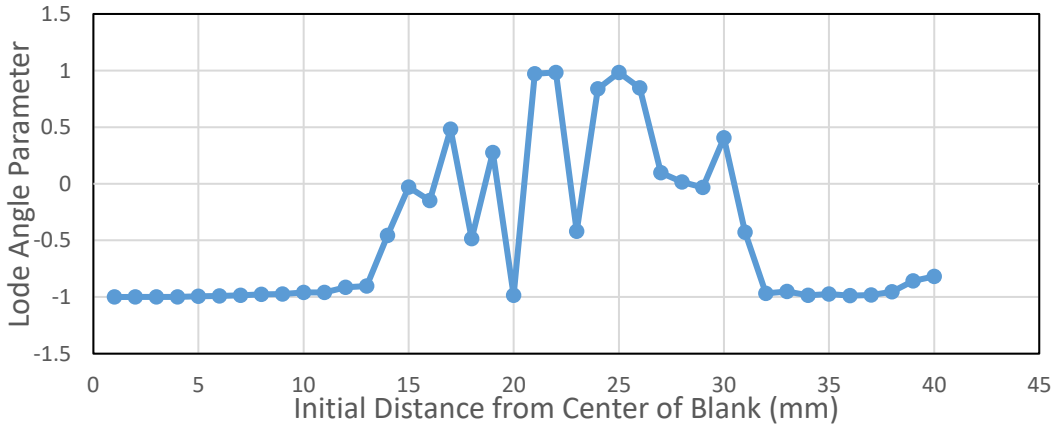

(c)

Figure 5.60. The variation of (a) Equivalent Plastic Strain (b) Stress Triaxiality and (c) Lode Angle Parameter along the transverse direction of the blank at 10 mm cup depth for Al2024 aluminum (VM-JC-HC)

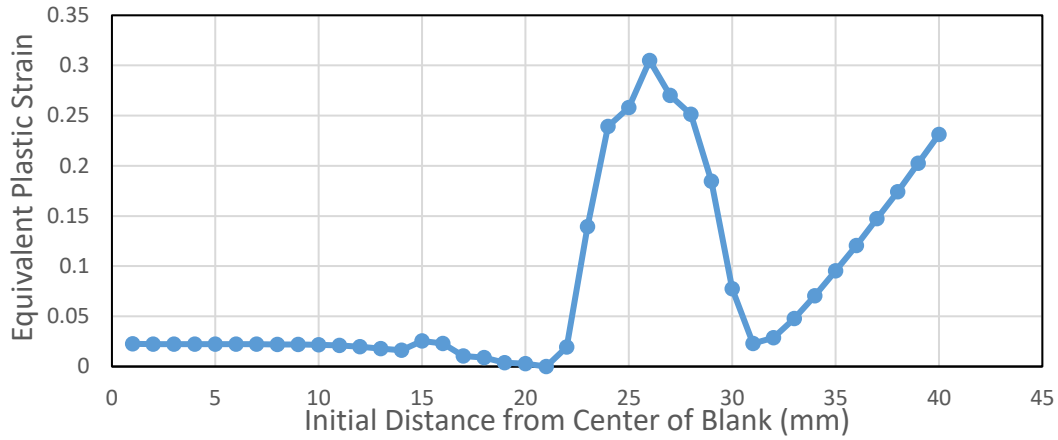

(a)

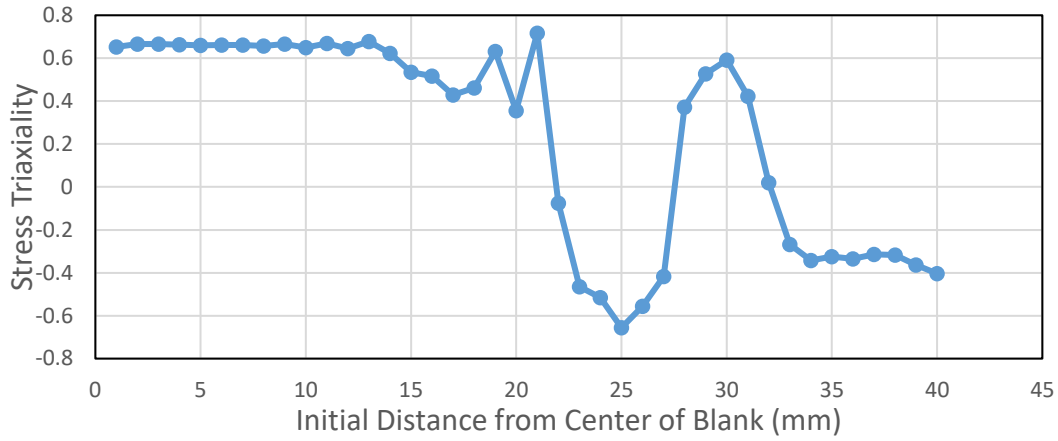

(b)

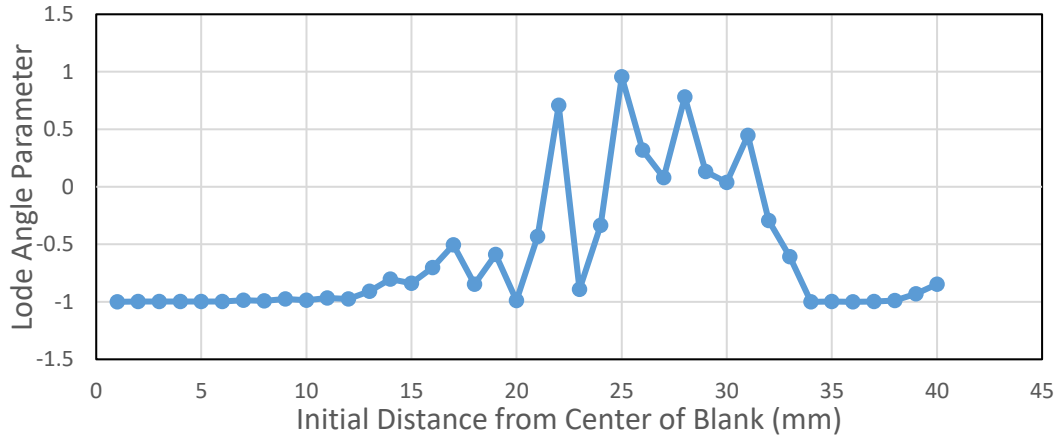

(c)

Figure 5.61. The variation of (a) Equivalent Plastic Strain (b) Stress Triaxiality and (c) Lode Angle Parameter along the transverse direction of the blank at 12 mm cup depth for Al2024 aluminum (VM-JC-HC)

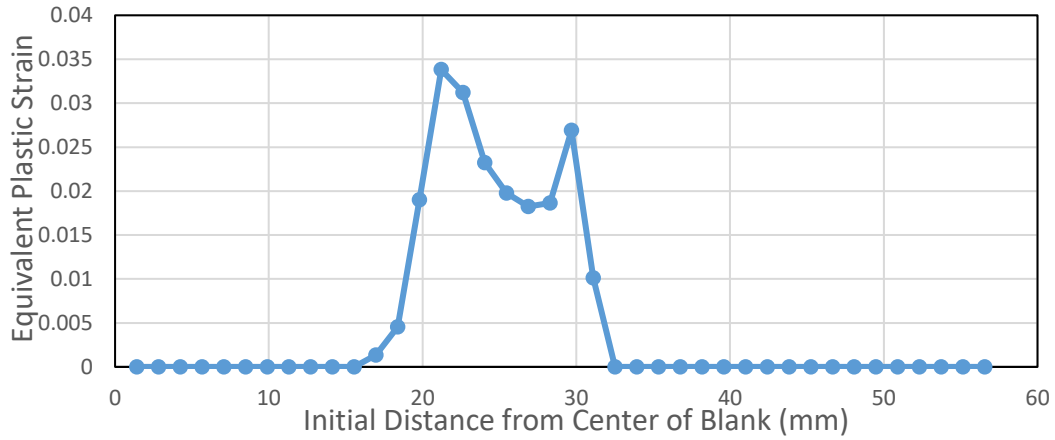

(a)

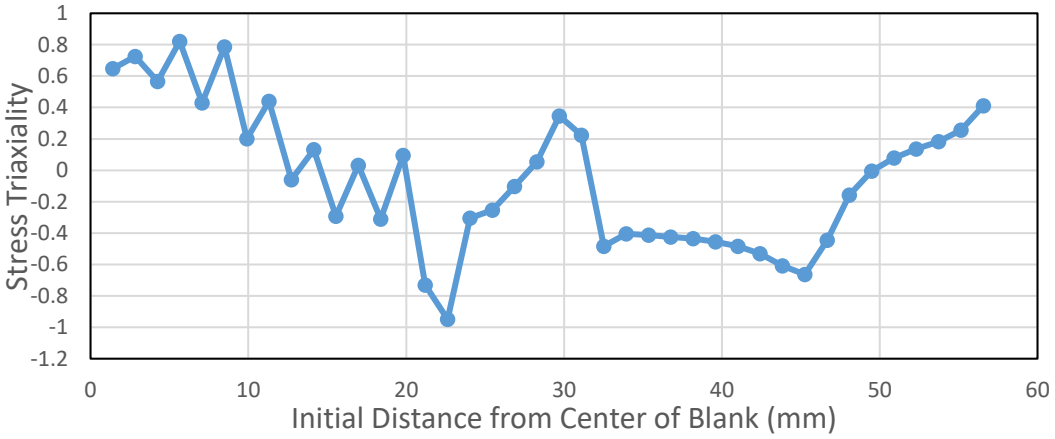

(b)

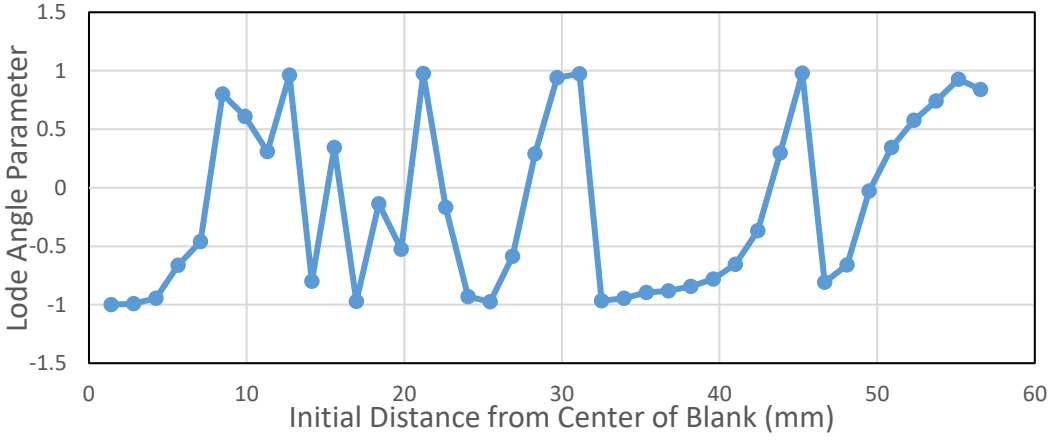

(c)

Figure 5.62. The variation of (a) Equivalent Plastic Strain (b) Stress Triaxiality and (c) Lode Angle Parameter along the diagonal of the blank at 2 mm cup depth for Al2024 aluminum (VM-JC-HC)

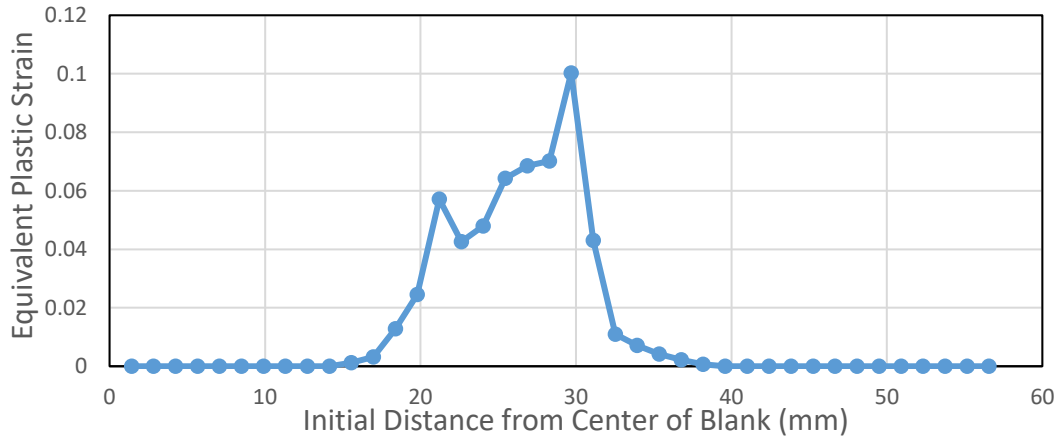

(a)

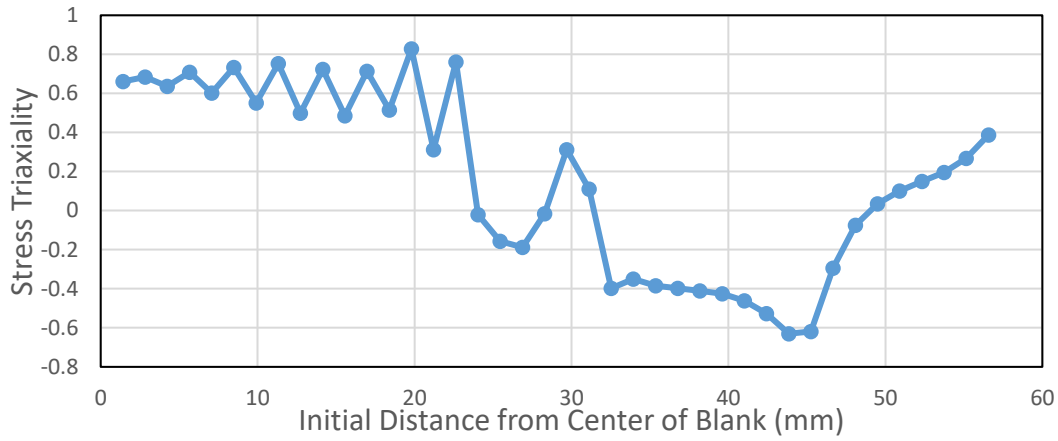

(b)

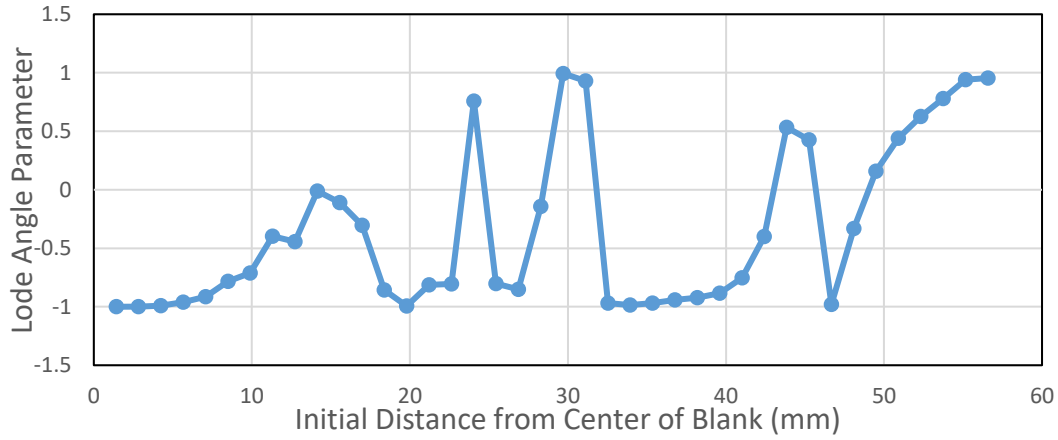

(c)

Figure 5.63. The variation of (a) Equivalent Plastic Strain (b) Stress Triaxiality and (c) Lode Angle Parameter along the diagonal of the blank at 4 mm cup depth for Al2024 aluminum (VM-JC-HC)

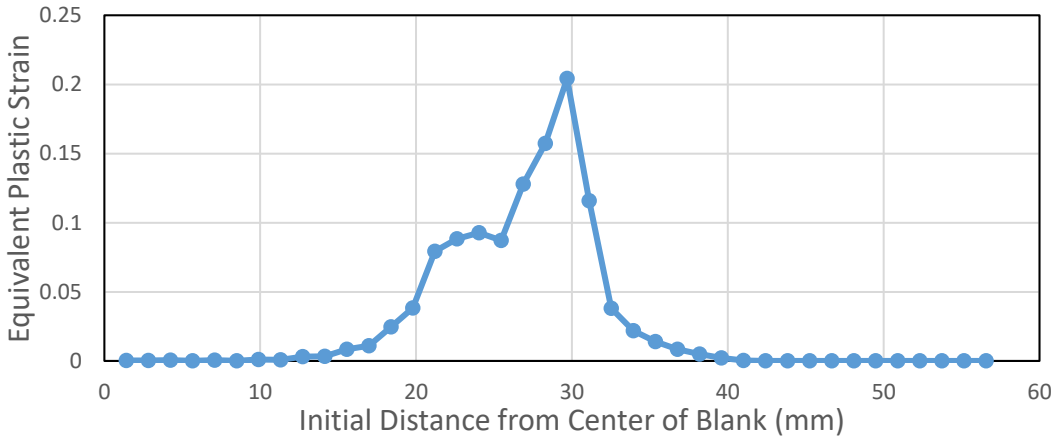

(a)

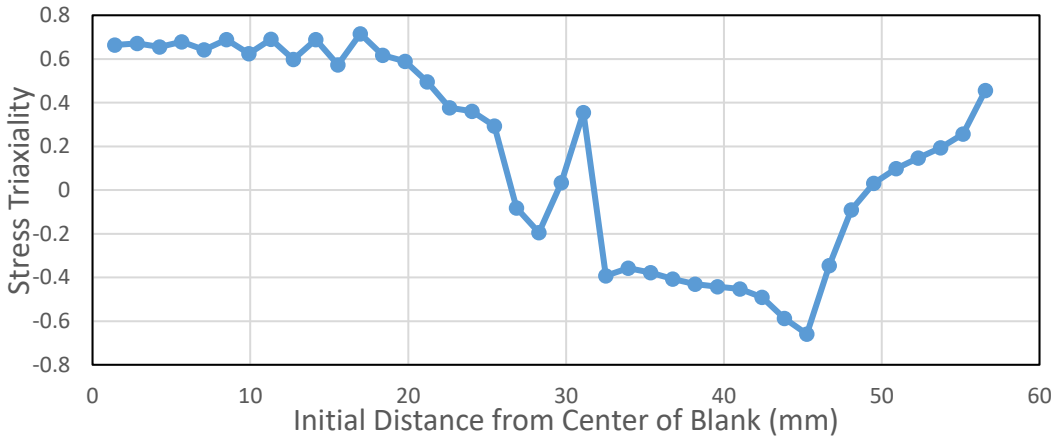

(b)

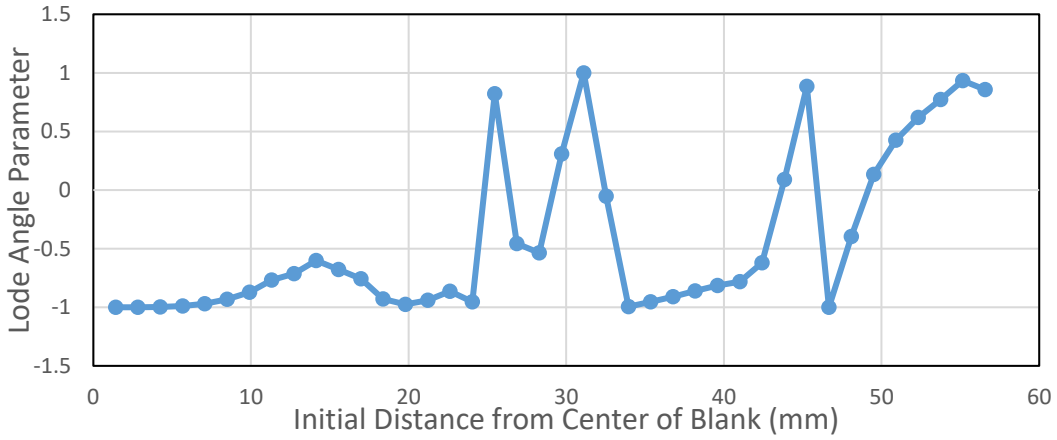

(c)

Figure 5.64 The variation of (a) Equivalent Plastic Strain (b) Stress Triaxiality and (c) Lode Angle Parameter along the diagonal of the blank at 6 mm cup depth for Al2024 aluminum (VM-JC-HC)

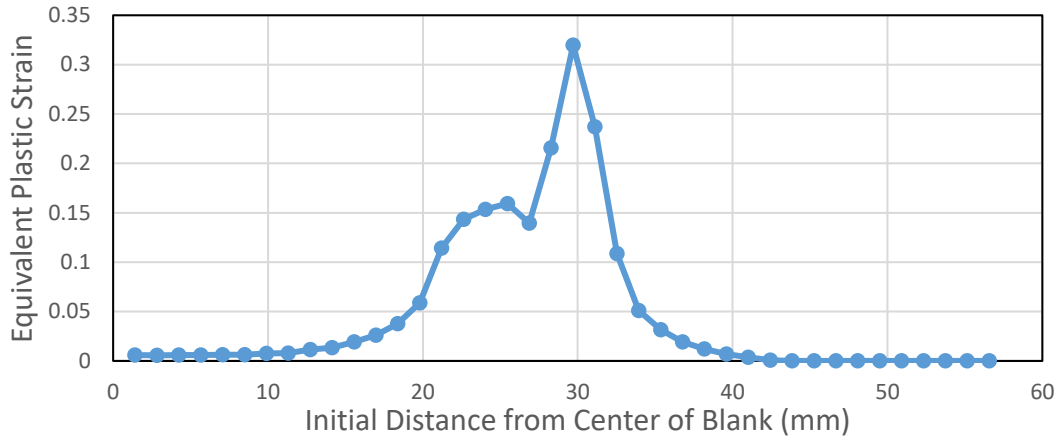

(a)

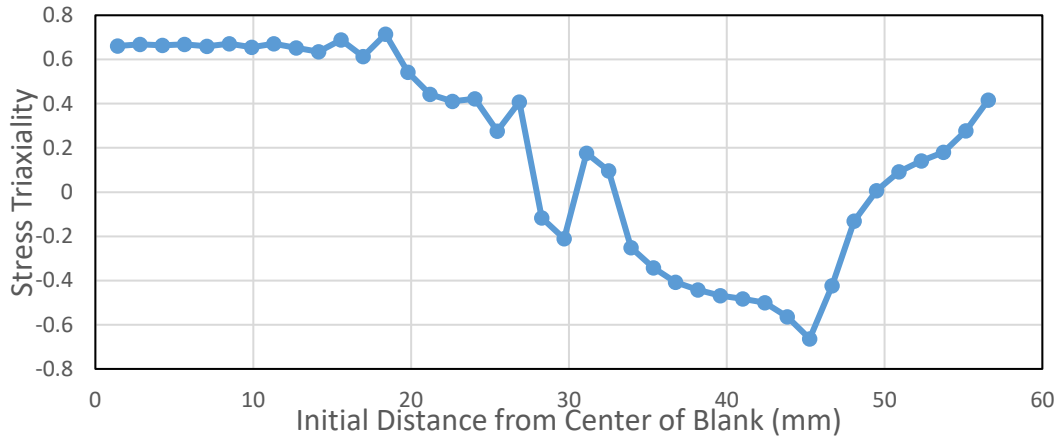

(b)

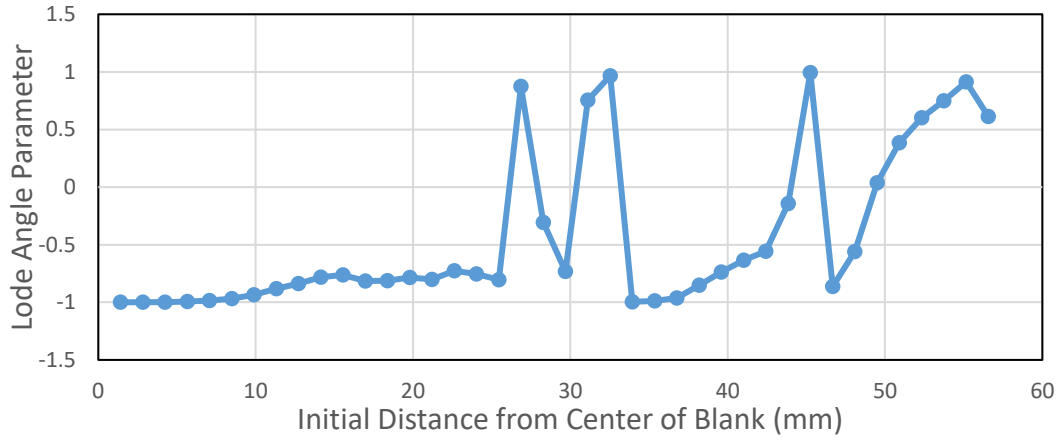

(c)

Figure 5.65. The variation of (a) Equivalent Plastic Strain (b) Stress Triaxiality and (c) Lode Angle Parameter along the diagonal of the blank at 8 mm cup depth for Al2024 aluminum (VM-JC-HC)

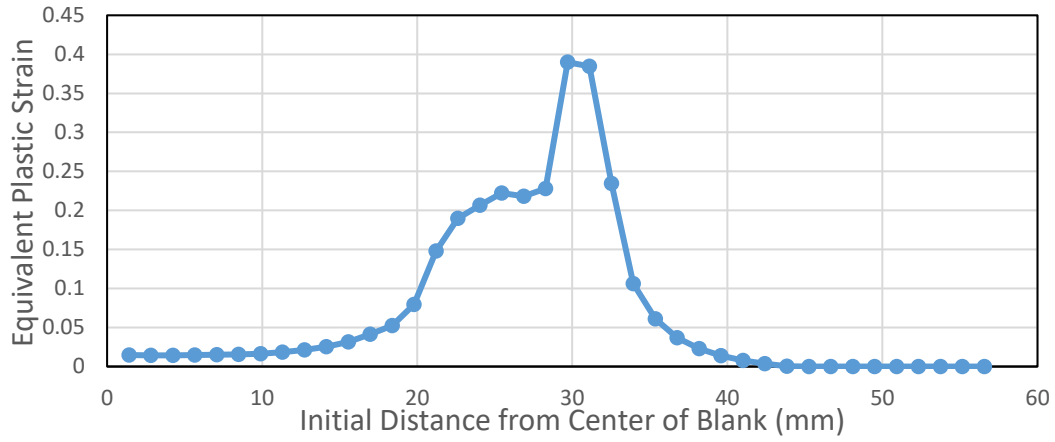

(a)

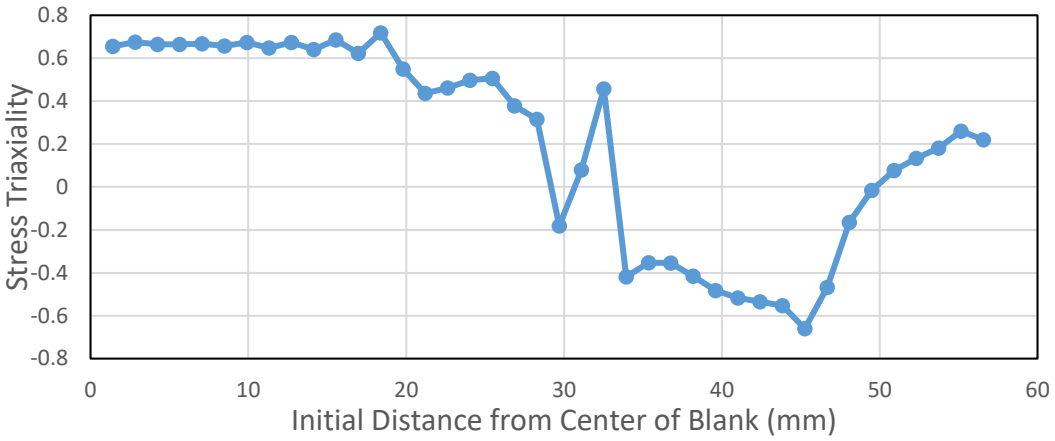

(b)

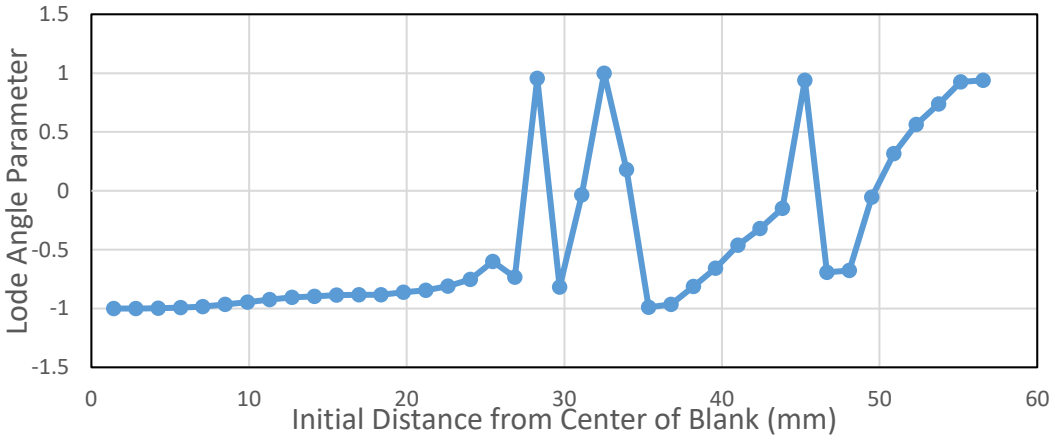

(c)

Figure 5.66. The variation of (a) Equivalent Plastic Strain (b) Stress Triaxiality and (c) Lode Angle Parameter along the diagonal of the blank at 10 mm cup depth for Al2024 aluminum (VM-JC-HC)

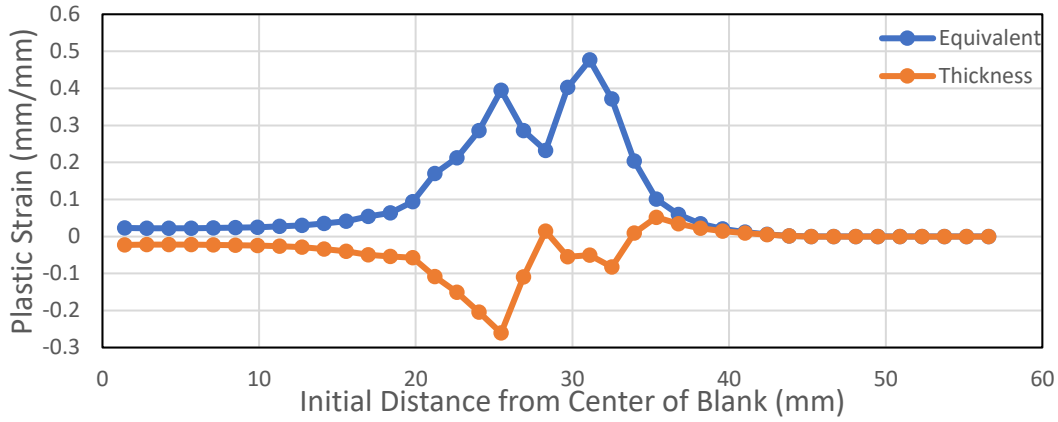

(a)

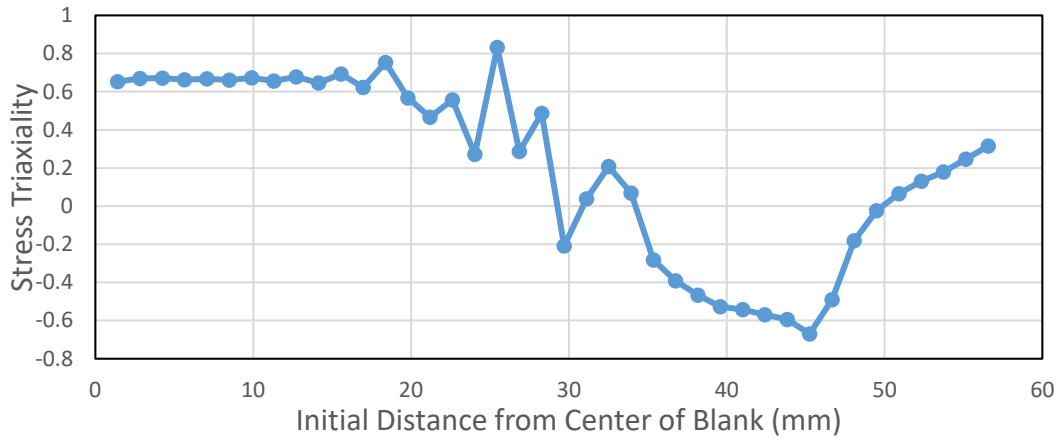

(b)

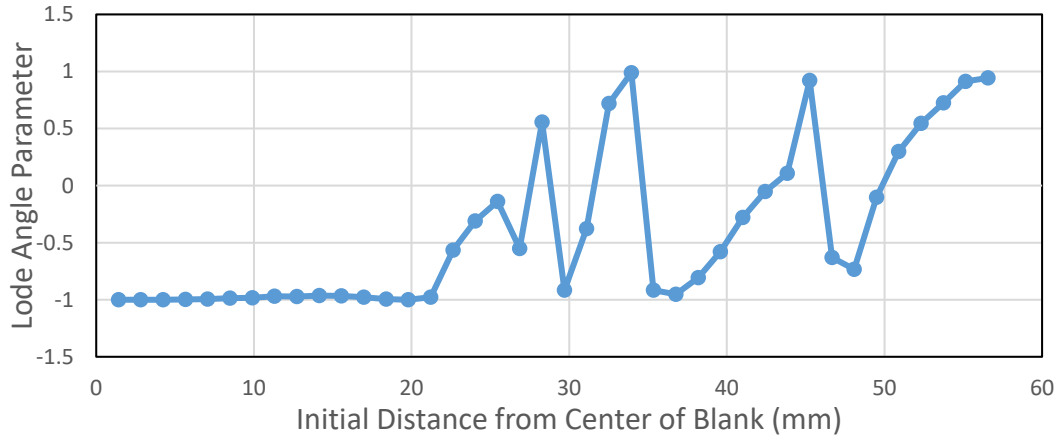

(c)

Figure 5.67. The variation of (a) Equivalent Plastic Strain and Thickness Plastic Strain (b) Stress Triaxiality and (c) Lode Angle Parameter along the diagonal of the blank at 12 mm cup depth for Al2024 aluminum (VM-JC-HC)

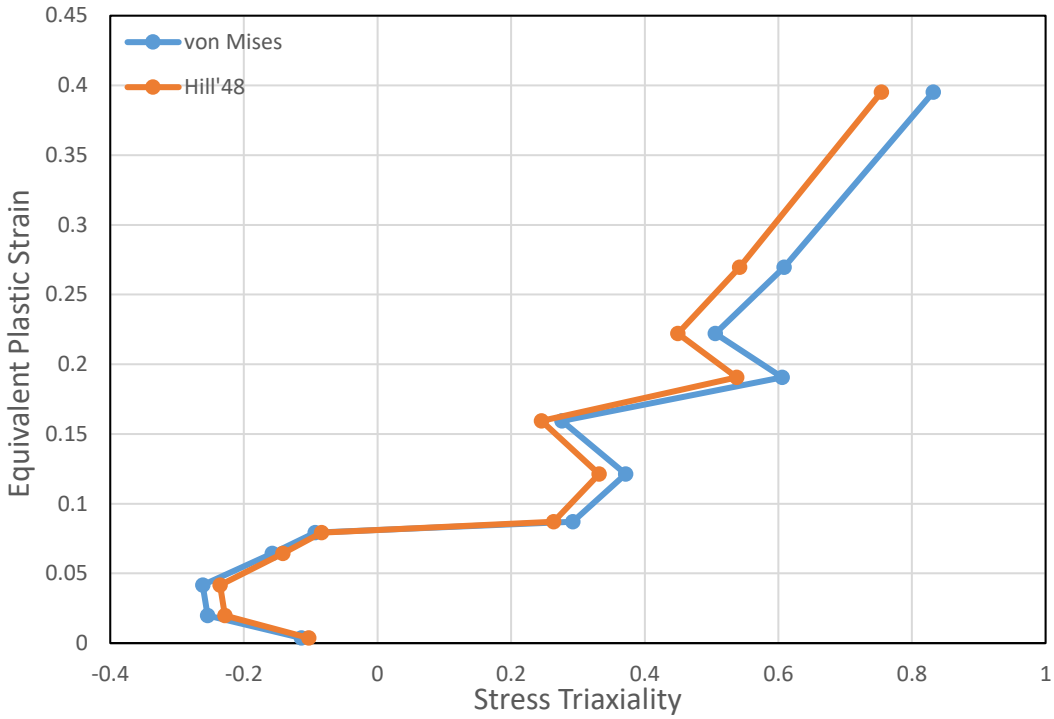

Figure 5.68. Equivalent Plastic Strain - Stress Triaxiality Plot of First Rupture Element (VM-JC-HC)

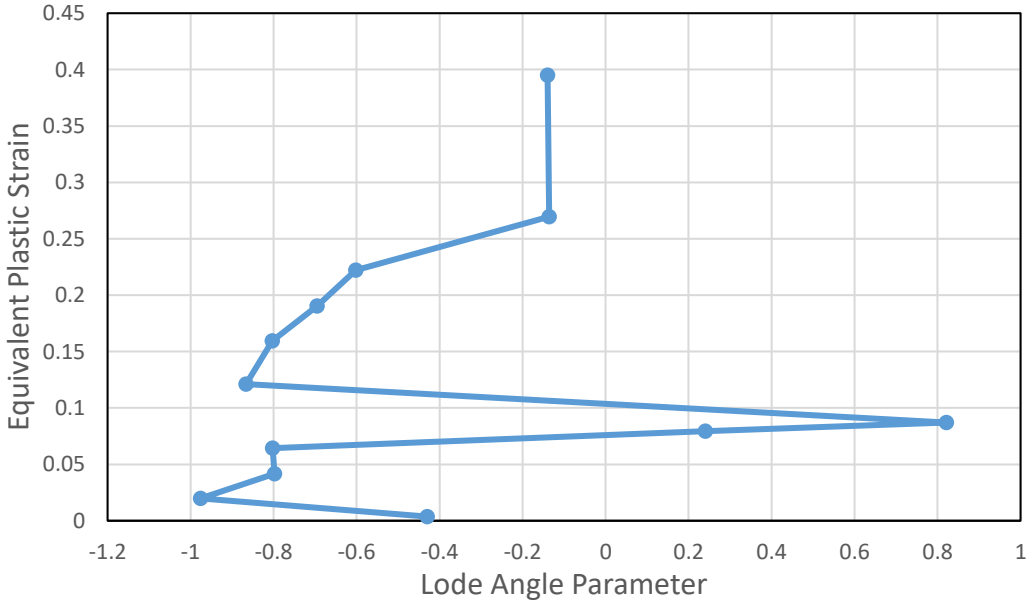

Figure 5.69. Equivalent Plastic Strain – Lode Angle Parameter Plot of First Rupture Element (VM-JC-HC)

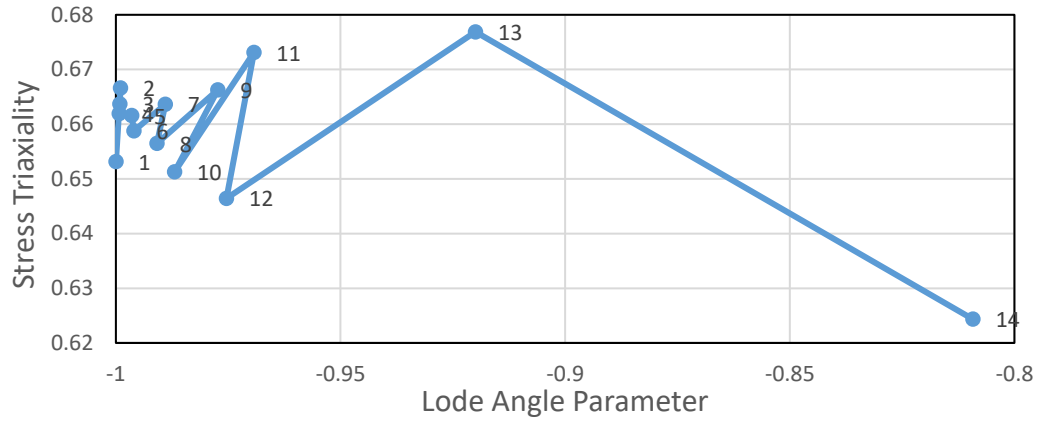
Stress Triaxiality
Lode Angle Parameter
0.68
0.67
0.66
0.65
0.64
0.63
0.62
-1
-0.95
-0.9
-0.85
-0.8
1
2
3
4
5
6
7
8
9
10
11
12
13
14

(a)

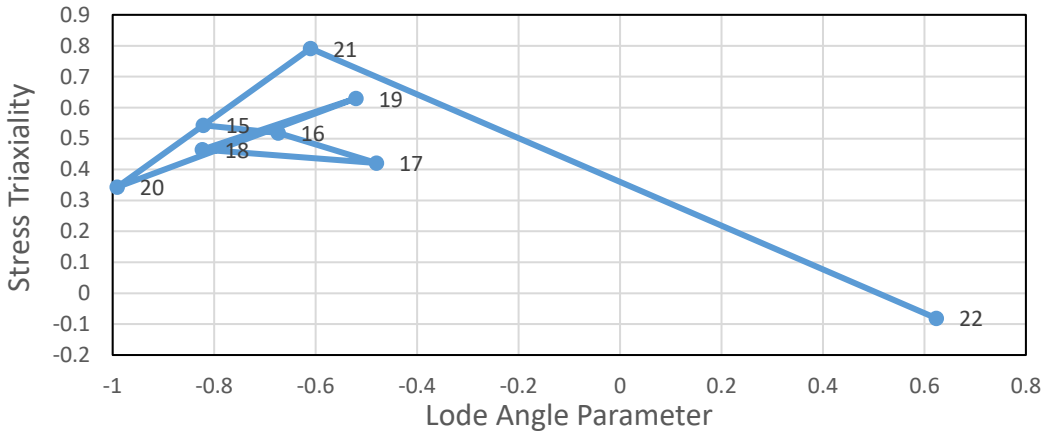
Stress Triaxiality
Lode Angle Parameter
0.9
0.8
0.7
0.6
0.5
0.4
0.3
0.2
0.1
0
-0.1
-0.2
-1
-0.8
-0.6
-0.4
-0.2
0
0.2
0.4
0.6
0.8
15
16
17
18
19
20
21
22

(b)

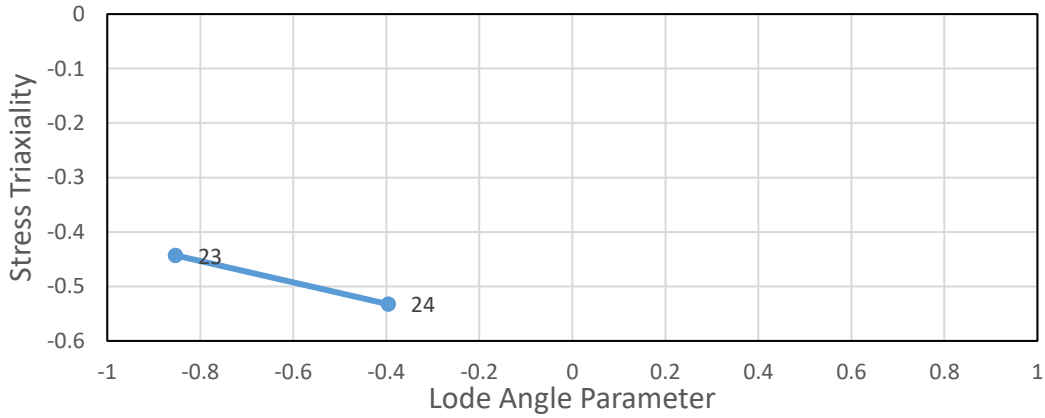
Stress Triaxiality
Lode Angle Parameter
0
-0.1
-0.2
-0.3
-0.4
-0.5
-0.6
-1
-0.8
-0.6
-0.4
-0.2
0
0.2
0.4
0.6
0.8
1
23
24

(c)

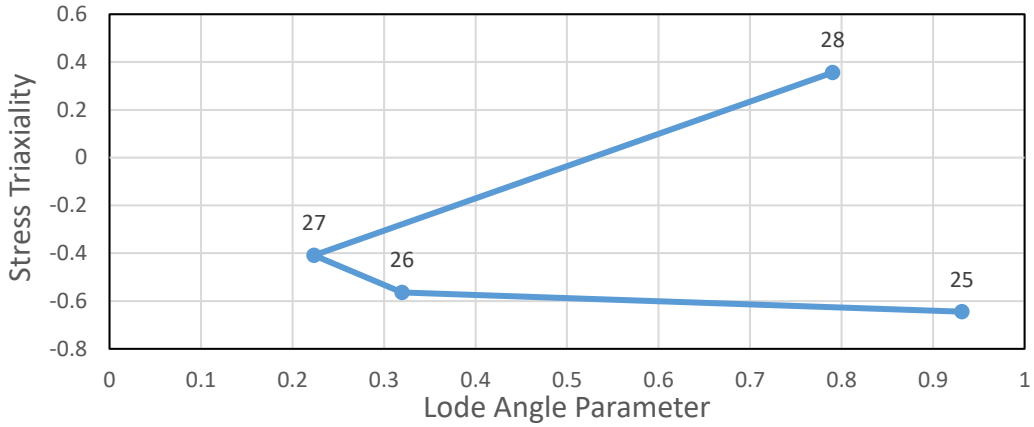

(d)

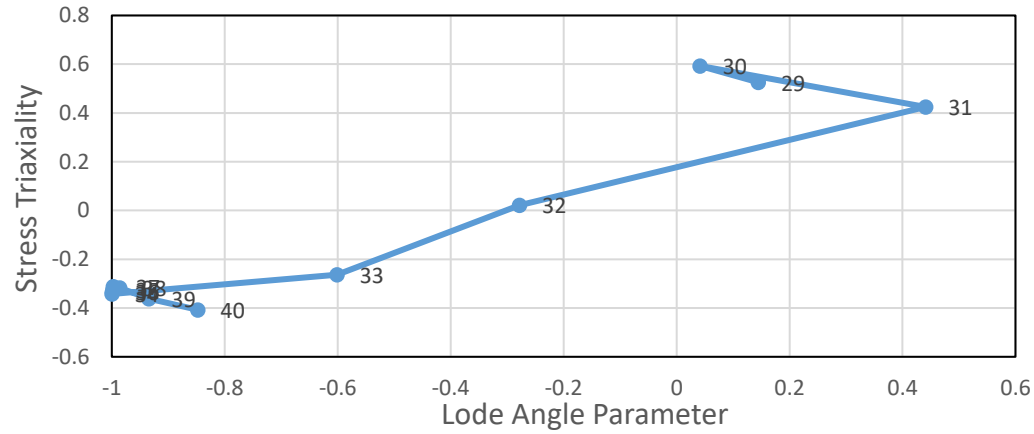

(e)

Figure 5.70. The variation of triaxiality values with respect to Lode angle parameter values in rolling direction (a) for punch (b) for punch shoulder or corner (c) for the clearance between die and punch (d) for die shoulder or corner and (e) for the blank holder regions of the blank at 12 mm cup depth for Al2024 aluminum (VM-JC-HC)

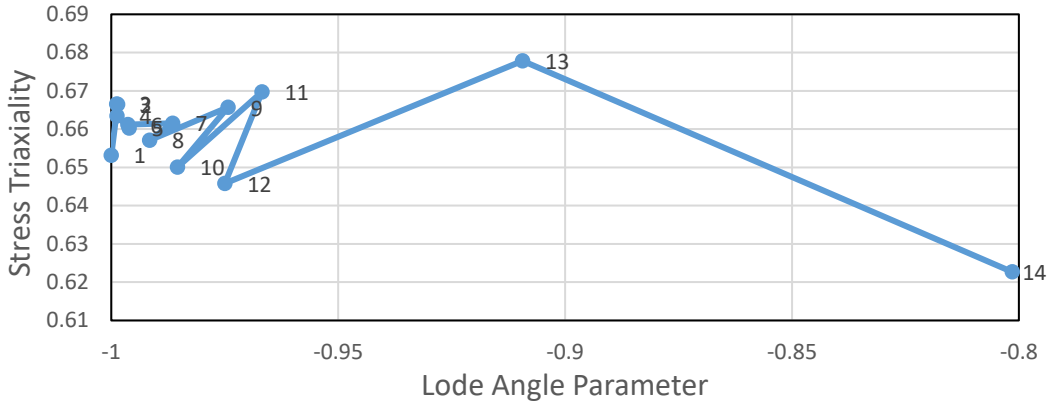
Stress Triaxiality
0.69
0.68
0.67
0.66
0.65
0.64
0.63
0.62
0.61
-1
-0.95
-0.9
-0.85
-0.8
Lode Angle Parameter
1
2
3
4
5
6
7
8
9
10
11
12
13
14

(a)

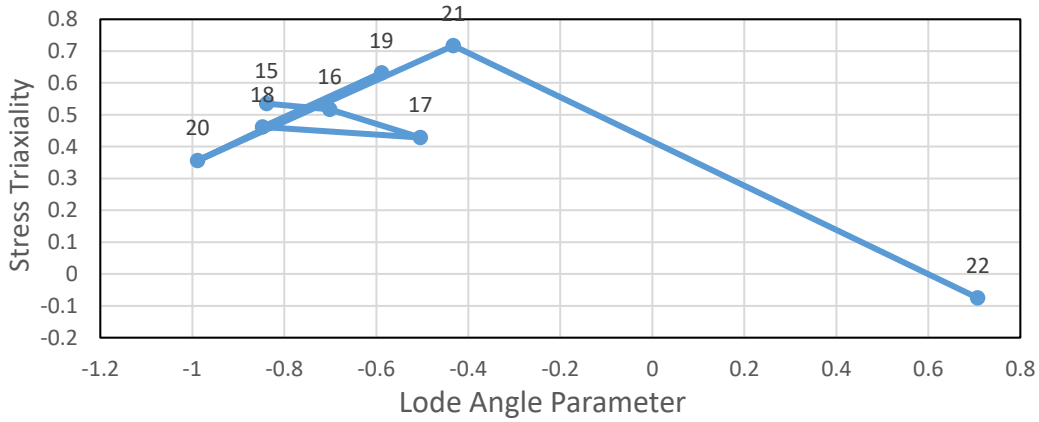
Stress Triaxiality
0.8
0.7
0.6
0.5
0.4
0.3
0.2
0.1
0
-0.1
-0.2
-1.2
-1
-0.8
-0.6
-0.4
-0.2
0
0.2
0.4
0.6
0.8
Lode Angle Parameter
15
16
17
18
19
20
21
22

(b)

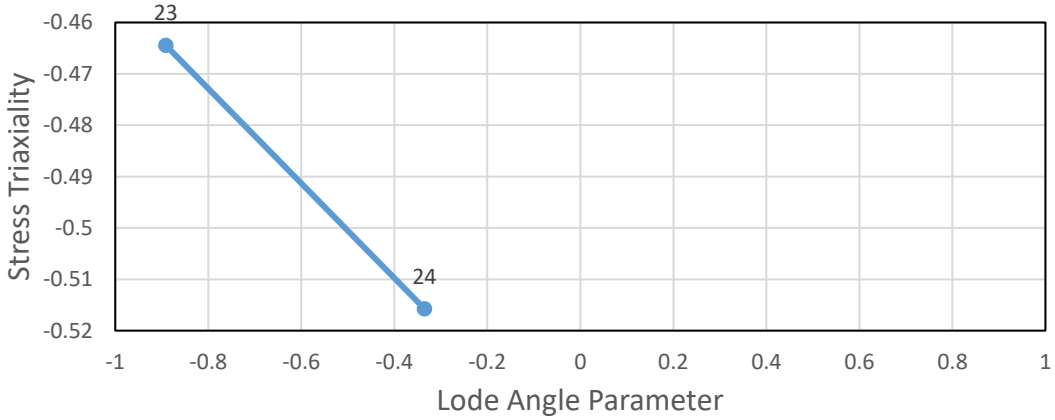
Stress Triaxiality
-0.46
-0.47
-0.48
-0.49
-0.5
-0.51
-0.52
-1
-0.8
-0.6
-0.4
-0.2
0
0.2
0.4
0.6
0.8
1
Lode Angle Parameter
23
24

(c)

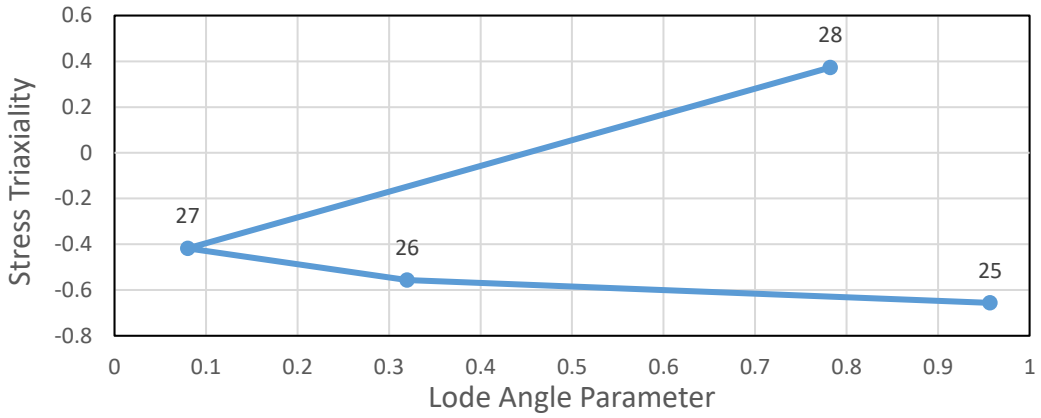

(d)

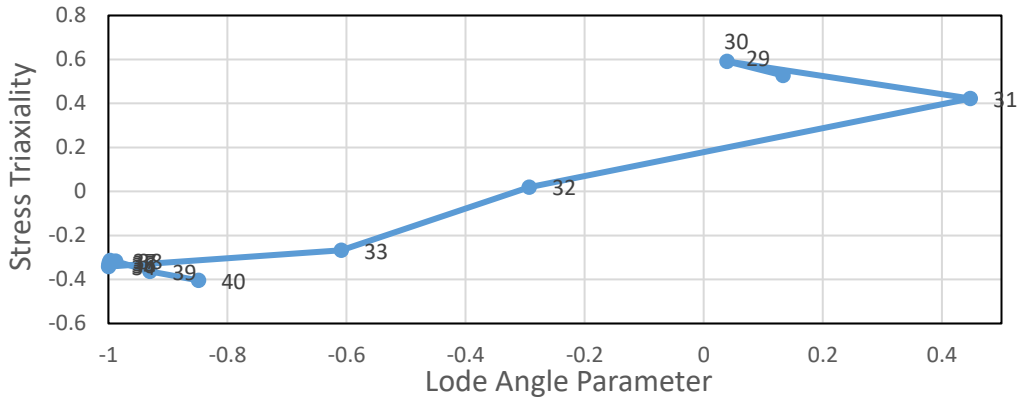

(e)

Figure 5.71. The variation of triaxiality values with respect to Lode angle parameter values in transverse direction (a) for punch (b) for punch shoulder or corner (c) for the clearance between die and punch (d) for die shoulder or corner and (e) for the blank holder regions of the blank at 12 mm cup depth for Al2024 aluminum (VM-JC-HC)

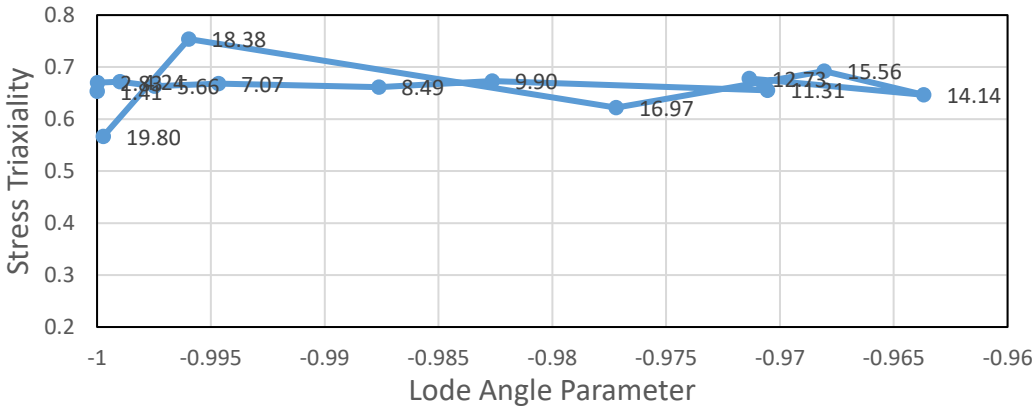
Stress Triaxiality
Lode Angle Parameter
0.8
0.7
0.6
0.5
0.4
0.3
0.2
-1
-0.995
-0.99
-0.985
-0.98
-0.975
-0.97
-0.965
-0.96
18.38
19.80
7.07
8.49
9.90
16.97
12.73
11.31
15.56
14.14

(a)

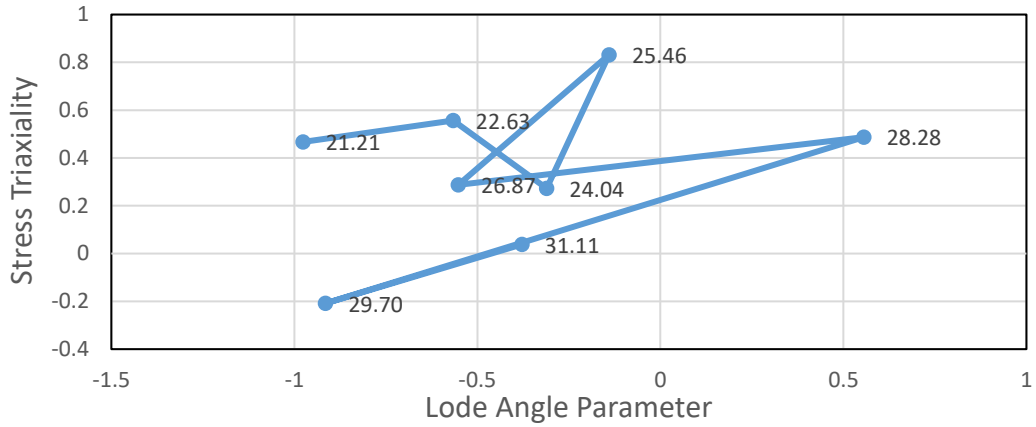
Stress Triaxiality
Lode Angle Parameter
1
0.8
0.6
0.4
0.2
0
-0.2
-0.4
-1.5
-1
-0.5
0
0.5
1
25.46
22.63
21.21
28.28
26.87
24.04
31.11
29.70

(b)

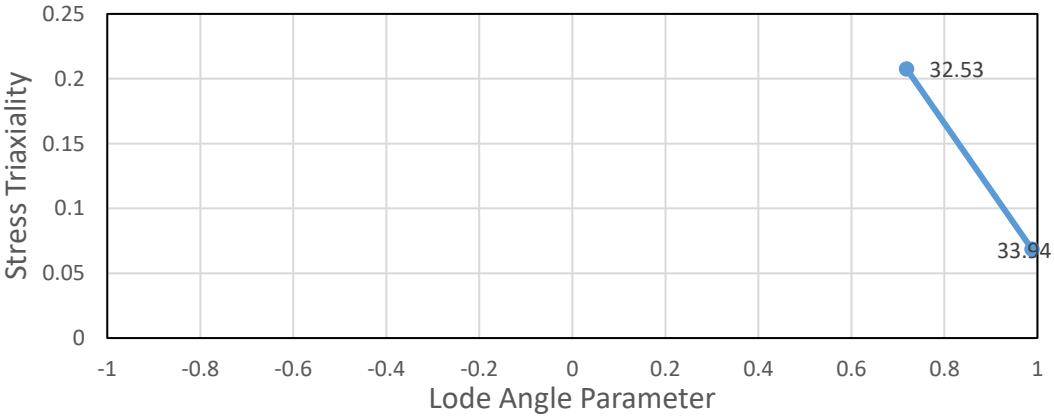
Stress Triaxiality
Lode Angle Parameter
0.25
0.2
0.15
0.1
0.05
0
-1
-0.8
-0.6
-0.4
-0.2
0
0.2
0.4
0.6
0.8
1
32.53
33.94

(c)

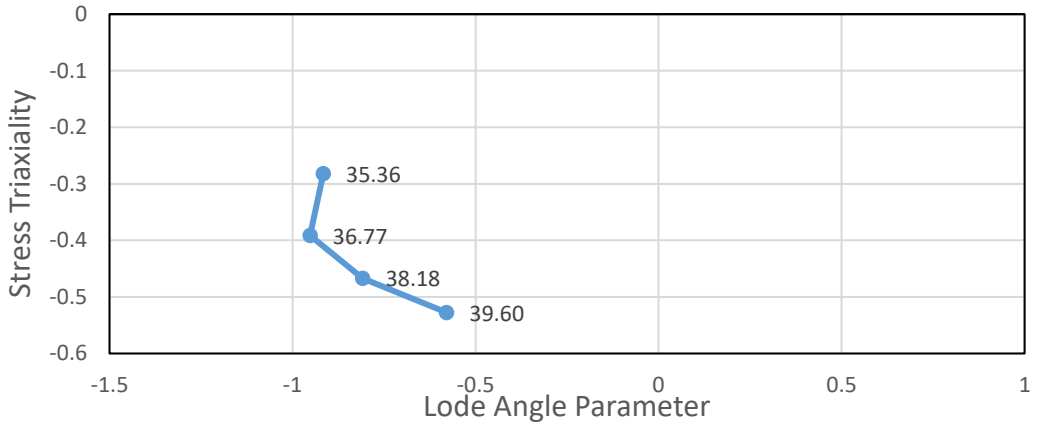

(d)

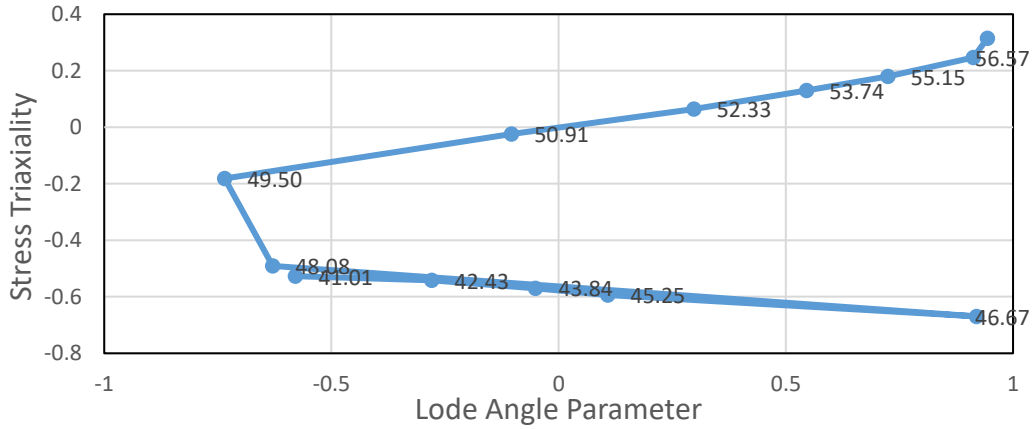

(e)

Figure 5.72. The variation of triaxiality values with respect to Lode angle parameter values in diagonal direction (a) for punch (b) for punch shoulder or corner (c) for the clearance between die and punch (d) for die shoulder or corner and (e) for the blank holder regions of the blank at 12 mm cup depth for Al2024 aluminum (VM-JC-HC)

In the rolling direction, the triaxiality values vary generally between 0.6 and 0.8 under the punch whereas the Lode angle parameter values change between -0.5 and -1. Up to the punch shoulder, it can be said that the deformation behavior is in equi-biaxial tension condition. At the punch shoulder triaxiality values are decreasing as the distance increases from the blank center. Under the blank holder the triaxiality values and Lode angle parameter values are negative, indicating thickening towards the rim.

The same tendency of rolling direction is observed in the transverse direction also. The differences are a result of anisotropy of the material.

In diagonal direction, equi-biaxial strain is dominating up to a distance of 20 mm from the center. At the punch corner, triaxiality values are still positive and the Lode angle parameter values are increasing, as the distance increases from the blank center. At the die corner the triaxiality values became negative, indication compressive type deformation with the Lode angle parameter values. At punch corner, fracture occurs in the situation close to the plain strain tension state.

5.1.5 Case 5: Square-Al2024-Hill48-Discrete-Johnson Cook Model

For the fifth case, Hill'48 yield criterion was applied with discrete hardening and the Johnson Cook ductile fracture criterion was used. It is observed that the fracture started after 8 mm punch travel as shown in Figure 5.73. The variations of equivalent plastic strain, stress triaxiality and Lode angle parameter values are presented as a function of the distance from the center of the blank for different cup heights up to fracture. The results are shown for rolling direction in Figure 5.74 to Figure 5.77, for transverse direction in Figure 5.78 to Figure 5.81 and for diagonal direction in Figure 5.82 to Figure 5.85. The thickness plastic strain distribution is also inserted into Figure 5.85 (a) in order to better visualize the deformation. Further, the variations of stress triaxiality values with respect to equivalent plastic strain are given by considering both von Mises and Hill'48 criteria as a function of the path of the element that fractured first in Figure 5.86. Along the same path, the variation of the Lode parameter with respect to equivalent plastic strain is also illustrated in Figure 5.87.

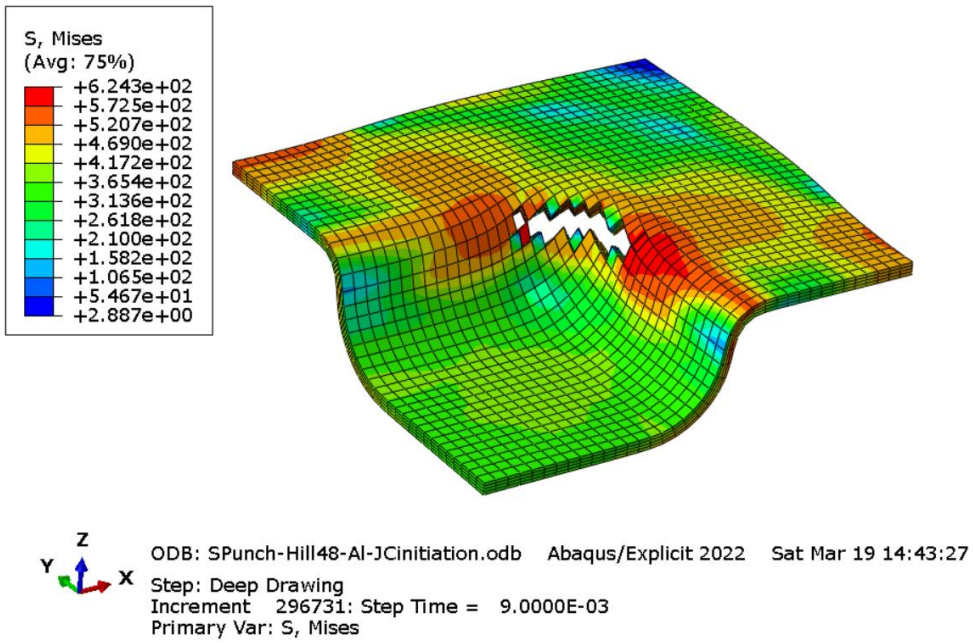

Figure 5.73. First Rupture Moment of Case 5

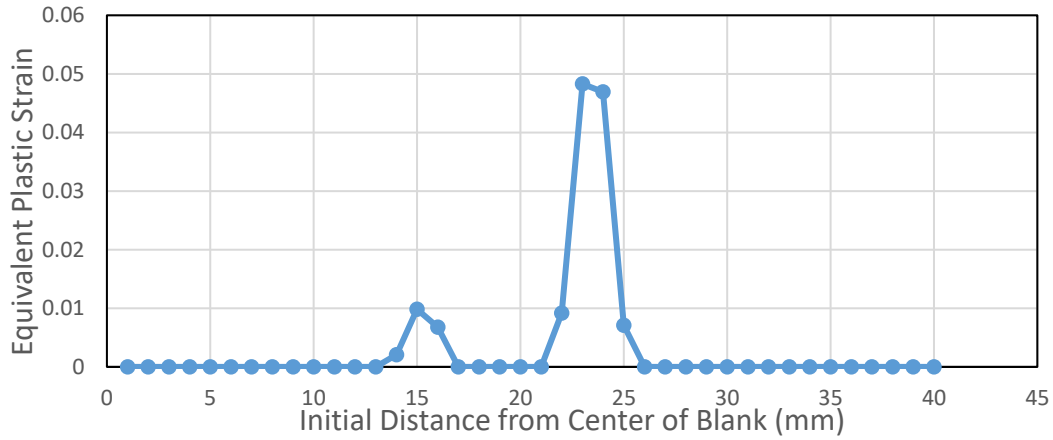

(a)

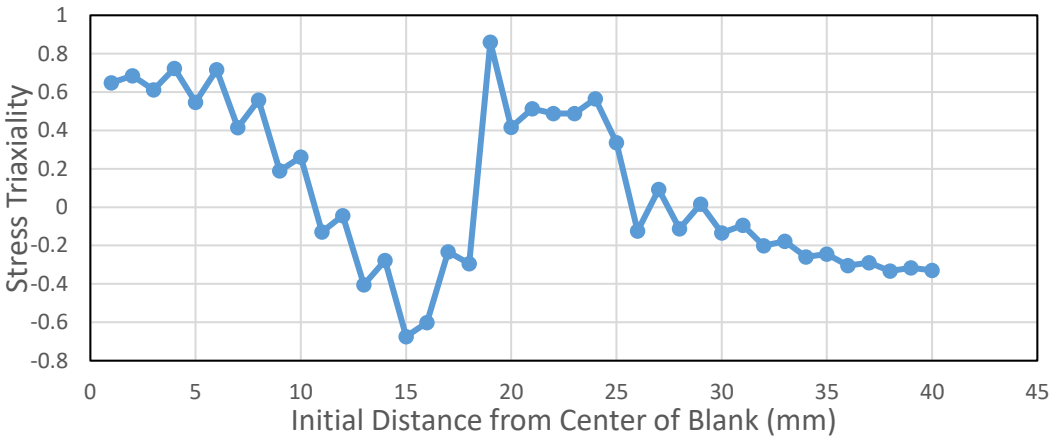

(b)

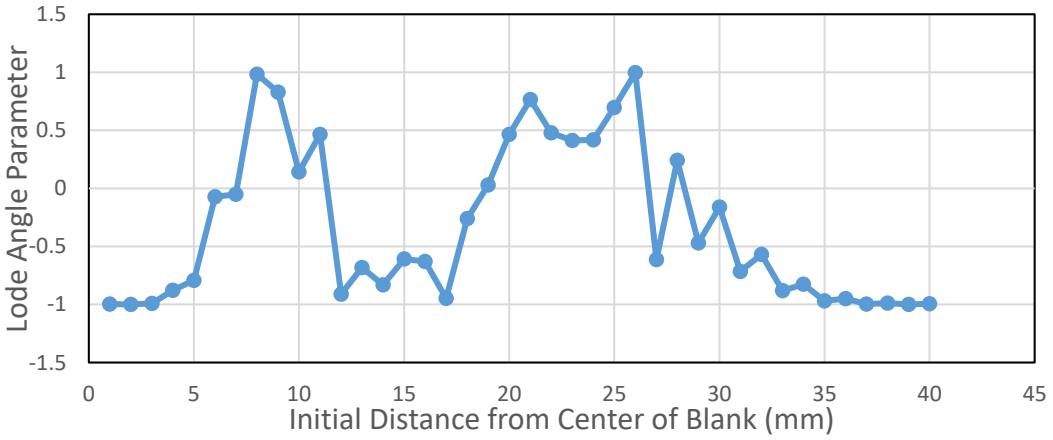

(c)

Figure 5.74. The variation of (a) Equivalent Plastic Strain (b) Stress Triaxiality and (c) Lode Angle Parameter along the rolling direction of the blank at 2 mm cup depth for Al2024 aluminum (Hill'48-Disc-JC)

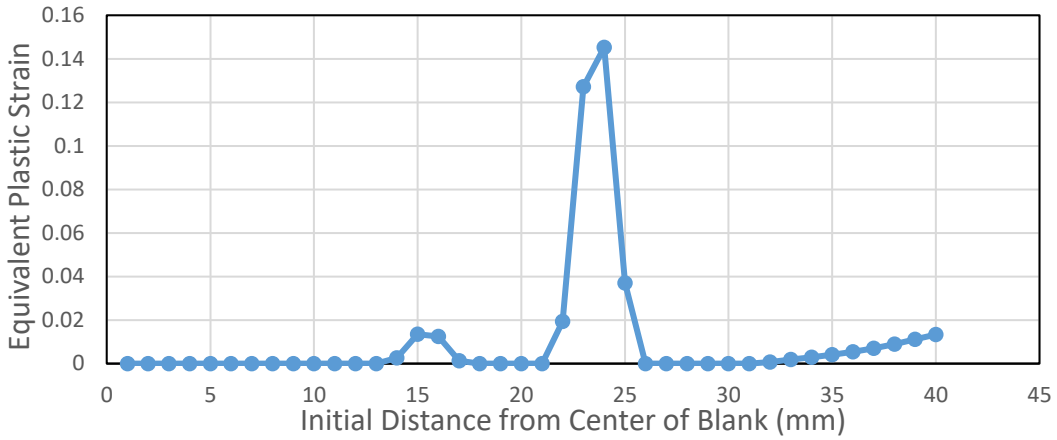

(a)

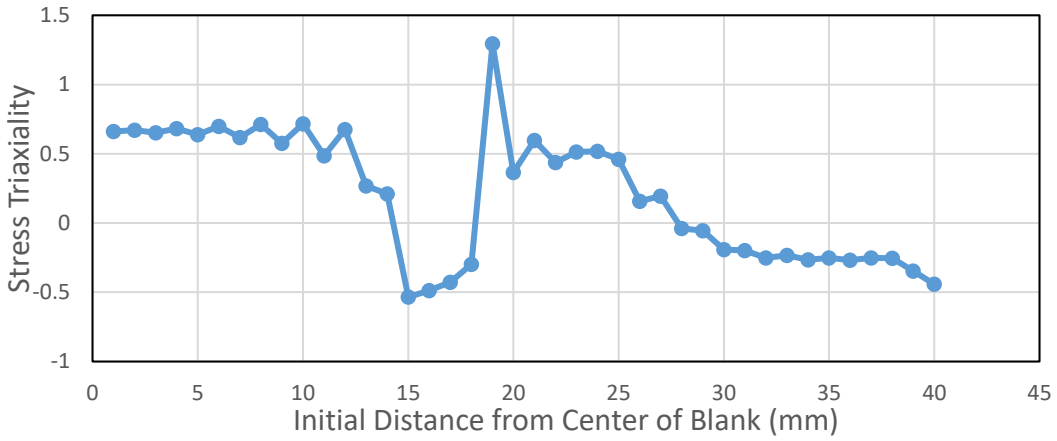

(b)

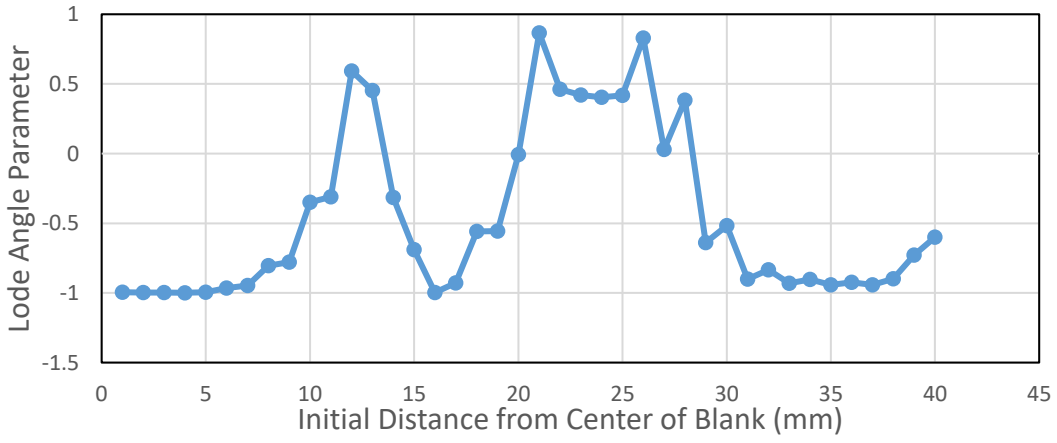

(c)

Figure 5.75. The variation of (a) Equivalent Plastic Strain (b) Stress Triaxiality and (c) Lode Angle Parameter along the rolling direction of the blank at 4 mm cup depth for Al2024 aluminum (Hill'48-Disc-JC)

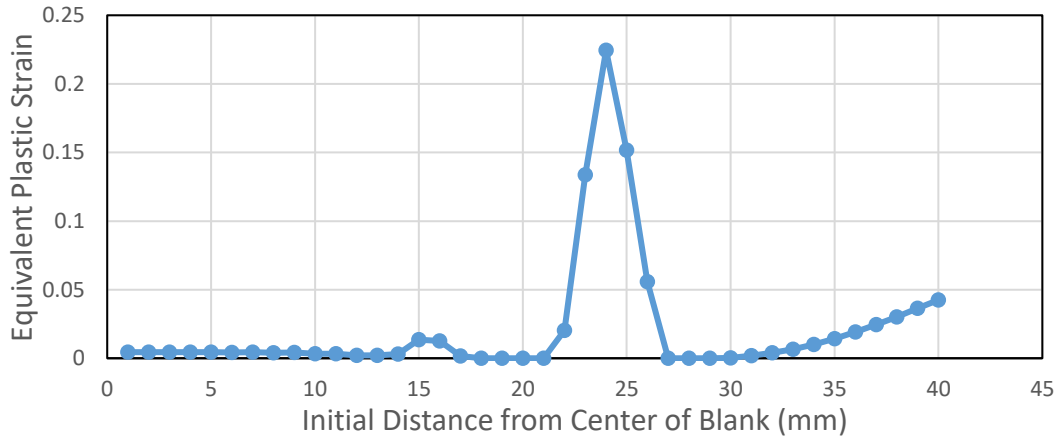

(a)

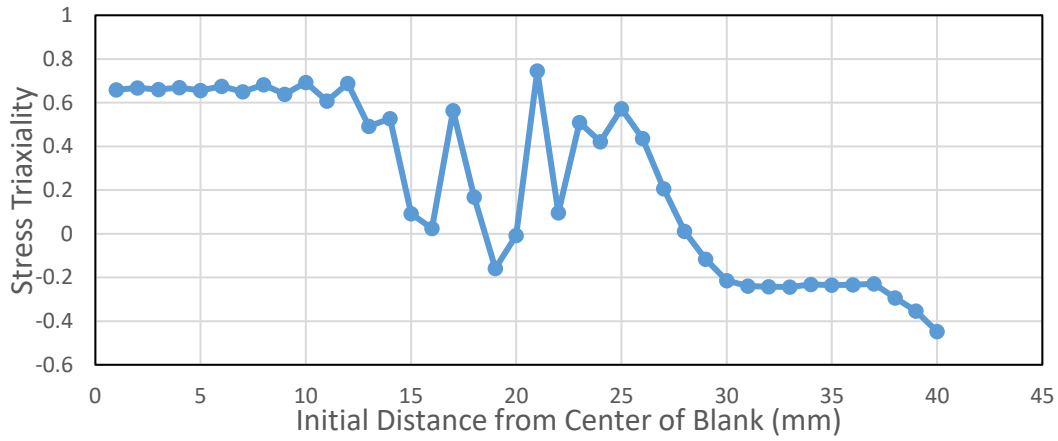

(b)

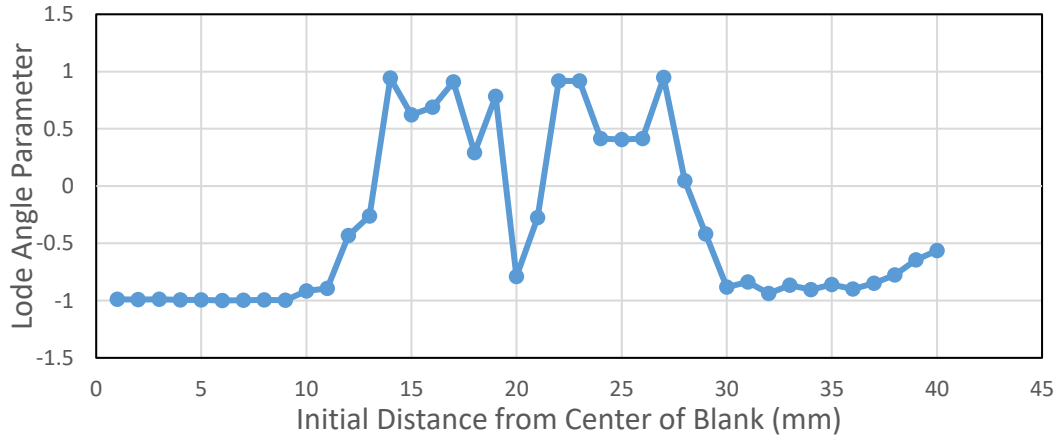

(c)

Figure 5.76. The variation of (a) Equivalent Plastic Strain (b) Stress Triaxiality and (c) Lode Angle Parameter along the rolling direction of the blank at 6 mm cup depth for Al2024 aluminum (Hill'48-Disc-JC)

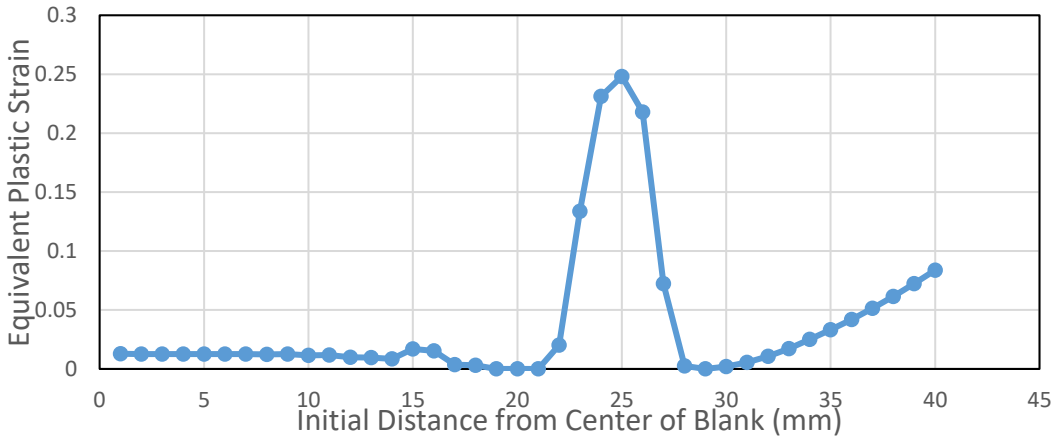

(a)

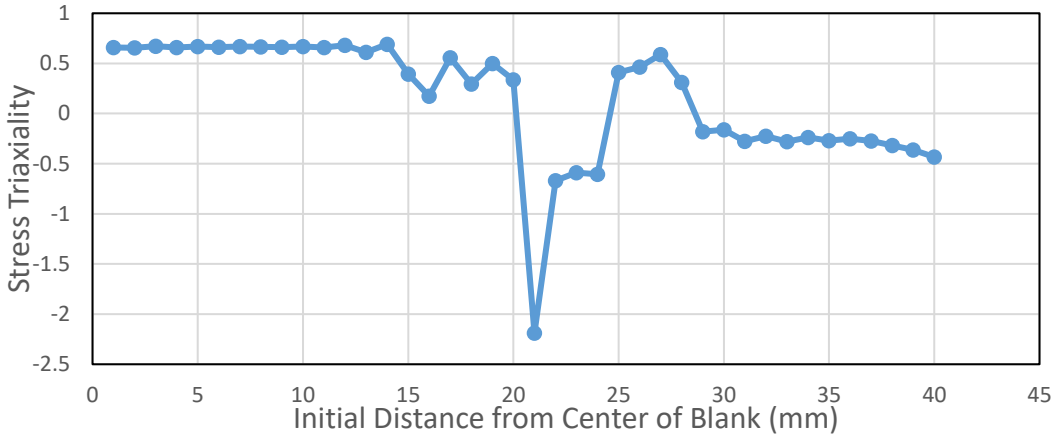

(b)

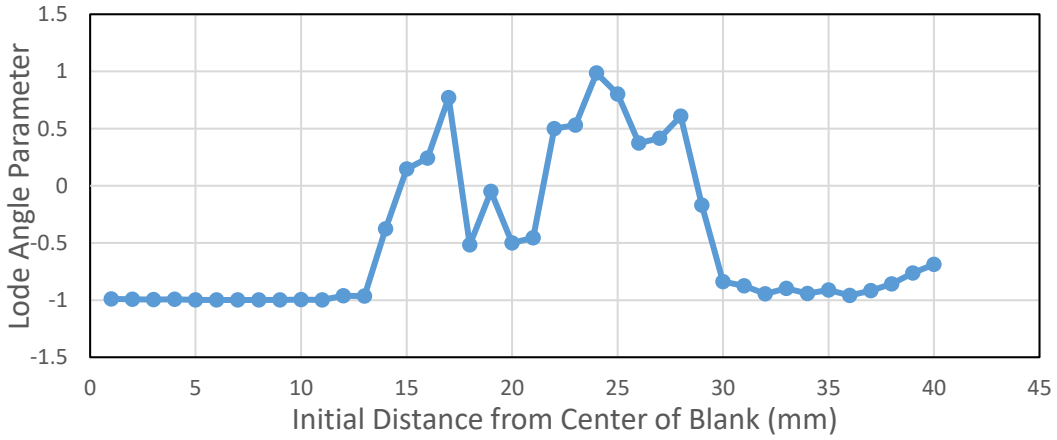

(c)

Figure 5.77. The variation of (a) Equivalent Plastic Strain (b) Stress Triaxiality and (c) Lode Angle Parameter along the rolling direction of the blank at 8 mm cup depth for Al2024 aluminum (Hill'48-Disc-JC)

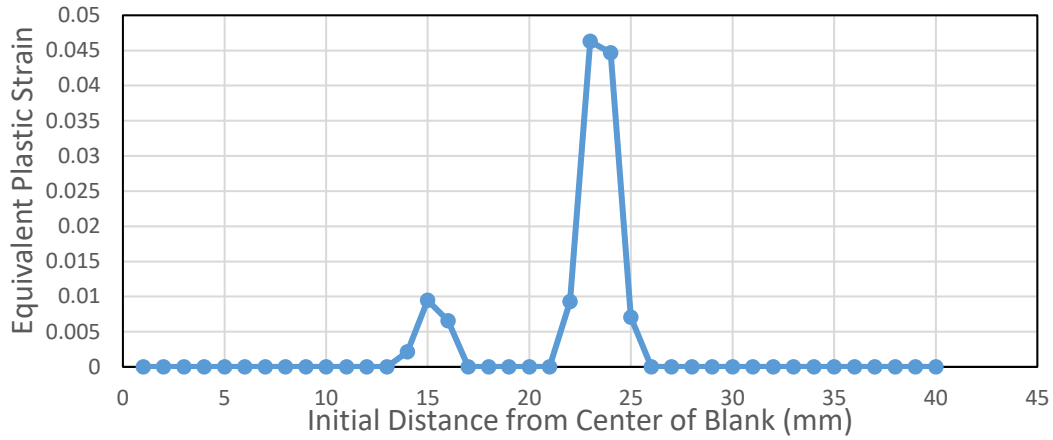

(a)

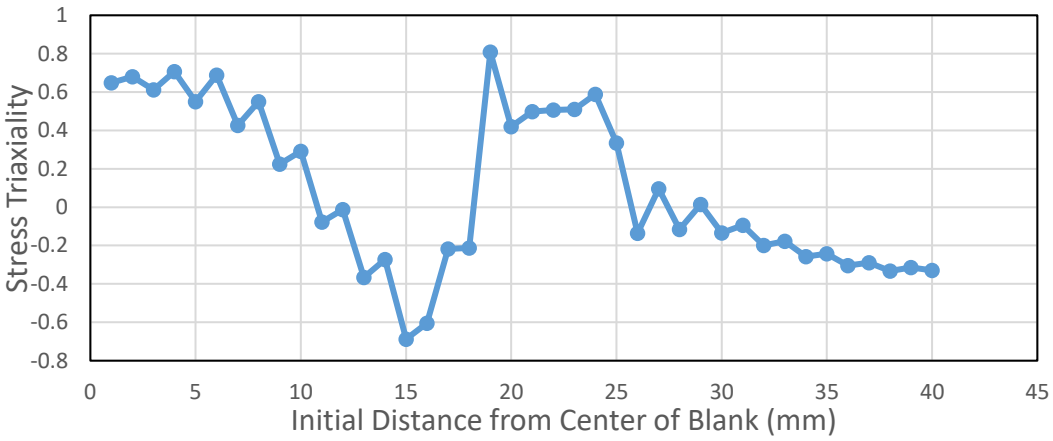

(b)

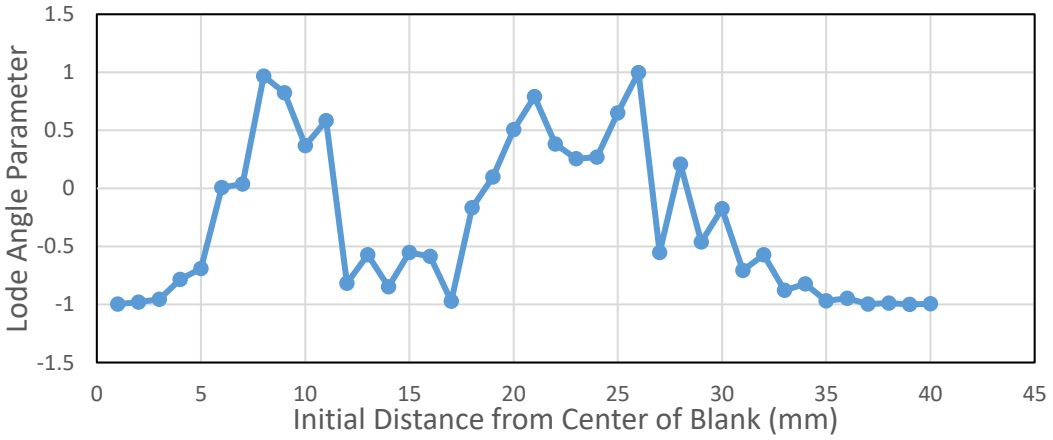

(c)

Figure 5.78. The variation of (a) Equivalent Plastic Strain (b) Stress Triaxiality and (c) Lode Angle Parameter along the transverse direction of the blank at 2 mm cup depth for Al2024 aluminum (Hill'48-Disc-JC)

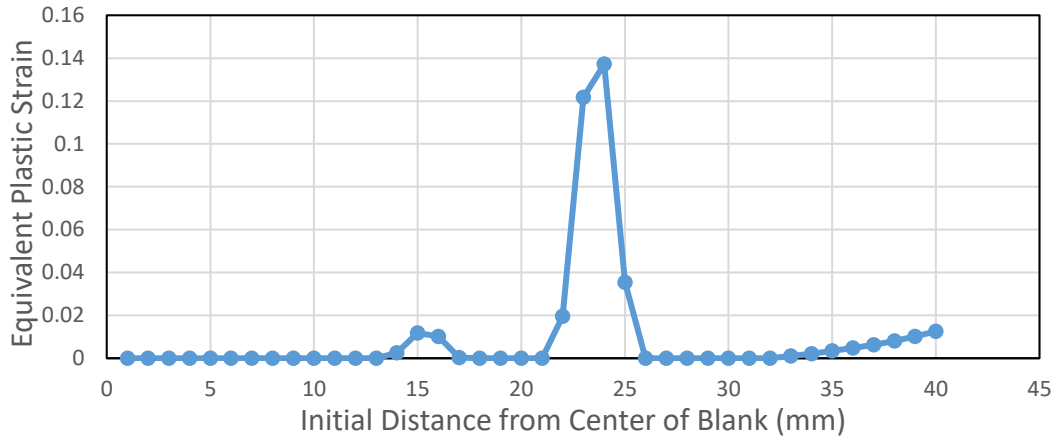

(a)

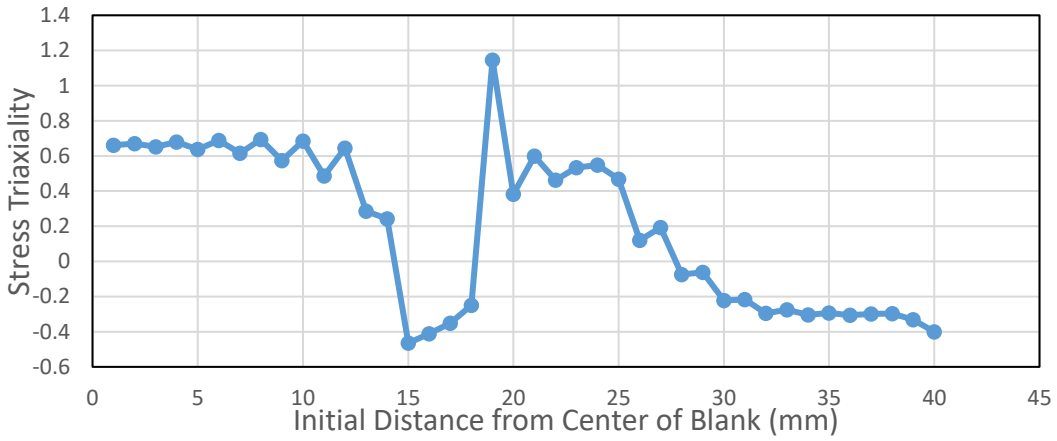

(b)

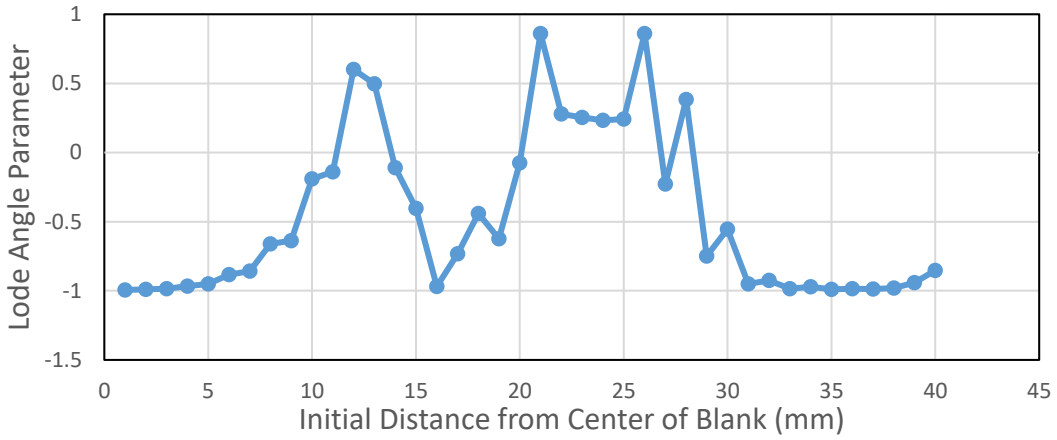

(c)

Figure 5.79. The variation of (a) Equivalent Plastic Strain (b) Stress Triaxiality and (c) Lode Angle Parameter along the transverse direction of the blank at 4 mm cup depth for Al2024 aluminum (Hill'48-Disc-JC)

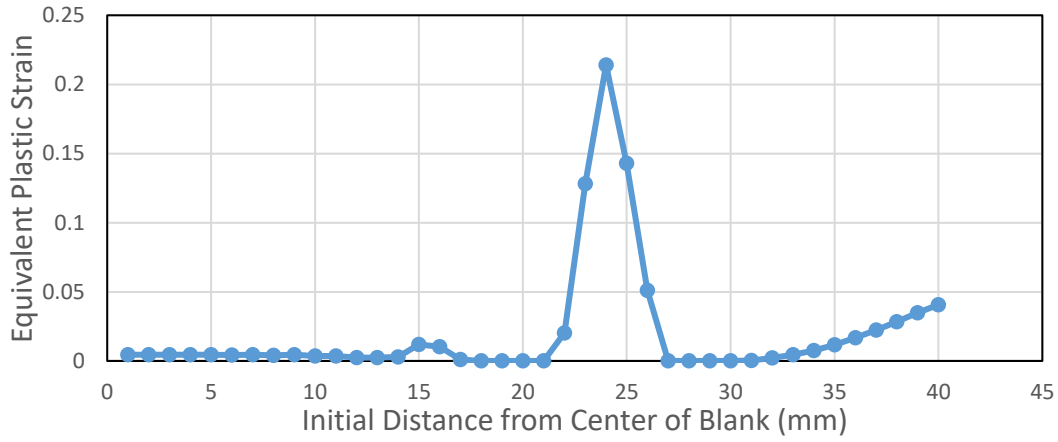

(a)

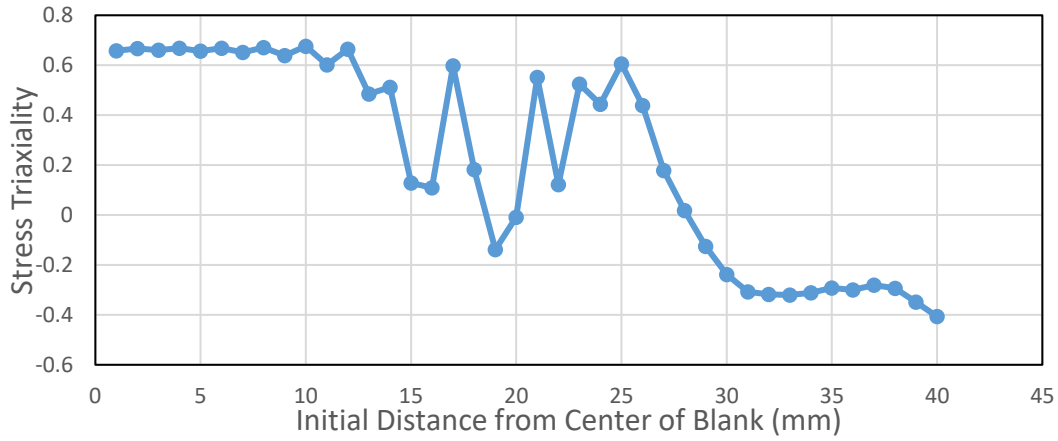

(b)

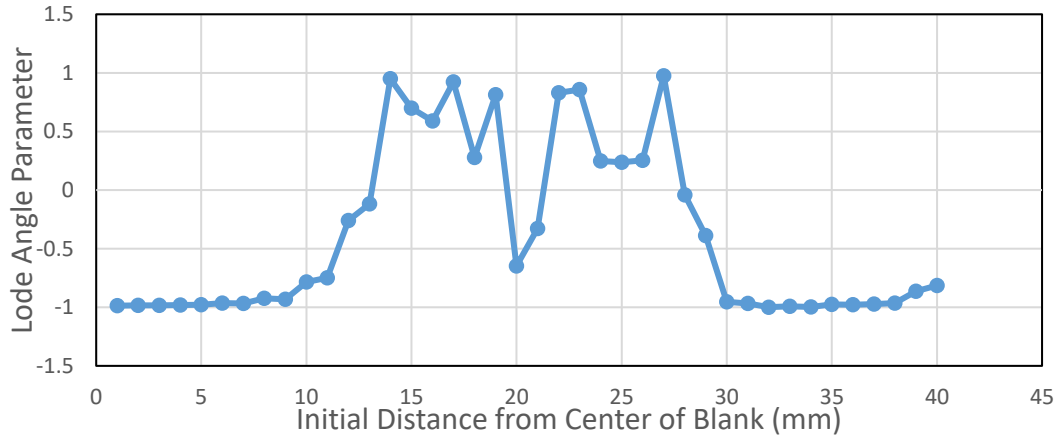

(c)

Figure 5.80. The variation of (a) Equivalent Plastic Strain (b) Stress Triaxiality and (c) Lode Angle Parameter along the transverse direction of the blank at 6 mm cup depth for Al2024 aluminum (Hill'48-Disc-JC)

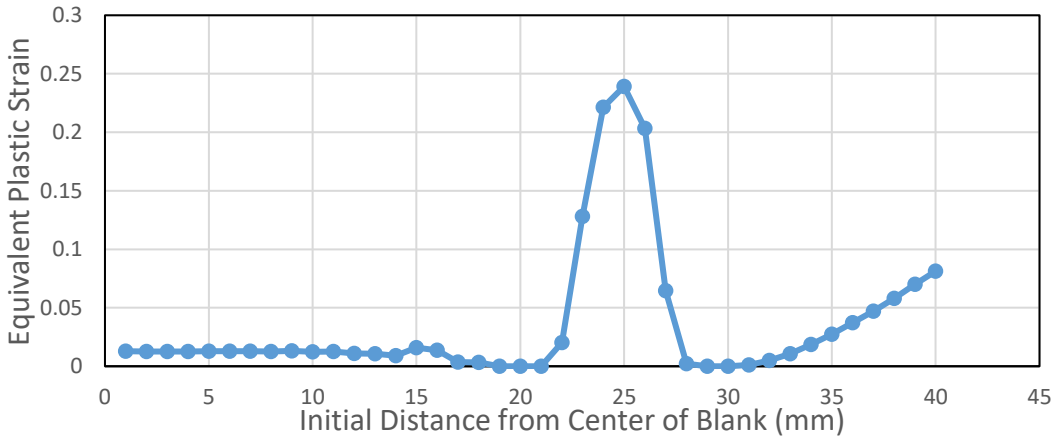

(a)

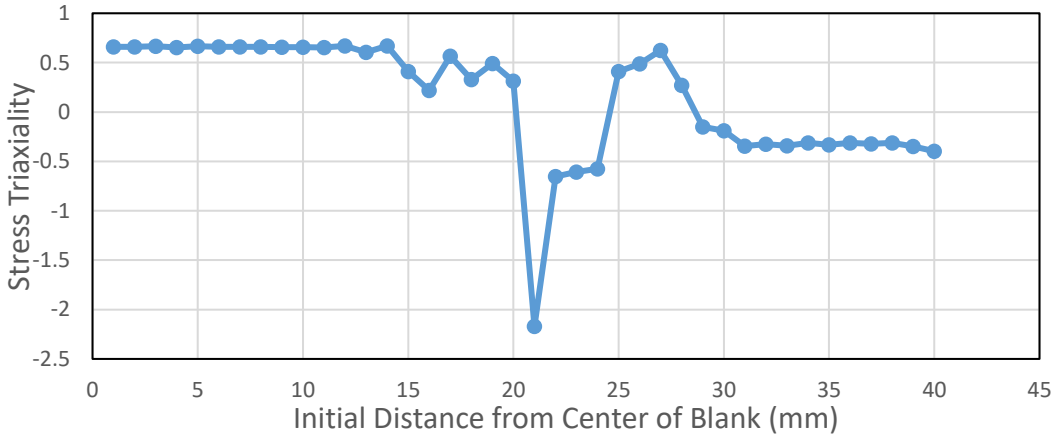

(b)

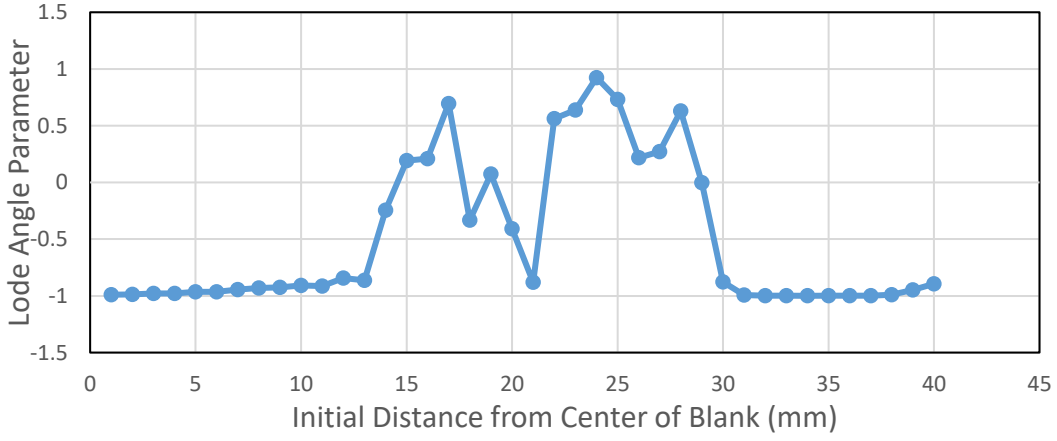

(c)

Figure 5.81. The variation of (a) Equivalent Plastic Strain (b) Stress Triaxiality and (c) Lode Angle Parameter along the transverse direction of the blank at 8 mm cup depth for Al2024 aluminum (Hill'48-Disc-JC)

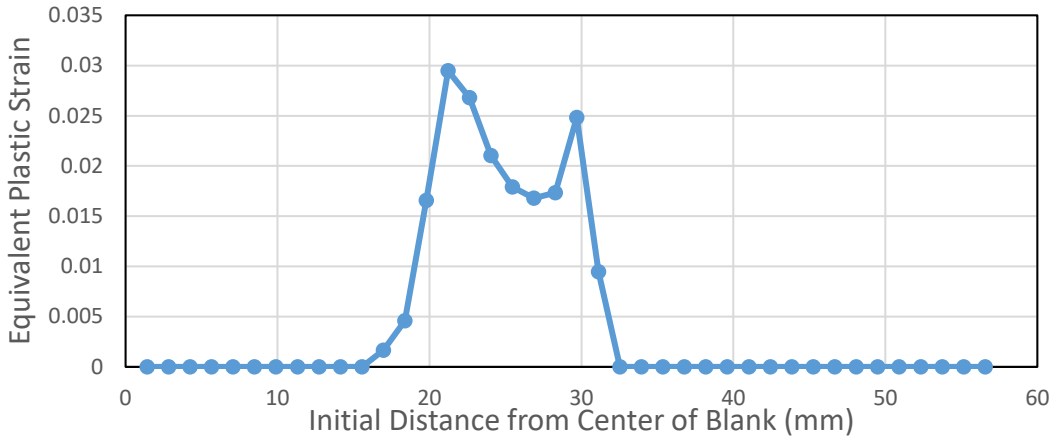

(a)

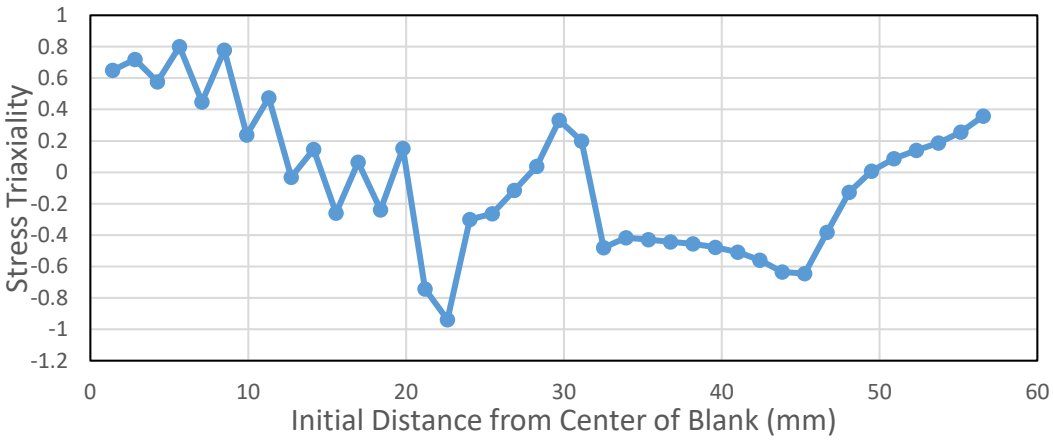

(b)

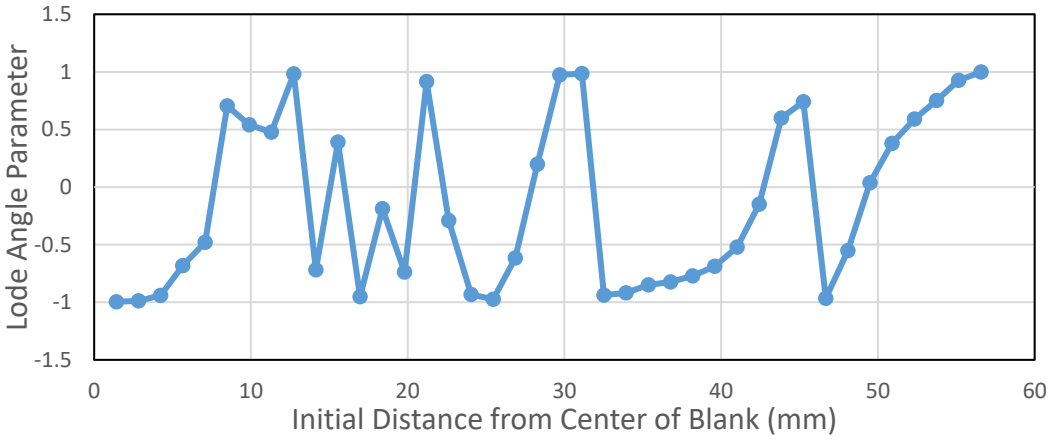

(c)

Figure 5.82. The variation of (a) Equivalent Plastic Strain (b) Stress Triaxiality and (c) Lode Angle Parameter along the diagonal of the blank at 2 mm cup depth for Al2024 aluminum (Hill'48-Disc-JC)

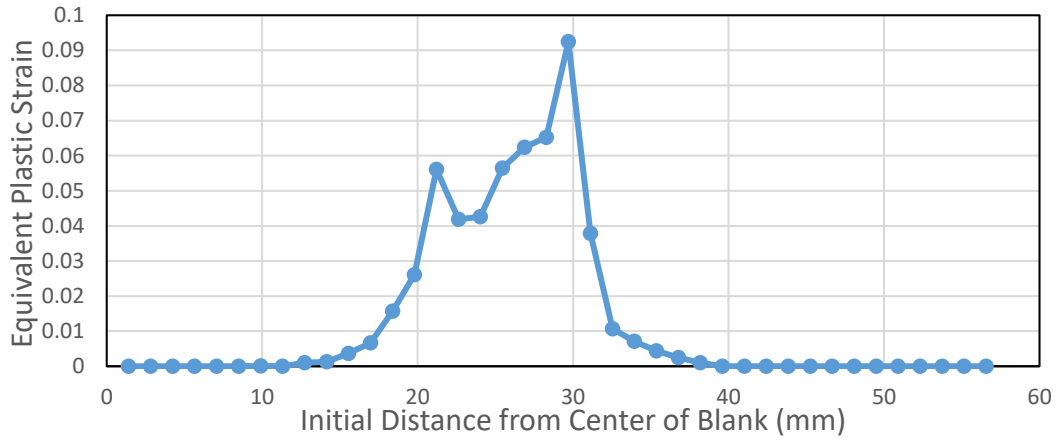

(a)

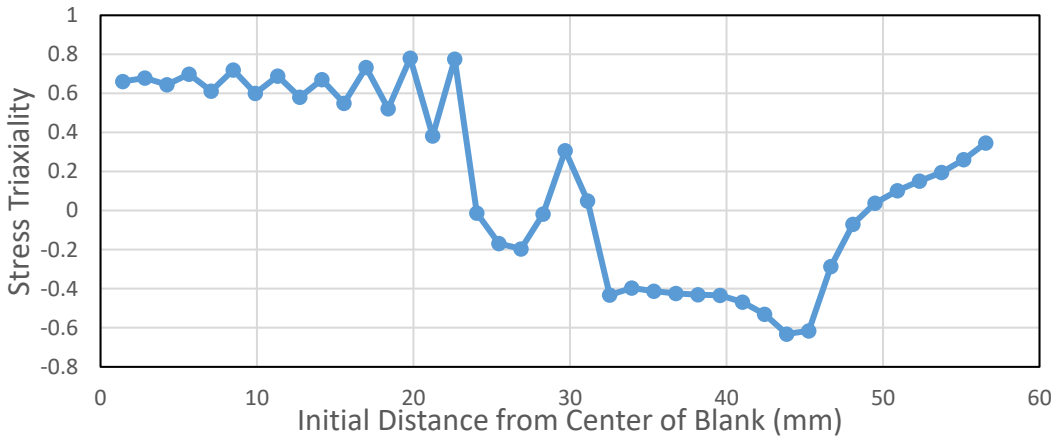

(b)

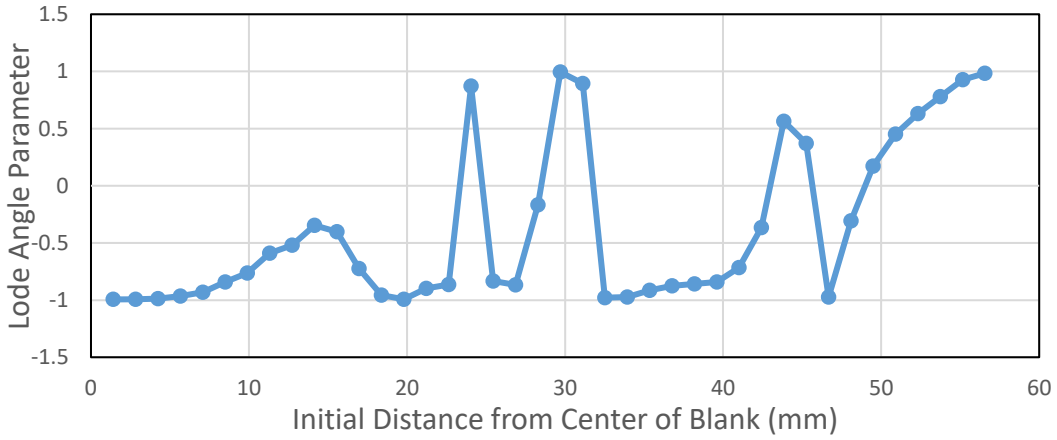

(c)

Figure 5.83. The variation of (a) Equivalent Plastic Strain (b) Stress Triaxiality and (c) Lode Angle Parameter along the diagonal of the blank at 4 mm cup depth for Al2024 aluminum (Hill'48-Disc-JC)

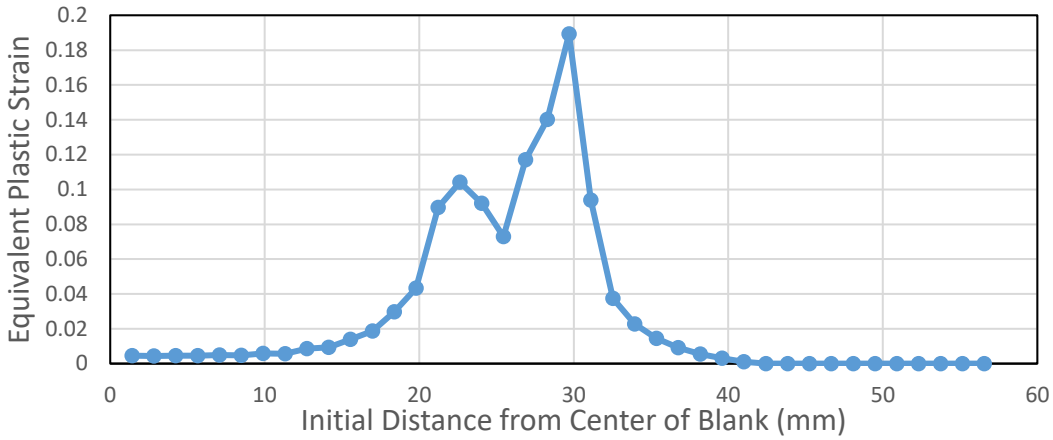

(a)

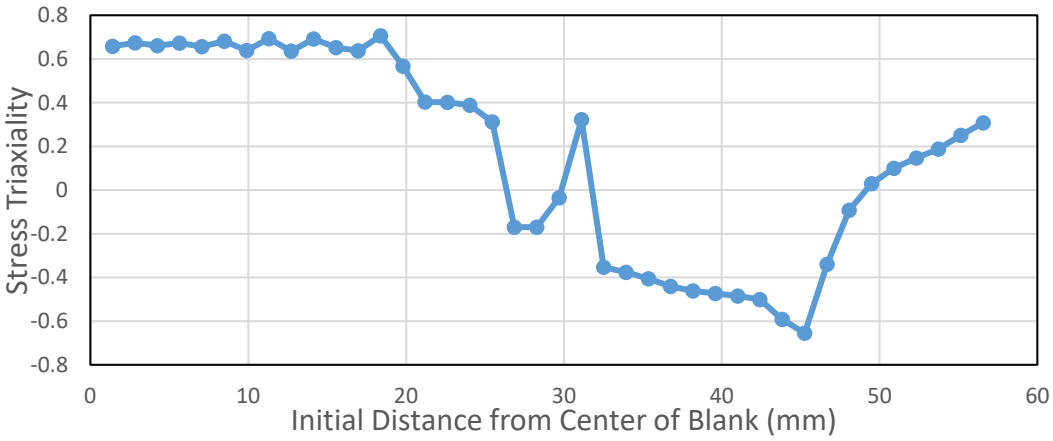

(b)

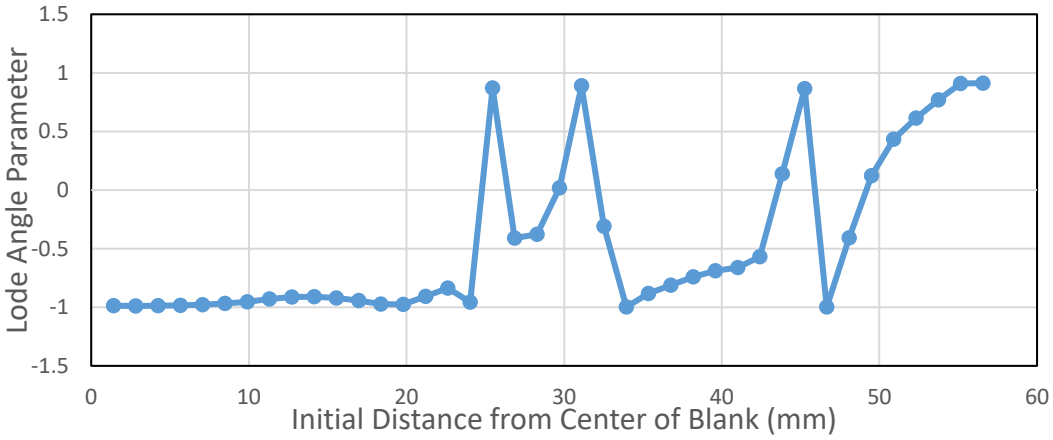

(c)

Figure 5.84. The variation of (a) Equivalent Plastic Strain (b) Stress Triaxiality and (c) Lode Angle Parameter along the diagonal of the blank at 6 mm cup depth for Al2024 aluminum (Hill'48-Disc-JC)

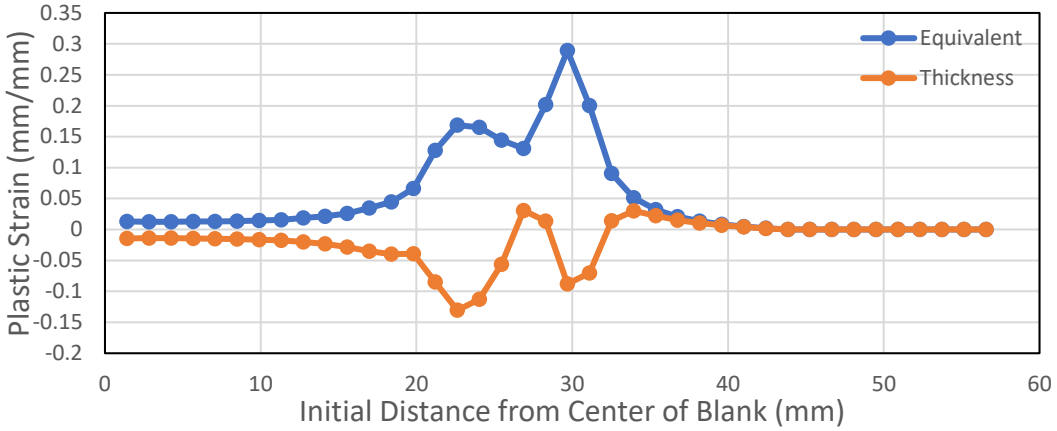

(a)

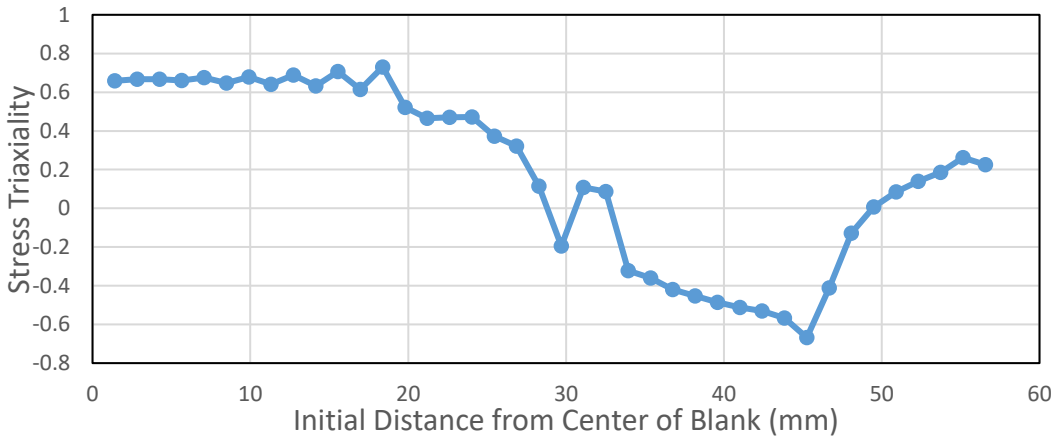

(b)

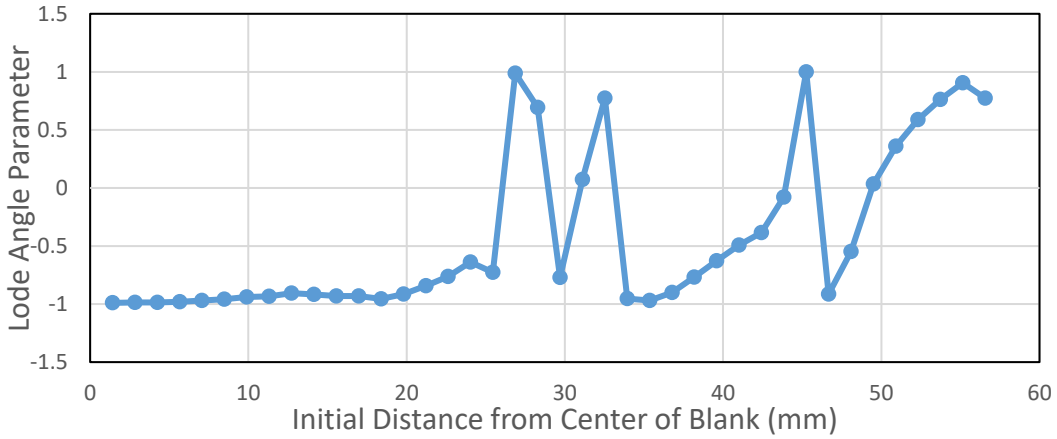

(c)

Figure 5.85. The variation of (a) Equivalent Plastic Strain and Thickness Plastic Strain (b) Stress Triaxiality and (c) Lode Angle Parameter along the diagonal of the blank at 8 mm cup depth for Al2024 aluminum (Hill'48-Disc-JC)

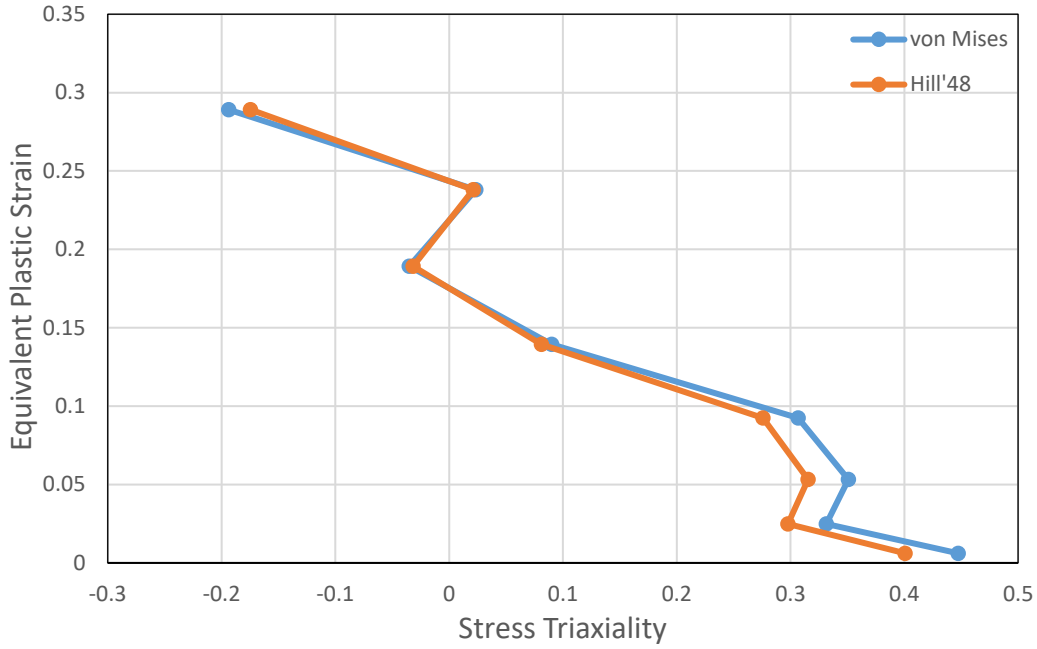

Figure 5.86. Equivalent Plastic Strain - Stress Triaxiality Plot of First Rupture Element (Hill'48-Disc-JC)

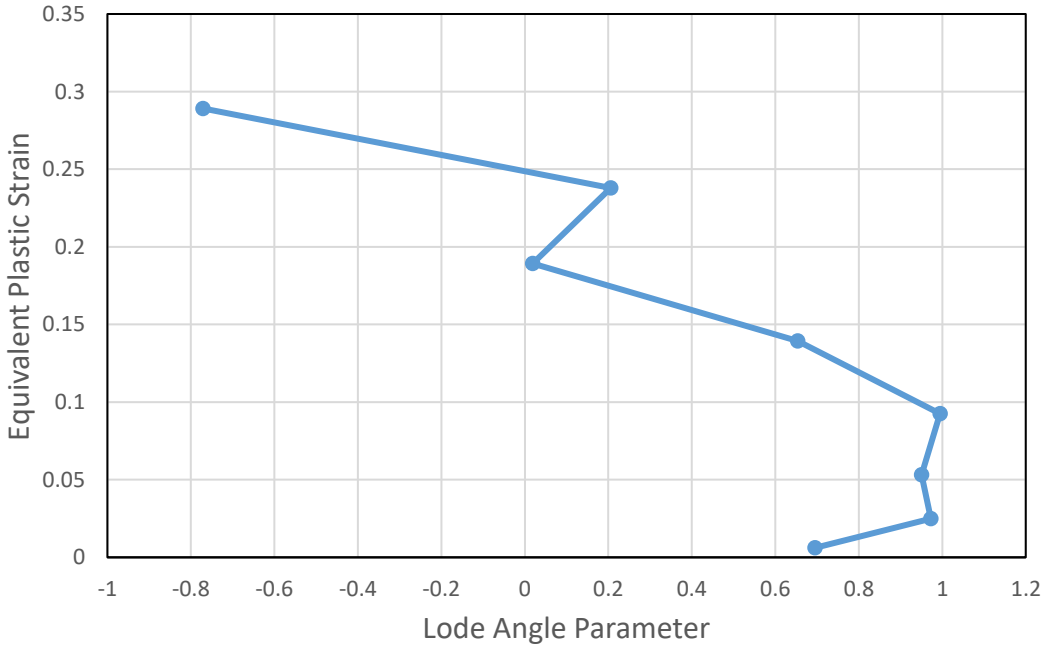

Figure 5.87. Equivalent Plastic Strain – Lode Angle Parameter Plot of First Rupture Element (Hill'48-Disc-JC)

In the rolling direction, the triaxiality values vary generally between 0.6 and 0.8 under the punch whereas the Lode angle parameter values change between -0.5 and -1. Up to the punch shoulder, it can be said that the deformation behavior is in equi-biaxial tension condition. However, for 2 mm punch travel the compressive punch force on the sheet surface dominates towards the punch shoulder where triaxiality values change towards negative where Lode angle parameter values show the same tendency. Here, only in the regions close to the center of the blank i.e., up to a distance of 5 mm from the center, the equi-biaxial tension conditions are observed. As the punch continues to move, the region with equi-biaxial tension conditions extend and reaches 10 mm from the center of the blank. When the pre-rupture state of sheet is examined, it is seen that equi-biaxial stress conditions dominates up to 15 mm from the center of the blank. At the punch shoulder triaxiality values are still positive but decreasing as the distance increases from the blank center. On the other hand, the Lode angle parameter values increases as with distance from the center of the blank. Hence, there is a tensile type deformation in this region. At the clearance between die and punch thinning continues. At the die shoulder, the triaxiality values are mostly positive with varying Lode angle parameter values. The deformation nature begins to change towards thickening. Under the blank holder the triaxiality values and Lode angle parameter values are negative, indicating thickening towards the rim.

The same tendency of rolling direction is observed in the transverse direction also. The differences are a result of anisotropy of the material.

In the diagonal direction, as in the transverse and rolling directions, equi-biaxial stress condition is observed under the punch. Still, for 2 mm punch travel the compressive punch force on the sheet surface dominates towards the punch corner. Here, the triaxiality values change towards negative whereas Lode angle parameter values show the same tendency. Only in the regions close to the center of the blank i.e., up to a distance of 5 mm from the center, the equi-biaxial tension conditions are observed. At the punch corner, triaxiality values are still positive but decreasing and the Lode angle parameter values are increasing, as the distance increases from the

blank center. Hence there is a tensile type deformation in this region. At the clearance between die and punch thinning continues, by changing the nature of deformation from equi-biaxial tension towards unidirectional tension. At the die corner the triaxiality values start to became negative, indication compressive type deformation with the Lode angle parameter values. Under the blank holder, the triaxiality values are negative and decreases, and finally become positive, similarly negative Lode angle parameter values turn into positive, indicating thickening towards the rim where the nature of the deformation changes from uniaxial dominant compression to equi-biaxial dominant compression.

5.1.6 Case 6: Square-Al2024- Hill48-Discrete-Hosford Coulomb Model

For the sixth case, Hill'48 yield criterion was applied with discrete hardening and the Hosford Coulomb ductile fracture criterion was used. It was observed that the fracture had started after 12 mm punch travel as shown in Figure 5.88. The variation of equivalent plastic strain, stress triaxiality and Lode angle parameter values are presented as a function of the distance from the center of the blank for different cup heights up to the fracture. The results are shown for rolling direction in Figure 5.89 to Figure 5.94, for transverse direction in Figure 5.95 to Figure 5.100 and for diagonal direction in Figure 5.101 to Figure 5.106. The thickness plastic strain distribution is also inserted into Figure 5.106 (a) in order to better visualize the deformation. Further, the variations of stress triaxiality values with respect to equivalent plastic strain are given by considering both von Mises and Hill'48 criteria as a function of the path of the element that fractured first in Figure 5.107. Along the same path, the variation of the Lode parameter with respect to equivalent plastic strain is also illustrated in Figure 5.108.

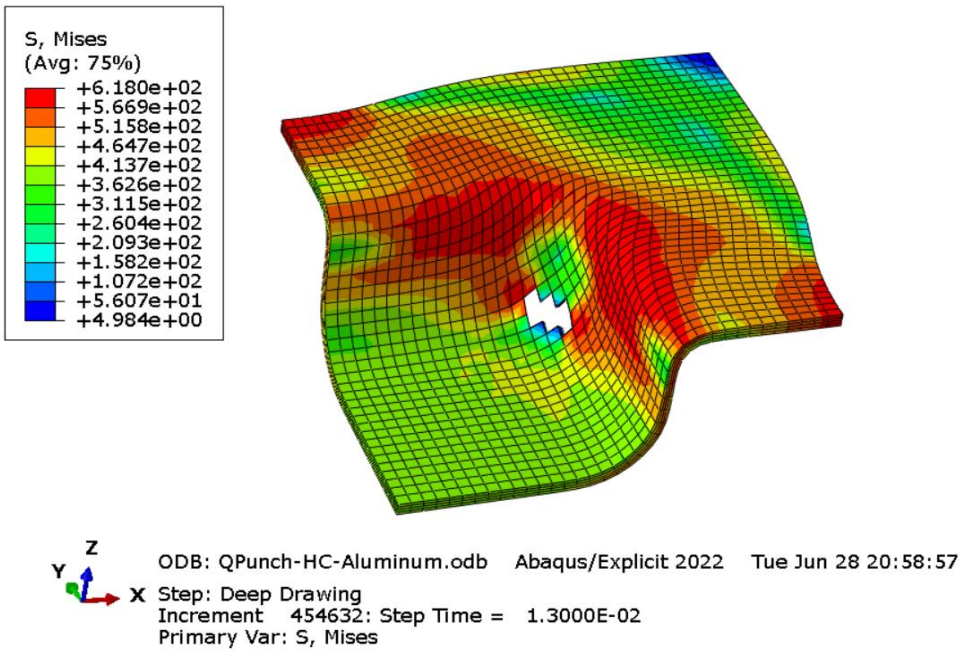

Figure 5.88. First Rupture Moment of Case 6

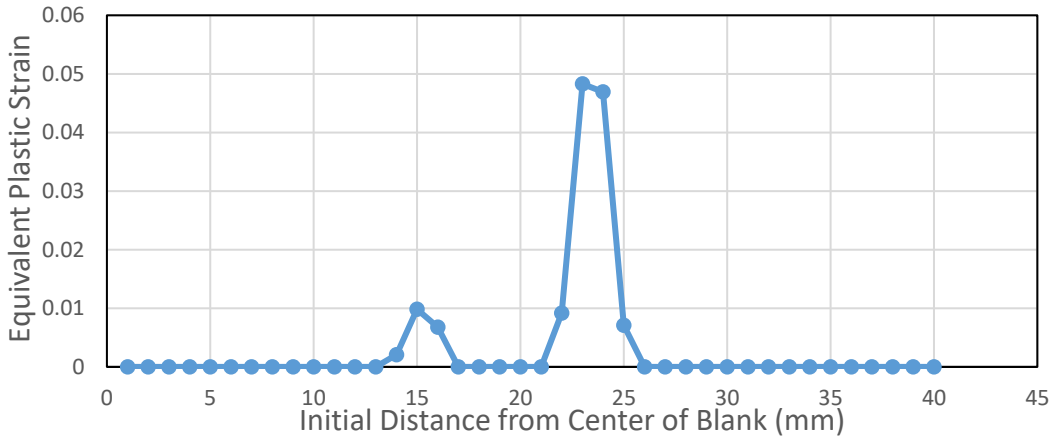

(a)

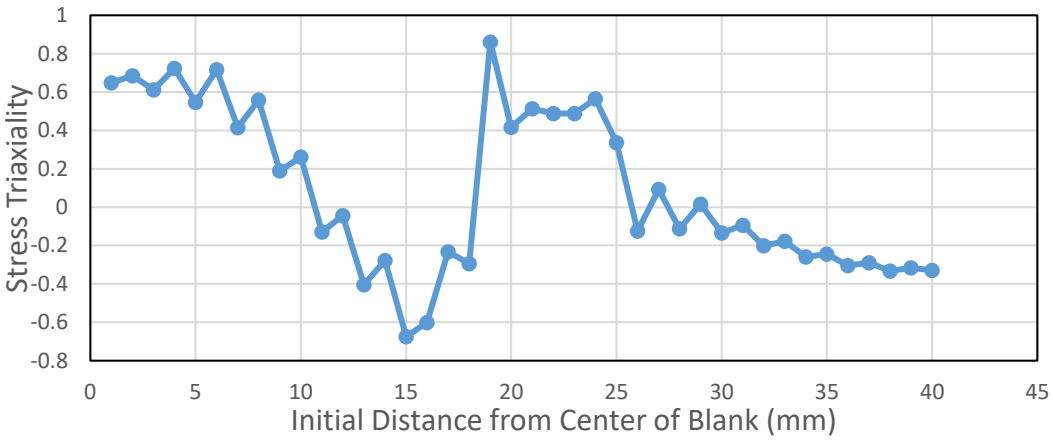

(b)

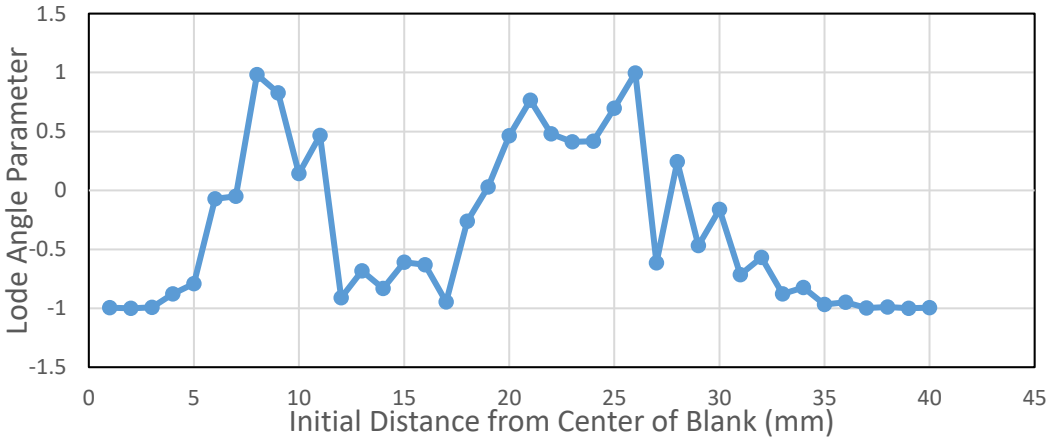

(c)

Figure 5.89. The variation of (a) Equivalent Plastic Strain (b) Stress Triaxiality and (c) Lode Angle Parameter along the rolling direction of the blank at 2 mm cup depth for Al2024 aluminum (Hill'48-Disc-HC)

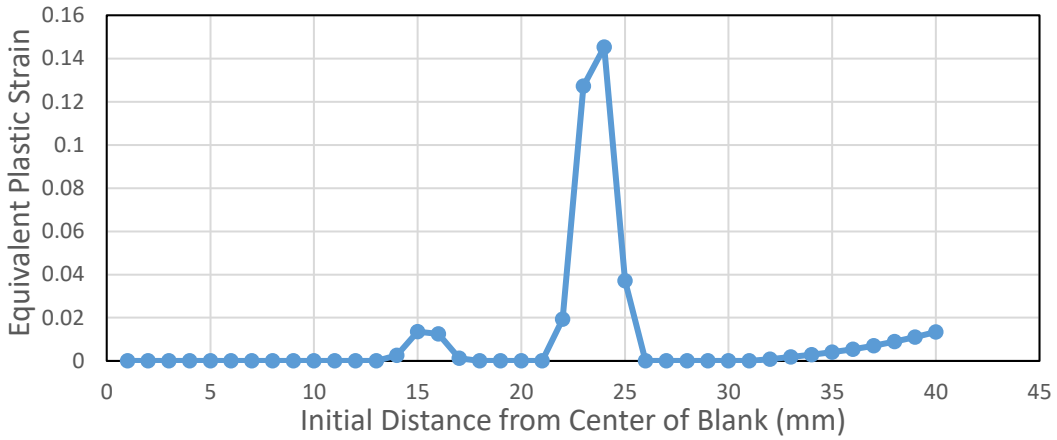

(a)

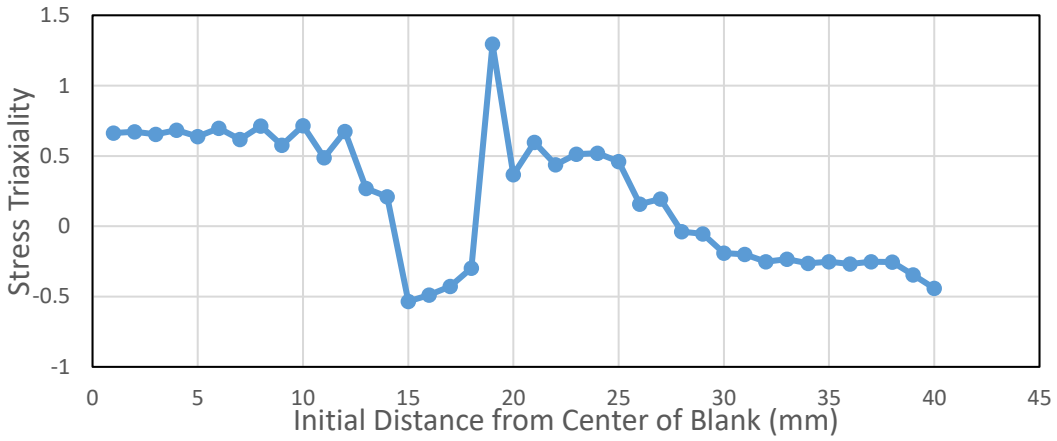

(b)

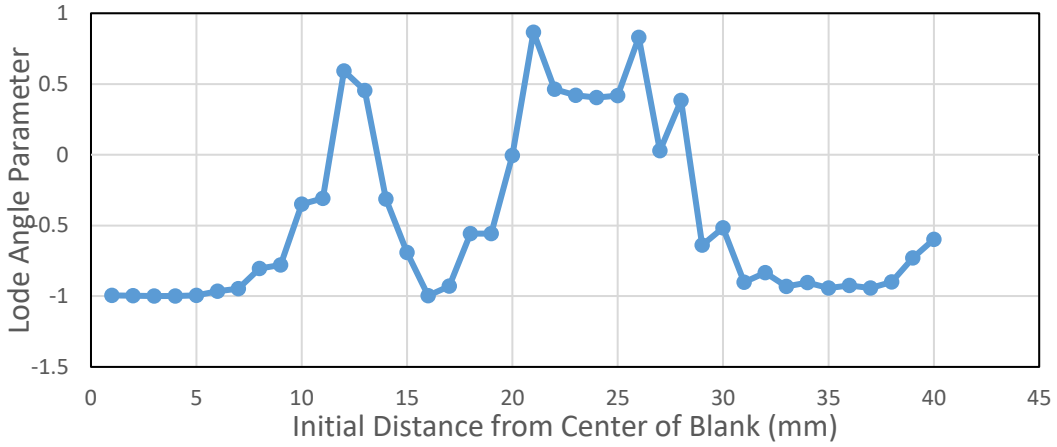

(c)

Figure 5.90. The variation of (a) Equivalent Plastic Strain (b) Stress Triaxiality and (c) Lode Angle Parameter along the rolling direction of the blank at 4 mm cup depth for Al2024 aluminum (Hill'48-Disc-HC)

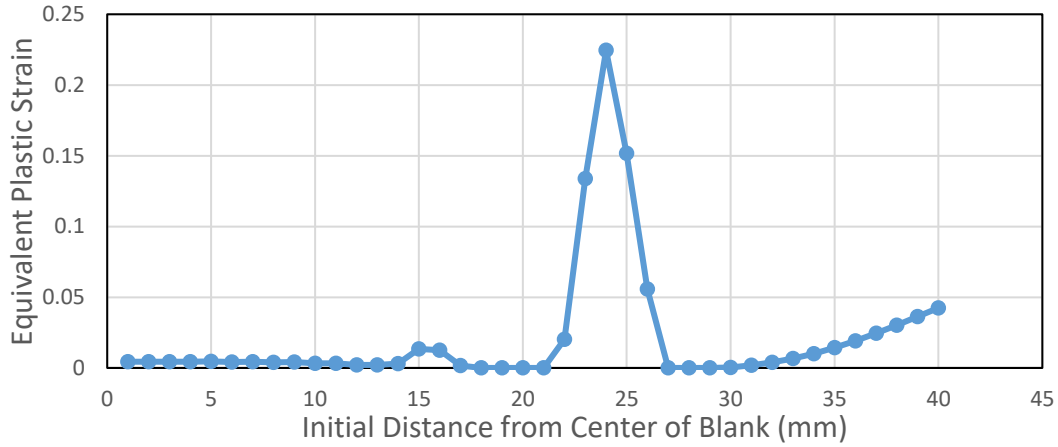

(a)

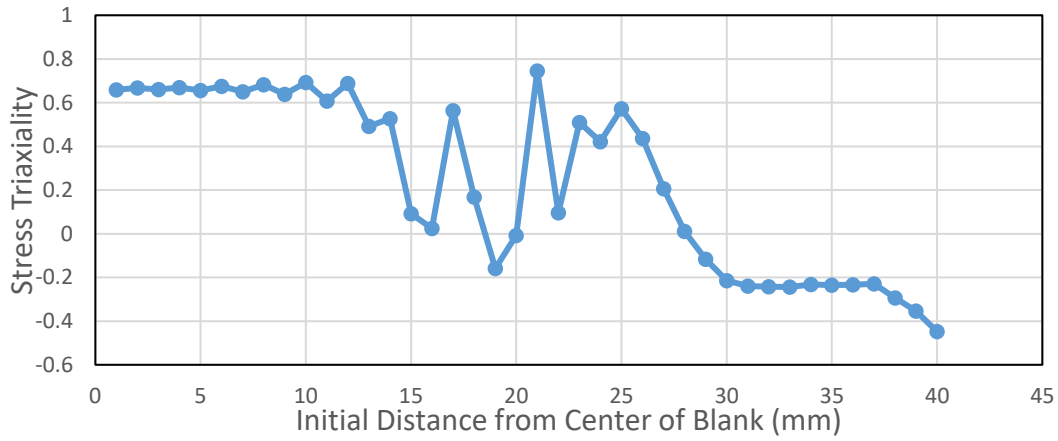

(b)

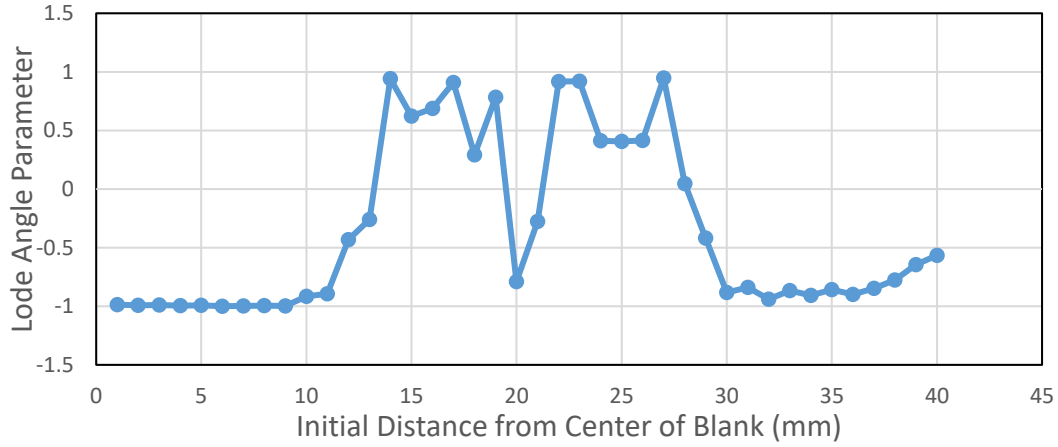

(c)

Figure 5.91. The variation of (a) Equivalent Plastic Strain (b) Stress Triaxiality and (c) Lode Angle Parameter along the rolling direction of the blank at 6 mm cup depth for Al2024 aluminum (Hill'48-Disc-HC)

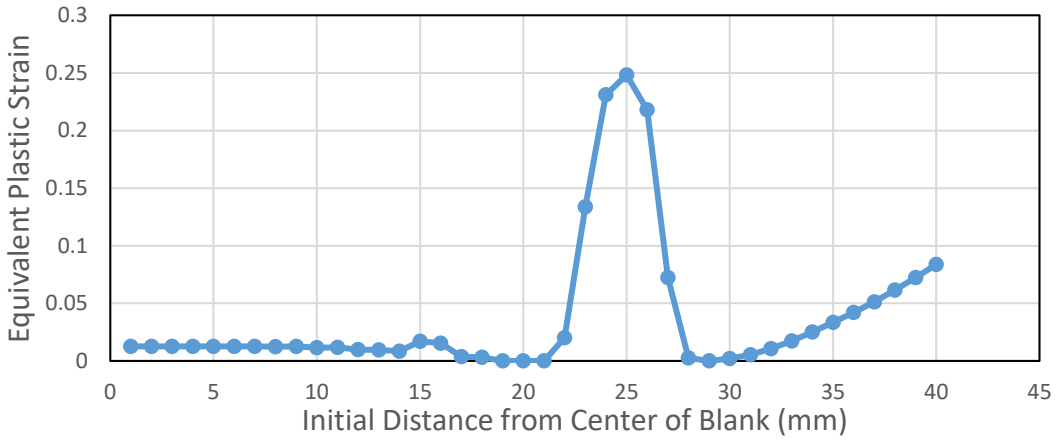

(a)

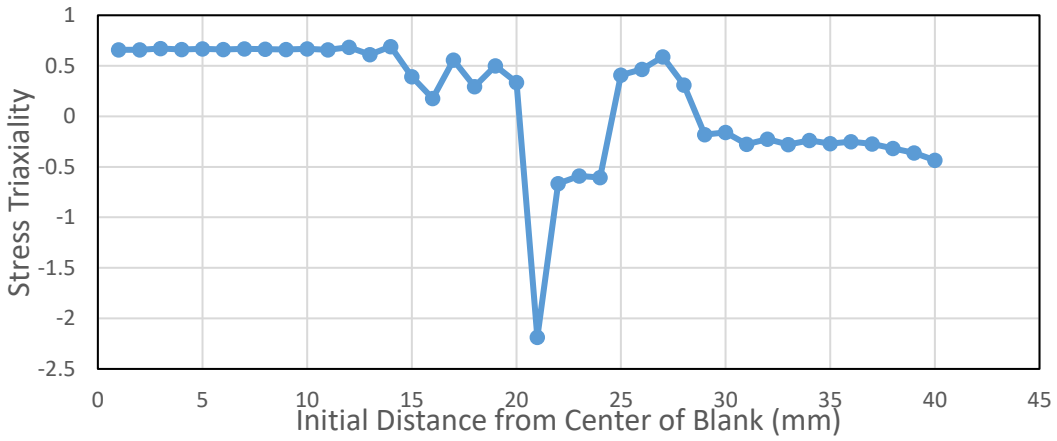

(b)

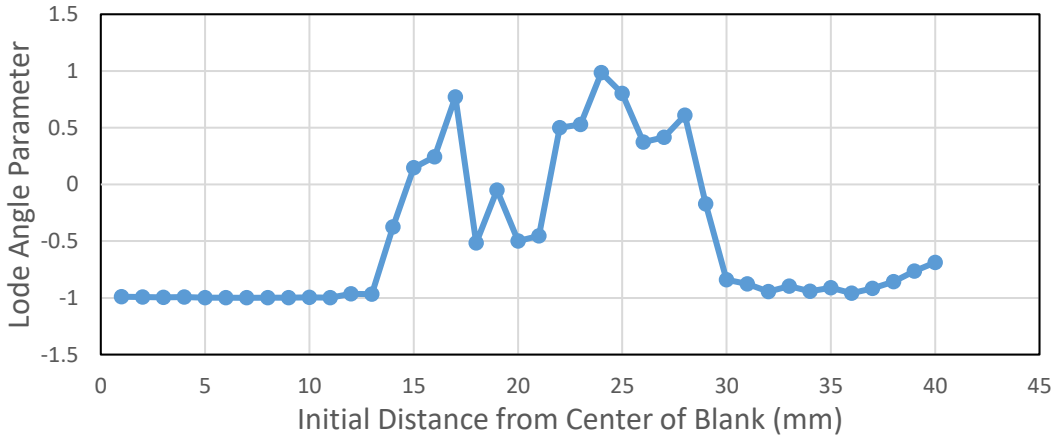

(c)

Figure 5.92. The variation of (a) Equivalent Plastic Strain (b) Stress Triaxiality and (c) Lode Angle Parameter along the rolling direction of the blank at 8 mm cup depth for Al2024 aluminum (Hill'48-Disc-HC)

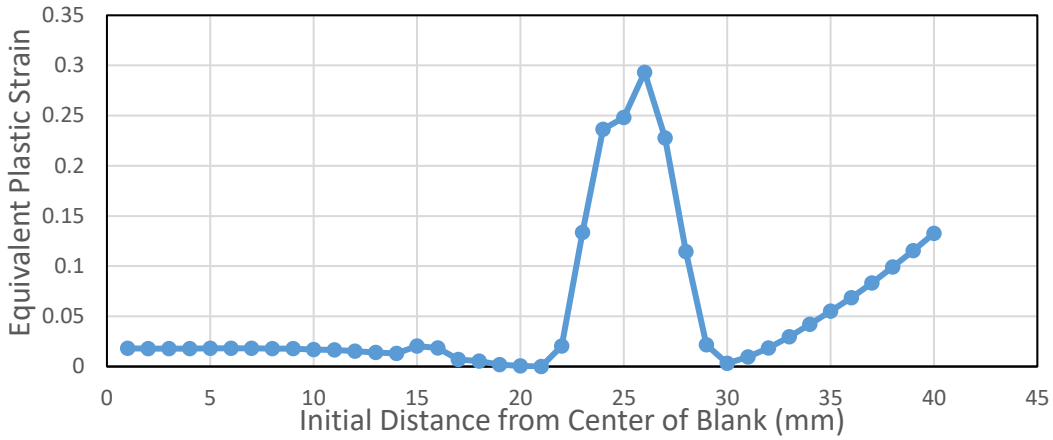

(a)

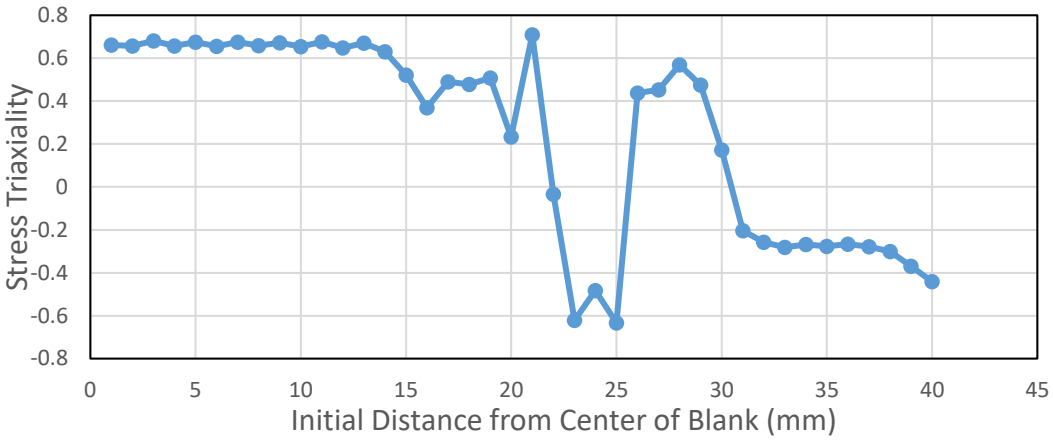

(b)

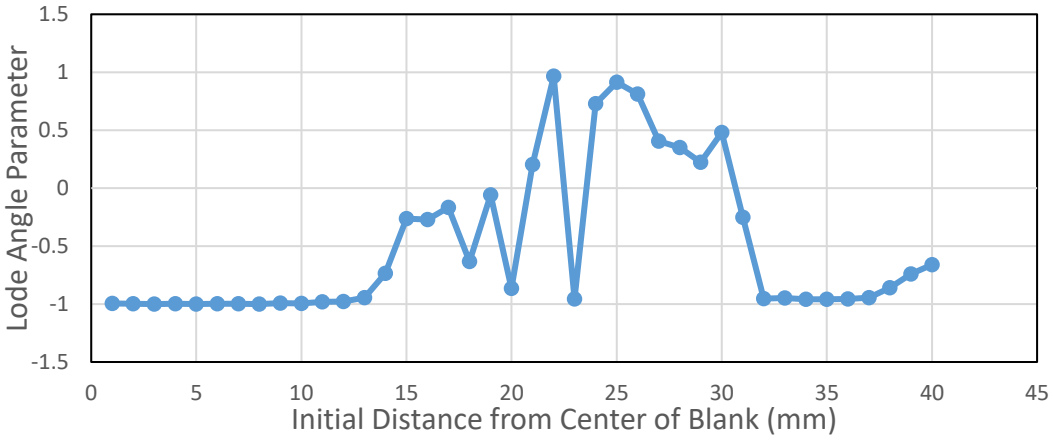

(c)

Figure 5.93. The variation of (a) Equivalent Plastic Strain (b) Stress Triaxiality and (c) Lode Angle Parameter along the rolling direction of the blank at 10 mm cup depth for Al2024 aluminum (Hill'48-Disc-HC)

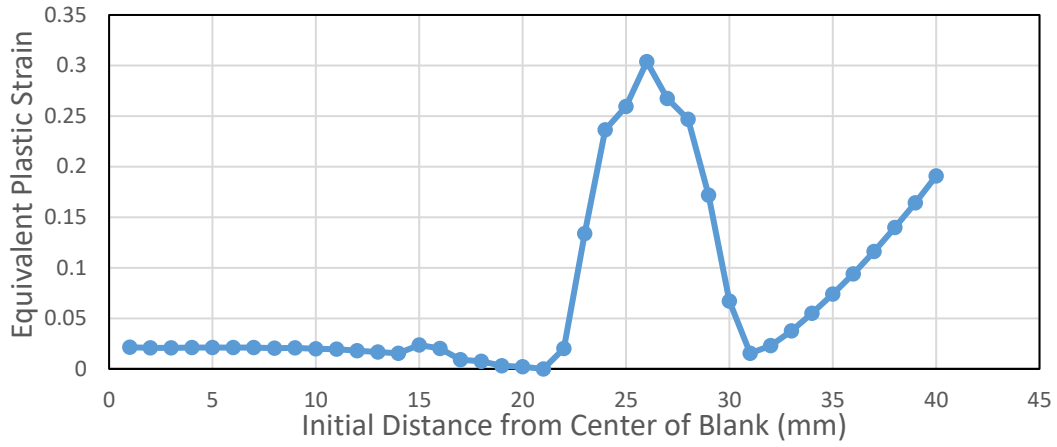

(a)

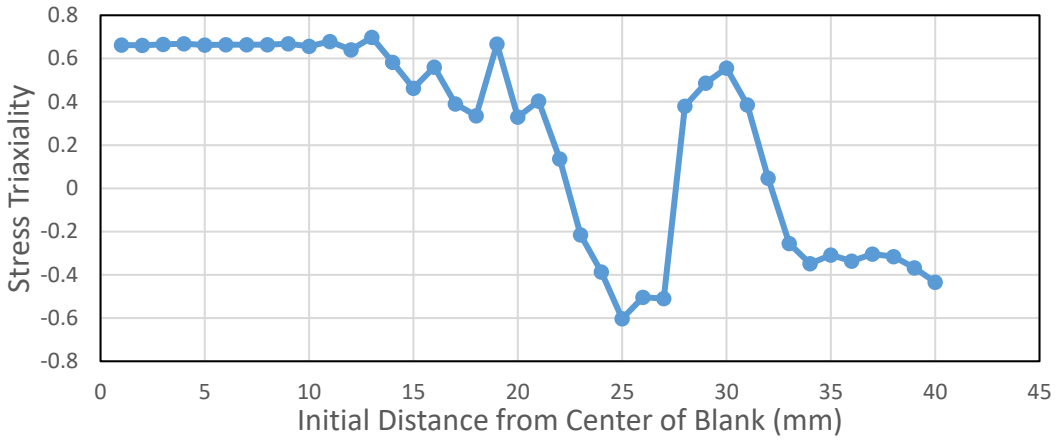

(b)

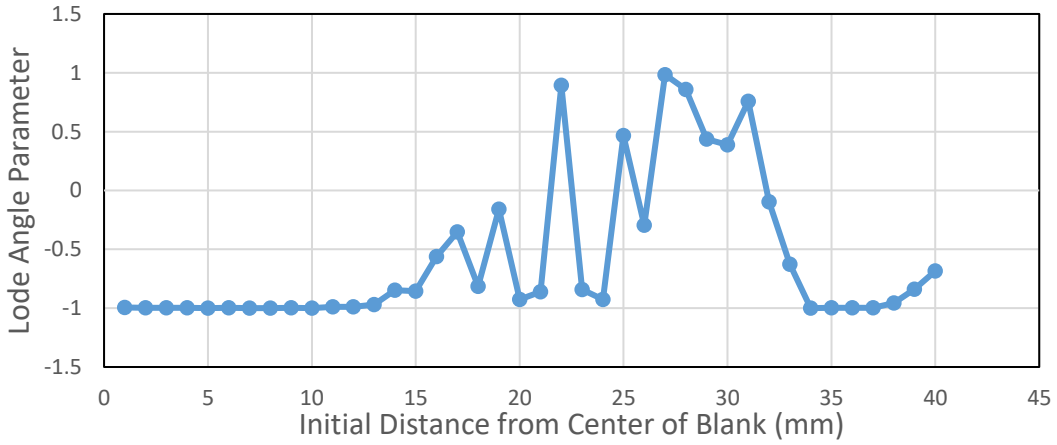

(c)

Figure 5.94 The variation of (a) Equivalent Plastic Strain (b) Stress Triaxiality and (c) Lode Angle Parameter along the rolling direction of the blank at 12 mm cup depth for Al2024 aluminum (Hill'48-Disc-HC)

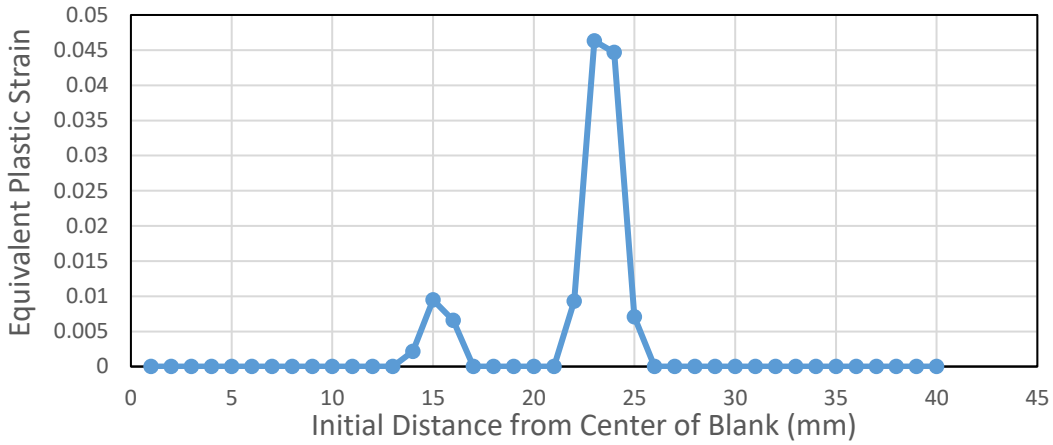

(a)

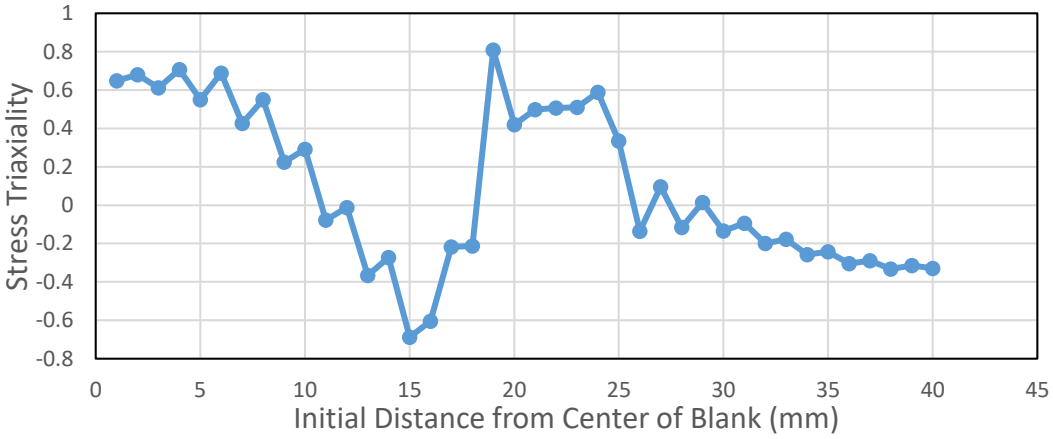

(b)

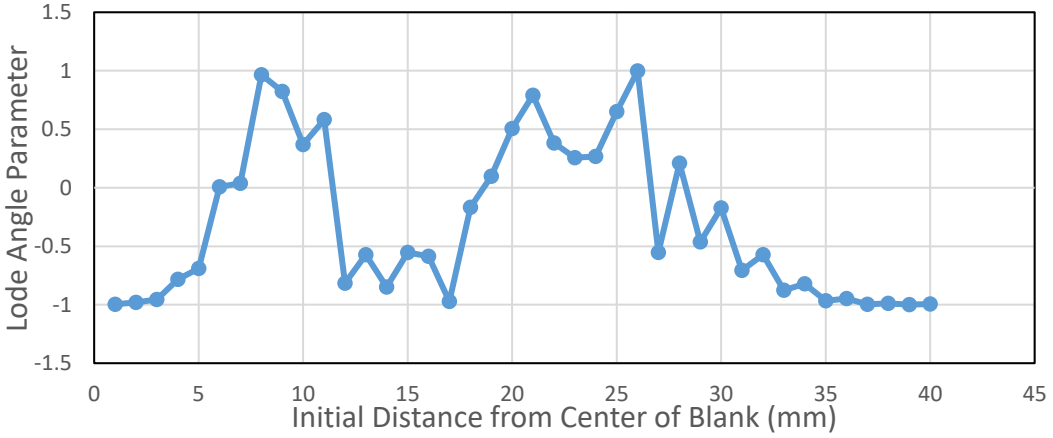

(c)

Figure 5.95. The variation of (a) Equivalent Plastic Strain (b) Stress Triaxiality and (c) Lode Angle Parameter along the transverse direction of the blank at 2 mm cup depth for Al2024 aluminum (Hill'48-Disc-HC)

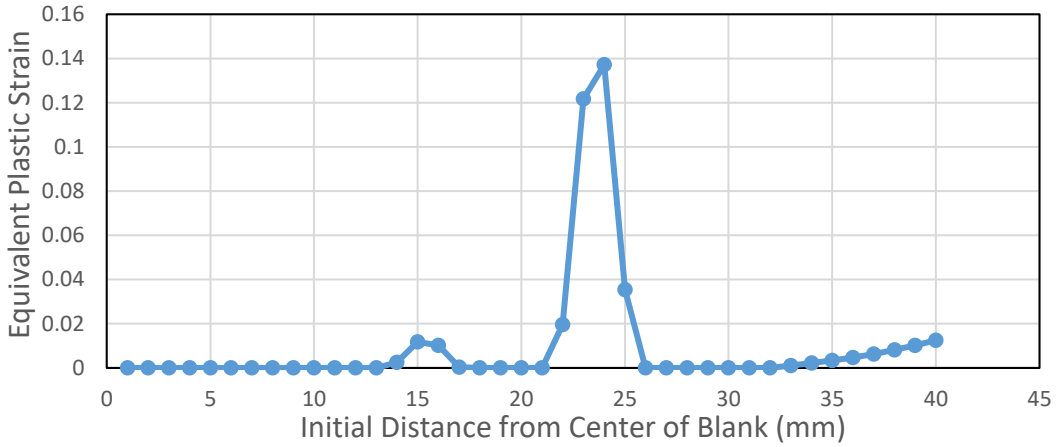

(a)

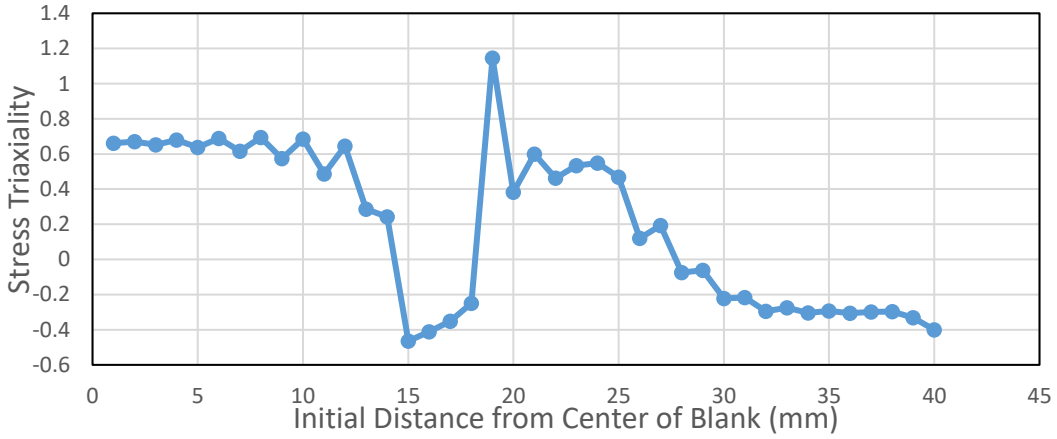

(b)

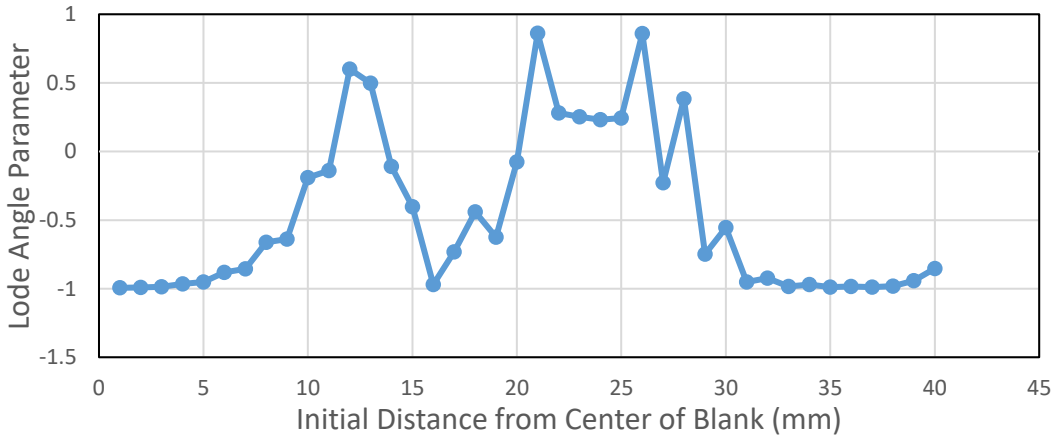

(c)

Figure 5.96. The variation of (a) Equivalent Plastic Strain (b) Stress Triaxiality and (c) Lode Angle Parameter along the transverse direction of the blank at 4 mm cup depth for Al2024 aluminum (Hill'48-Disc-HC)

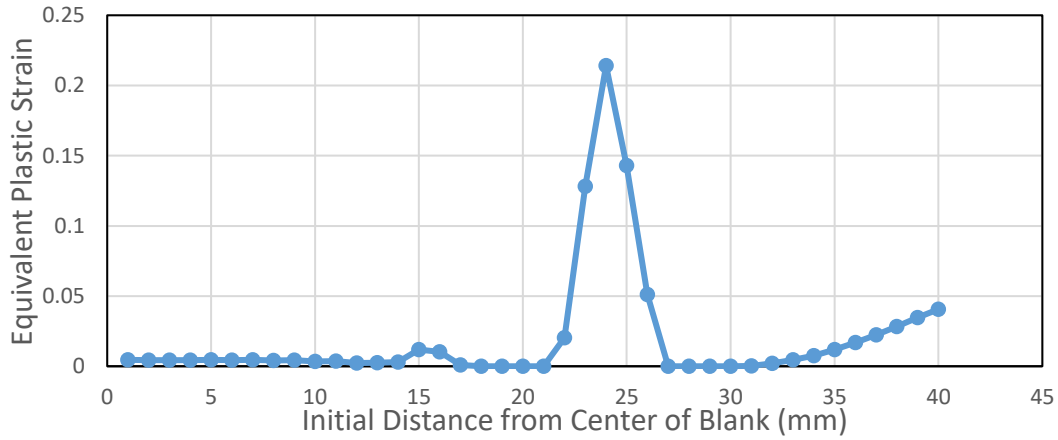

(a)

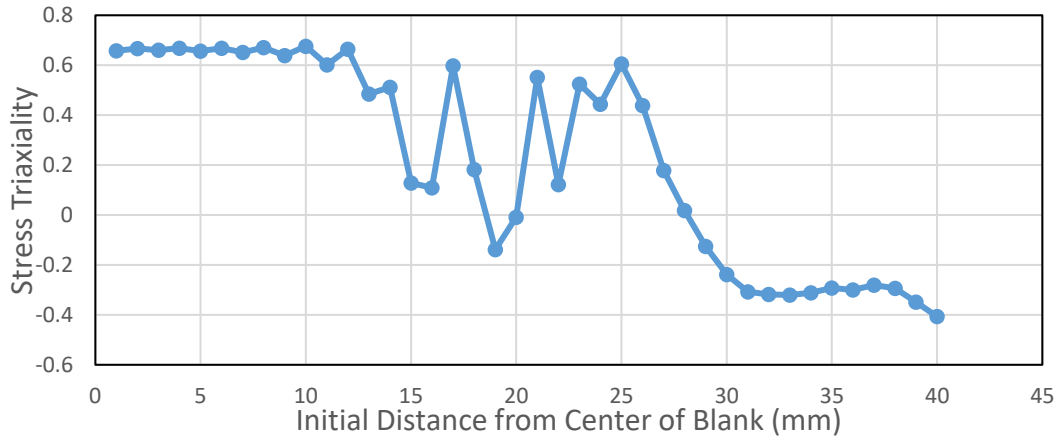

(b)

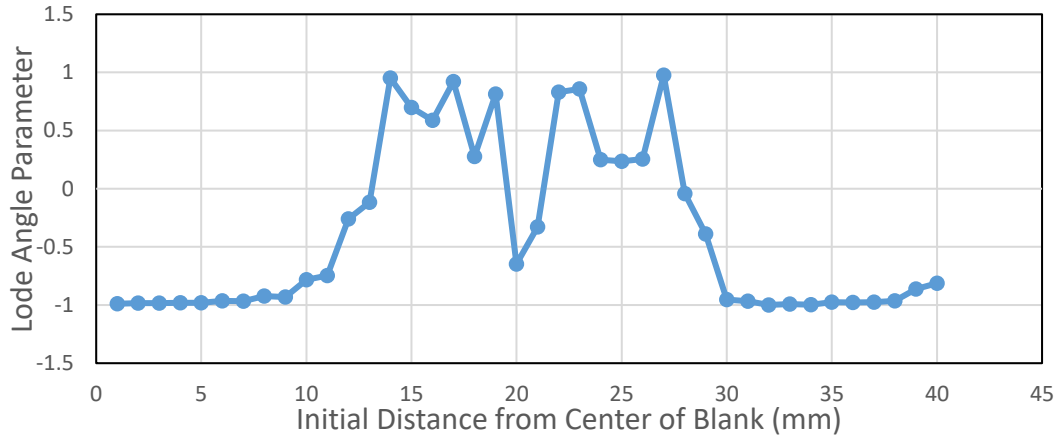

(c)

Figure 5.97. The variation of (a) Equivalent Plastic Strain (b) Stress Triaxiality and (c) Lode Angle Parameter along the transverse direction of the blank at 6 mm cup depth for Al2024 aluminum (Hill'48-Disc-HC)

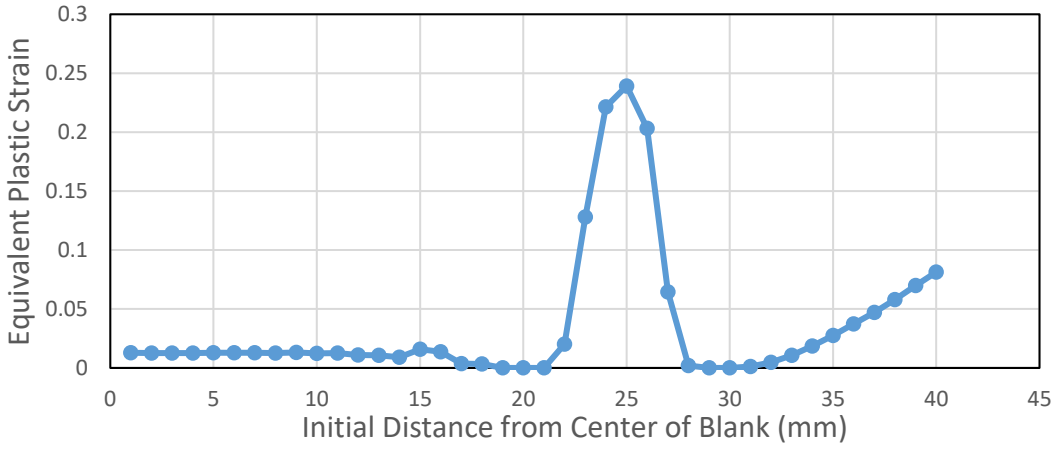

(a)

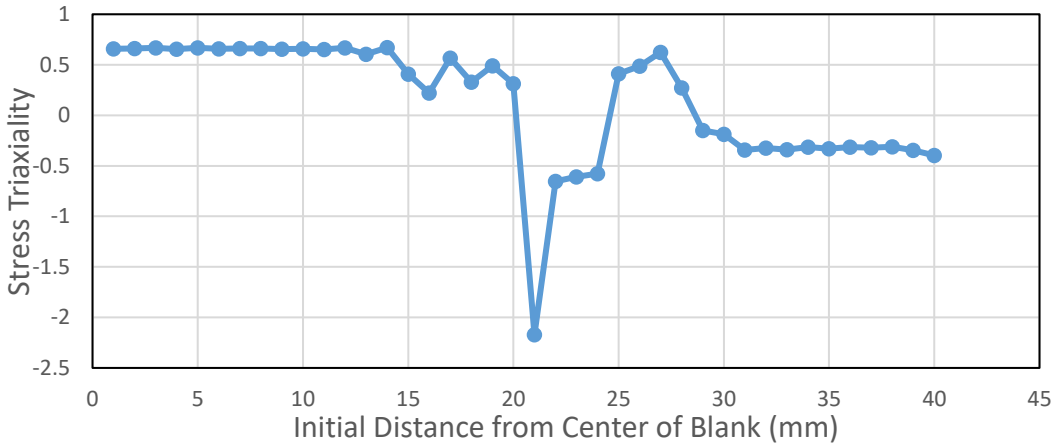

(b)

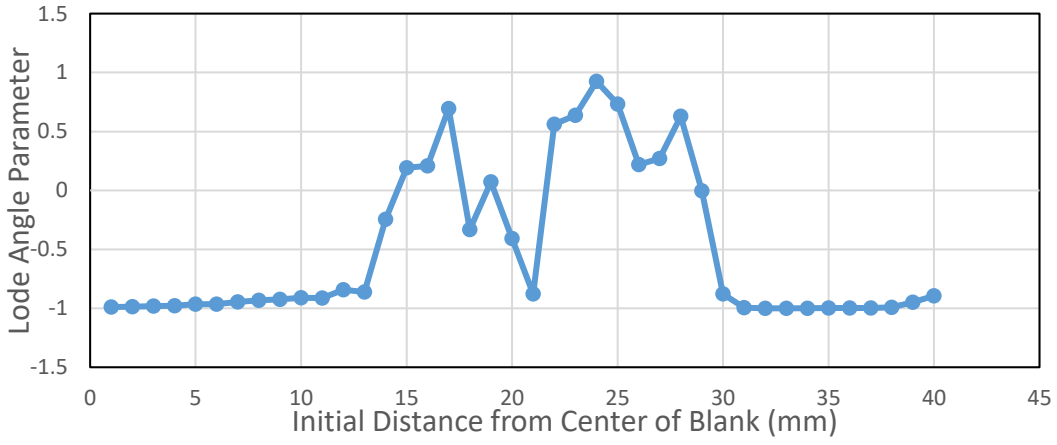

(c)

Figure 5.98. The variation of (a) Equivalent Plastic Strain (b) Stress Triaxiality and (c) Lode Angle Parameter along the transverse direction of the blank at 8 mm cup depth for Al2024 aluminum (Hill'48-Disc-HC)

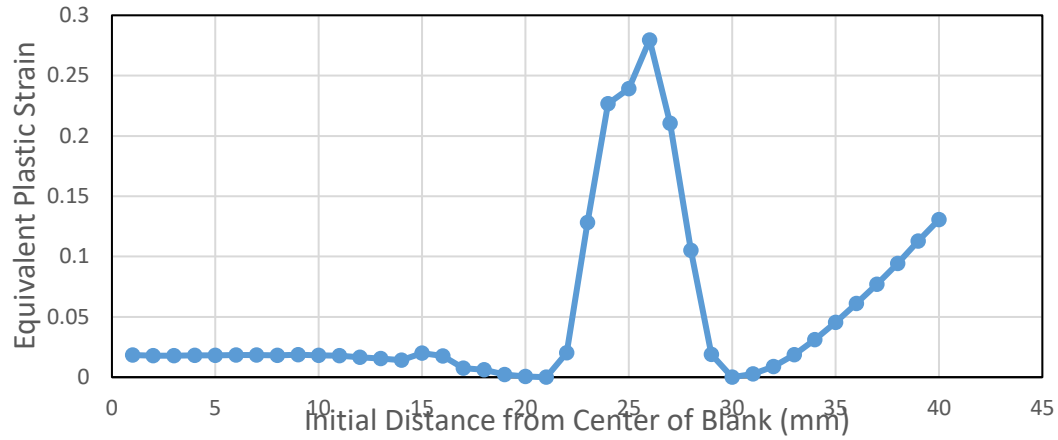

(a)

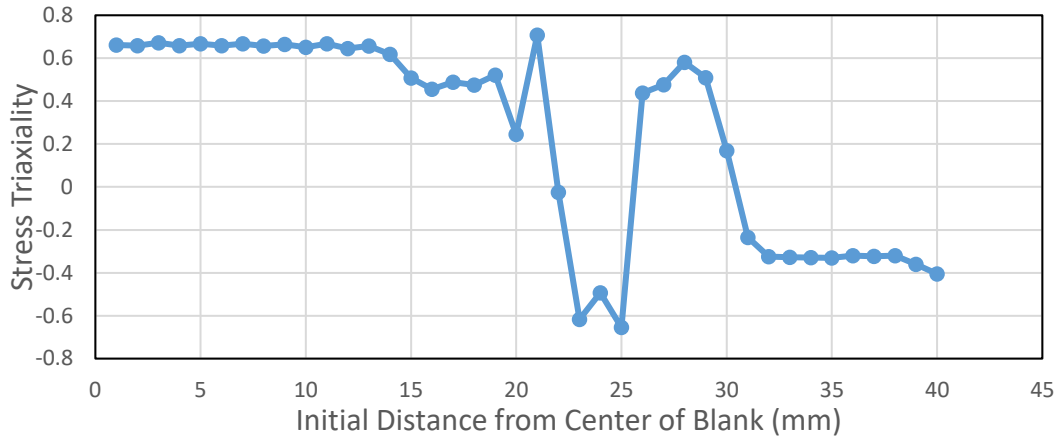

(b)

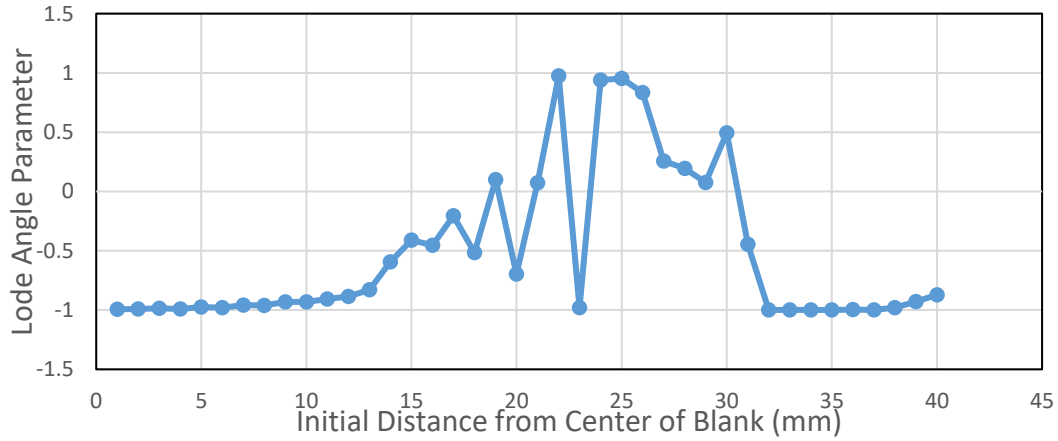

(c)

Figure 5.99. The variation of (a) Equivalent Plastic Strain (b) Stress Triaxiality and (c) Lode Angle Parameter along the transverse direction of the blank at 10 mm cup depth for Al2024 aluminum (Hill'48-Disc-HC)

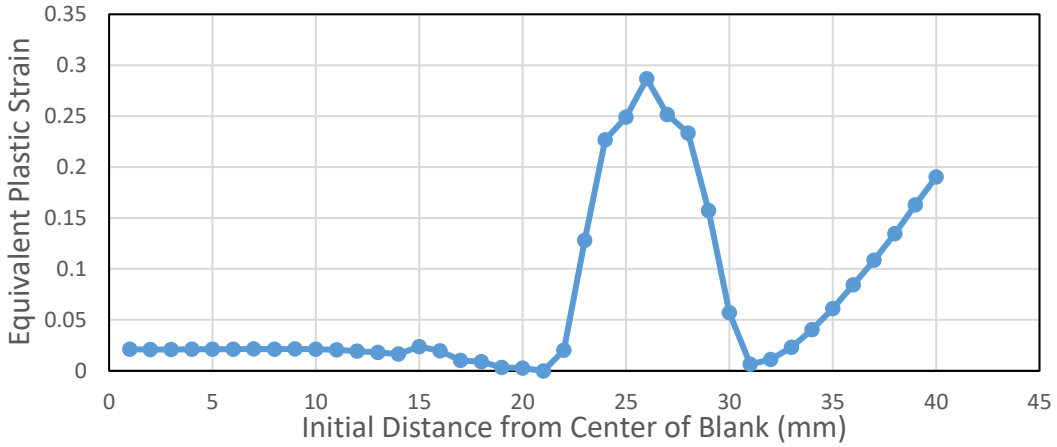

(a)

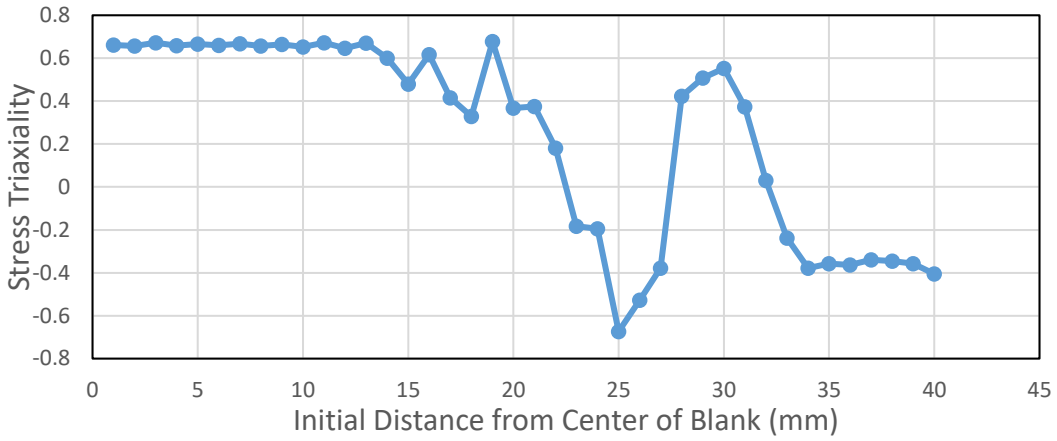

(b)

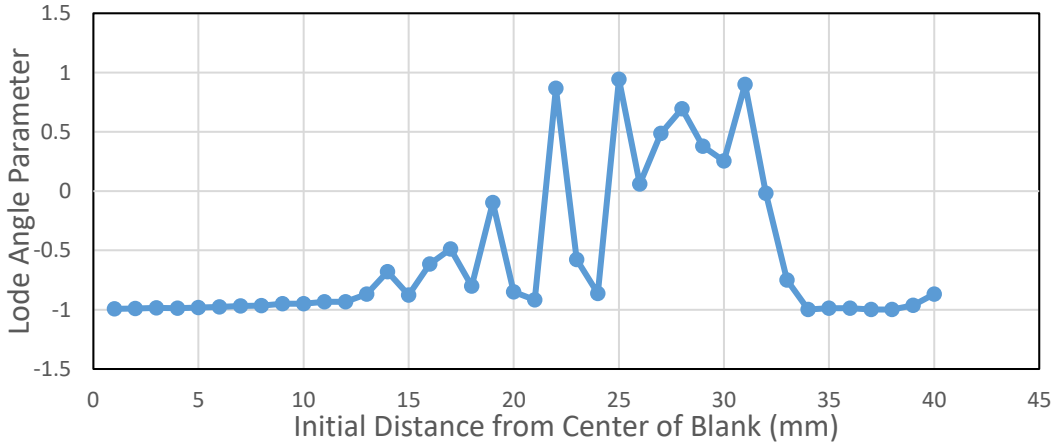

(c)

Figure 5.100. The variation of (a) Equivalent Plastic Strain (b) Stress Triaxiality and (c) Lode Angle Parameter along the transverse direction of the blank at 12 mm cup depth for Al2024 aluminum (Hill'48-Disc-HC)

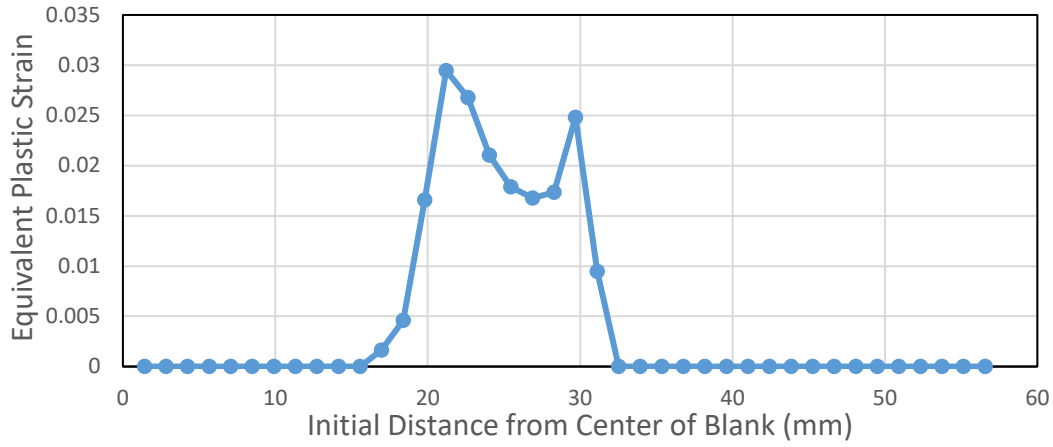

(a)

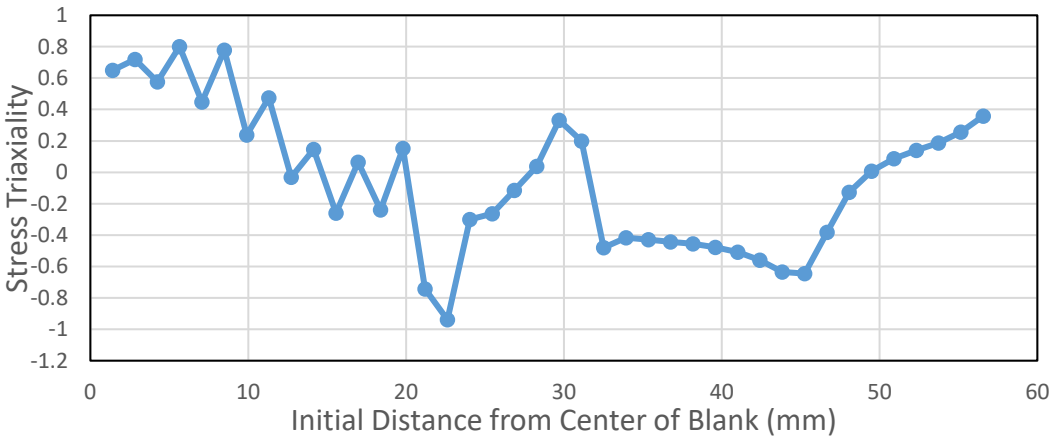

(b)

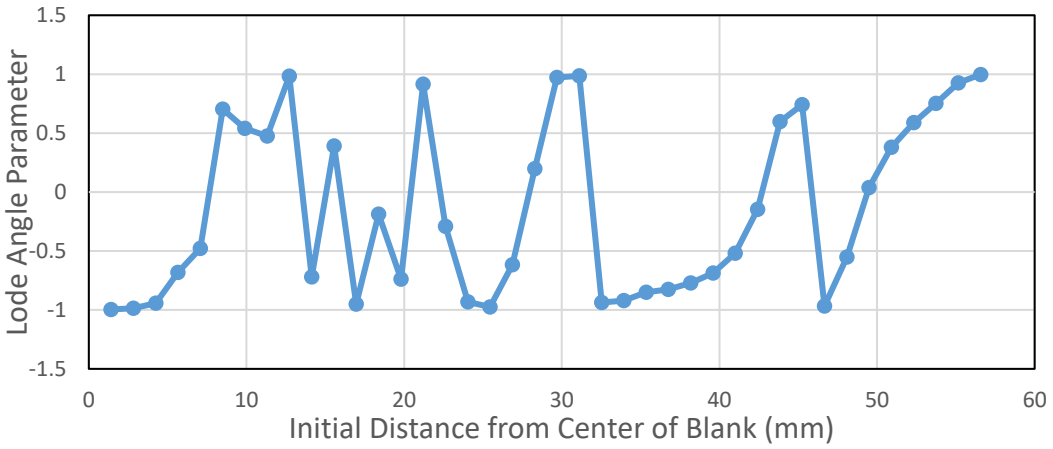

(c)

Figure 5.101. The variation of (a) Equivalent Plastic Strain (b) Stress Triaxiality and (c) Lode Angle Parameter along the diagonal of the blank at 2 mm cup depth for Al2024 aluminum (Hill'48-Disc-HC)

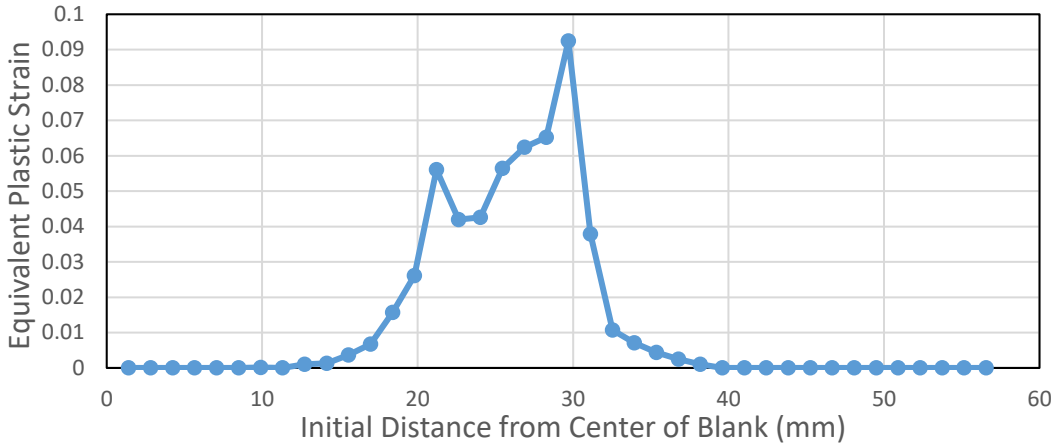

(a)

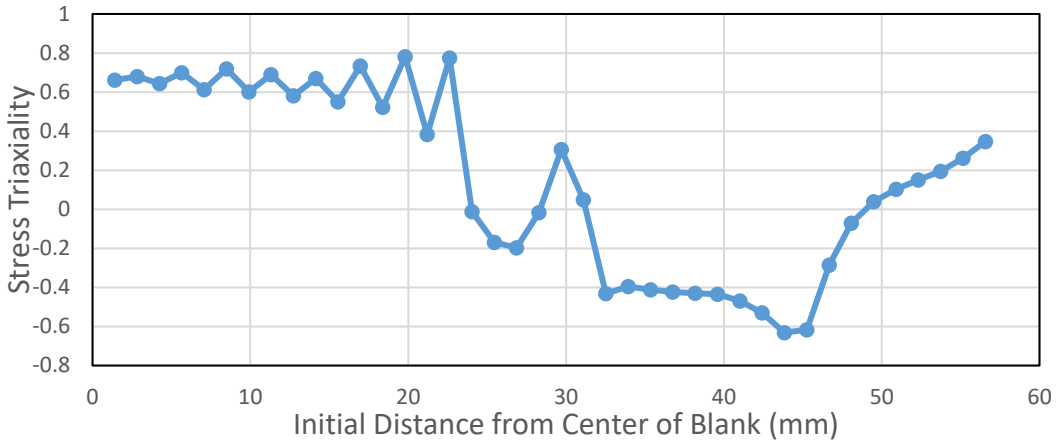

(b)

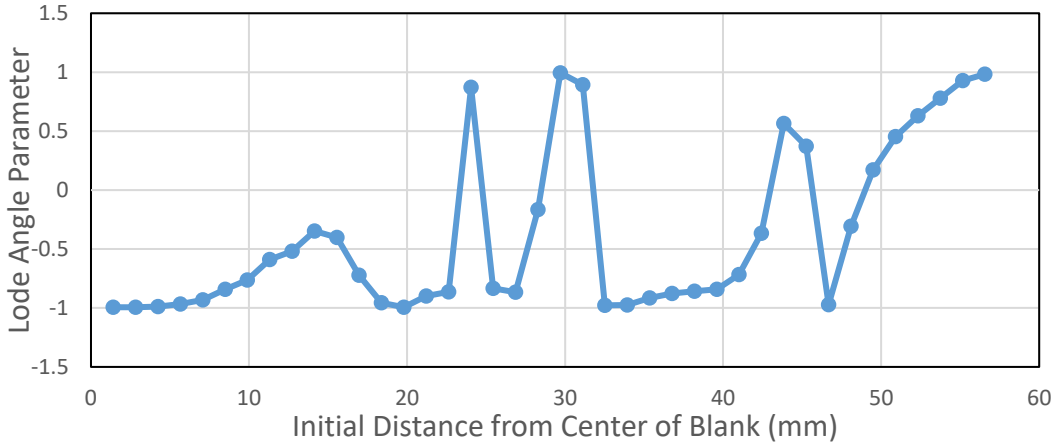

(c)

Figure 5.102. The variation of (a) Equivalent Plastic Strain (b) Stress Triaxiality and (c) Lode Angle Parameter along the diagonal of the blank at 4 mm cup depth for Al2024 aluminum (Hill'48-Disc-HC)

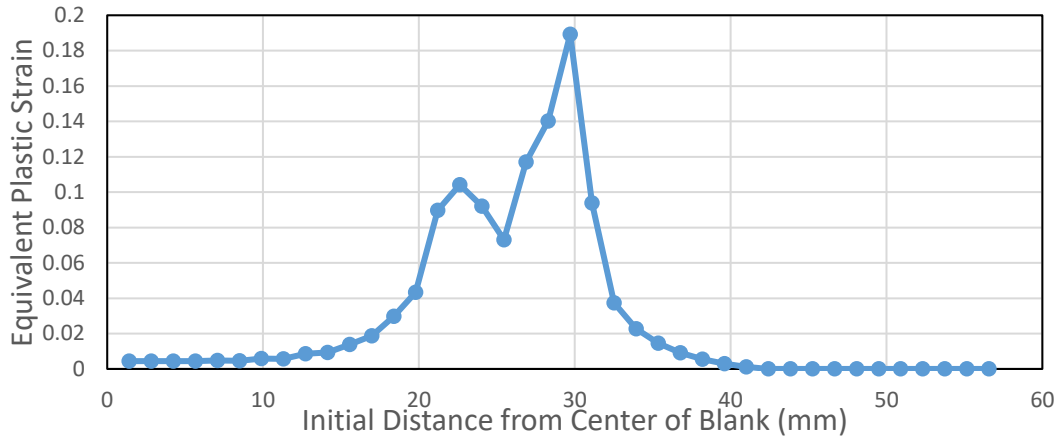

(a)

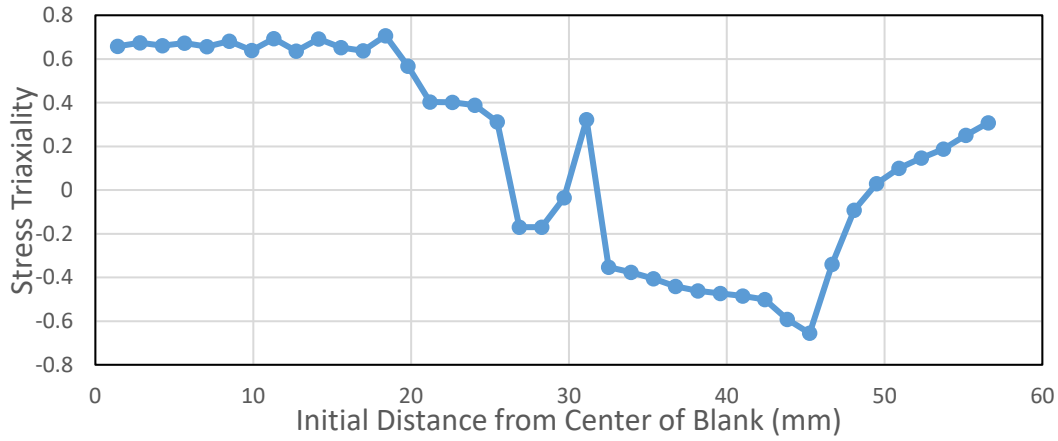

(b)

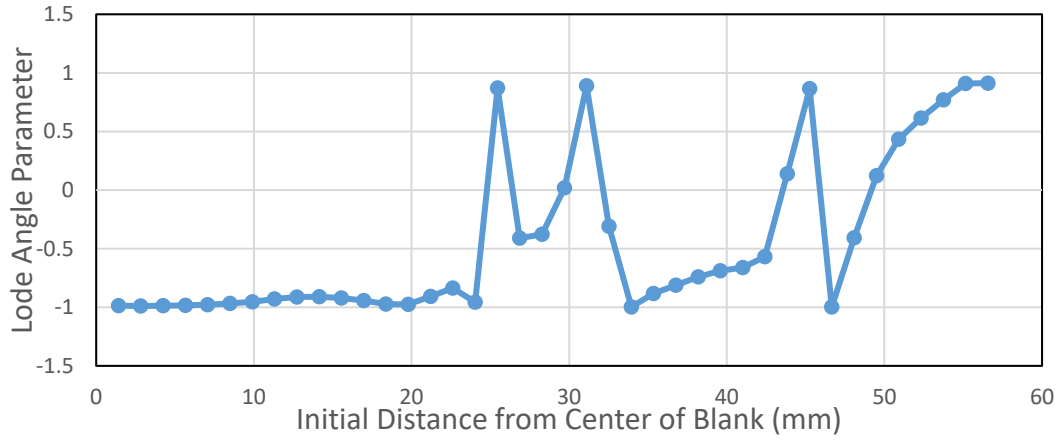

(c)

Figure 5.103 The variation of (a) Equivalent Plastic Strain (b) Stress Triaxiality and (c) Lode Angle Parameter along the diagonal of the blank at 6 mm cup depth for Al2024 aluminum (Hill'48-Disc-HC)

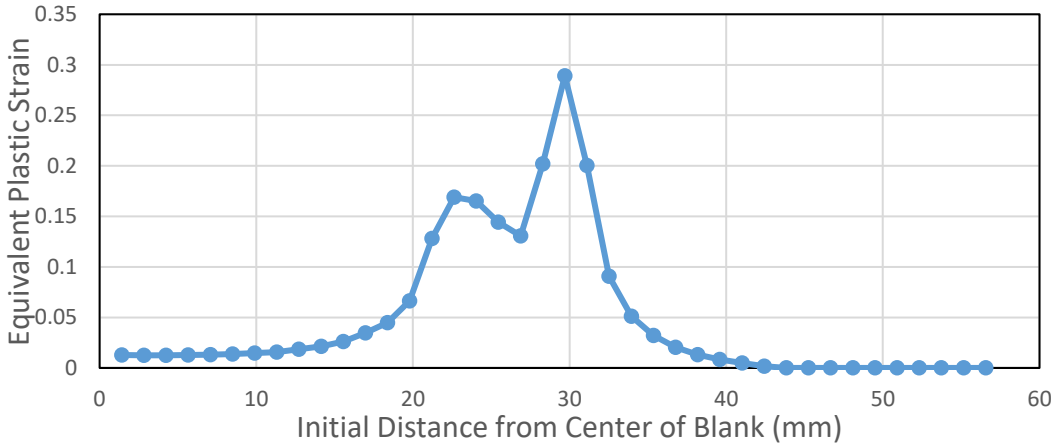

(a)

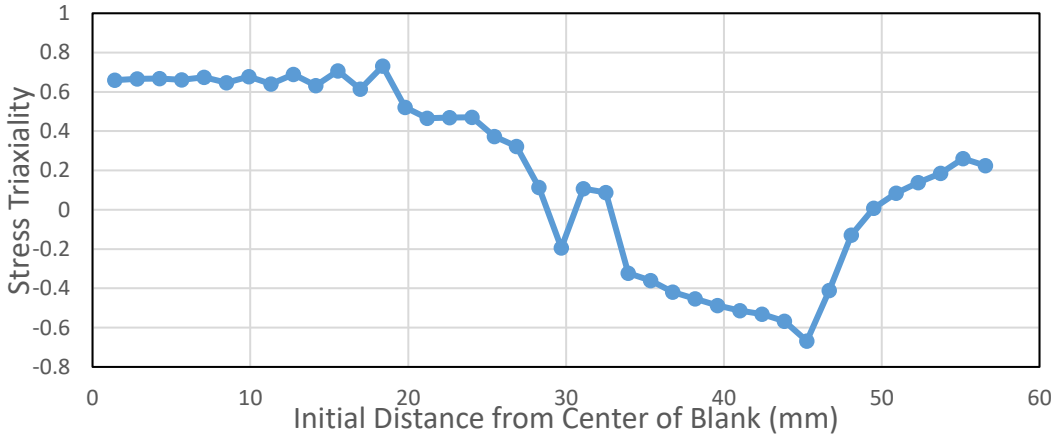

(b)

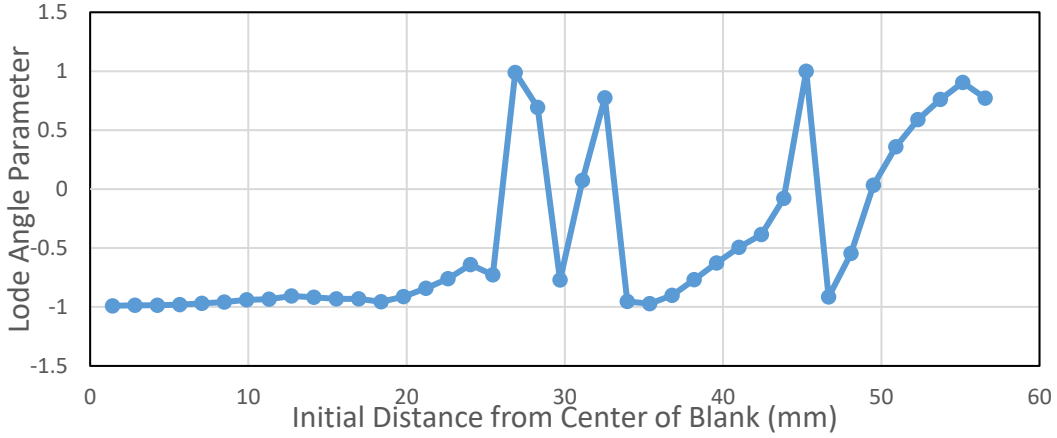

(c)

Figure 5.104 The variation of (a) Equivalent Plastic Strain (b) Stress Triaxiality and (c) Lode Angle Parameter along the diagonal of the blank at 8 mm cup depth for Al2024 aluminum (Hill'48-Disc-HC)

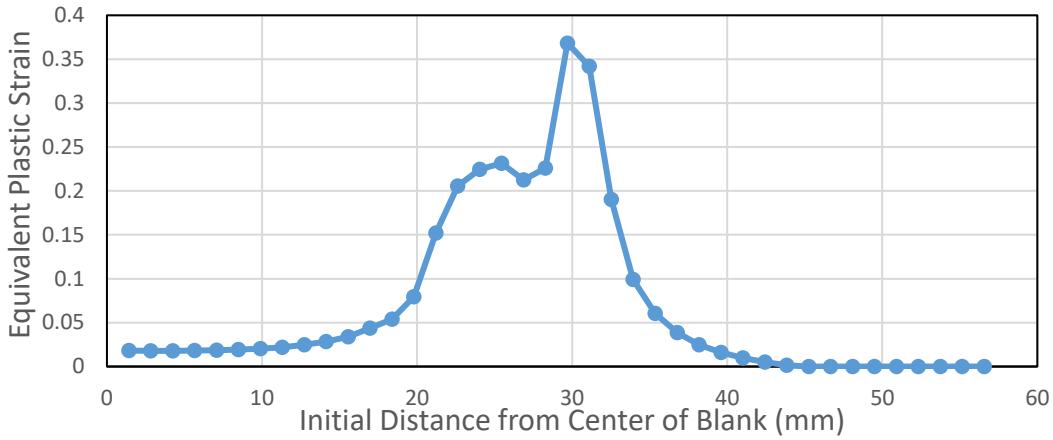

(a)

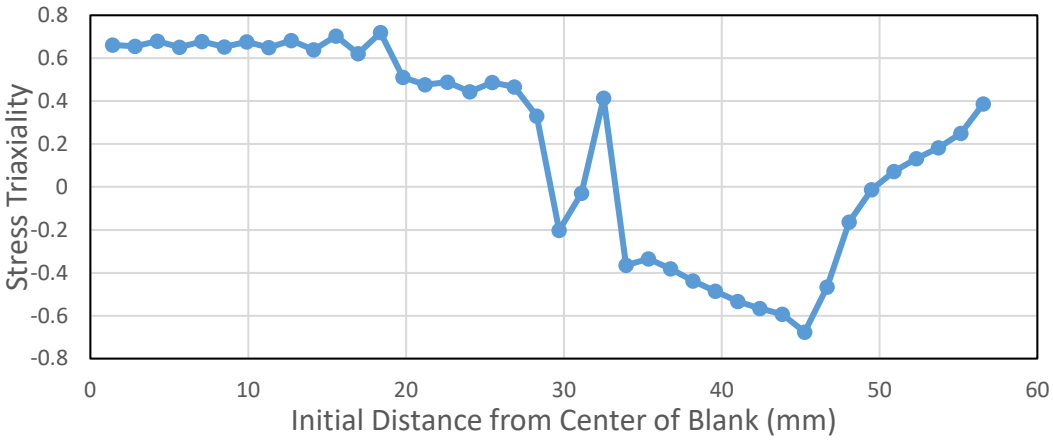

(b)

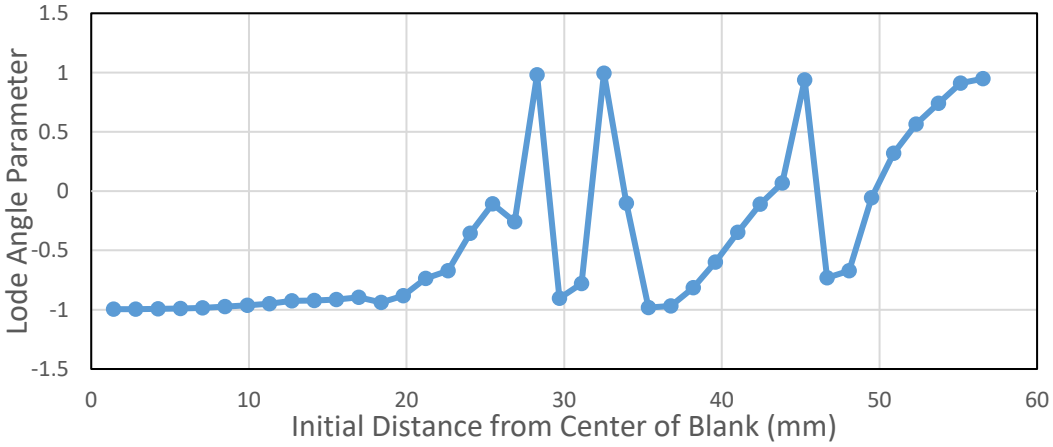

(c)

Figure 5.105. The variation of (a) Equivalent Plastic Strain (b) Stress Triaxiality and (c) Lode Angle Parameter along the diagonal of the blank at 10 mm cup depth for Al2024 aluminum (Hill'48-Disc-HC)

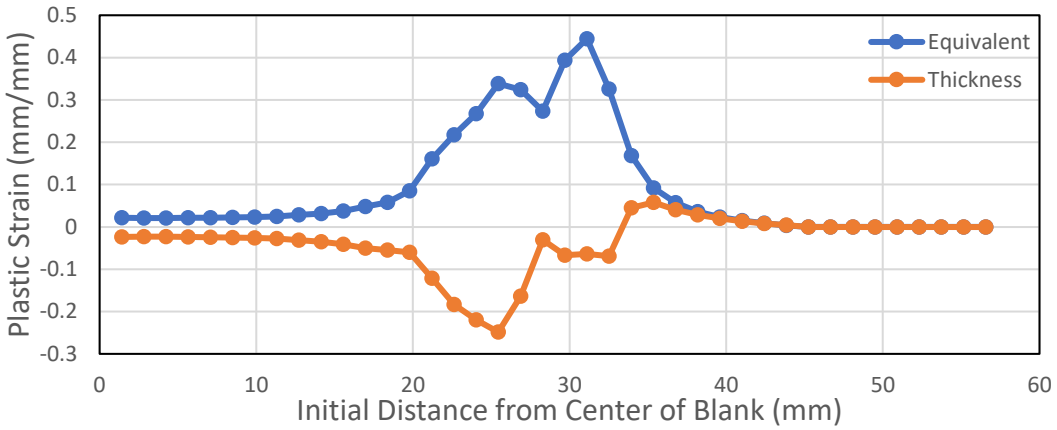

(a)

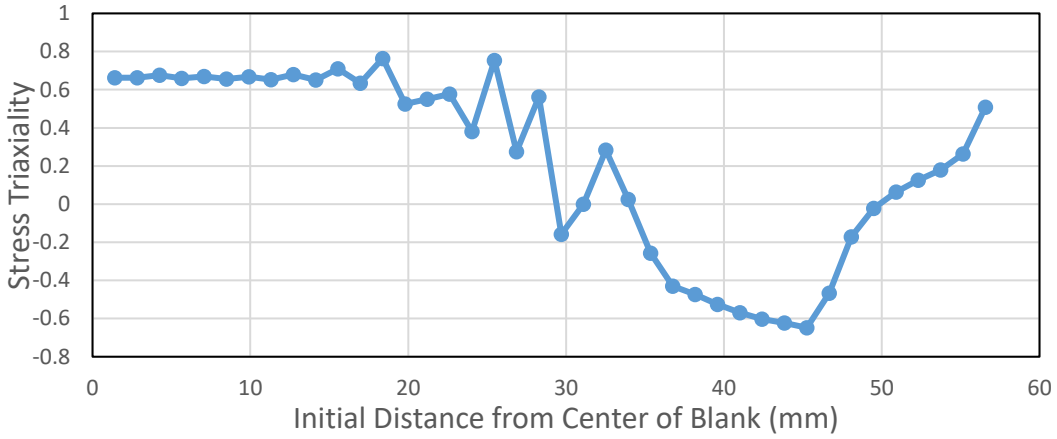

(b)

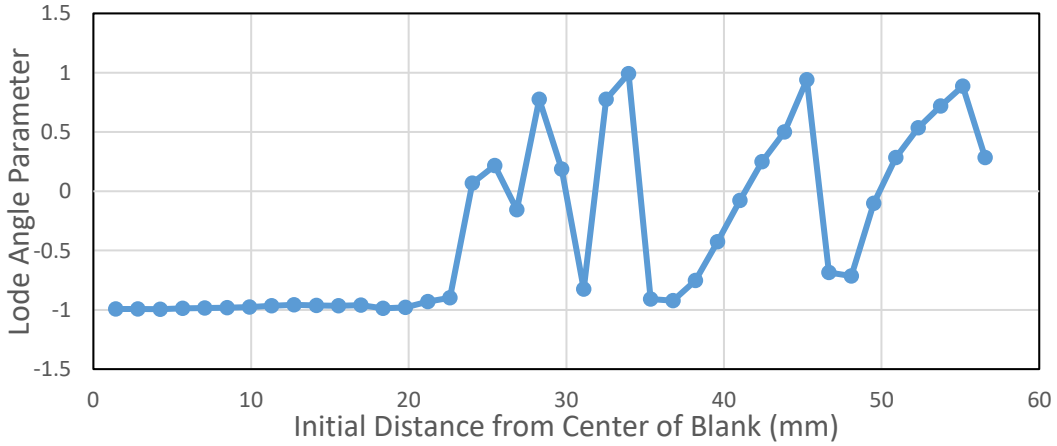

(c)

Figure 5.106. The variation of (a) Equivalent Plastic Strain and Thickness Plastic Strain (b) Stress Triaxiality and (c) Lode Angle Parameter along the diagonal of the blank at 12 mm cup depth for Al2024 aluminum (Hill'48-Disc-HC)

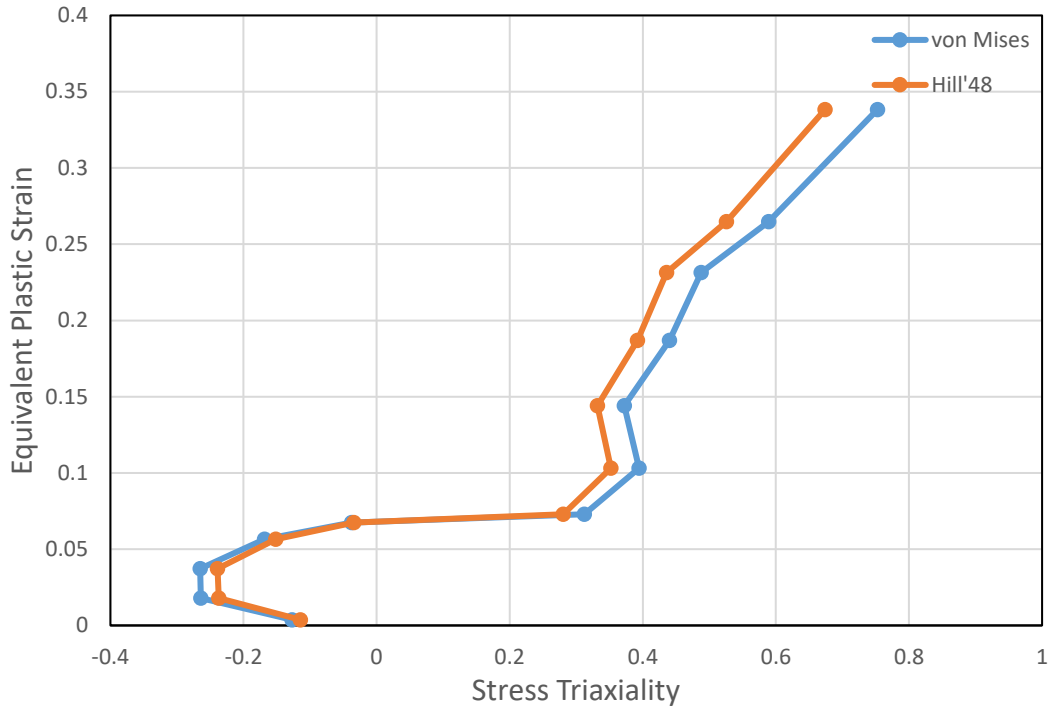

Figure 5.107. Equivalent Plastic Strain - Stress Triaxiality Plot of First Rupture Element (Hill'48-Disc-HC)

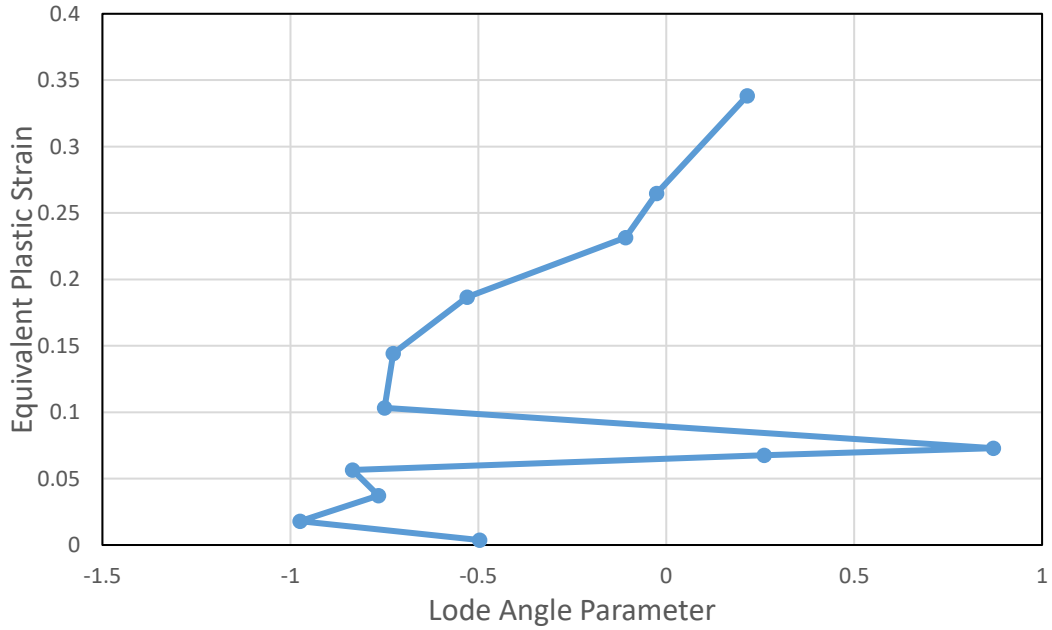

Figure 5.108. Equivalent Plastic Strain – Lode Angle Parameter Plot of First Rupture Element (Hill'48-Disc-HC)

In the rolling direction, the triaxiality values vary generally between 0.6 and 0.8 under the punch whereas the Lode angle parameter values change between -0.8 and -1 up to the punch shoulder, it is seen that equi-biaxial stress conditions dominates up to 15 mm from the center of the blank. Up to die corner, triaxiality values became negative with varying Lode angle parameter values.

The same tendency of rolling direction is observed in the transverse direction also. The differences are a result of anisotropy of the material.

In the diagonal direction, up to 20 mm from the center of the blank equi-biaxial stress condition is observed. From punch shoulder to die corner triaxiality values are decreasing with varying Lode angle parameter values. According to these values there is a transition from uniaxial compression to uniaxial tension at the die corner. Finally, fracture occurs in tension situation at the punch shoulder.

5.1.7 Case 7: Square- AISI304-von Mises-Discrete-Johnson Cook Model

For the seventh case, von Mises yield criterion was applied with discrete hardening and the Johnson Cook ductile fracture criterion was used. It was observed that the fracture had started after 20 mm punch travel as shown in Figure 5.109. The variation of equivalent plastic strain, stress triaxiality and Lode angle parameter values are presented as a function of the distance from the center of the blank for different cup heights up to the fracture. The results are shown for rolling direction in Figure 5.110 to Figure 5.114, for transverse direction in Figure 5.115 to Figure 5.119 and for diagonal direction in Figure 5.120 to Figure 5.124. The thickness plastic strain distribution is also inserted into Figure 5.124 (a) in order to better visualize the deformation. Further, the variations of stress triaxiality values with respect to equivalent plastic strain are given by considering both von Mises and Hill'48 criteria as a function of the path of the element that fractured first in Figure 5.125. Along the same path, the variation of the Lode parameter with respect to equivalent plastic strain is also illustrated in Figure 5.126.

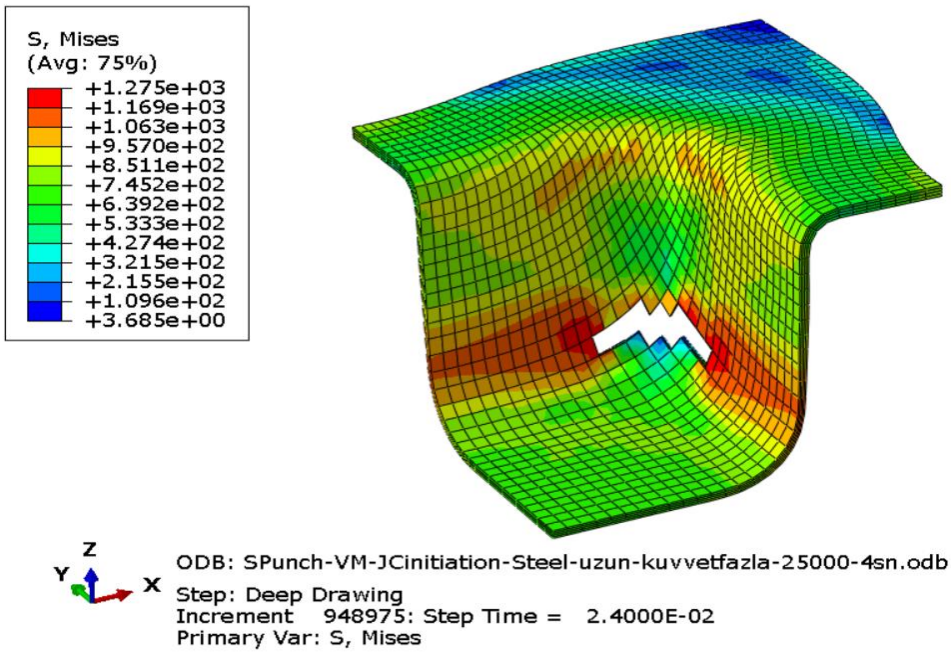

Figure 5.109. First Rupture Moment of Case 7

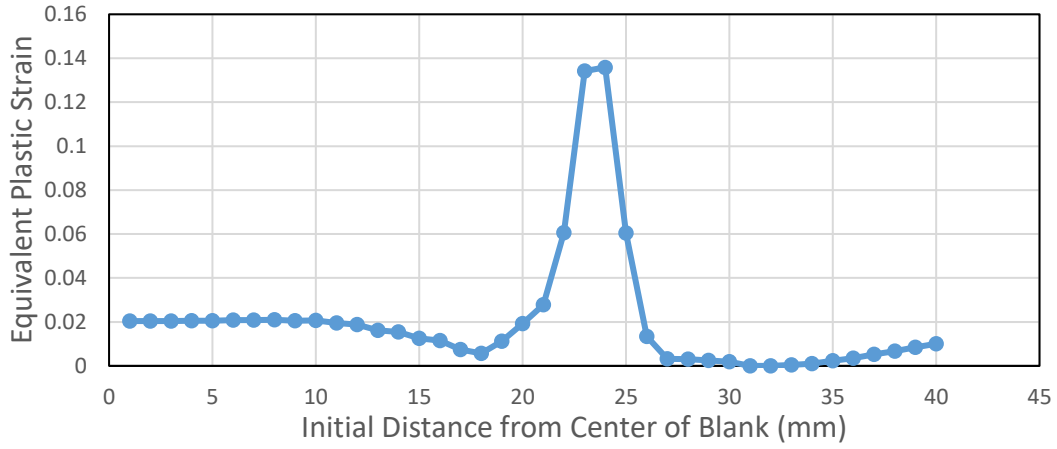

(a)

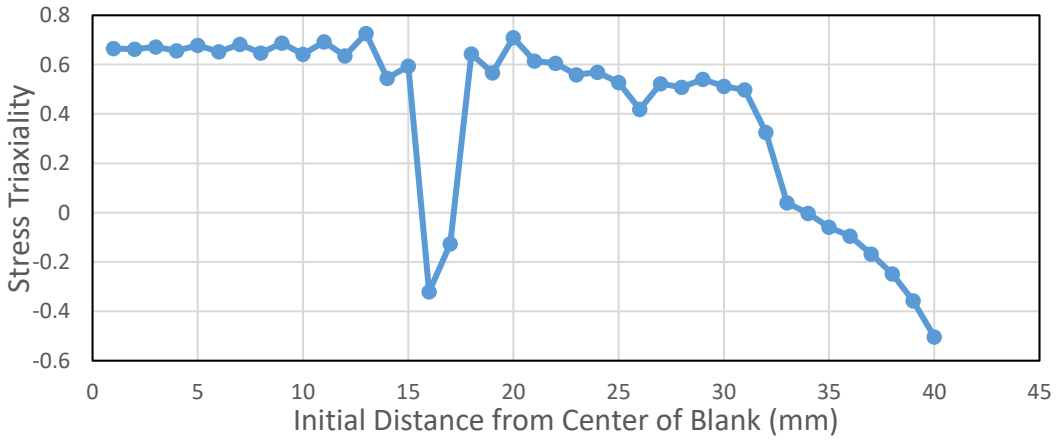

(b)

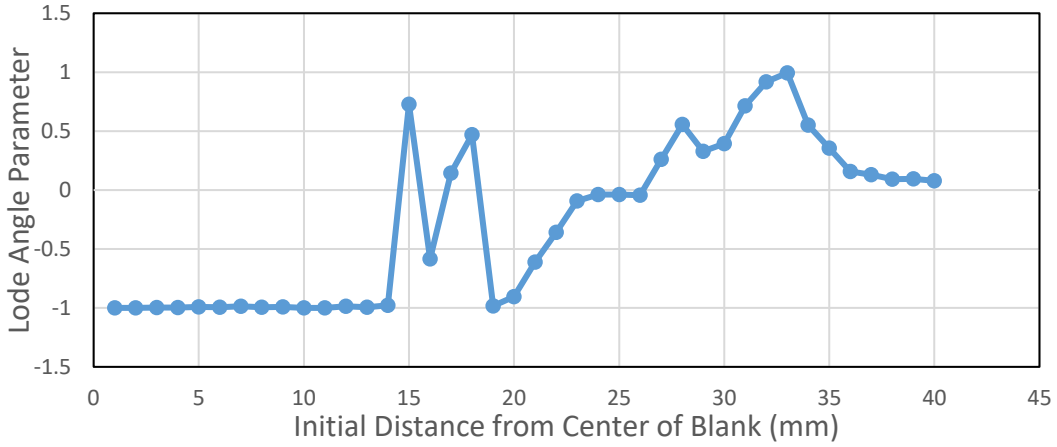

(c)

Figure 5.110. The variation of (a) Equivalent Plastic Strain (b) Stress Triaxiality and (c) Lode Angle Parameter along the rolling direction of the blank at 4 mm cup depth for AISI 304 steel (VM-Disc-JC)

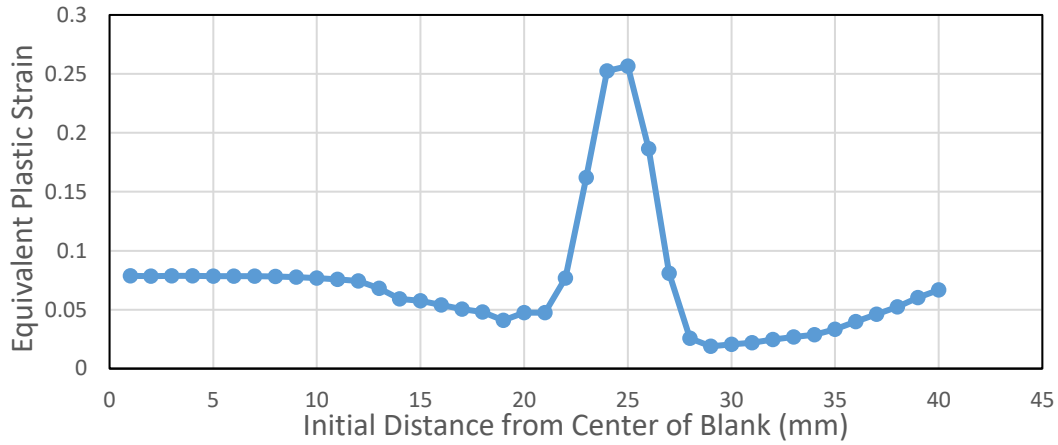

(a)

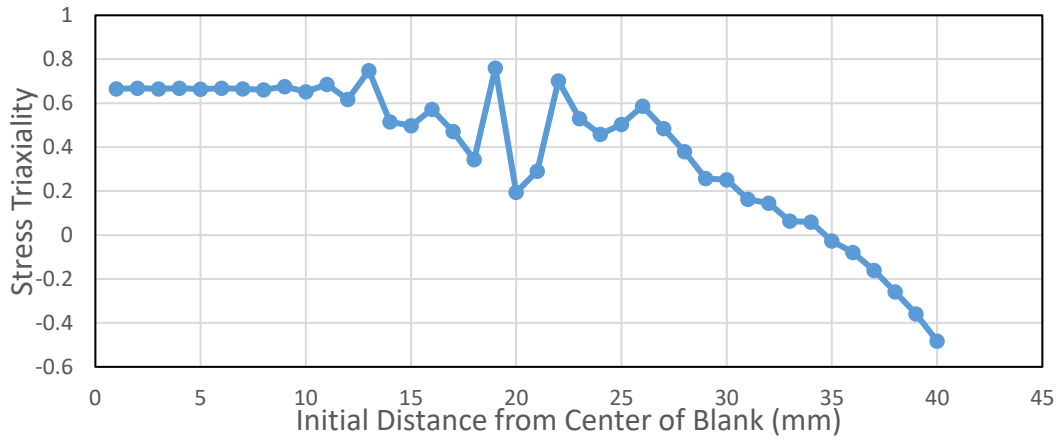

(b)

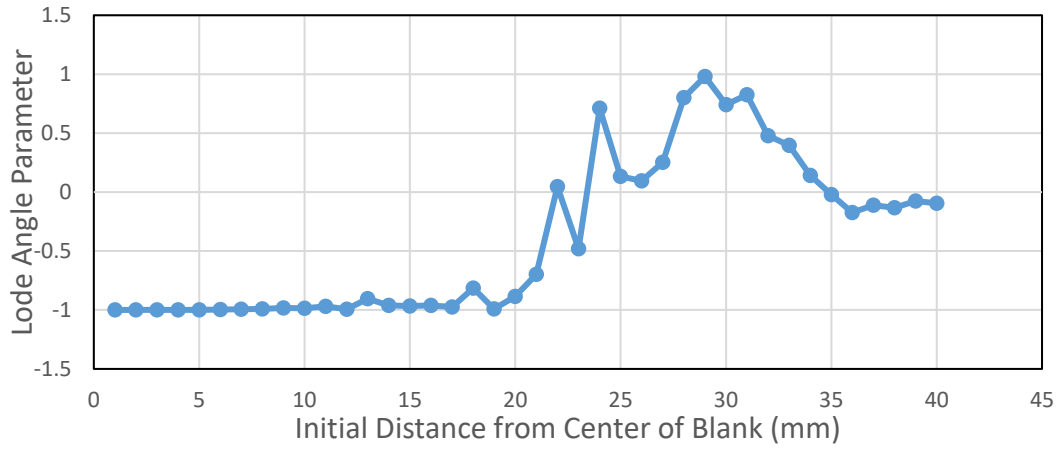

(c)

Figure 5.111. The variation of (a) Equivalent Plastic Strain (b) Stress Triaxiality and (c) Lode Angle Parameter along the rolling direction of the blank at 8 mm cup depth for AISI 304 steel (VM-Disc-JC)

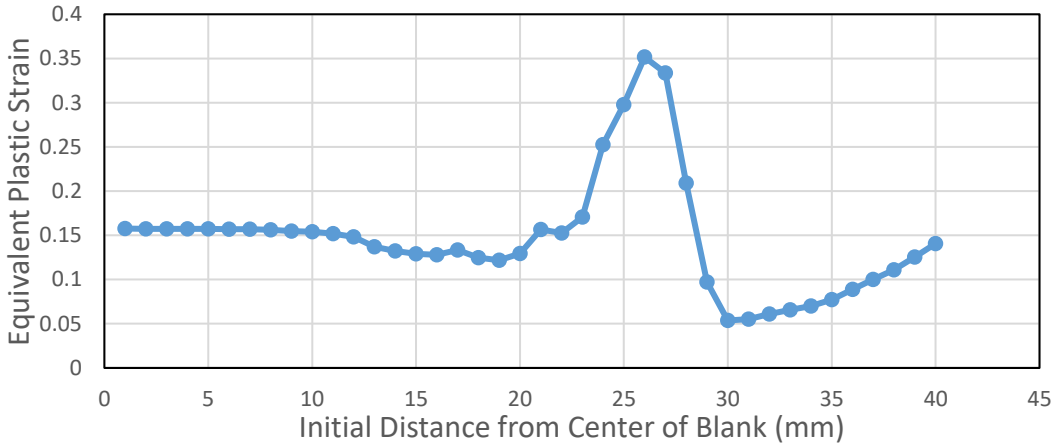

(a)

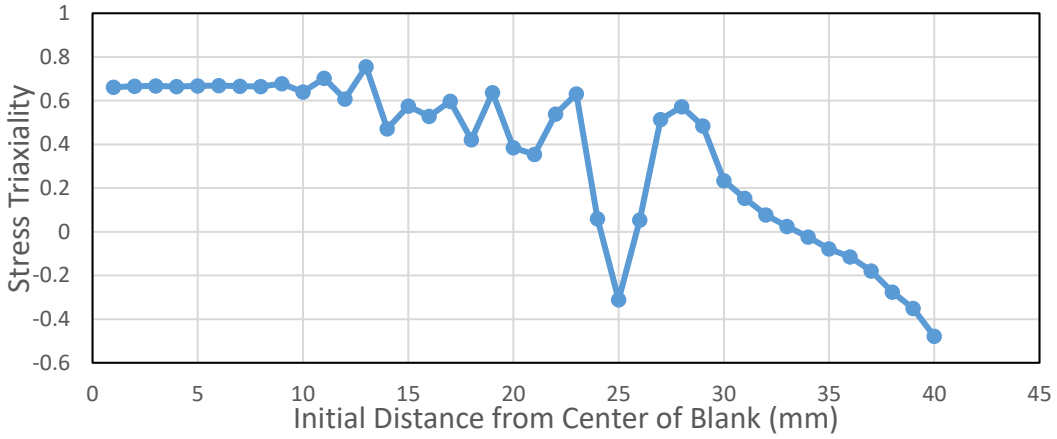

(b)

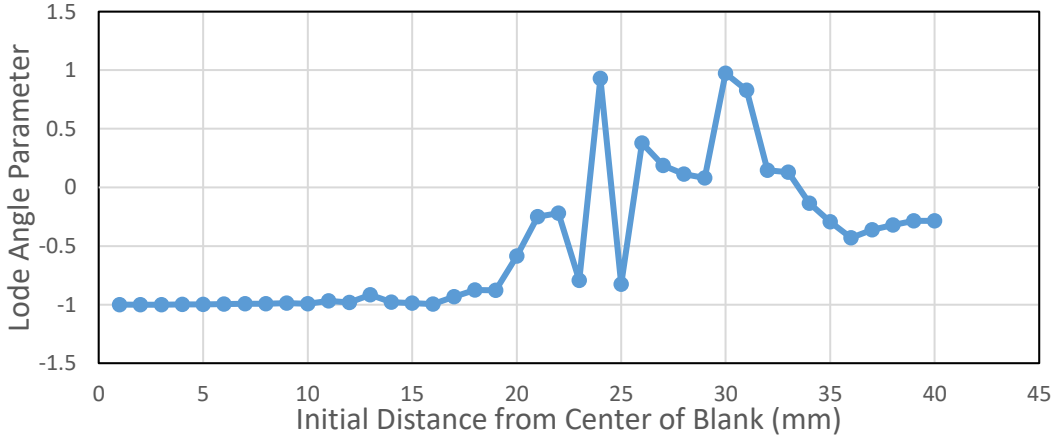

(c)

Figure 5.112. The variation of (a) Equivalent Plastic Strain (b) Stress Triaxiality and (c) Lode Angle Parameter along the rolling direction of the blank at 12 mm cup depth for AISI 304 steel (VM-Disc-JC)

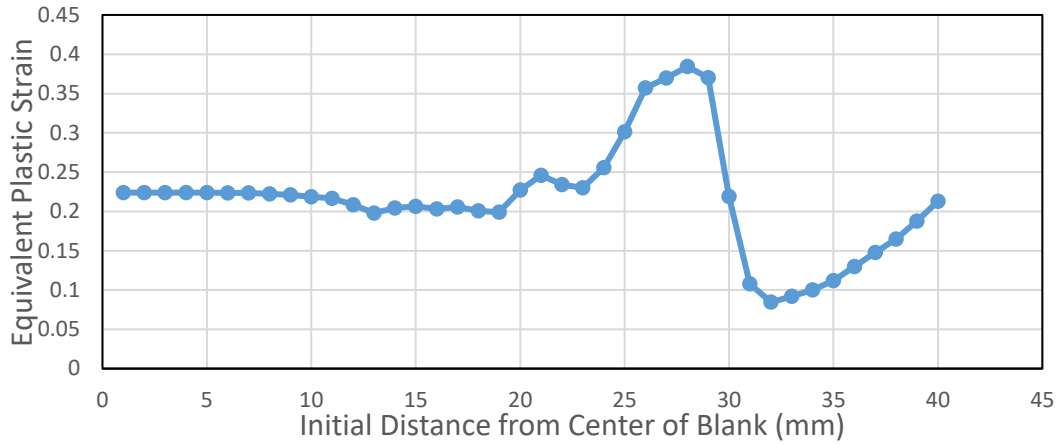

(a)

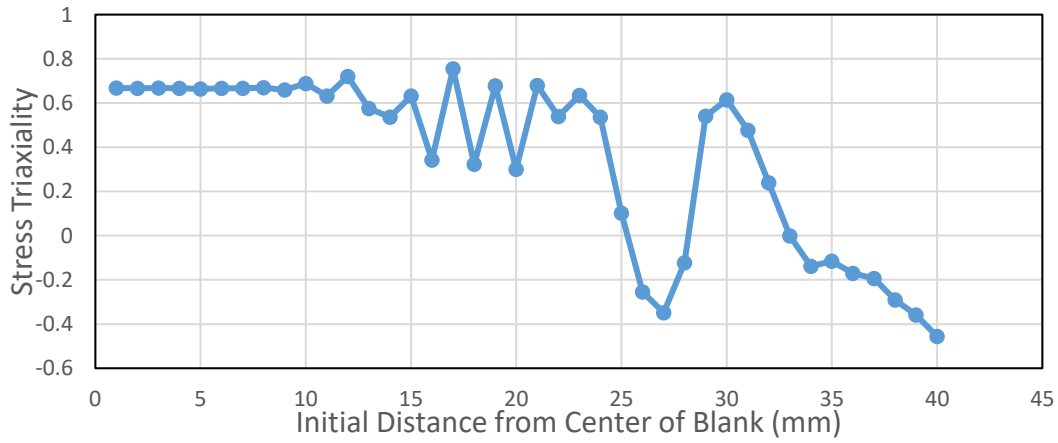

(b)

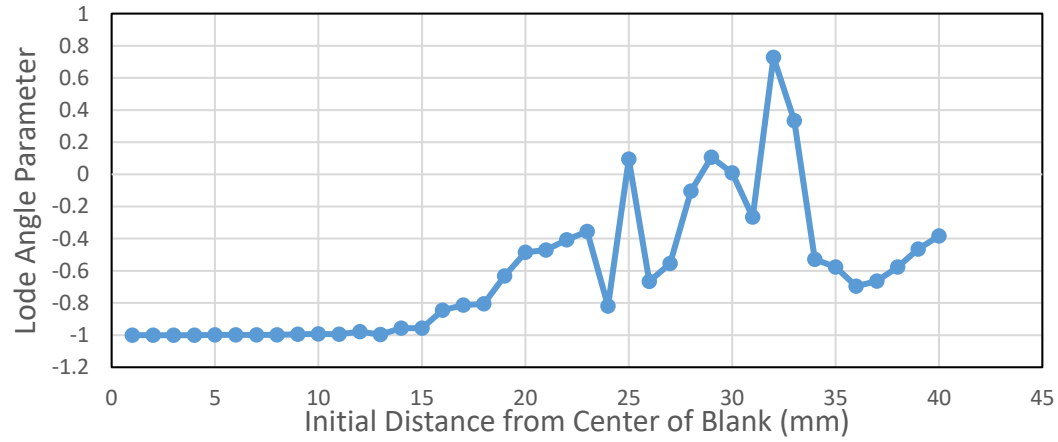

(c)

Figure 5.113. The variation of (a) Equivalent Plastic Strain (b) Stress Triaxiality and (c) Lode Angle Parameter along the rolling direction of the blank at 16 mm cup depth for AISI 304 steel (VM-Disc-JC)

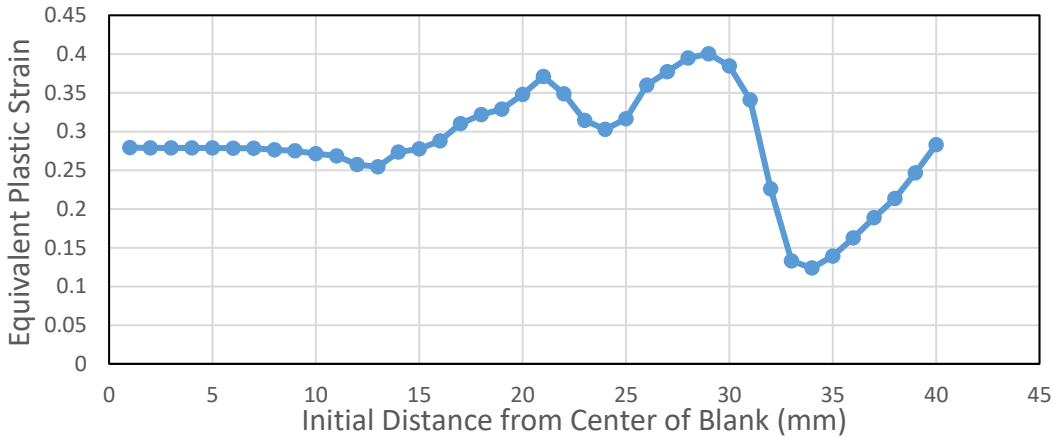

(a)

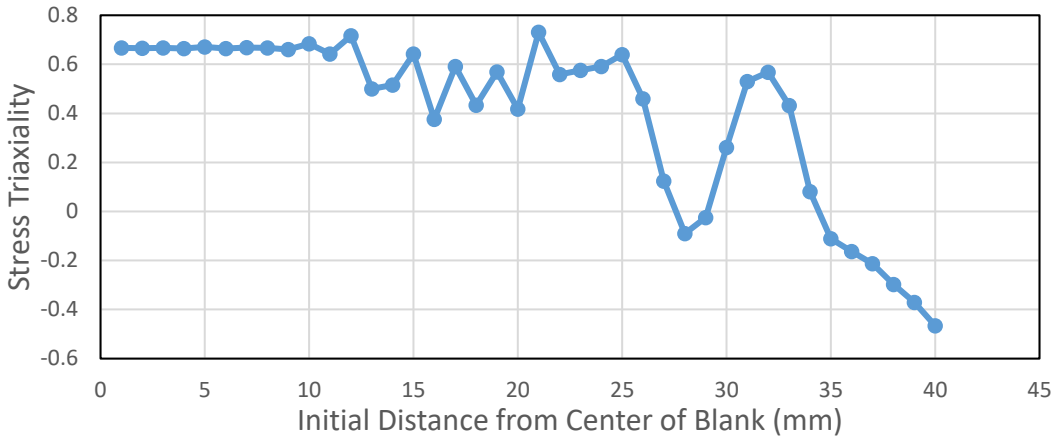

(b)

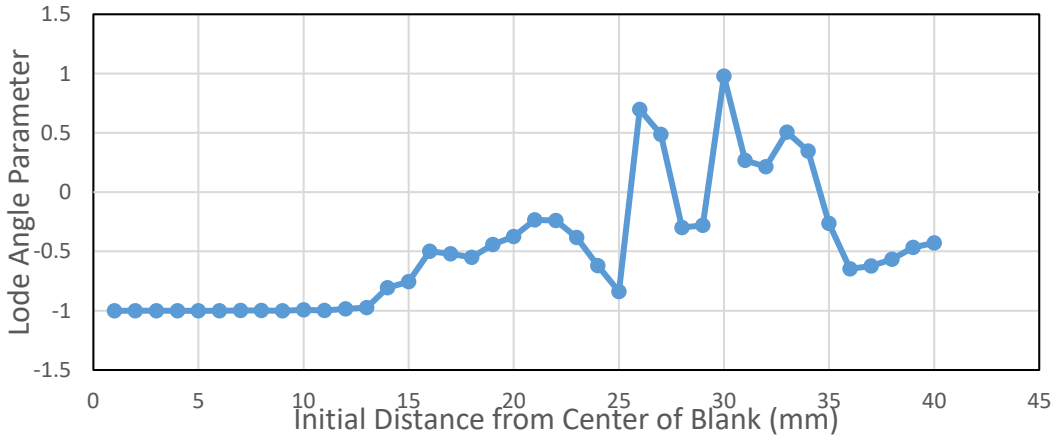

(c)

Figure 5.114. The variation of (a) Equivalent Plastic Strain (b) Stress Triaxiality and (c) Lode Angle Parameter along the rolling direction of the blank at 20 mm cup depth for AISI 304 steel (VM-Disc-JC)

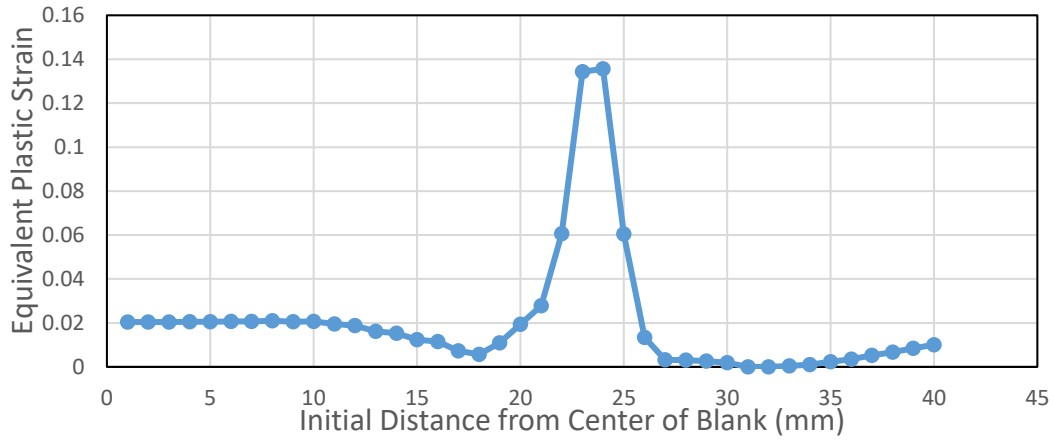

(a)

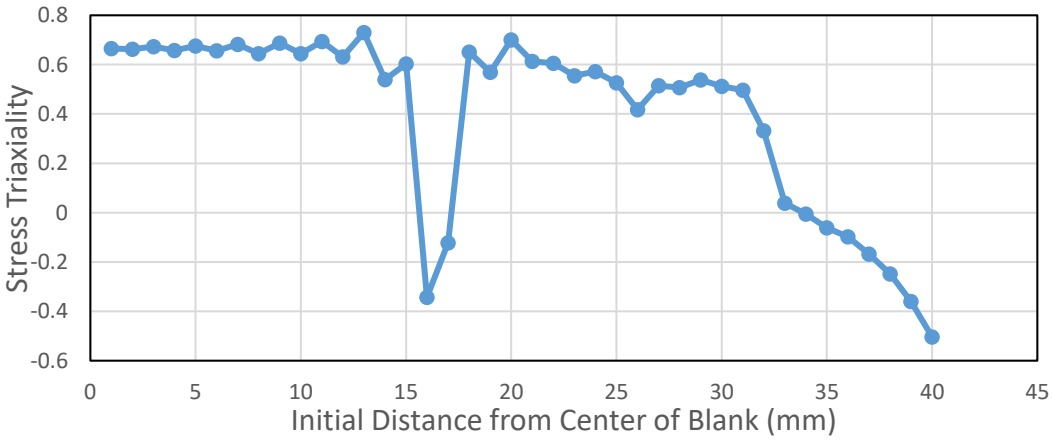

(b)

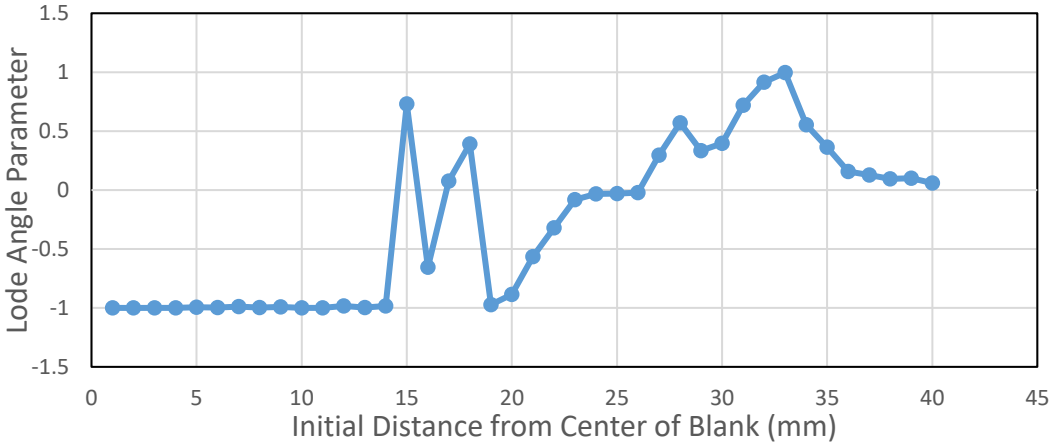

(c)

Figure 5.115. The variation of (a) Equivalent Plastic Strain (b) Stress Triaxiality and (c) Lode Angle Parameter along the transverse direction of the blank at 4 mm cup depth for AISI 304 steel (VM-Disc-JC)

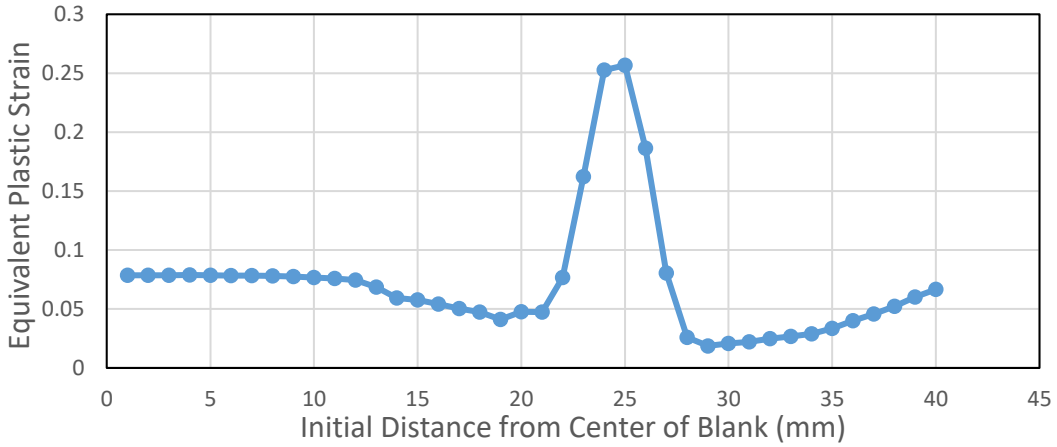

(a)

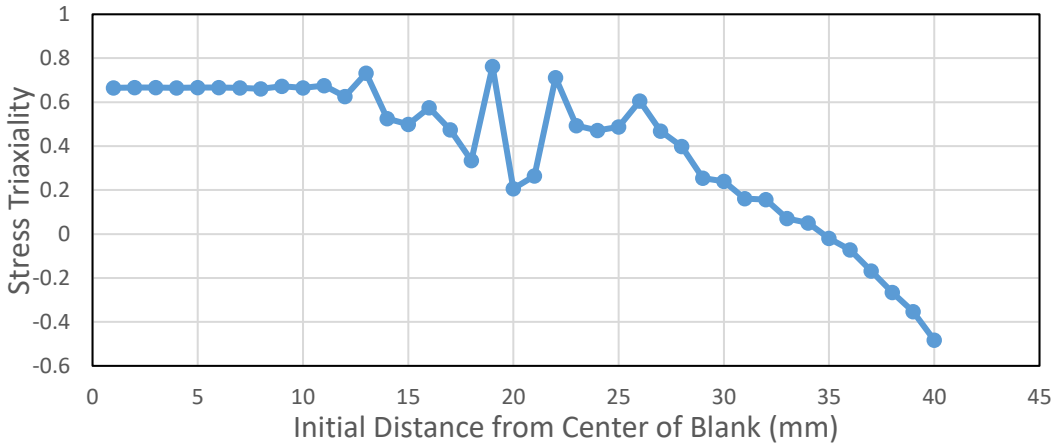

(b)

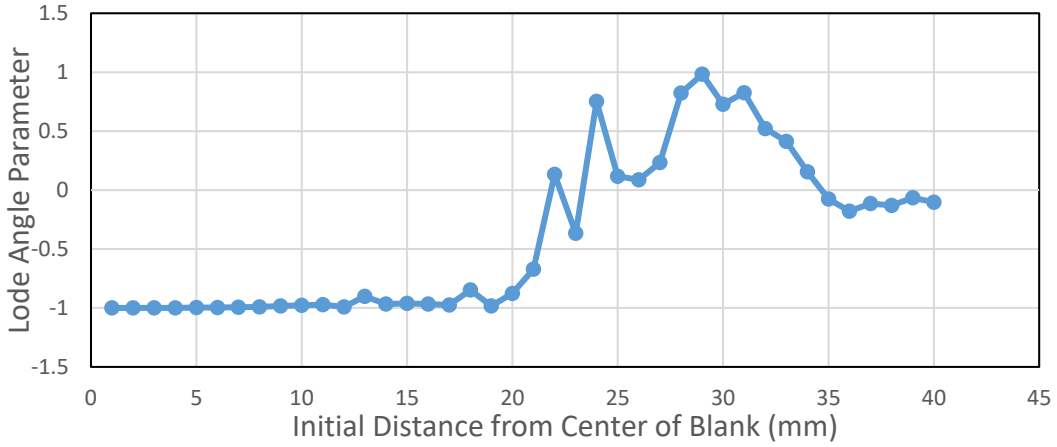

(c)

Figure 5.116. The variation of (a) Equivalent Plastic Strain (b) Stress Triaxiality and (c) Lode Angle Parameter along the transverse direction of the blank at 8 mm cup depth for AISI 304 steel (VM-Disc-JC)

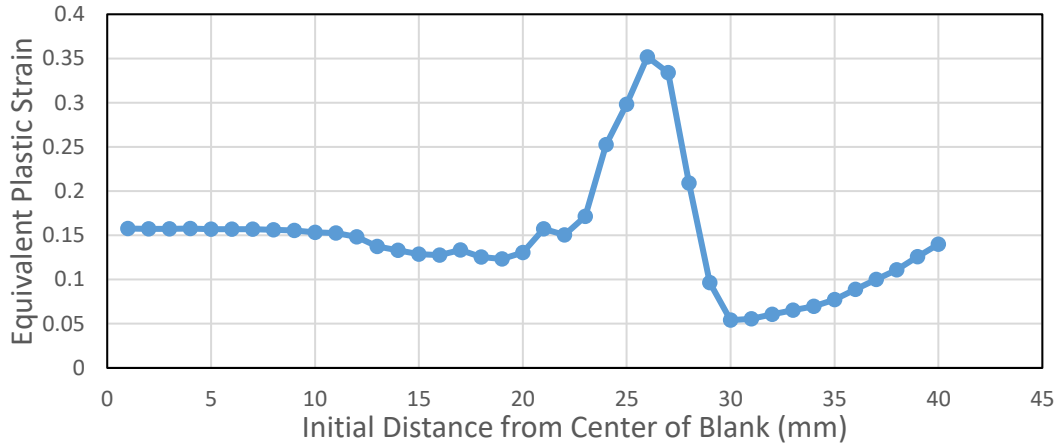

(a)

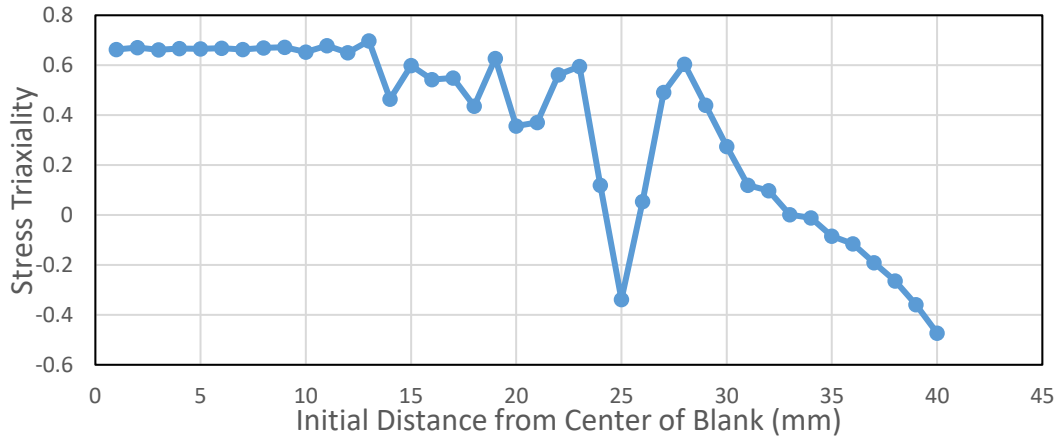

(b)

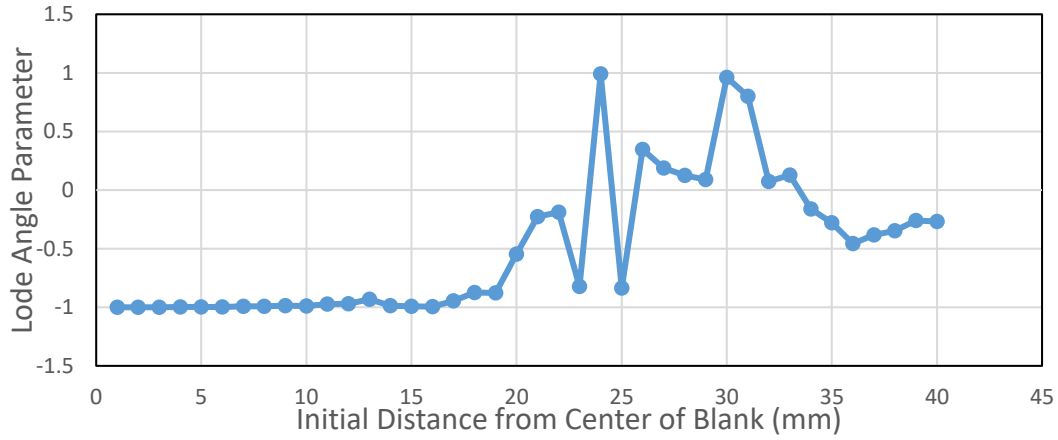

(c)

Figure 5.117. The variation of (a) Equivalent Plastic Strain (b) Stress Triaxiality and (c) Lode Angle Parameter along the transverse direction of the blank at 12 mm cup depth for AISI 304 steel (VM-Disc-JC)

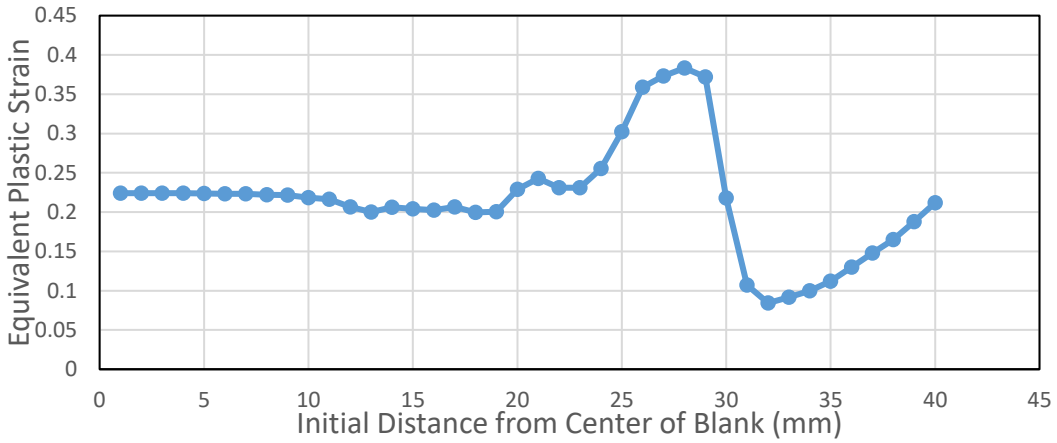

(a)

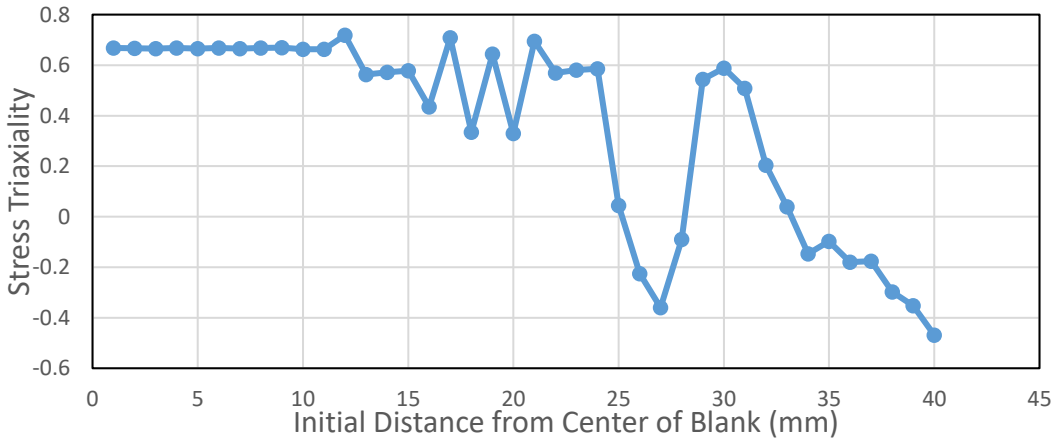

(b)

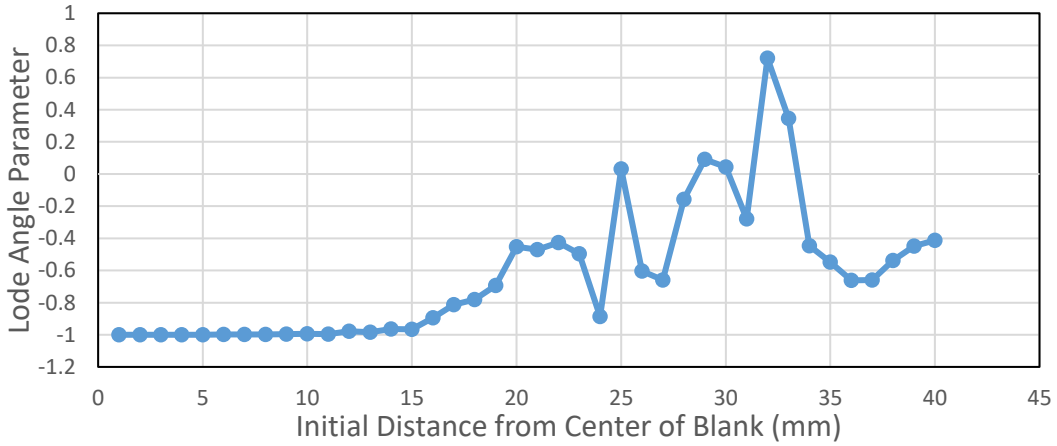

(c)

Figure 5.118. The variation of (a) Equivalent Plastic Strain (b) Stress Triaxiality and (c) Lode Angle Parameter along the transverse direction of the blank at 16 mm cup depth for AISI 304 steel (VM-Disc-JC)

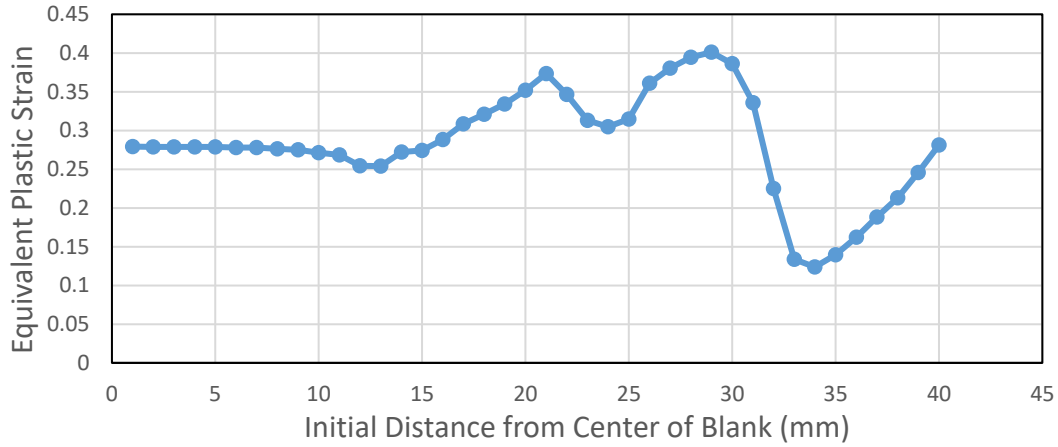

(a)

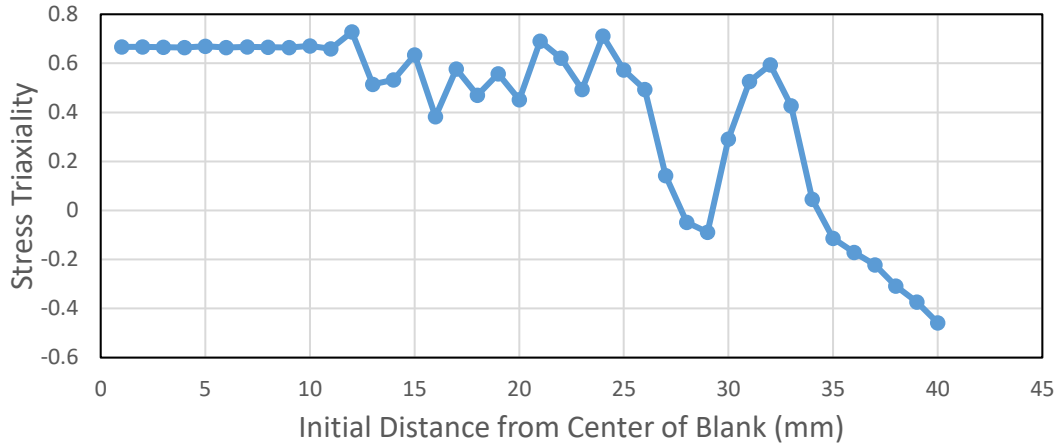

(b)

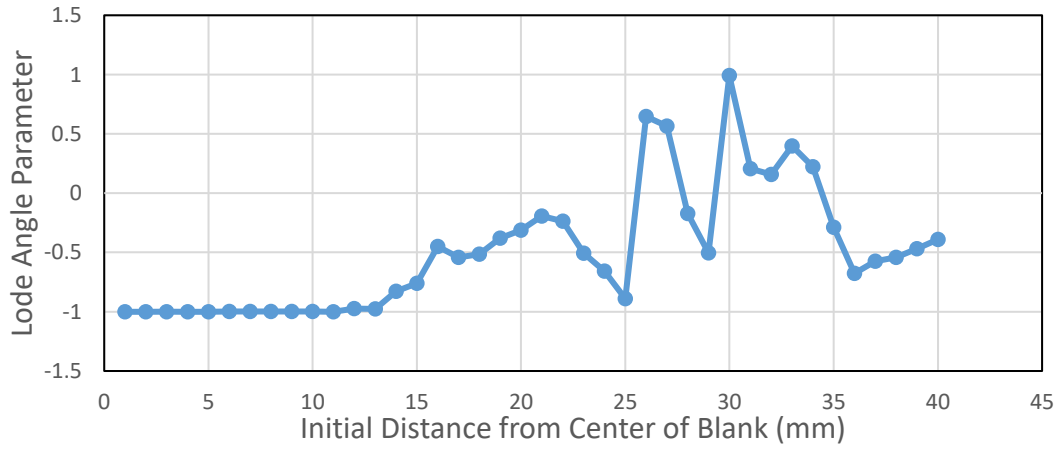

(c)

Figure 5.119. The variation of (a) Equivalent Plastic Strain (b) Stress Triaxiality and (c) Lode Angle Parameter along the transverse direction of the blank at 20 mm cup depth for AISI 304 steel (VM-Disc-JC)

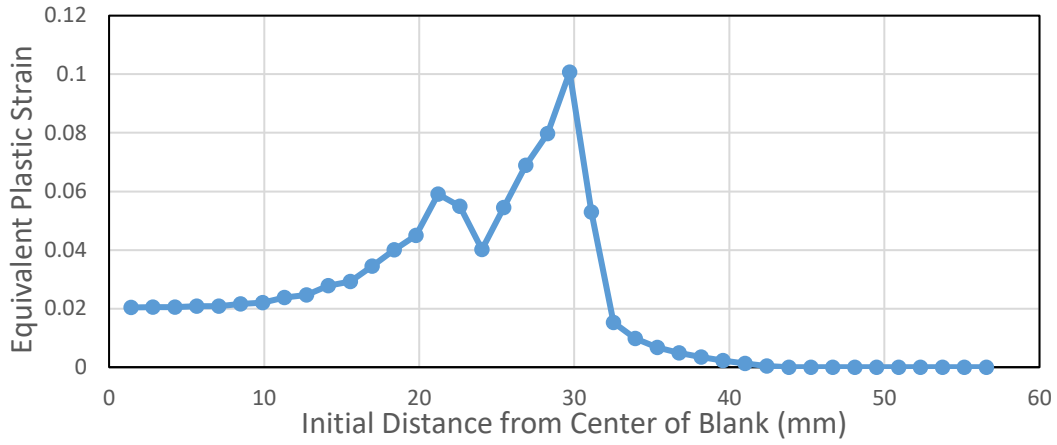

(a)

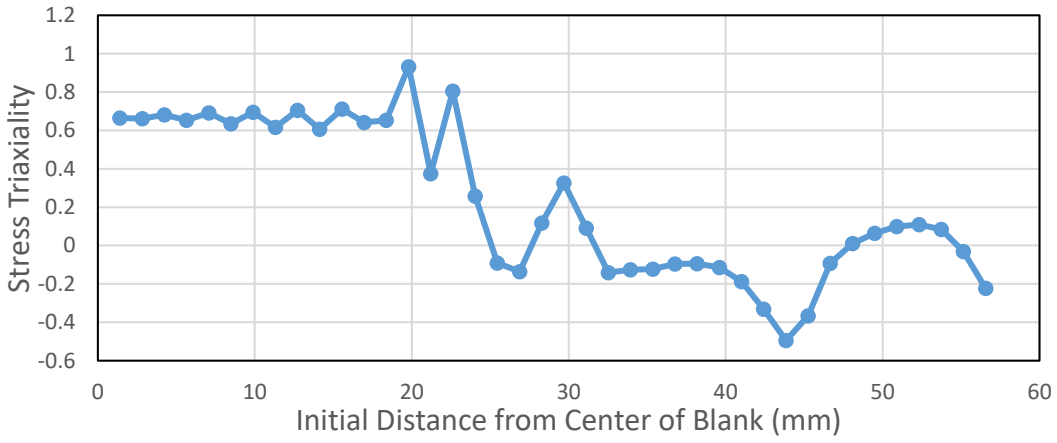

(b)

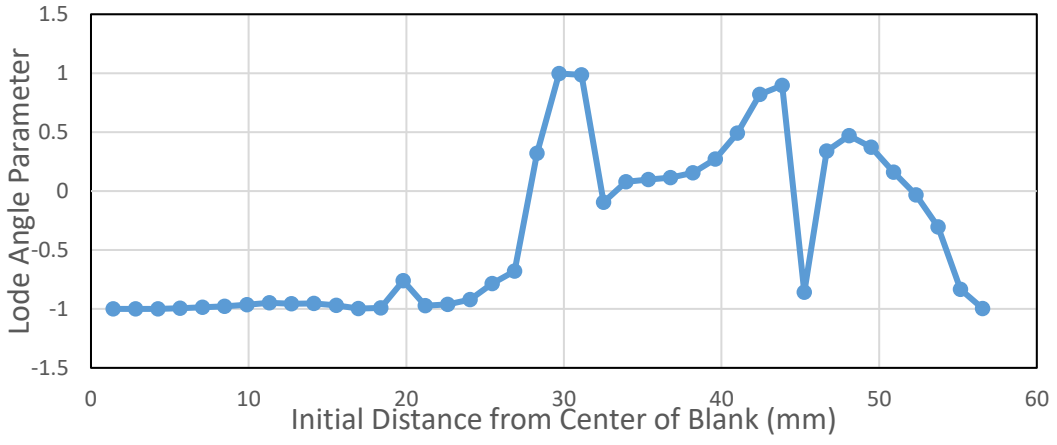

(c)

Figure 5.120. The variation of (a) Equivalent Plastic Strain (b) Stress Triaxiality and (c) Lode Angle Parameter along the diagonal of the blank at 4 mm cup depth for AISI 304 steel (VM-Disc-JC)

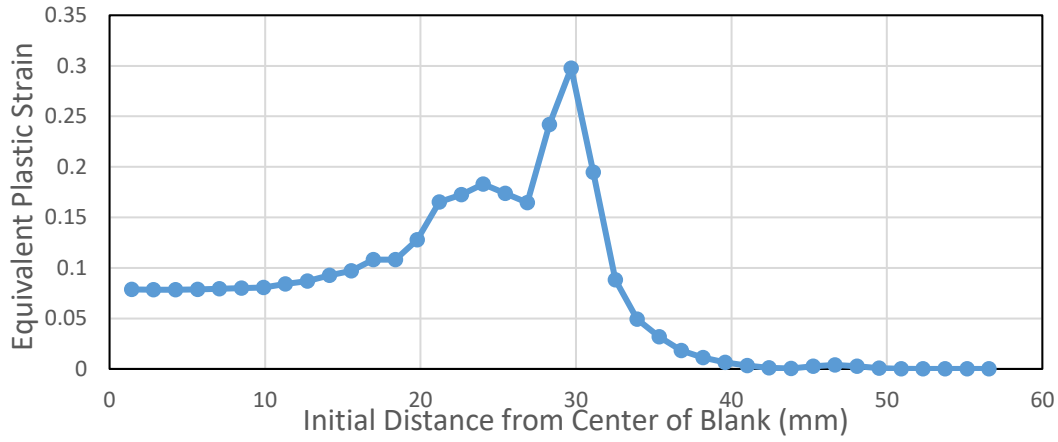

(a)

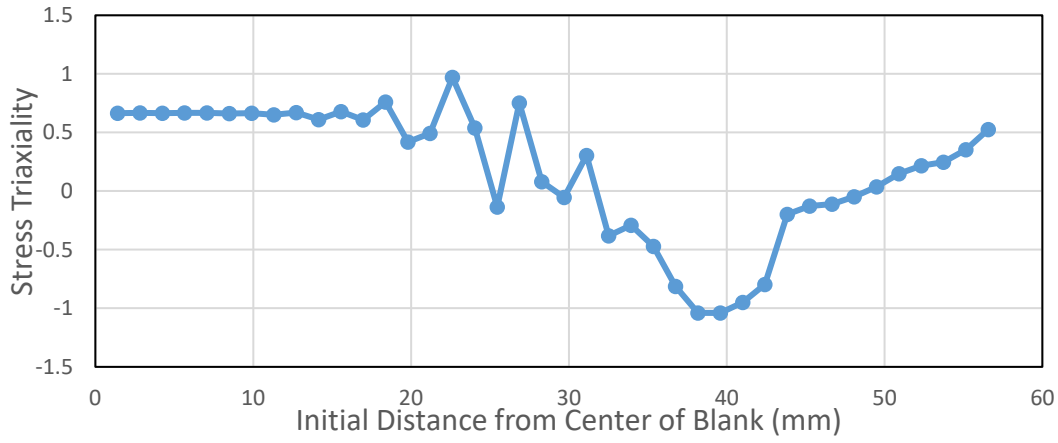

(b)

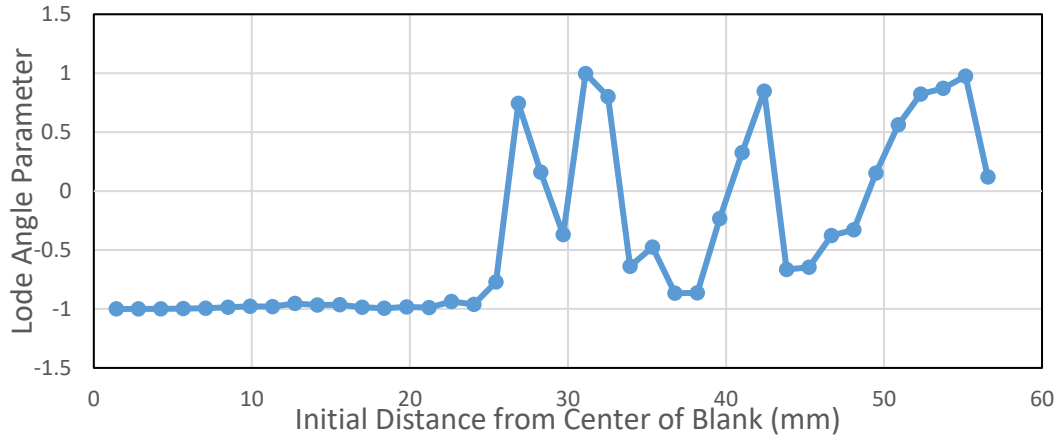

(c)

Figure 5.121. The variation of (a) Equivalent Plastic Strain (b) Stress Triaxiality and (c) Lode Angle Parameter along the diagonal of the blank at 8 mm cup depth for AISI 304 steel (VM-Disc-JC)

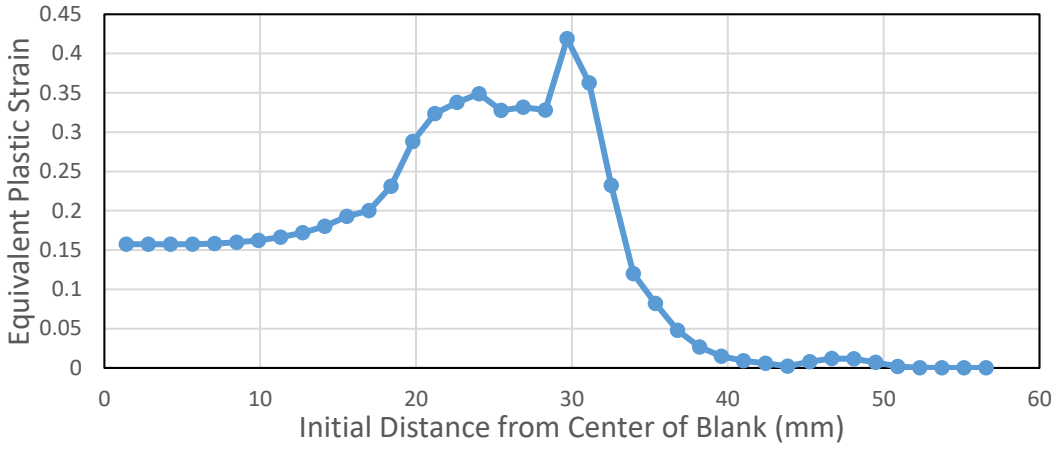

(a)

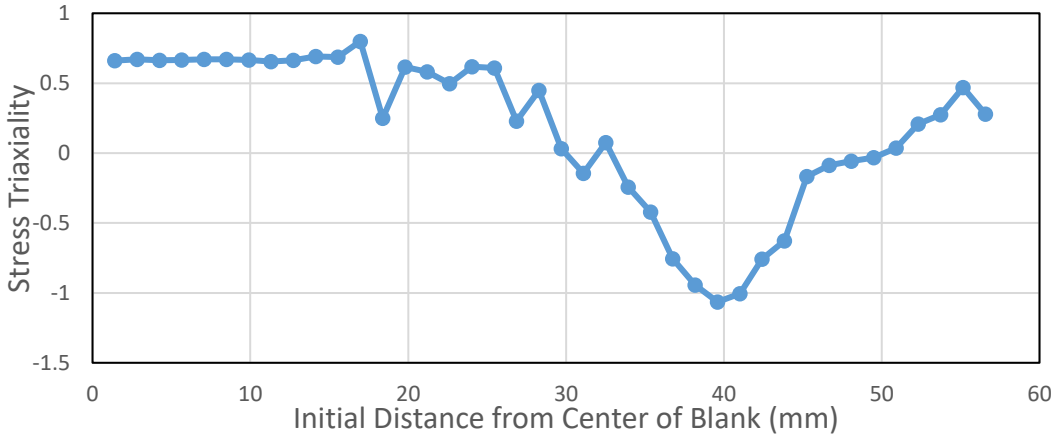

(b)

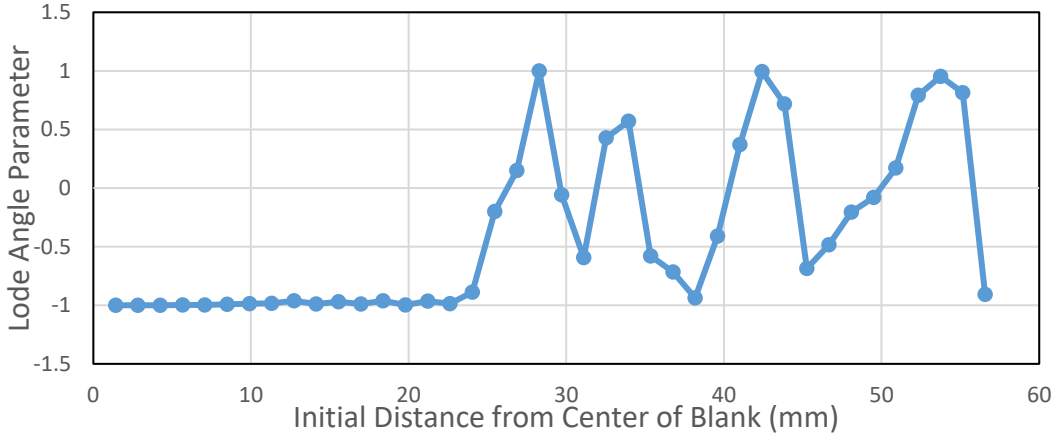

(c)

Figure 5.122 The variation of (a) Equivalent Plastic Strain (b) Stress Triaxiality and (c) Lode Angle Parameter along the diagonal of the blank at 12 mm cup depth for AISI 304 steel (VM-Disc-JC)

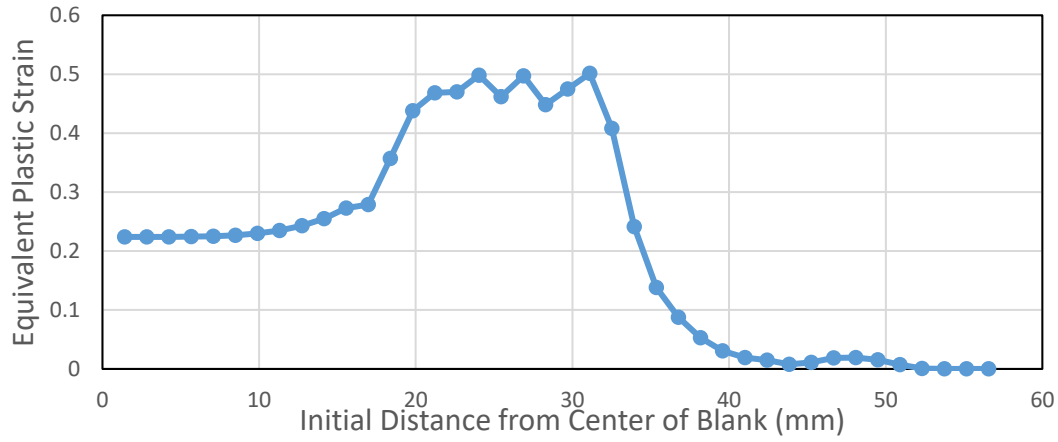

(a)

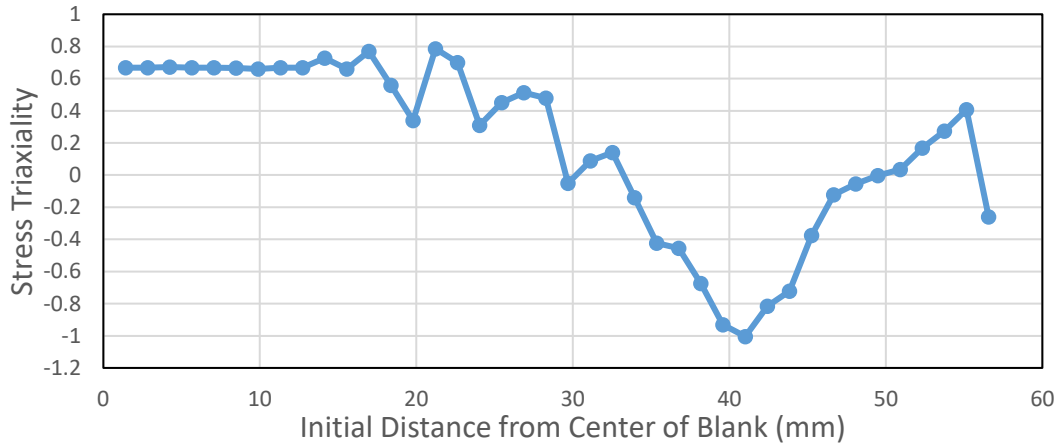

(b)

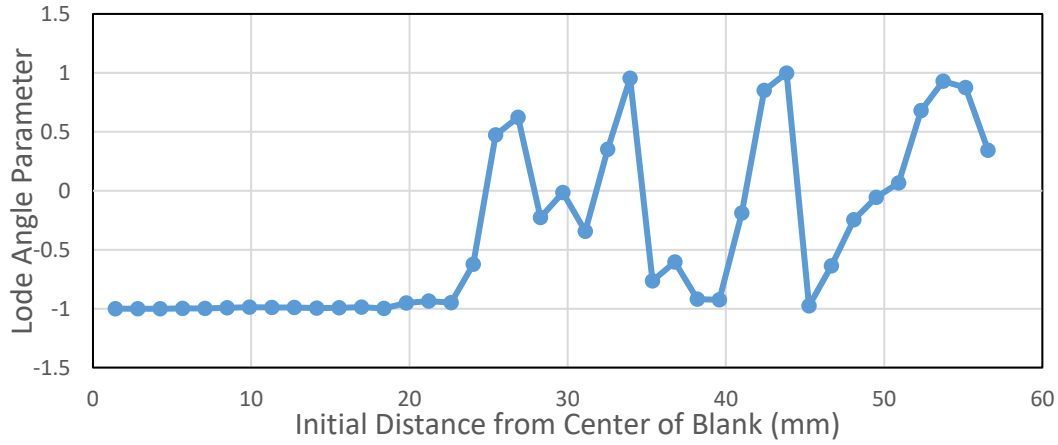

(c)

Figure 5.123 The variation of (a) Equivalent Plastic Strain (b) Stress Triaxiality and (c) Lode Angle Parameter along the diagonal of the blank at 16 mm cup depth for AISI 304 steel (VM-Disc-JC)

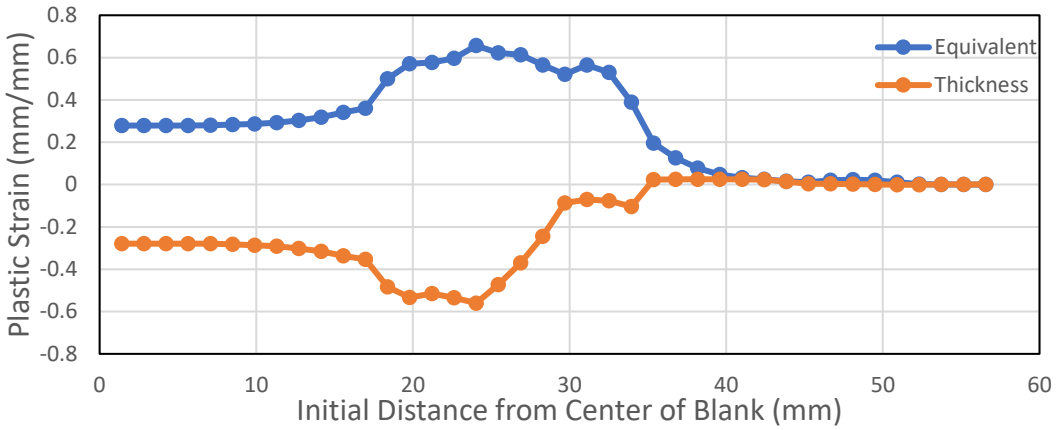

(a)

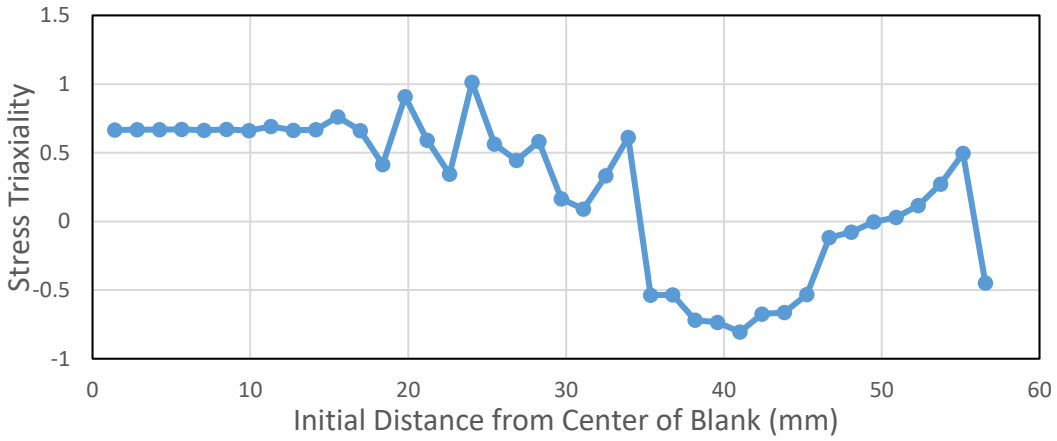

(b)

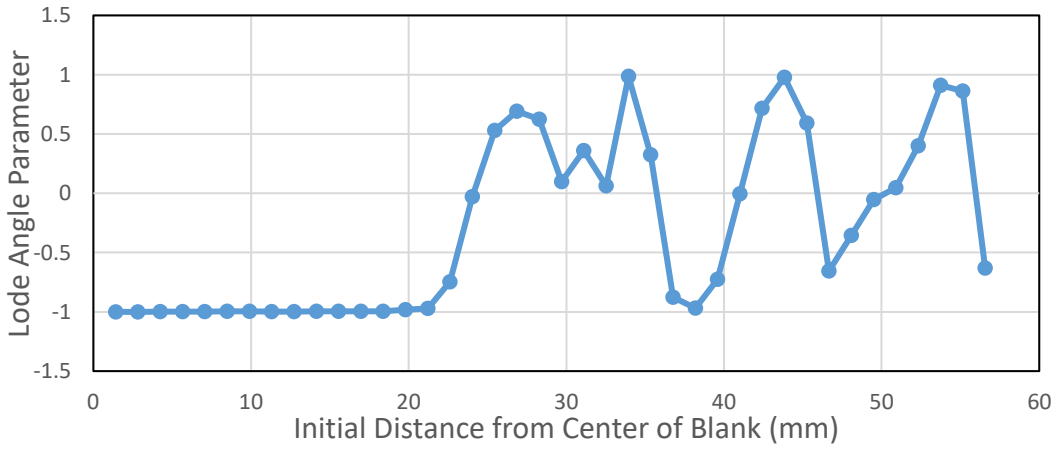

(c)

Figure 5.124. The variation of (a) Equivalent Plastic Strain and Thickness Plastic Strain (b) Stress Triaxiality and (c) Lode Angle Parameter along the diagonal of the blank at 20 mm cup depth for AISI 304 steel (VM-Disc-JC)

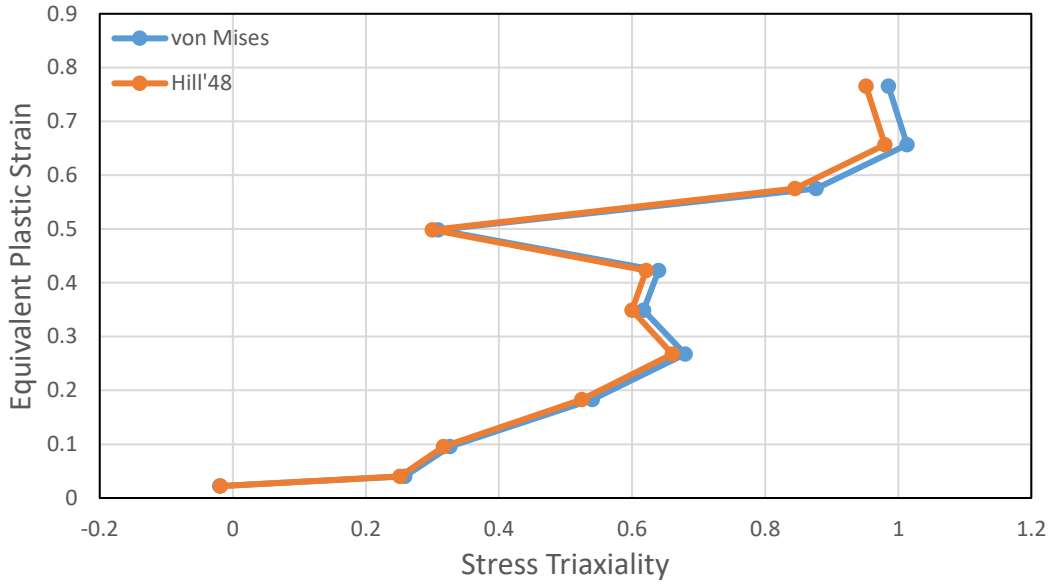

Figure 5.125. Equivalent Plastic Strain - Stress Triaxiality Plot of First Rupture Element (VM-Disc-JC)

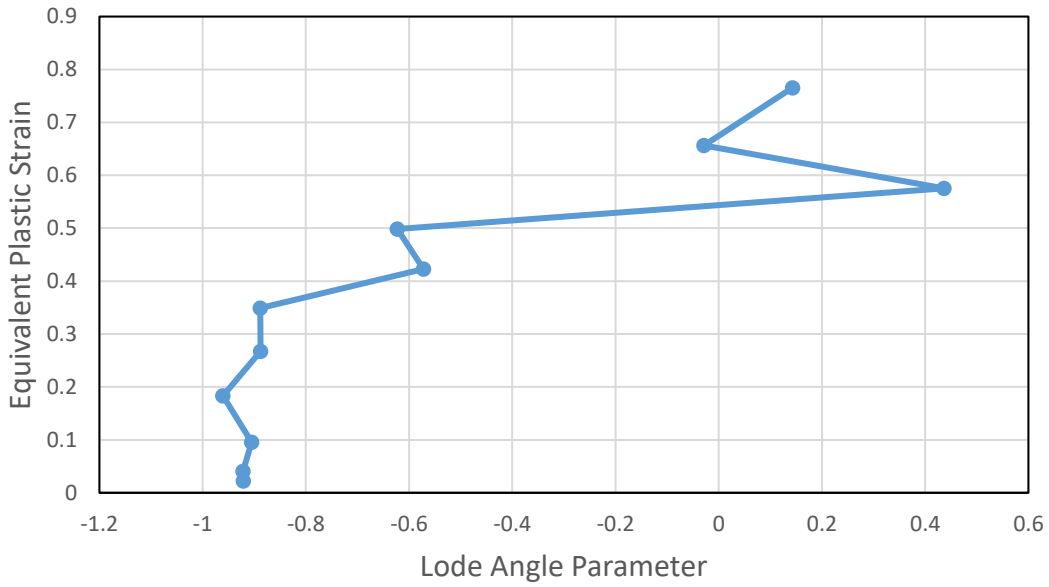

Figure 5.126. Equivalent Plastic Strain – Lode Angle Parameter Plot of First Rupture Element (VM-Disc-JC)

In the rolling direction, the triaxiality values vary generally between 0.6 and 0.8 under the punch whereas the Lode angle parameter values change between -0.8 and -1 up to a distance of 15 mm from the center, it can be said that the deformation behavior is in equi-biaxial tension condition. When the pre-rupture state of sheet is examined, after punch region, the stress triaxiality is positive while Lode angle parameter values are increasing up to a distance of 35 mm from the center. Finally, both of them became negative under blank holder, indicating thickening towards the rim.

The same tendency of rolling direction is observed in the transverse direction also. The differences are a result of anisotropy of the material.

In the diagonal direction, when the pre-rupture state of sheet is examined, equi-biaxial tension is dominant up to a distance of 20 mm from the center. It is observed that from punch corner to die corner, state of region shifts from tension to shear. Also, there is a transition from compression to equi-biaxial compression between 35 mm distance from the center of the blank to 45 mm distance. After this point, both of triaxiality values and Lode angle parameter values increasing and became positive. Finally, fracture occurs in the punch shoulder in tension state.

5.1.8 Case 8: Square- AISI304-von Mises-Discrete-Hosford Coulomb Model

For the eighth case, von Mises yield criterion was applied with discrete hardening and the Hosford Coulomb ductile fracture criterion was used. It was observed that the fracture had started after 16 mm punch travel as shown in Figure 5.127. The variation of equivalent plastic strain, stress triaxiality and Lode angle parameter values are presented as a function of the distance from the center of the blank for different cup heights up to the fracture. The results are shown for rolling direction in Figure 5.128 to Figure 5.131, for transverse direction in Figure 5.132 to Figure 5.135 and for diagonal direction in Figure 5.136 to Figure 5.139. The thickness plastic strain distribution is also inserted into Figure 5.139 (a) in order to better visualize the deformation. Further, the variations of stress triaxiality values with respect to equivalent plastic strain are given by considering both von Mises and Hill'48 criteria as a function of the path of the element that fractured first in Figure 5.140. Along the same path, the variation of the Lode parameter with respect to equivalent plastic strain is also illustrated in Figure 5.141.

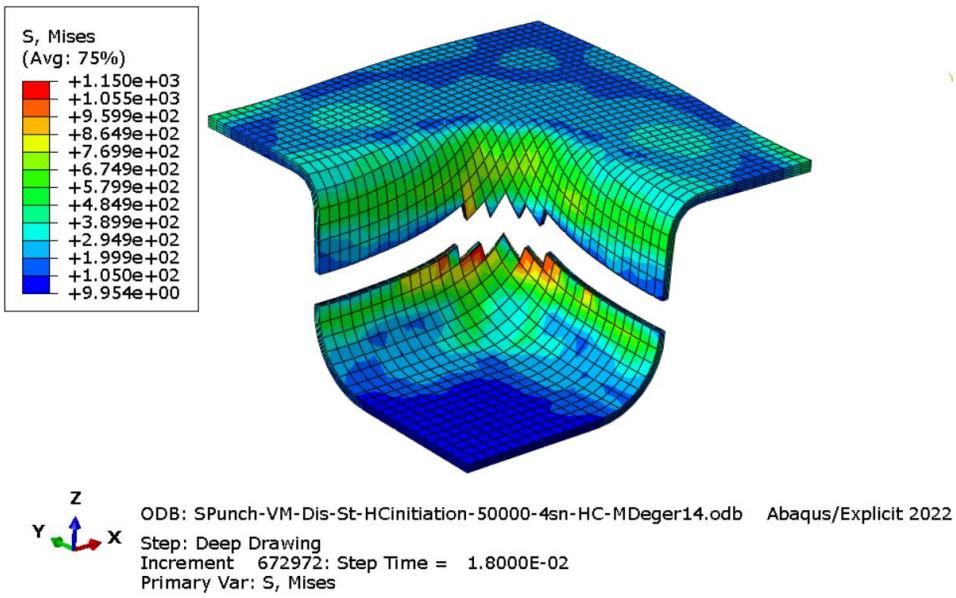

Figure 5.127. First Rupture Moment of Case 8

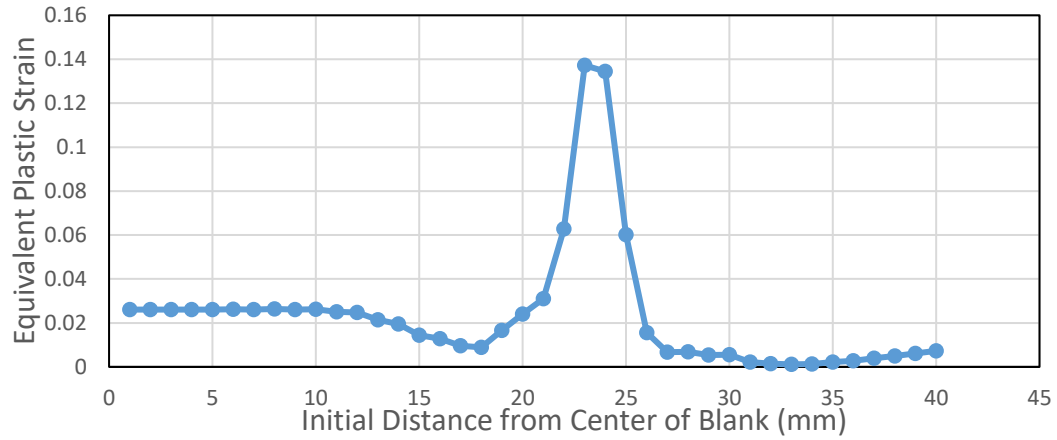

(a)

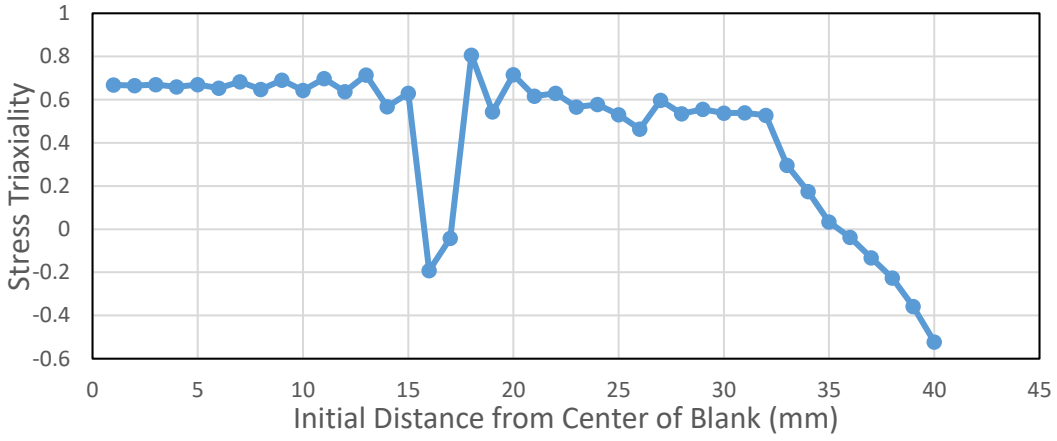

(b)

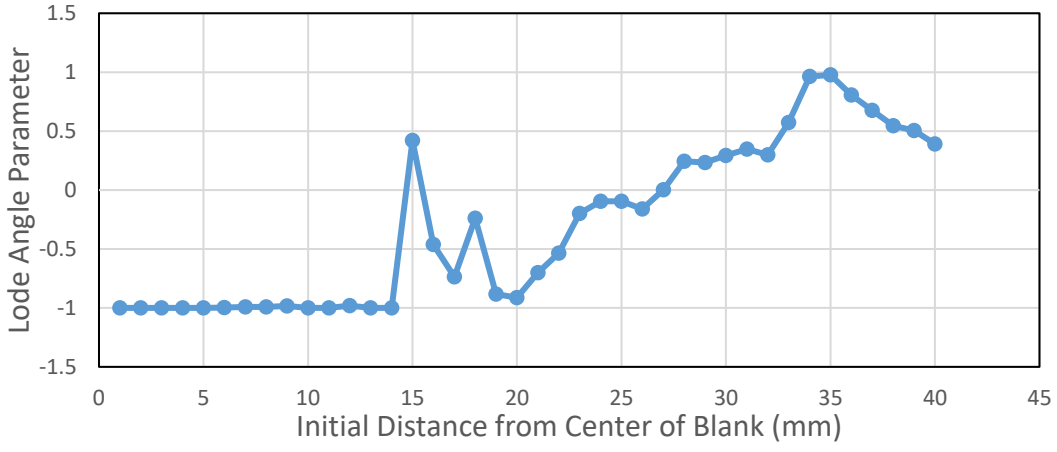

(c)

Figure 5.128. The variation of (a) Equivalent Plastic Strain (b) Stress Triaxiality and (c) Lode Angle Parameter along the rolling direction of the blank at 4 mm cup depth for AISI 304 steel (VM-Disc-HC)

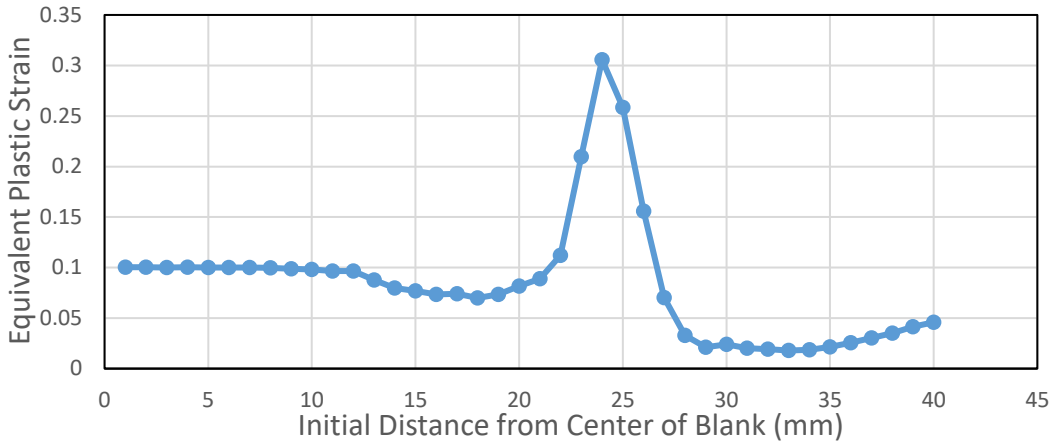

(a)

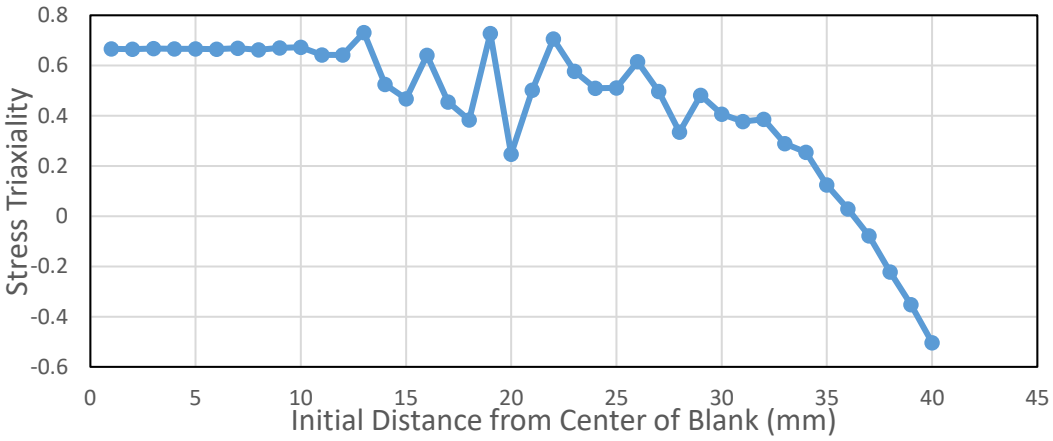

(b)

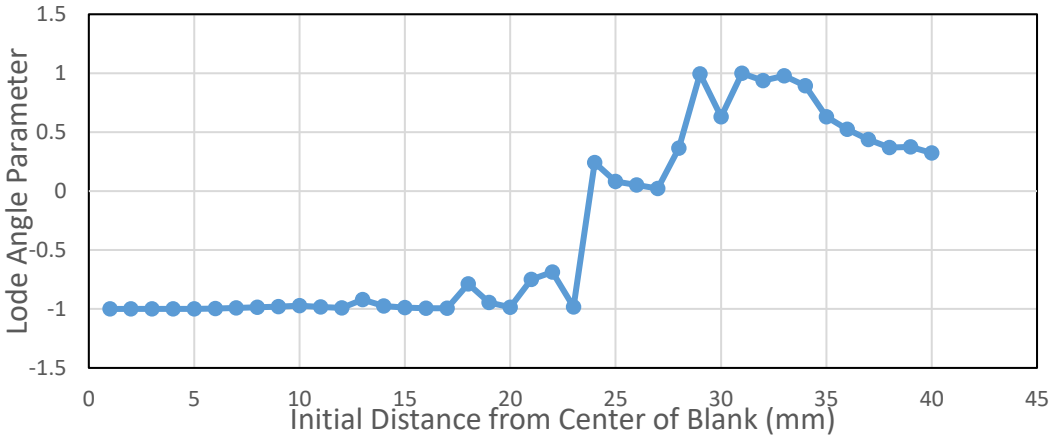

(c)

Figure 5.129. The variation of (a) Equivalent Plastic Strain (b) Stress Triaxiality and (c) Lode Angle Parameter along the rolling direction of the blank at 8 mm cup depth for AISI 304 steel (VM-Disc-HC)

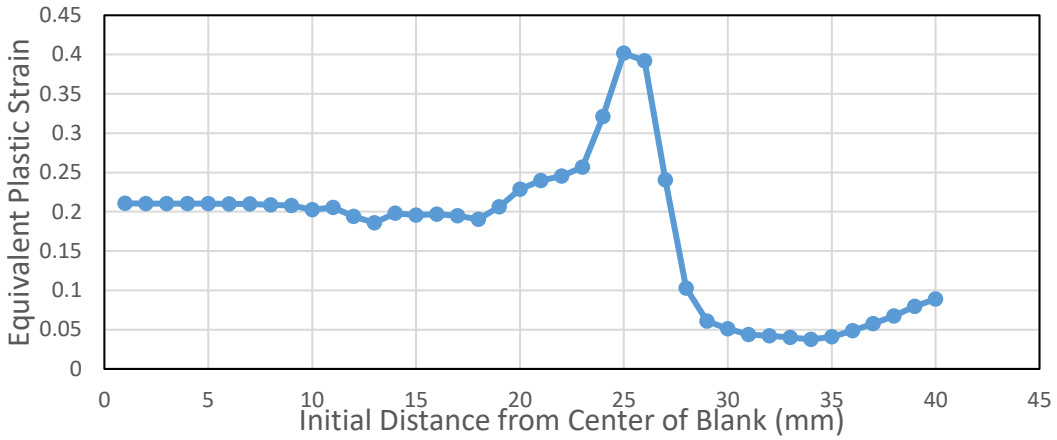

(a)

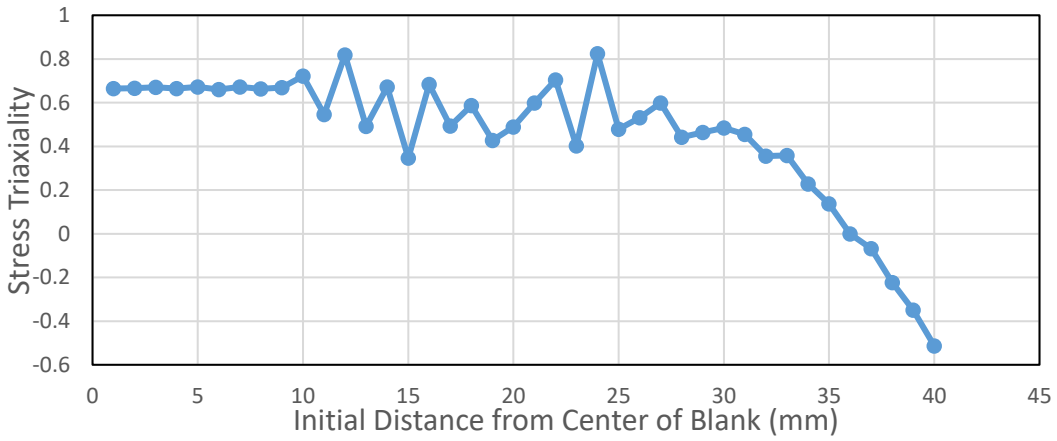

(b)

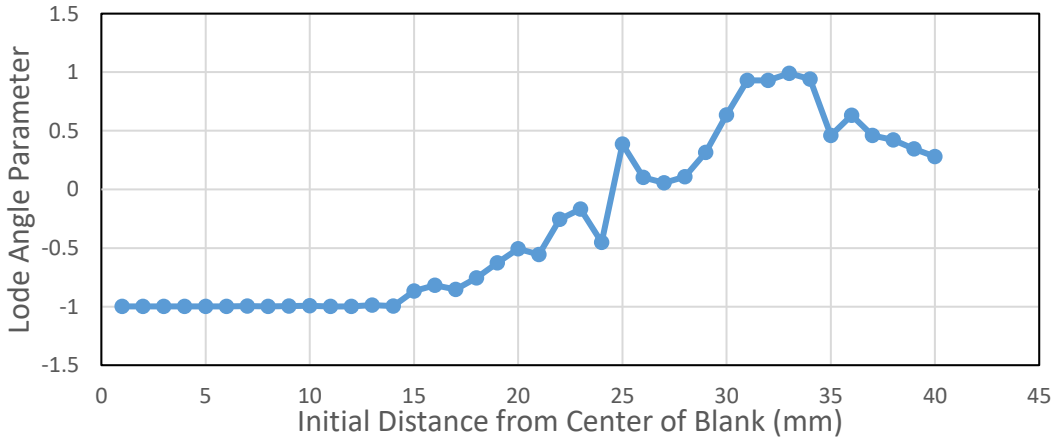

(c)

Figure 5.130. The variation of (a) Equivalent Plastic Strain (b) Stress Triaxiality and (c) Lode Angle Parameter along the rolling direction of the blank at 12 mm cup depth for AISI 304 steel (VM-Disc-HC)

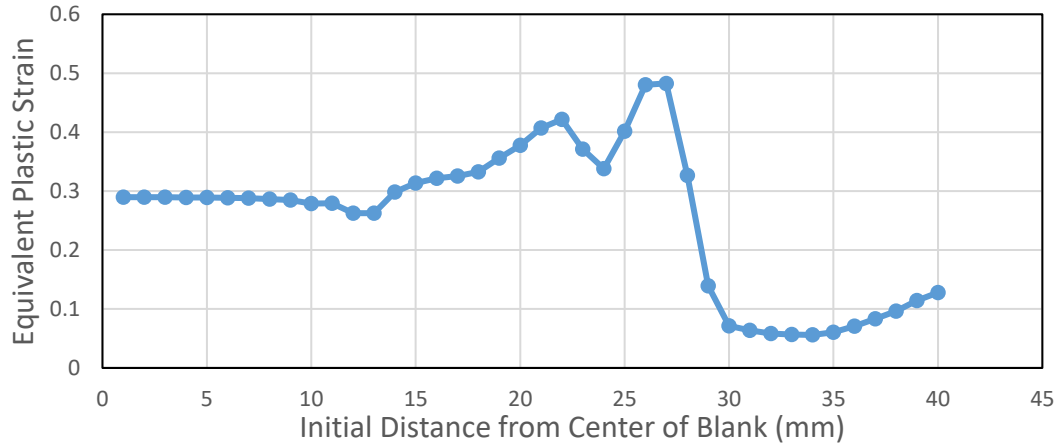

(a)

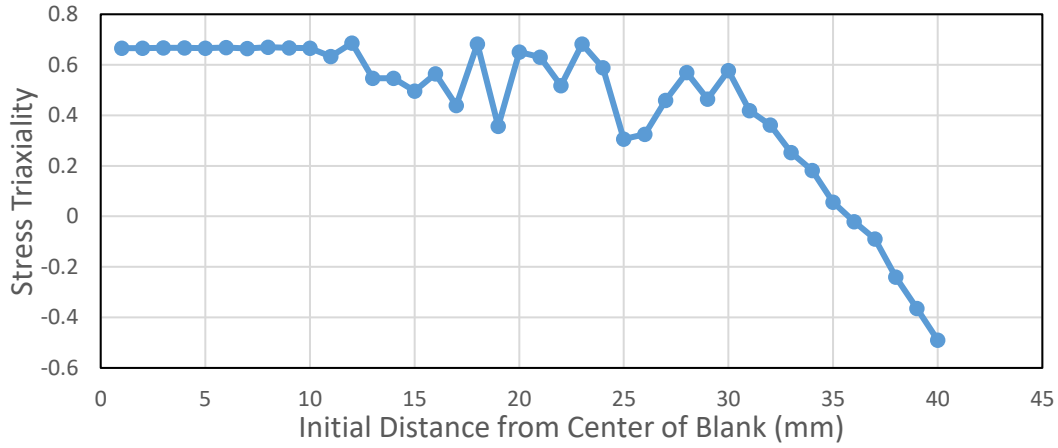

(b)

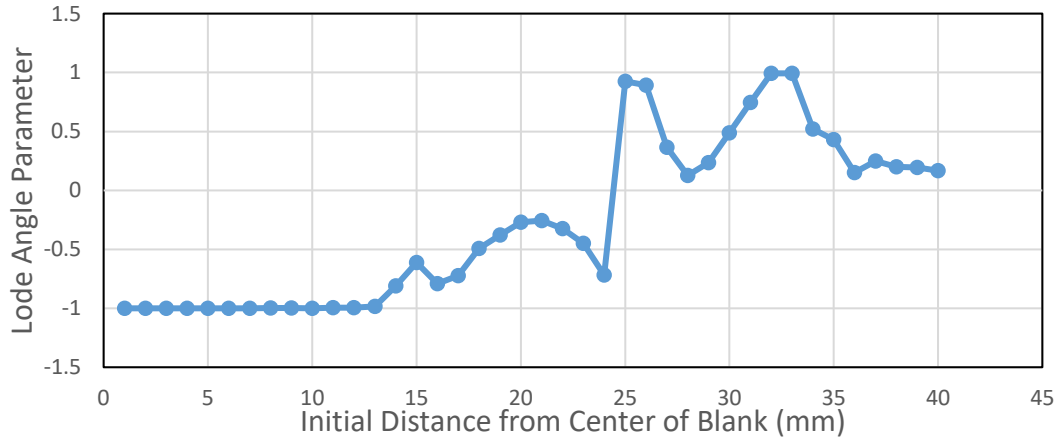

(c)

Figure 5.131. The variation of (a) Equivalent Plastic Strain (b) Stress Triaxiality and (c) Lode Angle Parameter along the rolling direction of the blank at 16 mm cup depth for AISI 304 steel (VM-Disc-HC)

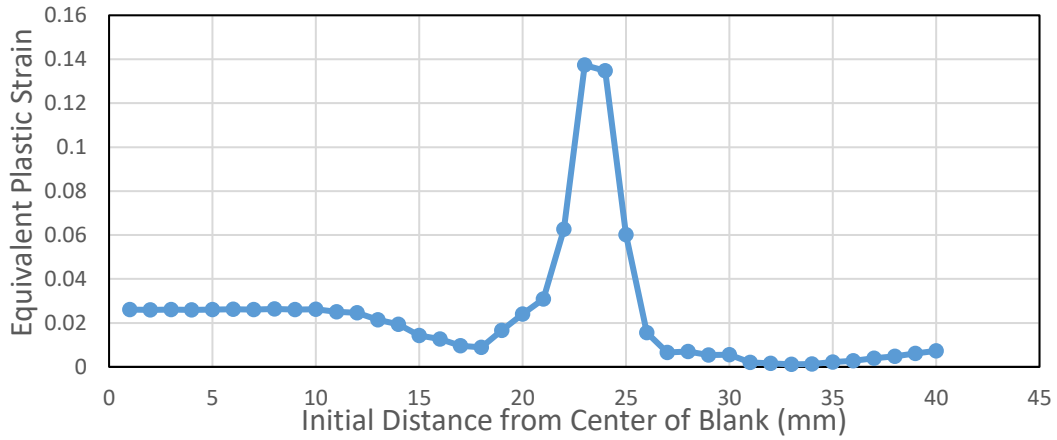

(a)

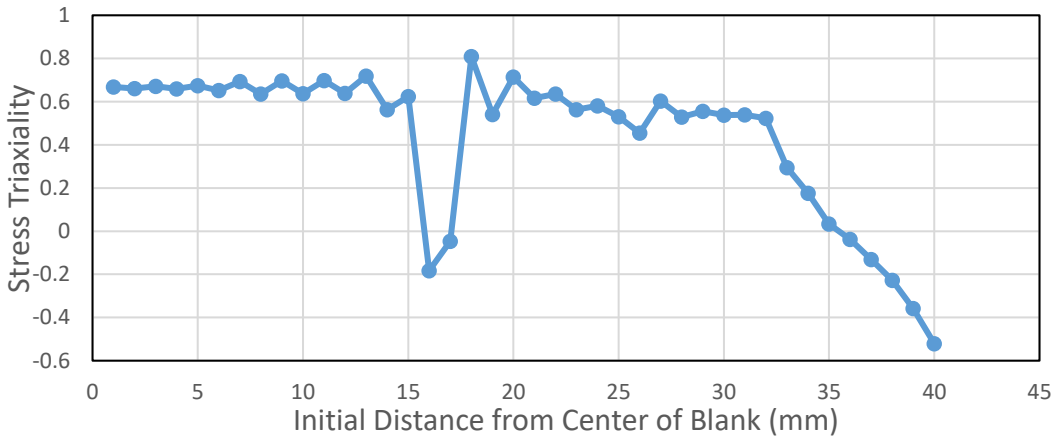

(b)

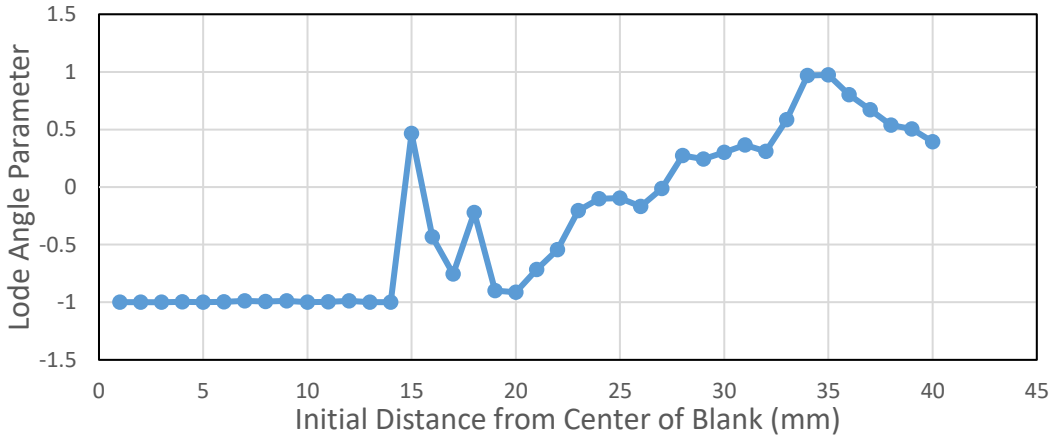

(c)

Figure 5.132. The variation of (a) Equivalent Plastic Strain (b) Stress Triaxiality and (c) Lode Angle Parameter along the transverse direction of the blank at 4 mm cup depth for AISI 304 steel (VM-Disc-HC)

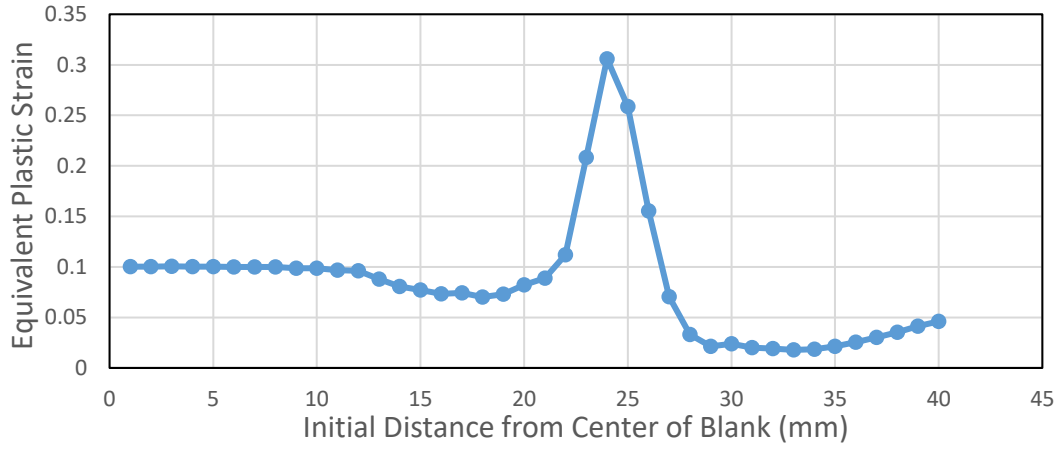

(a)

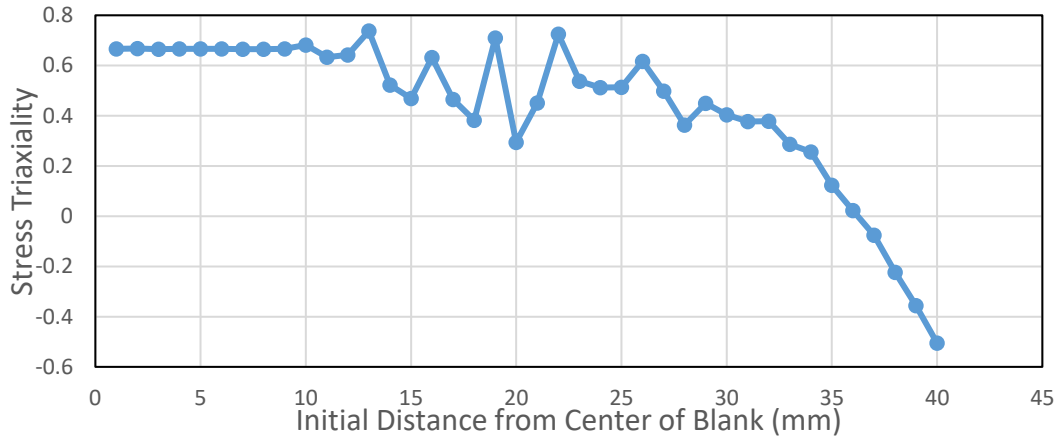

(b)

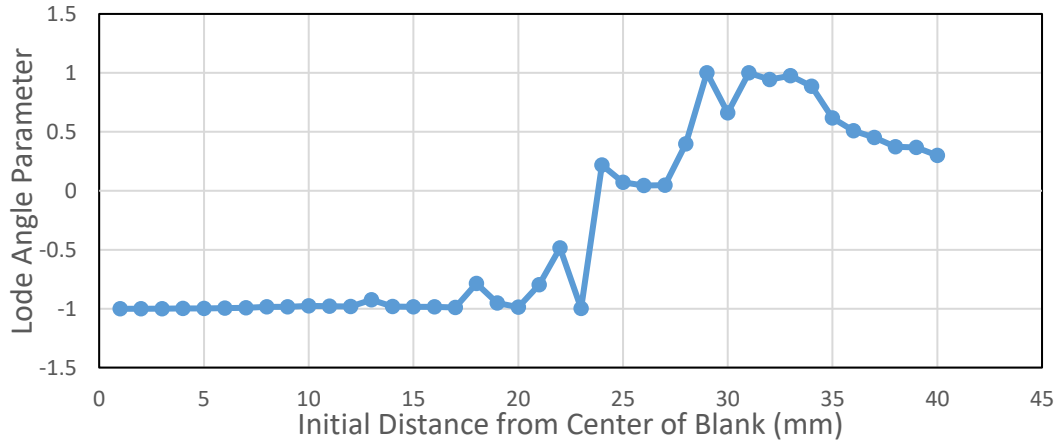

(c)

Figure 5.133. The variation of (a) Equivalent Plastic Strain (b) Stress Triaxiality and (c) Lode Angle Parameter along the transverse direction of the blank at 8 mm cup depth for AISI 304 steel (VM-Disc-HC)

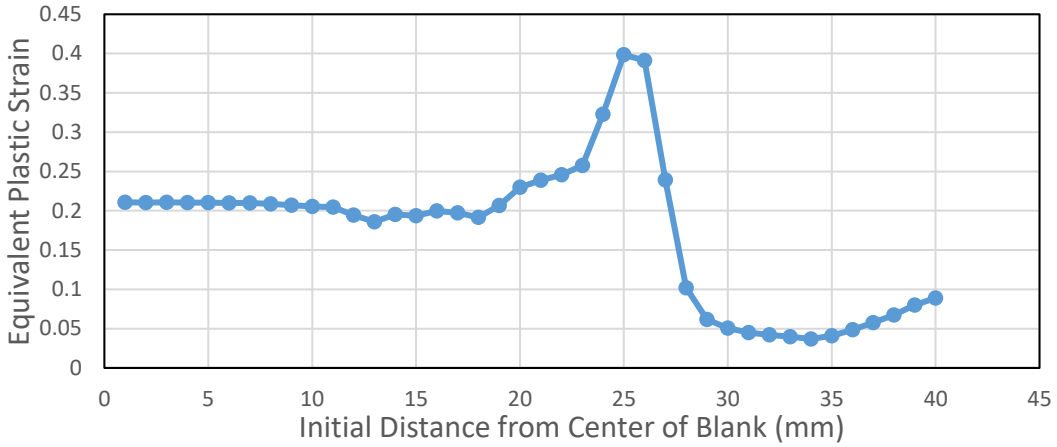

(a)

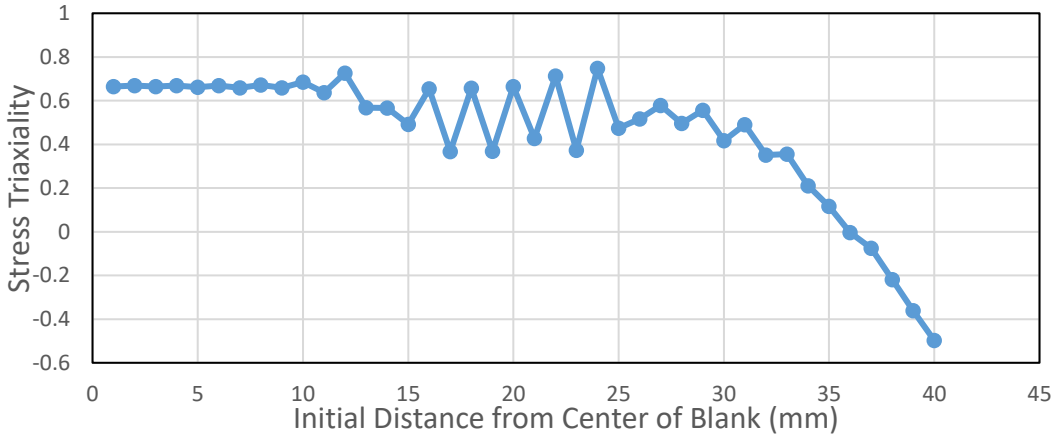

(b)

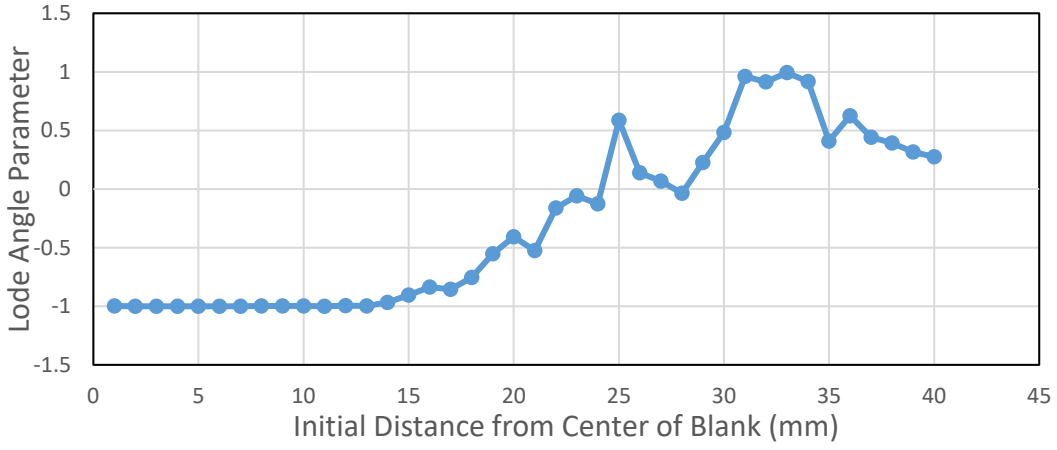

(c)

Figure 5.134. The variation of (a) Equivalent Plastic Strain (b) Stress Triaxiality and (c) Lode Angle Parameter along the transverse direction of the blank at 12 mm cup depth for AISI 304 steel (VM-Disc-HC)

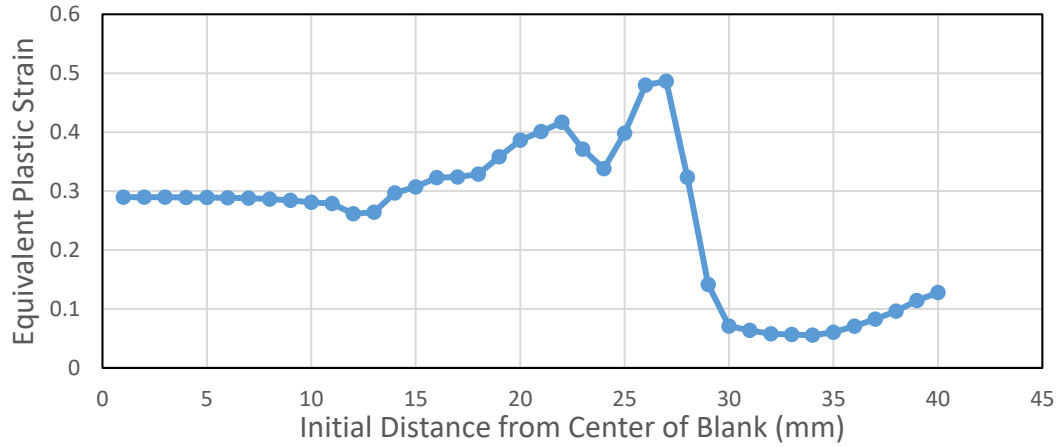

(a)

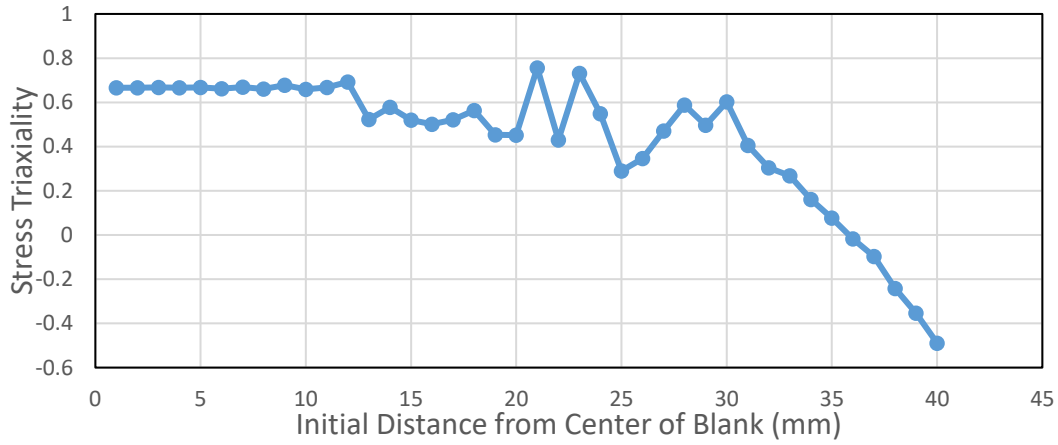

(b)

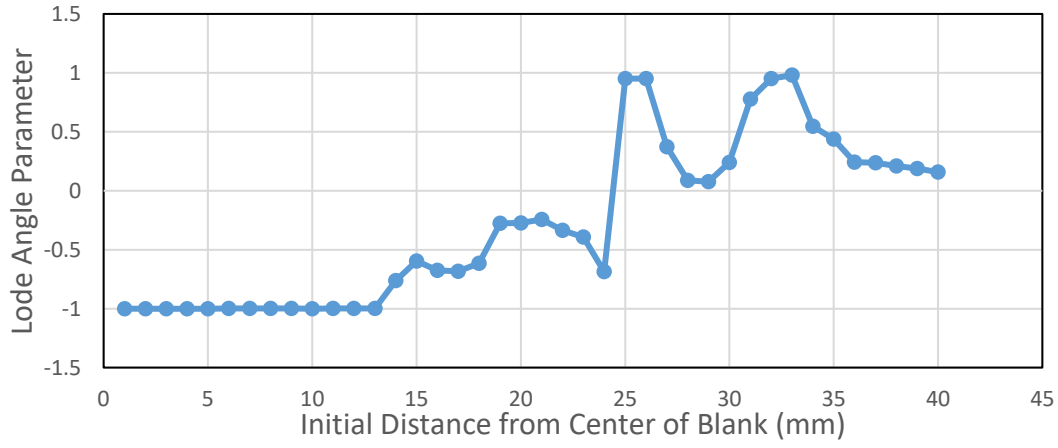

(c)

Figure 5.135. The variation of (a) Equivalent Plastic Strain (b) Stress Triaxiality and (c) Lode Angle Parameter along the transverse direction of the blank at 16 mm cup depth for AISI 304 steel (VM-Disc-HC)

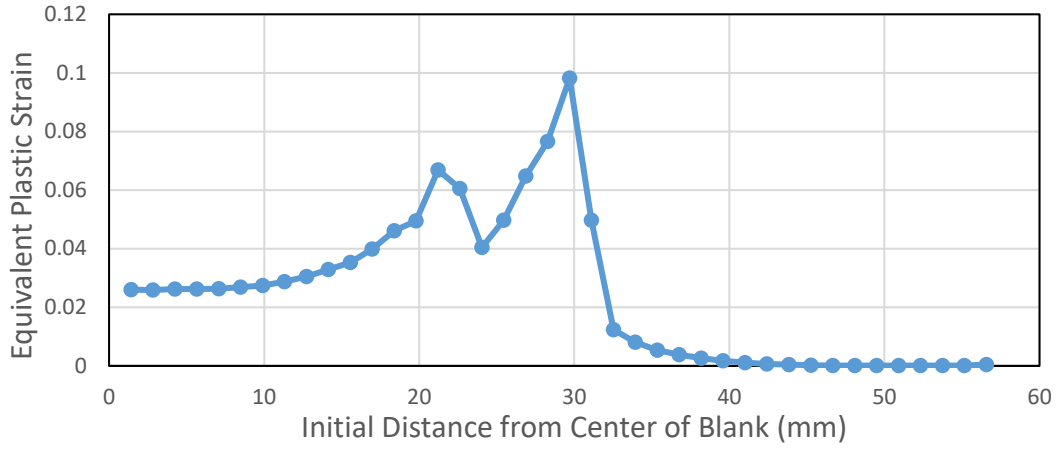

(a)

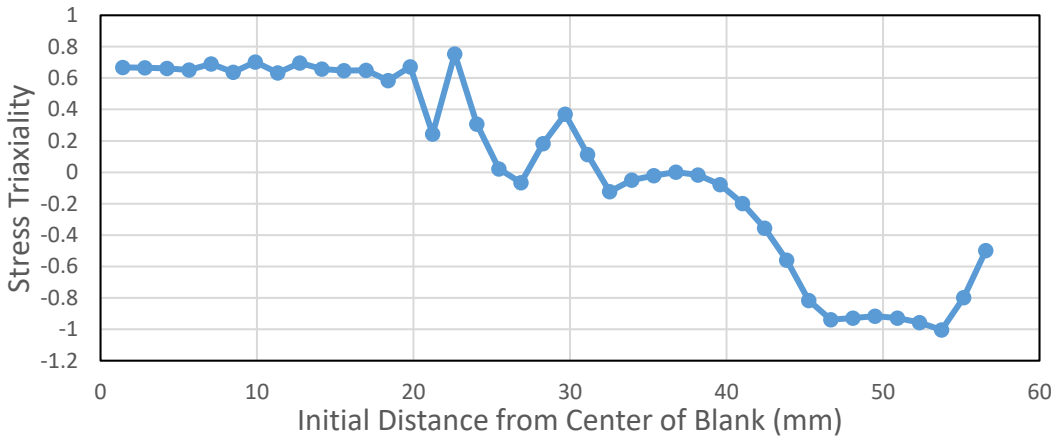

(b)

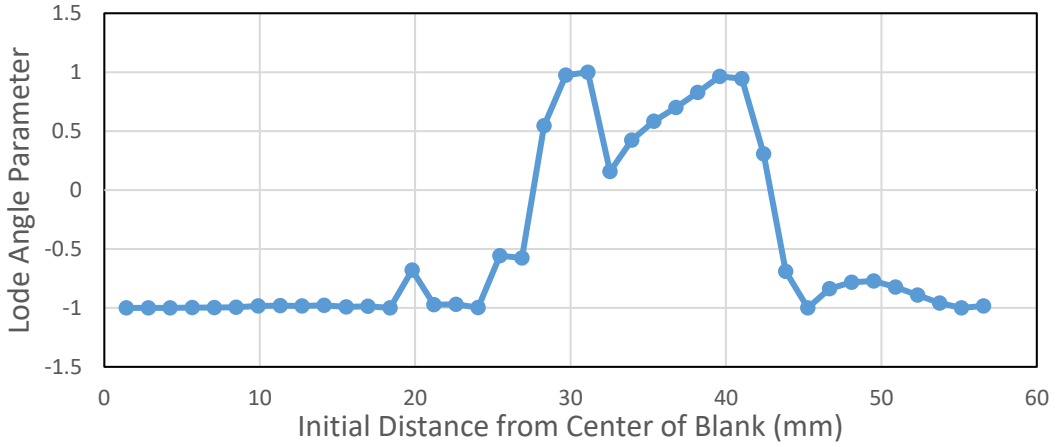

(c)

Figure 5.136. The variation of (a) Equivalent Plastic Strain (b) Stress Triaxiality and (c) Lode Angle Parameter along the diagonal of the blank at 4 mm cup depth for AISI 304 steel (VM-Disc-HC)

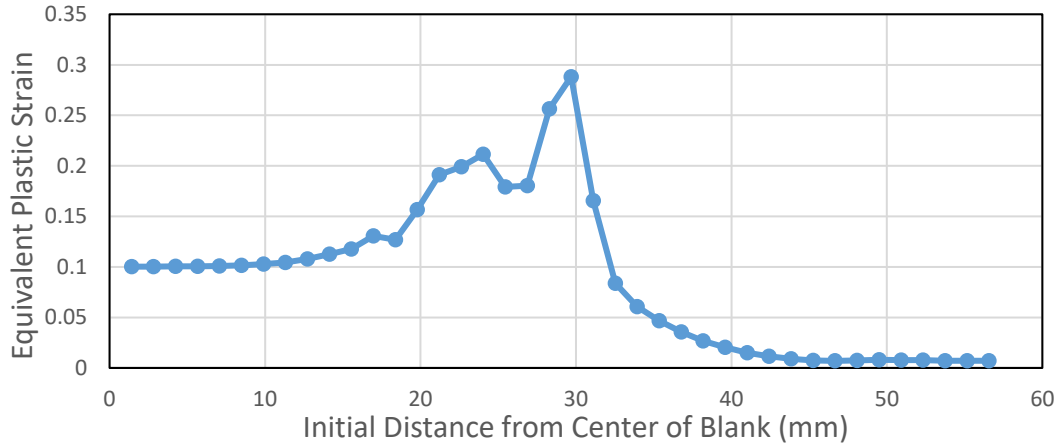

(a)

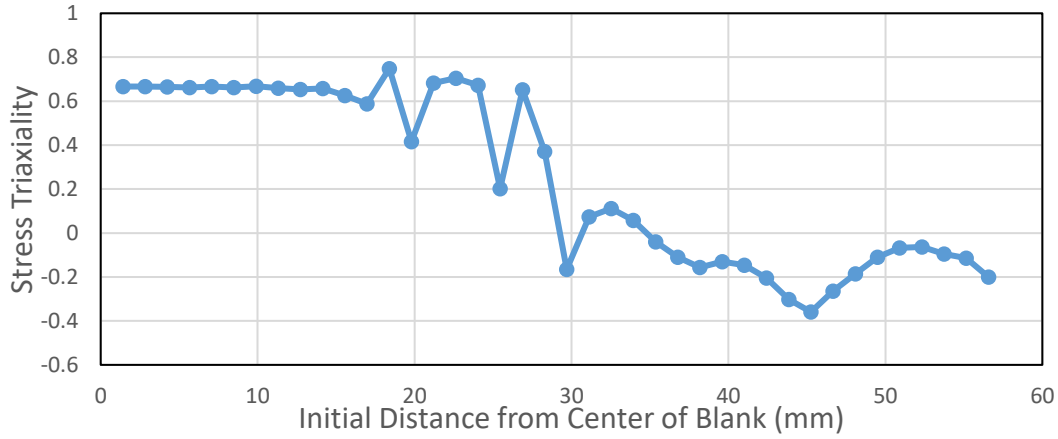

(b)

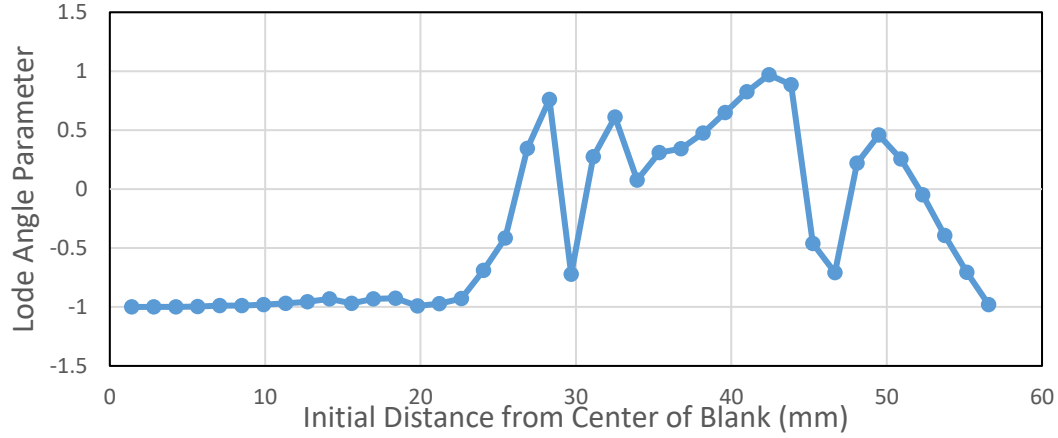

(c)

Figure 5.137. The variation of (a) Equivalent Plastic Strain (b) Stress Triaxiality and (c) Lode Angle Parameter along the diagonal of the blank at 8 mm cup depth for AISI 304 steel (VM-Disc-HC)

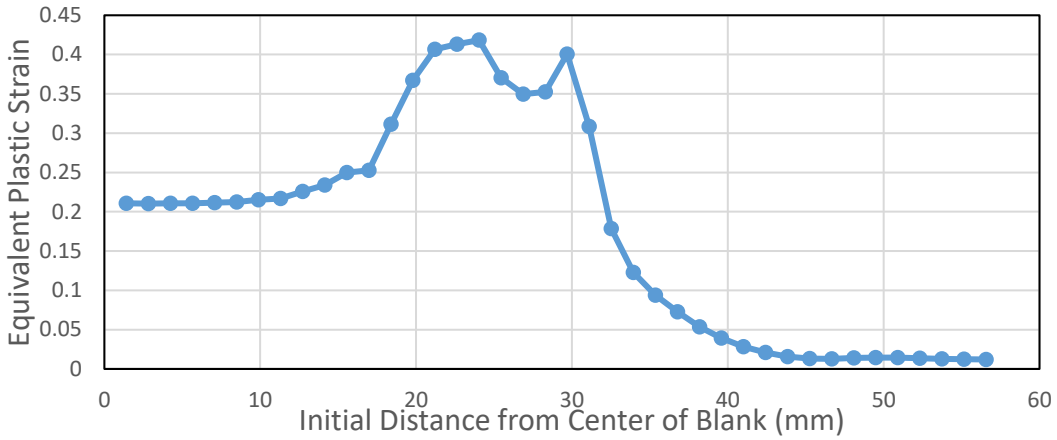

(a)

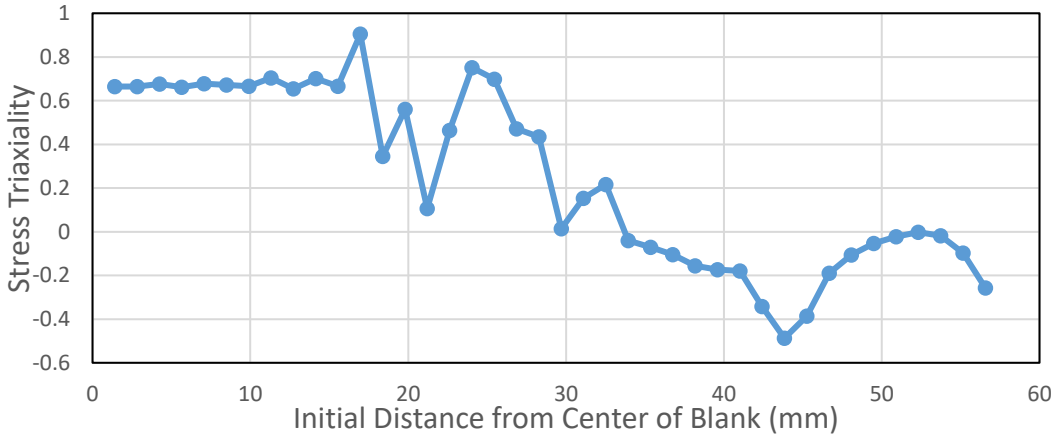

(b)

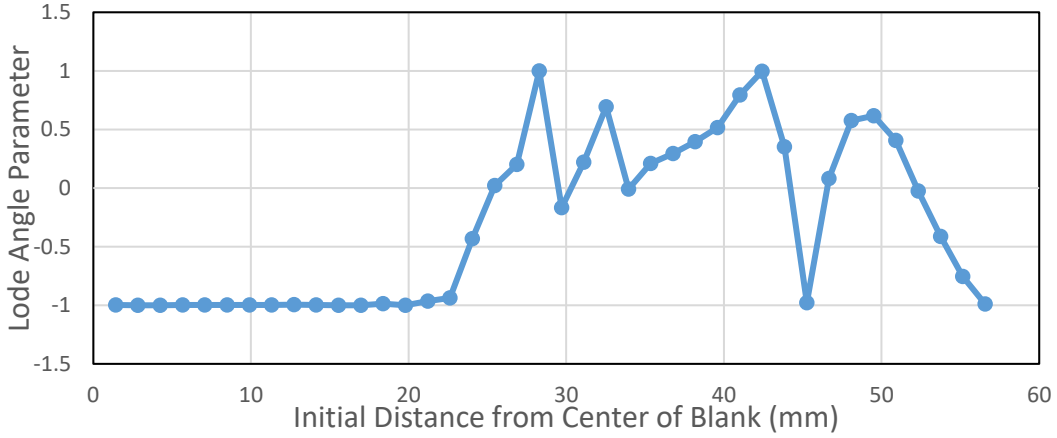

(c)

Figure 5.138 The variation of (a) Equivalent Plastic Strain (b) Stress Triaxiality and (c) Lode Angle Parameter along the diagonal of the blank at 12 mm cup depth for AISI 304 steel (VM-Disc-HC)

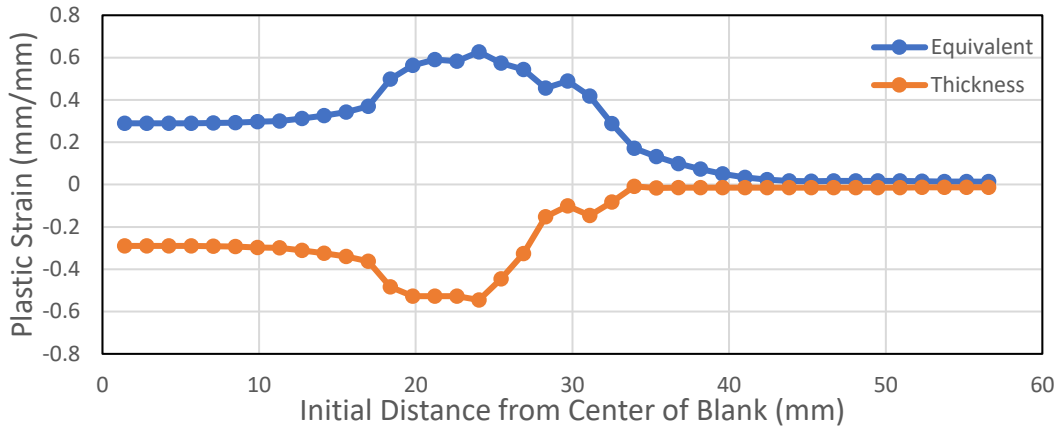

(a)

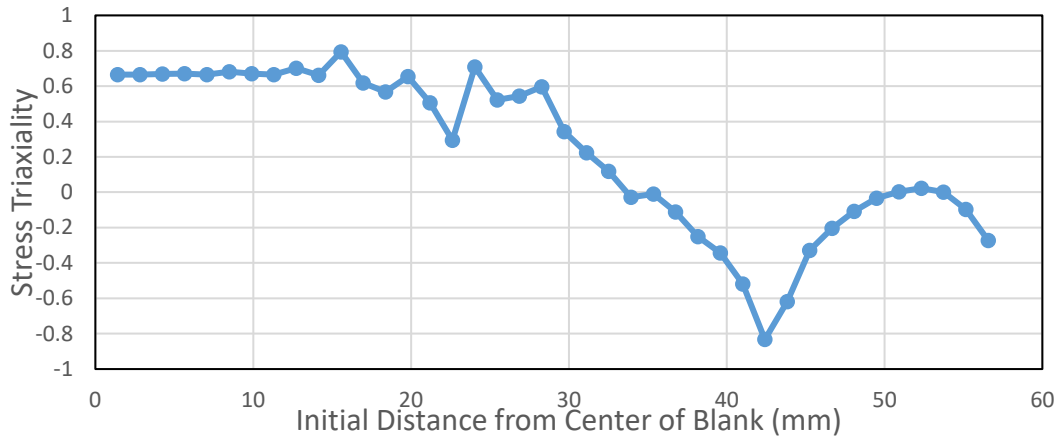

(b)

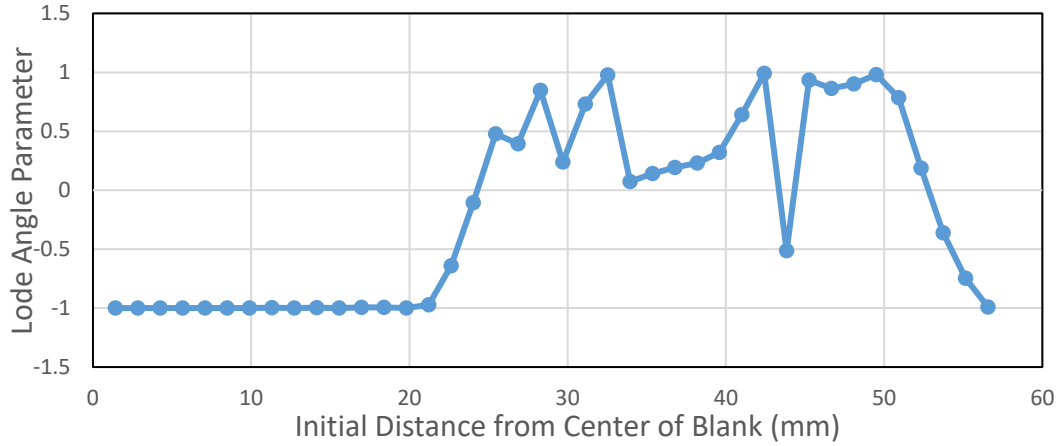

(c)

Figure 5.139 The variation of (a) Equivalent Plastic Strain and Thickness Plastic Strain (b) Stress Triaxiality and (c) Lode Angle Parameter along the diagonal of the blank at 16 mm cup depth for AISI 304 steel (VM-Disc-HC)

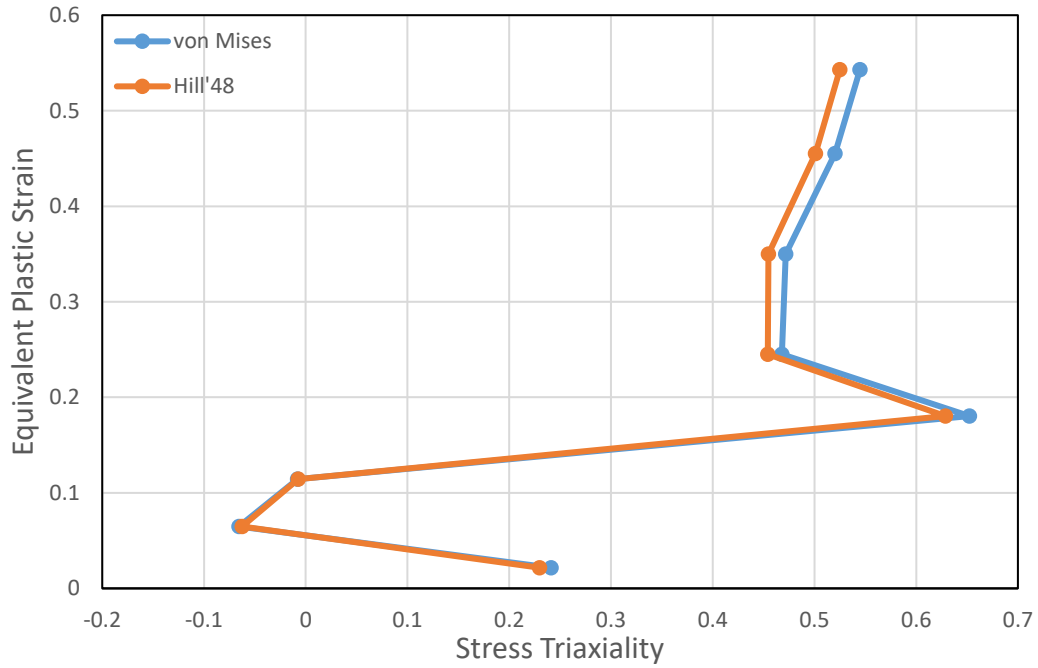

Figure 5.140. Equivalent Plastic Strain - Stress Triaxiality Plot of First Rupture Element (VM-Disc-HC)

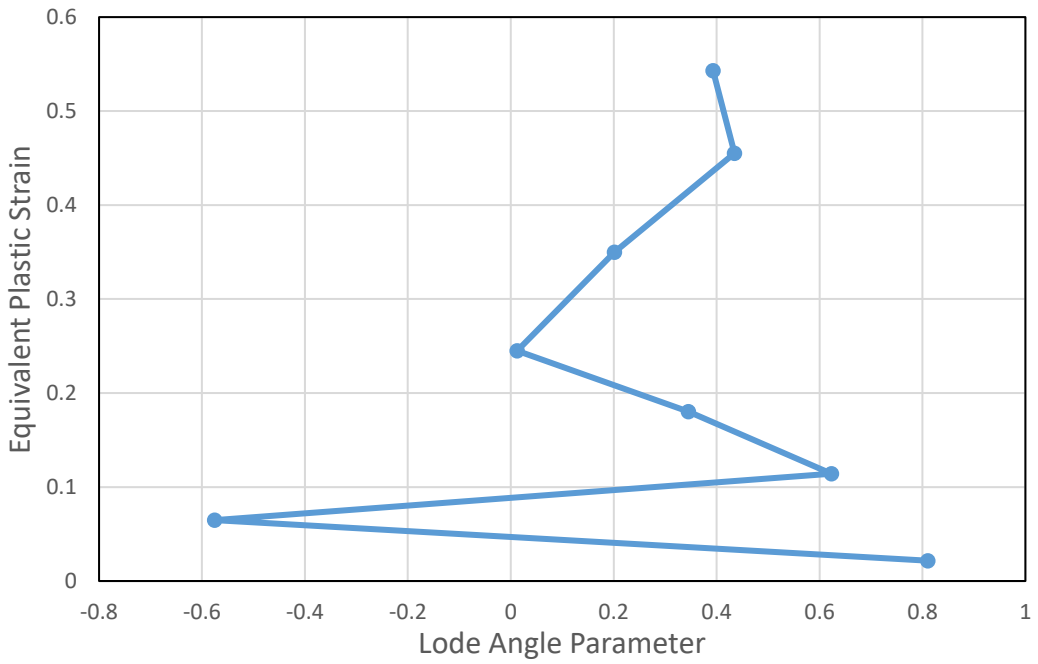

Figure 5.141. Equivalent Plastic Strain – Lode Angle Parameter Plot of First Rupture Element (VM-Disc-HC)

In the rolling direction, the triaxiality values vary generally between 0.6 and 0.8 under the punch whereas the Lode angle parameter values change between -0.8 and -1 up to a distance of 15 mm from the center, it can be said that the deformation behavior is in equi-biaxial tension condition. After 30 mm distance from blank center, under blank holder, triaxiality values decreasing with positive Lode angle parameter values. According to these values it can be said that, under blank holder region stress state is compressive.

The same tendency of rolling direction is observed in the transverse direction also. The differences are a result of anisotropy of the material.

In the diagonal direction, as in the transverse and rolling directions, equi-biaxial stress condition is observed under the punch. When the pre-rupture state of sheet is examined, it is seen that equi-biaxial stress conditions dominates up to 20 mm from the center of the blank. At the punch shoulder, stress state changes from tension to shear while triaxiality values decreasing. On the other hand, the Lode angle parameter values increases as with distance from the center of the blank. After this region, triaxiality values are increasing and Lode angle parameter values are decreasing. Fracture occurs at the punch shoulder in tension situation.

5.1.9 Case 9: Square- AISI304-von Mises -Johnson Cook-Johnson Cook Model

For the ninth case, von Mises yield criterion was applied with Johnson Cook hardening and the Johnson Cook ductile fracture criterion was used. It was observed that the fracture had started after 20 mm punch travel as shown in Figure 5.142 The variation of equivalent plastic strain, stress triaxiality and Lode angle parameter values are presented as a function of the distance from the center of the blank for different cup heights up to the fracture. The results are shown for rolling direction in Figure 5.143 to Figure 5.147, for transverse direction in Figure 5.148 to Figure 5.152 and for diagonal direction in Figure 5.153 to Figure 5.157. The thickness plastic strain distribution is also inserted into Figure 5.157 (a) in order to better visualize the deformation. Further, the variations of stress triaxiality values with respect to equivalent plastic strain are given by considering both von Mises and Hill'48 criteria as a function of the path of the element that fractured first in Figure 5.158 Along the same path, the variation of the Lode parameter with respect to equivalent plastic strain is also illustrated in Figure 5.159. Finally, the variation of triaxiality values with respect to Lode angle parameter values are given in Figure 5.160 to Figure 5.162 for rolling direction in Figure 5.160, for transverse direction Figure 5.161 and, in Figure 5.162 for diagonal direction. The variations are first given for the whole deformation and then for punch, punch shoulder or corner, the clearance between die and punch, punch shoulder or corner and for the blank holder regions.

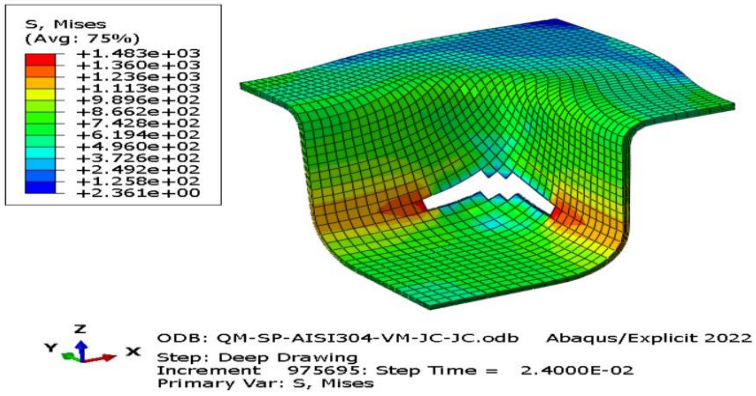

Figure 5.142. First Rupture Moment of Case 9

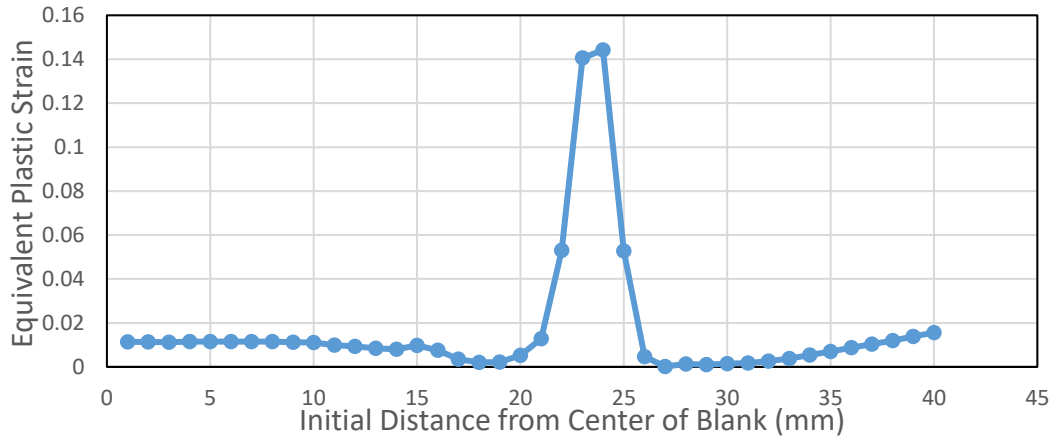

(a)

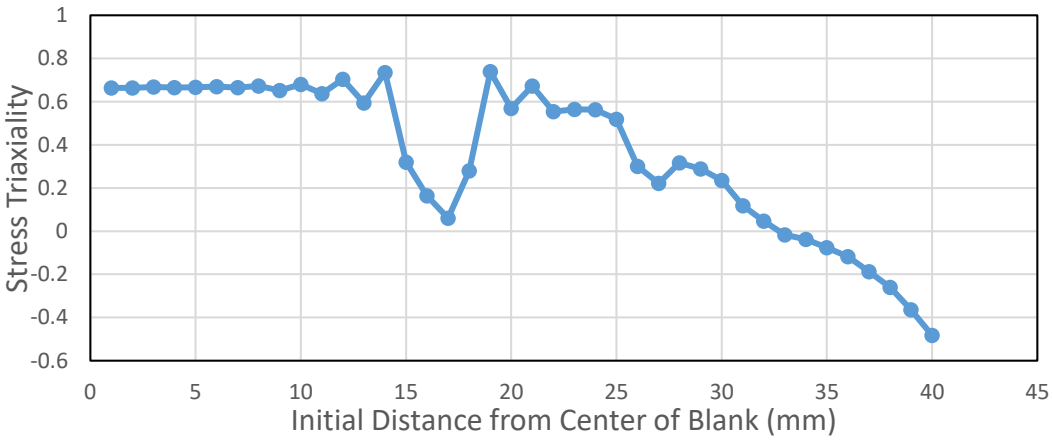

(b)

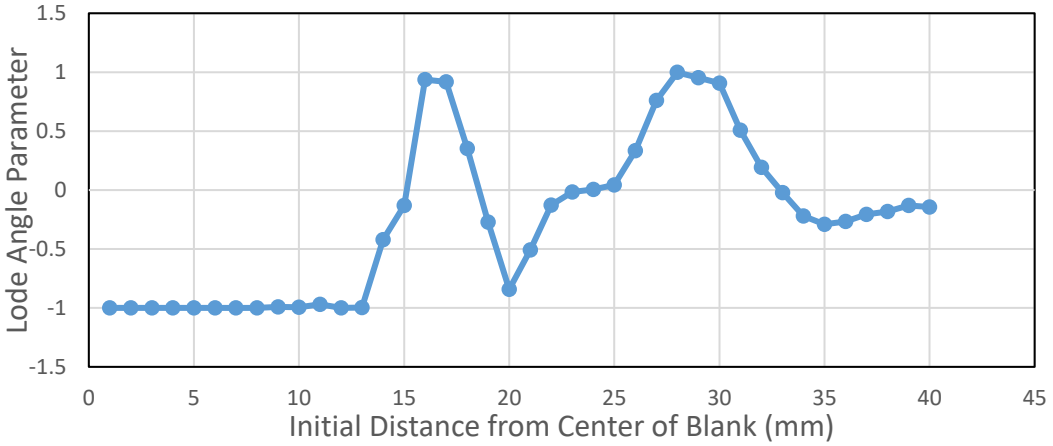

(c)

Figure 5.143. The variation of (a) Equivalent Plastic Strain (b) Stress Triaxiality and (c) Lode Angle Parameter along the rolling direction of the blank at 4 mm cup depth for AISI 304 steel (VM-JC-JC)

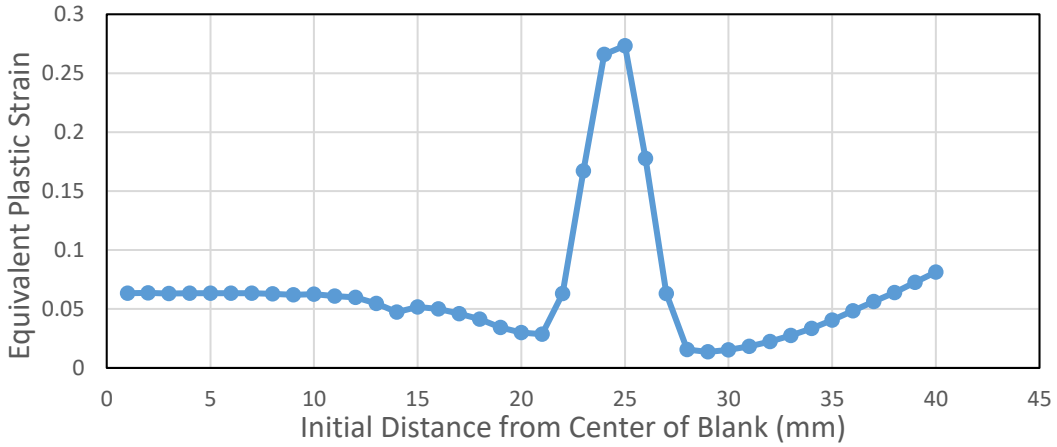

(a)

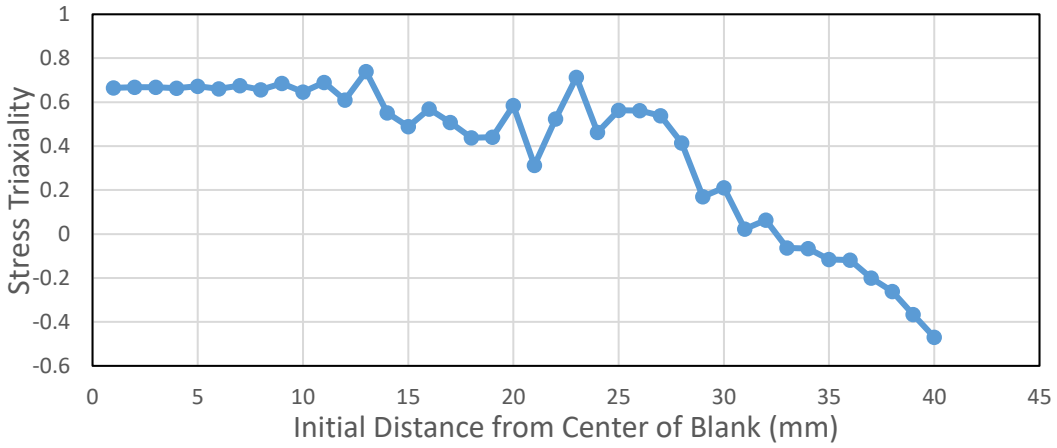

(b)

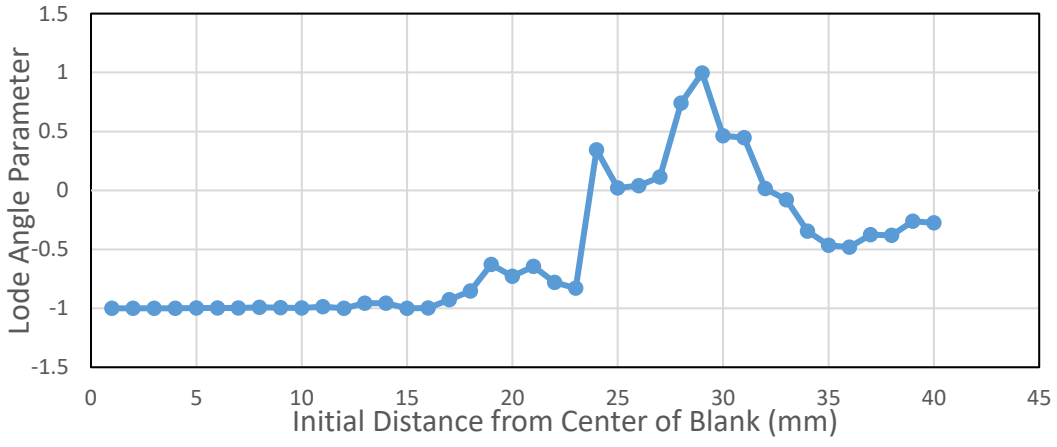

(c)

Figure 5.144. The variation of (a) Equivalent Plastic Strain (b) Stress Triaxiality and (c) Lode Angle Parameter along the rolling direction of the blank at 8 mm cup depth for AISI 304 steel (VM-JC-JC)

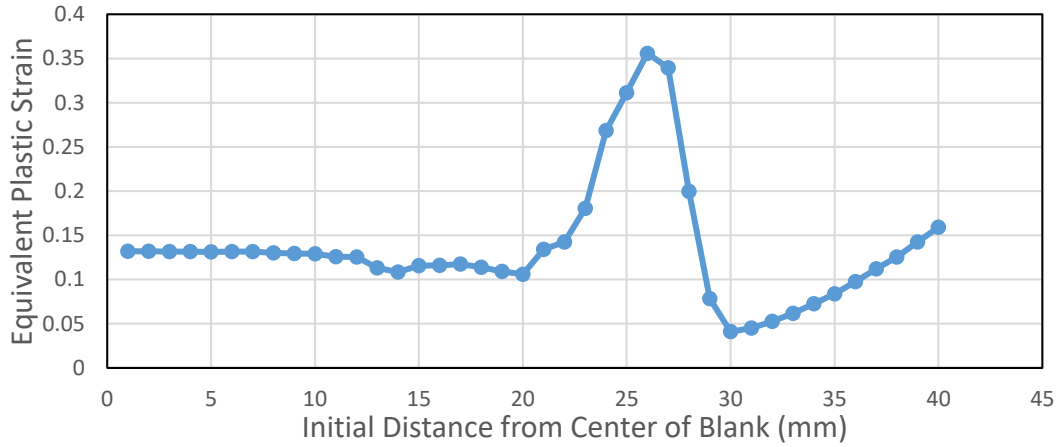

(a)

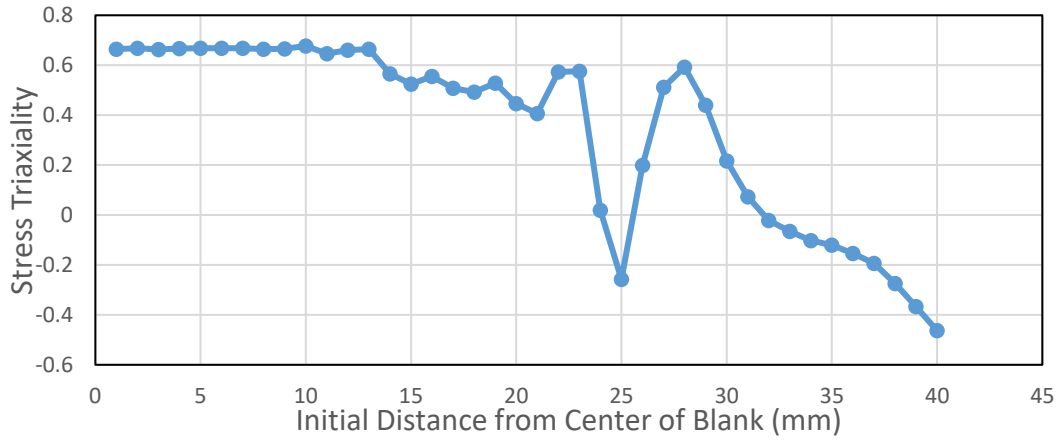

(b)

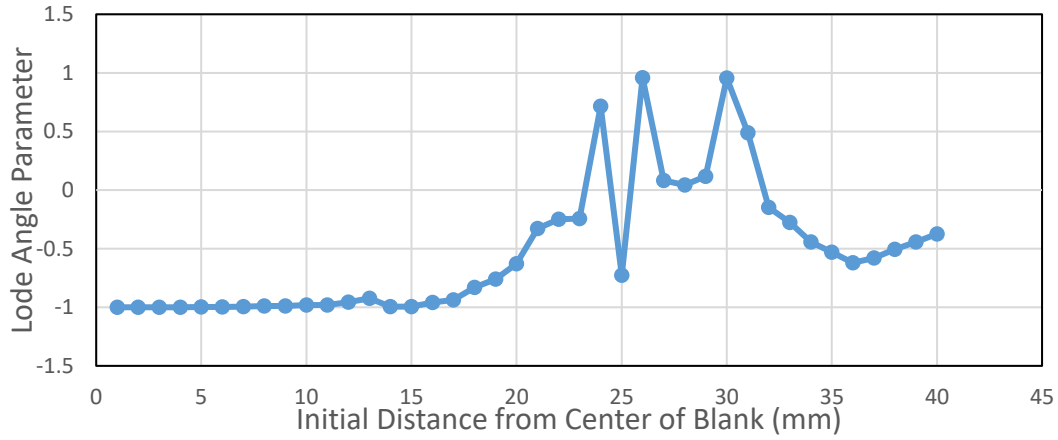

(c)

Figure 5.145. The variation of (a) Equivalent Plastic Strain (b) Stress Triaxiality and (c) Lode Angle Parameter along the rolling direction of the blank at 12 mm cup depth for AISI 304 steel (VM-JC-JC)

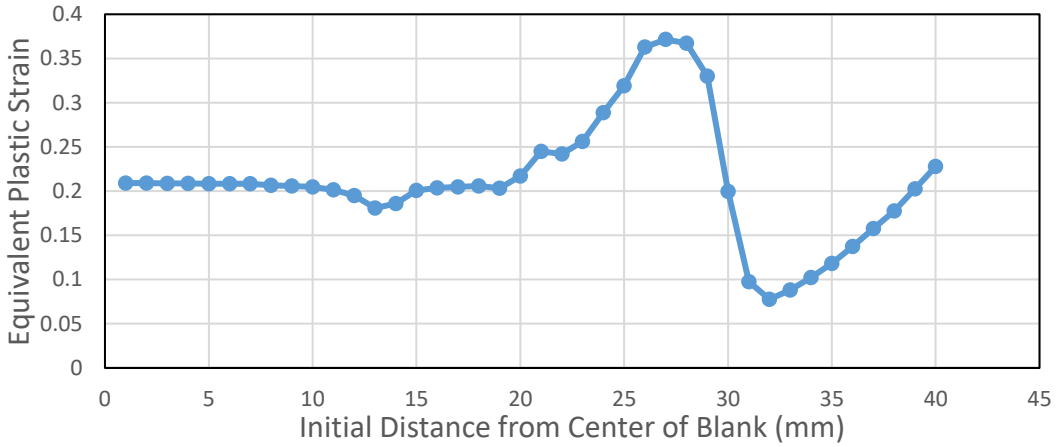

(a)

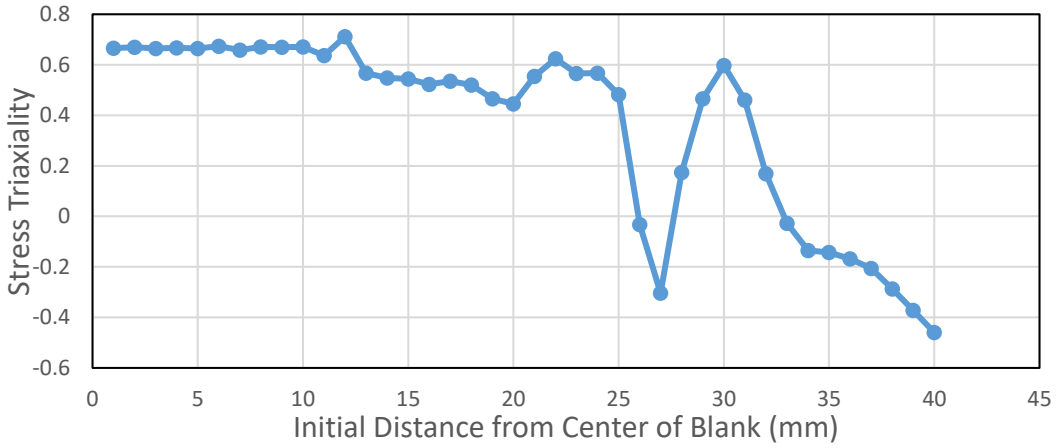

(b)

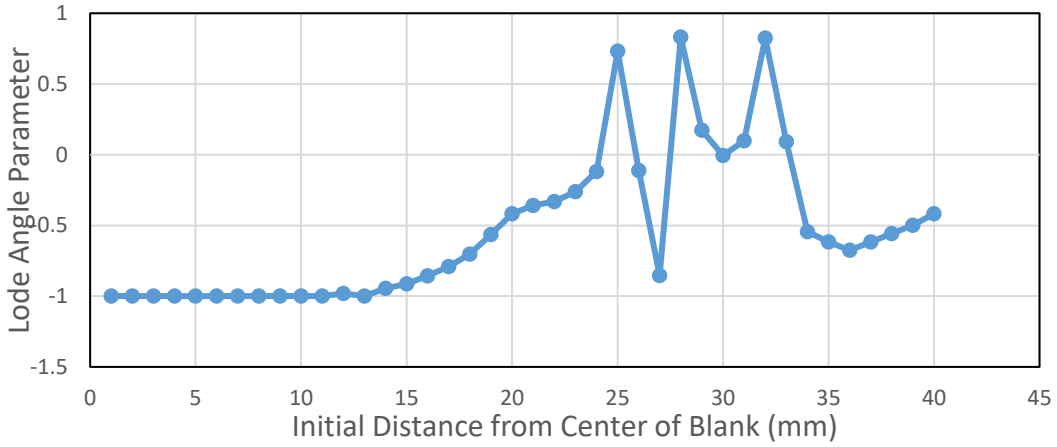

(c)

Figure 5.146. The variation of (a) Equivalent Plastic Strain (b) Stress Triaxiality and (c) Lode Angle Parameter along the rolling direction of the blank at 16 mm cup depth for AISI 304 steel (VM-JC-JC)

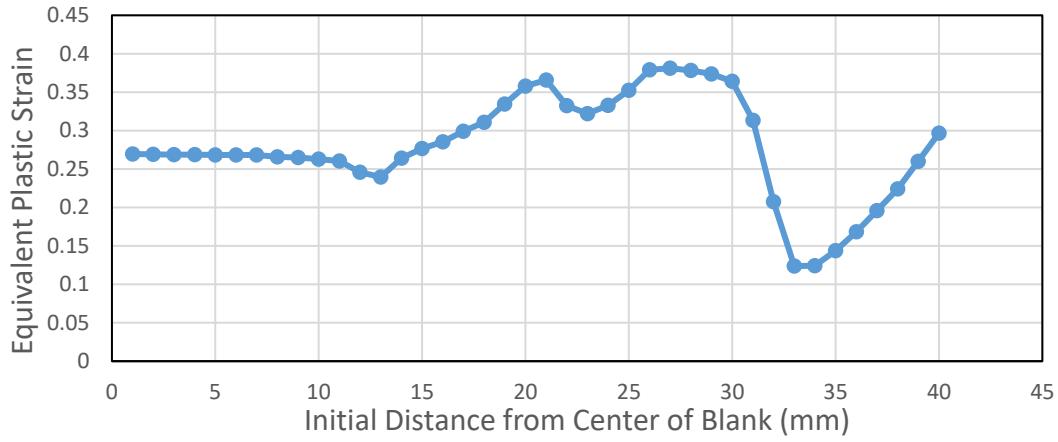

(a)

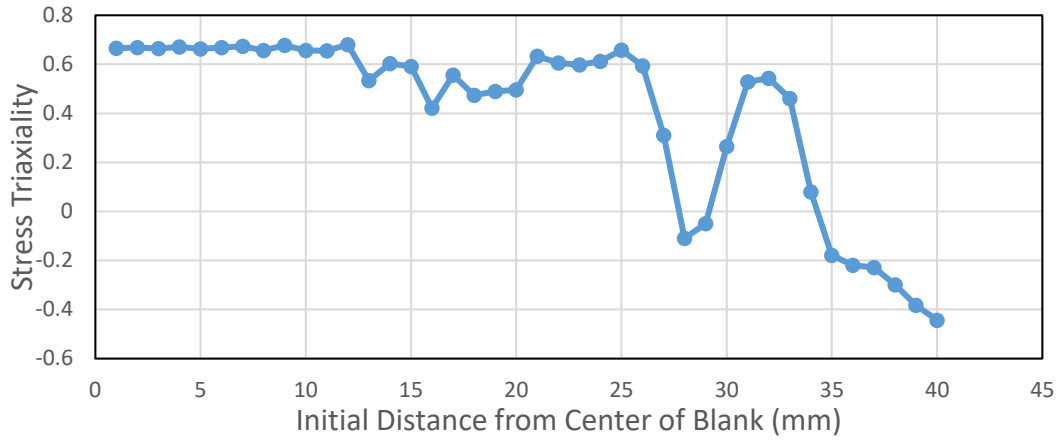

(b)

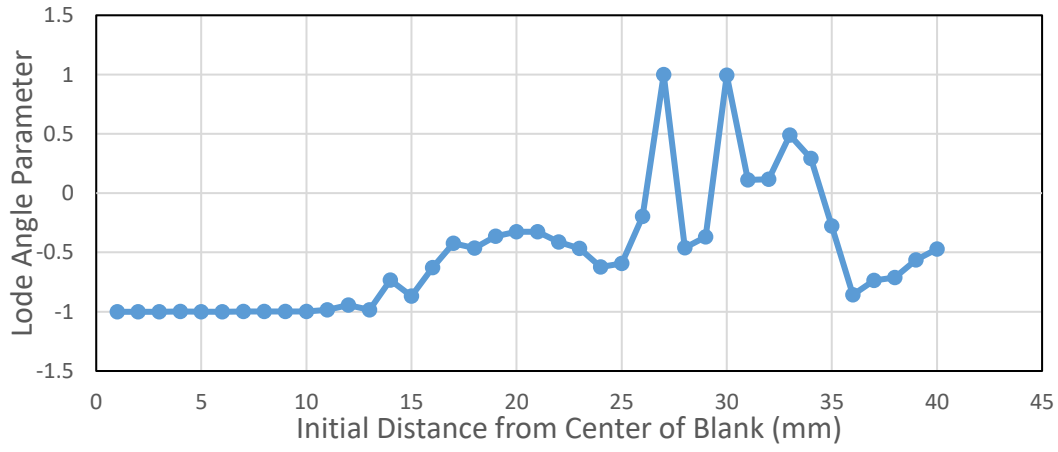

(c)

Figure 5.147. The variation of (a) Equivalent Plastic Strain (b) Stress Triaxiality and (c) Lode Angle Parameter along the rolling direction of the blank at 20 mm cup depth for AISI 304 steel (VM-JC-JC)

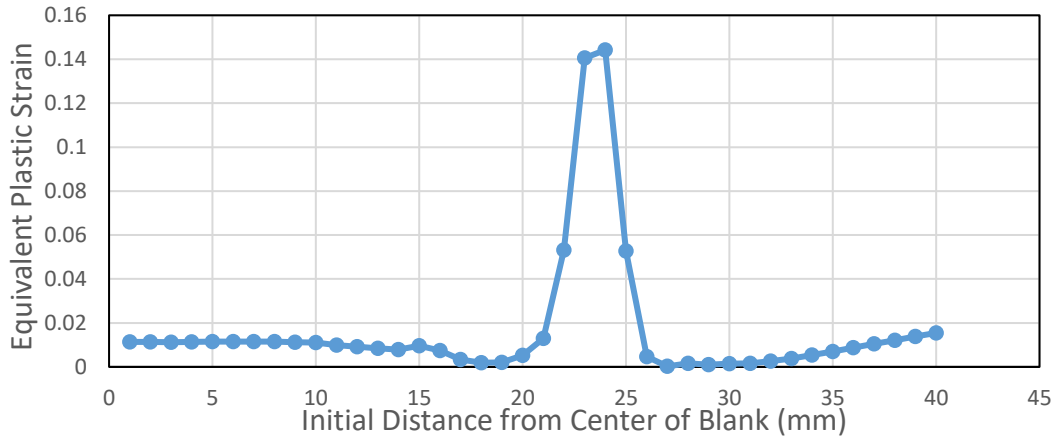

(a)

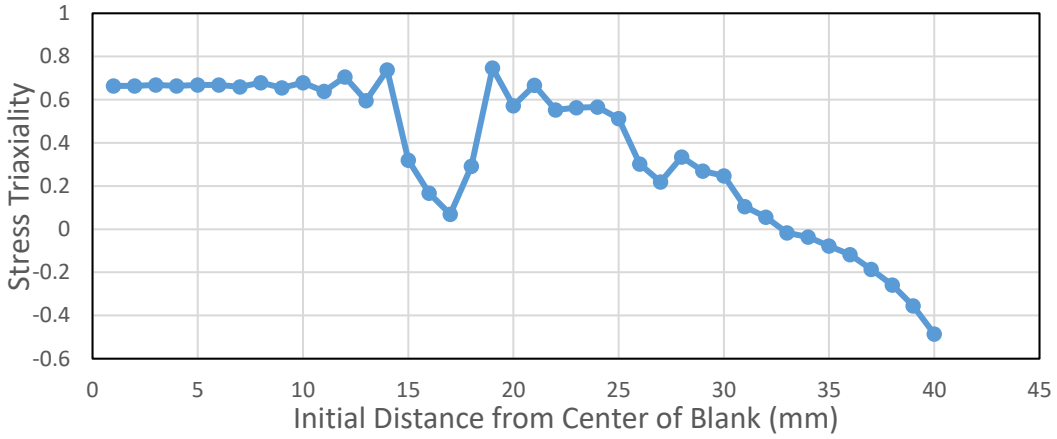

(b)

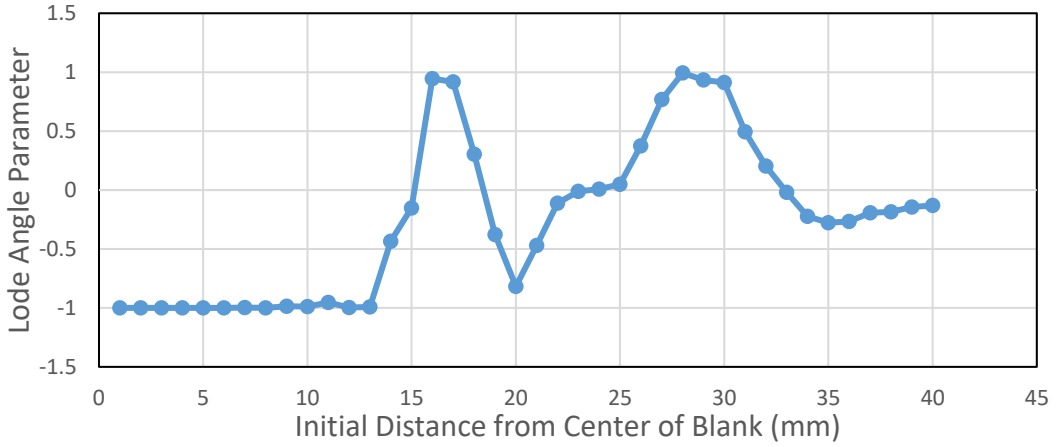

(c)

Figure 5.148. The variation of (a) Equivalent Plastic Strain (b) Stress Triaxiality and (c) Lode Angle Parameter along the transverse direction of the blank at 4 mm cup depth for AISI 304 steel (VM-JC-JC)

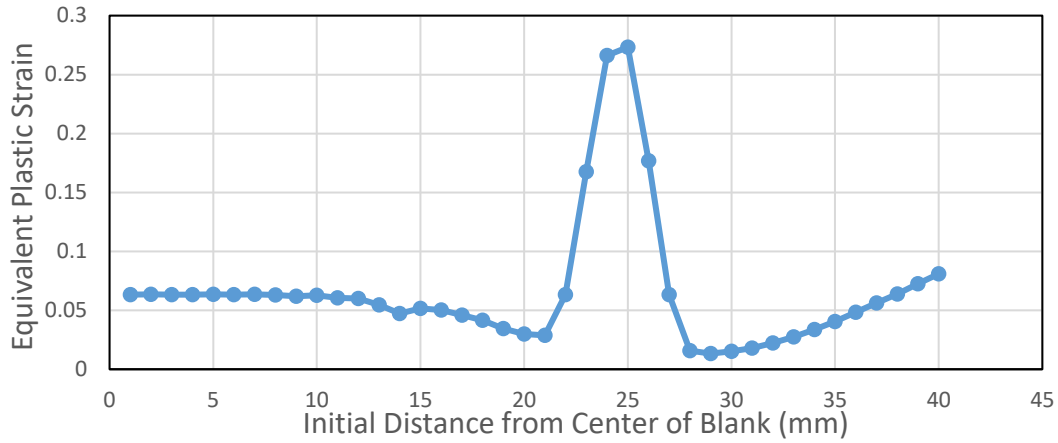

(a)

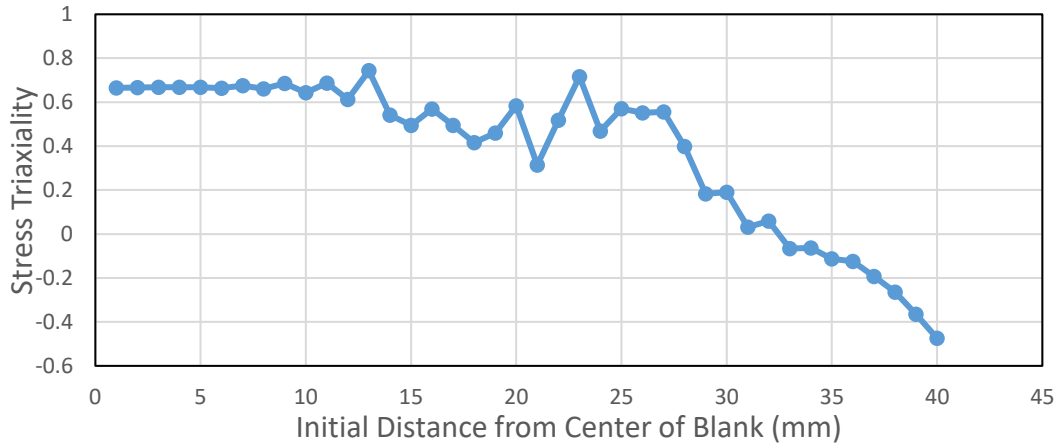

(b)

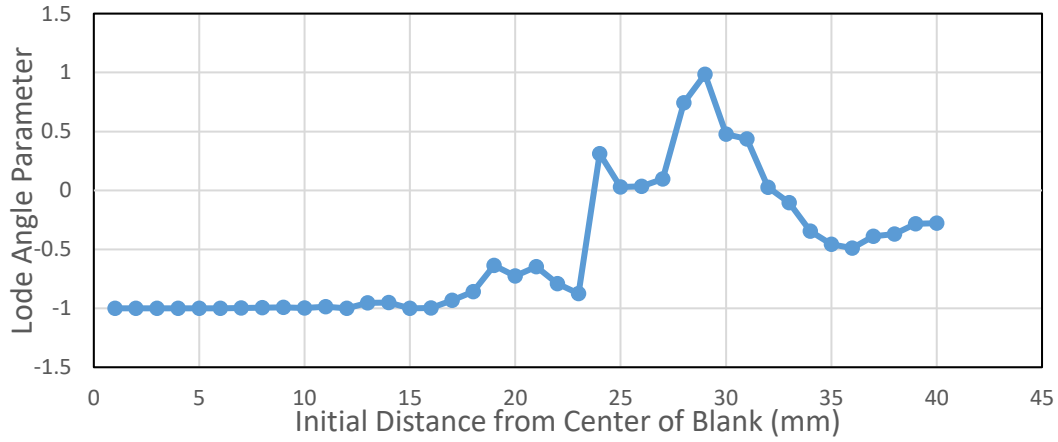

(c)

Figure 5.149. The variation of (a) Equivalent Plastic Strain (b) Stress Triaxiality and (c) Lode Angle Parameter along the transverse direction of the blank at 8 mm cup depth for AISI 304 steel (VM-JC-JC)

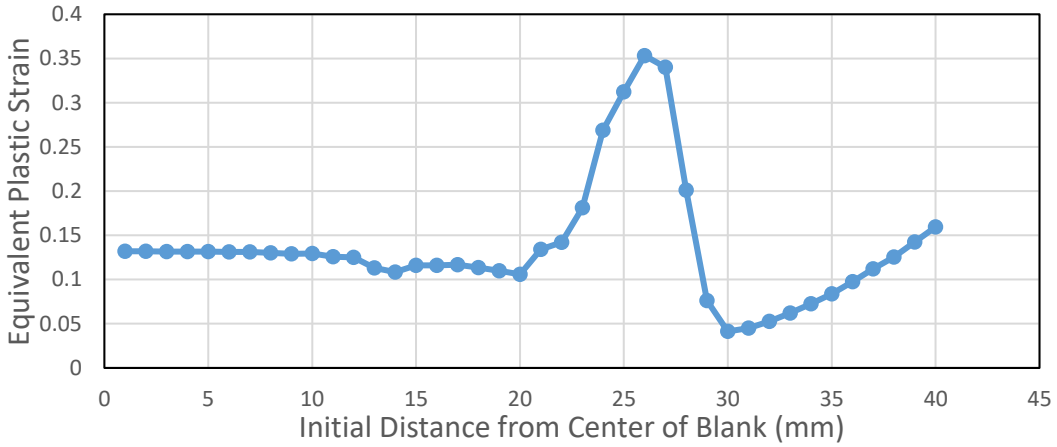

(a)

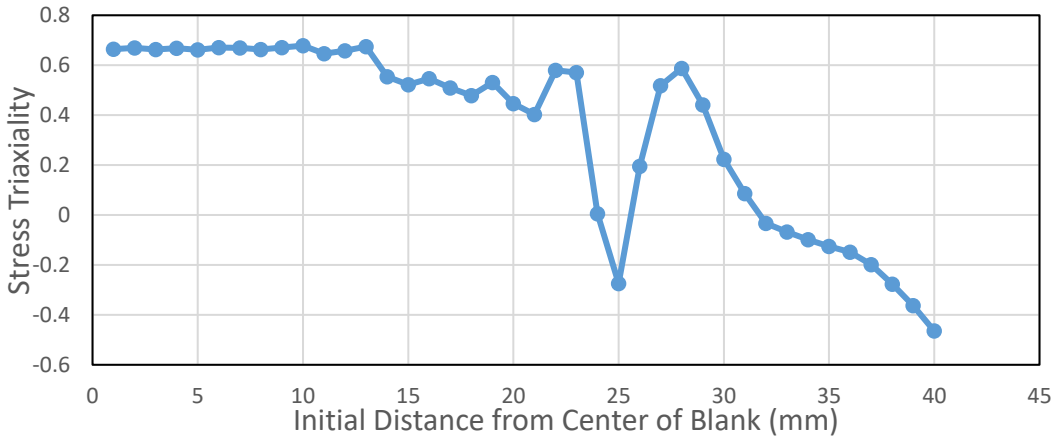

(b)

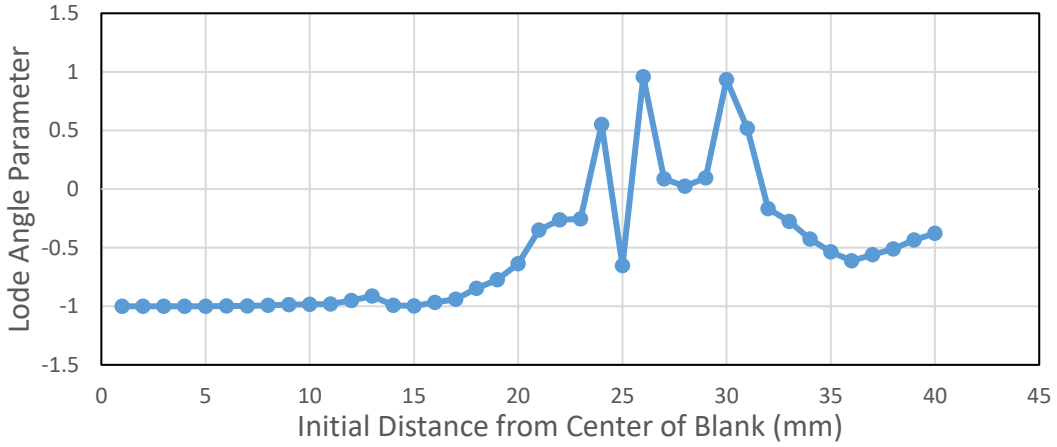

(c)

Figure 5.150. The variation of (a) Equivalent Plastic Strain (b) Stress Triaxiality and (c) Lode Angle Parameter along the transverse direction of the blank at 12 mm cup depth for AISI 304 steel (VM-JC-JC)

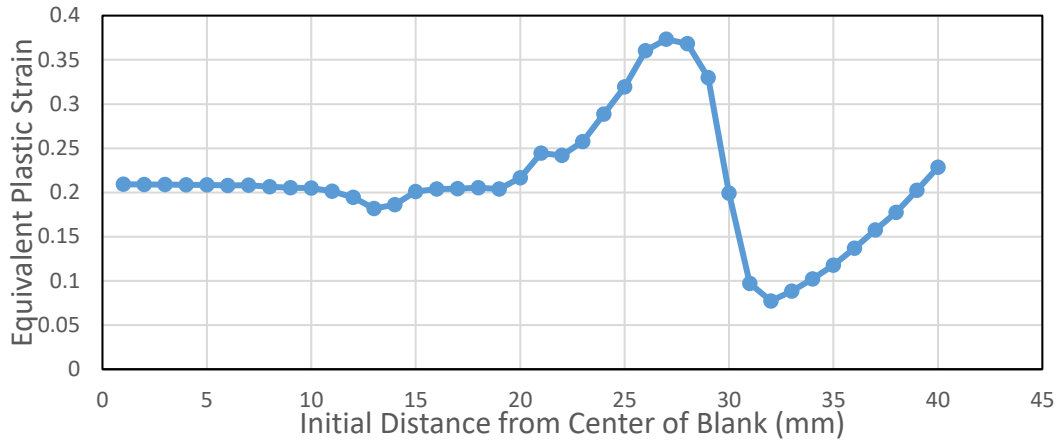

(a)

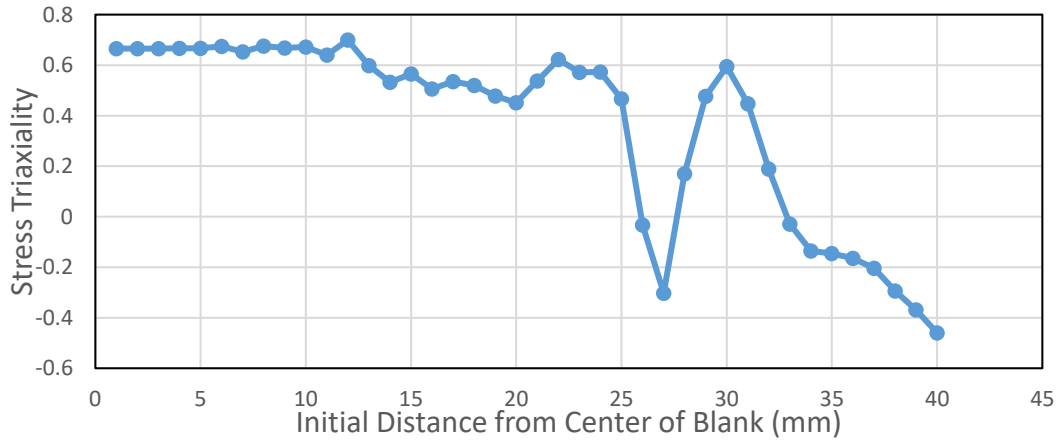

(b)

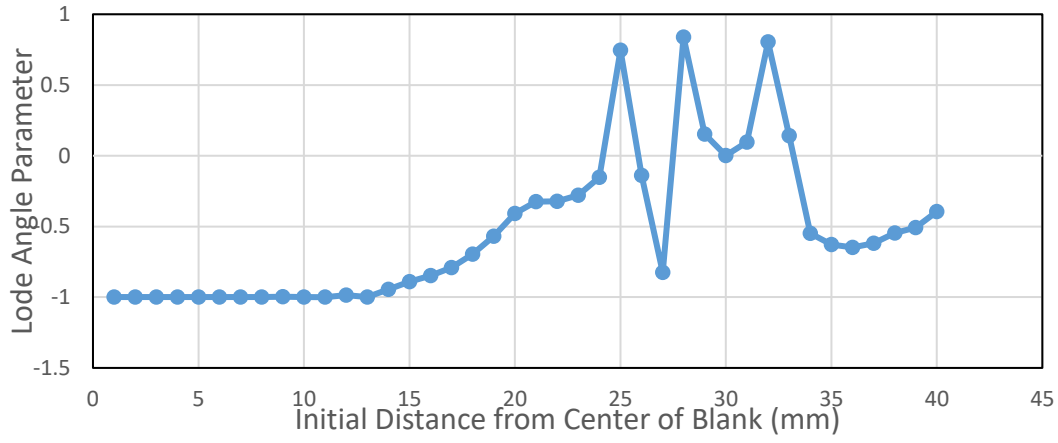

(c)

Figure 5.151. The variation of (a) Equivalent Plastic Strain (b) Stress Triaxiality and (c) Lode Angle Parameter along the transverse direction of the blank at 16 mm cup depth for AISI 304 steel (VM-JC-JC)

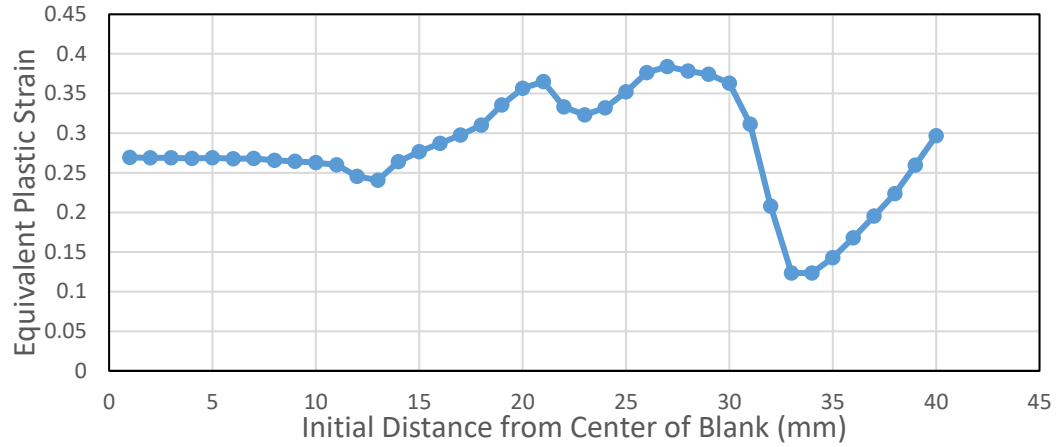

(a)

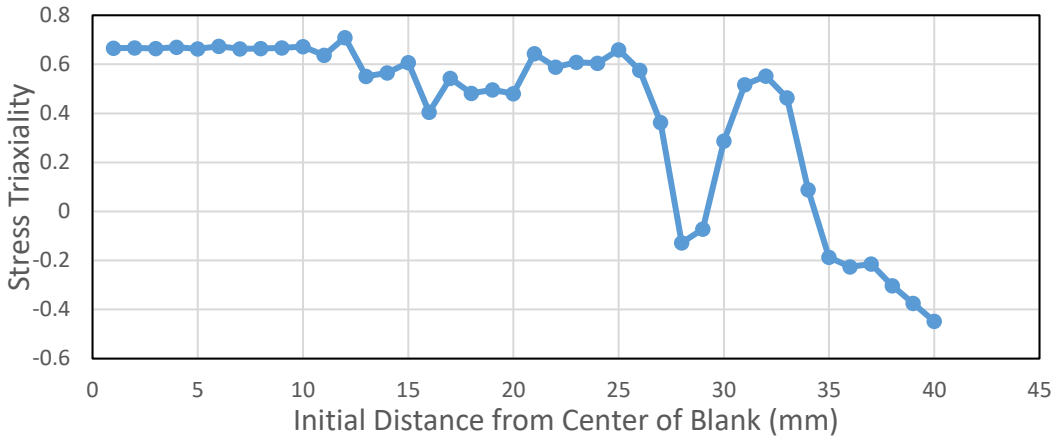

(b)

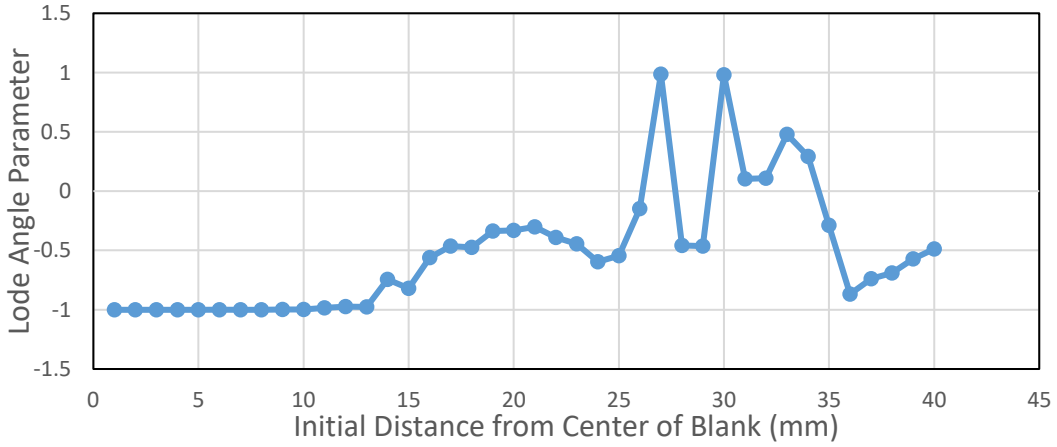

(c)

Figure 5.152. The variation of (a) Equivalent Plastic Strain (b) Stress Triaxiality and (c) Lode Angle Parameter along the transverse direction of the blank at 20 mm cup depth for AISI 304 steel (VM-JC-JC)

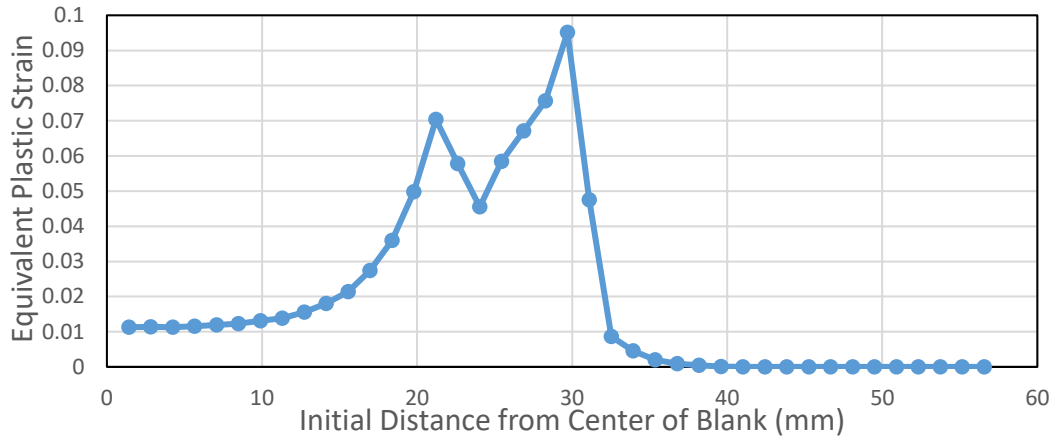

(a)

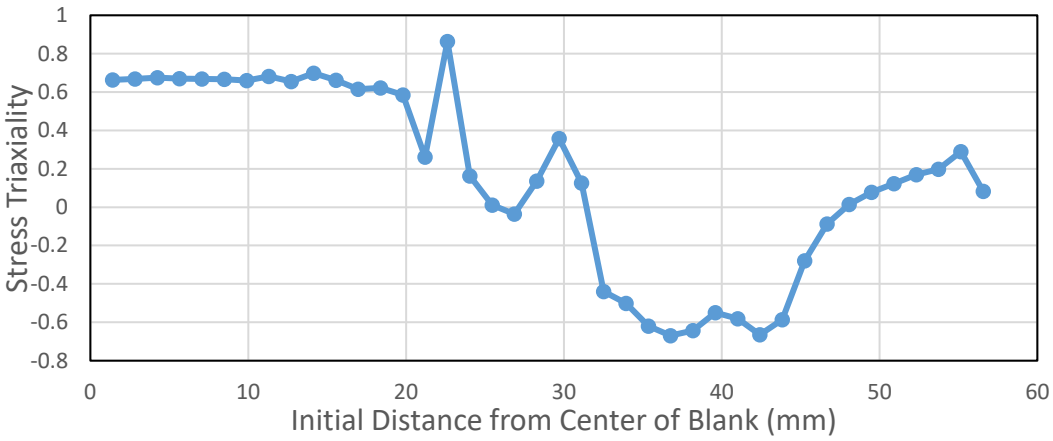

(b)

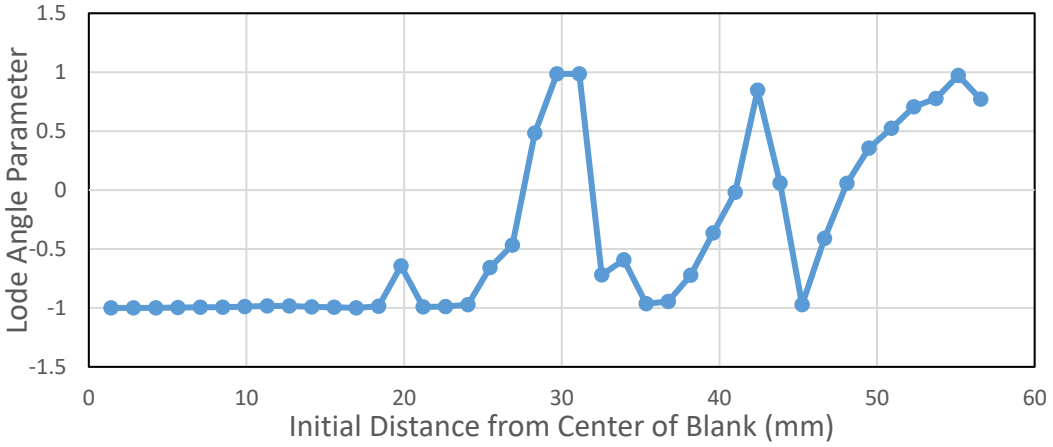

(c)

Figure 5.153. The variation of (a) Equivalent Plastic Strain (b) Stress Triaxiality and (c) Lode Angle Parameter along the diagonal of the blank at 4 mm cup depth for AISI 304 steel (VM-JC-JC)

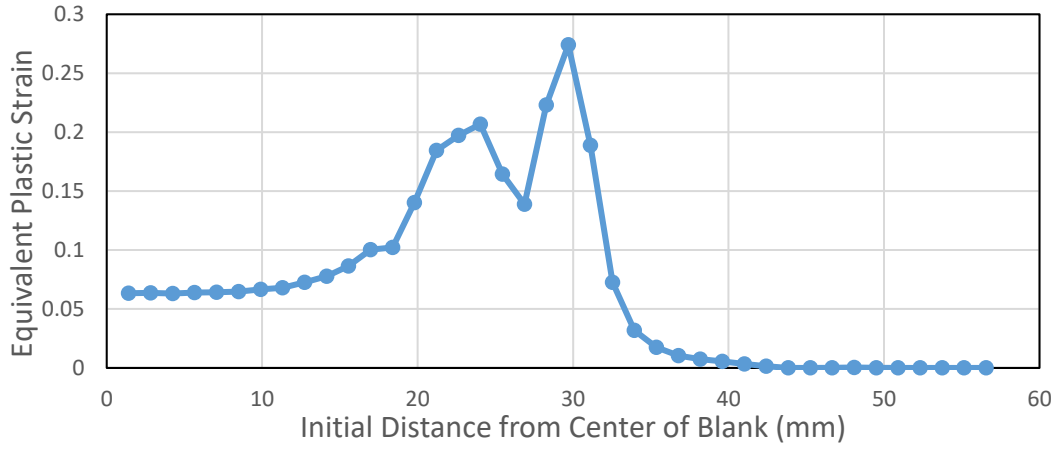

(a)

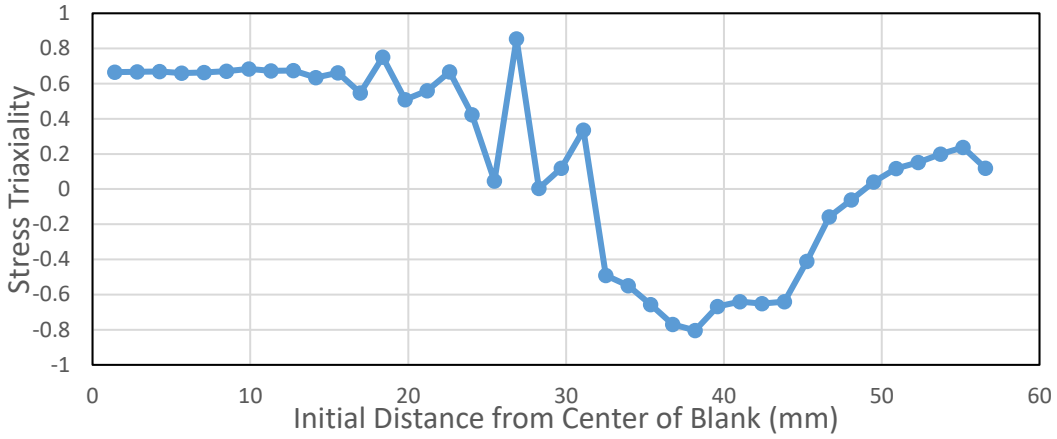

(b)

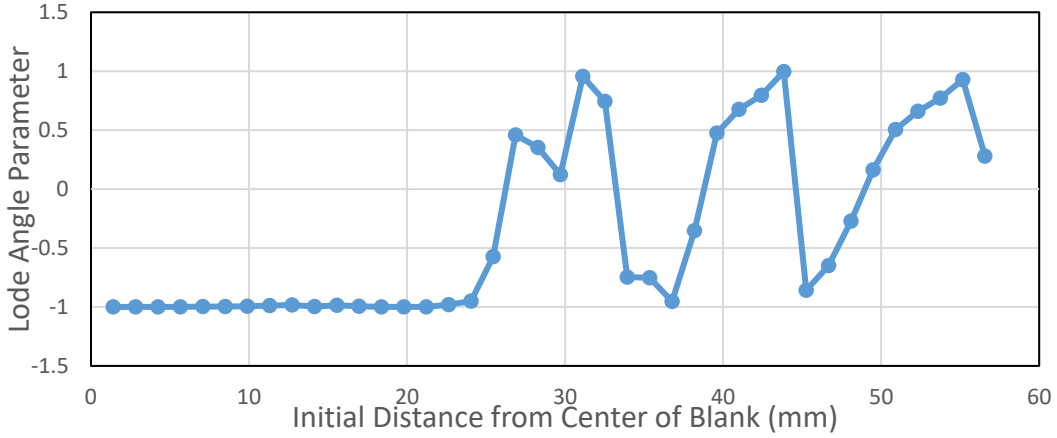

(c)

Figure 5.154. The variation of (a) Equivalent Plastic Strain (b) Stress Triaxiality and (c) Lode Angle Parameter along the diagonal of the blank at 8 mm cup depth for AISI 304 steel (VM-JC-JC)

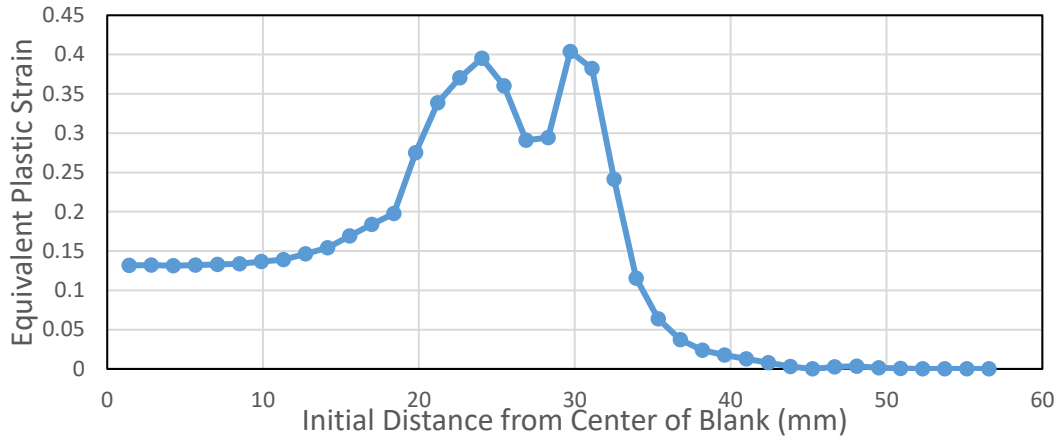

(a)

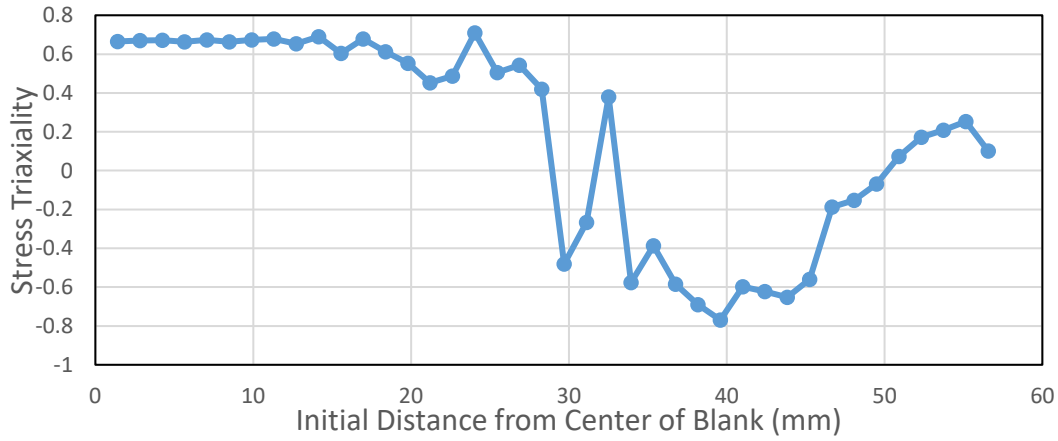

(b)

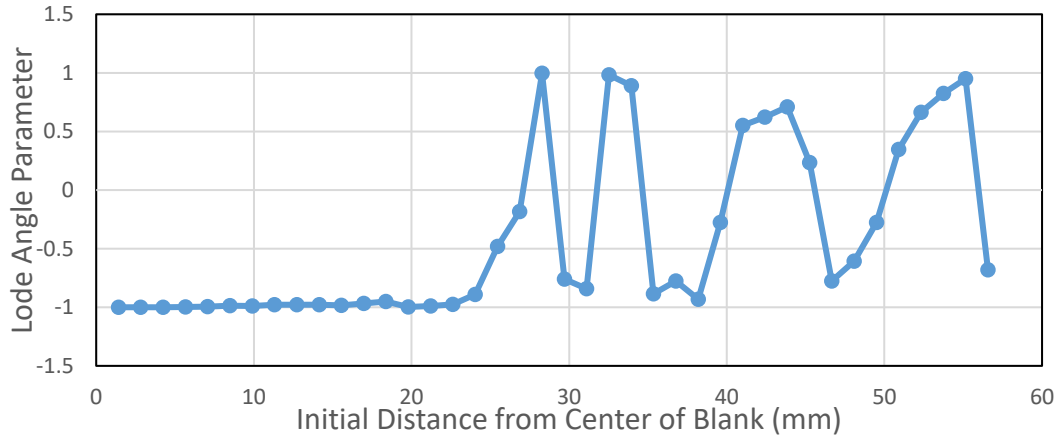

(c)

Figure 5.155 The variation of (a) Equivalent Plastic Strain (b) Stress Triaxiality and (c) Lode Angle Parameter along the diagonal of the blank at 12 mm cup depth for AISI 304 steel (VM-JC-JC)

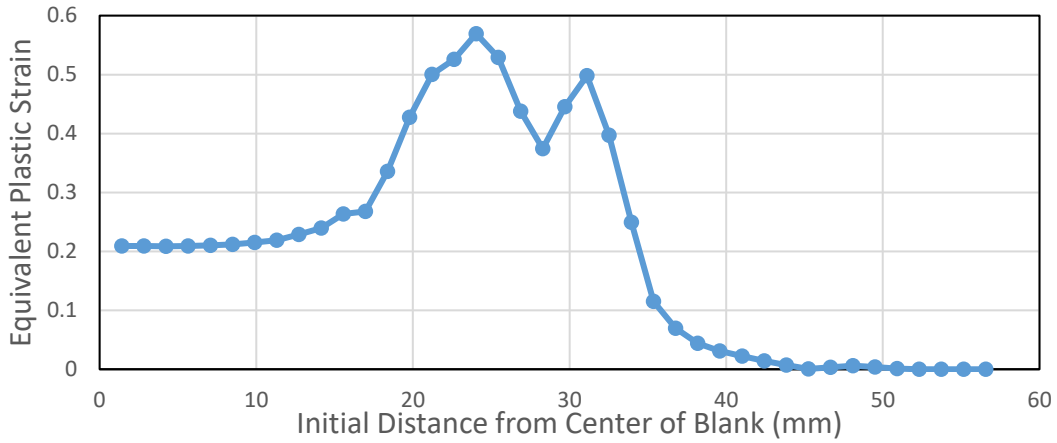

(a)

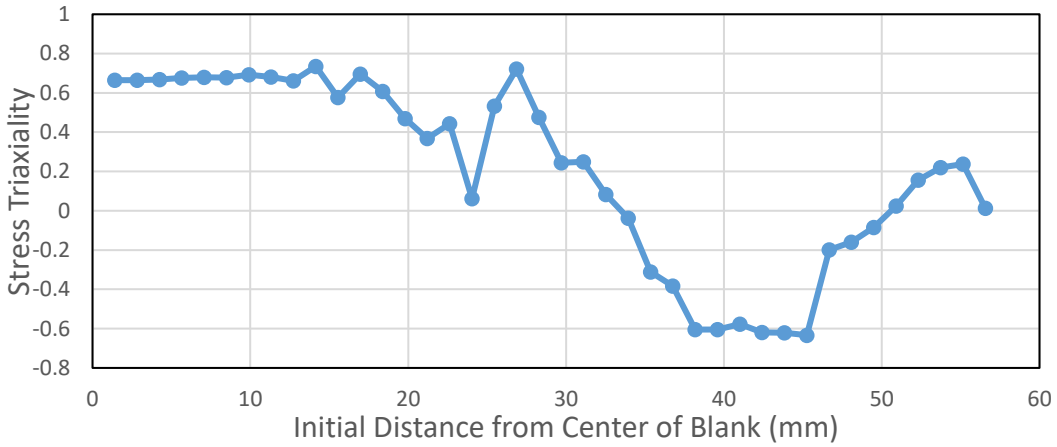

(b)

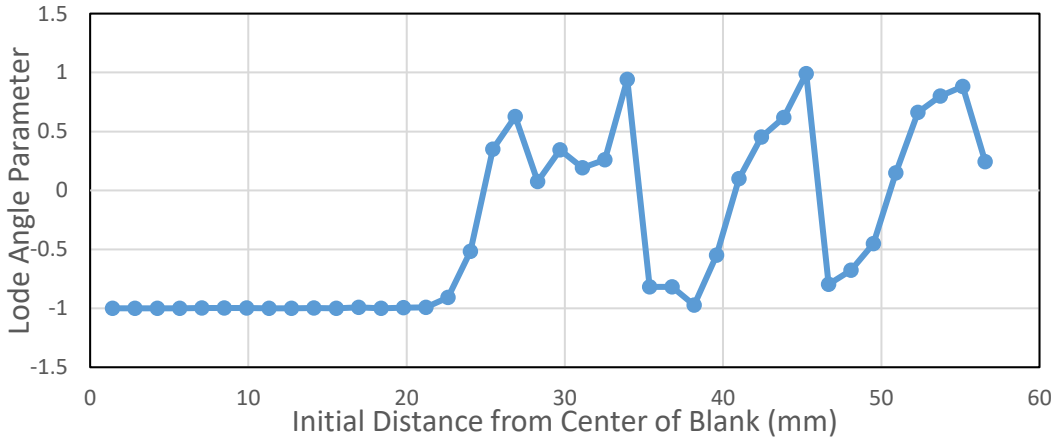

(c)

Figure 5.156 The variation of (a) Equivalent Plastic Strain (b) Stress Triaxiality and (c) Lode Angle Parameter along the diagonal of the blank at 16 mm cup depth for AISI 304 steel (VM-JC-JC)

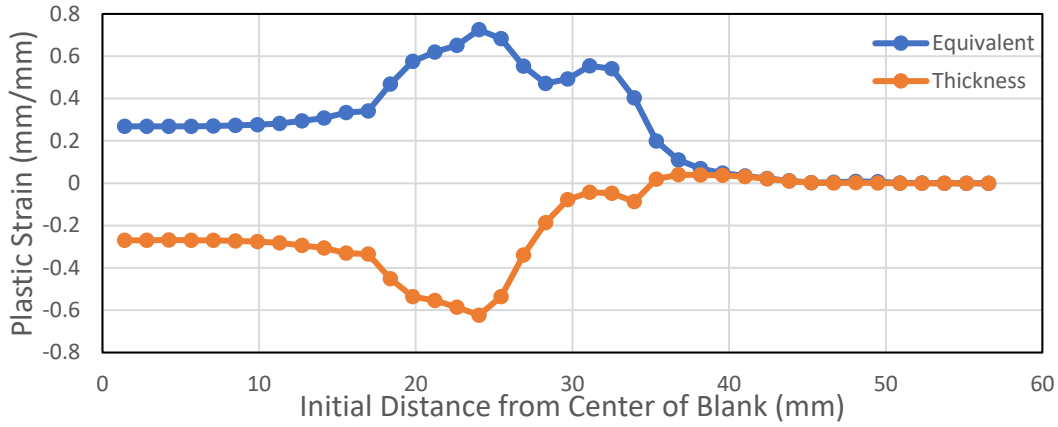

(a)

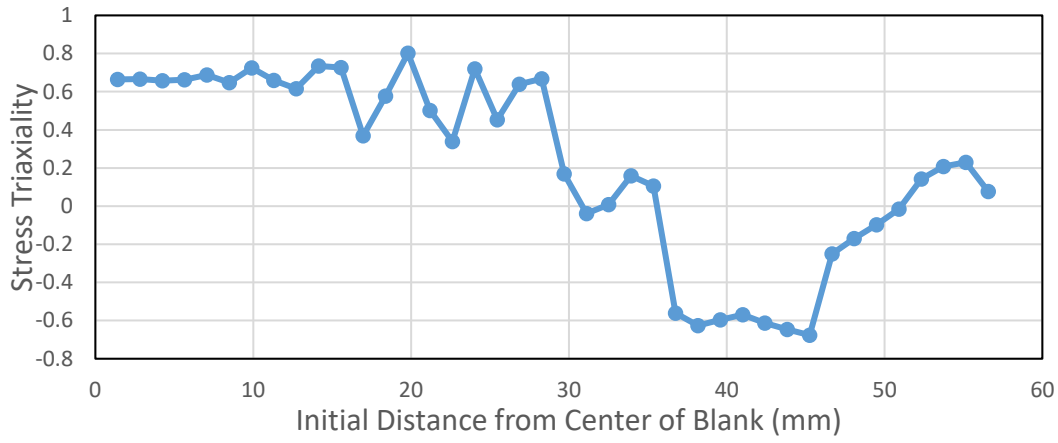

(b)

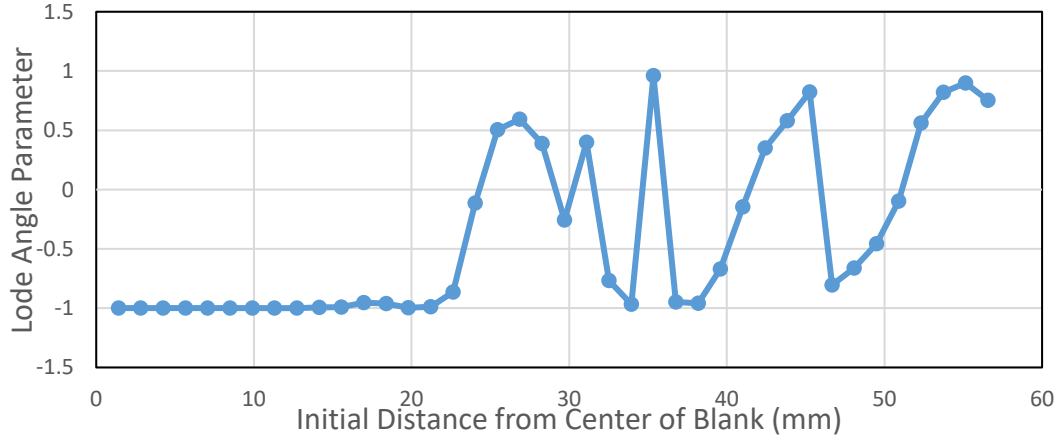

(c)

Figure 5.157. The variation of (a) Equivalent Plastic Strain (b) Stress Triaxiality and (c) Lode Angle Parameter along the diagonal of the blank at 20 mm cup depth for AISI 304 steel (VM-JC-JC)

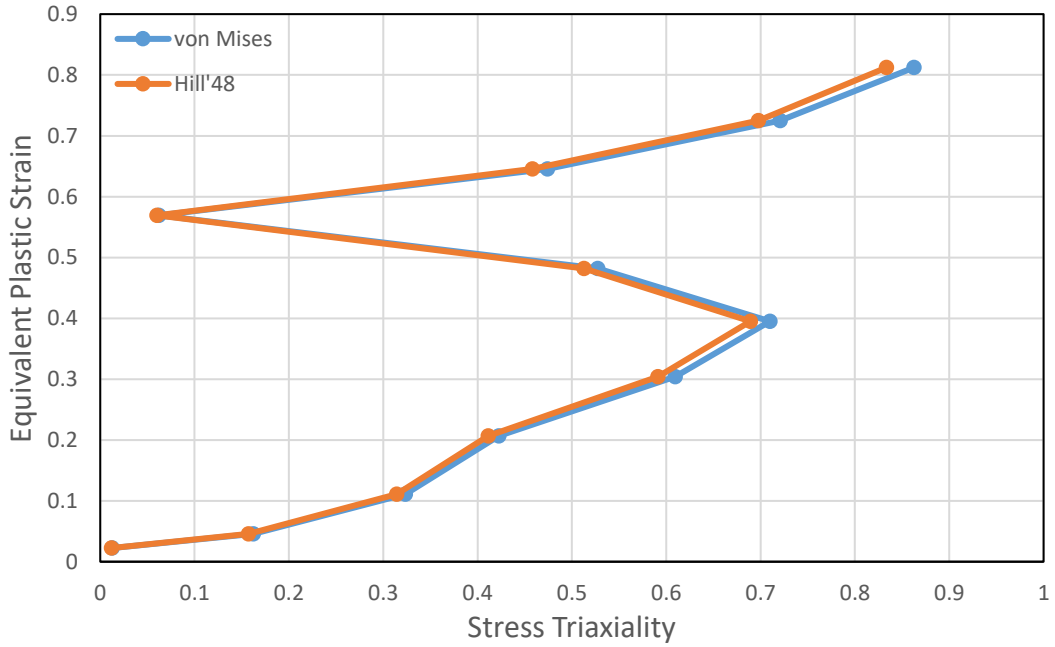

Figure 5.158. Equivalent Plastic Strain - Stress Triaxiality Plot of First Rupture Element (VM-JC-JC)

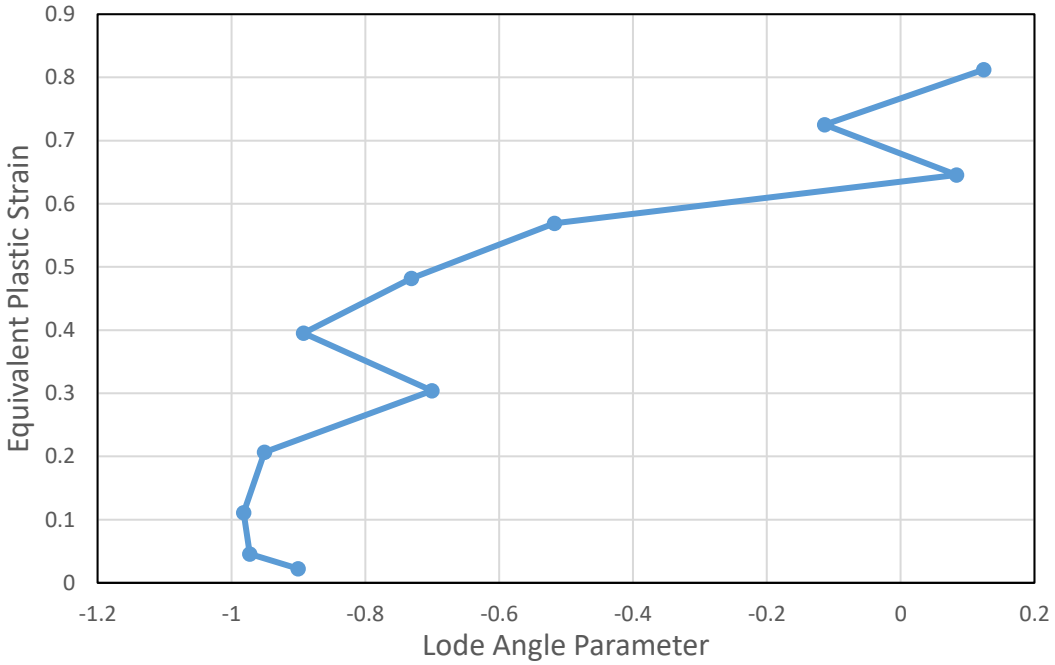

Figure 5.159. Equivalent Plastic Strain – Lode Angle Parameter Plot of First Rupture Element (VM-JC-JC)

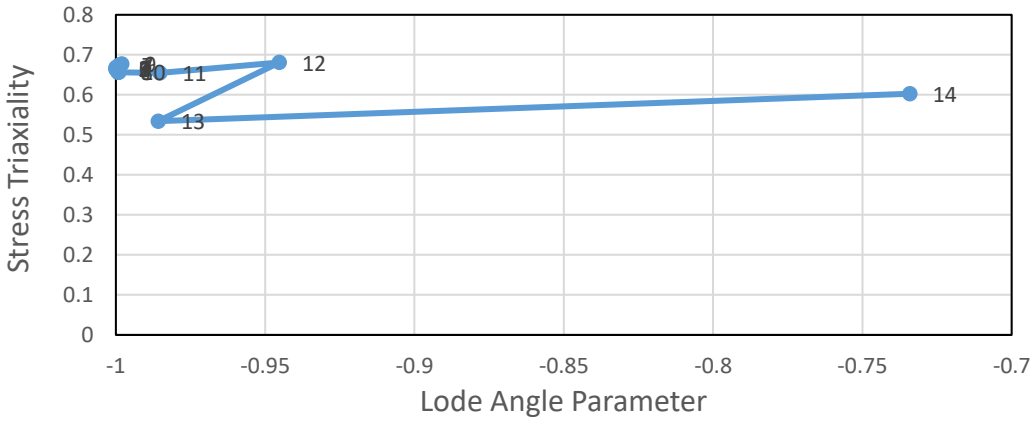
Stress Triaxiality
0.8
0.7
0.6
0.5
0.4
0.3
0.2
0.1
0
-1
-0.95
-0.9
-0.85
-0.8
-0.75
-0.7
Lode Angle Parameter
11
12
13
14

(a)

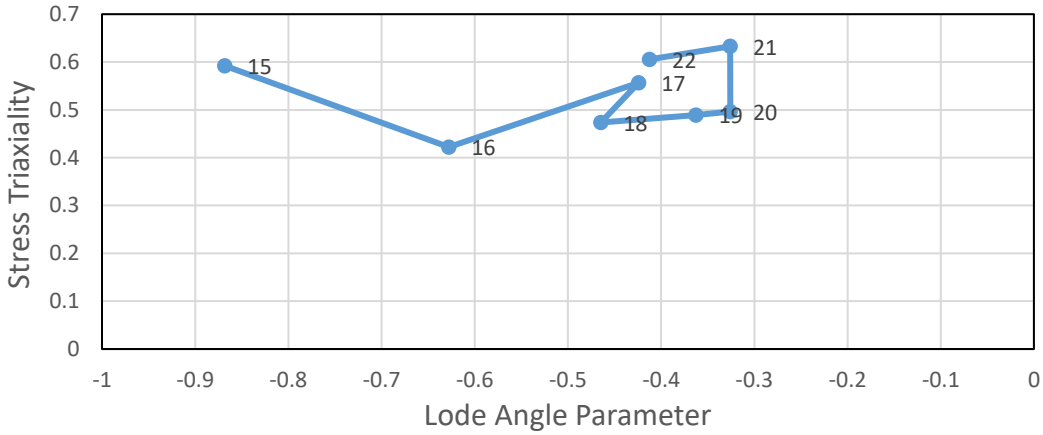
Stress Triaxiality
0.7
0.6
0.5
0.4
0.3
0.2
0.1
0
-1
-0.9
-0.8
-0.7
-0.6
-0.5
-0.4
-0.3
-0.2
-0.1
0
Lode Angle Parameter
15
16
17
18
19
20
21
22

(b)

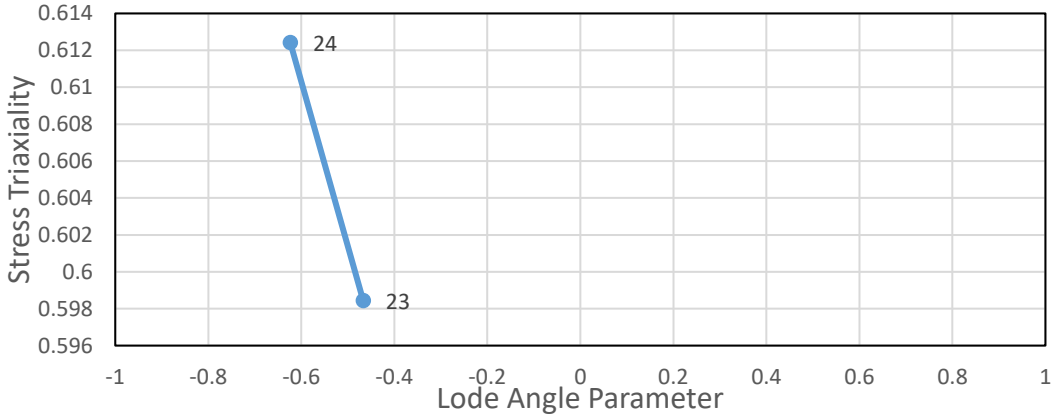
Stress Triaxiality
0.614
0.612
0.61
0.608
0.606
0.604
0.602
0.6
0.598
0.596
-1
-0.8
-0.6
-0.4
-0.2
0
0.2
0.4
0.6
0.8
1
Lode Angle Parameter
23
24

(c)

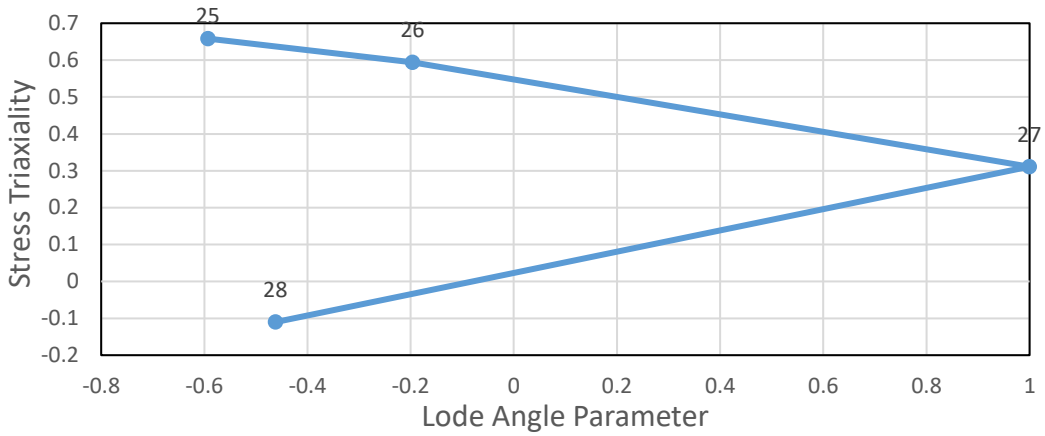

(d)

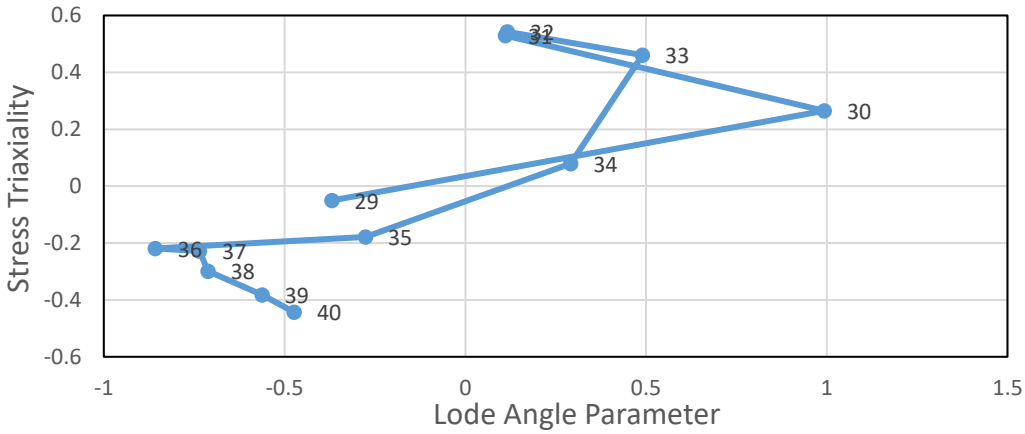

(e)

Figure 5.160. The variation of triaxiality values with respect to Lode angle parameter values in rolling direction (a) for punch (b) for punch shoulder or corner (c) for the clearance between die and punch (d) for die shoulder or corner and (e) for the blank holder regions of the blank at 20 mm cup depth for AISI304 steel (VM-JC-JC)

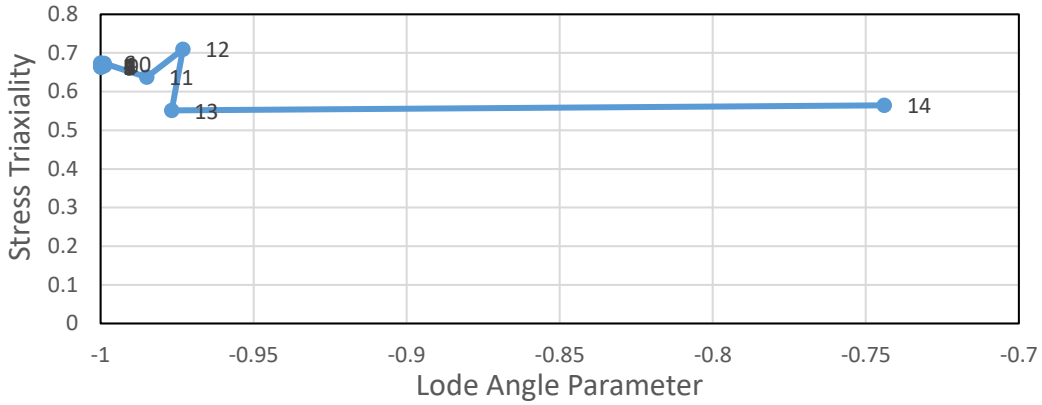
Stress Triaxiality
0.8
0.7
0.6
0.5
0.4
0.3
0.2
0.1
0
-1
-0.95
-0.9
-0.85
-0.8
-0.75
-0.7
Lode Angle Parameter
12
11
13
14

(a)

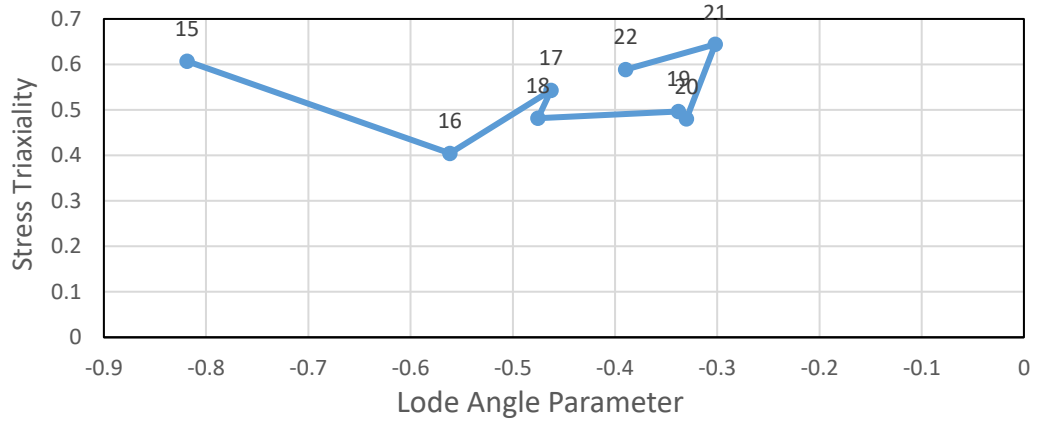
Stress Triaxiality
0.7
0.6
0.5
0.4
0.3
0.2
0.1
0
-0.9
-0.8
-0.7
-0.6
-0.5
-0.4
-0.3
-0.2
-0.1
0
Lode Angle Parameter
15
16
17
18
22
21
19
20

(b)

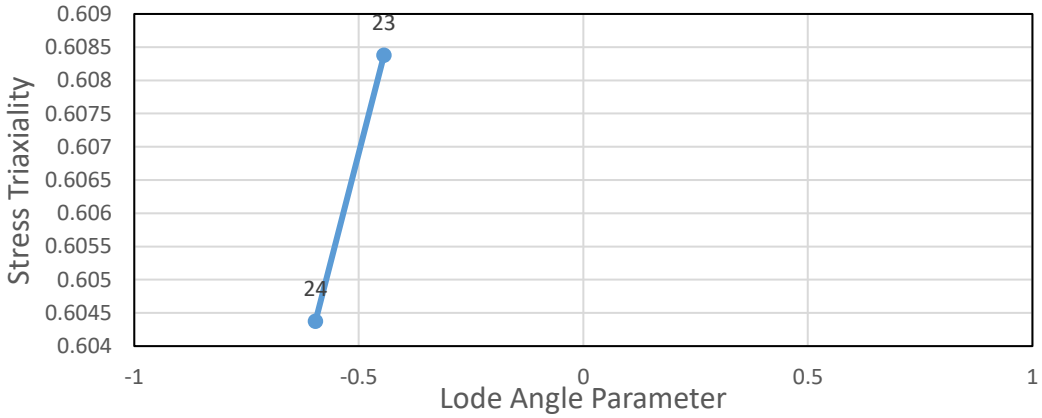
Stress Triaxiality
0.609
0.6085
0.608
0.6075
0.607
0.6065
0.606
0.6055
0.605
0.6045
0.604
-1
-0.5
0
0.5
1
Lode Angle Parameter
23
24

(c)

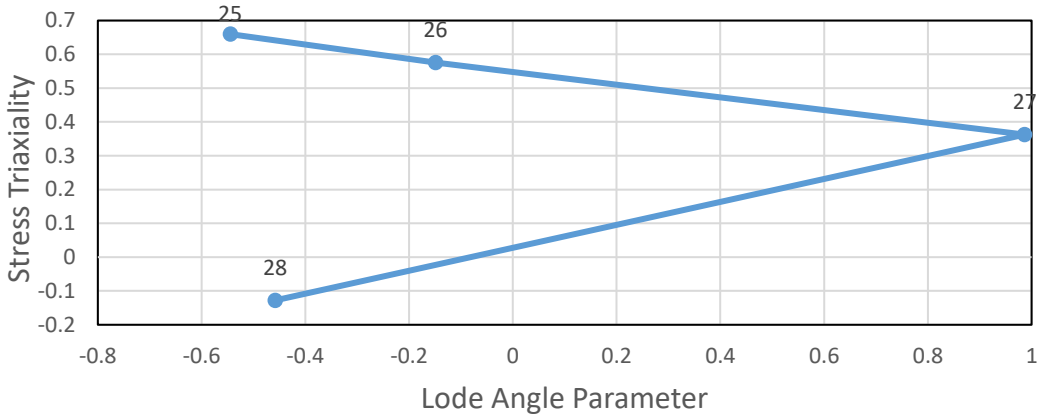

(d)

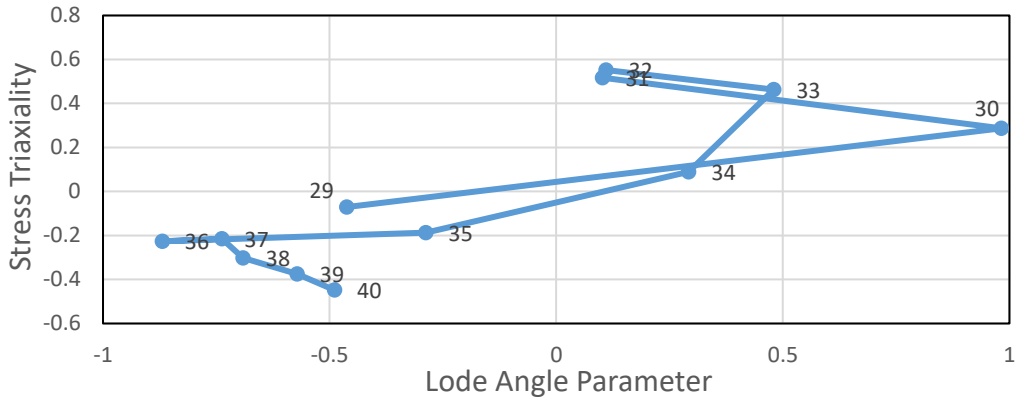

(e)

Figure 5.161. The variation of triaxiality values with respect to Lode angle parameter values in transverse direction (a) for punch (b) for punch shoulder or corner (c) for the clearance between die and punch (d) for die shoulder or corner and (e) for the blank holder regions of the blank at 20 mm cup depth for AISI304 steel (VM-JC-JC)

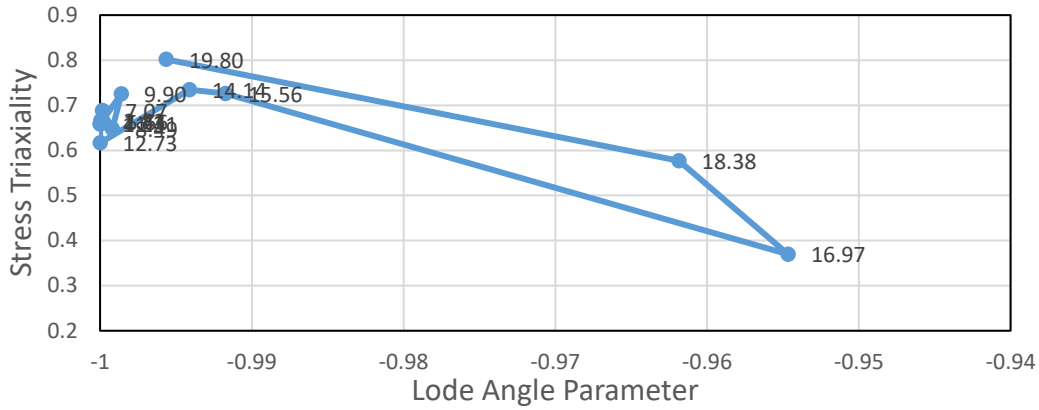
Stress Triaxiality
Lode Angle Parameter
19.80
9.90
14.14
15.56
7.07
12.73
18.38
16.97

(a)

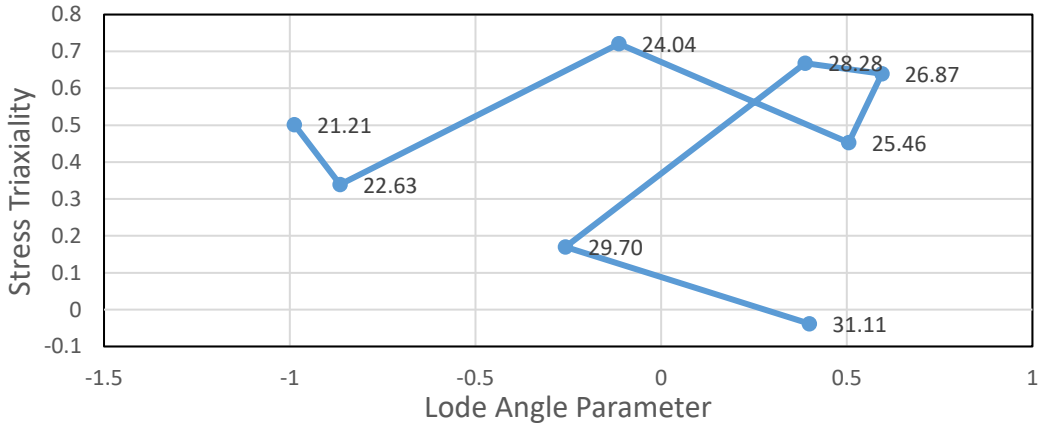
Stress Triaxiality
Lode Angle Parameter
24.04
28.28
26.87
21.21
25.46
22.63
29.70
31.11

(b)

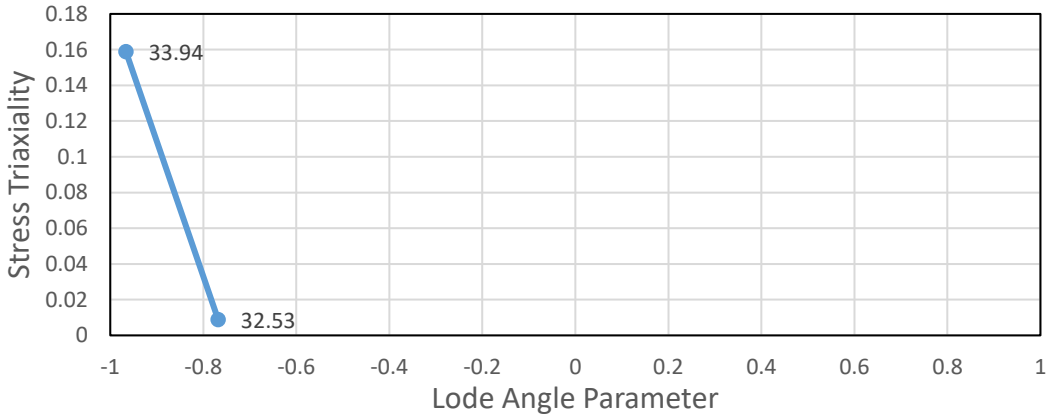
Stress Triaxiality
Lode Angle Parameter
33.94
32.53

(c)

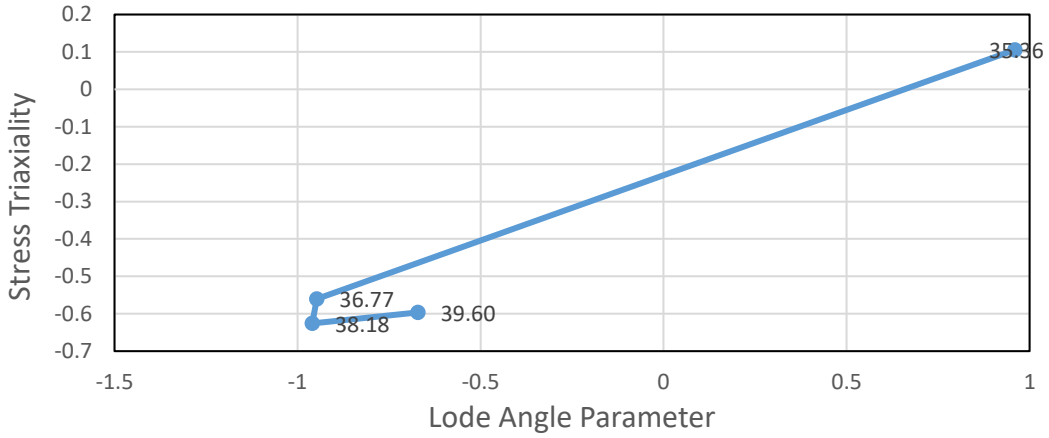

(d)

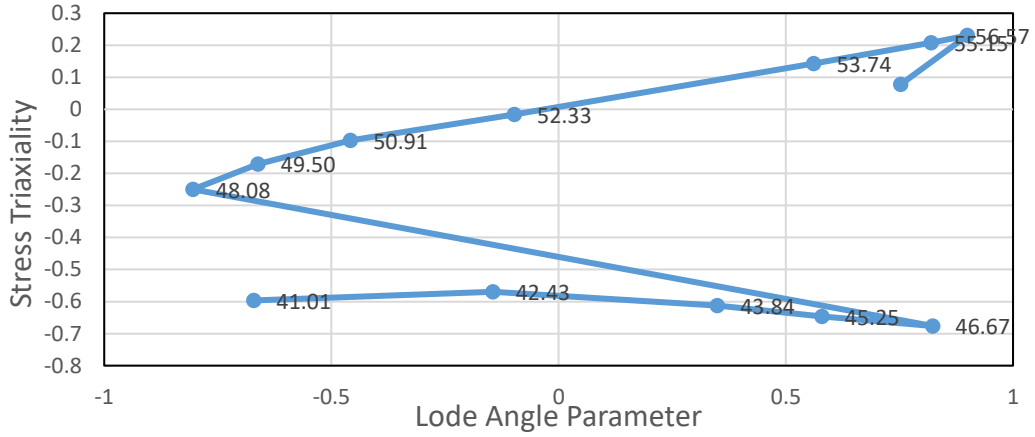

(e)

Figure 5.162. The variation of triaxiality values with respect to Lode angle parameter values in diagonal direction (a) for punch (b) for punch shoulder or corner (c) for the clearance between die and punch (d) for die shoulder or corner and (e) for the blank holder regions of the blank at 20 mm cup depth for AISI304 steel (VM-JC-JC)

In the rolling direction, the triaxiality values vary generally between 0.6 and 0.8 under the punch whereas the Lode angle parameter values change between -0.8 and -1 up to a distance of 15 mm from the center, it can be said that the deformation behavior is in equi-biaxial tension condition. At the punch shoulder triaxiality values are positive. On the other hand, the Lode angle parameter values increase with distance from the center of the blank. Hence, there is a tensile type deformation in this region. At the clearance between die and punch thinning continues. At the die shoulder, the triaxiality values are mostly positive with varying Lode angle parameter values. Under the blank holder the triaxiality values and Lode angle parameter values are negative, indicating thickening towards the rim.

The same tendency of rolling direction is observed in the transverse direction also. The differences are a result of anisotropy of the material.

In the diagonal direction, as in the transverse and rolling directions, equi-biaxial stress condition is observed under the punch. Here, the triaxiality values change towards negative whereas Lode angle parameter values show the same tendency. Only in the regions close to the center of the blank i.e., up to a distance of 10 mm from the center, the equi-biaxial tension conditions are observed. At the punch corner, triaxiality values are varying and the Lode angle parameter values are increasing, as the distance increases from the blank center. At the die corner the triaxiality values start to became negative, indication compressive type deformation with the Lode angle parameter values. Under the blank holder, the triaxiality values are negative, but finally become positive, similarly negative Lode angle parameter values turn into positive, indicating thickening towards the rim where the nature of the deformation changes to tension situation.

5.1.10 Case 10: Square-AISI304-von Mises-Johnson Cook-Hosford Coulomb Model

For the tenth case, von Mises yield criterion was applied with Johnson Cook hardening and the Hosford Coulomb ductile fracture criterion was used. It was observed that the fracture had started after 8 mm punch travel as shown in Figure 5.163. The variation of equivalent plastic strain, stress triaxiality and Lode angle parameter values are presented as a function of the distance from the center of the blank for different cup heights up to the fracture. The results are shown for rolling direction in Figure 5.164 to Figure 5.167, for transverse direction in Figure 5.168 to Figure 5.171 and for diagonal direction in Figure 5.172 to Figure 5.175. The thickness plastic strain distribution is also inserted into Figure 5.175 (a) in order to better visualize the deformation. Further, the variations of stress triaxiality values with respect to equivalent plastic strain are given by considering both von Mises and Hill'48 criteria as a function of the path of the element that fractured first in Figure 5.176 Along the same path, the variation of the Lode parameter with respect to equivalent plastic strain is also illustrated in Figure 5.177.

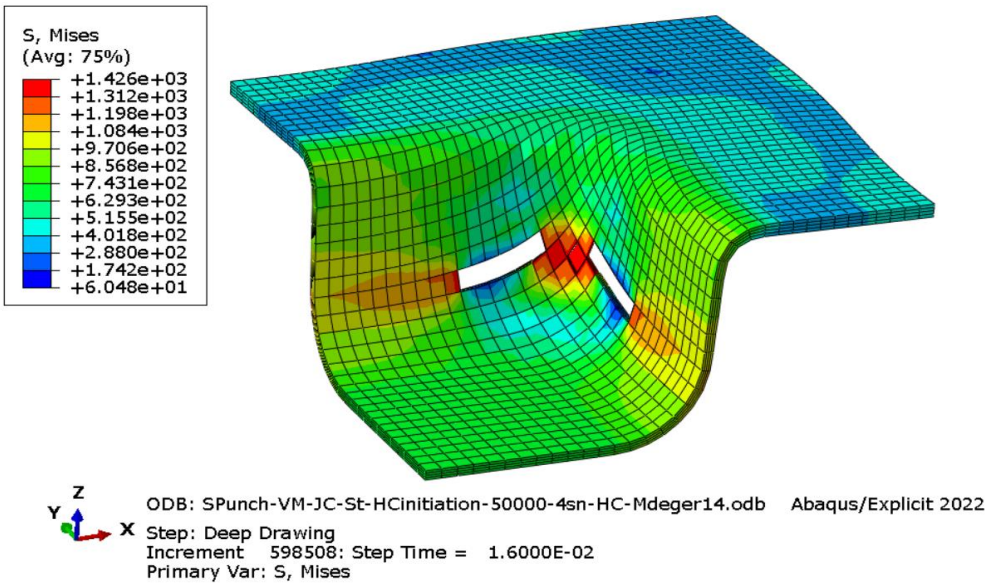

Figure 5.163. First Fracture Moment of Case 10

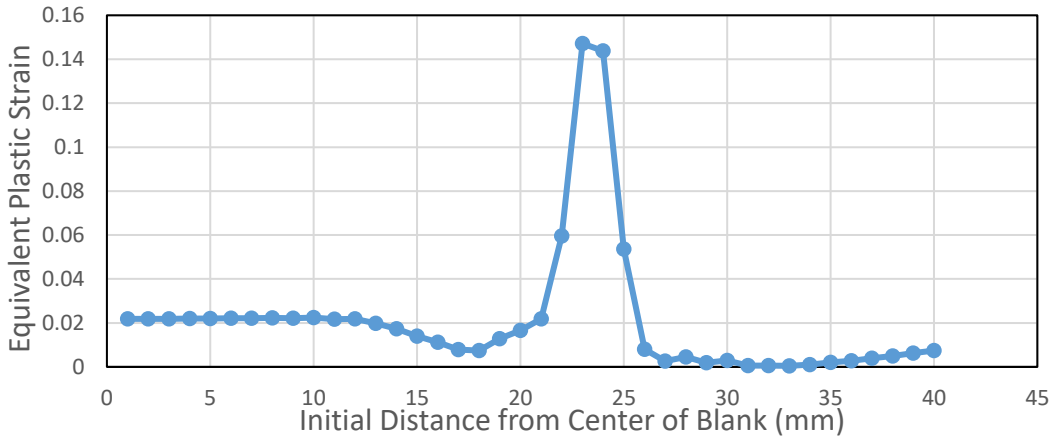

(a)

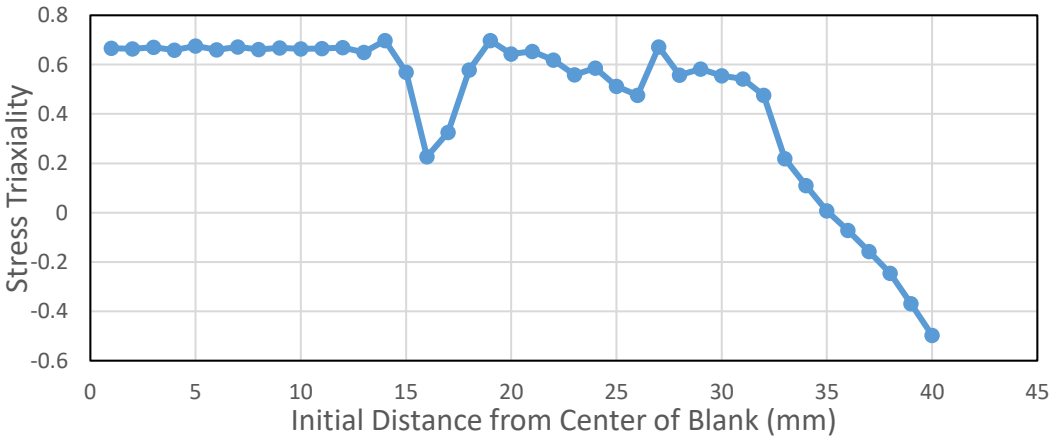

(b)

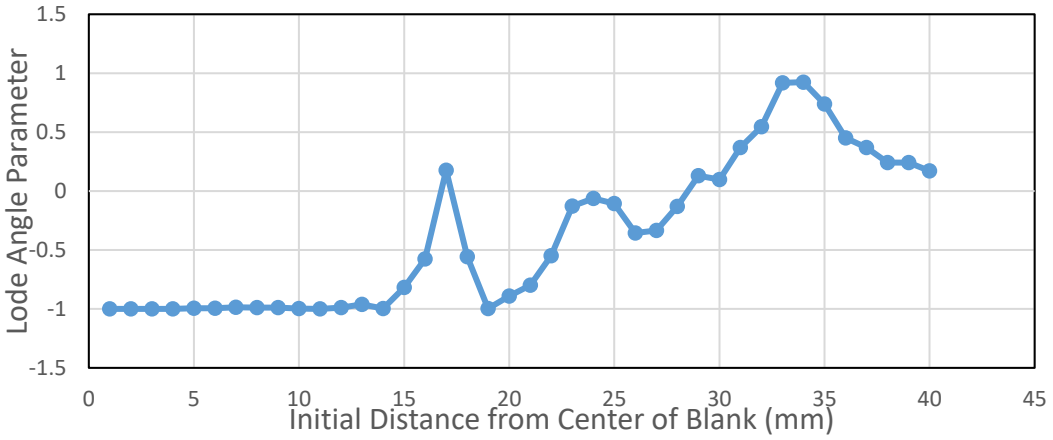

(c)

Figure 5.164. The variation of (a) Equivalent Plastic Strain (b) Stress Triaxiality and (c) Lode Angle Parameter along the rolling direction of the blank at 4 mm cup depth for AISI 304 steel (VM-JC-HC)

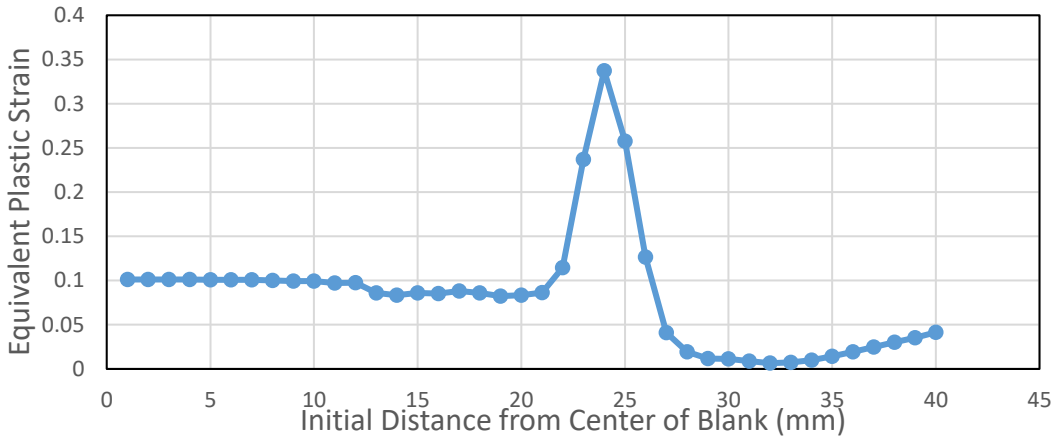

(a)

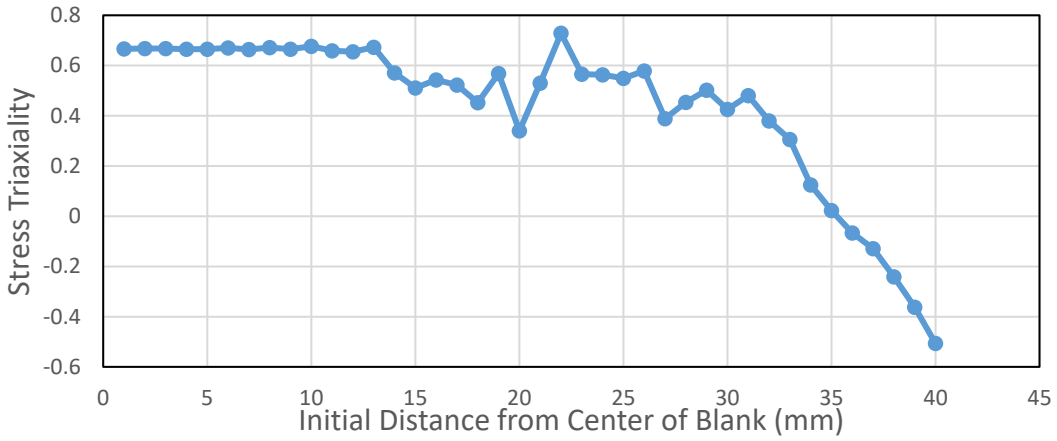

(b)

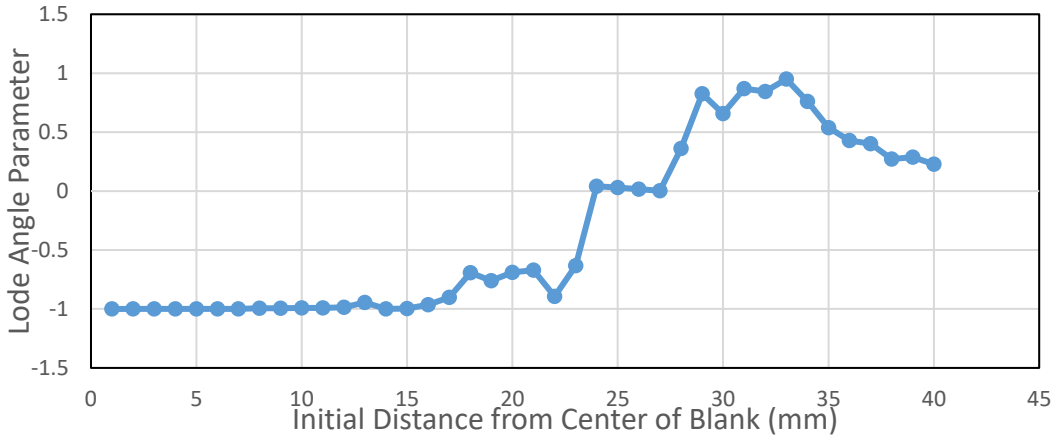

(c)

Figure 5.165. The variation of (a) Equivalent Plastic Strain (b) Stress Triaxiality and (c) Lode Angle Parameter along the rolling direction of the blank at 8 mm cup depth for AISI 304 steel (VM-JC-HC)

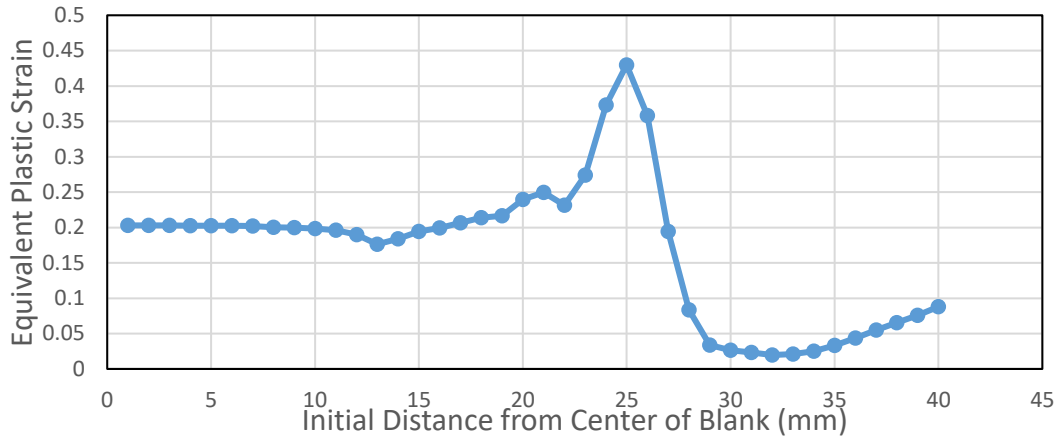

(a)

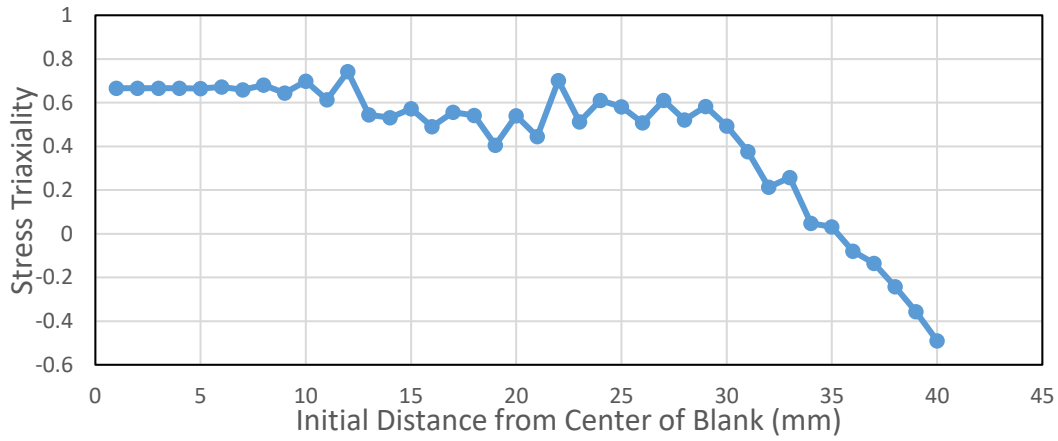

(b)

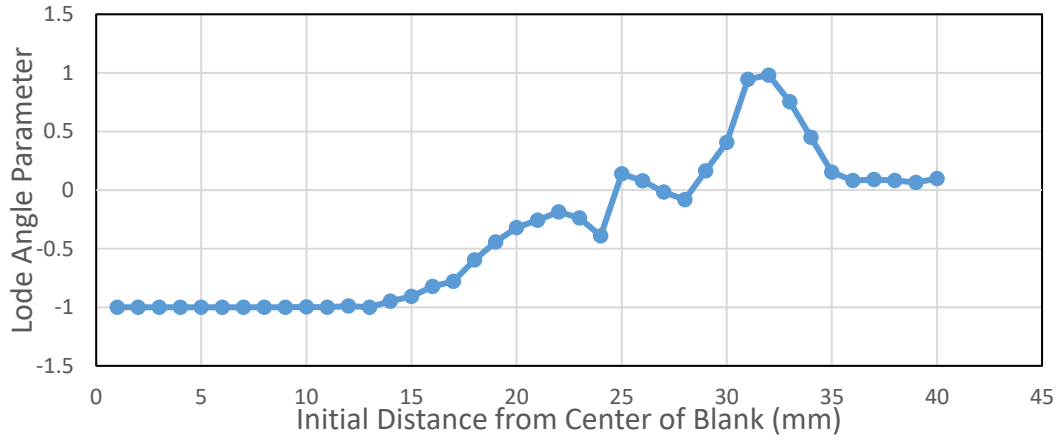

(c)

Figure 5.166. The variation of (a) Equivalent Plastic Strain (b) Stress Triaxiality and (c) Lode Angle Parameter along the rolling direction of the blank at 12 mm cup depth for AISI 304 steel (VM-JC-HC)

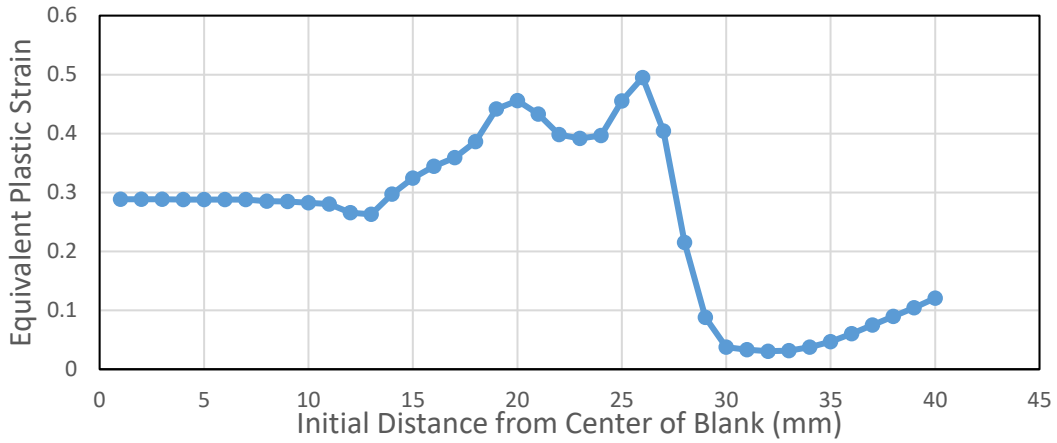

(a)

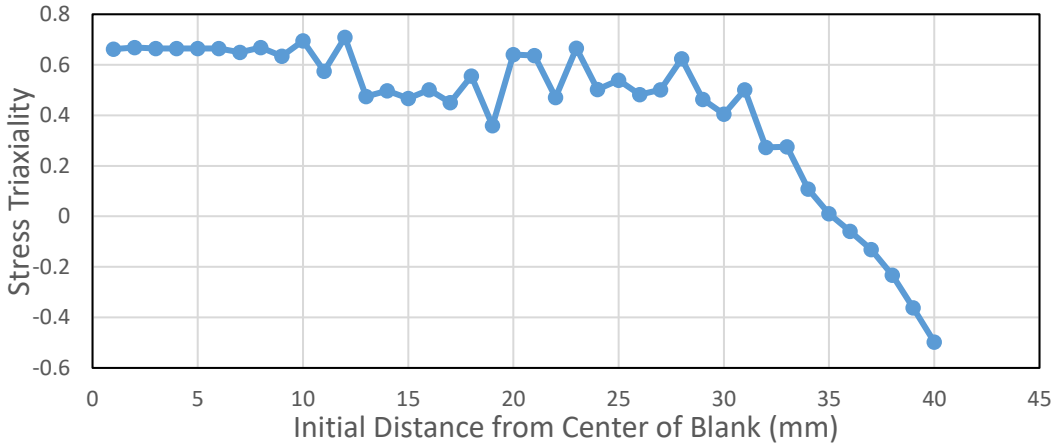

(b)

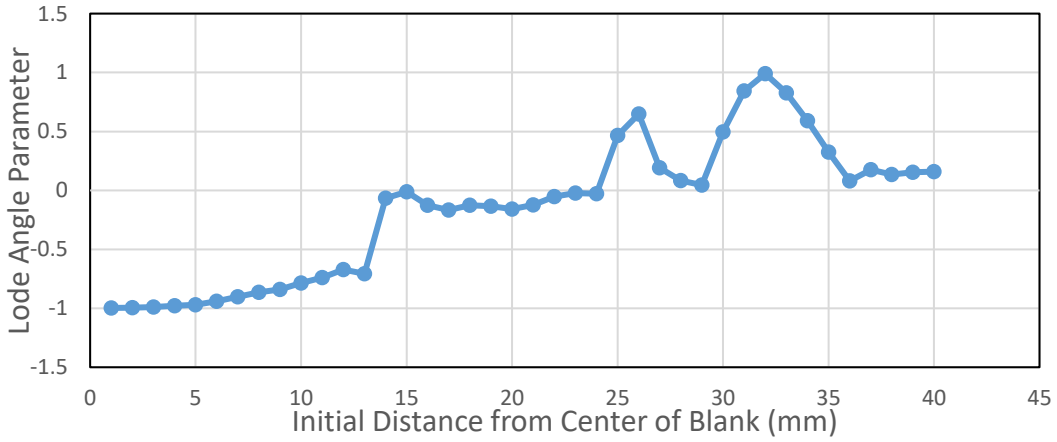

(c)

Figure 5.167. The variation of (a) Equivalent Plastic Strain (b) Stress Triaxiality and (c) Lode Angle Parameter along the rolling direction of the blank at 16 mm cup depth for AISI 304 steel (VM-JC-HC)

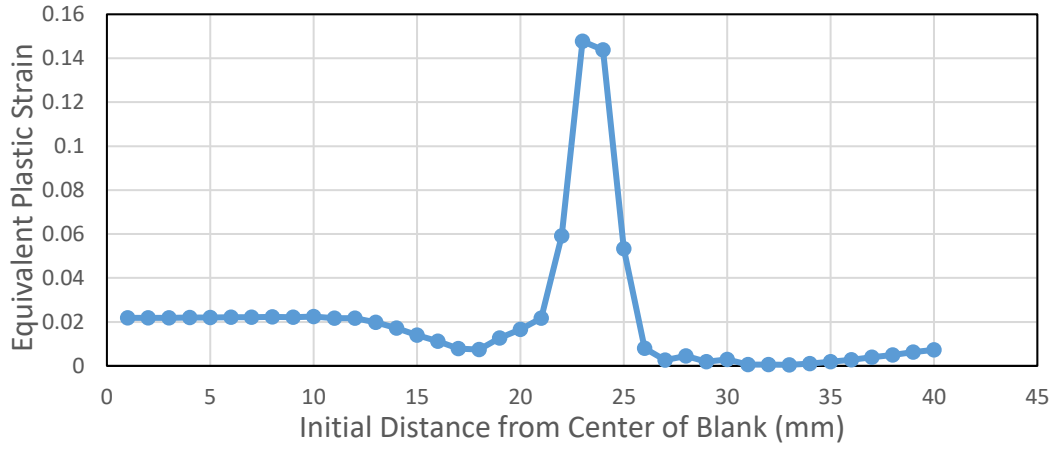

(a)

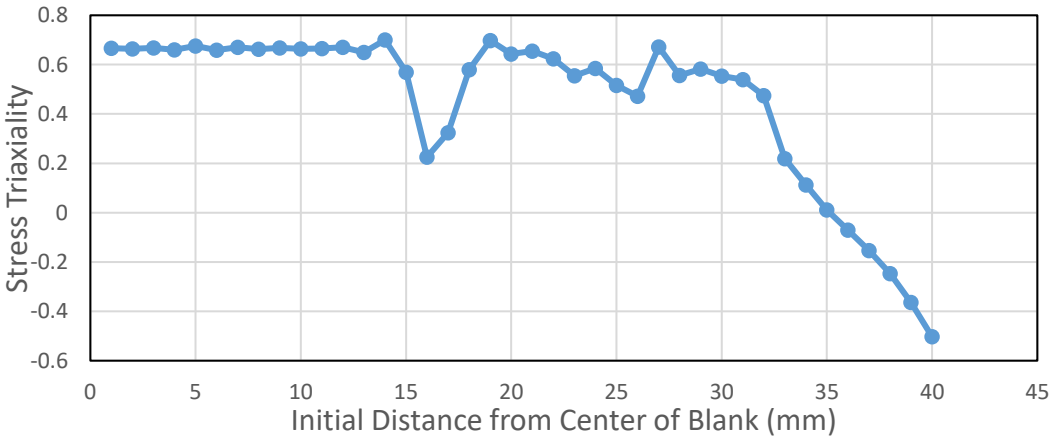

(b)

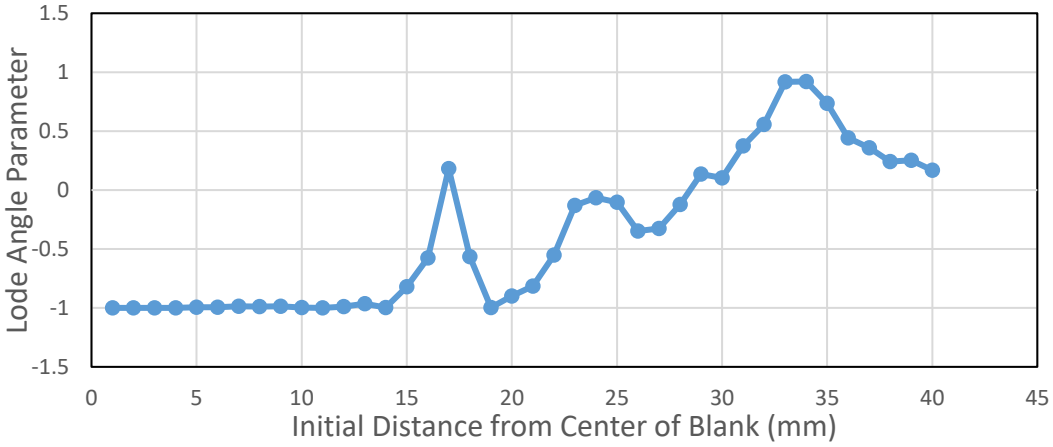

(c)

Figure 5.168. The variation of (a) Equivalent Plastic Strain (b) Stress Triaxiality and (c) Lode Angle Parameter along the transverse direction of the blank at 4 mm cup depth for AISI 304 steel (VM-JC-HC)

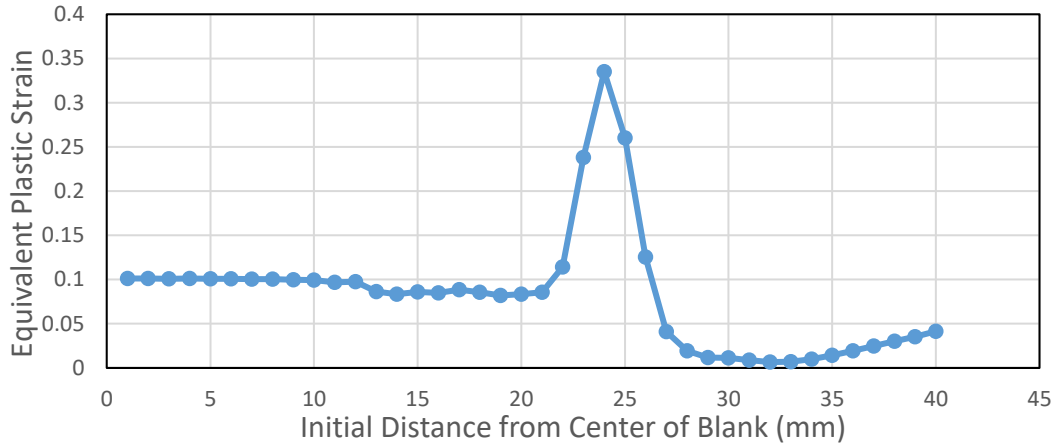

(a)

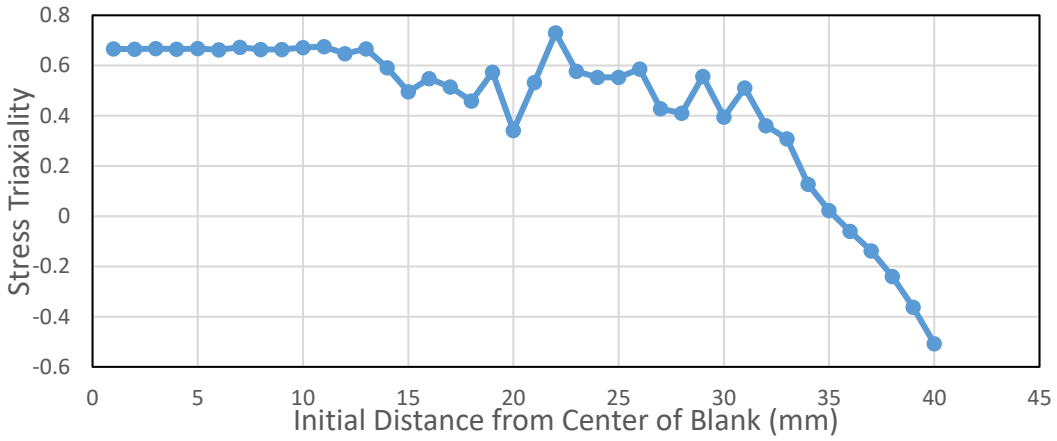

(b)

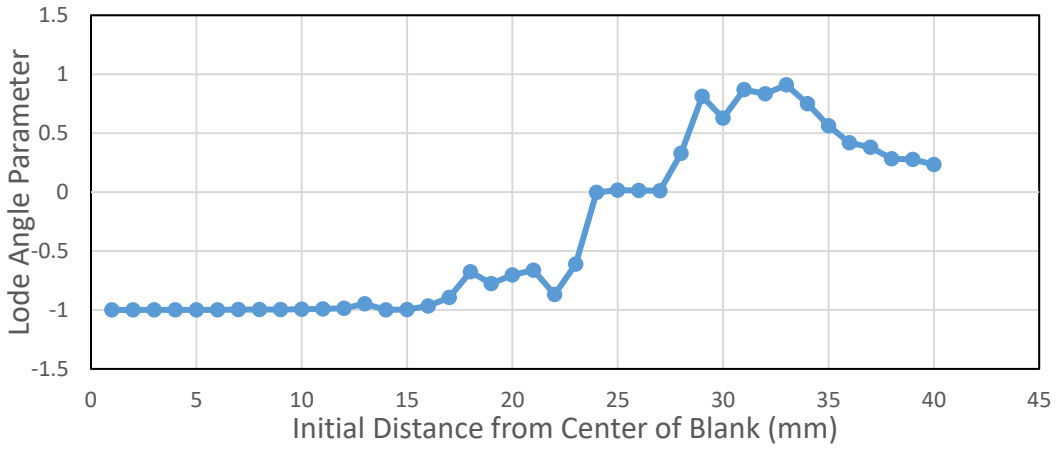

(c)

Figure 5.169. The variation of (a) Equivalent Plastic Strain (b) Stress Triaxiality and (c) Lode Angle Parameter along the transverse direction of the blank at 8 mm cup depth for AISI 304 steel (VM-JC-HC)

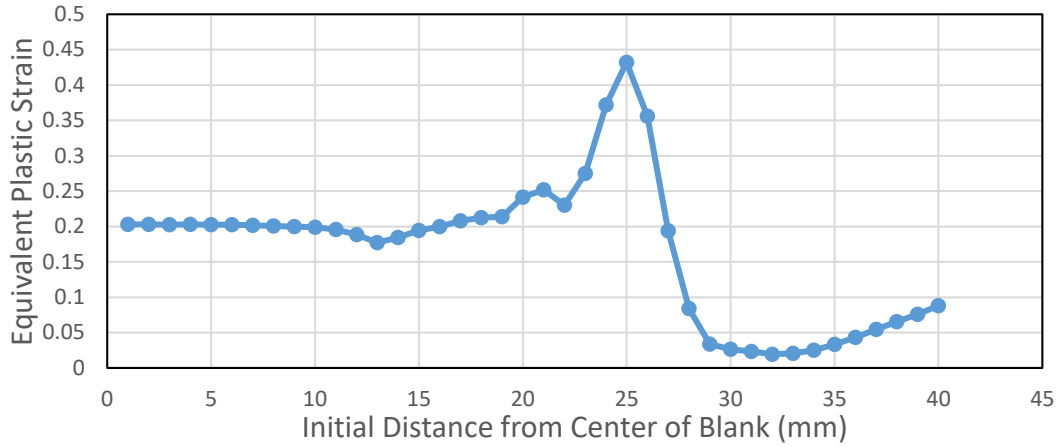

(a)

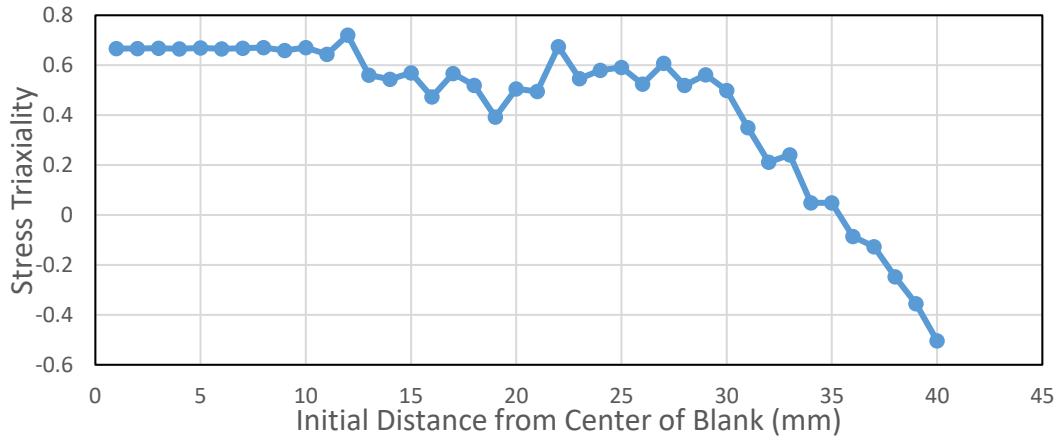

(b)

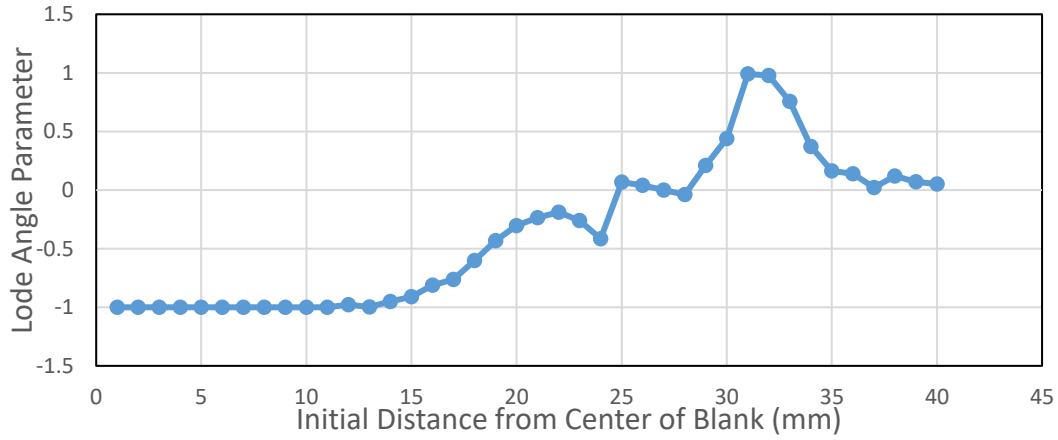

(c)

Figure 5.170. The variation of (a) Equivalent Plastic Strain (b) Stress Triaxiality and (c) Lode Angle Parameter along the transverse direction of the blank at 12 mm cup depth for AISI 304 steel (VM-JC-HC)

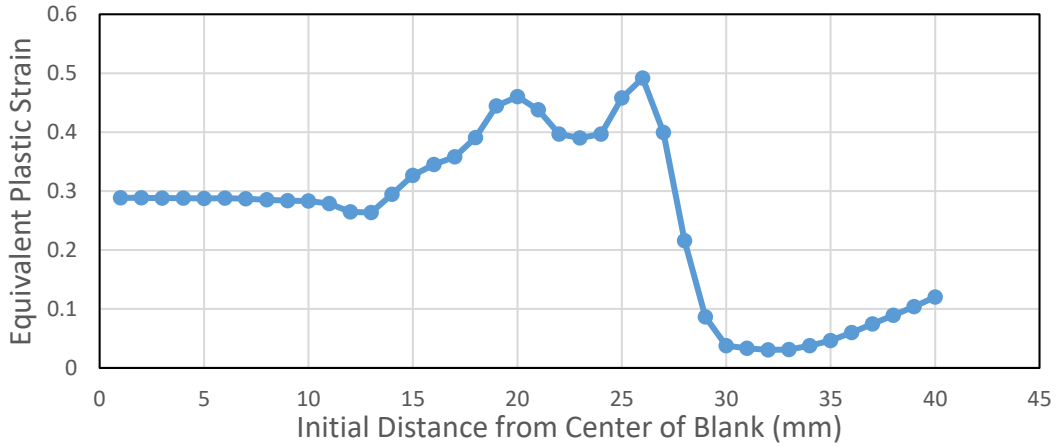

(a)

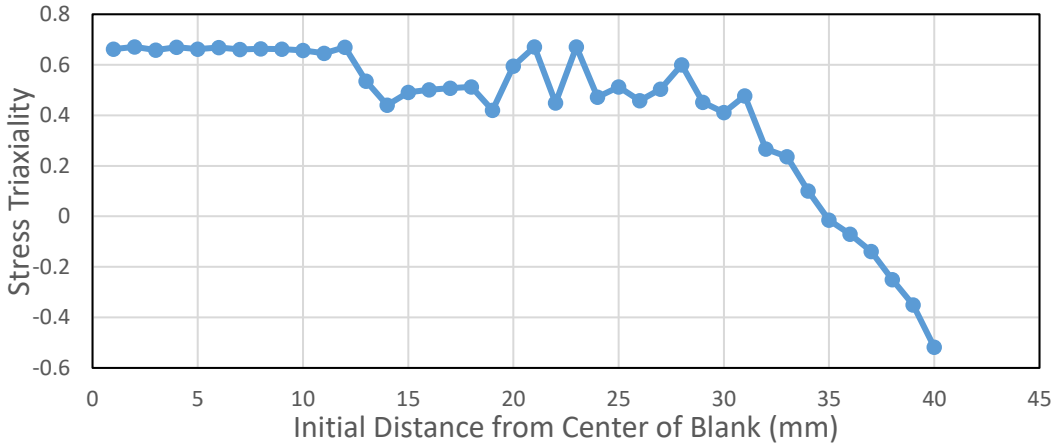

(b)

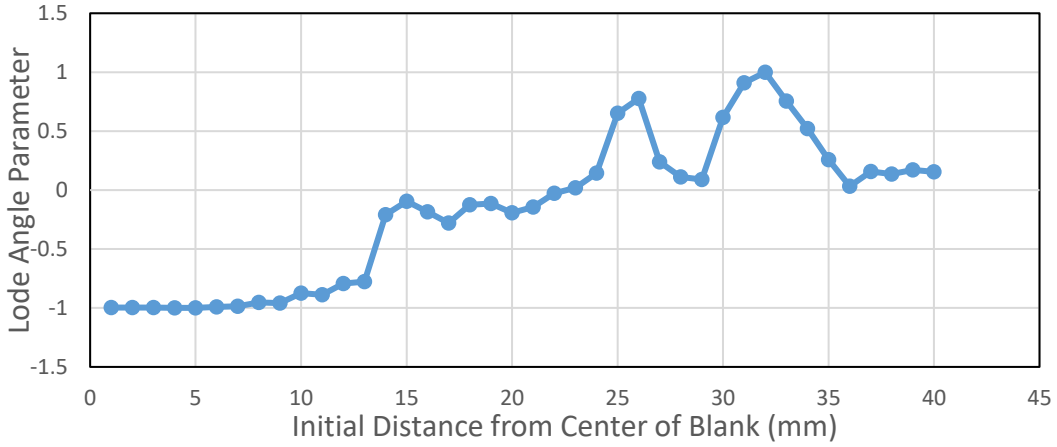

(c)

Figure 5.171. The variation of (a) Equivalent Plastic Strain (b) Stress Triaxiality and (c) Lode Angle Parameter along the transverse direction of the blank at 16 mm cup depth for AISI 304 steel (VM-JC-HC)

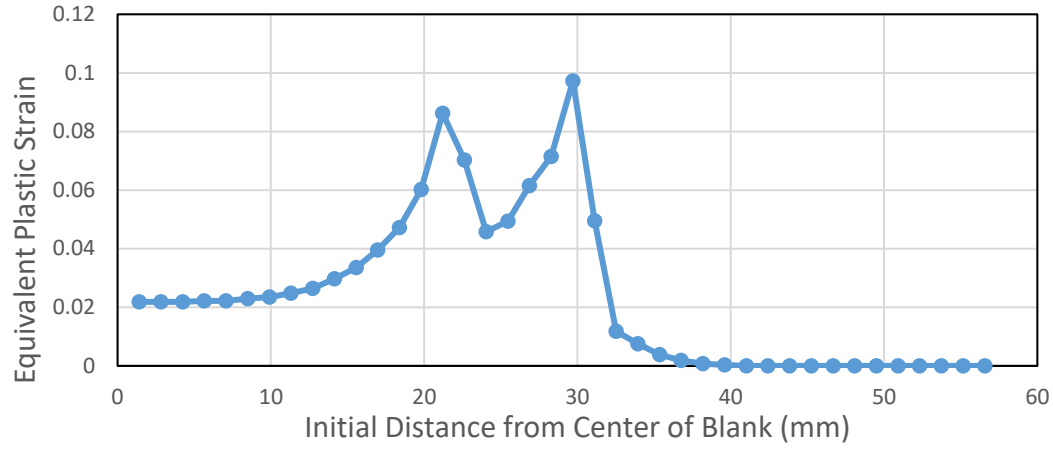

(a)

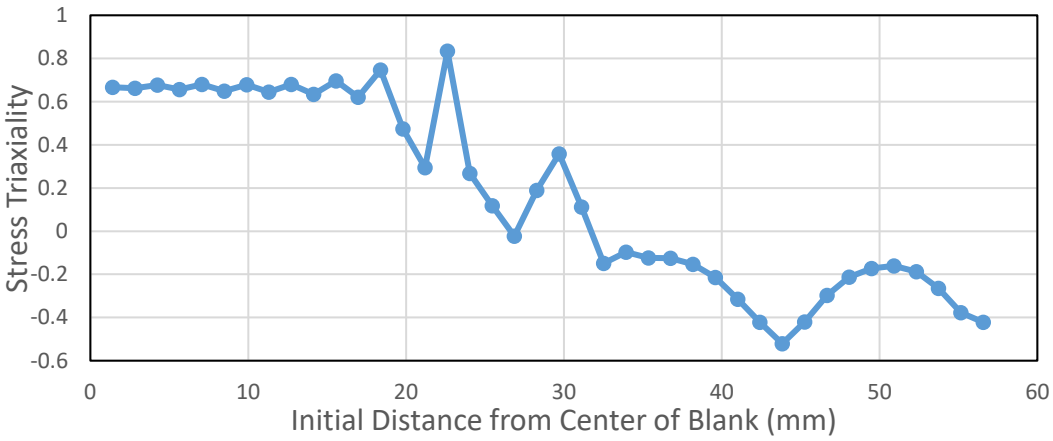

(b)

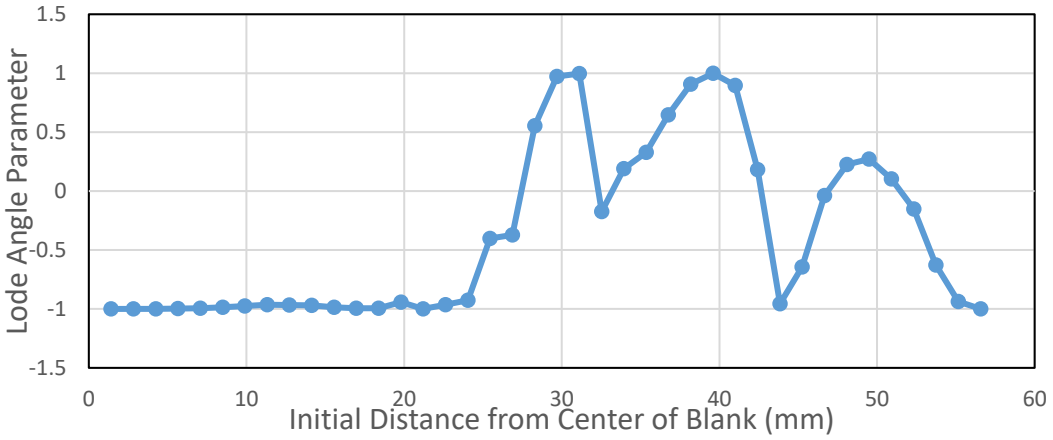

(c)

Figure 5.172. The variation of (a) Equivalent Plastic Strain (b) Stress Triaxiality and (c) Lode Angle Parameter along the diagonal of the blank at 4 mm cup depth for AISI 304 steel (VM-JC-HC)

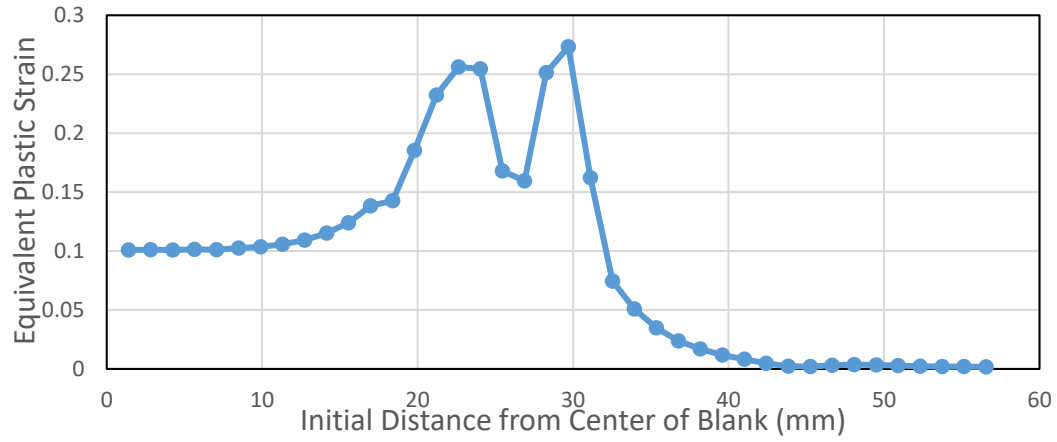

(a)

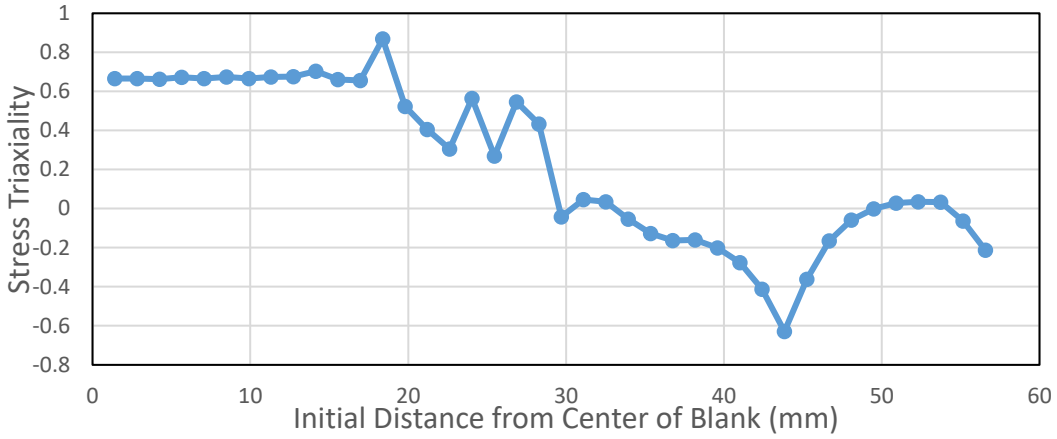

(b)

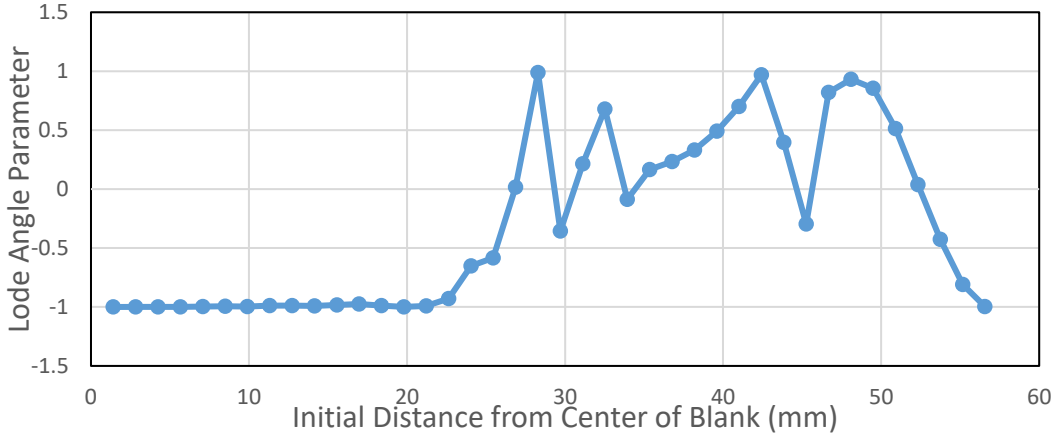

(c)

Figure 5.173. The variation of (a) Equivalent Plastic Strain (b) Stress Triaxiality and (c) Lode Angle Parameter along the diagonal of the blank at 8 mm cup depth for AISI 304 steel (VM-JC-HC)

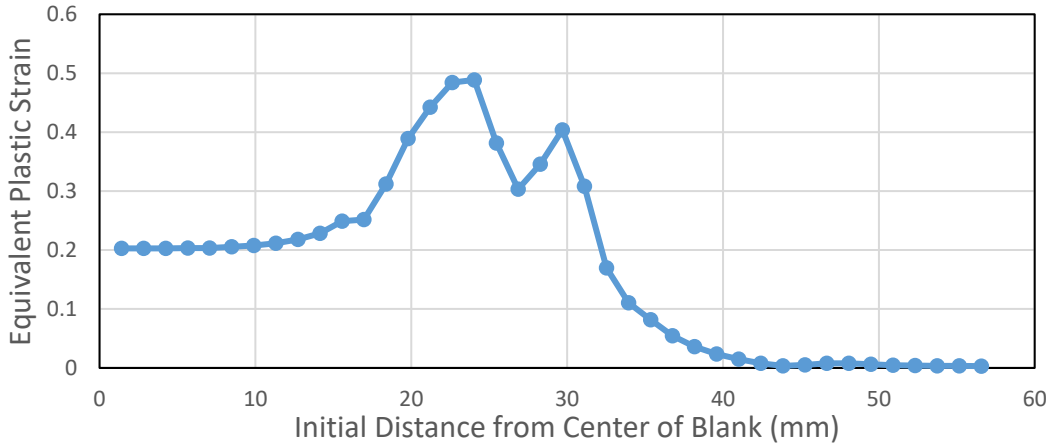

(a)

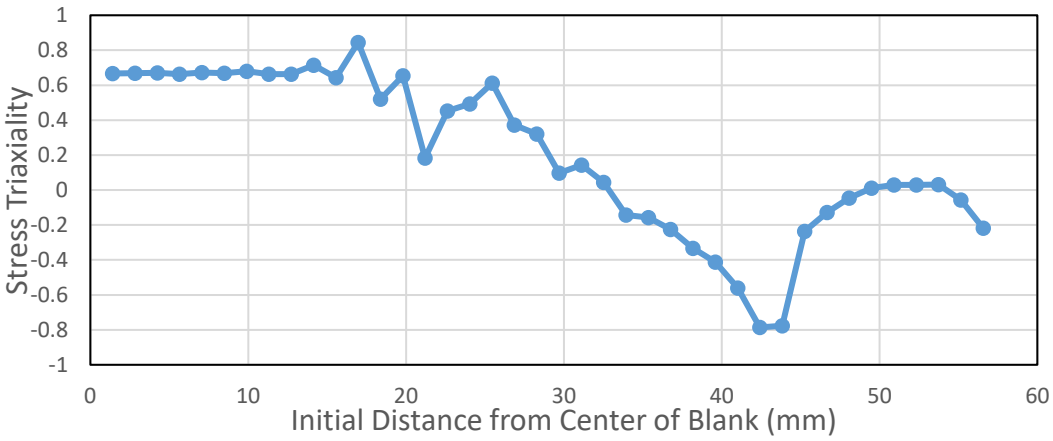

(b)

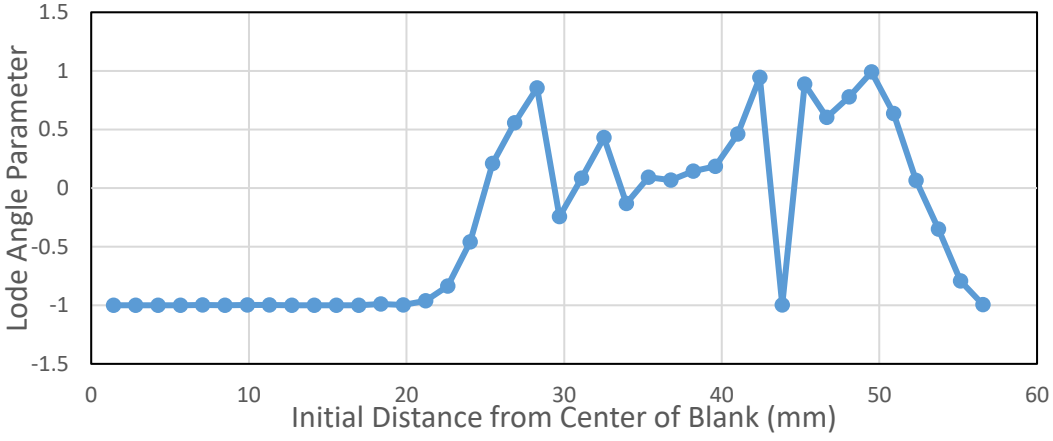

(c)

Figure 5.174 The variation of (a) Equivalent Plastic Strain (b) Stress Triaxiality and (c) Lode Angle Parameter along the diagonal of the blank at 12 mm cup depth for AISI 304 steel (VM-JC-HC)

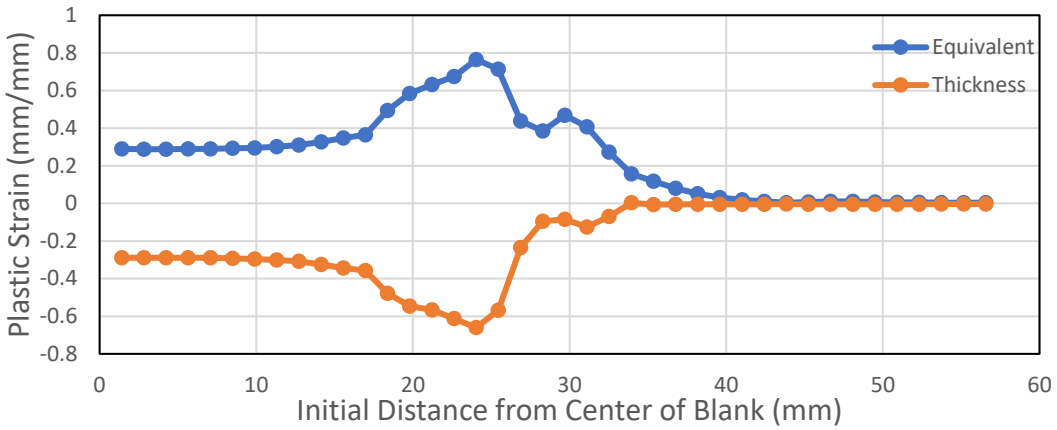

(a)

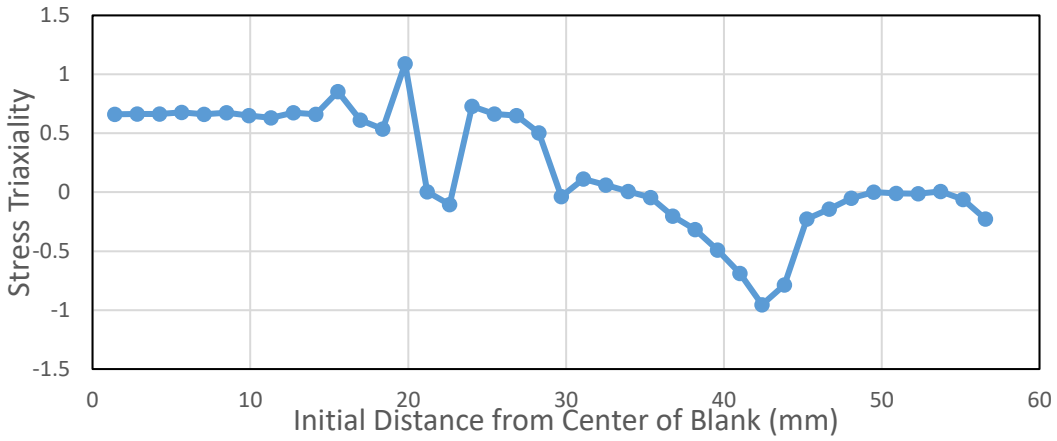

(b)

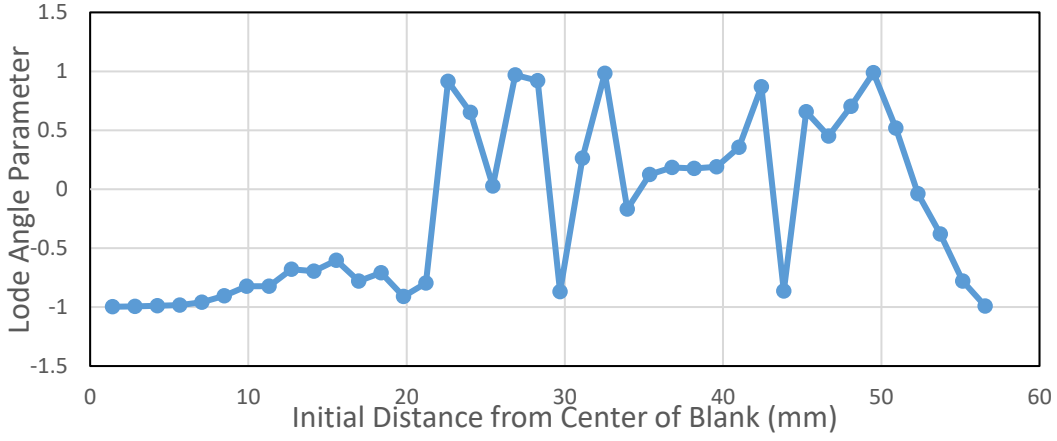

(c)

Figure 5.175 The variation of (a) Equivalent Plastic Strain and Thickness Plastic Strain (b) Stress Triaxiality and (c) Lode Angle Parameter along the diagonal of the blank at 16 mm cup depth for AISI 304 steel (VM-JC-HC)

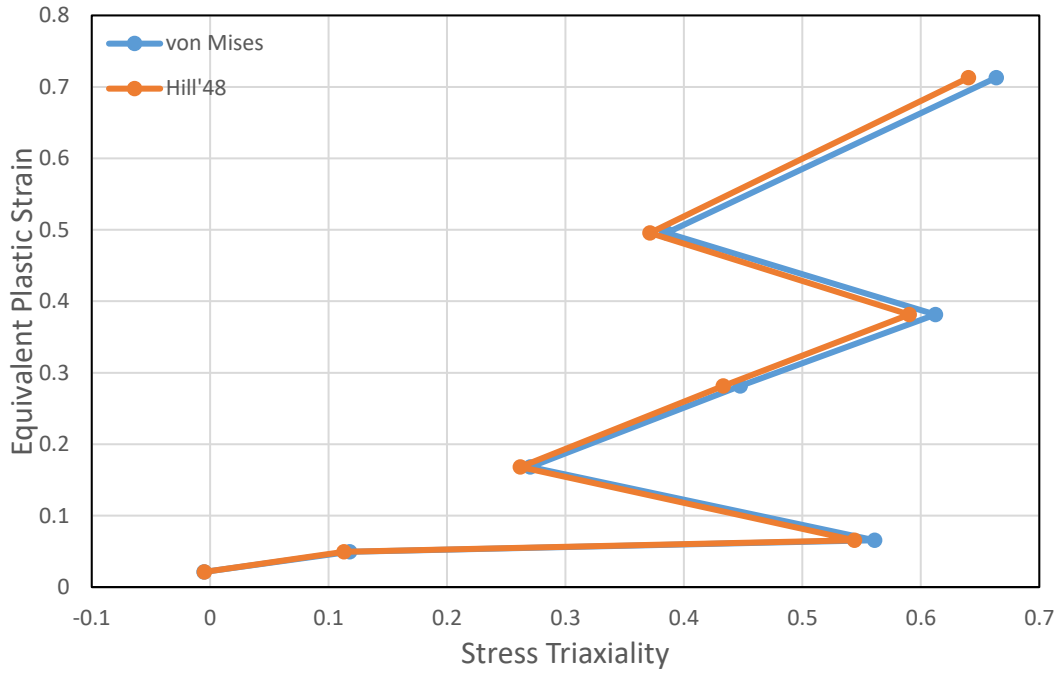

Figure 5.176. Equivalent Plastic Strain - Stress Triaxiality Plot of First Fracture Element (VM-JC-HC)

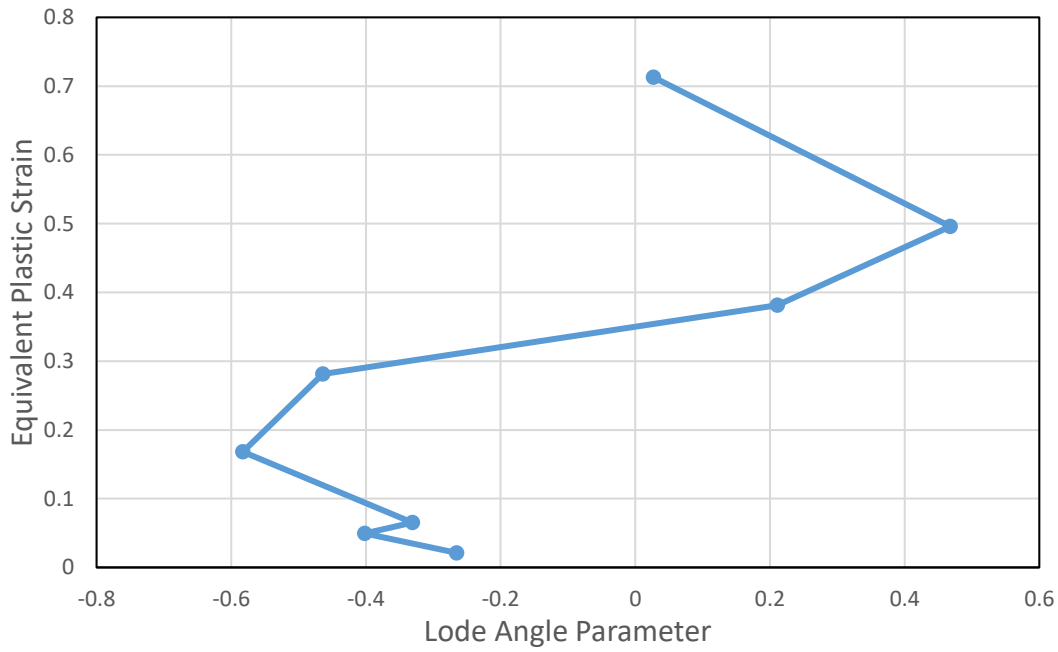

Figure 5.177. Equivalent Plastic Strain – Lode Angle Parameter Plot of First Fracture Element (VM-JC-HC)

In the rolling direction, the triaxiality values vary generally between 0.6 and 0.8 under the punch whereas the Lode angle parameter values change between -0.5 and -1. Up to the punch shoulder, it can be said that the deformation behavior is in equi-biaxial tension condition. After 30 mm from the blank center, triaxiality values became negative and the Lode angle parameter values became positive, indicating that the components are in a compressed condition. After 30 mm distance from blank center, under blank holder, triaxiality values decreasing with positive Lode angle parameter values. According to these values it can be said that, under blank holder region stress state is compressive.

The same tendency of rolling direction is observed in the transverse direction also. The differences are a result of anisotropy of the material.

In the diagonal direction, as in the transverse and rolling directions, equi-biaxial stress condition is observed under the punch until 20 mm distance from the center of blank. It is observed that from a distance from the center of blank of 20 mm to 35 mm, it shifts from tension to shear as it moves away from the center. There is a transition from compression to equi-biaxial compression between 35 mm distance from the center of the blank to 45 mm distance. After this point, stress triaxiality becomes zero and Lode angle parameter values decreasing so, state changes from uniaxial tension to uniaxial compression. Fracture occurs in tension situation at punch shoulder.

5.1.11 Case 11: Square-AISI304-Hill48-Discrete-Johnson Cook Model

For the eleventh case, Hill'48 yield criterion was applied with discrete hardening and the Johnson Cook ductile fracture criterion was used. It was observed that the fracture had started after 20 mm punch travel as shown in Figure 5.178. The variation of equivalent plastic strain, stress triaxiality and Lode angle parameter values are presented as a function of the distance from the center of the blank for different cup heights up to the fracture. The results are shown for rolling direction in Figure 5.179 to Figure 5.183, for transverse direction in Figure 5.184 to Figure 5.188 and for diagonal direction in Figure 5.189 to Figure 5.193. The thickness plastic strain distribution is also inserted into Figure 5.193 (a) in order to better visualize the deformation. Further, the variations of stress triaxiality values with respect to equivalent plastic strain are given by considering both von Mises and Hill'48 criteria as a function of the path of the element that fractured first in Figure 5.194. Along the same path, the variation of the Lode parameter with respect to equivalent plastic strain is also illustrated in Figure 5.195.

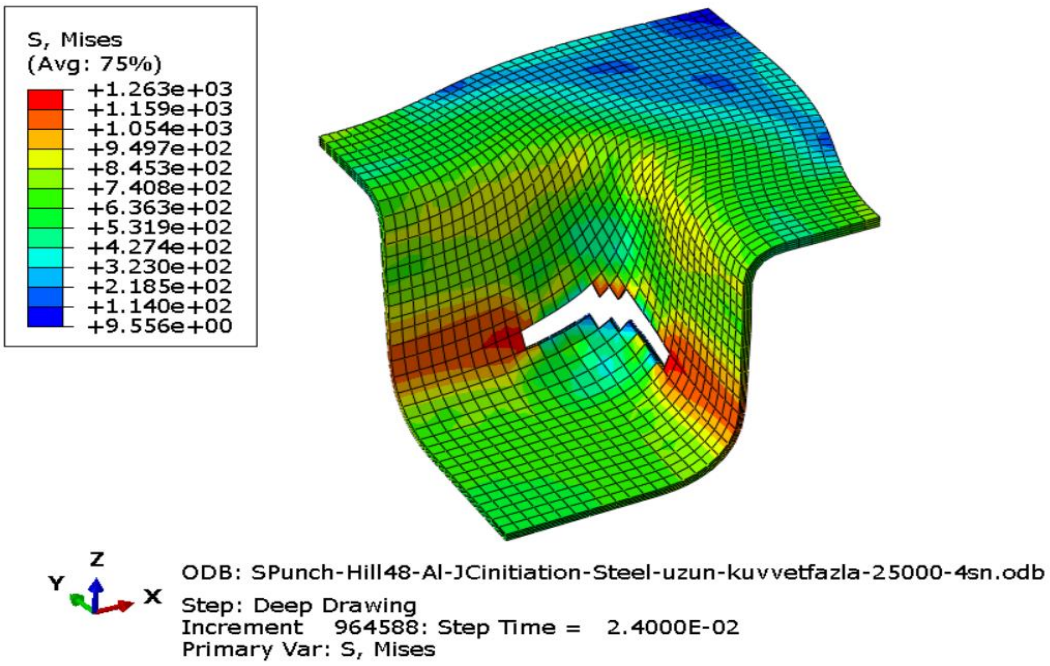

Figure 5.178. First Fracture Moment of Case 11

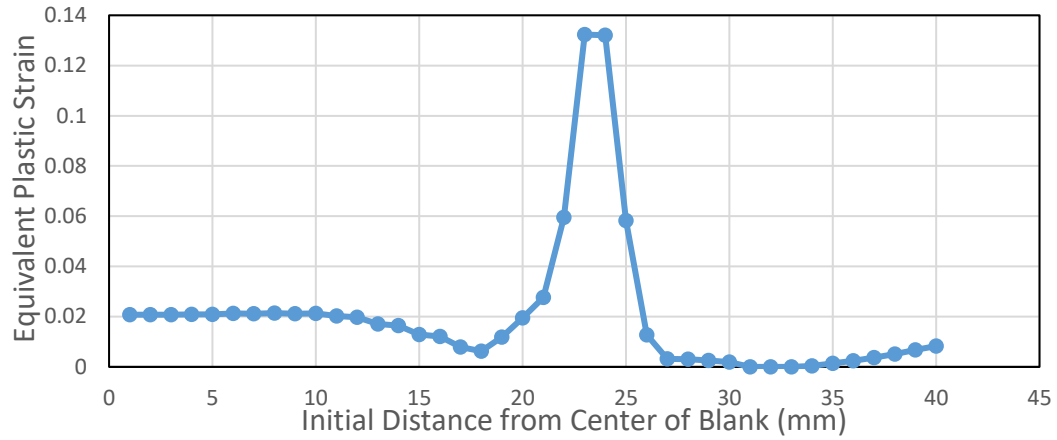

(a)

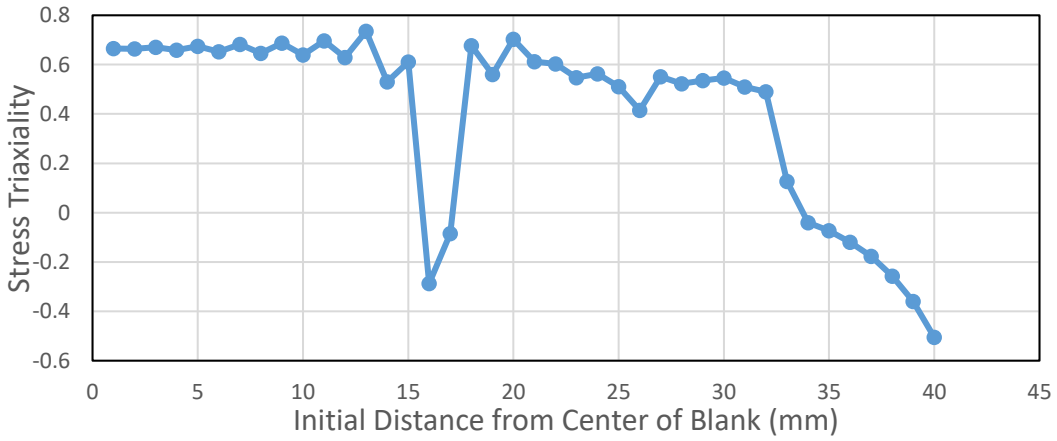

(b)

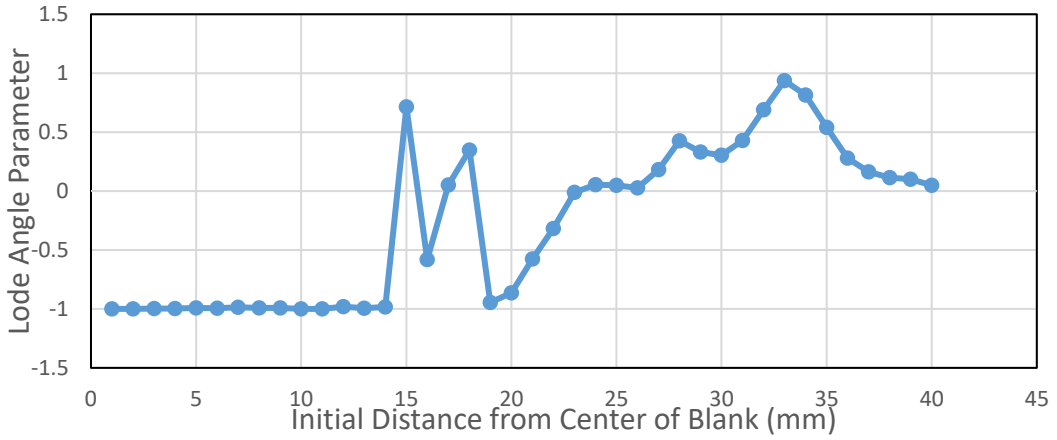

(c)

Figure 5.179. The variation of (a) Equivalent Plastic Strain (b) Stress Triaxiality and (c) Lode Angle Parameter along the rolling direction of the blank at 4 mm cup depth for AISI 304 steel (Hill'48-Disc-JC)

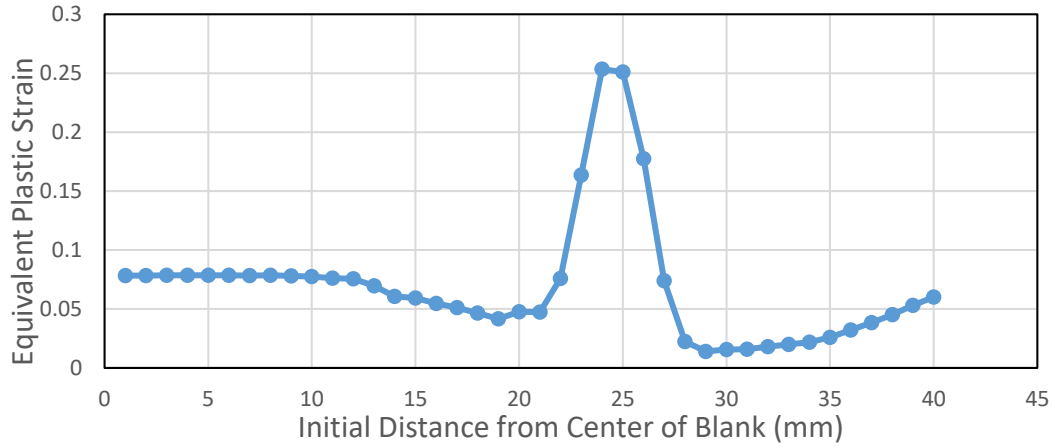

(a)

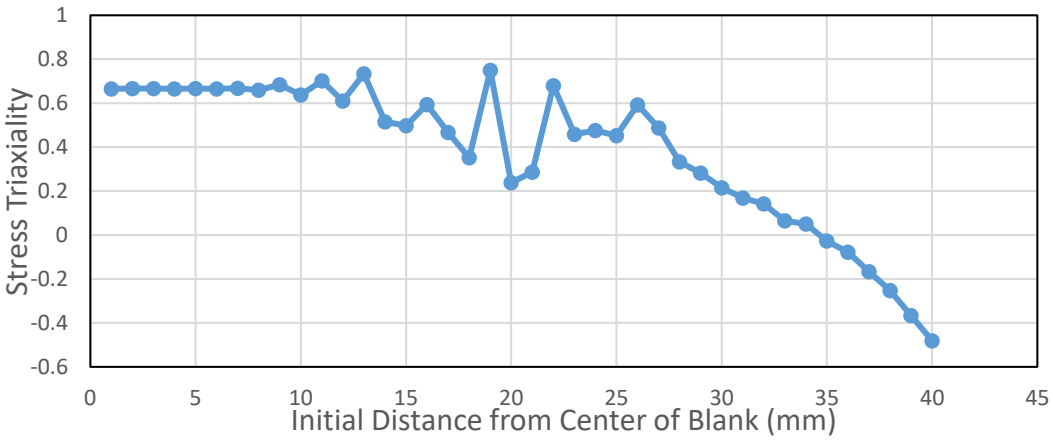

(b)

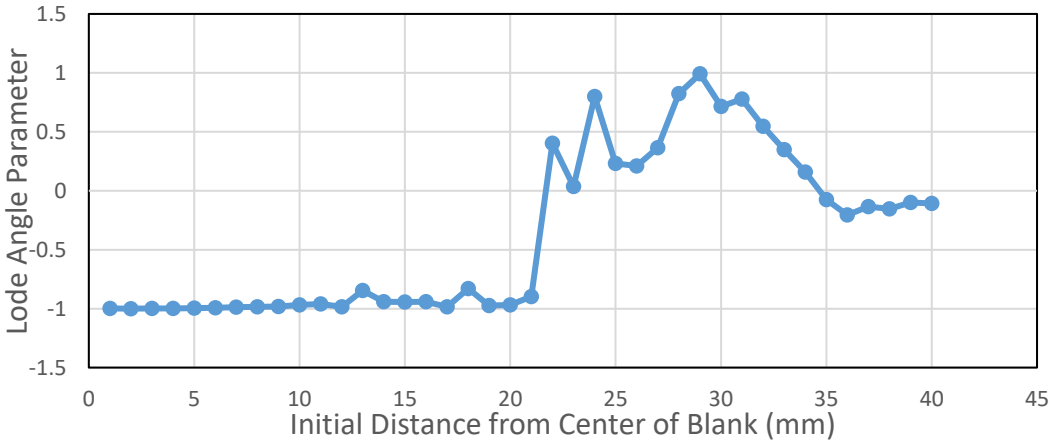

(c)

Figure 5.180. The variation of (a) Equivalent Plastic Strain (b) Stress Triaxiality and (c) Lode Angle Parameter along the rolling direction of the blank at 8 mm cup depth for AISI 304 steel (Hill'48-Disc-JC)

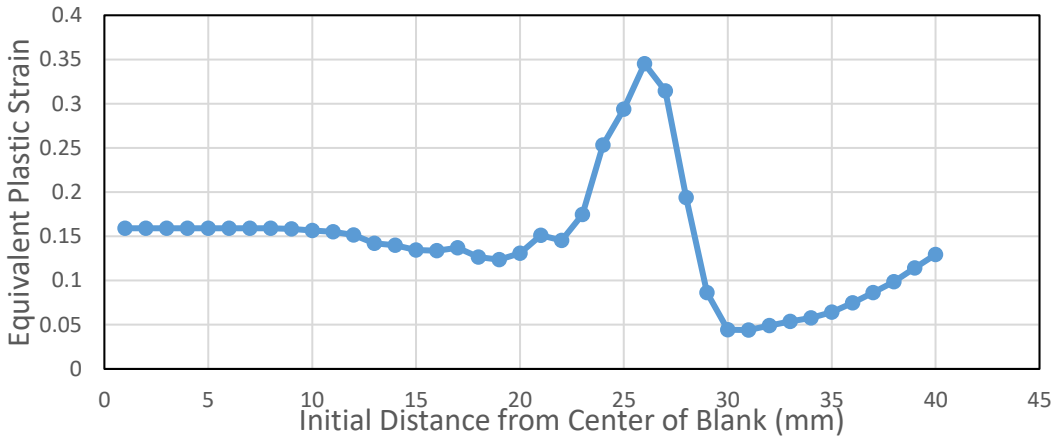

(a)

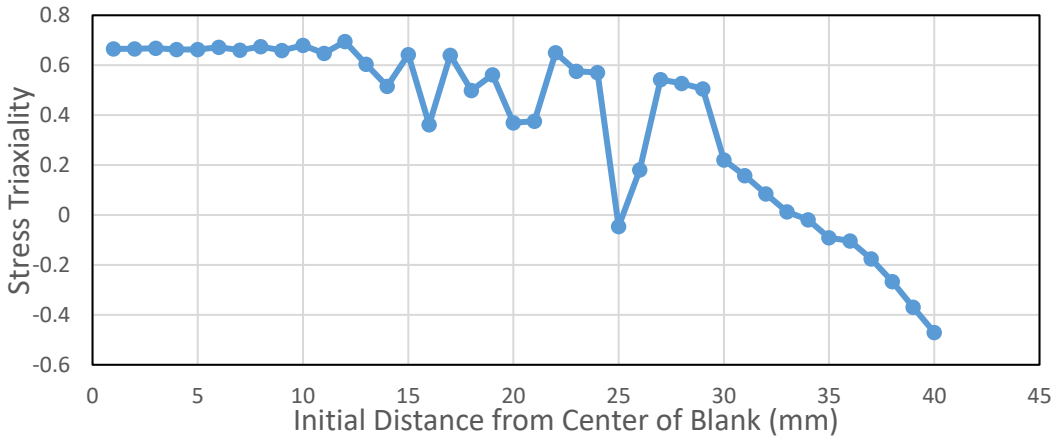

(b)

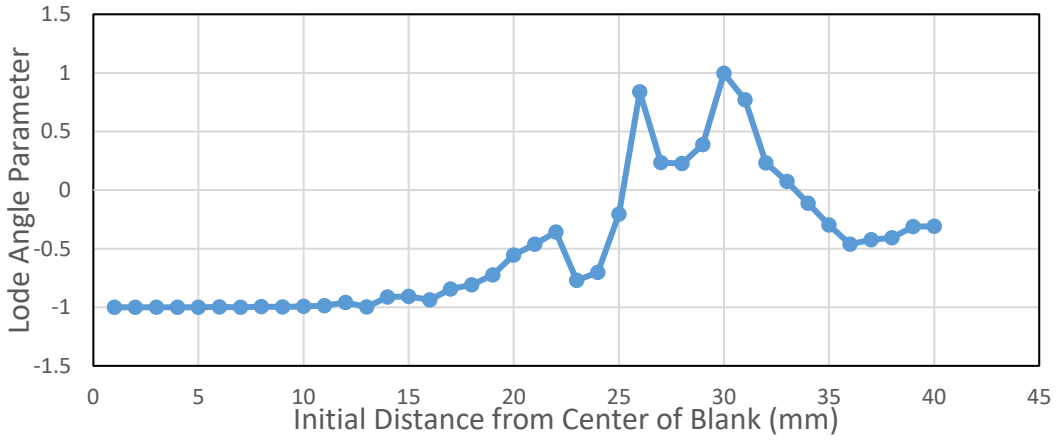

(c)

Figure 5.181. The variation of (a) Equivalent Plastic Strain (b) Stress Triaxiality and (c) Lode Angle Parameter along the rolling direction of the blank at 12 mm cup depth for AISI 304 steel (Hill'48-Disc-JC)

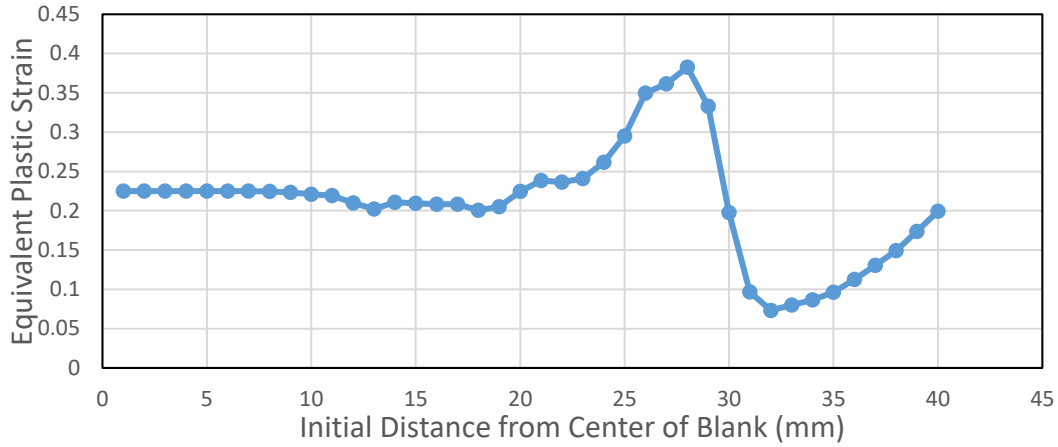

(a)

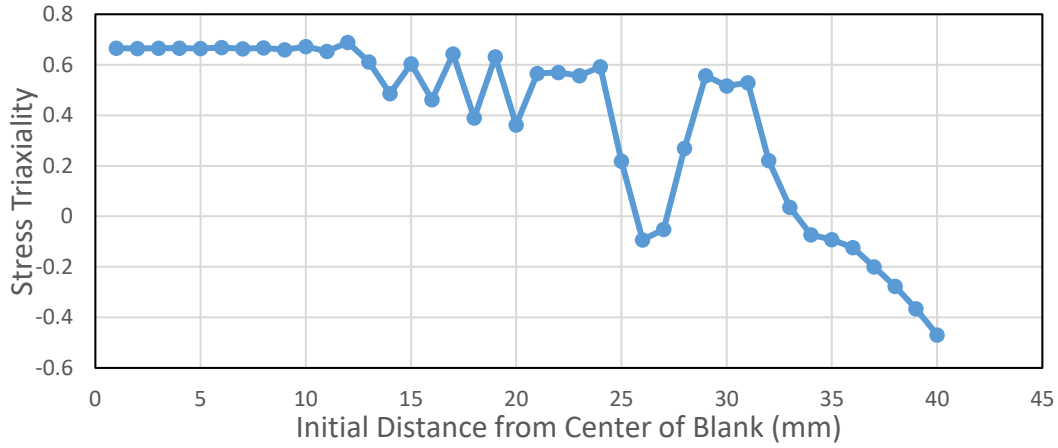

(b)

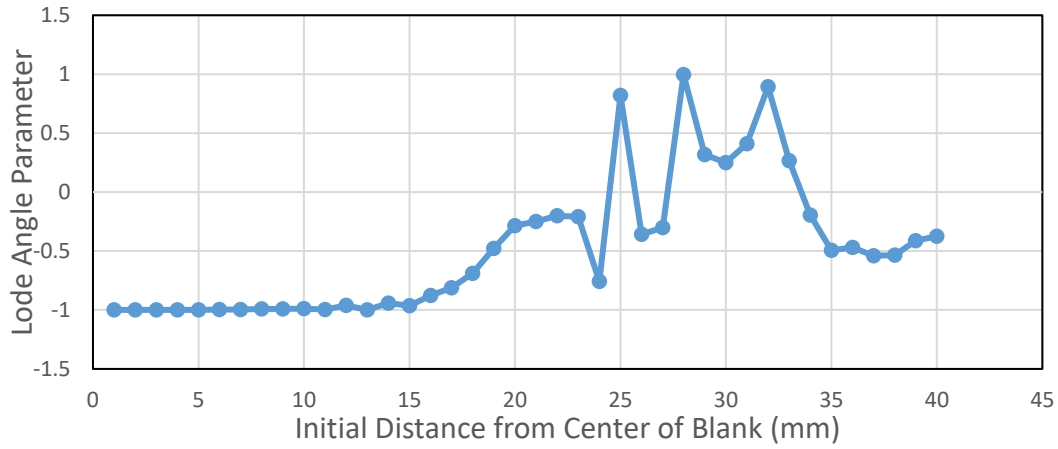

(c)

Figure 5.182. The variation of (a) Equivalent Plastic Strain (b) Stress Triaxiality and (c) Lode Angle Parameter along the rolling direction of the blank at 16 mm cup depth for AISI 304 steel (Hill'48-Disc-JC)

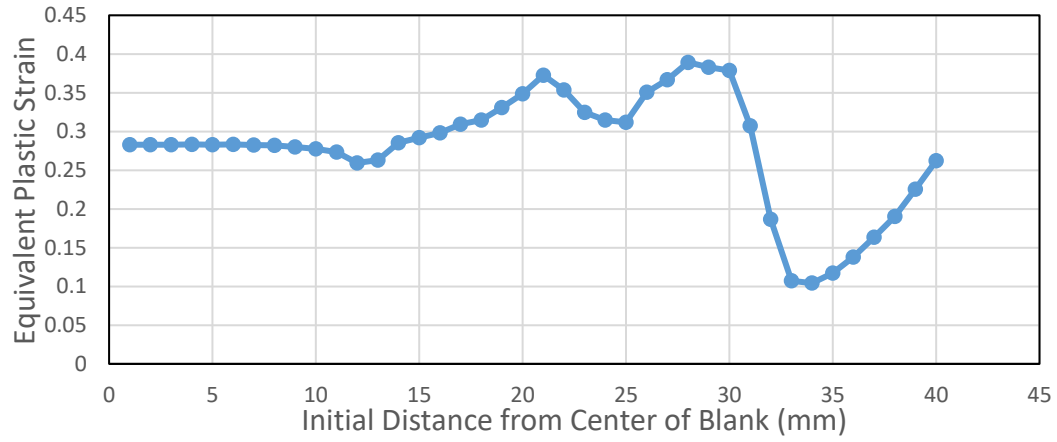

(a)

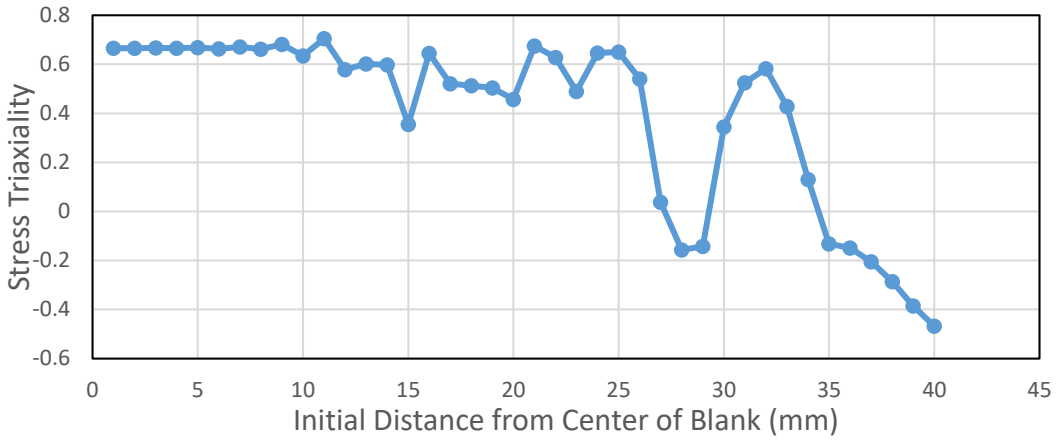

(b)

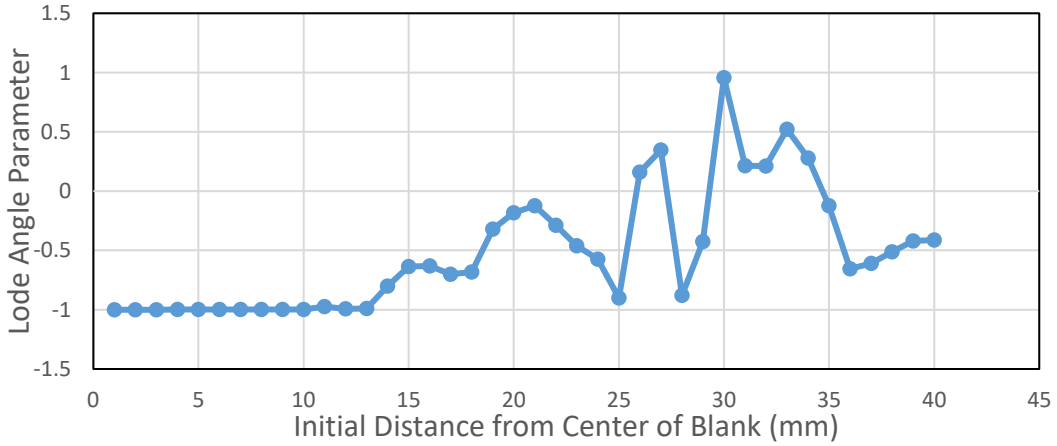

(c)

Figure 5.183. The variation of (a) Equivalent Plastic Strain (b) Stress Triaxiality and (c) Lode Angle Parameter along the rolling direction of the blank at 20 mm cup depth for AISI 304 steel (Hill'48-Disc-JC)

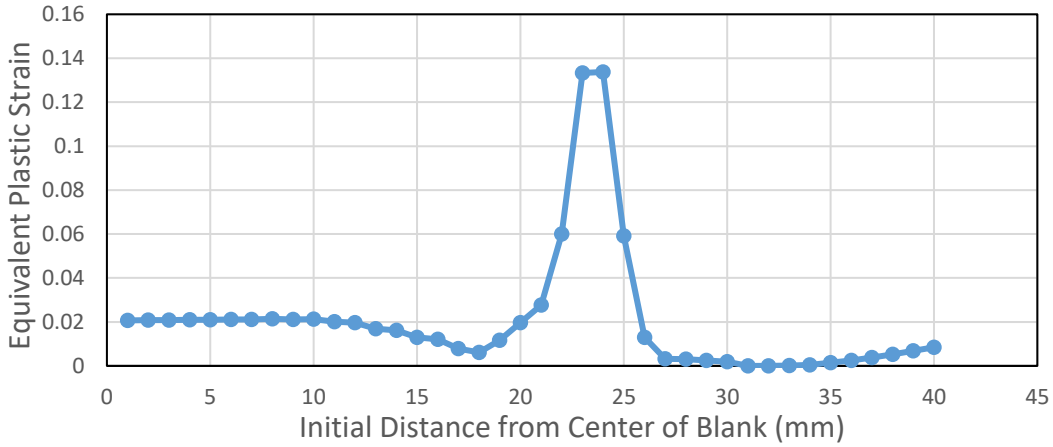

(a)

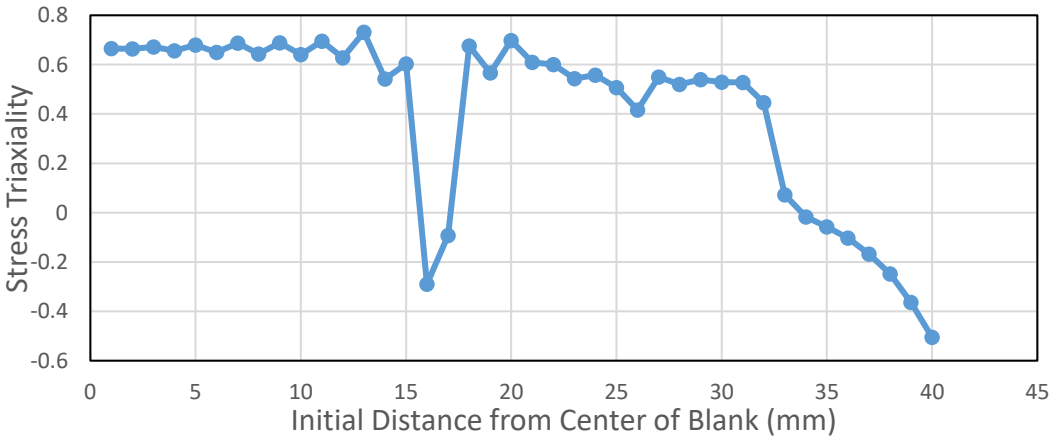

(b)

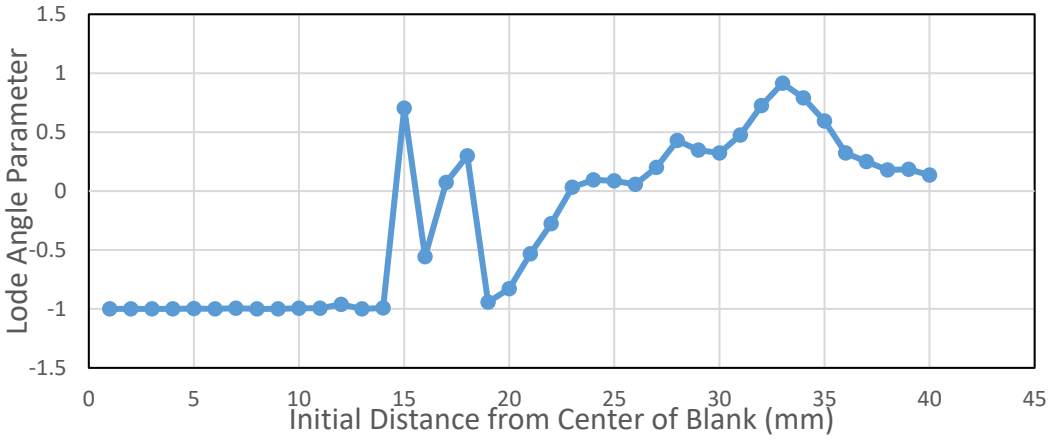

(c)

Figure 5.184. The variation of (a) Equivalent Plastic Strain (b) Stress Triaxiality and (c) Lode Angle Parameter along the transverse direction of the blank at 4 mm cup depth for AISI 304 steel (Hill'48-Disc-JC)

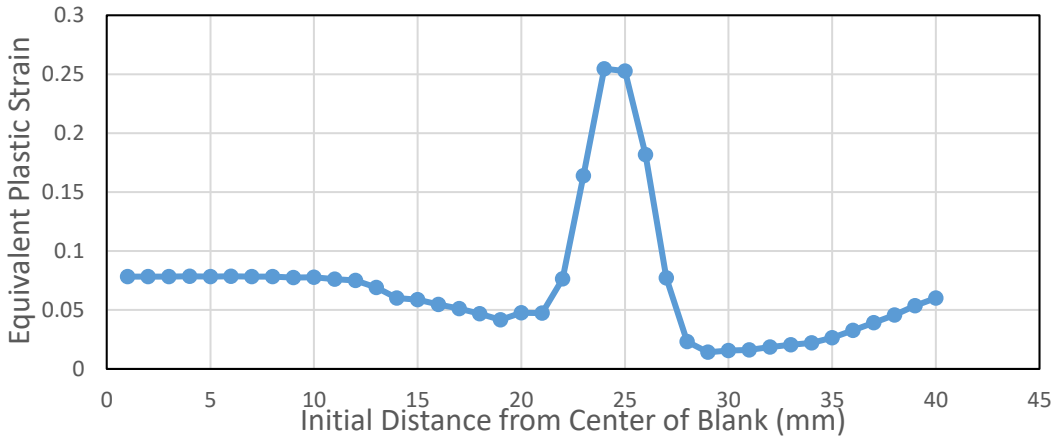

(a)

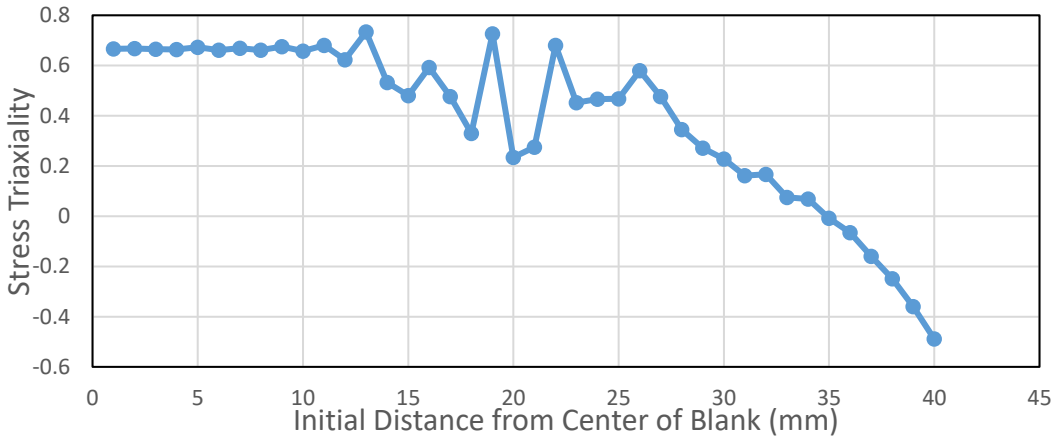

(b)

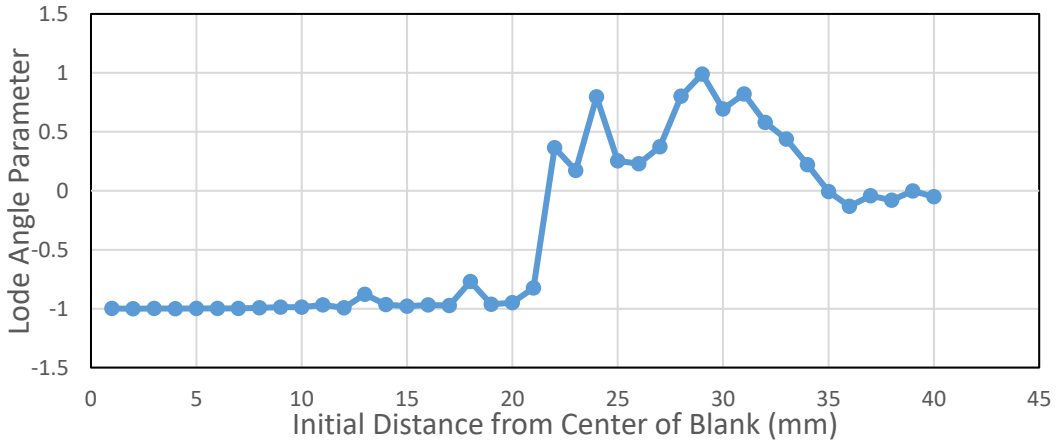

(c)

Figure 5.185. The variation of (a) Equivalent Plastic Strain (b) Stress Triaxiality and (c) Lode Angle Parameter along the transverse direction of the blank at 8 mm cup depth for AISI 304 steel (Hill'48-Disc-JC)

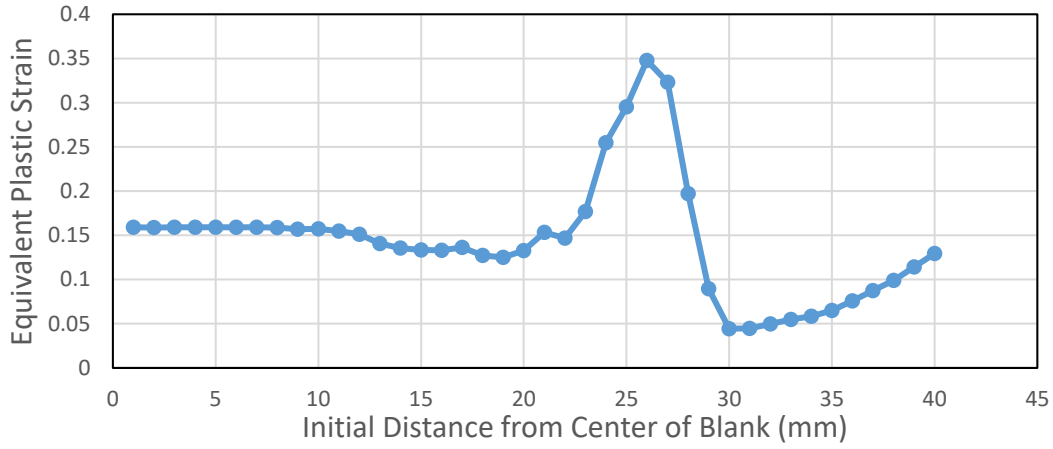

(a)

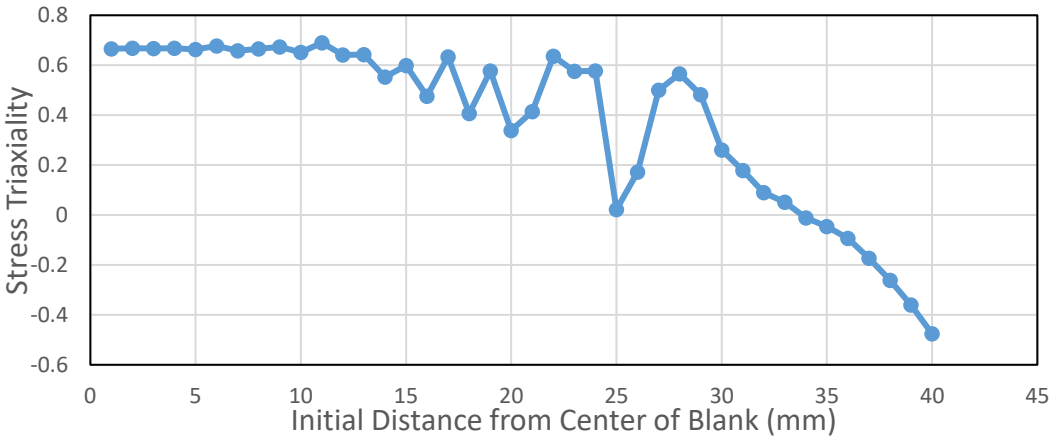

(b)

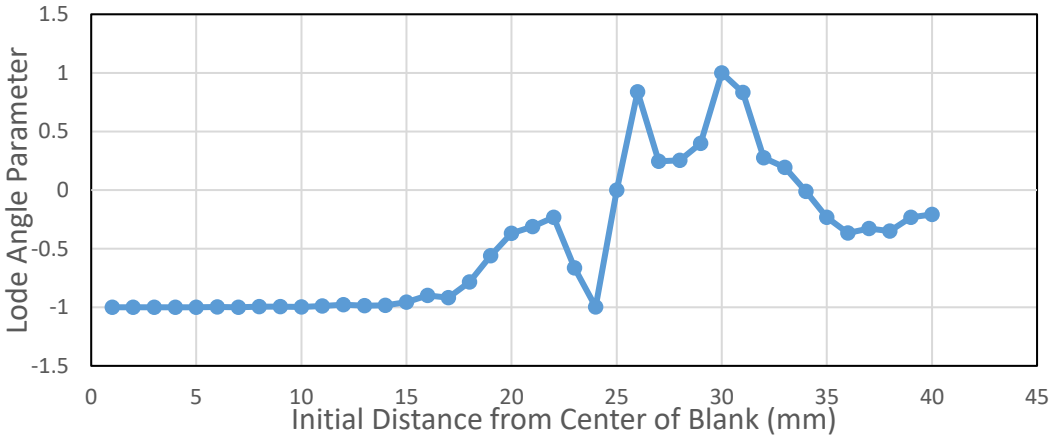

(c)

Figure 5.186. The variation of (a) Equivalent Plastic Strain (b) Stress Triaxiality and (c) Lode Angle Parameter along the transverse direction of the blank at 12 mm cup depth for AISI 304 steel (Hill'48-Disc-JC)

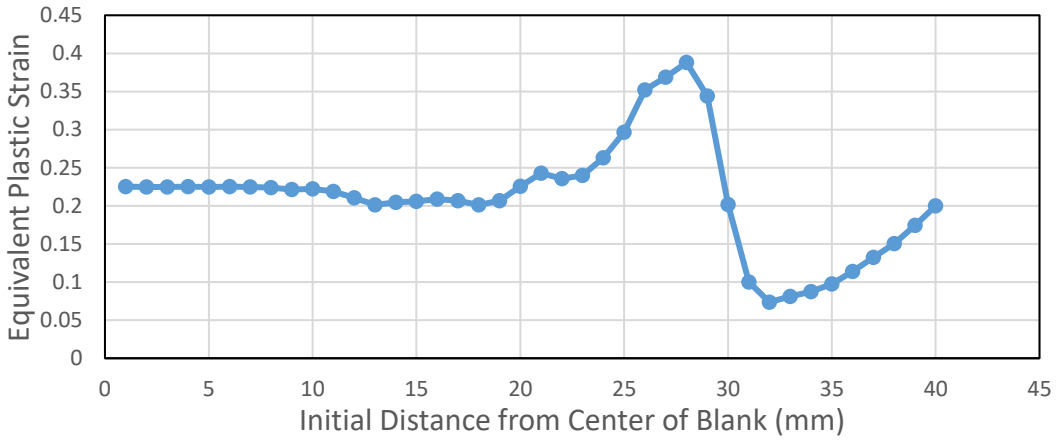

(a)

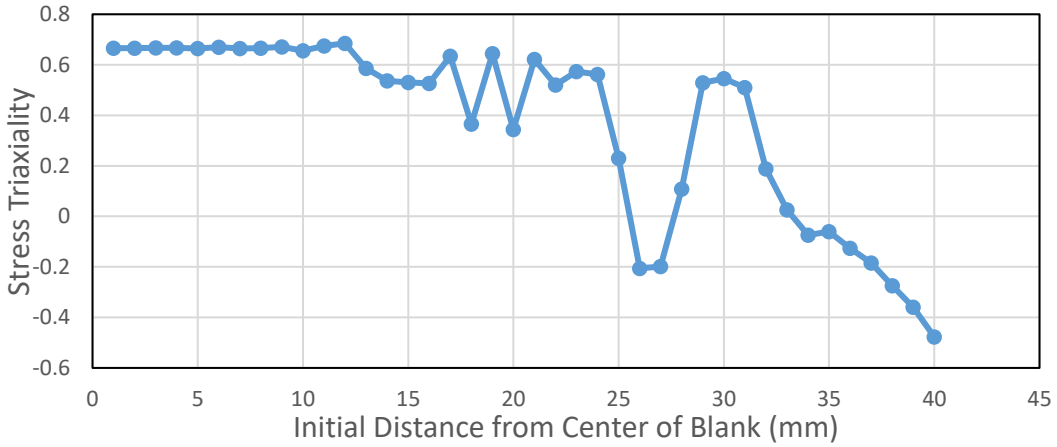

(b)

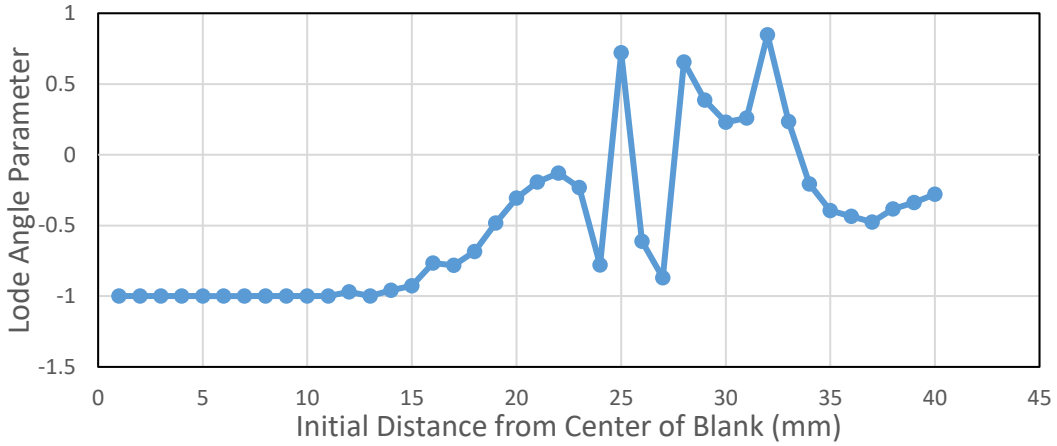

(c)

Figure 5.187. The variation of (a) Equivalent Plastic Strain (b) Stress Triaxiality and (c) Lode Angle Parameter along the transverse direction of the blank at 16 mm cup depth for AISI 304 steel (Hill'48-Disc-JC)

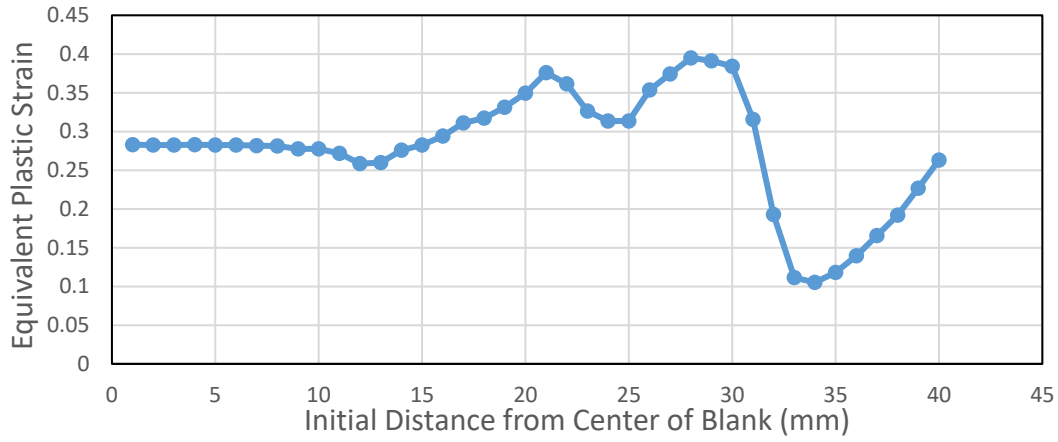

(a)

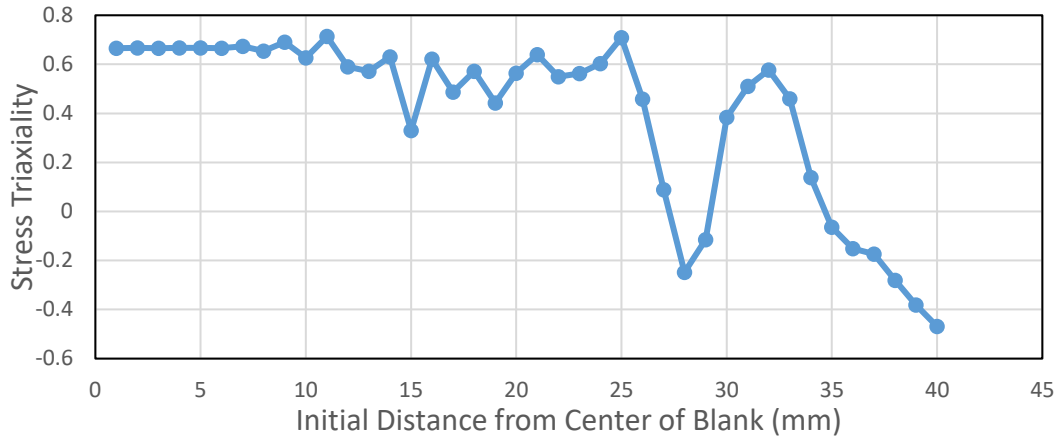

(b)

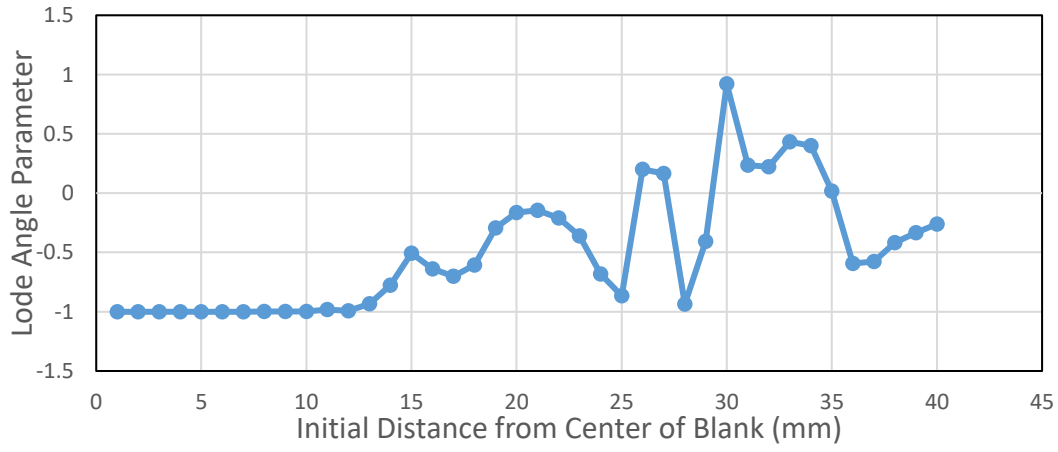

(c)

Figure 5.188. The variation of (a) Equivalent Plastic Strain (b) Stress Triaxiality and (c) Lode Angle Parameter along the transverse direction of the blank at 20 mm cup depth for AISI 304 steel (Hill'48-Disc-JC)

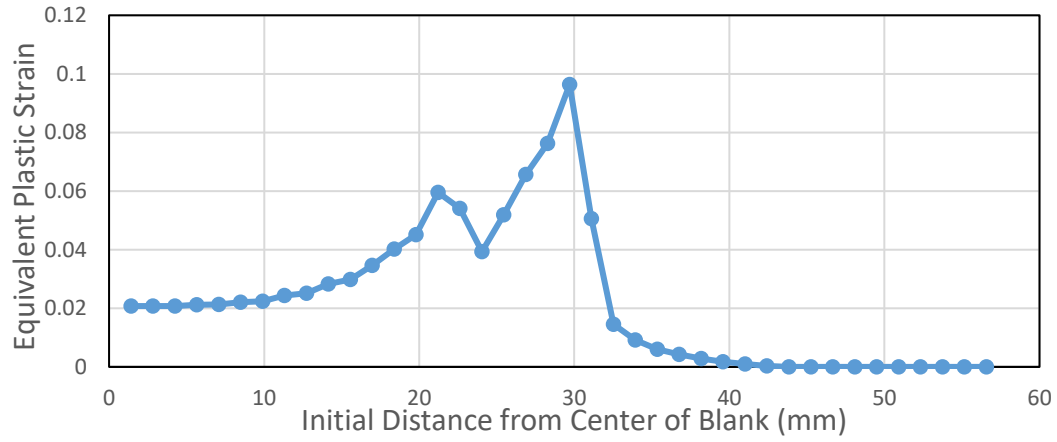

(a)

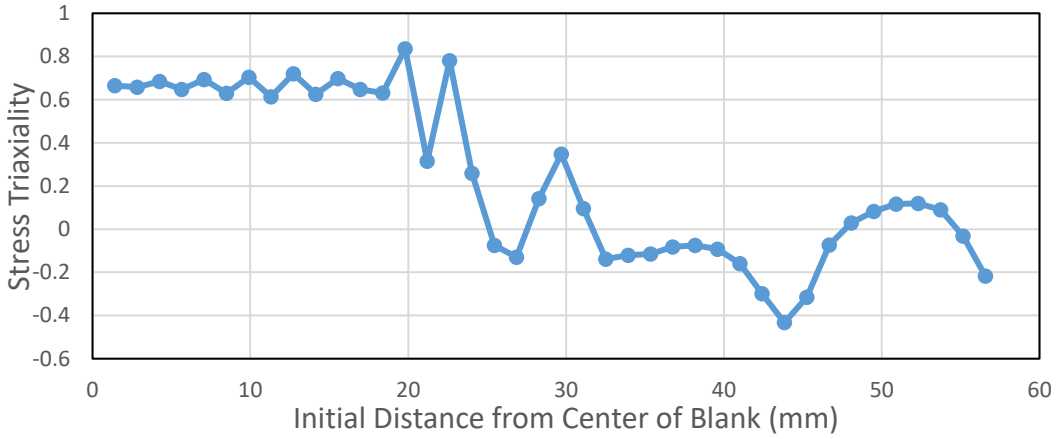

(b)

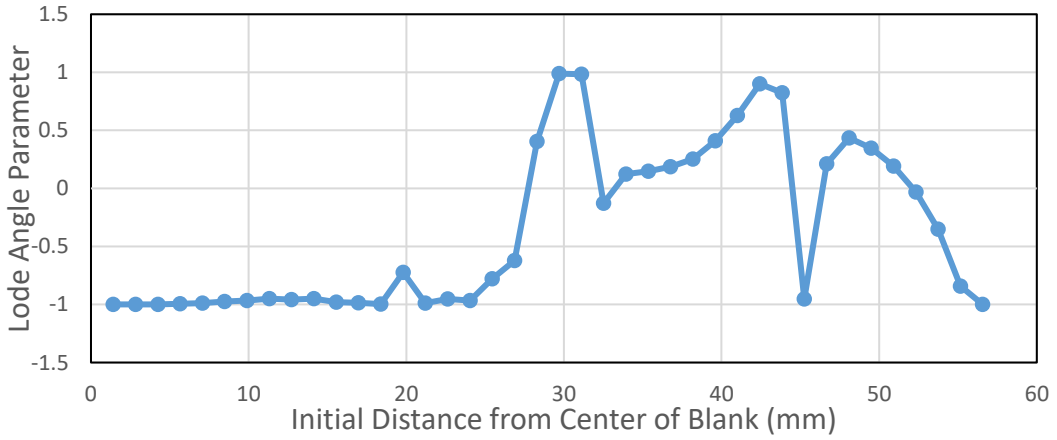

(c)

Figure 5.189. The variation of (a) Equivalent Plastic Strain (b) Stress Triaxiality and (c) Lode Angle Parameter along the diagonal of the blank at 4 mm cup depth for AISI 304 steel (Hill'48-Disc-JC)

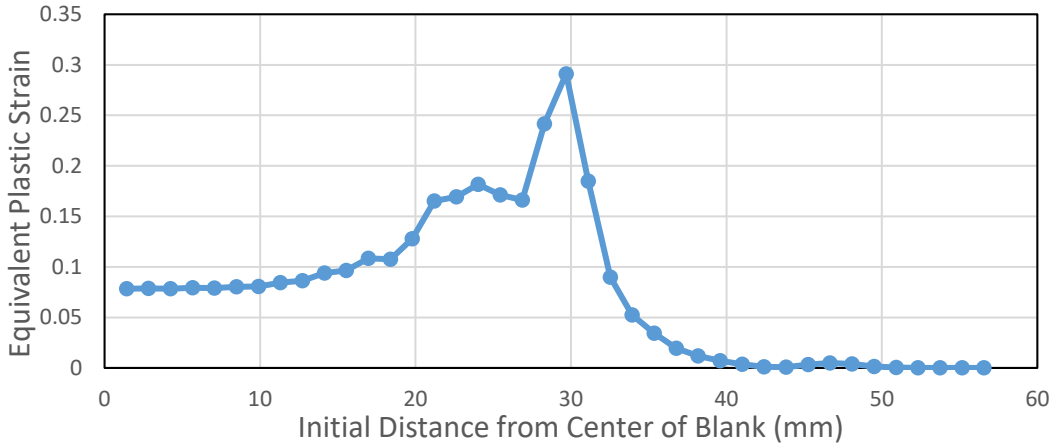

(a)

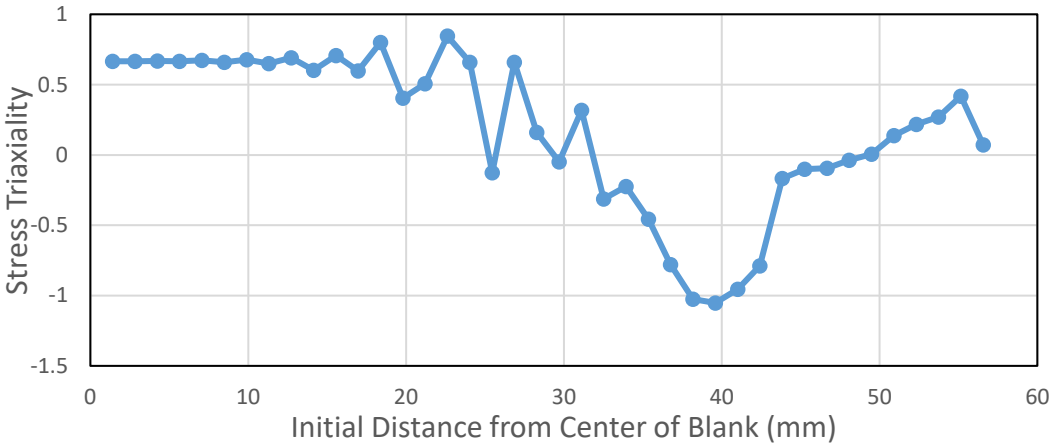

(b)

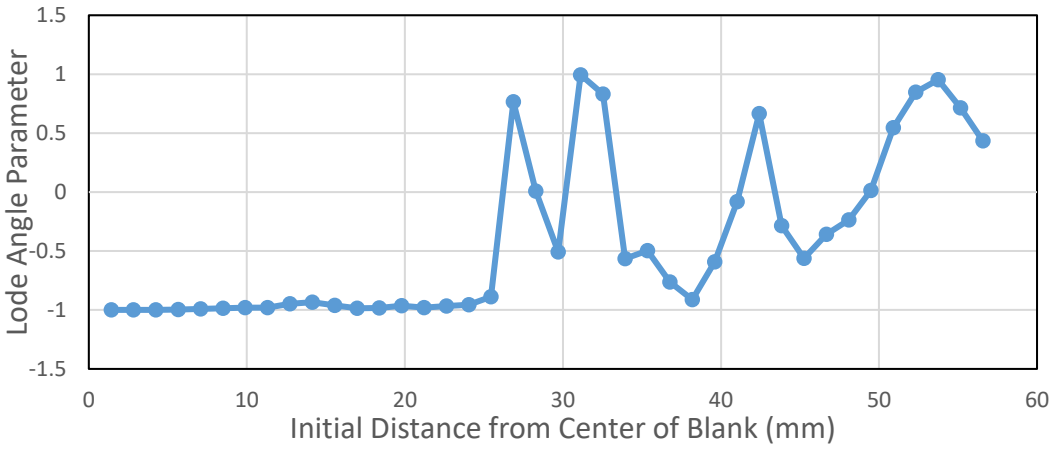

(c)

Figure 5.190. The variation of (a) Equivalent Plastic Strain (b) Stress Triaxiality and (c) Lode Angle Parameter along the diagonal of the blank at 8 mm cup depth for AISI 304 steel (Hill'48-Disc-JC)

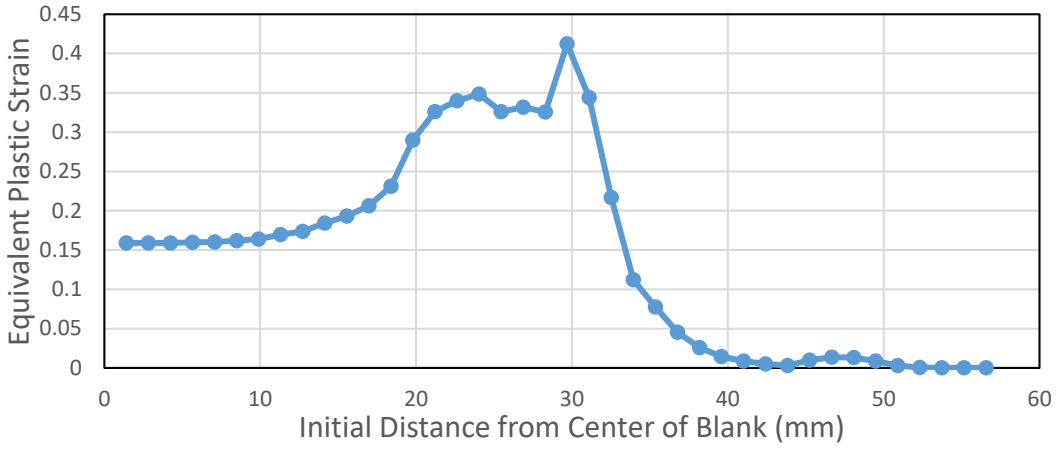

(a)

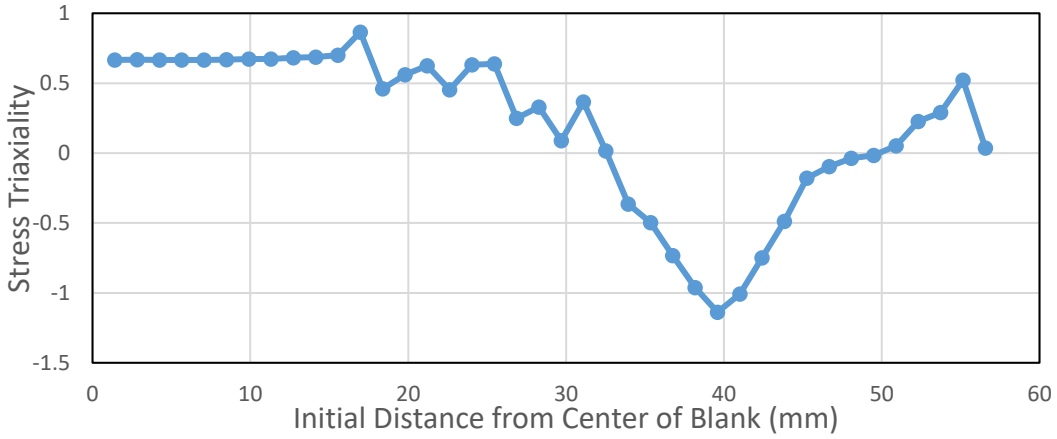

(b)

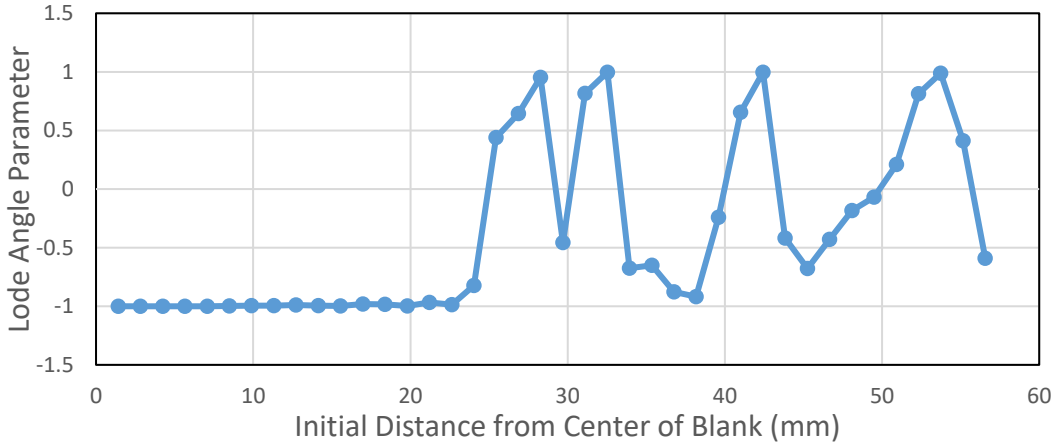

(c)

Figure 5.191 The variation of (a) Equivalent Plastic Strain (b) Stress Triaxiality and (c) Lode Angle Parameter along the diagonal of the blank at 12 mm cup depth for AISI 304 steel (Hill'48-Disc-JC)

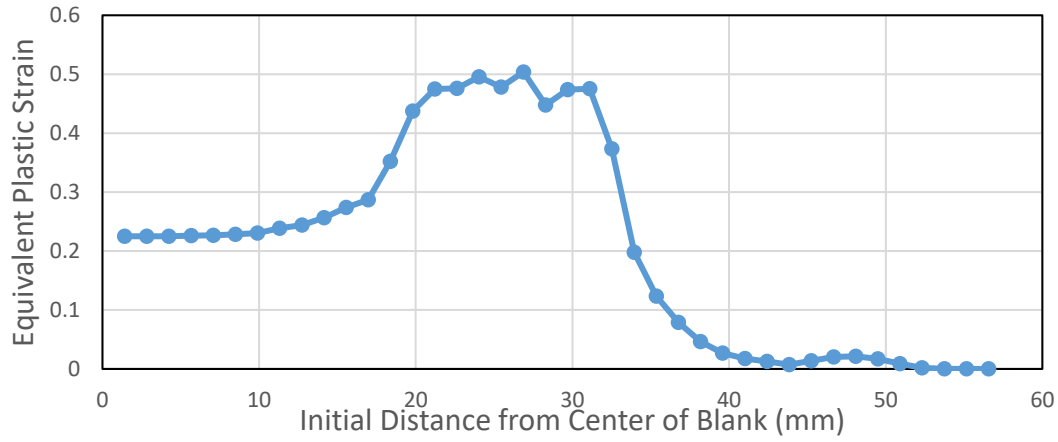

(a)

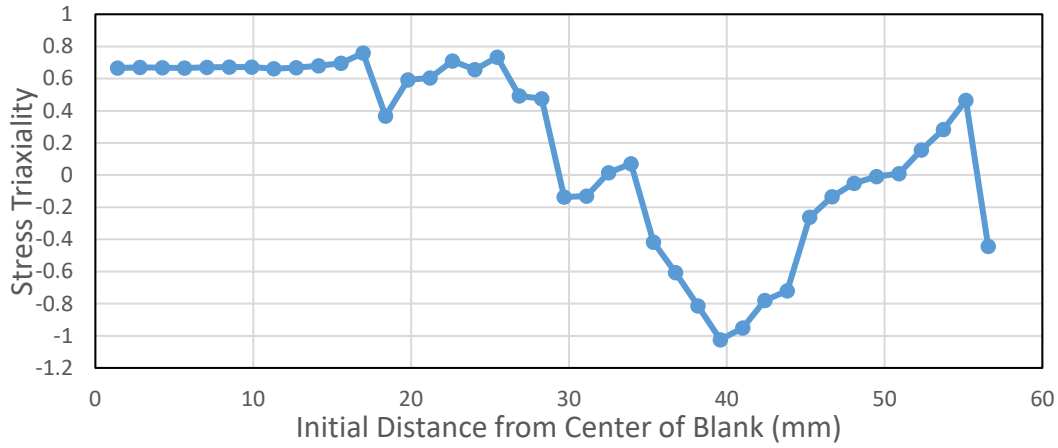

(b)

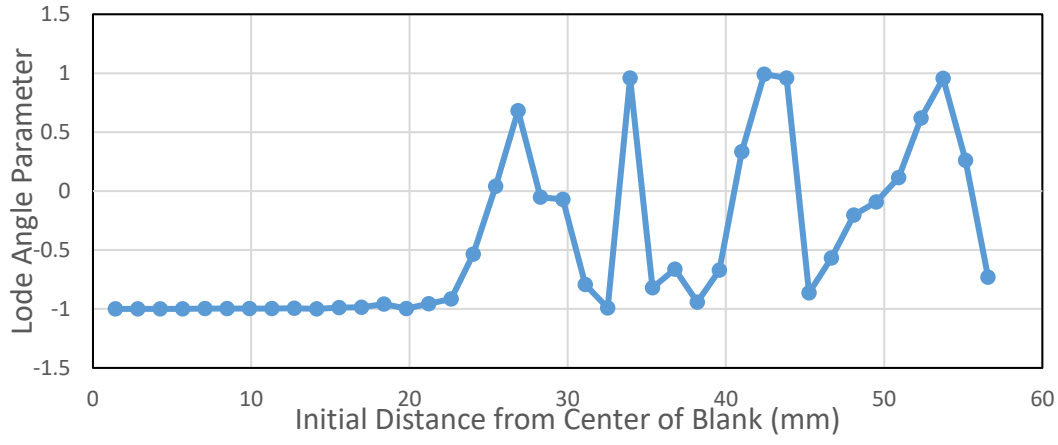

(c)

Figure 5.192 The variation of (a) Equivalent Plastic Strain (b) Stress Triaxiality and (c) Lode Angle Parameter along the diagonal of the blank at 16 mm cup depth for AISI 304 steel (Hill'48-Disc-JC)

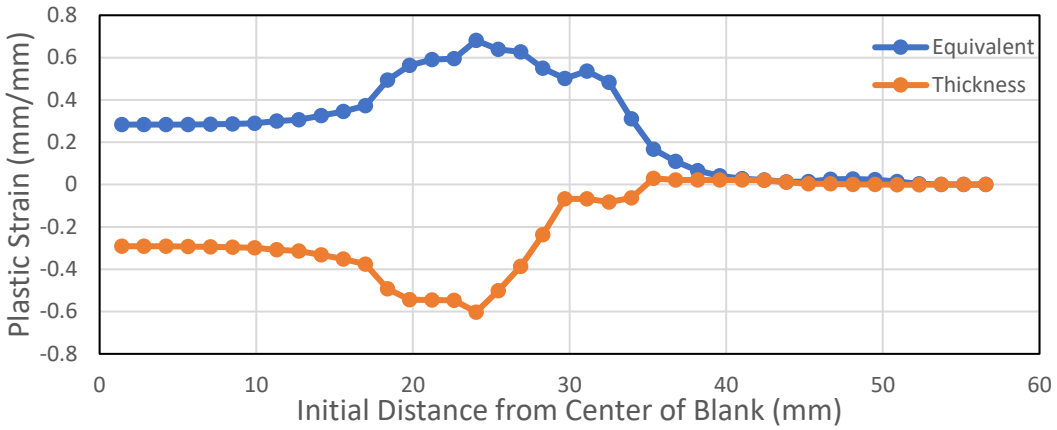

(a)

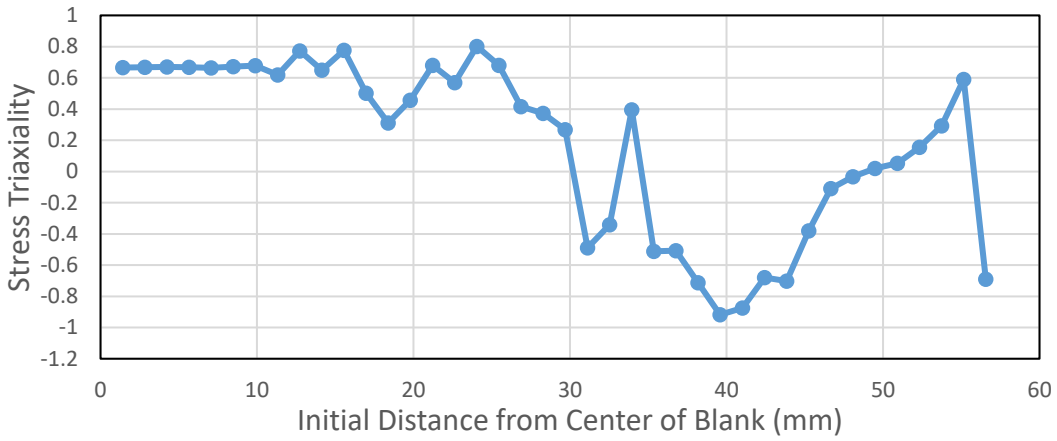

(b)

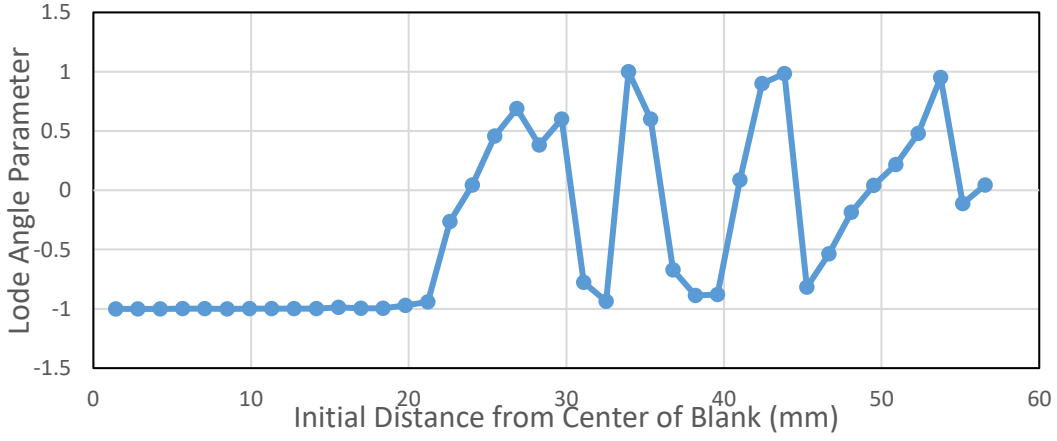

(c)

Figure 5.193. The variation of (a) Equivalent Plastic Strain and Thickness Plastic Strain (b) Stress Triaxiality and (c) Lode Angle Parameter along the diagonal of the blank at 20 mm cup depth for AISI 304 steel (Hill'48-Disc-JC)

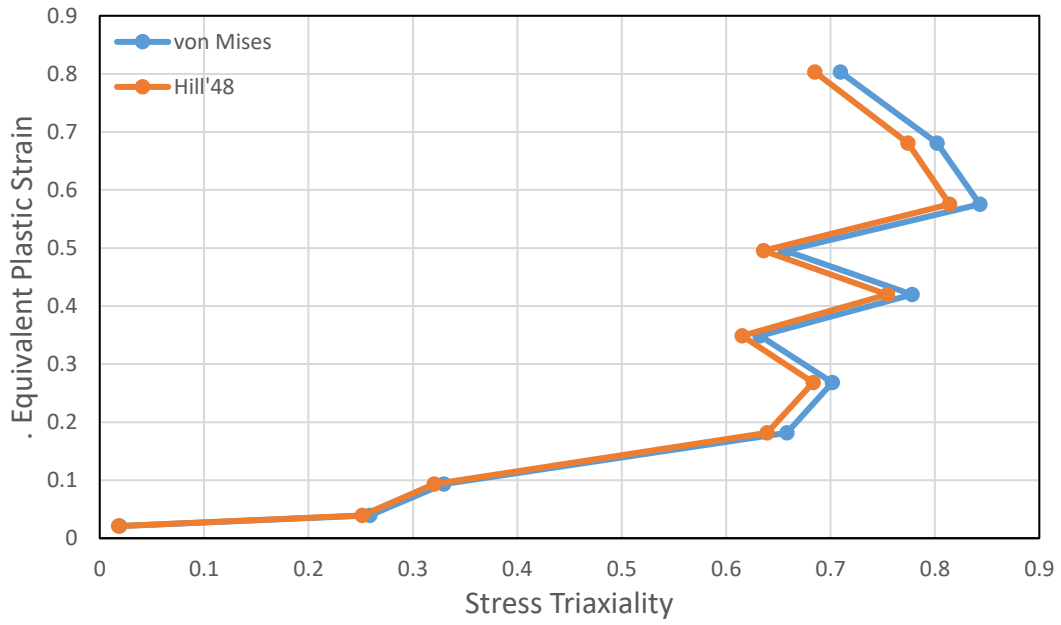

Figure 5.194. Equivalent Plastic Strain - Stress Triaxiality Plot of First Fracture Element (Hill'48-Disc-JC)

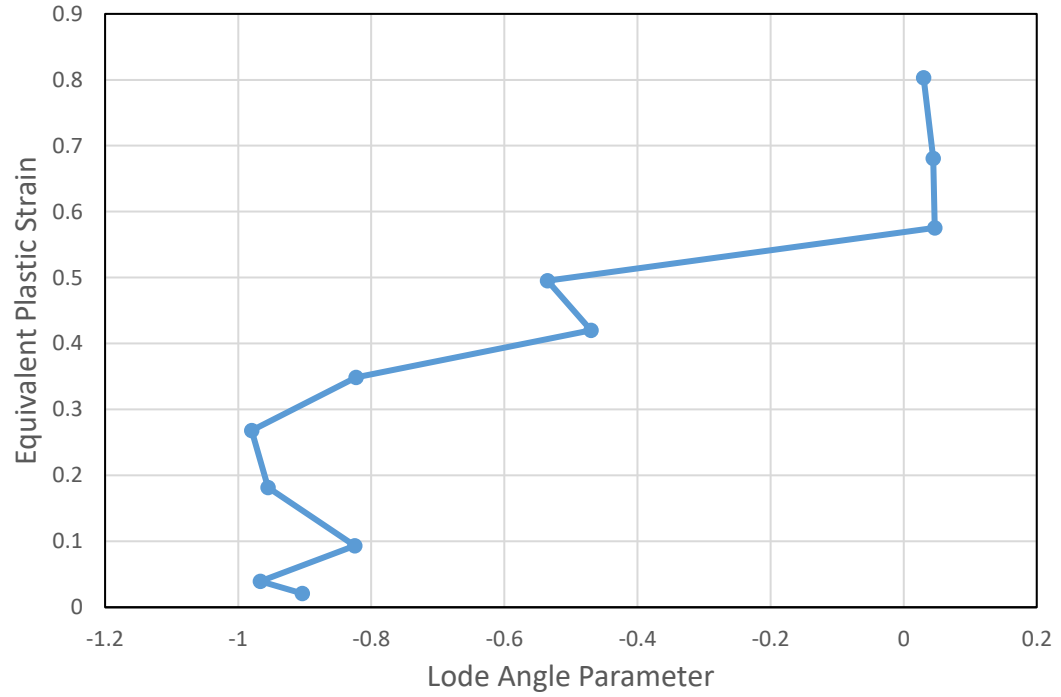

Figure 5.195. Equivalent Plastic Strain – Lode Angle Parameter Plot of First Fracture Element (Hill'48-Disc-JC)

In the rolling direction, the triaxiality values vary generally between 0.6 and 0.8 under the punch whereas the Lode angle parameter values change between -0.8 and -1 up to a distance of 15 mm from the center, it can be said that the deformation behavior is in equi-biaxial tension condition. When the pre-rupture state of sheet is examined, after punch region, the stress triaxiality is positive while Lode angle parameter values are increasing up to a distance of 35 mm from the center. Under blank holder, triaxiality values and Lode angle parameter values became negative, indicating thickening towards the rim.

The same tendency of rolling direction is observed in the transverse direction also. The differences are a result of anisotropy of the material.

In the diagonal direction, when the pre-rupture state of the sheet is examined, equi-biaxial tension state dominates up to a distance of 20 mm from the center of blank. It has been noted that the stress situation of the region changes from tension to shear from punch corner to die corner. Between 35 mm and 45 mm from the center of the blank, there is a change of stress state from compression to equi-biaxial compression. Following this, the values of the Lode angle parameter and the triaxiality both increasing and became positive. Finally, fracture occurs in the punch shoulder in tension state.

5.1.12 Case 12: Square-AISI304-Hill48-Discrete-Hosford Coulomb Model

For the twelfth case, Hill'48 yield criterion was applied with discrete hardening and the Hosford Coulomb ductile fracture criterion was used. It was observed that the fracture had started after 16 mm punch travel as shown in Figure 5.196. The variation of equivalent plastic strain, stress triaxiality and Lode angle parameter values are presented as a function of the distance from the center of the blank for different cup heights up to the fracture. The results are shown for rolling direction in Figure 5.197 to Figure 5.200, for transverse direction in Figure 5.201 to Figure 5.204 and for diagonal direction in Figure 5.205 to Figure 5.208. The thickness plastic strain distribution is also inserted into Figure 5.208 (a) in order to better visualize the deformation. Further, the variations of stress triaxiality values with respect to equivalent plastic strain are given by considering both von Mises and Hill'48 criteria as a function of the path of the element that fractured first in Figure 5.209 Along the same path, the variation of the Lode parameter with respect to equivalent plastic strain is also illustrated in Figure 5.210.

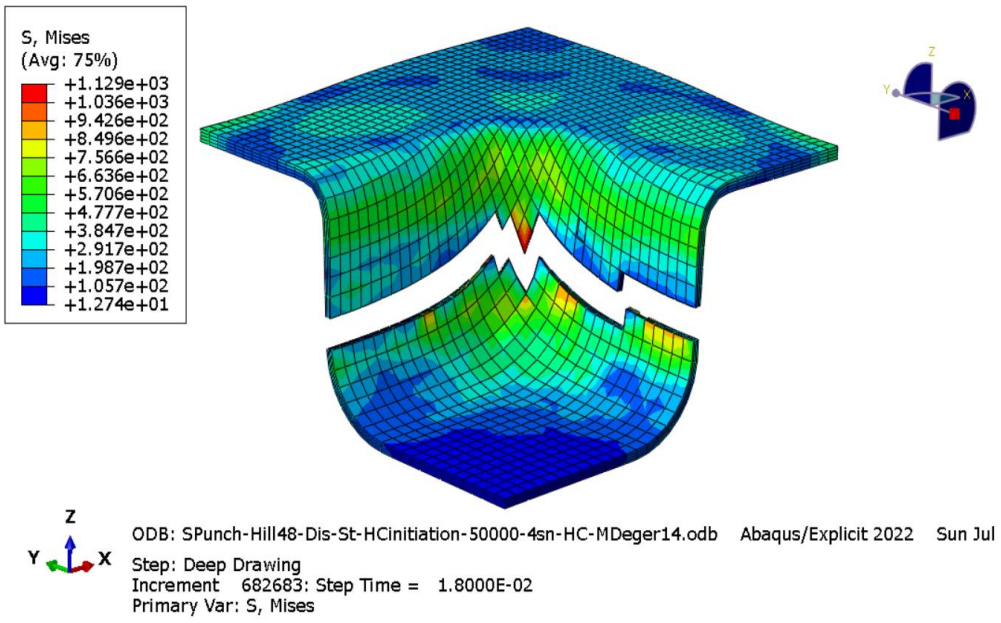

Figure 5.196. First Fracture Moment of Case 12

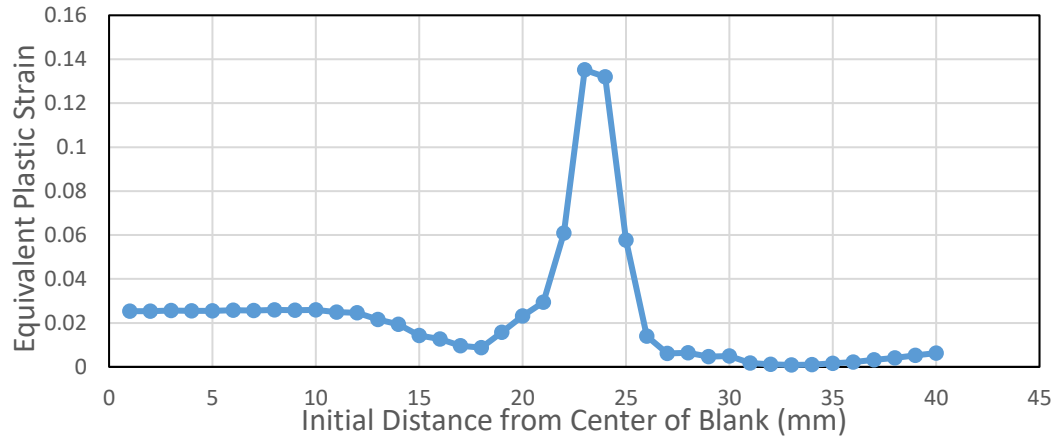

(a)

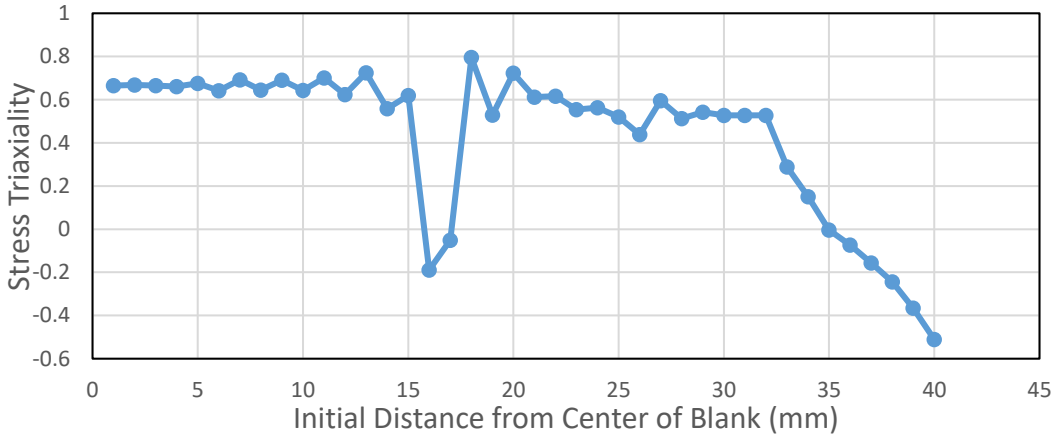

(b)

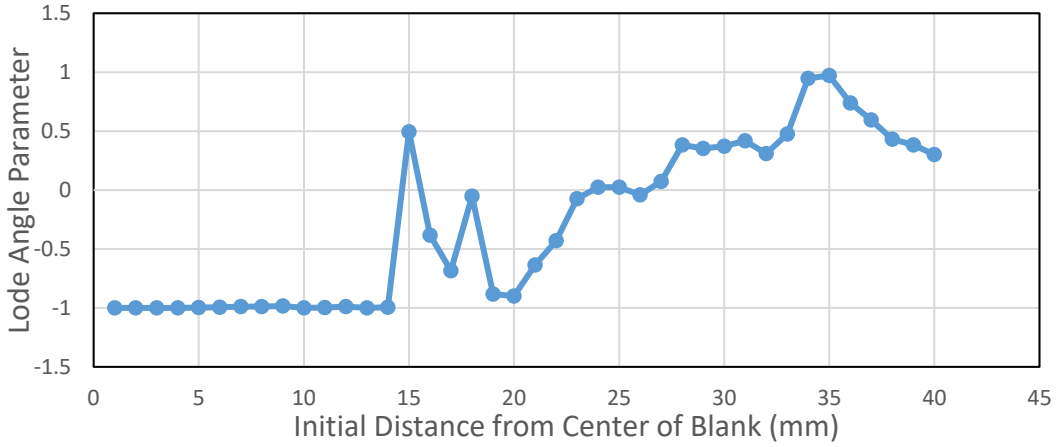

(c)

Figure 5.197. The variation of (a) Equivalent Plastic Strain (b) Stress Triaxiality and (c) Lode Angle Parameter along the rolling direction of the blank at 4 mm cup depth for AISI 304 steel (Hill'48-Disc-HC)

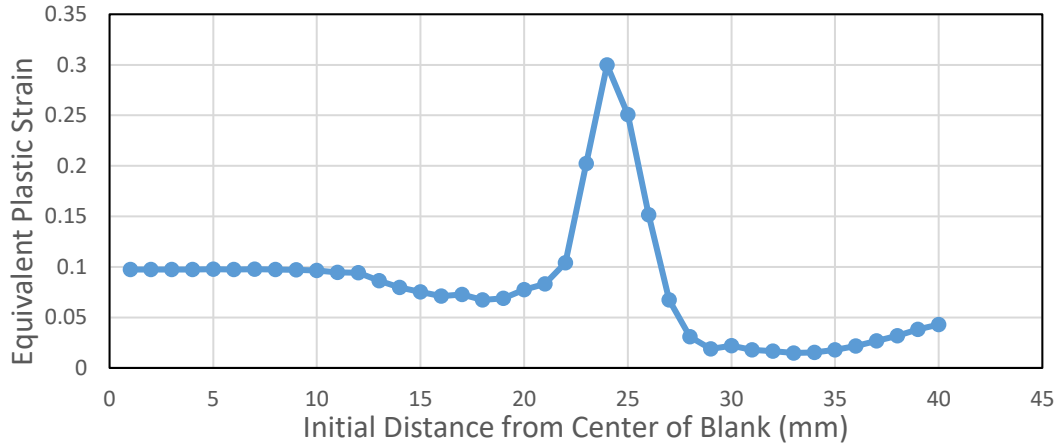

(a)

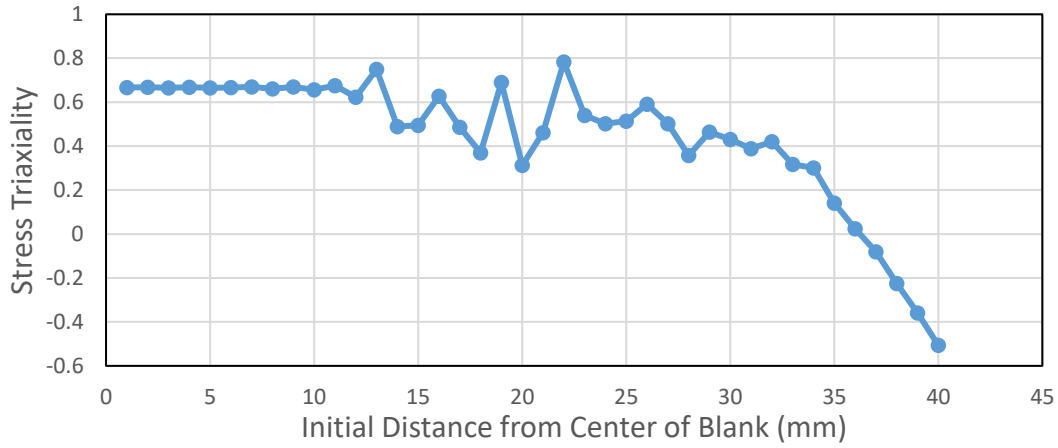

(b)

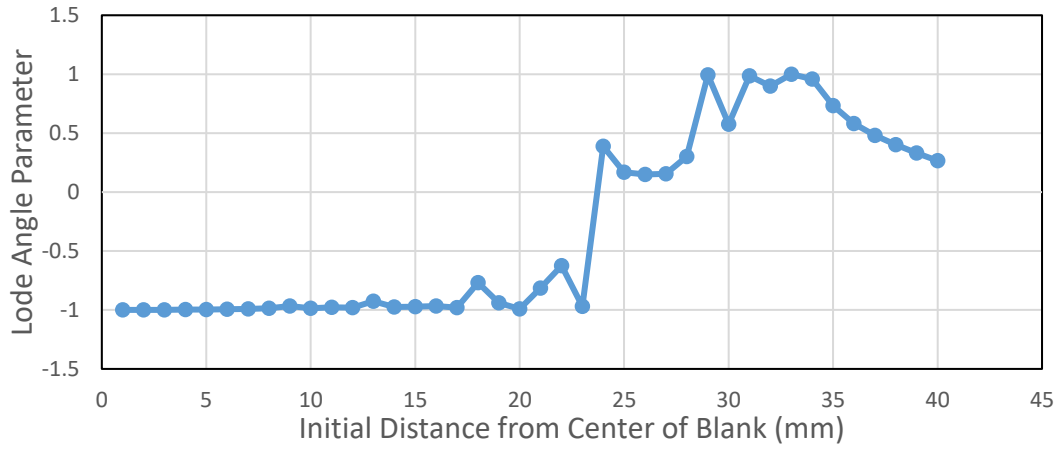

(c)

Figure 5.198. The variation of (a) Equivalent Plastic Strain (b) Stress Triaxiality and (c) Lode Angle Parameter along the rolling direction of the blank at 8 mm cup depth for AISI 304 steel (Hill'48-Disc-HC)

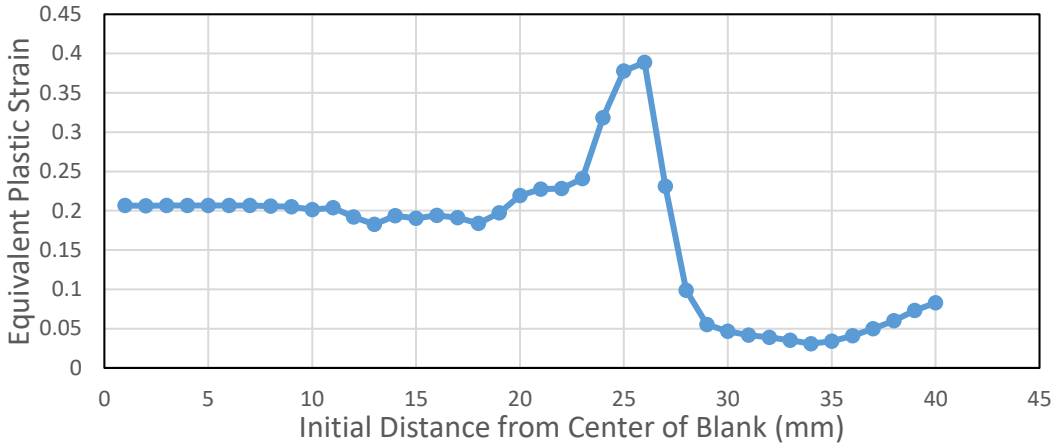

(a)

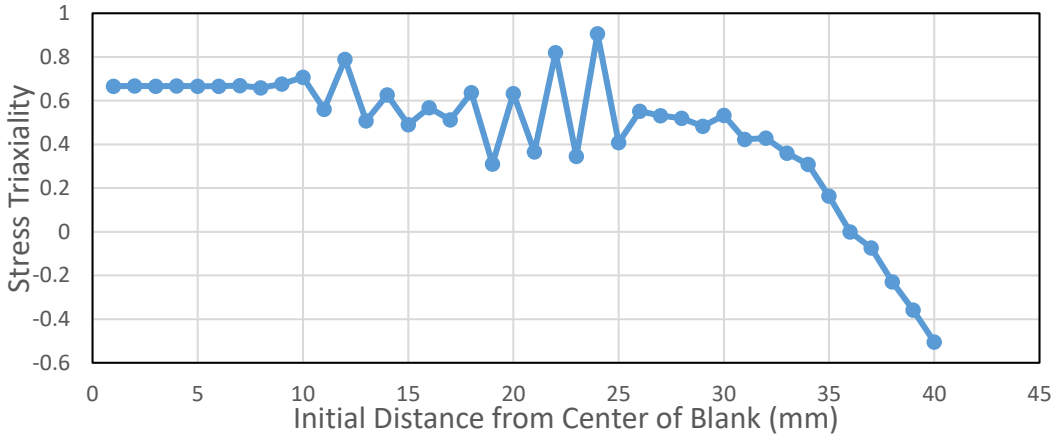

(b)

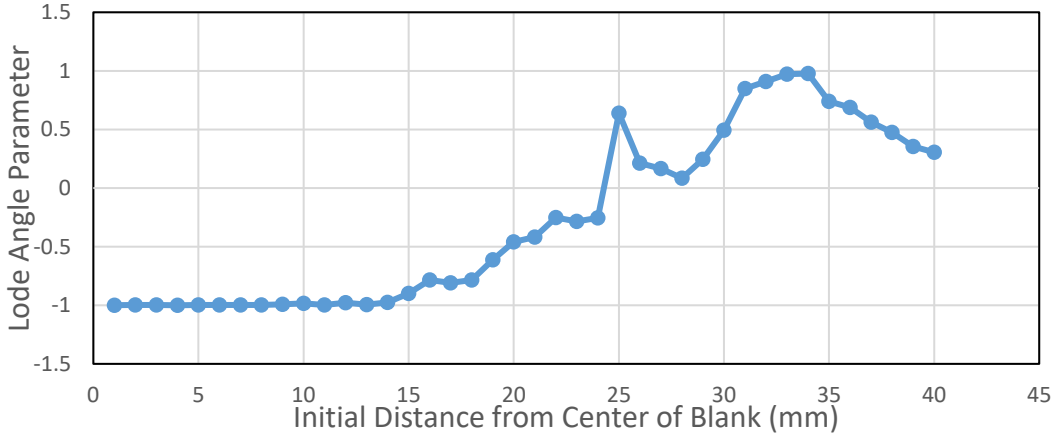

(c)

Figure 5.199. The variation of (a) Equivalent Plastic Strain (b) Stress Triaxiality and (c) Lode Angle Parameter along the rolling direction of the blank at 12 mm cup depth for AISI 304 steel (Hill'48-Disc-HC)

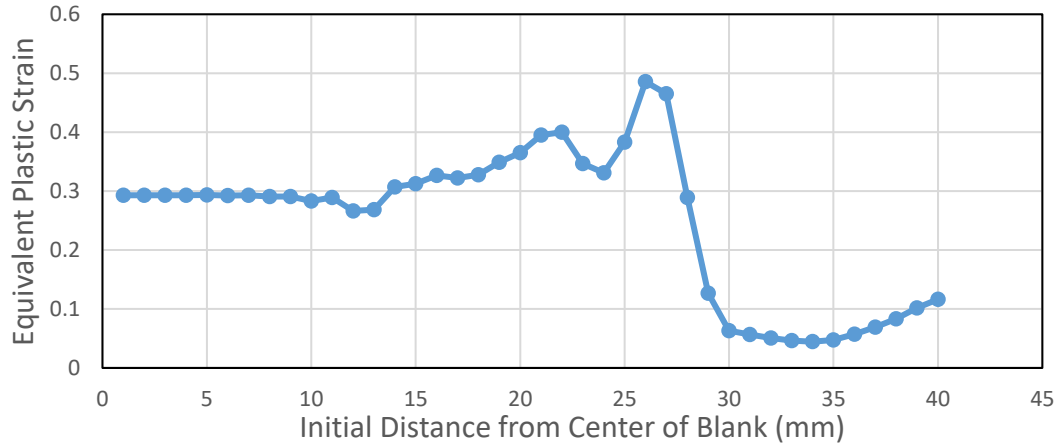

(a)

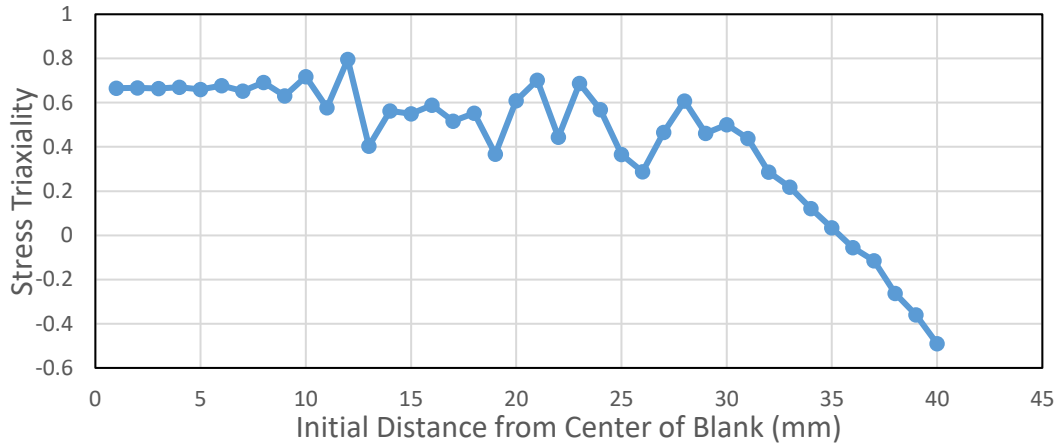

(b)

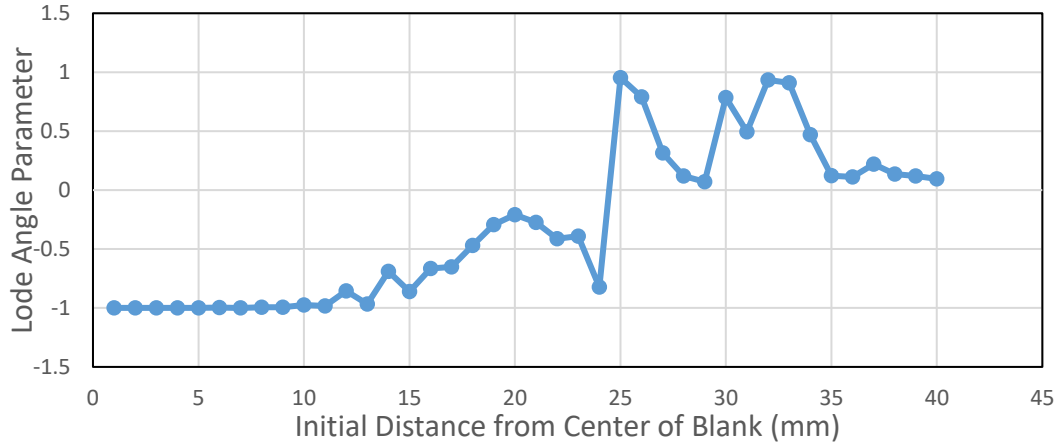

(c)

Figure 5.200. The variation of (a) Equivalent Plastic Strain (b) Stress Triaxiality and (c) Lode Angle Parameter along the rolling direction of the blank at 16 mm cup depth for AISI 304 steel (Hill'48-Disc-HC)

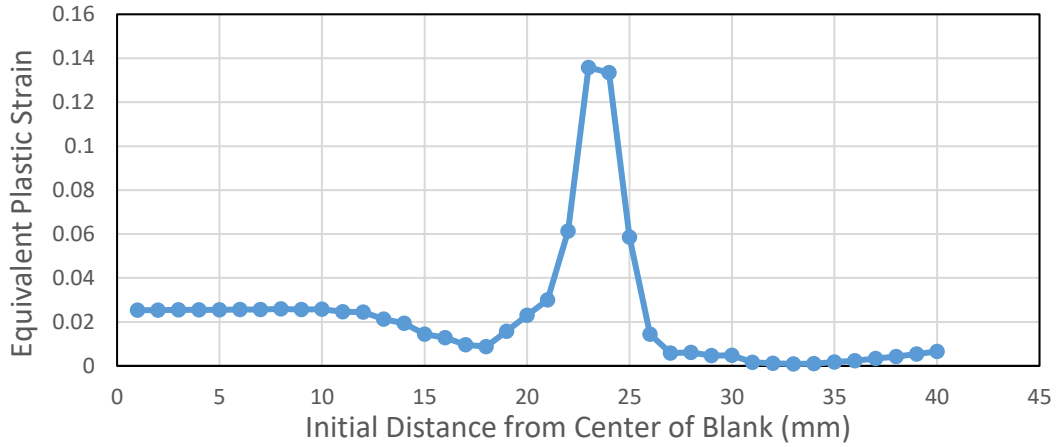

(a)

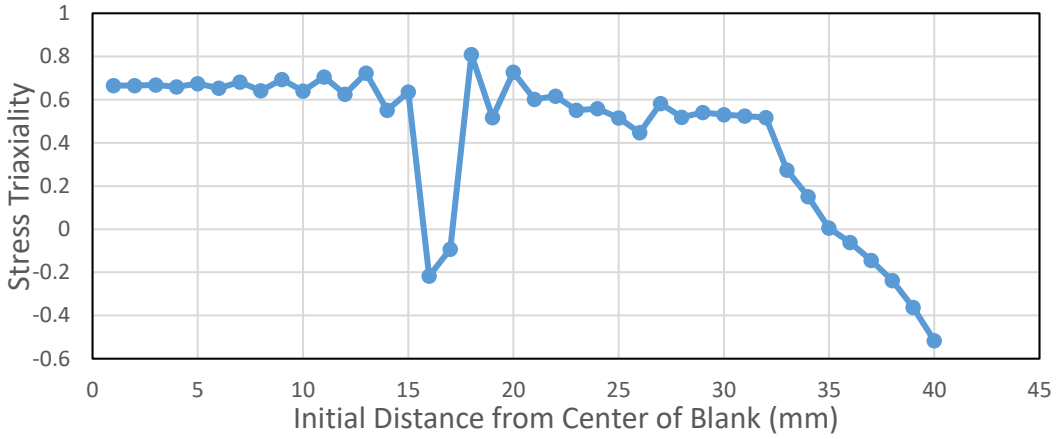

(b)

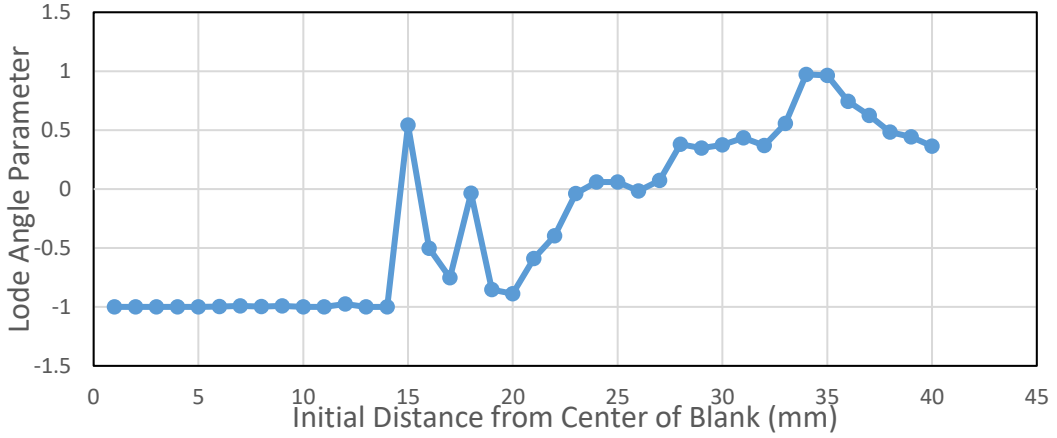

(c)

Figure 5.201. The variation of (a) Equivalent Plastic Strain (b) Stress Triaxiality and (c) Lode Angle Parameter along the transverse direction of the blank at 4 mm cup depth for AISI 304 steel (Hill'48-Disc-HC)

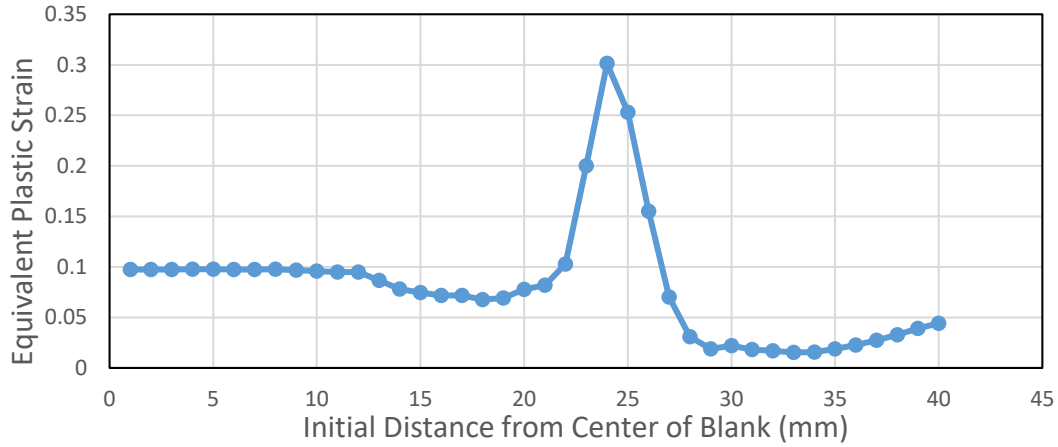

(a)

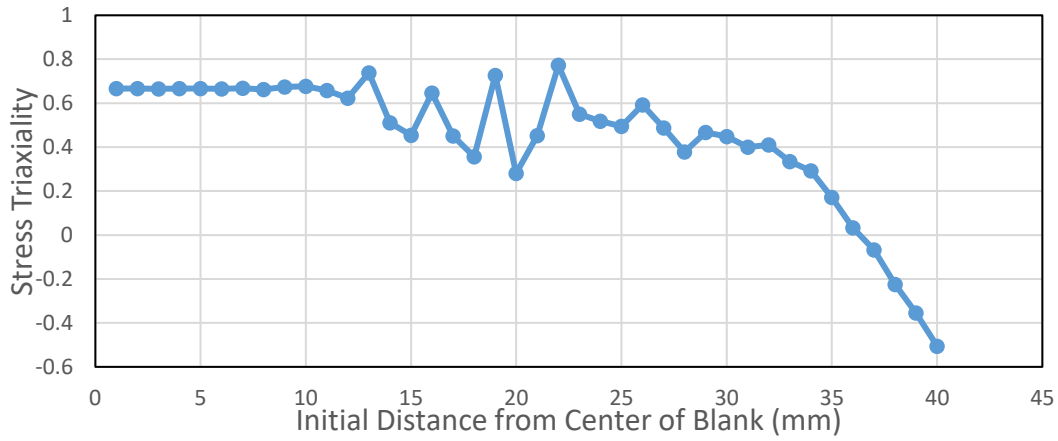

(b)

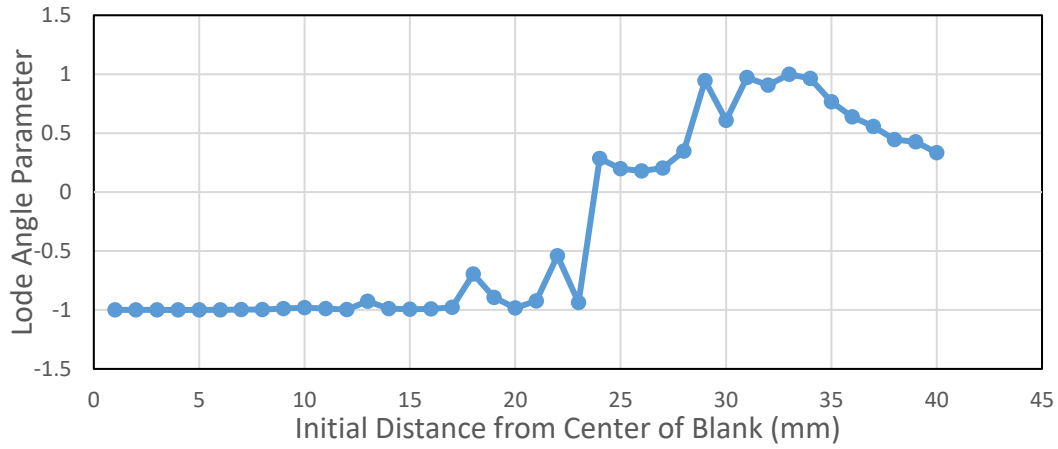

(c)

Figure 5.202. The variation of (a) Equivalent Plastic Strain (b) Stress Triaxiality and (c) Lode Angle Parameter along the transverse direction of the blank at 8 mm cup depth for AISI 304 steel (Hill'48-Disc-HC)

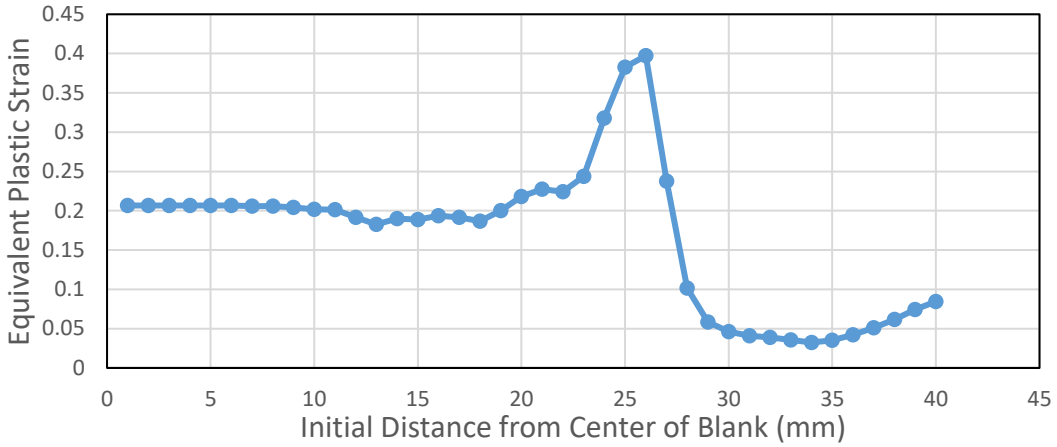

(a)

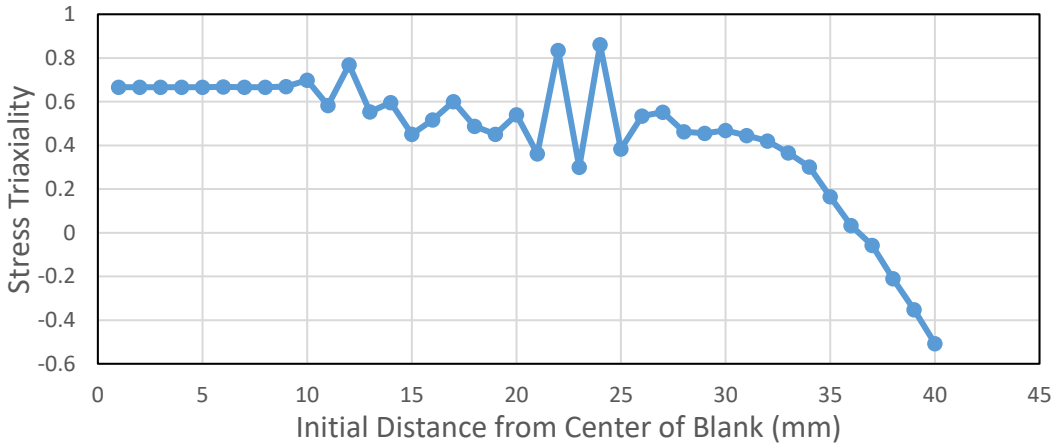

(b)

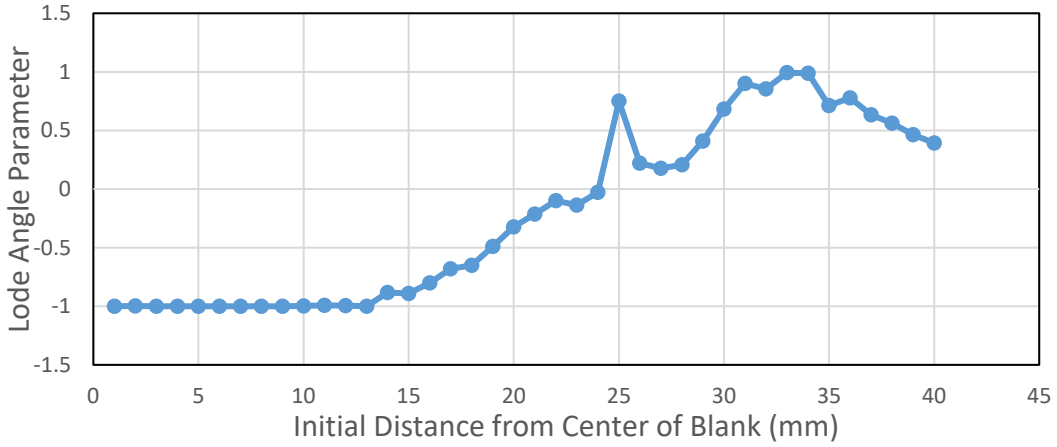

(c)

Figure 5.203. The variation of (a) Equivalent Plastic Strain (b) Stress Triaxiality and (c) Lode Angle Parameter along the transverse direction of the blank at 12 mm cup depth for AISI 304 steel (Hill'48-Disc-HC)

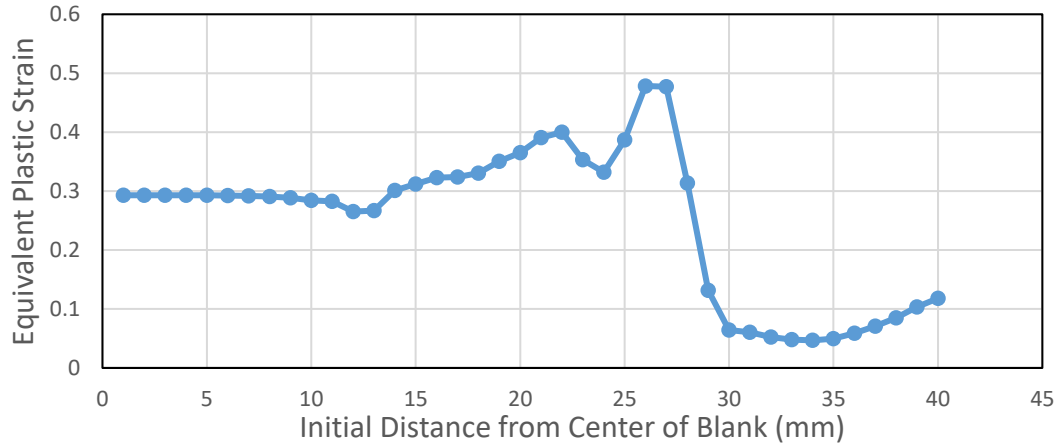

(a)

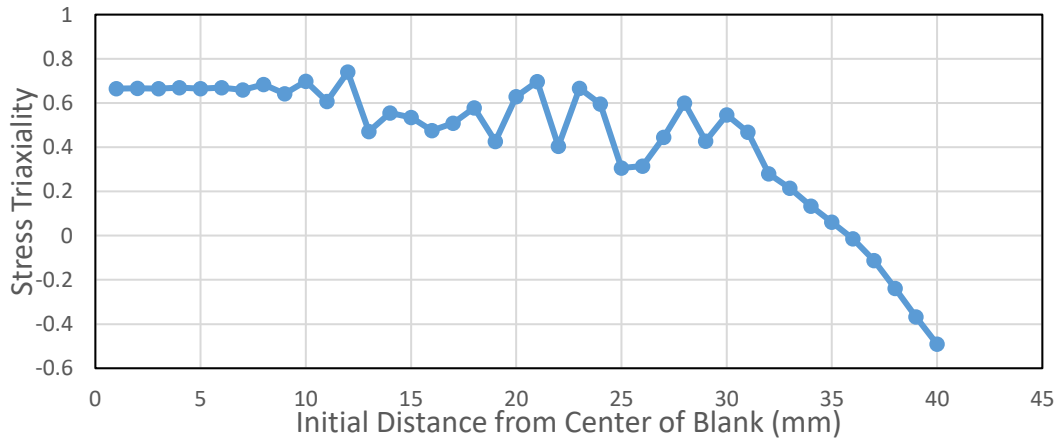

(b)

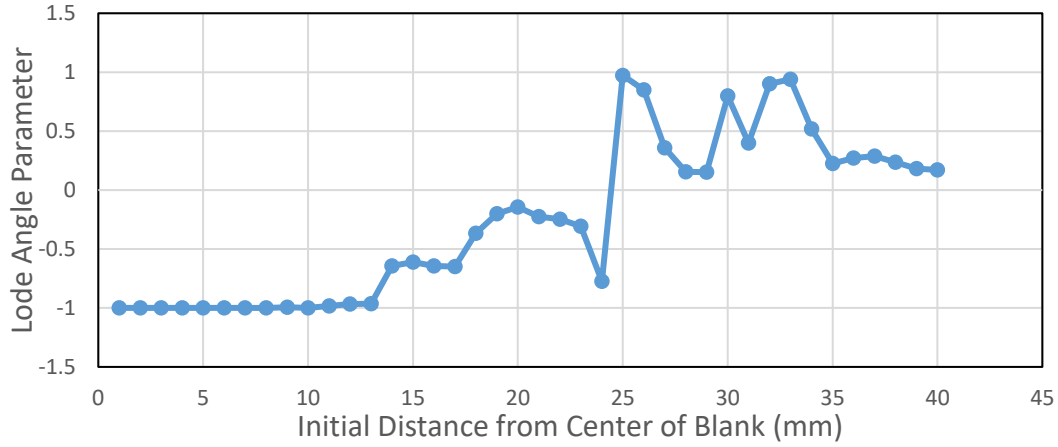

(c)

Figure 5.204. The variation of (a) Equivalent Plastic Strain (b) Stress Triaxiality and (c) Lode Angle Parameter along the transverse direction of the blank at 16 mm cup depth for AISI 304 steel (Hill'48-Disc-HC)

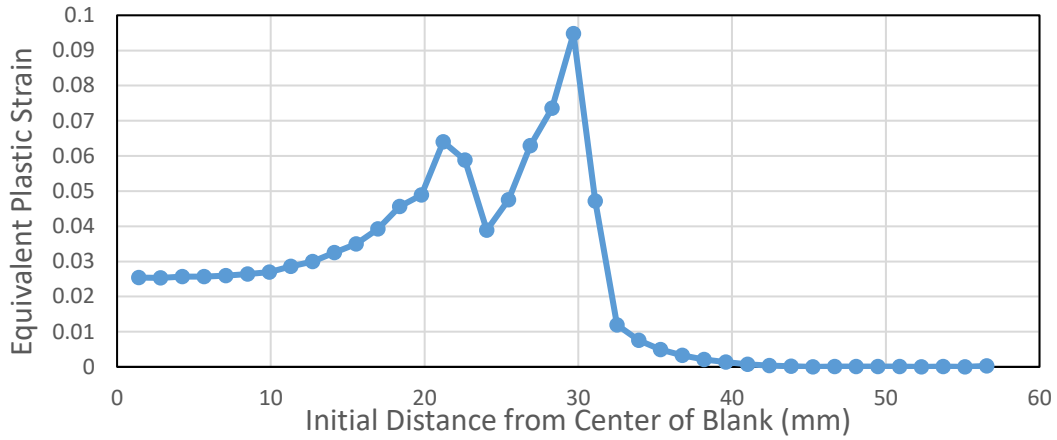

(a)

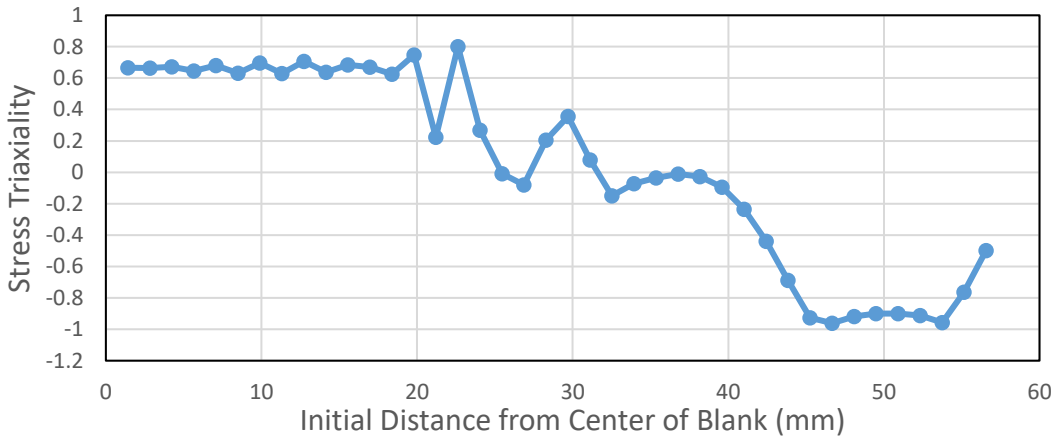

(b)

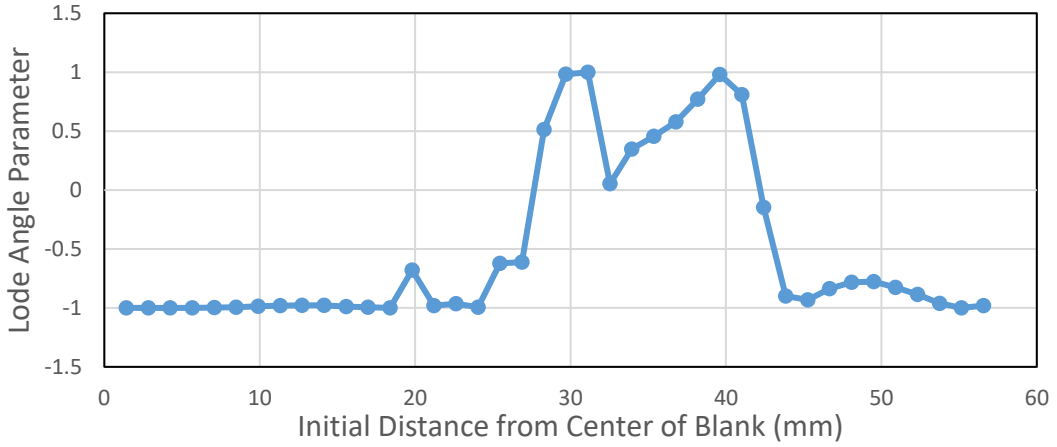

(c)

Figure 5.205. The variation of (a) Equivalent Plastic Strain (b) Stress Triaxiality and (c) Lode Angle Parameter along the diagonal of the blank at 4 mm cup depth for AISI 304 steel (Hill'48-Disc-HC)

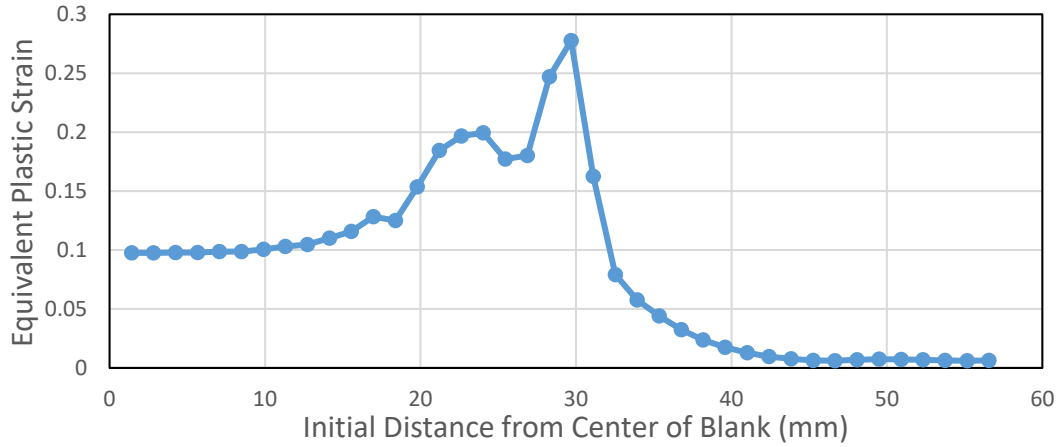

(a)

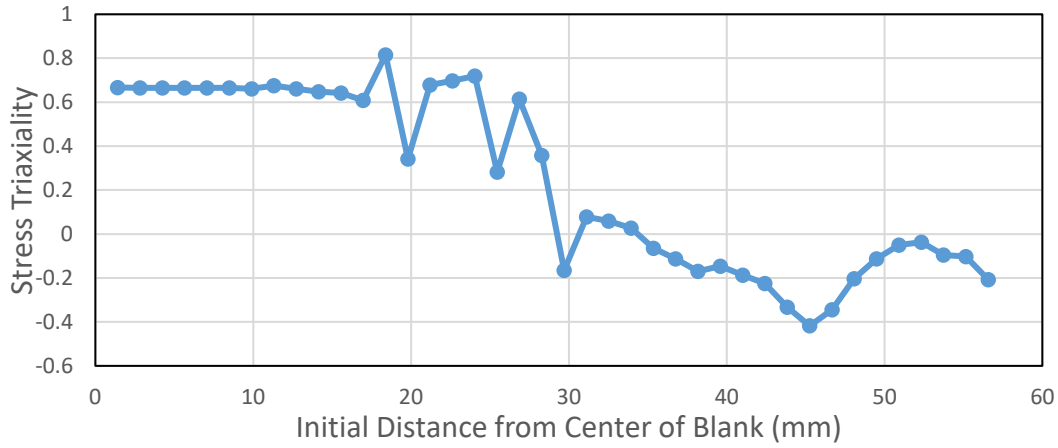

(b)

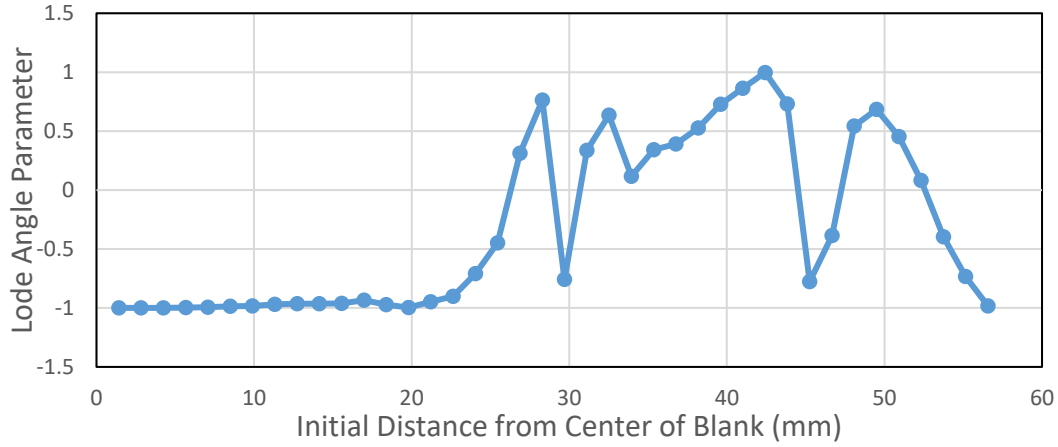

(c)

Figure 5.206. The variation of (a) Equivalent Plastic Strain (b) Stress Triaxiality and (c) Lode Angle Parameter along the diagonal of the blank at 8 mm cup depth for AISI 304 steel (Hill'48-Disc-HC)

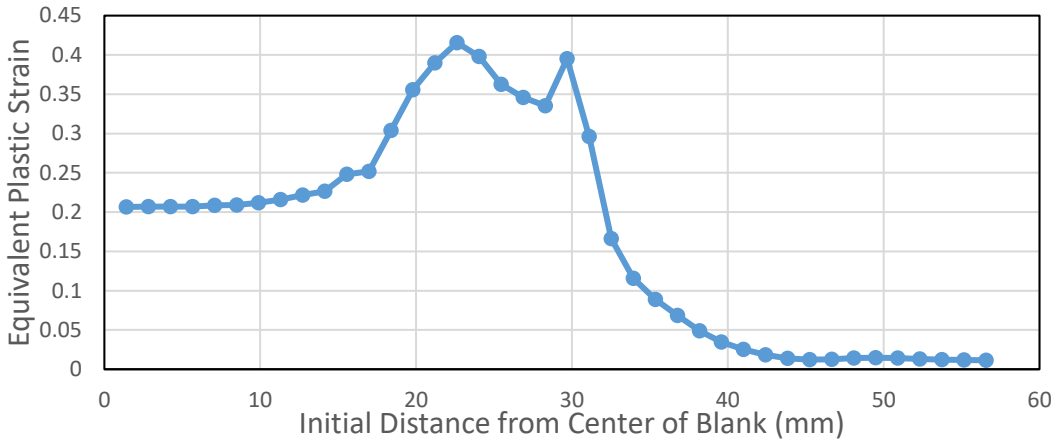

(a)

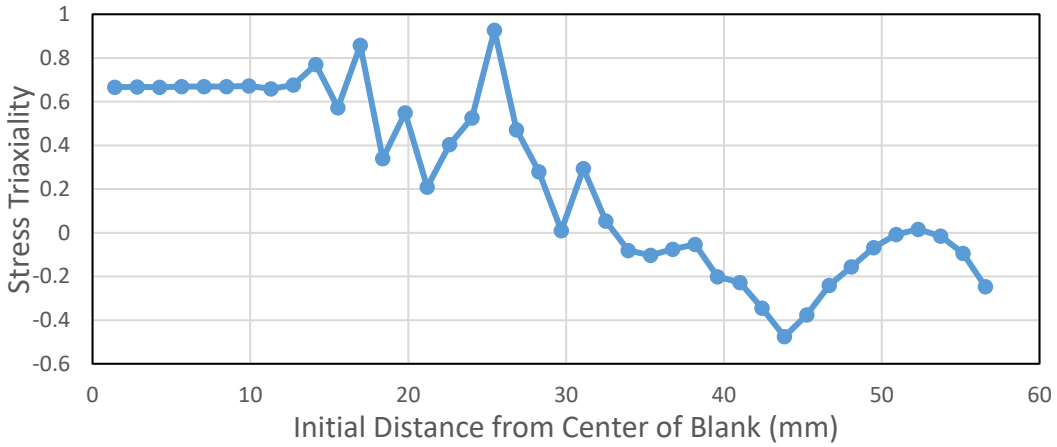

(b)

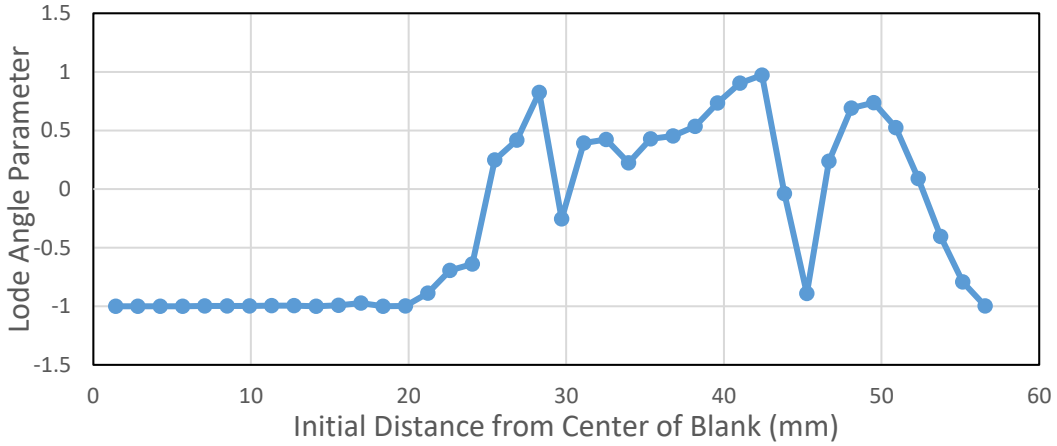

(c)

Figure 5.207 The variation of (a) Equivalent Plastic Strain (b) Stress Triaxiality and (c) Lode Angle Parameter along the diagonal of the blank at 12 mm cup depth for AISI 304 steel (Hill'48-Disc-HC)

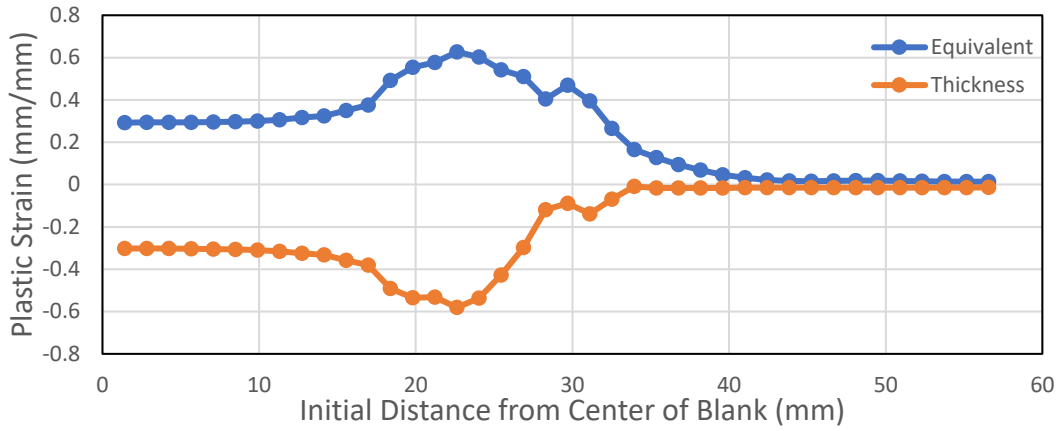

(a)

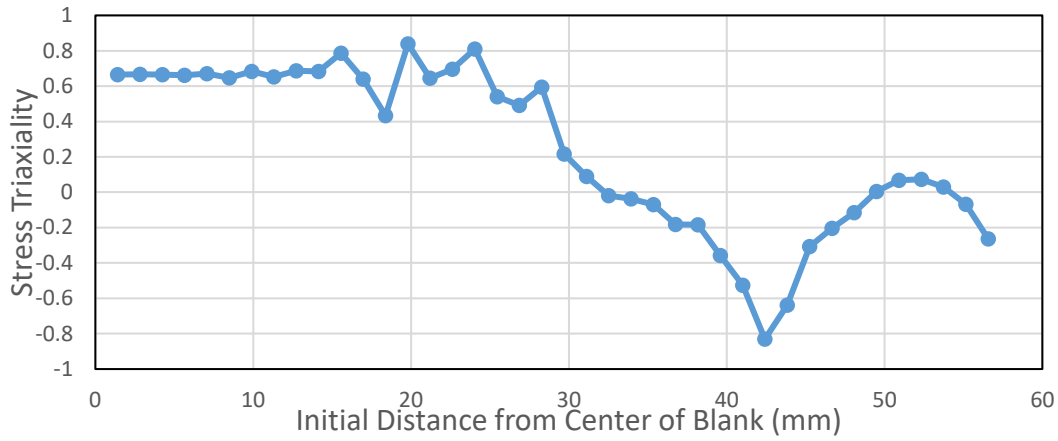

(b)

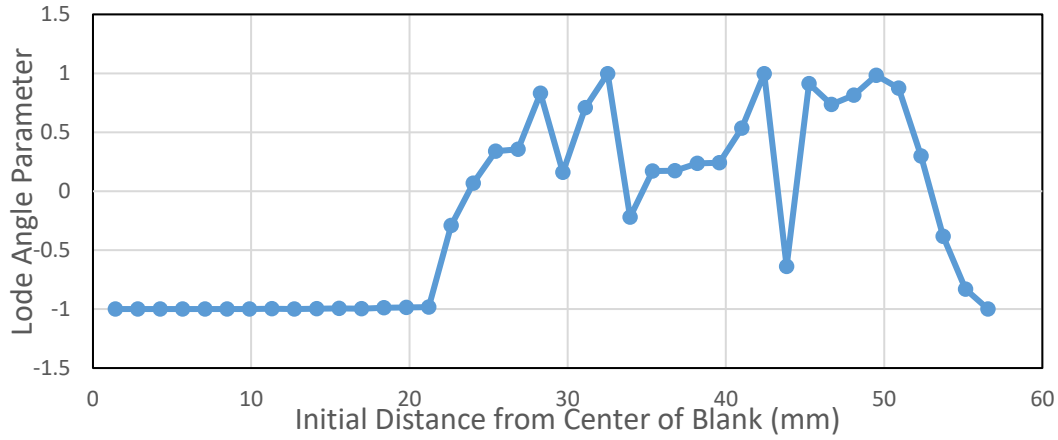

(c)

Figure 5.208 The variation of (a) Equivalent Plastic Strain and Thickness Plastic Strain (b) Stress Triaxiality and (c) Lode Angle Parameter along the diagonal of the blank at 16 mm cup depth for AISI 304 steel (Hill'48-Disc-HC)

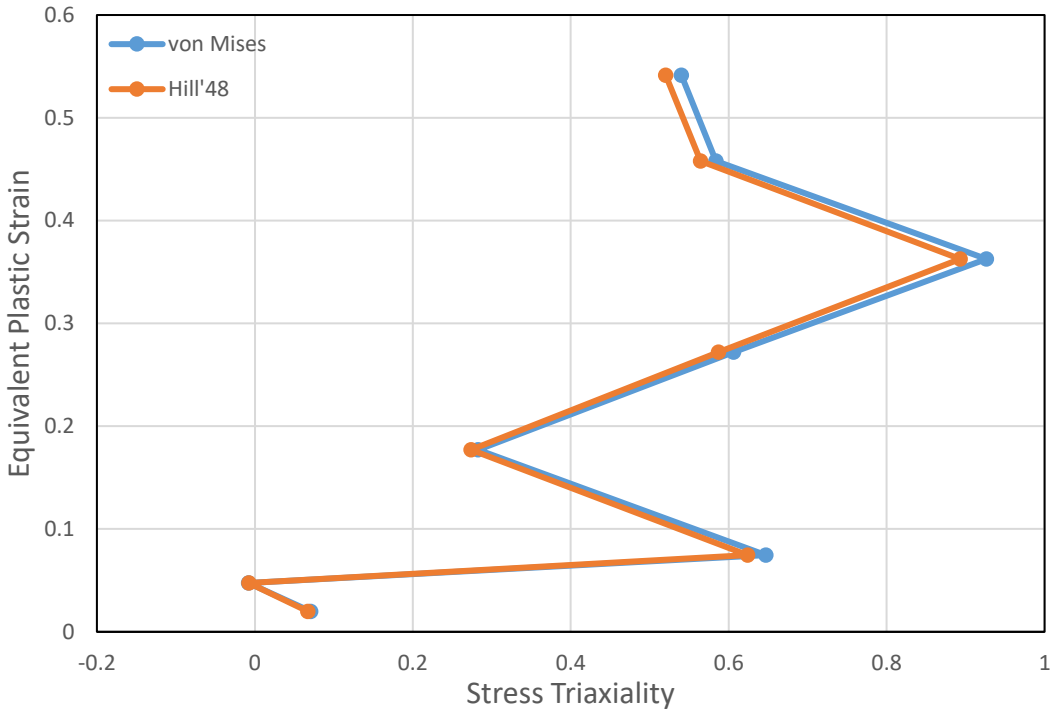

Figure 5.209. Equivalent Plastic Strain - Stress Triaxiality Plot of First Fracture Element (Hill'48-Disc-HC)

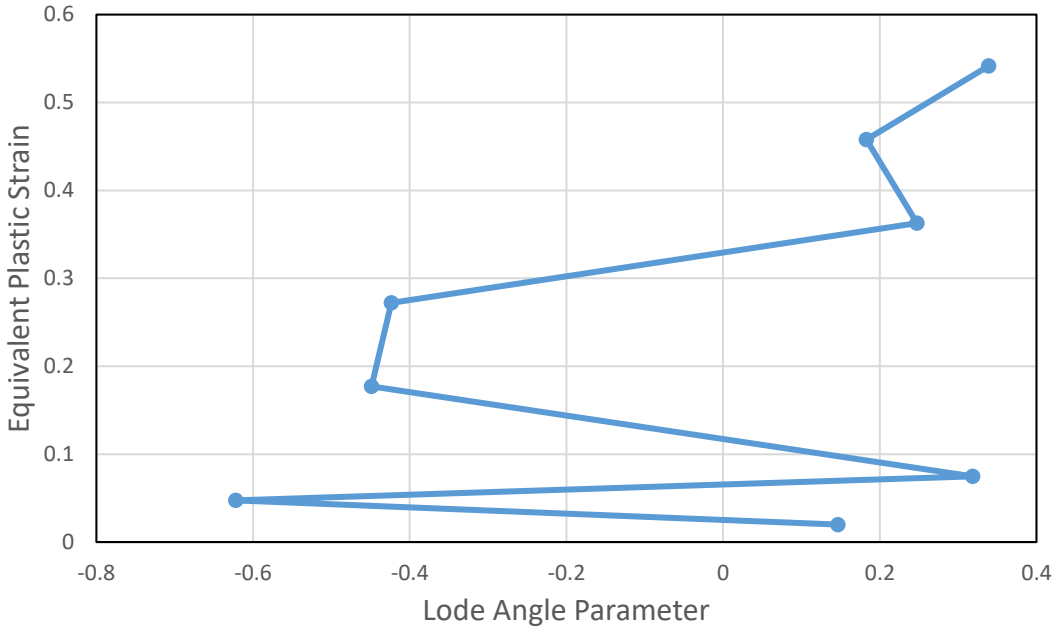

Figure 5.210. Equivalent Plastic Strain – Lode Angle Parameter Plot of First Fracture Element (Hill'48-Disc-HC)

In the rolling direction, the triaxiality values vary generally between 0.6 and 0.8 under the punch whereas the Lode angle parameter values change between -0.8 and -1 up to a distance of 15 mm from the center, it can be said that the deformation behavior is in equi-biaxial tension condition. After 30 mm distance from blank center, under blank holder, triaxiality values decreasing with positive Lode angle parameter values. According to these values it can be said that, under blank holder region stress state is compressive.

The same tendency of rolling direction is observed in the transverse direction also. The differences are a result of anisotropy of the material.

In the diagonal direction, as in the transverse and rolling directions, equi-biaxial stress condition is observed under the punch. When the pre-rupture state of sheet is examined, it is seen that equi-biaxial stress conditions dominates up to 20 mm from the center of the blank. At the punch shoulder, stress state changes from tension to shear while triaxiality values decreasing. On the other hand, the Lode angle parameter values increases as with distance from the center of the blank. After this region, triaxiality values are increasing and Lode parameter values are decreasing. Fracture occurs at the punch shoulder in tension situation.

5.2 Cylindrical Bottom Punch Deep-Drawing Analysis

5.2.1 Case 13-Al2024-von Mises-Johnson Cook-Hosford Coulomb Model

For the cylindrical cup drawing case, von Mises yield criterion was applied with Johnson Cook hardening and the Hosford Coulomb ductile fracture criterion was used. It was observed that the fracture had started after 12 mm punch travel as shown in Figure 5.211. The variation of equivalent plastic strain, stress triaxiality and Lode angle parameter values are presented as a function of the distance from the center of the blank for different cup heights up to the fracture. The results are shown in Figure 5.212 to Figure 5.215. The thickness plastic strain distribution is also inserted into Figure 5.215 (a) in order to better visualize the deformation. Further, the variations of stress triaxiality values with respect to equivalent plastic strain are given by considering both von Mises and Hill'48 criteria as a function of the path of the element that fractured first in Figure 5.216. Along the same path, the variation of the Lode parameter with respect to equivalent plastic strain is also illustrated in Figure 5.217. Finally, the variation of triaxiality values with respect to Lode angle parameter values are given in Figure 5.218.

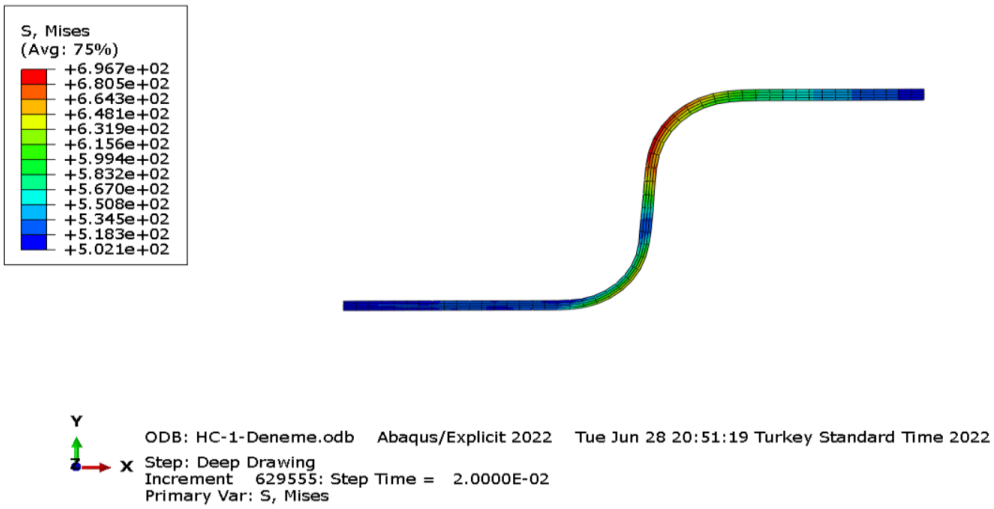

Figure 5.211. First Fracture Moment of Case 13

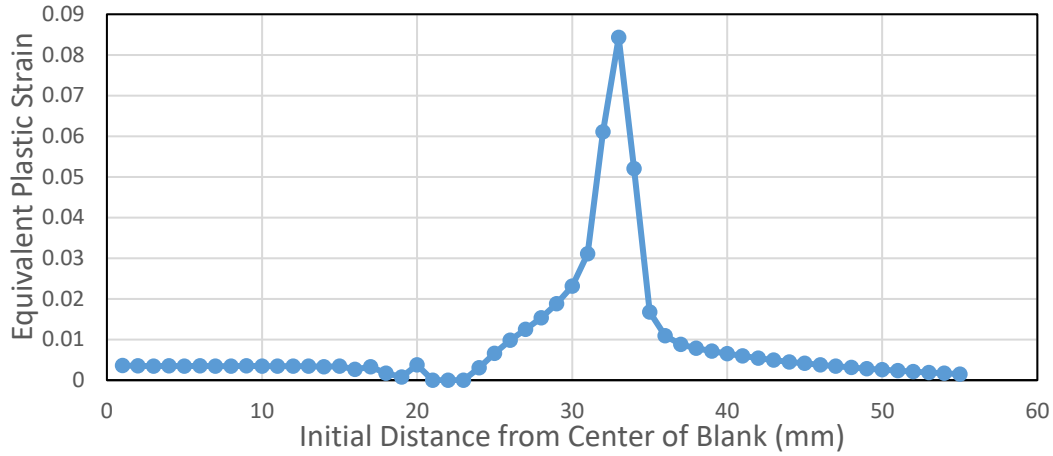

(a)

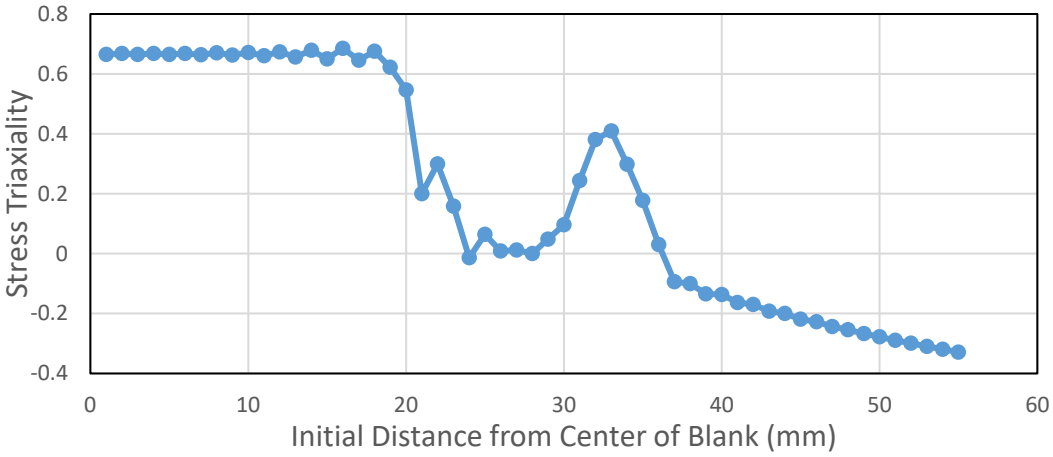

(b)

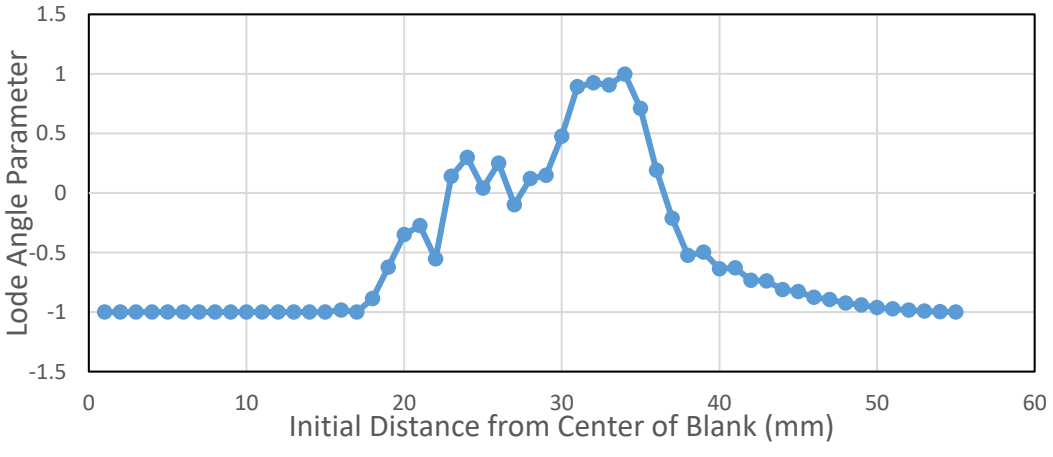

(c)

Figure 5.212. The variation of (a) Equivalent Plastic Strain (b) Stress Triaxiality and (c) Lode Angle Parameter of the blank at 5 mm cup depth for Al2024 aluminum (VM-JC-HC)

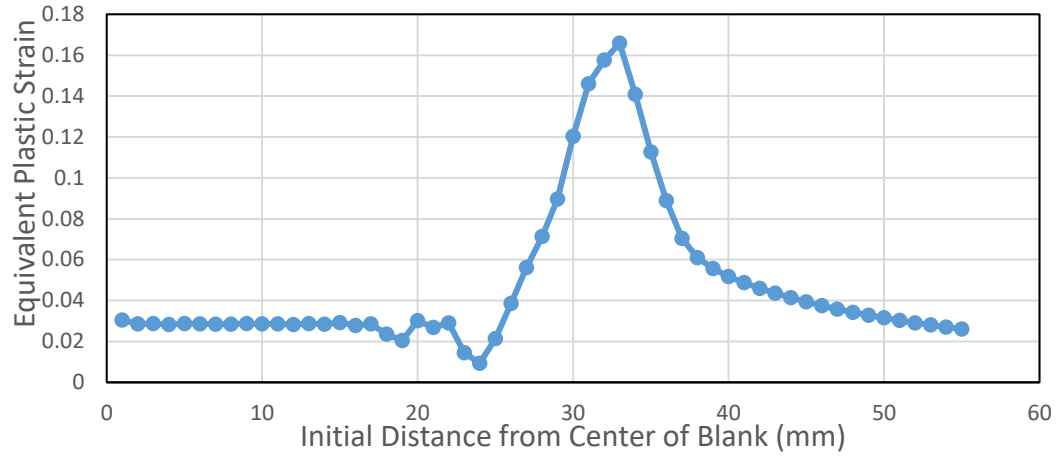

(a)

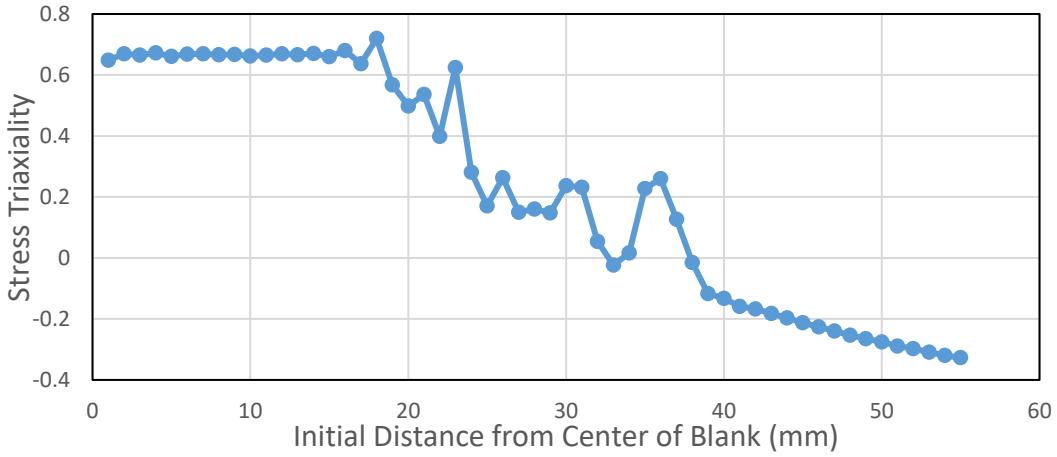

(b)

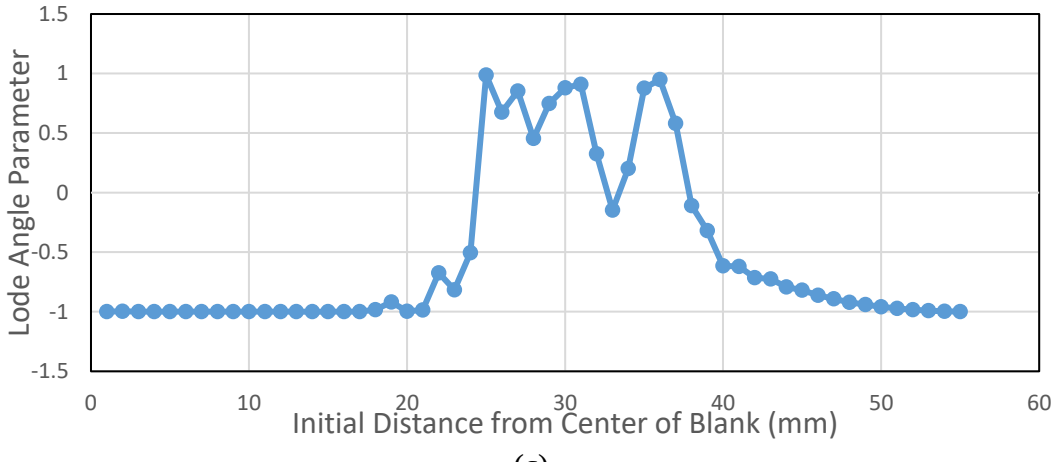

(c)

Figure 5.213. The variation of (a) Equivalent Plastic Strain (b) Stress Triaxiality and (c) Lode Angle Parameter of the blank at 10 mm cup depth for Al2024 aluminum (VM-JC-HC)

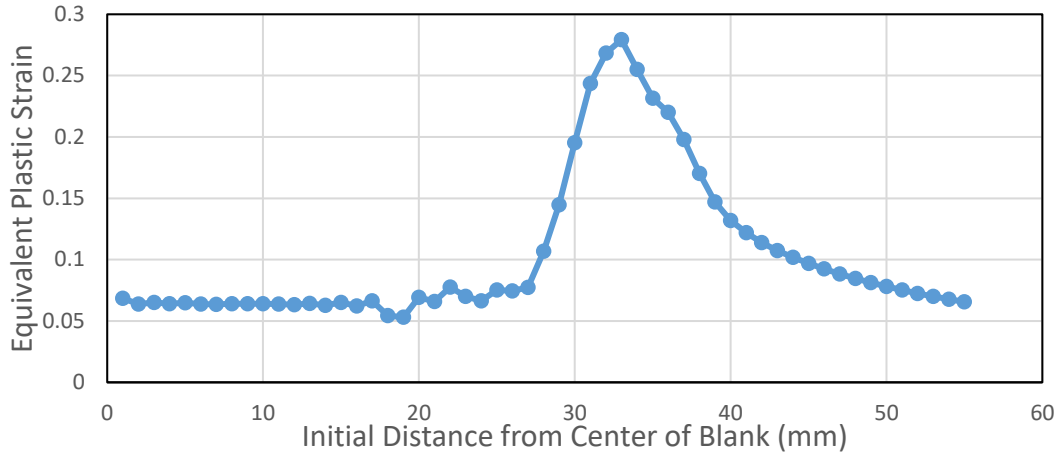

(a)

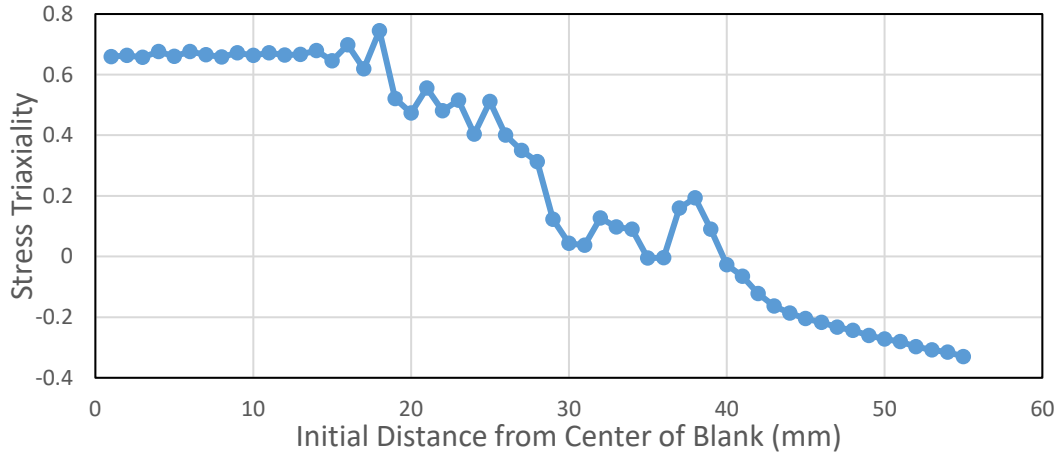

(b)

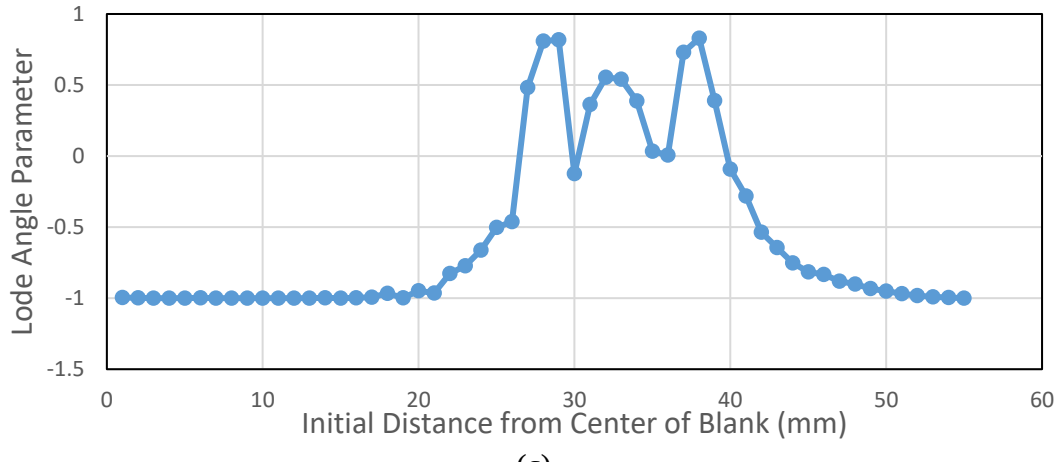

(c)

Figure 5.214. The variation of (a) Equivalent Plastic Strain (b) Stress Triaxiality and (c) Lode Angle Parameter of the blank at 15 mm cup depth for Al2024 aluminum (VM-JC-HC)

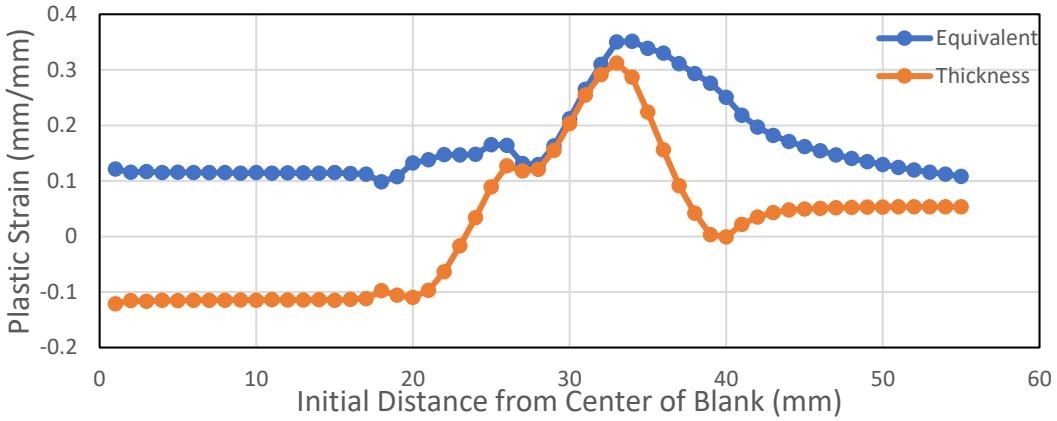

(a)

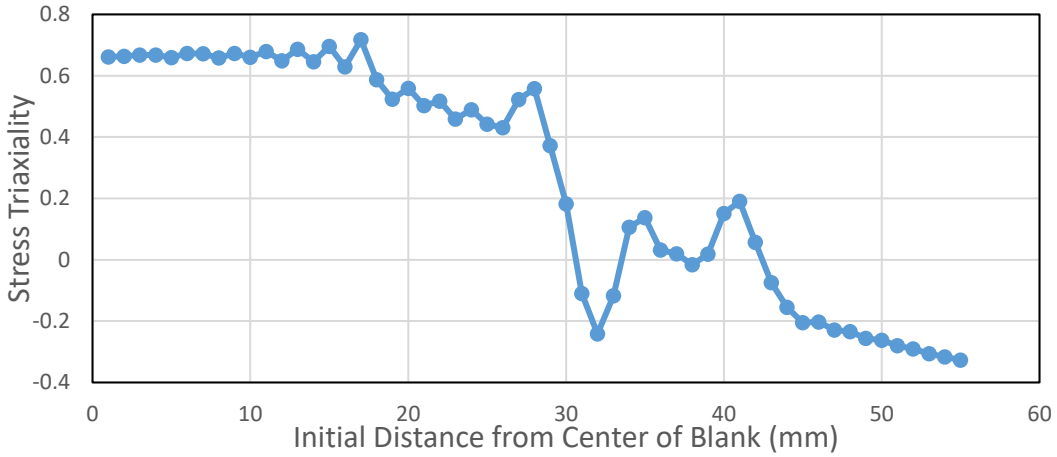

(b)

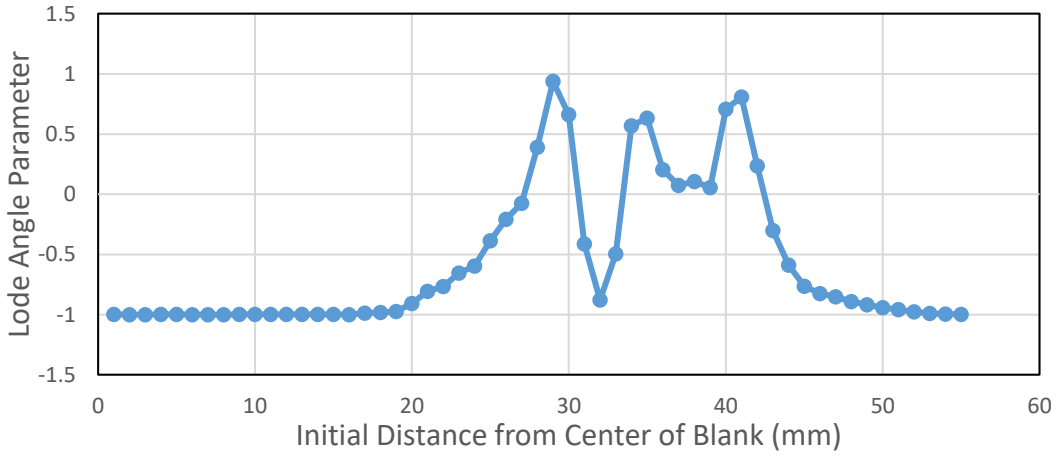

(c)

Figure 5.215. The variation of (a) Equivalent Plastic Strain and Thickness Plastic Strain (b) Stress Triaxiality and (c) Lode Angle Parameter of the blank at 20 mm cup depth for Al2024 aluminum (VM-JC-HC)

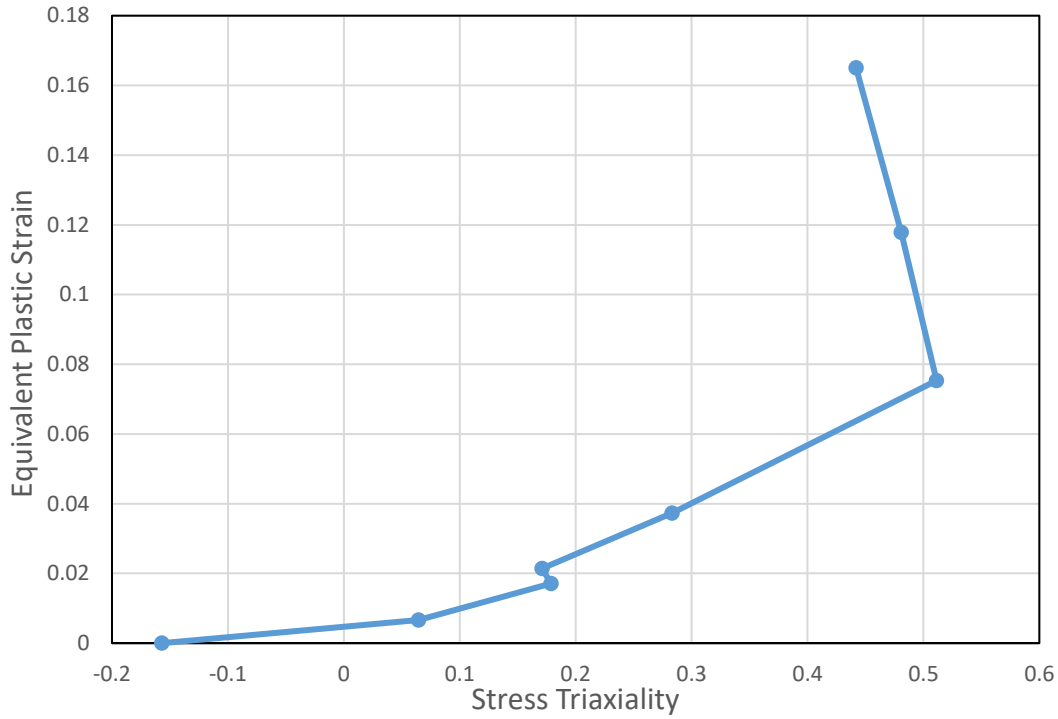

Figure 5.216. Equivalent Plastic Strain - Stress Triaxiality Plot of First Fracture Element (VM-JC-HC)

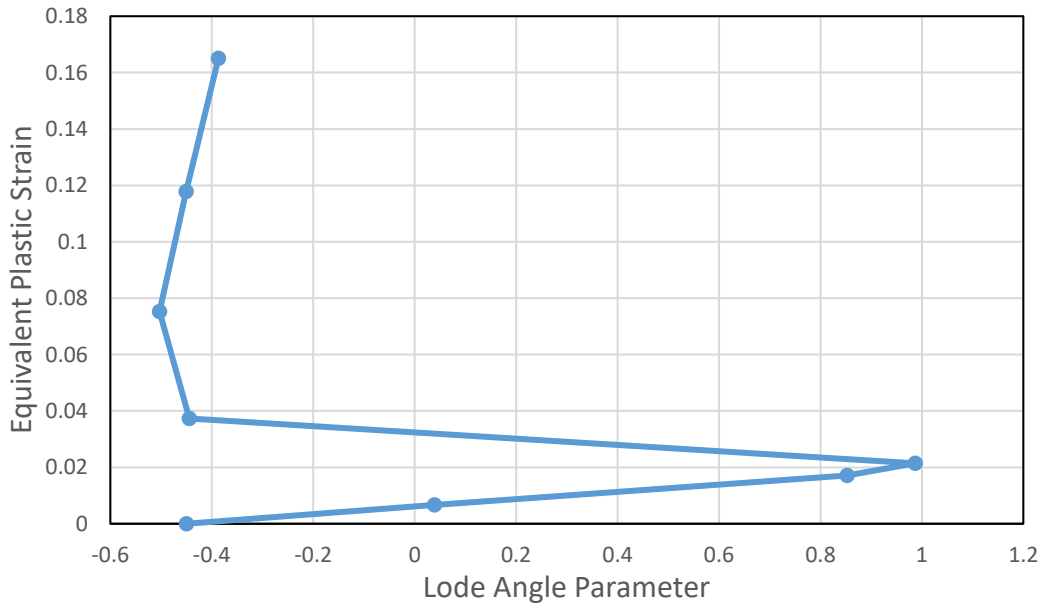

Figure 5.217. Equivalent Plastic Strain – Lode Angle Parameter Plot of First Fracture Element (VM-JC-HC)

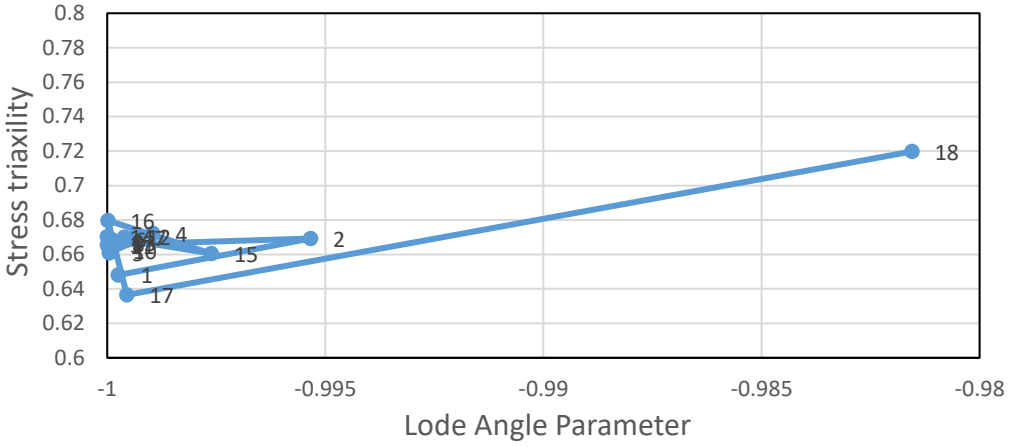
Stress triaxility
0.8
0.78
0.76
0.74
0.72
0.7
0.68
0.66
0.64
0.62
0.6
-1
-0.995
-0.99
-0.985
-0.98
Lode Angle Parameter
18
16
2
15
1
17

(a)

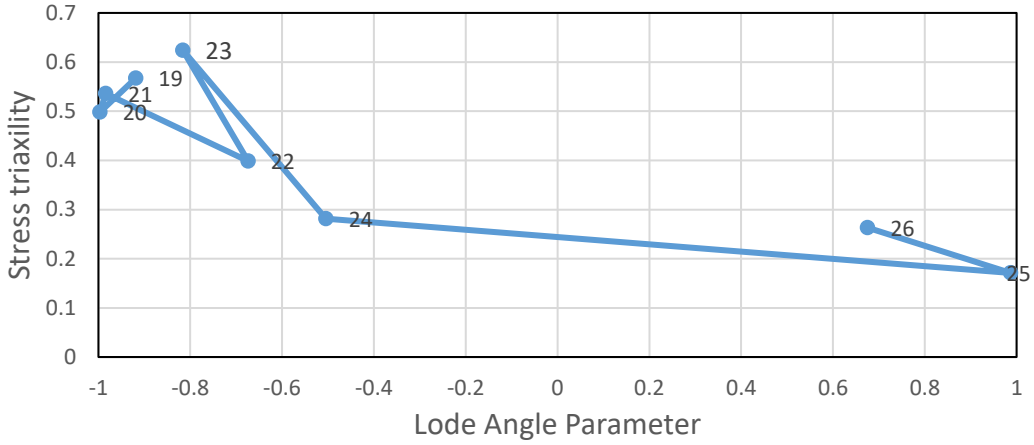
Stress triaxility
0.7
0.6
0.5
0.4
0.3
0.2
0.1
0
-1
-0.8
-0.6
-0.4
-0.2
0
0.2
0.4
0.6
0.8
1
Lode Angle Parameter
23
19
21
20
22
24
26
25

(b)

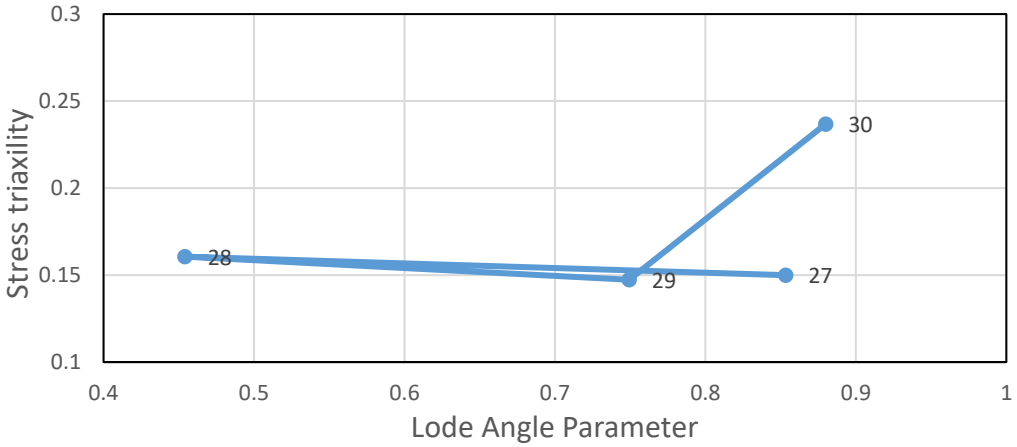
Stress triaxility
0.3
0.25
0.2
0.15
0.1
0.4
0.5
0.6
0.7
0.8
0.9
1
Lode Angle Parameter
30
28
29
27

(c)

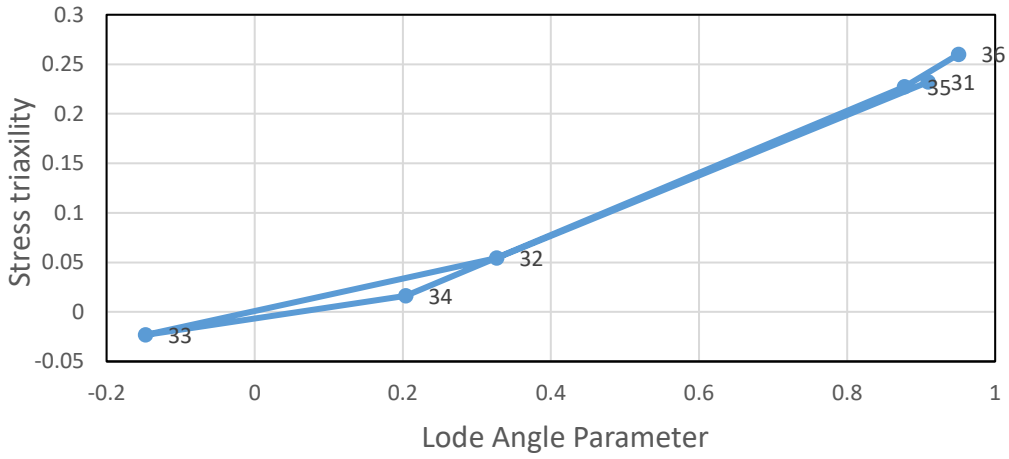

(d)

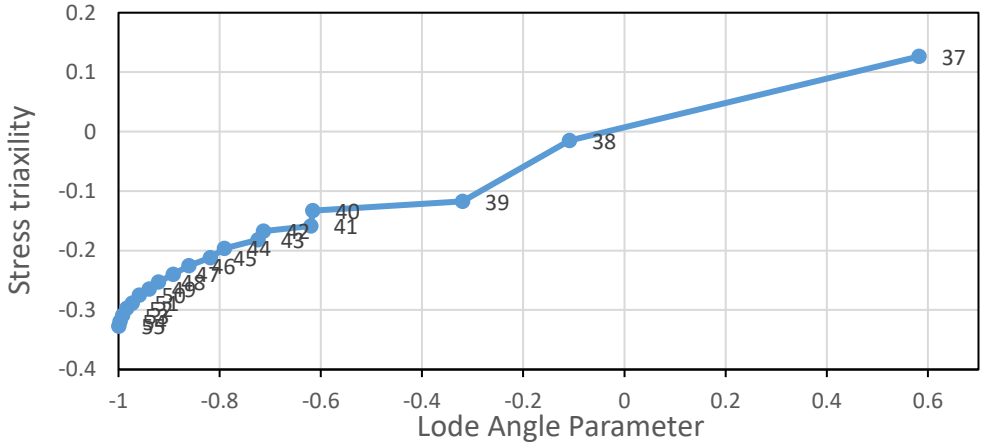

(e)

Figure 5.218. The variation of triaxiality values with respect to Lode angle parameter values (a) for punch (b) for punch shoulder or corner (c) for the clearance between die and punch (d) for die shoulder or corner and (e) for the blank holder regions of the blank at 20 mm cup depth for Al2024 aluminum (VM-JC-HC)

The triaxiality values vary generally between 0.6 and 0.8 under the punch whereas the Lode angle parameter values change between -0.8 and -1 up to a distance of 20 mm from the center. When the pre-rupture state of sheet is examined, it is seen that equi-biaxial stress conditions dominates up to 20 mm from the center of the blank. At punch shoulder, triaxiality values are positive with varying Lode angle parameter values. After this region, triaxiality values are decreasing with negative Lode angle parameter values. At the die corner, the dominant state is shear. Fracture occurs at the punch shoulder in tension situation. Also, under blank holder region both values of triaxiality and Lode angle parameter are negative so, it is in compression state. Fracture occurs in the tension situation at the punch shoulder.

CHAPTER 6

CONCLUSION & FUTURE WORKS

6.1 Conclusion

In this study, von Mises and Hill48 yield criteria, and Hosford Coulomb and Johnson Cook ductile fracture criteria are considered to simulate the square cup drawing process for two different sheet materials. Cylindrical cup drawing is also analyzed by using von Mises yield criterion and Hosford Coulomb ductile fracture criterion. In the simulations different hardening criteria are used. The following conclusions are acquired:

1. For the square cup drawing in the rolling and the transverse directions;
    - the part of the sheet under the punch is in equi-biaxial tension condition,
    - on the punch shoulder the sheet is in tension and the dominant deformation type changes from equi-biaxial tension to uniaxial tension as the distance from the center of the blank increases,
    - at the clearance between die and the punch sheet is in tension and the uniaxial tension condition is the dominant deformation type,
    - on the die shoulder tension type deformation is observed,
    - under the blank holder the sheet is in compression condition and the thickness increases towards the rim,
    - although similar deformation conditions are observed along the rolling and the transverse directions, there are differences in the variations due to anisotropy.
2. For the square cup drawing in the diagonal direction;
    - the part of the sheet under the punch is equi-biaxial tension condition,

- on the punch shoulder the sheet is in tension and the dominant deformation type changes from equi-biaxial tension to uniaxial tension as the distance from the center of the blank increases,
- at the clearance between die and the punch sheet is in tension and the uniaxial tension condition is the dominant deformation type,
- on the die shoulder the deformation type changes from tension to compression,
- under the blank holder the sheet is in compression condition; however, the thickness decreases towards the rim.

3. For the cylindrical cup drawing;
   - the part of the sheet under the punch is equi-biaxial tension condition,
   - on the punch shoulder the sheet is in tension and the dominant deformation type changes from equi-biaxial tension condition to uniaxial tension condition as the distance from the center of the blank increases.
   - at the clearance between die and the punch sheet is in tension and the uniaxial tension condition is the dominant deformation type,
   - on the die shoulder the deformation type for the sheet changes from tension to compression,
   - under the blank holder the sheet is in compression condition and the thickness increases towards the rim.
4. For all analyses made with aluminum Al-2024 and steel AISI-304 the deformation conditions show the same tendency.
5. For all the cases of square cup drawing, high variations are observed for the Lode angle parameter and stress triaxiality values in the region between die and punch.
6. Significant differences are observed in determining the fracture point depending on the ductile fracture criterion and yield criterion used.
7. For all square cup drawing cases fracture occurs along the diagonal direction.
8. For Al-2024 material, fracture is noticed due to the shear state at the die corner when Johnson Cook ductile fracture criterion is used. However, fracture is

observed at the punch corner due to tension state when Hosford Coulomb ductile fracture criterion is applied.

9. It is observed that triaxiality and Lode angle parameter values can be efficiently used to determine the deformation nature of the cup drawing and determine the fracture.

6.2 Future Works

Possible future works that can be realized are suggested below,

- Analyzes can be repeated by increasing the number of materials
- Analyzes can be repeated by using different ductile criteria and yield criteria.
- Different materials can be used by conducting the relating tests.
- Deep drawing analyzes can be performed with more complicated shapes.

REFERENCES

[1] A. K. Rana, S. Datta, and S. Kundu, “Deformation behaviour during deep drawing operation under simple loading path: A simulation study,” *Mater. Today Proc.*, vol. 26, pp. 750–755, 2019, doi: 10.1016/j.matpr.2019.12.413.

[2] R. Padmanabhan, M. C. Oliveira, J. L. Alves, and L. F. Menezes, “Influence of process parameters on the deep drawing of stainless steel,” *Finite Elem. Anal. Des.*, vol. 43, no. 14, pp. 1062–1067, 2007, doi: 10.1016/j.finel.2007.06.011.

[3] E. J. Obermeyer and S. A. Majlessi, “A review of recent advances in the application of blank-holder force towards improving the forming limits of sheet metal parts,” *J. Mater. Process. Technol.*, vol. 75, no. 1–3, pp. 222–234, 1998, doi: 10.1016/S0924-0136(97)00368-3.

[4] N. Krishnan and J. Cao, “Estimation of optimal blank holder force trajectories in segmented binders using an ARMA model,” *J. Manuf. Sci. Eng.*, vol. 125, no. 4, pp. 763–770, 2003, doi: 10.1115/1.1616948.

[5] Z. Q. Sheng, S. Jirathearanat, and T. Altan, “Adaptive FEM simulation for prediction of variable blank holder force in conical cup drawing,” *Int. J. Mach. Tools Manuf.*, vol. 44, no. 5, pp. 487–494, 2004, doi: 10.1016/j.ijmachtools.2003.11.001.

[6] S. Yoshihara, K. I. Manabe, and H. Nishimura, “Effect of blank holder force control in deep-drawing process of magnesium alloy sheet,” *J. Mater. Process. Technol.*, vol. 170, no. 3, pp. 579–585, 2005, doi: 10.1016/j.jmatprotec.2005.06.028.

[7] M. Colgan and J. Monaghan, “Deep drawing process: Analysis and experiment,” *J. Mater. Process. Technol.*, vol. 132, no. 1–3, pp. 35–41, 2003, doi: 10.1016/S0924-0136(02)00253-4.

[8] J. Wang, “Principles of the draw-bend springback test,” *ProQuest Diss. Theses*, pp. 185-185 p., 2004, [Online]. Available: http://search.proquest.com/docview/305140046?accountid=26400%5Cnhttp:

//www.yidu.edu.cn/educhina/educhina.do?artifact=&svalue=Principles+of+the+draw-bend+springback+test&stype=2&s=on%5Cnhttp://pqdt.calis.edu.cn/Detail.aspx?pid=3148224%5Cnhttp://sfx.bit.edu

[9] W. Hu, “An orthotropic yield criterion in a 3-D general stress state,” *Int. J. Plast.*, vol. 21, no. 9, pp. 1771–1796, 2005, doi: 10.1016/j.ijplas.2004.11.004.

[10] R. Hill, *The Mathematical Theory of Plasticity*. Clarendon Press, 1998.

[11] L. M. Kachanov, *Fundamentals of the Theory of Plasticity*. Dover Publications, 2004.

[12] A. S. Khan and S. Huang, *Continuum Theory of Plasticity*. John Wiley and Sons, 1995.

[13] M. B. Gorji and D. Mohr, “Predicting shear fracture of aluminum 6016-T4 during deep drawing: Combining Yld-2000 plasticity with Hosford–Coulomb fracture model,” *Int. J. Mech. Sci.*, vol. 137, no. January, pp. 105–120, 2018, doi: 10.1016/j.ijmecsci.2018.01.008.

[14] D. Mohr and S. J. Marcadet, “Micromechanically-motivated phenomenological Hosford-Coulomb model for predicting ductile fracture initiation at low stress triaxialities,” *Int. J. Solids Struct.*, vol. 67–68, pp. 40–55, 2015, doi: 10.1016/j.ijsolstr.2015.02.024.

[15] F. Barlat, H. Aretz, J. W. Yoon, M. E. Karabin, J. C. Brem, and R. E. Dick, “Linear transfomation-based anisotropic yield functions,” *Int. J. Plast.*, vol. 21, no. 5, pp. 1009–1039, 2005, doi: 10.1016/j.ijplas.2004.06.004.

[16] F. Barlat *et al.*, “Plane stress yield function for aluminum alloy sheets - Part 1: Theory,” *Int. J. Plast.*, vol. 19, no. 9, pp. 1297–1319, 2003, doi: 10.1016/S0749-6419(02)00019-0.

[17] A. P. Karafillis and M. C. Boyce, “A general anisotropic yield criterion using bounds and a transformation weighting tensor,” *J. Mech. Phys. Solids*, vol. 41, pp. 1859–1886, 1993.

[18] R. Hill, *Theoretical plasticity of textured aggregates*. Math. Proc. Camb. Philos. Soc., 1979.

[19] Y. Lou and H. Huh, "Extension of a shear-controlled ductile fracture model considering the stress triaxiality and the Lode parameter," *Int. J. Solids Struct.*, vol. 50, no. 2, pp. 447–455, 2013, doi: 10.1016/j.ijsolstr.2012.10.007.

[20] Y. Bao and T. Wierzbicki, "On fracture locus in the equivalent strain and stress triaxiality space," *Int. J. Mech. Sci.*, vol. 46, no. 1, pp. 81–98, 2004, doi: 10.1016/j.ijmecsci.2004.02.006.

[21] M. Dunand and D. Mohr, "Hybrid experimental-numerical analysis of basic ductile fracture experiments for sheet metals," *Int. J. Solids Struct.*, vol. 47, no. 9, pp. 1130–1143, 2010, doi: 10.1016/j.ijsolstr.2009.12.011.

[22] F. A. McClintock, "A criterion of ductile fracture by growth of holes.," *J. Appl. Mech.*, vol. 35, pp. 363–371, 1968.

[23] R. JR and Tracey DM, "On the ductile enlargement of voids in triaxial stress fields," *J. Mech. Phys. Solids*, vol. 17, pp. 17–201, 1969.

[24] A. L. Gurson, "Continuum theory of ductile Fracture by void nucleation and growth. Part I: Yield criteria and flow rules for porous ductile media," *J. Eng. Mater. Technol*, vol. 99, pp. 2–15, 1975.

[25] Y. Bai and T. Wierzbicki, "A new model of metal plasticity and fracture with pressure and Lode dependence," *Int. J. Plast.*, vol. 24, no. 6, pp. 1071–1096, 2008, doi: 10.1016/j.ijplas.2007.09.004.

[26] Y. Bao, "Prediction of Ductile Crack Formation in Uncracked Bodies," *PhD Thesis*, pp. 1–253, 2003.

[27] J. W. Hancock and A. C. Mackenzie, "On the mechanisms of ductile failure in high-strength steels subjected to multi-axial stress states," *J. Mech. Phys. Solids*, vol. 24, pp. 147–160, 1976.

[28] J. R. Rice, "The localization of plastic deformation," *14th Int. Congr. Theoratical Appl. Mech.*, pp. 207–220, 1976, doi: 10.1.1.160.6740.

[29] Y. Bai and T. Wierzbicki, “Application of extended Mohr-Coulomb criterion to ductile fracture,” *Int. J. Fract.*, vol. 161, no. 1, pp. 1–20, 2010, doi: 10.1007/s10704-009-9422-8.

[30] Y. Bai and T. Wierzbicki., “Predicting fracture of AHSS sheets on the punch and die radii and sidewall.,” in *In Proceedings: Numisheet*, 2008, pp. 297–306.

[31] Y. Li and D. G. Karr, “Prediction of ductile fracture in tension by bifurcation, localization, and imperfection analyses,” *Int. J. Plast.*, vol. 25, no. 6, pp. 1128–1153, 2009, doi: 10.1016/j.ijplas.2008.07.001.

[32] X. Sun, K. S. Choi, W. N. Liu, and M. A. Khaleel, “Predicting failure modes and ductility of dual phase steels using plastic strain localization,” *Int. J. Plast.*, vol. 25, no. 10, pp. 1888–1909, 2009, doi: 10.1016/j.ijplas.2008.12.012.

[33] R. Hill, “A theory of the yielding and plastic flow of anisotropic metals,” *Proc. Roy. Soc. London*, vol. 193, pp. 281–297, 1948.

[34] S. D. Kumar, T. R. Amjith, and C. Anjaneyulu, “Forming Limit Diagram Generation of Aluminum Alloy AA2014 Using Nakazima Test Simulation Tool,” *Procedia Technol.*, vol. 24, pp. 386–393, 2016, doi: 10.1016/j.protcy.2016.05.053.

[35] R. K. Boger, “Non-Monotonic Strain Hardening and Its Constitutive Representations,” Ohio State University, 2006.

[36] M. Luo, “Anisotropic ductile fracture of metal sheets: experimental investigation and constitutive modeling,” p. 311, 2012, [Online]. Available: http://dspace.mit.edu/handle/1721.1/74983

[37] D. Systems, “Johson Cook Damage Criterion,” *3DS*.

[38] D. Systems, “Hosford Coulomb Damage Criterion,” *3DS*. https://help.3ds.com/2022x/english/dsdoc/SIMA3DXKEYRefMap/simakey-r-damageinitiation.htm?contextscope=cloud#simakey-r-damageinitiation

[39] C. C. Roth and D. Mohr, “Ductile fracture experiments with locally

proportional loading histories," *Int. J. Plast.*, vol. 79, pp. 328–354, 2016, doi: 10.1016/j.ijplas.2015.08.004.

[40] D. Mohr, "Dynamic behavior of materials and structures [Lecture Notes].," 2015. [Online]. Available: https://ethz.ch/

[41] K. Wang, "Edge fracture of AHSS sheets under out-of-plane loading followed by in-plane loading," 2015.

[42] N. Park, H. Huh, S. J. Lim, Y. Lou, Y. S. Kang, and M. H. Seo, "Fracture-based forming limit criteria for anisotropic materials in sheet metal forming," *Int. J. Plast.*, vol. 96, pp. 1–35, 2017, doi: 10.1016/j.ijplas.2016.04.014.

[43] J. Peng, P. Zhou, Y. Wang, Q. Dai, D. Knowles, and M. Mostafavi, "Stress triaxiality and lode angle parameter characterization of flat metal specimen with inclined notch," *Metals (Basel).*, vol. 11, no. 10, 2021, doi: 10.3390/met11101627.

[44] Y. Bai, "Effect of Loading History on Necking and Fracture," *Technology*, no. 2000, pp. 1–262, 2008.

[45] S. Neto, D. Peric, and D. Owen, *Computational Methods for Plasticity, Theory and Applications*. Willey, 2008.

[46] D. W. Pepper and J. C. Heinrich, *The Finite Element Method*, 3rd ed. Taylor & Francis Group, 2017.

[47] U. . Dixit, "Finite Element Method: Introduction [Lecture Notes]," India.

[48] I. Koutromanos, *Fundamentals of Finite Element Analysis: Linear Finite Element Analysis*. John Wiley and Sons, 2018.

[49] D. V. Hutton, "Fundamentals of finite element analysis." McGraw-Hill, 2004.

[50] T. Wierzbicki, Y. Bao, Y. W. Lee, and Y. Bai, "Calibration and evaluation of seven fracture models," *Int. J. Mech. Sci.*, vol. 47, no. 4-5 SPEC. ISS., pp. 719–743, 2005, doi: 10.1016/j.ijmecsci.2005.03.003.

[51] C. Wang, D. Li, B. Meng, and M. Wan, "Effect of anisotropic yield

functions on prediction of critical process window and deformation behavior for hydrodynamic deep drawing of aluminum alloys," *Metals (Basel).*, vol. 10, no. 4, 2020, doi: 10.3390/met10040492.

[52] L. Xue, "Ductile fracture modeling: theory, experimental investigation and numerical verification," *PhD Thesis*, no. January 2009, p. 251, 2007, [Online]. Available: http://dspace.mit.edu/handle/1721.1/40876

[53] K. Senthil, B. Arindam, R. Mittal, M. A. Iqbal, and N. K. Gupta, "Numerical Investigations on the Impact of Hemi Spherically Tipped Projectiles on Thin Plates," *Procedia Eng.*, vol. 173, pp. 1926–1931, 2017, doi: 10.1016/j.proeng.2016.12.254.

[54] J. Papasidero, V. Doquet, and D. Mohr, "Ductile fracture of aluminum 2024-T351 under proportional and non-proportional multi-axial loading: Bao-Wierzbicki results revisited," *Int. J. Solids Struct.*, vol. 69–70, pp. 459–474, 2015, doi: 10.1016/j.ijsolstr.2015.05.006.

[55] H. Do Kweon, J. W. Kim, O. Song, and D. Oh, "Determination of true stress-strain curve of type 304 and 316 stainless steels using a typical tensile test and finite element analysis," *Nucl. Eng. Technol.*, vol. 53, no. 2, pp. 647–656, 2021, doi: 10.1016/j.net.2020.07.014.

[56] T. Manninen, A. S. Korhonen, and P. Aspegren, "Identifying the material parameters of a combined isotropic and non-linear kinematic hardening model for AISI 304 stain- less steel sheet," vol. 1, no. 3, pp. 451–455, 2004.

[57] J. Lian *et al.*, "An evolving non-associated Hill48 plasticity model accounting for anisotropic hardening and r-value evolution and its application to forming limit prediction," *Int. J. Solids Struct.*, vol. 151, pp. 20–44, 2018, doi: 10.1016/j.ijsolstr.2017.04.007.

[58] J. J. Berthelier, J. Forest, X. Chen, and J. Yang, "Experimental analysis and numerical simulation of the operation of the DEMETER electric field instrument in deep equatorial plasma depletions," *IEEE Trans. Plasma Sci.*, vol. 36, no. 5 SUPPL. 4, pp. 2859–2866, 2008, doi:

10.1109/TPS.2008.2003078.

[59] S. Qin, Z. Wang, and A. M. Beese, “Orientation and stress state dependent plasticity and damage initiation behavior of stainless steel 304L manufactured by laser powder bed fusion additive manufacturing,” *Extrem. Mech. Lett.*, vol. 45, p. 101271, 2021, doi: 10.1016/j.eml.2021.101271.